frontiers | Research Topics

Biomedical applications of natural polymers

Edited by
Yongsheng Yu, Qian Feng, Kunyu Zhang and Boguang Yang

Published in
Frontiers in Bioengineering and Biotechnology
Frontiers in Materials

ISSN 1664-8714
ISBN 978-2-8325-2501-2
DOI 10.3389/978-2-8325-2501-2

About Frontiers

Frontiers is more than just an open access publisher of scholarly articles: it is a pioneering approach to the world of academia, radically improving the way scholarly research is managed. The grand vision of Frontiers is a world where all people have an equal opportunity to seek, share and generate knowledge. Frontiers provides immediate and permanent online open access to all its publications, but this alone is not enough to realize our grand goals.

Frontiers journal series

The Frontiers journal series is a multi-tier and interdisciplinary set of open-access, online journals, promising a paradigm shift from the current review, selection and dissemination processes in academic publishing. All Frontiers journals are driven by researchers for researchers; therefore, they constitute a service to the scholarly community. At the same time, the *Frontiers journal series* operates on a revolutionary invention, the tiered publishing system, initially addressing specific communities of scholars, and gradually climbing up to broader public understanding, thus serving the interests of the lay society, too.

Dedication to quality

Each Frontiers article is a landmark of the highest quality, thanks to genuinely collaborative interactions between authors and review editors, who include some of the world's best academicians. Research must be certified by peers before entering a stream of knowledge that may eventually reach the public - and shape society; therefore, Frontiers only applies the most rigorous and unbiased reviews. Frontiers revolutionizes research publishing by freely delivering the most outstanding research, evaluated with no bias from both the academic and social point of view. By applying the most advanced information technologies, Frontiers is catapulting scholarly publishing into a new generation.

What are Frontiers Research Topics?

Frontiers Research Topics are very popular trademarks of the *Frontiers journals series*: they are collections of at least ten articles, all centered on a particular subject. With their unique mix of varied contributions from Original Research to Review Articles, Frontiers Research Topics unify the most influential researchers, the latest key findings and historical advances in a hot research area.

Find out more on how to host your own Frontiers Research Topic or contribute to one as an author by contacting the Frontiers editorial office: frontiersin.org/about/contact

Biomedical applications of natural polymers

Topic editors
Yongsheng Yu — Chinese Academy of Sciences, China
Qian Feng — Chongqing University, China
Kunyu Zhang — South China University of Technology, China
Boguang Yang — The Chinese University of Hong Kong, China

Topic coordinator
Wei Kang — Dalian University of Technology, China

Citation
Yu, Y., Feng, Q., Zhang, K., Yang, B., eds. (2023). *Biomedical applications of natural polymers*. Lausanne: Frontiers Media SA. doi: 10.3389/978-2-8325-2501-2

Table of contents

frontiers | Frontiers in Bioengineering and Biotechnology

TYPE Editorial
PUBLISHED 24 November 2022
DOI 10.3389/fbioe.2022.1077823

OPEN ACCESS

EDITED AND REVIEWED BY
Hasan Uludag,
University of Alberta, Canada

*CORRESPONDENCE
Yongsheng Yu,
yuyongsheng@cigit.ac.cn

SPECIALTY SECTION
This article was submitted to Biomaterials, a section of the journal Frontiers in Bioengineering and Biotechnology

RECEIVED 23 October 2022
ACCEPTED 03 November 2022
PUBLISHED 24 November 2022

CITATION
Feng Q, Zhang K, Yang B and Yu Y (2022), Editorial: Biomedical applications of natural polymers. *Front. Bioeng. Biotechnol.* 10:1077823. doi: 10.3389/fbioe.2022.1077823

Editorial: Biomedical applications of natural polymers

Qian Feng[1,2,3], Kunyu Zhang[4], Boguang Yang[5] and Yongsheng Yu[1,2]*

[1]Chongqing Institute of Green and Intelligent Technology, Chinese Academy of Sciences, Chongqing, China, [2]Chongqing School, University of Chinese Academy of Sciences, Chongqing, China, [3]Bioengineering College, Chongqing University, Chongqing, China, [4]School of Biomedical Sciences and Engineering, South China University of Technology, Guangzhou, China, [5]Department of Biomedical Engineering, The Chinese University of Hong Kong, Hong kong, China

KEYWORDS

biomedical applications, natural polymers, tissues repair, wearable sensor, hydrogel

Editorial on the Research Topic
Biomedical applications of natural polymers

Introduction

Natural polymers are attracting a lot of interest for use in biomedical applications due to their high biocompatibilities and ease of modification. Regenerative medicine, drug delivery, and targeted therapy are the main biomedical applications for natural polymers. For biomedical applications, natural polymers are chosen for their biocompatibilities, porosities, hydrophobicities/hydrophilicities, surface energies, degradation rates, and other desirable characteristics. Moreover, they can undergo a diverse range of chemical or physical modifications to fulfill the requirements for specific biomedical applications.

This Research Topic is designed to attract recent, novel findings in regenerative medicine, peptide/protein modulators of protein-protein interactions, natural polymer-based biosensors in biomedical applications, natural polymers for drug delivery, computer-aided design of original natural polymers, design and preparation of antibiosis natural polymers, and functionalization of virus-like particles. The Research Topic incudes 14 high-quality papers focused on the research areas highlighted above.

Applications in tissue repair

Nature polymers are frequently used to construct scaffolds with customized structures and functionalities that can improve cell growth and the formation of new tissue. Zheng et al. reported a linearly cross-linked sodium HA hydrogel (HA-engineered hydrogel) used as a retinal patch in the rabbit rhegmatogenous retinal detachment (RRD) model. The HA-engineered hydrogel exhibited a similar dynamic viscosity, cohesiveness, and G′ compared

with the commercial HA hydrogel. The findings demonstrated that the HA-engineered hydrogel can facilitate complete retinal reattachment without the need for silicone oil endotamponade or expansile gas. It may serve as a promising retinal patch for sealing retinal breaks during retinal detachment repair.

By cross-linking GO-arabinoxylan and polyvinyl alcohol (PVA) with tetraethyl orthosilicate (TEOS), Ul-Haq and coworkers functionalized arabinoxylan and graphene oxide (GO) using a hydrothermal method to produce multifunctional composite hydrogels. The hydrogel accelerated wound healing and promoted vascularization, with no major inflammation observed within 7 days. In order to improve the efficiency of ginsenosides (GS) transdermal absorption, Jin et al. prepared delivery vehicles using GS liposomes (GSLs) and GS niosomes (GSNs). The vehicles suppressed skin lipid peroxidation caused by ultraviolet (UV) radiation and reduced the amounts of MMPs and inflammatory cytokines in skin tissue.

Chen et al. summarized recent progress in natural polymer-based scaffolds for soft tissue repair. Furthermore, the authors discussed challenges in clinical translations and materials design. Zhang et al. reviewed the physicochemical properties and the latest applications of hydrogels in premature ovarian failure and intrauterine adhesion. The authors also summarized the limitations in clinical application of hydrogels and provide future prospects. Yan et al. proved that human umbilical cord mesenchymal stem cell-derived exosomes can accelerate diabetic cutaneous wound healing, providing a promising therapeutic strategy for chronic diabetic wound repair. Yang et al. reviewed the various structures of natural polysaccharides with high commercial values, and their various applications in treating various oral diseases such as drug delivery, tissue regeneration, material modification, and tissue repair.

Applications as wearable sensors

Owing to the advantages of hydrogels, hydrogel-based flexible electronic devices were developed for future healthcare and biomedical applications. Chen et al. designed a mechanically resilient and conductive hydrogel exhibiting a double-network structure. The first dense network comprised Ca^{2+}-crosslinked alginate, and the second loose network consisted of ionic pair-crosslinked polyzwitterion. The results demonstrated the enduring accuracy and sensitivity of the hydrogel in detecting human motions, including large joint flexion, foot planter pressure measurement, and local muscle movement. Hu et al. developed a natural polymer-based conductive hydrogel formed by the Schiff base reaction between hydrazide-grafted hyaluronic acid and oxidized chitosan, with added KCl employed as a conductive filler. The hydrogel exhibited excellent mechanical properties, good sensitivity (GF = 2.64), durability, and stability, even in cold conditions (−37°C).

Applications in other fields

There is no effective treatment for placental dysfunction. Therefore, Jiang et al. reviewed nanotechnologies for placental dysfunctional. In order to provide a foundational understanding of placental dysfunction, potential delivery targets, and recent research on placenta-targeted nanoparticle delivery systems for the potential treatment of placental dysfunction, the authors highlighted candidate nanoparticle-loaded molecules. Xia et al. summarized the structures and biological characteristics of chitosan and its derivatives. Moreover, the authors reviewed their applications in therapeutics, drug delivery, anti-infection, wound healing, tissue regeneration, and anticancer. Although absorbable plates and screws are used to treat rib fractures in clinical settings, it is unclear which type of screw fixation method is more effective. Thus, Xue et al. evaluated five different types of screw fixation methods on anterior ribs, lateral ribs, and posterior ribs, using finite element analysis. The authors provided a basis and a reference for clinical application, and presented the best screw fixation method on an absorbable plate for rib fractures. Chen et al. developed an injectable hyaluronic acid (HA)/oxidized chitosan (OCS) hydrogel that slowly released micro hypochlorous acid (HClO). The positive charge of OCS can introduce a sustainable antibacterial effect. This hydrogel may be a promising wound dressing material in clinical treatments.

Outlook

Natural polymers have been broadly utilized in tissue culture, wound treatment, implantation, controlled drug delivery, targeted therapy of diseases, etc. However, their expansion in biomedical applications has encountered two main challenges: 1) limited strategies for functional modification of natural polymers, and 2) limited new fields of application. Fourteen top-quality articles have been published in this Research Topic on biomedical applications of natural polymers. We hope that this Research Topic proves meaningful for novel natural

polymer designs, the evolution of advanced fabrication techniques, and biomedical applications.

Author contributions

QF and YY drafted the manuscript. KZ and BY corrected the draft. All authors listed approved it for publication.

Funding

This study was supported by the National Natural Science Foundation of China (No. 81902622).

Conflict of interest

The authors declare that the research was conducted in the absence of any commercial or financial relationships that could be construed as a potential conflict of interest.

Publisher's note

frontiers in Bioengineering and Biotechnology

ORIGINAL RESEARCH
published: 31 January 2022
doi: 10.3389/fbioe.2022.829868

Human Umbilical Cord Mesenchymal Stem Cell-Derived Exosomes Accelerate Diabetic Wound Healing *via* Ameliorating Oxidative Stress and Promoting Angiogenesis

Chenchen Yan[1†], Yan Xv[1†], Ze Lin[1†], Yori Endo[2], Hang Xue[1], Yiqiang Hu[1], Liangcong Hu[1], Lang Chen[1], Faqi Cao[1], Wu Zhou[1], Peng Zhang[3]* and Guohui Liu[1]**

[1]Department of Orthopedics, Union Hospital, Tongji Medical College, Huazhong University of Science and Technology, Wuhan, China, [2]Department of Plastic Surgery, Brigham and Women's Hospital, Harvard Medical School, Boston, MA, United States, [3]Department of Orthopedics, Suzhou Science and Technology Town Hospital, The Affiliated Suzhou Science and Technology Town Hospital of Nanjing Medical University, Suzhou, China

Diabetic wounds remain a great challenge for clinicians due to the multiple bacterial infections and oxidative damage. Exosomes, as an appealing nanodrug delivery system, have been widely applied in the treatment of diabetic wounds. Endovascular cells are important component cells of the vascular wall. Herein, we investigated the effects of HUCMSCs and HUC-Exos (exosomes secreted by HUCMSCs) on diabetic wound healing. In this study, HUVECs were coincubated with HUCMSCs, and HUC-Exos were utilized for *in vitro* and *in vivo* experiments to verify their roles in the regulation of diabetic wound healing. Our results demonstrated that HUCMSCs have the ability to regulate oxidative stress injuries of endothelial cells through exosomes and accelerate diabetic cutaneous wound healing *in vitro*. The present study suggests that HUC-Exos accelerate diabetic cutaneous wound healing, providing a promising therapeutic strategy for chronic diabetic wound repair.

Keywords: diabetes, exosome, wound healing, stem cells, endothelial cells

OPEN ACCESS

Edited by:
Kunyu Zhang,
Johns Hopkins University,
United States

Reviewed by:
Zuolin Wang,
Tongji University, China
Dongyang Qian,
Guangzhou Medical University, China

****Correspondence:***
Guohui Liu
liuguohui@medmail.com.cn
Peng Zhang
zp801223@njmu.edu.cn
Wu Zhou
wuzhoutjmu1986@163.com

[†]These authors have contributed equally to this work

Specialty section:
This article was submitted to Biomaterials, a section of the journal Frontiers in Bioengineering and Biotechnology

Received: *06 December 2021*
Accepted: *03 January 2022*
Published: *31 January 2022*

Citation:
Yan C, Xv Y, Lin Z, Endo Y, Xue H, Hu Y, Hu L, Chen L, Cao F, Zhou W, Zhang P and Liu G (2022) Human Umbilical Cord Mesenchymal Stem Cell-Derived Exosomes Accelerate Diabetic Wound Healing via Ameliorating Oxidative Stress and Promoting Angiogenesis. Front. Bioeng. Biotechnol. 10:829868. doi: 10.3389/fbioe.2022.829868

INTRODUCTION

With the diet changes and rising average age of the global population, the prevalence of diabetes is on the rise (Martinengo et al., 2019; Kowluru, 2020). The main comorbidities of diabetes include chronic recalcitrant cutaneous wounds due to multiple drug-resistant bacterial infections, angiopathy, and oxidative damage to the microenvironment (Castleberry et al., 2016; Armstrong et al., 2017). Complications of diabetes are not only leading causes of disability and mortality worldwide but also a significant economic burden to the community (Bowling et al., 2015; Sen, 2019; Chang and Nguyen, 2021). About 22.3 million people in the United States were diagnosed with diabetes. Of which, 15%–25% are at risk for diabetic foot (Reardon et al., 2020). Specifically, up to 2%–3% of diabetics are at risk of developing active diabetic ulcer foot (Lavery et al., 2016). In addition, the recurrence rate of diabetic foot cannot be ignored. According to statistics, 40% of diabetic foot patients have onset symptoms after 1 year, and the probability of recurrence symptoms within 5 years is 65% (Lim et al., 2017). While many therapeutic strategies have been adopted to treat recalcitrant cutaneous wounds, the clinical results for those have been unsatisfactory (An et al., 2021; Deng et al., 2021). In order to

solve the problem of refractory wound healing and improve the prognosis, we aim to address the underlying angiopathy by restoring blood supply to the skin and tissue integrity (Wong et al., 2015; Qu et al., 2018; Wang et al., 2019).

Angiogenesis is the basis of blood supply and an important physiological response required to cure diabetic skin wounds. It has been known that vascular endothelial cells are the main driver of angiogenesis (Chen et al., 2018). Previous studies have reported that, under the high-glucose environment caused by diabetes, vascular endothelial cells are damaged by oxidative stress, resulting in low cell activity and decreased proliferation ability (Zhang et al., 2021). For example, the nicotinamide adenine dinucleotide phosphate (NADPH) oxidase (NOX) family is involved in bacterial inhibition, neutrophil chemotaxis, and signal transduction necessary for skin wound healing (Shinohara et al., 2007). Among them, NOX1 and NOX4 play a role in regulating the proliferation and differentiation of HUVECs. In addition, oxygen is essential for wound healing as the wound healing process relies on adenosine triphosphate (ATP) for energy (Thi et al., 2020). Nevertheless, oxygen makes contributions to the expression of other reactive oxygen species (ROS) on the condition that it was transformed into superoxide. Previous studies have shown that NOX activation and ROS release are both related to skin wound healing (Sadjadi et al., 2019).

HUCMSCs are high-profile due to their pluripotency. In recent years of research, HUCMSCs have been applied in many clinical fields, such as *in vitro* organ culture and heart and lung injury repair, made possible due to characteristics such as easier separation, purification, and culture (Pavlou et al., 2018). Some studies have shown that HUCMSCs can promote the formation of new blood vessels and strengthen tissue regeneration (Yin et al., 2021). In the research focusing on the mechanism of HUCMSCs, it was found that the exosomes derived from them have good stability and immunogenicity, with the ability to transport proteins and growth factors of different functions to exert different effects (Zhuang et al., 2020). Recent studies have shown that exosomes derived from HUCMSCs regulate the differentiation and proliferation of bone marrow mesenchymal stem cells (Wen et al., 2020). Studies have also shown that exosomes derived from HUCMSCs can regulate oxidative stress and inhibit cell hypoxia damage (Xue et al., 2018). Based on these findings, exosomes may serve as a promising candidate to promote angiogenesis in wound healing.

This study is thus intended to verify that exosomes from HUCMSCs can enhance angiogenesis by endothelial cells and to determine the effects of HUC-Exos (exosomes secreted by HUCMSCs) on cutaneous wound healing *in vivo*.

RESULTS

Hyperglycemia drives oxidative stress damage and impairs cellular function in HUVECs

To evaluate the oxidative stress damage caused by the hyperglycemic environment, we set up three groups of HUVECs in a culture medium with different glucose concentrations. The glucose concentrations in the culture medium were the normal physiological level (physiological levels quoted in our article refer to glucose concentration in the medium itself) and supranormal level (15 and 30 mM), respectively. Then we measured the oxidative stress level of each group at three time points: 24, 48, and 72 h after the incubation. Based on a previous study, DCFH-DA (2′,7′-dichlorodihydrofluorescein diacetate), as a ROS indicator, has the ability to visualize intracellular ROS variations (Jang and Sharkis, 2007). ROS flow fluorescence assay was performed in each group at the designated time points. Results show that the cells treated with high-level glucose concentrations had higher fluorescence intensity compared with the low-level group and middle-level group. Under the same conditions, the fluorescence intensity increased with the increase of culture time (**Figure 1A**). The same result is illustrated in the fluorescence intensity statistics (**Figures 1B–D**). Thus, the results showed that a high-glucose environment indeed induces oxidative stress in cells, and this effect increases with the duration of hyperglycemia. As mentioned above, NOX1 and NOX4, as oxidative stress-related factors, play an important role in the oxidative stress of endothelial cells. Besides, we detected the expression levels of oxidative stress-related factors at different time points in each group through Western blotting, and its outcome confirms that the expression levels of oxidative stress-related factors increased with time (**Figure 1E**). With the intention to detect endothelial cell activity, the tube formation experiment was performed, and the results showed that tube formation is reduced in a high-glucose environment (**Figure 1F**). The statistics of the tube formation experiment show the same result (**Figures 1G, H**). Cell proliferation-related factors cyclin D1 and cyclin D3 were analyzed by RT-qPCR, and the results of each group were consistent with Cell Counting Kit-8 (CCK-8) (**Figure 1I**). In addition, we evaluated the level of cell damage on HUVECs as reflected by the inflammatory response. The inflammatory factors IL-1β, IL-6, and TNF-α were analyzed by RT-qPCR, and the results showed that the intensity of the inflammatory response increased with the increase of glucose concentration (**Figures 1J–L**). The proliferation ability of HUVECs in each group was detected by Cell Counting Kit-8 (CCK-8) technology, and the results showed that the proliferation level of cells in the high-glucose group decreased compared with other groups, and this result became more significant over time (Supplementary Figure S1A). Together, these findings reflected that hyperglycemia drives oxidative stress damage and impairs cellular function in HUVECs.

HUCMSCs can regulate oxidative stress damage of HUVECs through exosomes

The effect of HUCMSCs on the regulation of oxidative stress damage in HUVECs was assessed. According to a previous study, GW4869 (hydrochloride hydrate) was utilized as an exosome secretion inhibitor (Dinkins et al., 2014). We established three groups of growth environments for HUVECs. The first group was HUVECs incubated in a 30-mM glucose medium. The second group was a coincubated system consisting of HUCMSCs and HUVECs incubated in a 30-mM glucose medium. Based on the

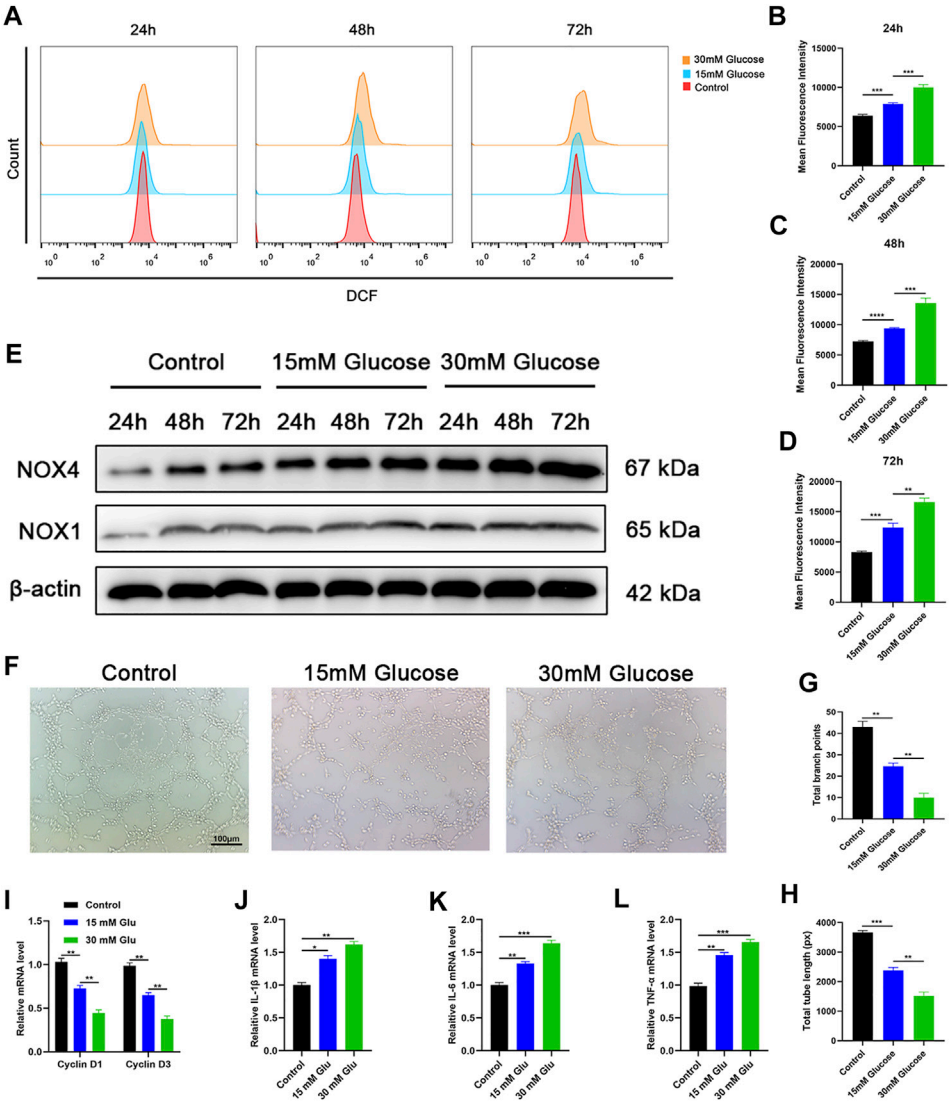

FIGURE 1 | Hyperglycemia drives oxidative stress damage and impairs cellular function in HUVECs. **(A)** Reduction of reactive oxygen species (ROS) in HUVECs assessed *via* flow cytometry with the DCFH-DA (2′,7′-dichlorodihydrofluorescein diacetate) probe following different treatments. **(B–D)** Quantitation of ROS depletion measured by the intensity of fluorescence of HUVECs. **(E)** Western blotting results of NOX1 and NOX4 in HUVECs following different treatments at varied time points. **(F)** A tube formation assay was performed to visualize the cell capillary network formation of HUVECs. Scale bar: 100 μm. **(G, H)** Quantitative analysis of the tube formation of HUVECs in the three groups. **(I)** RT-qPCR results of cyclin D1 and cyclin D3 expressions in the HUVECs following different treatments; **(J–L)** RT-qPCR results of IL-1β, IL-6, and TNF-α expressions in the HUVECs following different treatments. Differences were measured by one-way ANOVA followed by a Tukey *post hoc* test for pairwise comparison. Data presented as means ± SD. ****$p < 0.0001$, ***$p < 0.001$, **$p < 0.01$, and *$p < 0.05$.

condition of the second group, GW4869 was added into the third group to inhibit the secretion of exosomes. Based on the outcome shown in **Figure 1E**, we evaluated the expression levels of NOX1 and NOX4 in each group at the time point of 72 h through Western blotting. The results revealed that the first and third groups express increased levels of oxidative stress-related factors, while the second group showed the opposite consequence (**Figure 2A**). ROS flow fluorescence assay demonstrated that HUCMSCs reduced the fluorescence in the second group compared with the others. The third group, on the other hand, demonstrated a strong fluorescence. The statistical significance was detected between the groups (**Figures 2B, C**). Tube formation was performed to evaluate the capillary network formation by HUVECs. As shown in the results, the endothelial cells of the second group showed higher tube-forming ability, while the cells in the third group were hardly better than the first group in tube formation (**Figures 2D–F**). Then we conducted RT-qPCR, as a supplement, to analyze the expression levels of cyclin D1 and cyclin D3. The results showed that proliferation-related factors in the second group had higher levels than the other groups (**Figure 2G**). In order to evaluate the inflammatory response, we then employed RT-qPCR to detect IL-1β, IL-6, and

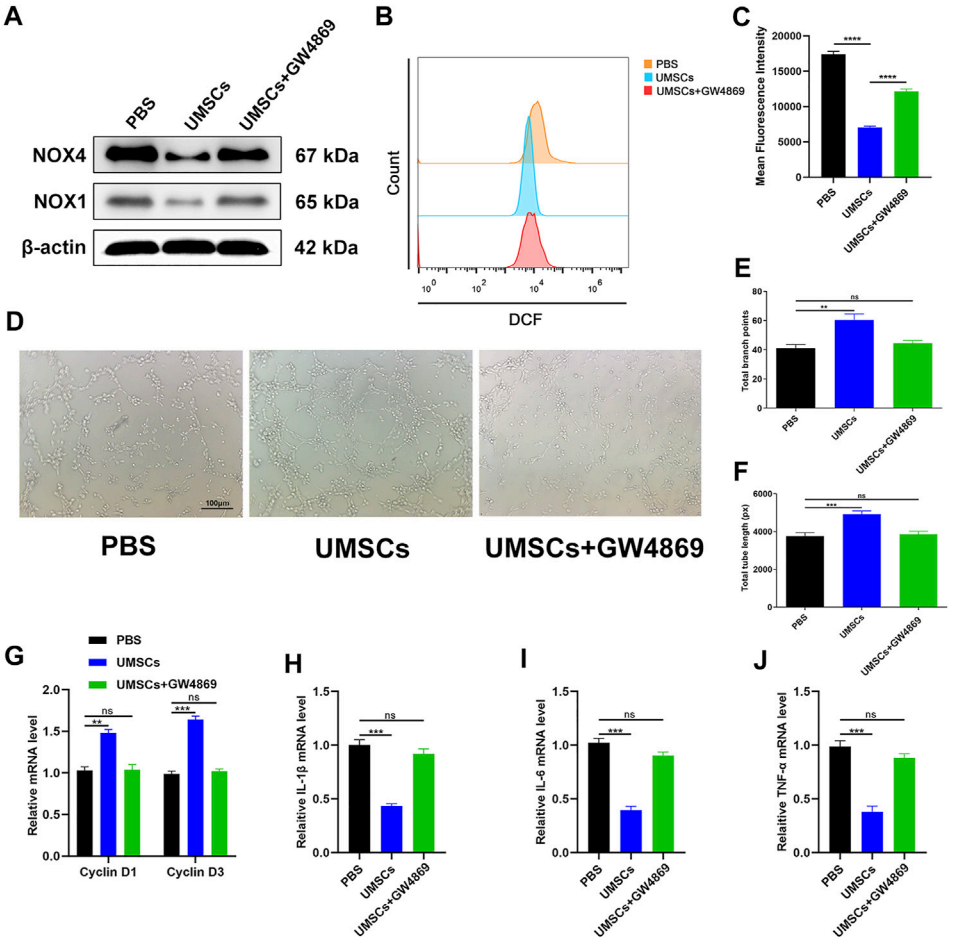

FIGURE 2 | HUCMSCs can regulate oxidative stress damage of HUVECs through exosomes. **(A)** Western blotting results of NOX1 and NOX4 in HUVECs following different treatments. **(B)** Reduction of ROS in HUVECs assessed through flow cytometry with the DCFH-DA probe following different treatments. **(C)** Quantitation of ROS depletion measured by the intensity of fluorescence of HUVECs. **(D)** A tube formation assay was performed to visualize the cell capillary network formation of HUVECs. Scale bar: 100 μm. **(E, F)** Quantitative analysis of the tube formation of HUVECs in the three groups. **(G)** RT-qPCR results of cyclin D1 and cyclin D3 expressions in the HUVECs following different treatments. **(H–J)** RT-qPCR results of IL-1β, IL-6, and TNF-α expressions in the HUVECs following different treatments. Differences were measured by one-way ANOVA followed by a Tukey *post hoc* test for pairwise comparison. Data presented as means ± SD. $^{****}p < 0.0001$, $^{***}p < 0.001$, $^{**}p < 0.01$, and $^{*}p < 0.05$.

TNF-α as surrogate markers of cell damage. The results showed that the levels of inflammatory factors in the second group were lower than that of the other groups, and the third group had no significant difference from the first group (**Figures 2H–J**). A CCK-8 experiment was conducted, and the outcome reflected that the cell proliferation ability of the second group was significantly better than the other groups, and the third group was slightly higher than the first group (Supplementary Figure S1B). These data indicated that HUCMSCs improve oxidative stress damage of HUVECs through exosomes derived from HUCMSCs.

Identification of exosomes secreted by HUCMSCs

To investigate the effect of HUC-Exos (exosomes secreted by HUCMSCs) on diabetic cutaneous wound healing, we assessed HUC-Exos through transmission electron microscopy (TEM), dynamic light scattering (DLS), and Western blotting. We began by collecting HUCMSCs to isolate exosomes. Analyzing the TEM data, we found that HUC-Exos included typical structures of exosomes, known to be homogeneous, spherical, and membrane vesicles (**Figure 3A**). The TEM images of HUC-Exos are also in agreement with a previous study. DLS was conducted to verify the particle size of HUC-Exos and to further identify the characteristic of HUC-Exos. According to the DLS data, particle sizes of HUC-Exos ranged from 30 to 150 nm (**Figure 3B**). Western blotting demonstrated that these isolated particles had high expression levels of CD9, CD81, and tumor susceptibility gene 101 (TSG101), which are typical markers of exosomes (**Figure 3C**). Together, these results revealed that the nanoparticles isolated from HUCMSCs were exosomes.

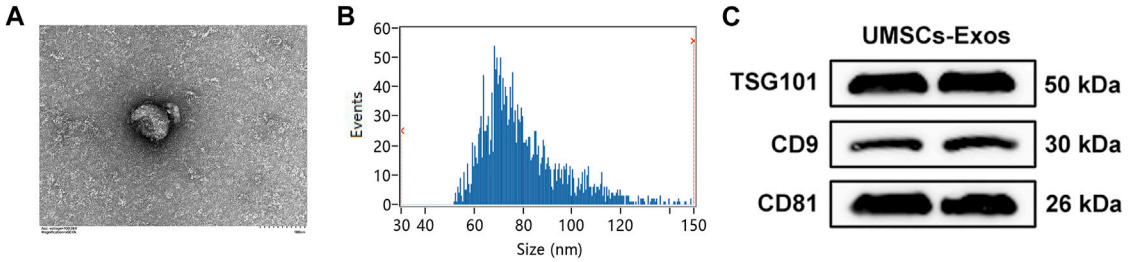

FIGURE 3 | Identification of HUC-Exos (exosomes secreted by HUCMSCs). **(A)** Representative picture of the ultrastructure of exosomes observed by transmission electron microscopy (TEM). **(B)** The average particle size distribution of normal-Exos and diabetes-Exos was measured by dynamic light scattering (DLS). **(C)** The marker protein levels of CD9, CD81, and TSG101 in the isolated exosomes were detected with Western blotting. Differences were measured by one-way ANOVA followed by a Tukey *post hoc* test for pairwise comparison. Data presented as means ± SD. ****$p < 0.0001$, ***$p < 0.001$, **$p < 0.01$, and *$p < 0.05$.

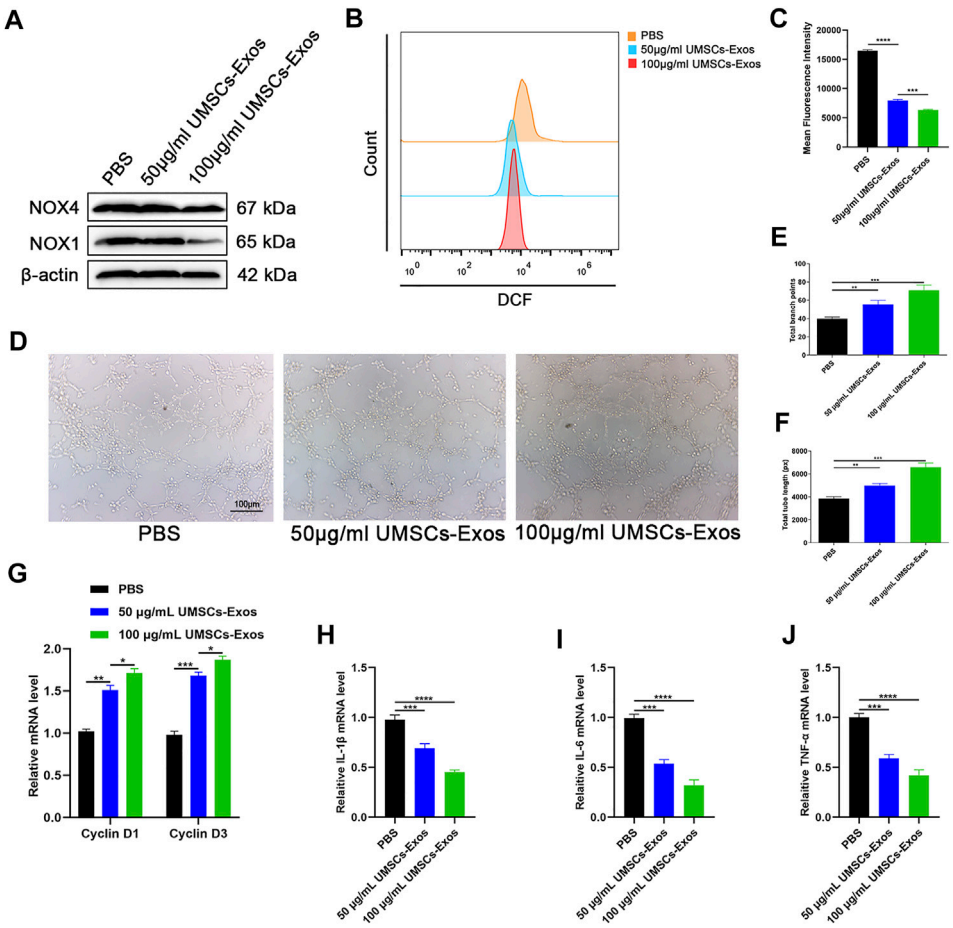

FIGURE 4 | HUC-Exos can improve oxidative stress injury caused by hyperglycemia *in vitro*. **(A)** Western blotting results of NOX1 and NOX4 in HUVECs following different treatments. **(B)** Reduction of ROS in HUVECs assessed by flow cytometry with the DCFH-DA probe following different treatments. **(C)** Quantitation of ROS depletion measured by the intensity of fluorescence of HUVECs. **(D)** A tube formation assay was performed to visualize the cell capillary network formation of HUVECs. Scale bar: 100 μm. **(E, F)** A tube formation assay was performed to visualize the cell capillary network formation of HUVECs. Scale bar: 100 μm. **(G)** RT-qPCR results of cyclin D1 and cyclin D3 expressions in the HUVECs following different treatments. **(H–J)** RT-qPCR results of IL-1β, IL-6, and TNF-α expressions in the HUVECs following different treatments. Differences were measured by one-way ANOVA followed by a Tukey *post hoc* test for pairwise comparison. Data presented as means ± SD. ****$p < 0.0001$, ***$p < 0.001$, **$p < 0.01$, and *$p < 0.05$.

Exosomes secreted by HUCMSCs are the mechanism underlying the beneficial effect of HUCMSCs on HUVECs

To determine the effect of HUC-Exos in improving oxidative stress injury, three groups were founded based on the medium. The common feature of the three groups was that HUVECs were cultured in the medium with a glucose concentration of 30 mM. The three groups were successively supplemented with 0, 50, and 100 μg/ml of HUC-Exos. Then according to the results above, we selected the time point of 72 h to evaluate the expression levels of NOX1 and NOX4 in HUVECs through Western blotting. It was shown that oxidative stress factors were expressed at lower levels in higher concentrations of exosomes (**Figure 4A**). ROS flow fluorescence assay was conducted, and the results showed that fluorescence intensity decreased with the increase in the exosome concentrations, as highlighted by the results of the statistical analyses (**Figures 4B, C**). With the intention to verify the function of HUVECs, we performed a tube formation experiment. The results showed that endothelial cell tubule formation in the high-concentration exosome group was higher than that in the low-concentration group (**Figures 4D–F**). In addition, endothelial cell proliferation was detected *via* RT-qPCR, and data showed that the expression levels of cyclin D1 and cyclin D3 increased with the elevation of the HUC-Exos concentrations in the culture medium (**Figure 4G**). Further, RT-qPCR was performed to detect the expression of endothelial inflammatory factors in a high-glucose environment. We found that the expression levels of IL-1β, IL-6, and TNF-α were negatively correlated with the concentration of exosomes in the medium (**Figures 4H–J**). CCK-8 was performed to further identify the proliferation ability of endothelial cells, and the data reflected that endothelial cell proliferation was positively correlated with exosome concentration (Supplementary Figure S1C). Based on these data above, it can be concluded that HUC-Exos improve oxidative stress injury caused by hyperglycemia *in vitro*.

Exosomes secreted by HUCMSCs accelerate diabetic cutaneous wound healing and enhance angiogenesis *in vivo*

To characterize the effect HUC-Exos exerted on accelerating diabetic cutaneous wound healing, a mouse model of diabetic cutaneous wounds was produced, and the effects of HUC-Exos were studied. Three groups were established, and each group was given an equal amount of PBS, 50 μg/ml of UMSCs-Exos, and 100 μg/ml of UMSCs-Exos to the wound site through local injections. As shown in **Figures 5A**, B, the wound healing of the high-concentration exosome group was fastest among the groups, followed by the low-concentration exosome group. So the healing curve is shown (**Figures 5A, B**). In addition, we collected the tissue around the wound site from each group 14 days after induction of the wounds. Dihydroethidium (DHE) staining was carried out to evaluate the ROS content. Wounds treated with HUC-Exos showed a better granulation tissue formation than the other groups, and the group treated with the high concentration of exosomes showed the highest level of tissue formation (**Figure 5C**). The fluorescence intensity statistics also reflect the same results (**Figure 5D**). To evaluate whether angiogenesis was regulated by HUC-Exos, we collected the tissue around the wound site from each group 10 days after induction of the wounds for small-animal Doppler examination. The data demonstrated that the high-concentration exosome group had better blood perfusion as reflected by the mean perfusion unit (MPU) ratio, which is consistent with the result expressed by the Doppler intensity graph (**Figures 6A, B**). Further, immunohistochemistry (IHC) staining was applied to wound tissue samples 14 days after induction of the wounds, and the CD31 (+) cells were used as the main indicator of angiogenesis. As shown in the results, the density of CD31 (+) cells was significantly higher in the group with a high level of HUC-Exos, indicating greater angiogenesis (**Figure 6C**). Immunofluorescence intensity statistics also reflect the same results (**Figure 6D**). Taking all these data into consideration, we found that HUC-Exos do accelerate diabetic cutaneous wound healing *in vivo*.

DISCUSSION

In this study, we found that HUCMSCs significantly inhibited oxidative stress damage induced by high glucose in HUVECs, thereby regulating their activity, proliferation, and angiogenesis. HUCMSCs enter HUVECs by secreting exosomes through endocytosis. HUC-Exos regulate endothelial cell activity and function by inhibiting oxidative stress and reducing inflammatory response, thereby promoting angiogenesis at the macrolevel. In addition, we found that HUC-Exos promote wound healing primarily by regulating reepithelialization, collagen deposition, and ECM remodeling. Combined with these results, it appears that HUC-Exos regulate endothelial cell function by reducing oxidative stress and inflammatory response, thereby promoting angiogenesis and ultimately accelerating diabetic wound healing. It offers a promising strategy for improving diabetes.

Diabetic cutaneous wounds are typified by drug-resistant bacterial infections, compromised angiogenesis, and oxidative damage to the microenvironment (Luo et al., 2021). The reconstruction of skin integrity and conservation of appropriate blood supply are the key factors for wound healing (Wong et al., 2015; Castleberry et al., 2016; Wang et al., 2019). According to previous studies, vascular complications caused by diabetes lead to endothelial dysfunction and hinder vascular repair (Zhang and Sun, 2020). More evidence indicates that the important cause of vascular dysfunction is endothelial cell function impairment induced by hyperglycemia, which leads to the occurrence of diabetic complications (Luo et al., 2020). Mechanistically, high glucose can induce endothelial cell apoptosis and dysfunction by activating the NF-κB signaling pathway, thereby inhibiting angiogenesis at the tissue level (Lee et al., 2019). In addition, a previous study reported that a high-glucose environment can inhibit endothelial cell activity, induce cell apoptosis, and induce

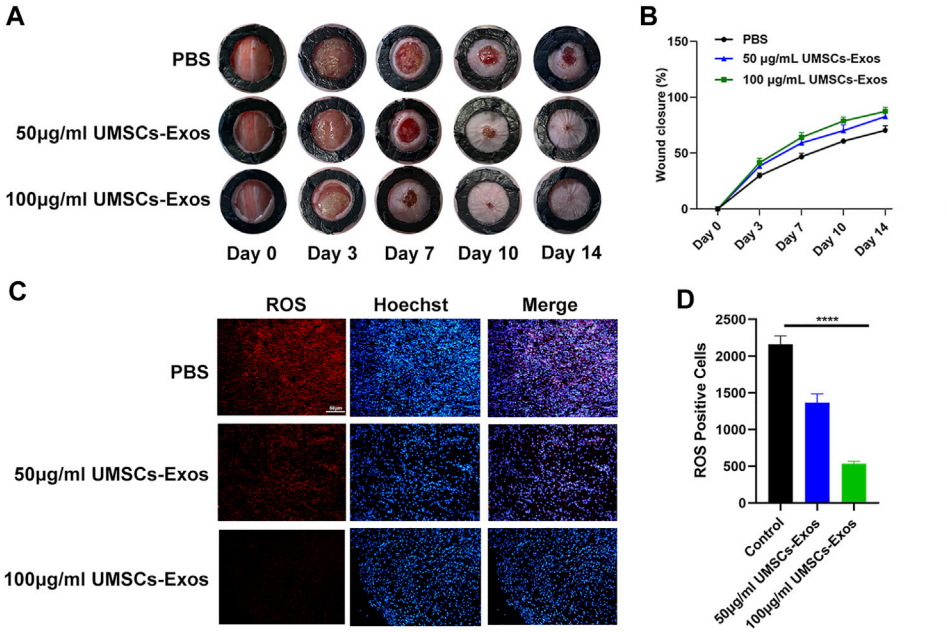

FIGURE 5 | HUC-Exos accelerate diabetic cutaneous wound healing *in vivo*. **(A)** Representative images of the wound healing process of mice treated with PBS, 50 μg/ml of UMSCs-Exos, and 100 μg/ml of UMSCs-Exos (n = 10). **(B)** *In vivo* wound closure rates of the five groups at different time points. **(C)** ROS level assessed by immunohistochemistry (IHC) staining. **(D)** Fluorescence quantification of the wound length at day 14. Scale bar: 50 μm. Differences were measured by one-way ANOVA followed by a Tukey *post hoc* test for pairwise comparison. Data presented as means ± SD. ****$p < 0.0001$, ***$p < 0.001$, **$p < 0.01$, and *$p < 0.05$.

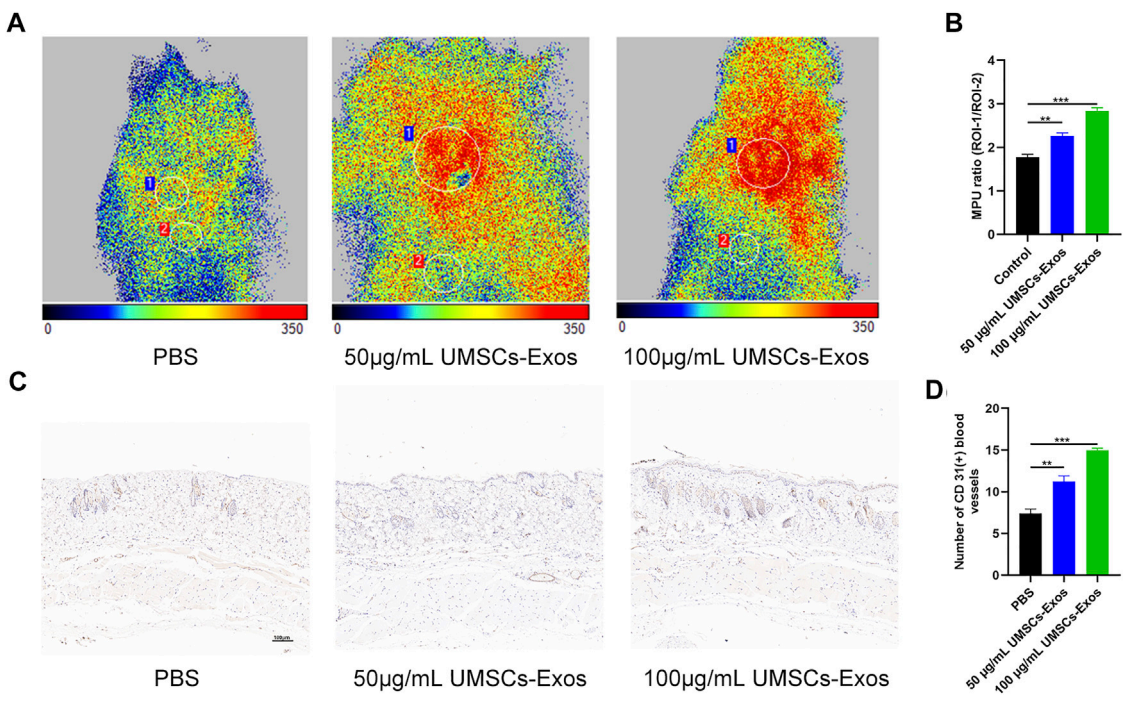

FIGURE 6 | HUC-Exos enhanced angiogenesis *in vivo*. Mice were treated with PBS, 50 μg/ml of UMSCs-Exos, and 100 μg/ml of UMSCs-Exos (n = 10). **(A)** The perfusion of the wound area in the three groups was assessed using a small-animal Doppler analysis. Scale bar: 100 μm. **(B)** Quantitative perfusion intensity of the wound area in the three groups. **(C)** Immunofluorescence assay with marker CD31 (+), n = 10. Scale bar: 100 μm. **(D)** Fluorescence quantification of the wound length at day 14. Scale bar: 50 μm. Differences were measured by one-way ANOVA followed by a Tukey *post hoc* test for pairwise comparison. Data presented as means ± SD. ****$p < 0.0001$, ***$p < 0.001$, **$p < 0.01$, and *$p < 0.05$.

oxidative stress injuries of HUVECs, making diabetic patients vulnerable to vascular diseases (Liu et al., 2020). In this study, our data also supported the above conclusion that a high-glucose environment caused oxidative stress damage and inflammatory response in endothelial cells and inhibited the functional activity and proliferation ability of endothelial cells (**Figure 1**).

HUCMSCs are pluripotent stem cells with omnidirectional differentiation potentials, which can regulate the functional and repair ability of various tissues and cells (Toh et al., 2017; Philipp et al., 2018). Our study showed that HUCMSCs regulate the functional activity and proliferation of endothelial cells (**Figure 2**). In addition, according to previous reports, HUCMSCs play a therapeutic role in tissue repair, mainly through paracrine exosomes (Corley et al., 2017; Wang et al., 2021). Exosomes are small vesicles secreted into the circulation by a series of cell types in the body and internalized by proximal or distal cells. These small molecules (including proteins and nucleic acids) in exosomes regulate the function of the recipient cells after internalization (Yang et al., 2019; Isaac et al., 2021). The outside secrete body has proven to be an ideal nanomaterial because it protects its contents, such as microRNAs, lncRNAs, and proteins. From the interference of external factors, the material is passed to the target cell, thus regulating gene expression and function in the target cell, allowing paracrine and endocrine communications between different tissues (Liu and Su, 2019). Exosome-based cell-free therapy avoids side effects associated with cell therapy, such as immune rejection and ectopic tissue formation (Mi et al., 2020; Wang et al., 2021). Our results showed that HUC-Exos entered endothelial cells through endocytosis and had the effect of inhibiting inflammatory response and alleviating oxidative stress (**Figure 4**). *In vitro* experiments also supported the above conclusions (**Figure 5**).

There is no doubt that the specific mechanism of HUC-Exos on endothelial cells in our study needs to be further studied. According to recent reports, the proliferation and tubulogenesis of vascular endothelial cells transfected with miR-20b-5p from peripheral blood exosomes in diabetic patients were significantly reduced, and the apoptosis rate was significantly increased (Niemiec et al., 2020). In addition, exosome-derived miR-146a significantly decreased phosphorylated IκB-α and NF-κB, thereby regulating the function of vascular endothelial cells (Xiong et al., 2020). From a therapeutic perspective, previous studies have pointed out that the self-levitating nanofiber gel-encapsulated polydeoxyribonucleotide benefits chronic ulcer in diabetic rats (Chen et al., 2016). The research of Xiong Y et al. indicates that chronic diabetic wound repair benefits from the nanohydrogel material loaded with growth factors (Xiong et al., 2021). At present, clinical trials have confirmed that miRNA is a key regulatory molecule of fracture healing and is likely to be a pathway to promote normal physiologic fracture healing. Its easy combination with agonists or antagonists makes it an ideal target for the treatment of fracture nonunion (Komatsu et al., 2021). All these provide possible directions for further research on the mechanism. In this study, human umbilical vein mesenchymal stem cells modulated endothelial cell injury and promoted fracture healing by secreting exosomes. However, the regulation from secretory exosomes to endothelial cells has not been further discussed. Although possible modes of action and potential targets were listed in the discussion section, they were not reflected in the experiment. This will be the direction of our further research in the future.

CONCLUSION

Taken together, our results show that HUC-Exos accelerate diabetic cutaneous wound healing *via* ameliorating oxidative stress and enhancing angiogenesis. From the point of view of clinical utility, this research could lead to addressing diabetic cutaneous wounds in the form of one-step mixed injection, thus reducing the medical burden and simultaneously increasing economic benefits. To summarize, our research provides a promising therapeutic approach to promote diabetic wound healing in the future.

METHODS AND MATERIALS

Cell culture and transfection

Experiments enrolled in this study were authorized by the Ethics Committee, Tongji Medical College, Huazhong University of Science and Technology, China.

HUVECs were offered by the Cell Bank of the Chinese Academy of Science, Shanghai, China. The cell culture medium is RPMI 1640 (Sigma-Aldrich, USA, cat. no. R8758), containing 10% exosome-depleted FBS (BI Israel).

For HUCMSCs, fresh umbilical cords were derived from informed pregnant women at the Wuhan Union Hospital (China). PBS was utilized to rinse the umbilical cords twice, and 5% penicillin-and-streptomycin PBS was used to rinse the umbilical cords three times.

Researchers removed cord vessels, and the processed cords were subsequently divided into small pieces that were individually attached to the substrate of culture plates. The stem cell culture medium (Beyotime, China, cat. no. S0154s) was hired, and the cells were incubated at 37°C with 5% CO_2. Then the cells changed the medium every 3 days.

And 10 days after the first incubation, the cells were well-developed and ready for experiments.

Inclusion criteria for pregnant women are as follows: 1) adult females aged 22–28; 2) the delivery condition was good, and the BPS score was more than 8; 3) pregnant women have no other adverse diseases; and 4) pregnant women who signed informed consent.

Exclusion criteria for pregnant women are as follows: 1) pregnant women with twins or more at the same time, 2) pregnant women with severe obstetric complications, and 3) pregnant women with poor prognosis after secretion.

HUCMSCs were grown in the RPMI 1640 medium (Sigma-Aldrich, USA, cat. no. R8758) supplemented with 10% fetal bovine serum (Gibco) and 1% pen/strep (Gibco). The cells were incubated in 5% CO_2 at 37°C.

Exosome purification and characterization

HUCMSCs were filtered through a 0.2-μm filter (122-0020PK, Thermo Fisher Scientific) at 4°C. The pellet was washed in PBS,

resuspended, and centrifuged for further 20 min at 100,000 × *g*, and the exosome-containing pellet was resuspended in PBS. Transmission electron microscopy (TEM, Tecnai G2) was used to evaluate the morphology of Exos. A Nanosizer instrument (Malvern Instruments, Malvern, UK) was used for dynamic light scattering analysis, and Western blotting was performed to analyze exosomal surface markers. The expressions of surface markers were determined by flow cytometry.

Tube formation assay

Cells (2×10^5 per well) were incubated in 24-well plates and grown for 1 day with mentioned treatment. HUVECs (2×10^4/well) were plated in 96-well plates precoated with Matrigel, incubated for 45 min, and then incubated for further 8 h. Three randomly chosen fields were examined using an inverted microscope, and the branch points and tube lengths were measured using ImageJ. We use gray analysis and other quantitative functions to transform pictures and tables.

GW4869

Product specification is cat. no. 52321ES10, 10 mg, YEASEN Biotech Co., Ltd., China. A 1.5-mm storage solution was prepared with DMSO and stored at −80°C. Before use, 5% MSA was dissolved into GW4869 storage solution, making GW4869 1.43 mM. The suspension is thoroughly mixed and heated at 37°C until clear. Then the GW4869 inhibitor was added to the cell culture medium at a concentration range of 10–20 μM, and the cells were treated for 30 min.

Western blotting analysis

The proteins of HUVECs were isolated using a RIPA lysis solution (Gibco, China). After treatment, HUVECs were rinsed with cold PBS twice, and RIPA lysis solution was added to the cells. The protein extracts were harvested at 12,000 *g* at 4°C for 10 min. Protein concentration was detected using a BCA protein assay kit (Beyotime, China). Equal amounts of protein were separated by 10%–12% sodium dodecyl sulfate–polyacrylamide gel electrophoresis and transferred to PVDF membranes (MilliporeSigma, USA). The membranes were blocked with 5% nonfat milk and incubated with the primary antibodies overnight at 4°C. The membranes were rinsed with PBS-T twice and incubated with the appropriate secondary antibodies at room temperature for 1 h. Subsequently, the proteins of the membranes were visualized according to the instructions of the manufacturer. The following antibodies were used: anti-TSG101 (1:1,000; Abcam, cat. no. Ab125011), anti-CD9 (1:1,000; Abcam, cat. no. Ab92726), anti-CD81 (1:1,000; Abcam, cat. no. Ab82452), anti-NOX1 (OCN; 1:500; Abcam, cat. no. Ab153241), anti-NOX4 (OCN; 1:500; Abcam, cat. no. Ab198213), and anti-GAPDH (1:10,000; Abcam, cat. no. Ab37168). All experiments were performed in triplicate.

RT-qPCR analysis

TRIzol (Invitrogen) was utilized to extract total RNA, and a Verso cDNA Synthesis Kit (Thermo Fisher Scientific) was used to reverse-transcribe the RNA according to the instructions of the kit. The SeraMir Exosome RNA Purification Kit (System Biosciences, Mountain View, USA) was used to extract exosomal miRNAs, and the TaqMan microRNA assay kit (Applied Biosystems, Foster City, USA) was utilized for cDNA synthesis. The StepOne Real-Time PCR System (Life Technologies, Carlsbad, CA, USA) was used for RT-qPCR reactions. GAPDH and U6 were used for the normalization of mRNA and miRNA expressions, respectively, and the $2^{-\Delta\Delta Ct}$ method was used to quantify relative expressions: IL-1β (Abcam, UK), IL-6 (Abcam, UK), TNF-α (Abcam, UK), cyclin D1 (Abcam, UK), and cyclin D3 (Abcam, UK).

Reactive oxygen species assay

The ROS Assay Kit (Beyotime, China, cat. no. S033SS), containing DCFH-DA (the fluorescent probe) and ROSup (ROS positive control), was stored at −20°C. After the cells were removed from the culture medium, 1 ml of 10 mm/L DCFH-DA was added. The cells were then incubated in an incubator at 37°C for 20 min. The cells were then washed three times in a serum-free culture medium. For flow cytometry detection, the excitation wavelength was 488nm and the emission wavelength was 525 nm.

Generation of diabetic mice

The diabetes model was established in male C57BL/6J mice (6 weeks old) by feeding on a high-fat diet for 4 weeks, followed by daily intraperitoneal administration of streptozotocin (STZ; 40 mg kg^{-1} day^{-1}) for 7 days. If the fasting blood glucose level was over 11.1 mmol L^{-1} for two successive measurements, the mice were considered to be diabetic and were used for the following experiments.

Murine wound model

The STZ-induced diabetic mice were anesthetized with intraperitoneal pentobarbital sodium (50 mg kg^{-1}; Sigma-Aldrich), and 1.0 cm × 1.0 cm full-thickness excision skin wounds were made. The mice were randomly divided into groups and injected with 100 μl of PBS, 50 μg/ml of UMSCs-Exos, and 100 μg/ml of UMSCs-Exos on days 0, 3, 5, 7, 9, and 11 after the establishment of the wound (n = 6). The wounds were covered with transparent dressings (Tegaderm™ Film) and were photographed and measured with a caliper on days 0, 3, 5, 7, 10, and 14. The degree of wound closure was determined by ImageJ as follows:

$$C_n = \frac{(A_0 - A_n)}{A_0} \times 100\%$$

where C_n is the percentage reduction of the wound area on the respective days; A_0 is the size of the original wound; A_n is the area of the wound on the respective days after the injury.

Dihydroethidium staining

Half of the wound tissue samples were collected on days 3, 7, and 14, fixed (4% formaldehyde), and paraffin-embedded. Sections (5 μm) were used in the DHE assay. Wound samples, including full-thickness skin layers, were cryosectioned. DHE staining (5 μm) was used to measure intracellular ROS. Images were

acquired using the IX53 microscope (DHE kit; Abcam, cat. no. ab236206).

Small-animal Doppler analysis

Ten days after the operation, a laser speckle contrast imaging (LSCI) system was utilized to examine local blood perfusion, while the PSI-ZR PeriCam system (Perimed Ltd., Stockholm, Sweden) was used to acquire images of the wounds. An invisible near-infrared (NIR) laser at 785 nm was used to determine blood perfusion, expressed as perfusion units. The wounds were photographed at a constant distance, using the same dimensions for the area. The MPU ratio was determined using PIMSoft (Moor Instruments Ltd., Axminster, UK) using flux images of individual wound sites, expressed as the correlation of the MPU of the wound area (ROI-1) to the MPU of the region surrounding the wound (ROI-2). The statistical map of fluorescence intensity was converted by FlowJ software.

Immunohistochemistry staining

The mice were sacrificed on day 14, and the wound tissues were embedded in paraffin and stained for CD31. Antigen retrieval was performed for 1 min in citrate buffer, followed by blocking for 30 min in goat serum. The samples were stained with anti-CD31 (1:100; Abcam, ab28364) antibodies overnight at 4°C, washed in PBS, and stained and counterstained with DAB and hematoxylin, respectively. The sections were evaluated under a microscope (Nikon, Japan). The statistical map of fluorescence intensity was converted by FlowJ software.

Origin of laboratory rats

Description of laboratory rats is as follows: variety: C57BL/6J; incubation company: Beijing Vital River, China; gender: 70 males and 70 females; age: 42 days; level: SPF; and license number: SCXK 2021-0010.

Cell coculture system

A Transwell plate was used (Corning, China, the no.: 3,470, 1 μm). 1. For the preparation of the cell suspension, the cells were digested, the culture medium was discarded by centrifugation after the termination of digestion, washed once or twice with PBS, and the cell density was adjusted by resuspension with a serum-free medium containing BSA. 2. For cultured cells, Transwell was used to inoculate human umbilical cord mesenchymal stem cells and endothelial cells. 3. The morphological changes of the cells in the upper and lower chambers were observed under the microscope, and the staining identification could be carried out if necessary. 4. Results were statistically analyzed.

Statistical analysis

The data were expressed as means ± standard deviation (SD). Differences between two groups were measured by Student's t-tests, and differences between multiple groups were measured by one-way ANOVA followed by a Tukey *post hoc* test for pairwise comparison. Analyses were conducted with GraphPad Prism 9.0. $p < 0.05$ was set as the significance threshold.

DATA AVAILABILITY STATEMENT

The original contributions presented in the study are publicly available. This data can be found here: https://doi.org/10.6084/m9.figshare.17696024.v1.

ETHICS STATEMENT

The studies involving human participants were reviewed and approved by the Ethics Committee, Tongji Medical College, Huazhong University of Science and Technology, China. The patients/participants provided their written informed consent to participate in this study. The animal study was reviewed and approved by the Ethics Committee, Tongji Medical College, Huazhong University of Science and Technology, China.

AUTHOR CONTRIBUTIONS

CY, YX, and ZL contributed equally to this work. CY, YX, and ZL designed and implemented the main content of the project. YX, BM, and YE were in charge of editing and cell experiments. HX, YH, and LH were responsible for the *in vitro* studies. CL and FC took charge of data analysis. GL, PZ, and WZ were responsible for project progress.

FUNDING

This study was supported by the National Natural Science Foundation of China (No. 31600754 and No. 81472144) and the National Key Research and Development Program of China (2018YFB200152).

ACKNOWLEDGMENTS

We thank the Cell Bank of the Chinese Academy of Science, Shanghai, China, for its help and guidance on our project.

REFERENCES

An, T., Chen, Y., Tu, Y., and Lin, P. (2021). Mesenchymal Stromal Cell-Derived Extracellular Vesicles in the Treatment of Diabetic Foot Ulcers: Application and Challenges. *Stem Cel Rev Rep* 17, 369–378. doi:10.1007/s12015-020-10014-9

Armstrong, D. G., Boulton, A. J. M., and Bus, S. A. (2017). Diabetic Foot Ulcers and Their Recurrence. *N. Engl. J. Med.* 376, 2367–2375. doi:10.1056/nejmra1615439

Bowling, F. L., Rashid, S. T., and Boulton, A. J. M. (2015). Preventing and Treating Foot Complications Associated with Diabetes Mellitus. *Nat. Rev. Endocrinol.* 11, 606–616. doi:10.1038/nrendo.2015.130

Castleberry, S. A., Almquist, B. D., Li, W., Reis, T., Chow, J., Mayner, S., et al. (2016). Self-Assembled Wound Dressings Silence MMP-9 and Improve

Diabetic Wound Healing *In Vivo*. *Adv. Mater.* 28, 1809–1817. doi:10.1002/adma.201503565

Chang, M., and Nguyen, T. T. (2021). Strategy for Treatment of Infected Diabetic Foot Ulcers. *Acc. Chem. Res.* 54, 1080–1093. doi:10.1021/acs.accounts.0c00864

Chen, C.-Y., Rao, S.-S., Ren, L., Hu, X.-K., Tan, Y.-J., Hu, Y., et al. (2018). Exosomal DMBT1 from Human Urine-Derived Stem Cells Facilitates Diabetic Wound Repair by Promoting Angiogenesis. *Theranostics* 8, 1607–1623. doi:10.7150/thno.22958

Chen, X., Zhou, W., Zha, K., Liu, G., Yang, S., Ye, S., et al. (2016). Treatment of Chronic Ulcer in Diabetic Rats with Self Assembling Nanofiber Gel Encapsulated-Polydeoxyribonucleotide. *Am. J. Transl Res.* 8, 3067–3076.

Corley, S. M., Mackenzie, K. L., Beverdam, A., Roddam, L. F., and Wilkins, M. R. (2017). Differentially Expressed Genes from RNA-Seq and Functional Enrichment Results Are Affected by the Choice of Single-End versus Paired-End Reads and Stranded versus Non-stranded Protocols. *BMC genomics* 18, 399. doi:10.1186/s12864-017-3797-0

Deng, L., Du, C., Song, P., Chen, T., Rui, S., Armstrong, D. G., et al. (2021). The Role of Oxidative Stress and Antioxidants in Diabetic Wound Healing. *Oxidative Med. Cell. longevity* 2021, 8852759. doi:10.1155/2021/8852759

Dinkins, M. B., Dasgupta, S., Wang, G., Zhu, G., and Bieberich, E. (2014). Exosome Reduction *In Vivo* Is Associated with Lower Amyloid Plaque Load in the 5XFAD Mouse Model of Alzheimer's Disease. *Neurobiol. Aging* 35, 1792–1800. doi:10.1016/j.neurobiolaging.2014.02.012

Isaac, R., Reis, F. C. G., Ying, W., and Olefsky, J. M. (2021). Exosomes as Mediators of Intercellular Crosstalk in Metabolism. *Cel Metab.* 33, 1744–1762. doi:10.1016/j.cmet.2021.08.006

Jang, Y.-Y., and Sharkis, S. J. (2007). A Low Level of Reactive Oxygen Species Selects for Primitive Hematopoietic Stem Cells that May Reside in the Low-Oxygenic Niche. *Blood* 110, 3056–3063. doi:10.1182/blood-2007-05-087759

Komatsu, D. E., Duque, E., and Hadjiargyrou, M. (2021). MicroRNAs and Fracture Healing: Pre-clinical Studies. *Bone* 143, 115758. doi:10.1016/j.bone.2020.115758

Kowluru, R. A. (2020). Retinopathy in a Diet-Induced Type 2 Diabetic Rat Model and Role of Epigenetic Modifications. *Diabetes* 69, 689–698. doi:10.2337/db19-1009

Lavery, L. A., Davis, K. E., Berriman, S. J., Braun, L., Nichols, A., Kim, P. J., et al. (2016). WHS Guidelines Update: Diabetic Foot Ulcer Treatment Guidelines. *Wound Rep. Reg.* 24, 112–126. doi:10.1111/wrr.12391

Lee, E., Ko, J.-Y., Kim, J., Park, J.-W., Lee, S., and Im, G.-I. (2019). Osteogenesis and Angiogenesis Are Simultaneously Enhanced in BMP2-/vegf-Transfected Adipose Stem Cells through Activation of the YAP/TAZ Signaling Pathway. *Biomater. Sci.* 7, 4588–4602. doi:10.1039/c9bm01037h

Lim, J. Z. M., Ng, N. S. L., and Thomas, C. (2017). Prevention and Treatment of Diabetic Foot Ulcers. *J. R. Soc. Med.* 110, 104–109. doi:10.1177/0141076816688346

Liu, C., and Su, C. (2019). Design Strategies and Application Progress of Therapeutic Exosomes. *Theranostics* 9, 1015–1028. doi:10.7150/thno.30853

Liu, W., Yu, M., Xie, D., Wang, L., Ye, C., Zhu, Q., et al. (2020). Melatonin-stimulated MSC-Derived Exosomes Improve Diabetic Wound Healing through Regulating Macrophage M1 and M2 Polarization by Targeting the PTEN/AKT Pathway. *Stem Cel Res Ther* 11, 259. doi:10.1186/s13287-020-01756-x

Luo, E.-F., Li, H.-X., Qin, Y.-H., Qiao, Y., Yan, G.-L., Yao, Y.-Y., et al. (2021). Role of Ferroptosis in the Process of Diabetes-Induced Endothelial Dysfunction. *Wjd* 12, 124–137. doi:10.4239/wjd.v12.i2.124

Luo, E., Wang, D., Yan, G., Qiao, Y., Zhu, B., Liu, B., et al. (2020). The NF-κB/miR-425-5p/MCT4 axis: A Novel Insight into Diabetes-Induced Endothelial Dysfunction. *Mol. Cell. Endocrinol.* 500, 110641. doi:10.1016/j.mce.2019.110641

Martinengo, L., Olsson, M., Bajpai, R., Soljak, M., Upton, Z., Schmidtchen, A., et al. (2019). Prevalence of Chronic Wounds in the General Population: Systematic Review and Meta-Analysis of Observational Studies. *Ann. Epidemiol.* 29, 8–15. doi:10.1016/j.annepidem.2018.10.005

Mi, B., Chen, L., Xiong, Y., Yan, C., Xue, H., Panayi, A. C., et al. (2020). Saliva Exosomes-Derived UBE2O mRNA Promotes Angiogenesis in Cutaneous Wounds by Targeting SMAD6. *J. Nanobiotechnol* 18, 68. doi:10.1186/s12951-020-00624-3

Niemiec, S. M., Louiselle, A. E., Hilton, S. A., Dewberry, L. C., Zhang, L., Azeltine, M., et al. (2020). Nanosilk Increases the Strength of Diabetic Skin and Delivers CNP-miR146a to Improve Wound Healing. *Front. Immunol.* 11, 590285. doi:10.3389/fimmu.2020.590285

Pavlou, S., Lindsay, J., Ingram, R., Xu, H., and Chen, M. (2018). Sustained High Glucose Exposure Sensitizes Macrophage Responses to Cytokine Stimuli but Reduces Their Phagocytic Activity. *BMC Immunol.* 19, 24. doi:10.1186/s12865-018-0261-0

Philipp, D., Suhr, L., Wahlers, T., Choi, Y.-H., and Paunel-Görgülü, A. (2018). Preconditioning of Bone Marrow-Derived Mesenchymal Stem Cells Highly Strengthens Their Potential to Promote IL-6-dependent M2b Polarization. *Stem Cel Res Ther* 9, 286. doi:10.1186/s13287-018-1039-2

Qu, J., Zhao, X., Liang, Y., Zhang, T., Ma, P. X., and Guo, B. (2018). Antibacterial Adhesive Injectable Hydrogels with Rapid Self-Healing, Extensibility and Compressibility as Wound Dressing for Joints Skin Wound Healing. *Biomaterials* 183, 185–199. doi:10.1016/j.biomaterials.2018.08.044

Reardon, R., Simring, D., Kim, B., Mortensen, J., Williams, D., and Leslie, A. (2020). The Diabetic Foot Ulcer. *Aust. J. Gen. Pract.* 49, 250–255. doi:10.31128/ajgp-11-19-5161

Sadjadi, J., Strumwasser, A. M., and Victorino, G. P. (2019). Endothelial Cell Dysfunction during Anoxia-Reoxygenation Is Associated with a Decrease in Adenosine Triphosphate Levels, Rearrangement in Lipid Bilayer Phosphatidylserine Asymmetry, and an Increase in Endothelial Cell Permeability. *J. Trauma Acute Care Surg.* 87, 1247–1252. doi:10.1097/ta.0000000000002489

Sen, C. K. (2019). Human Wounds and its Burden: An Updated Compendium of Estimates. *Adv. Wound Care* 8, 39–48. doi:10.1089/wound.2019.0946

Shinohara, M., Shang, W.-H., Kubodera, M., Harada, S., Mitsushita, J., Kato, M., et al. (2007). Nox1 Redox Signaling Mediates Oncogenic Ras-Induced Disruption of Stress Fibers and Focal Adhesions by Down-Regulating Rho. *J. Biol. Chem.* 282, 17640–17648. doi:10.1074/jbc.m609450200

Thi, P. L., Lee, Y., Tran, D. L., Thi, T. T. H., Kang, J. I., Park, K. M., et al. (2020). *In Situ* forming and Reactive Oxygen Species-Scavenging Gelatin Hydrogels for Enhancing Wound Healing Efficacy. *Acta Biomater.* 103, 142–152. doi:10.1016/j.actbio.2019.12.009

Toh, W. S., Lai, R. C., Hui, J. H. P., and Lim, S. K. (2017). MSC Exosome as a Cell-free MSC Therapy for Cartilage Regeneration: Implications for Osteoarthritis Treatment. *Semin. Cel Develop. Biol.* 67, 56–64. doi:10.1016/j.semcdb.2016.11.008

Wang, C., Wang, M., Xu, T., Zhang, X., Lin, C., Gao, W., et al. (2019). Engineering Bioactive Self-Healing Antibacterial Exosomes Hydrogel for Promoting Chronic Diabetic Wound Healing and Complete Skin Regeneration. *Theranostics* 9, 65–76. doi:10.7150/thno.29766

Wang, Y., Xu, X., Chen, X., and Li, J. (2021). Multifunctional Biomedical Materials Derived from Biological Membranes. *Adv. Mater.*, e2107406. Deerfield Beach, Fla. doi:10.1002/adma.202107406

Wen, Z., Mai, Z., Zhu, X., Wu, T., Chen, Y., Geng, D., et al. (2020). Mesenchymal Stem Cell-Derived Exosomes Ameliorate Cardiomyocyte Apoptosis in Hypoxic Conditions through microRNA144 by Targeting the PTEN/AKT Pathway. *Stem Cel Res Ther* 11, 36. doi:10.1186/s13287-020-1563-8

Wong, S. L., Demers, M., Martinod, K., Gallant, M., Wang, Y., Goldfine, A. B., et al. (2015). Diabetes Primes Neutrophils to Undergo NETosis, Which Impairs Wound Healing. *Nat. Med.* 21, 815–819. doi:10.1038/nm.3887

Xiong, Y., Chen, L., Liu, P., Yu, T., Lin, C., Yan, C., et al. (2021). All-in-One: Multifunctional Hydrogel Accelerates Oxidative Diabetic Wound Healing through Timed-Release of Exosome and Fibroblast Growth Factor. *Small*, e2104229. Weinheim an der Bergstrasse, Germany. doi:10.1002/smll.202104229

Xiong, Y., Chen, L., Yu, T., Yan, C., Zhou, W., Cao, F., et al. (2020). Inhibition of Circulating Exosomal microRNA-15a-3p Accelerates Diabetic Wound Repair. *Aging* 12, 8968–8986. doi:10.18632/aging.103143

Xue, C., Shen, Y., Li, X., Li, B., Zhao, S., Gu, J., et al. (2018). Exosomes Derived from Hypoxia-Treated Human Adipose Mesenchymal Stem Cells Enhance Angiogenesis through the PKA Signaling Pathway. *Stem Cell Dev.* 27, 456–465. doi:10.1089/scd.2017.0296

Yang, B., Chen, Y., and Shi, J. (2019). Exosome Biochemistry and Advanced Nanotechnology for Next-Generation Theranostic Platforms. *Adv. Mater.* 31, e1802896. doi:10.1002/adma.201802896

Yin, Y., Li, Y., Wang, S., Dong, Z., Liang, C., Sun, J., et al. (2021). MSCs-Engineered Biomimetic PMAA Nanomedicines for Multiple Bioimaging-Guided and Photothermal-Enhanced Radiotherapy of NSCLC. *J. Nanobiotechnol* 19, 80. doi:10.1186/s12951-021-00823-6

Zhang, J.-R., and Sun, H.-J. (2020). Roles of Circular RNAs in Diabetic Complications: From Molecular Mechanisms to Therapeutic Potential. *Gene* 763, 145066. doi:10.1016/j.gene.2020.145066

Zhang, K., Feng, Q., Fang, Z., Gu, L., and Bian, L. (2021). Structurally Dynamic Hydrogels for Biomedical Applications: Pursuing a Fine Balance between Macroscopic Stability and Microscopic Dynamics. *Chem. Rev.* 121, 11149–11193. doi:10.1021/acs.chemrev.1c00071

Zhuang, L., Xia, W., Chen, D., Ye, Y., Hu, T., Li, S., et al. (2020). Exosomal LncRNA-NEAT1 Derived from MIF-Treated Mesenchymal Stem Cells Protected against Doxorubicin-Induced Cardiac Senescence through Sponging miR-221-3p. *J. Nanobiotechnol* 18, 157. doi:10.1186/s12951-020-00716-0

Conflict of Interest: The authors declare that the research was conducted in the absence of any commercial or financial relationships that could be construed as a potential conflict of interest.

Publisher's Note: All claims expressed in this article are solely those of the authors and do not necessarily represent those of their affiliated organizations, or those of the publisher, the editors, and the reviewers. Any product that may be evaluated in this article, or claim that may be made by its manufacturer, is not guaranteed or endorsed by the publisher.

frontiers in Bioengineering and Biotechnology

ORIGINAL RESEARCH
published: 07 February 2022
doi: 10.3389/fbioe.2022.846401

Highly Transparent, Self-Healing, and Self-Adhesive Double Network Hydrogel for Wearable Sensors

Kai Chen[1,2], Mingxiang Liu[1], Feng Wang[1], Yunping Hu[1], Pei Liu[1], Cong Li[3], Qianqian Du[3], Yongsheng Yu[4], Xiufeng Xiao[1]* and Qian Feng[1,5]**

[1]Fujian Provincial Key Laboratory of Advanced Materials Oriented Chemical Engineering, College of Chemistry and Materials Science, Fujian Normal University, Fuzhou, China, [2]School of Resources and Chemical Engineering, Sanming University, Sanming, China, [3]Department of Biomaterial, College of Life Sciences, Mudanjiang Medical University, Mudanjiang, China, [4]Chongqing Institute of Green and Intelligent Technology, Chinese Academy of Sciences, Chongqing, China, [5]Key Laboratory of Biorheological Science and Technology, Ministry of Education College of Bioengineering, Chongqing University, Chongqing, China

OPEN ACCESS

Edited by:
Yilong Cheng,
Xi'an Jiaotong University, China

Reviewed by:
Haitao Cui,
George Washington University, United States
Shaojun Chen,
Shenzhen University, China

***Correspondence:**
Qian Feng
qianfeng@cqu.edu.cn
Xiufeng Xiao
xfxiao@fjnu.edu.cn
Yongsheng Yu
yongshengy@126.com

Specialty section:
This article was submitted to Biomaterials, a section of the journal Frontiers in Bioengineering and Biotechnology

Received: 31 December 2021
Accepted: 17 January 2022
Published: 07 February 2022

Citation:
Chen K, Liu M, Wang F, Hu Y, Liu P, Li C, Du Q, Yu Y, Xiao X and Feng Q (2022) Highly Transparent, Self-Healing, and Self-Adhesive Double Network Hydrogel for Wearable Sensors. Front. Bioeng. Biotechnol. 10:846401. doi: 10.3389/fbioe.2022.846401

Hydrogel-based flexible electronic devices are essential in future healthcare and biomedical applications, such as human motion monitoring, advanced diagnostics, physiotherapy, etc. As a satisfactory flexible electronic material, the hydrogel should be conductive, ductile, self-healing, and adhesive. Herein, we demonstrated a unique design of mechanically resilient and conductive hydrogel with double network structure. The Ca^{2+} crosslinked alginate as the first dense network and the ionic pair crosslinked polyzwitterion as the second loose network. With the synthetic effect of these two networks, this hydrogel showed excellent mechanical properties, such as superior stretchability (1,375%) and high toughness (0.57 MJ/m^3). At the same time, the abundant ionic groups of the polyzwitterion network endowed our hydrogel with excellent conductivity (0.25 S/m). Moreover, due to the dynamic property of these two networks, our hydrogel also performed good self-healing performance. Besides, our experimental results indicated that this hydrogel also had high optical transmittance (92.2%) and adhesive characteristics. Based on these outstanding properties, we further explored the utilization of this hydrogel as a flexible wearable strain sensor. The data strongly proved its enduring accuracy and sensitivity to detect human motions, including large joint flexion (such as finger, elbow, and knee), foot planter pressure measurement, and local muscle movement (such as eyebrow and mouth). Therefore, we believed that this hydrogel had great potential applications in wearable health monitoring, intelligent robot, human-machine interface, and other related fields.

Keywords: double network hydrogel, transparent, self-healing, adhesive, wearable strain sensor

INTRODUCTION

Conventional semiconductor-based strain sensors have limitations in the next generation of electronics due to their inherent deficiencies (Liu et al., 2020), including brittleness, rigidity, and low biocompatibility (Zhang et al., 2022). In recent years, the applications of conductive hydrogel in wearable devices, soft robots, and artificial skin have attracted researchers' attention (Shen et al., 2021; Sun et al., 2021; Zhu et al., 2021). Among these application scenarios, conductive hydrogel as

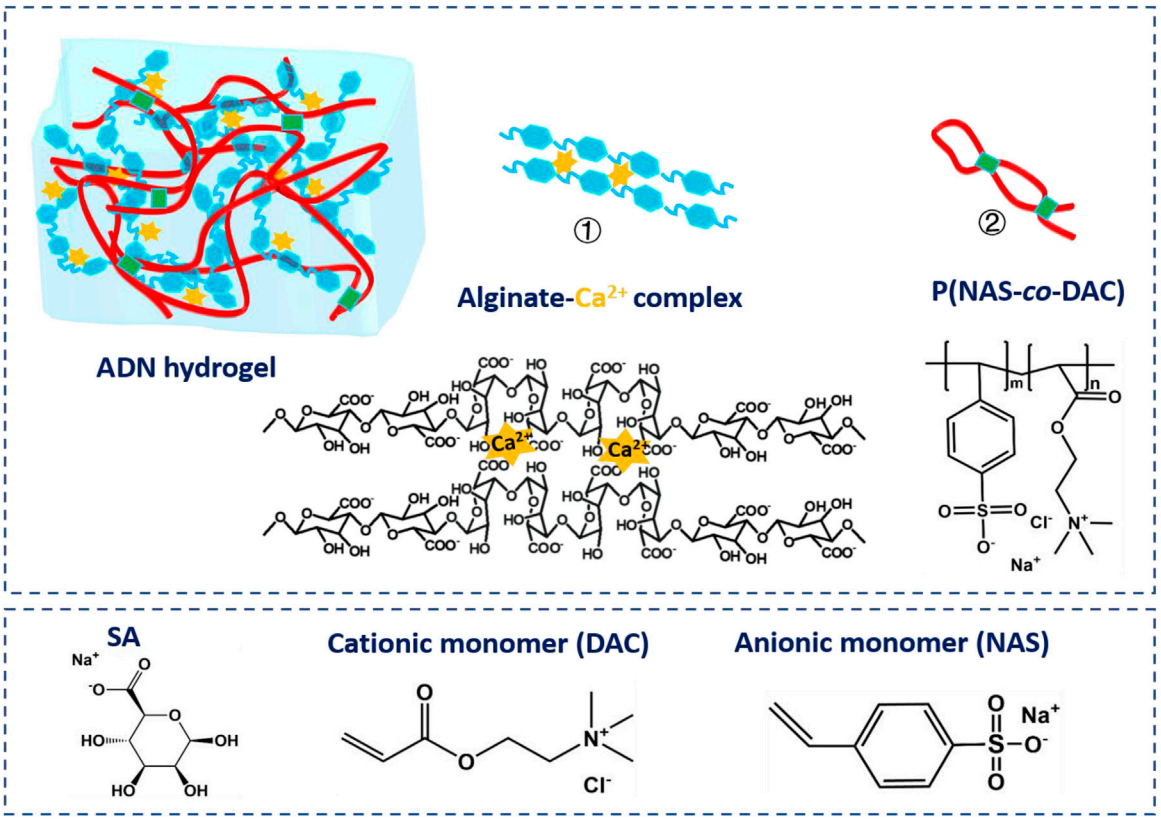

FIGURE 1 | Schematic of the preparation process of the ADN hydrogel.

wearable strain sensor for human movement monitoring is one of the most studied and reported directions (Ma et al., 2021; Yu et al., 2021; Zhang et al., 2021; Yang et al., 2022a). According to previous reports, the wearable strain sensor should be able to attach to human skin comfortably and monitor human motions with wide sensing range, high precision and good durability (Fan et al., 2018; Nam et al., 2020). In addition, it also must meet the requirements of flexibility, low power consumption, biocompatibility, and portability. In order to meet all of these demands, a series of multifunctional conductive hydrogels have been prepared through the precise design of the hydrogel component and internal network structure (Chimene et al., 2020).

Hydrogel is a kind of viscoelastic material with three-dimensional network structure, which can absorb and retain a large amount of water (Dai et al., 2020; Shen et al., 2021). It is usually composed of chemically or physically crosslinked hydrophilic polymers (Li W. et al., 2021). Ionic conductive hydrogels are considered as promising candidates for the development of flexible strain sensors with large strain ranges and high sensitivity (Liu et al., 2018; Zhou et al., 2019). It has a unique porous structure and can provide an effective channel for ion transport (Zhao X. et al., 2019), so it has high ionic conductivity. At the same time, they have high flexibility, transparency, and good biocompatibility (Luo et al., 2021; Ding et al., 2022). Although highly tensile and self-healing ionic hydrogels are usually reported, most synthetic ionic hydrogels exhibit strain-softening properties (Peng et al., 2022; Zhou et al., 2022). For stretchable ionic hydrogels, there are often conflicts between tensile properties, self-healing properties and high mechanical strength (Yang et al., 2022b; Zhao et al., 2022). In general, good tensile properties, self-healing property, and self-adhesion are favorable for the use of hydrogels in wearable devices (Chen Z. et al., 2021). Excellent tensile property makes hydrogel-based wearable devices suitable for large strain of human body, thus expanding the application range of sensors (Sun et al., 2021). He et al. designed a silk fibroin-based hydrogel with considerable tensile and compressive properties, which enabled it to be assembled as a strain/pressure sensor with a wide sensing range (> 600%) (He et al., 2020). The self-healing property can increase the service life of the device, which is critical to improve the durability of flexible wearable sensing devices (Pei et al., 2021). Lin et al. synthesized a multifunctional biomimetic hydrogel inspired by natural skin for use in wearable devices, achieving high self-healing (98.6% in 10 min) (Lin et al., 2019). The self-adhesive hydrogel can establish a stable and reliable interface with the measured target and improve the detection of weak and physiological signals (Jin et al., 2021). Wu et al. constructed a mussel-inspired PDA/BT/PAA glycerol-hydrogel (G-hydrogel), which exhibited wonderful self-adhesive performances (adhesion strength to porcine skin of 18 kPa) (Wu et al., 2020). Therefore, we tend to find solution from the

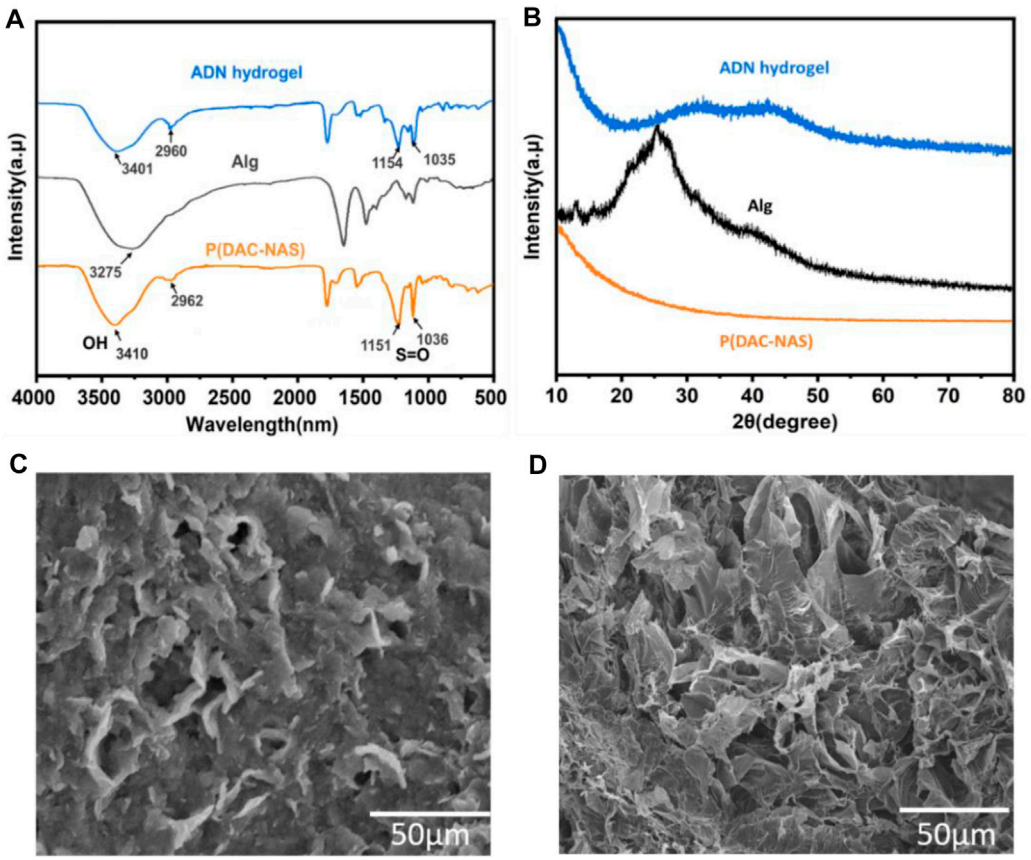

FIGURE 2 | Characterization of the hydrogels. **(A)** FTIR spectra of Alg, P (DAC-co-NAS) and $ADN_{1.5}$ hydrogels. **(B)** XRD pattern of Alg, P (DAC-co-NAS) and $ADN_{1.5}$ hydrogels. SEM images of Alg **(C)** and $ADN_{1.5}$ hydrogels **(D)**.

double network hydrogel system with outstanding mechanical properties.

Double network hydrogel is proposed by Gong Jianping group (Wen et al., 2020). Unlike traditional single-network hydrogels, double network hydrogels are composed of two different polymer networks with asymmetric structure (Wang T. et al., 2022; Kim et al., 2022), including a rigid and brittle first network and a soft and stretchable second network (Ahmed et al., 2020; Kim et al., 2020). The toughening mechanism of the double network structure is mainly based on the "sacrificial bond theory" (Sun et al., 2013). When an external force is applied to the hydrogel, the first network is disconnected to effectively dissipate the energy and protects the second network, which can maintain pressure and store elasticity to strengthen the hydrogel (Ling et al., 2021; Xu et al., 2022; Yao et al., 2022). Studies based on this theory have succeeded in producing tough hydrogels that are partially or completely self-healing after internal ruptures (Kim et al., 2022). These hydrogels combine the advantages of conductive medium and three-dimensional hydrogels, such as softness, self-healing property, adhesivity, biocompatibility, and electrical-responsive, which are beneficial to their applications in flexible wearable strain sensors (El-Atab et al., 2020; Feng et al., 2022). Therefore, the design of the double network hydrogel provides a new thinking for the development of wearable electronic materials (Qin et al., 2020; Li X. et al., 2021).

In this work, a novel conductive double network hydrogel was prepared by a one-pot and two-step procedure. This hydrogel was synthesized by an alginate network physically cross-linked by calcium ions and interpenetrating copolymers consisting of anionic monomer sodium p-styrene sulfonate (NAS) and cationic monomer acryloxyethyl trimethyl ammonium chloride (DAC) (**Figure 1**). The reversible physical cross-link brought advantages such as energy dissipation, super elasticity, and adaptive self-adhesion due to the ion dipole or dipole-dipole interaction created by strong dipolar zwitterionic units (Huang et al., 2021; Mirzaei et al., 2021). The obtained hydrogels were denoted as ADN, where A refers to sodium alginate, D refers to DAC, N refers to NAS. This hydrogel showed remarkable stretchability (~1,375%), toughness (0.57 MJ/m^3), high optical transmittance (~92.2%, **Supplementary Figure S1**), and self-adhesion to diverse substrates. The hydrogels also present high ionic conductivity (0.25 S/m) and sensitivity (up to 3.21 of the gauge factor for the tensile strain responses). Our research also demonstrated that our ADN hydrogel could work well as a wearable strain sensor directly to respond to a variety of large joint flexion (such as finger, elbow and knee) and local muscle

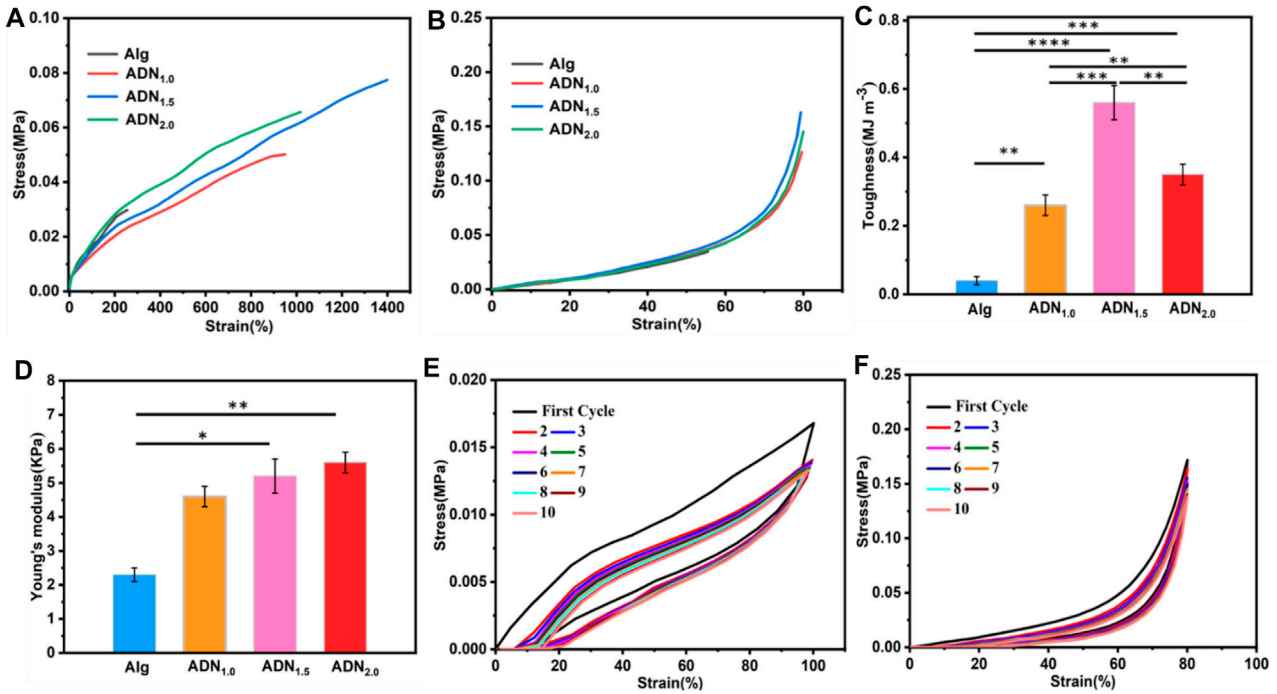

FIGURE 3 | Mechanical properties of the ADN hydrogels. **(A)** Tensile strain vs. stress curves of the ADN hydrogels. **(B)** Compressive strain vs. stress curves of the hydrogels at 80% strain. Toughness **(C)** and Young's modulus **(D)** of the hydrogels. **(E)** Ten successive cyclic tensile loading–unloading curves of the $ADN_{1.5}$ hydrogel at 100% strain. **(F)** Ten successive cyclic compressive tests of the $ADN_{1.5}$ hydrogel at 80% strain. $^{****}p < 0.0001$, $^{***}p < 0.001$, $^{**}p < 0.01$, $^{*}p < 0.05$.

movement (such as eyebrow and mouth). All of these verified its great potential in personalized healthcare monitoring, human–machine interfaces, and artificial intelligence.

EXPERIMENTAL SECTION

Materials

Sodium p-styrene sulfonate (NAS), acryloxyethyl trimethyl ammonium chloride (DAC), 2-azobis (2-methyl-propionamidine) dihydrochloride (V-50, 98%), D-(+)-gluconic acid δ-lactone (GDL), ethylenediaminetetraacetic acid calcium disodium salt hydrate ($EDTANa_2Ca$), sodium alginate, and they were purchased from Sinopharm Chemical Reagent Co., LTD. All the chemicals were purchased commercially and used directly without further purification. Deionized water (DI water) was used in all the experiments.

Preparation of ADN Hydrogel

The ADN hydrogel was prepared by a one-pot/two-step method. In the synthesis process, sodium alginate (3 wt%) aqueous solution was prepared at 60°C. After the addition of $EDTANa_2Ca$, NAS, DAC and initiator V-50 were added into the solution immediately. The mixture was stirred for another 30 min to form a thick solution. The formulation is shown in **Supplementary Table S1**. All the solutions were centrifugally degassed at 5,000 r/min. Then GDL was added into the solution to trigger the release of the Ca^{2+} to crosslink the alginate. After centrifugally degassing at 3,000 r/min, the mixed precursor solution was transferred to a mold. The precursor was stored at room temperature for 3 h to form the alginate network crosslinked by Ca^{2+} ions. Finally, the precursor was placed in a water bath of 45°C for 12 h to initiate the *in-situ* copolymerization of NAS and DAC. Hydrogels with different NAS contents and sole calcium alginate hydrogels (Alg) were prepared (**Supplementary Table S1**).

Characterization

The crystalline nature of the hydrogels was analyzed by X-ray diffraction (Japanese Ultima IV) with copper as the target and operating voltage range of 20–60 kV. The sample was placed horizontally with a scanning range of 5°–80° and a scanning speed of 20°/min. FEI Inspect F50 scanning electron microscopy (SEM) was used to analyze the microstructure of the composite hydrogel. The hydrogel was treated with liquid nitrogen to expose its internal structure. The freeze-dried hydrogel sample was mounted on a copper stud and coated with gold/palladium sputtering for 60 s. The infrared absorption spectra of the prepared hydrogels were measured using a Fourier Transform infrared (FTIR) spectrometer (Nicolet 5,700) in transmission mode under potassium bromide pellets. All spectra were obtained by 16 scans in the range of 4,000–500 cm^{-1}. The transmission spectrum of hydrogel with thickness of 1.6 mm in the wavelength range of 800–400 nm was characterized by UV-visible spectrophotometer.

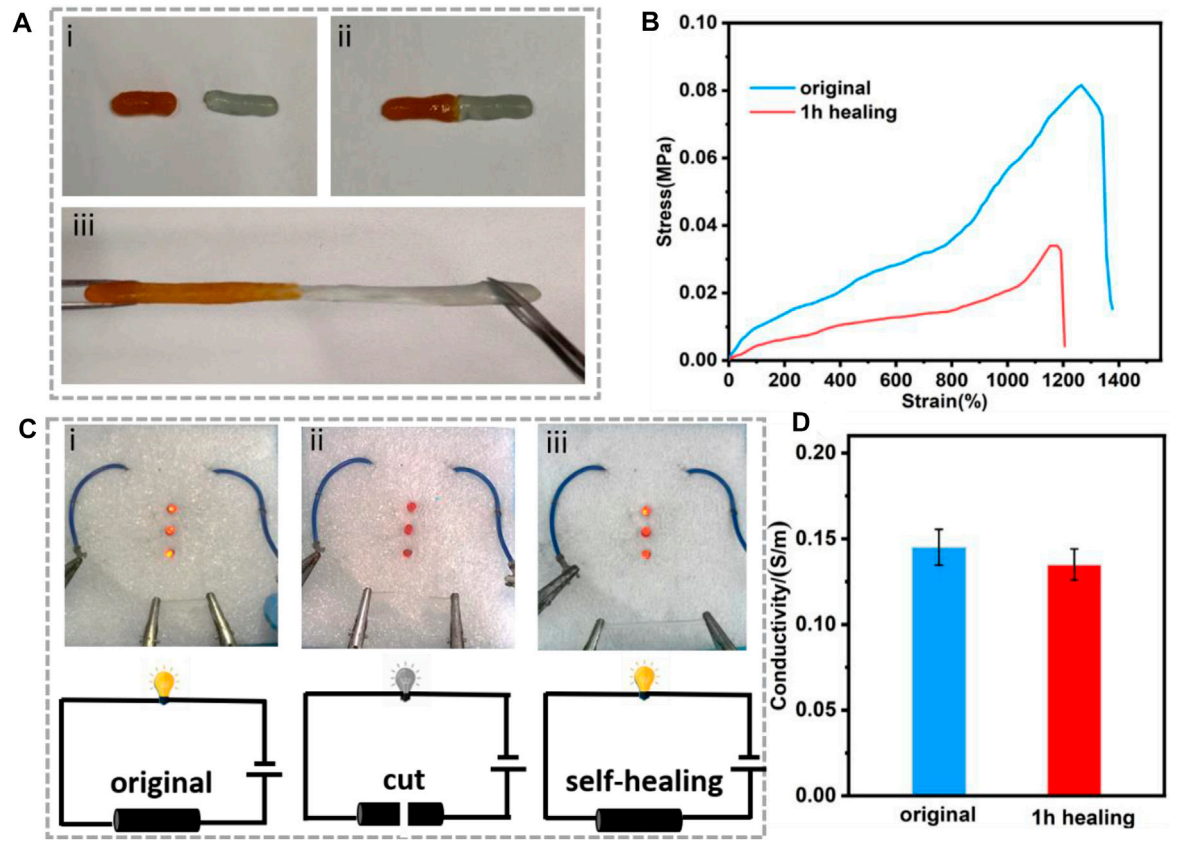

FIGURE 4 | (A) The self-healing behavior of the $ADN_{1.5}$ hydrogel: (i) original hydrogel, (ii) completely broken hydrogel, (iii) stretched hydrogel after self-healing. **(B)** Tensile strain vs. stress curves of the hydrogel after self-healing. **(C)** A circuit consisting of the hydrogel in series with red LED bulbs: (i) original hydrogel, (ii) completely broken hydrogel, (ii) self-healed hydrogel, and the corresponding schematic diagrams of the circuit. **(D)** The conductivity of the $ADN_{1.5}$ hydrogel after 1 h healing.

Mechanical Testing of the Hydrogels

The mechanical properties of the hydrogels were investigated using an electrical universal material testing machine (WDW-05) at room temperature. For tensile tests, the samples were prepared as the cylindrical-shaped strip with a 40 mm of length and 2.8 mm of diameter and stretched with a strain rate of 60 mm/min. For compression tests, a cylindrical hydrogel sample with a diameter of 10 mm and a height of 15 mm was placed on the bottom plate and the top plate was compressed at a strain rate of 10 mm/min. The adhesion strength of the hydrogels on different kinds of surfaces were performed by using a universal material testing machine. Each sample was tested at least three times and the results were reported with an average standard deviation. The adhesion strength was calculated by dividing the maximum force by the overlapping area of the adhesive position.

Electrical Measurements of the Hydrogels

The resistivity of the hydrogels was measured by a digital four-probe tester (Suzhou Crystal Lattice). Resistance change of the hydrogels with mechanical deformation was tested by LCR meter (TH 2832). The two ends of hydrogels were inserted into copper wires to connect the LCR meter, and the changes of hydrogels resistance were recorded in real time.

Fabrication and Testing of the Hydrogel-Based Flexible Wearable Strain Sensor

During the preparation of the hydrogel-based wearable strain sensor, the ADN hydrogel was made into strips of 30 mm × 8 mm × 1.5 mm in size. Two conductive copper sheets with conducting wires were tightly fixed on the two ends of the sample to assemble the strain sensor. The ADN hydrogel was sandwiched between two medical PU tapes. The function of PU tapes was mainly to prevent the evaporation of water in the hydrogel. During the monitoring of human movements, the wearable strain sensor was directly attached to the volunteers' skin, and the real-time change of the resistance of the sensor was recorded with an LCR meter. All experiments for monitoring human movements were performed with the consent of the volunteers. The experimental scheme was approved by the Human Experimental Ethics Committee of Fujian Normal University (Approve No.20200039).

Statistical Analysis

All the data were expressed as the means standard deviations (SD). Statistical analysis was executed with Student's t-test. If the

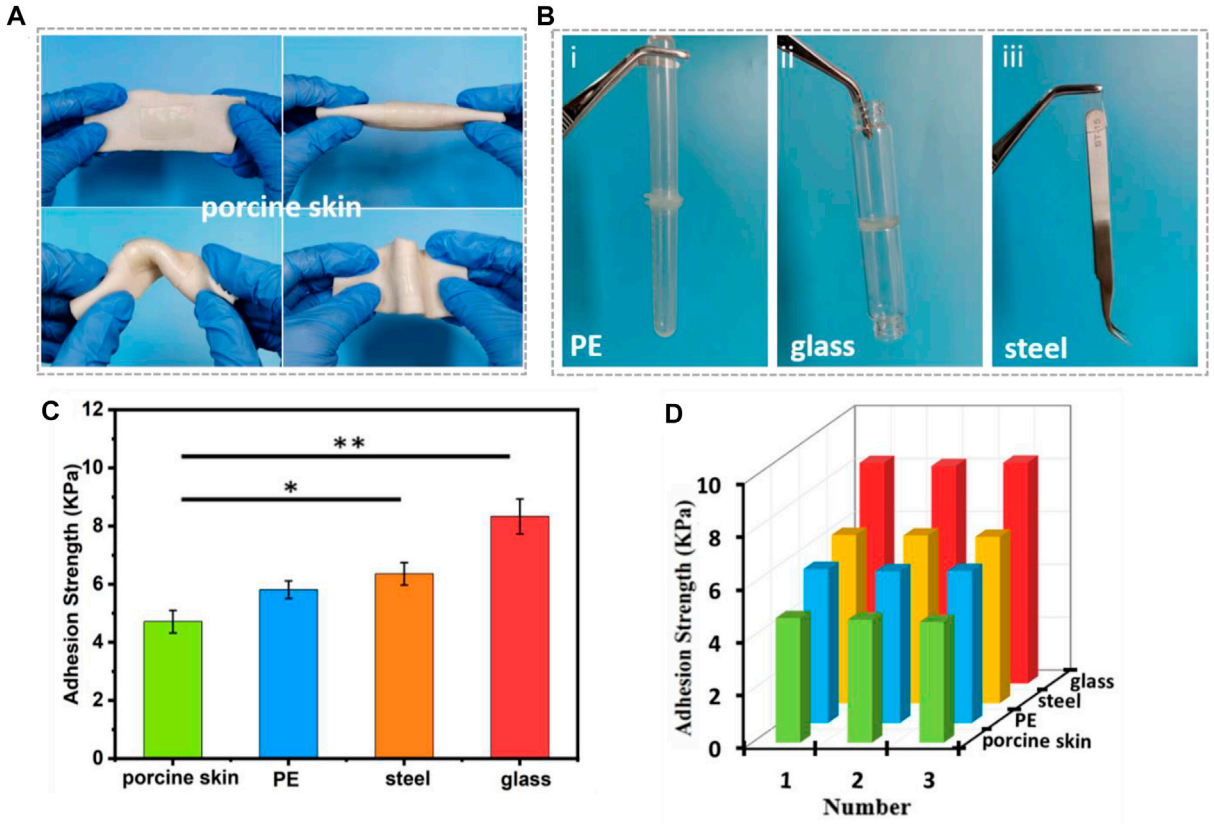

FIGURE 5 | Adhesion performance of the $ADN_{1.5}$ hydrogels. Photos of the self-adhesive hydrogels attached on porcine skin. **(A)** Photos of the self-adhesive hydrogels attached on porcine skin. **(B)** Photos of the self-adhesive hydrogels attached on PE (i), glass (ii), stainless steel (iii). **(C)** Adhesive strength of the $ADN_{1.5}$ hydrogels to different substrates. **(D)** Repeatable self-adhesive behavior of the hydrogels to different substrates. $^{**}p < 0.01$, $^{*}p < 0.05$.

p-value was lower than 0.05, the difference was considered significant.

RESULTS AND DISCUSSION

Design Principles and Material Synthesis

In the ADN double network hydrogel system, alginate and Ca^{2+} were physically cross-linked to form the first layer network, and anionic monomer NAS and cationic monomer DAC were polymerized to form the second layer network via ionic pair. Naturally derived alginate contains consecutive or alternating (1,4)-linked β-D-mannuronate (M) blocks and α-L-guluronate (G) blocks, where the adjacent G blocks can chelate divalent or multivalent metal ions to form an ionic crosslinking network. In order to avoid the formation of a heterogeneous network due to the rapid ion release process, we chose the ($EDTANa_2Ca$)/D-(+)-gluconic acid δ-lactone (GDL) system to delay the Ca^{2+} release during the alginate-Ca^{2+} crosslinking formation (Akay et al., 2017; Yang et al., 2021). Sulfonic anions of NAS interact with ammonium ions via electrostatic forces to produce the second physical crosslinking network. Furthermore, the rich hydroxyl and carboxyl groups in alginate trigged slightly crosslinking between the two networks with hydrogen bonds and electrostatic interactions, which could be determined by the shift of the O-H and S=O peaks in the FTIR (**Figure 2A**) (Ilcikova et al., 2015). The XRD analysis on the samples was performed to further evaluate the impact of physical blending conditions on crystalline structure as shown in **Figure 2B**. The diffractogram of Alg presented a broad peak at 2θ = 24, indicating its amorphous nature (Feng et al., 2022). An explicit decrease in the crystallization of alginate was observed in the XRD spectrum of the $ADN_{1.5}$ hydrogel, which might be contributed to its high optical transparency. SEM images of the morphology of Alg hydrogel, $ADN_{1.5}$ hydrogel, and P(NAS-co-DAC) hydrogel were presented in **Figure 2C,D** and **Supplementary Figure S2**, respectively. As could be seen from **Figure 1A**, the surface of the Alg hydrogel was rough and dense without obvious porous structure. This might be due to the dense structure formed by sufficient cross-linking between alginate and calcium ions in Alg hydrogels (Qu et al., 2016). This structure also led to the hard and brittle properties of Alg hydrogels (Zhao Y. et al., 2019). As could be seen from **Supplementary Figure S2**, the P(NAS-co-DAC) hydrogel had obvious porous structure, the hole was large and the structure was loose. Whereas, the surface of the $ADN_{1.5}$ hydrogel exhibited a reticulate structure (**Figure 1C**), which was highly beneficial to its toughness and stretchability (Zeng et al., 2020). This difference might be caused by the insufficiently cross-linking

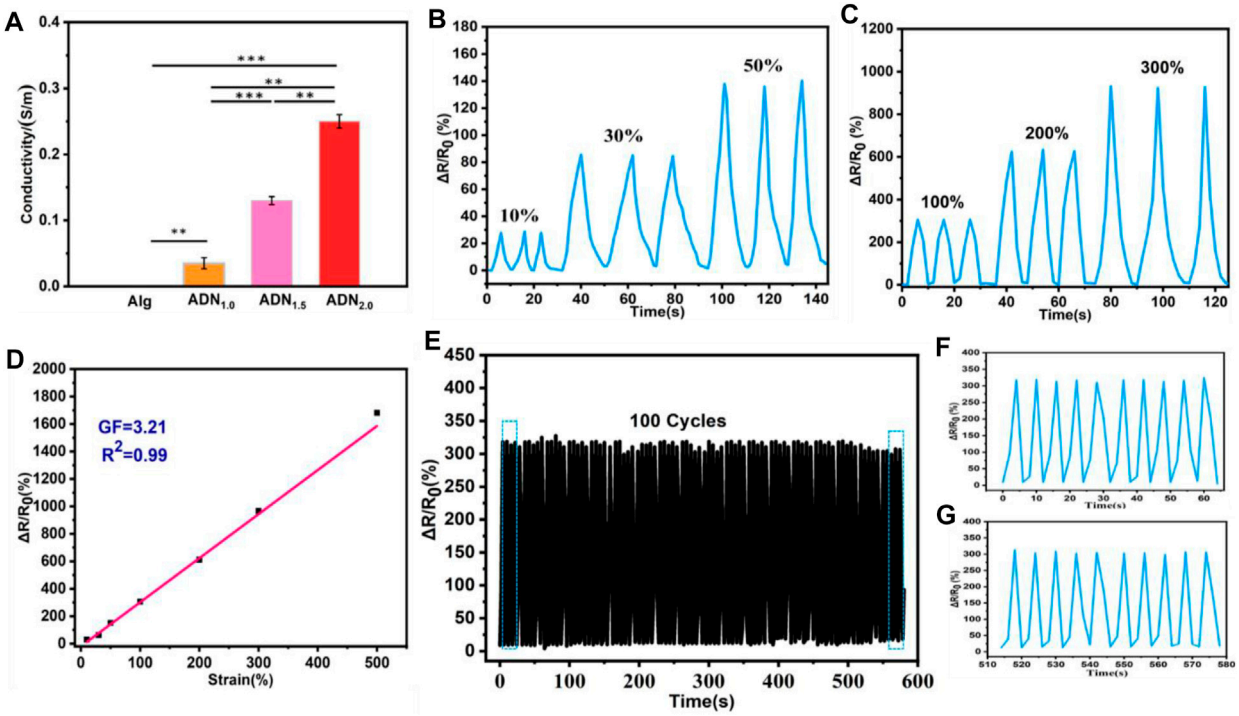

FIGURE 6 | Electromechanical performances of the $ADN_{1.5}$ hydrogel applicated as flexible strain sensor. **(A)** Conductivity comparison of hydrogels. The cyclic relative resistance changes of this hydrogel strain sensor under low strains **(B)** and high strains **(C)**, respectively. **(D)** The linear fitting of the relationship between the relative resistance changes and the strain of this hydrogel sensor. **(E)** The durability test of the hydrogel sensor under 0–100% strain. **(F)** Magnified signal during 1–10 cycles. **(G)** Magnified signal during 91–100 cycles.

of the calcium alginate network in $ADN_{1.5}$ hydrogels due to the introduction of P(NAS-co-DAC) network, which showed a looser structure than Alg hydrogels and a denser structure than P(NAS-co-DAC) hydrogel.

Mechanical Properties of the Hydrogels

The mechanical properties of Alg hydrogel were significantly enhanced by introducing the second P (DAC-co-NAS) network. As shown in **Figure 3A**, the tensile properties of ADN hydrogel were greatly improved compared with Alg hydrogel. In terms of the hydrogel stretchability, the $ADN_{1.5}$ hydrogel exhibited the maximum tensile fracture length of 1,375%, which was superior to reported hydrogels in some literatures. On the contrary, the Alg hydrogel presented a fracture tensile strain of only 212%. A similar result also presented in the following compressive test (**Figure 3B**). Furthermore, compared with Alg hydrogel, the elastic modulus and toughness of ADN hydrogel were also significantly increased (**Figure 3C,D**). Photographs of the mechanical performances of the ADN hydrogels were shown in **Supplementary Figure S3**. Herein, in view of the excellent stretchability and toughness of the $ADN_{1.5}$ hydrogel, we selected it as the best group for further test. **Figure 3E** showed 10 tensile-relaxation cycles at 100% strain. The tensile strength decreased after the first tensile cycle due to the inevitable viscosity of the polymer matrix and some permanently broken chemical bonds (Liu et al., 2021; Xue et al., 2021). The subsequent coincident tensile cycles, indicating that the reversible bond fracture and recombination had high repeatability and stability. As for the compressive cycle experiment, 10 cycles were basically consistent with the stress curves, which strongly proved that the hydrogel had good elasticity and fatigue resistance (**Figure 3F**). We speculated that it was because that compression was difficult to cause irreversible dissociation of the hydrogel crosslinking.

The ADN hydrogel exhibited the ability of self-healing due to its dynamic crosslinking (Chen G. et al., 2021; Huang et al., 2021). As shown in **Figure 4A,** the $ADN_{1.5}$ hydrogel was cut in half with a razor blade and then reassembled. After 30 min at room temperature, we observed that the two parts had healed into complete one, which still showed good stretchability (**Figure 4B**). The self-healing rate is defined as $\varepsilon = E/E_0$, where E_0 is the initial elongation at break and E is the elongation at break after self-healing (Deng et al., 2022). After calculation, the self-healing rate of composite hydrogel reached 86.5%. As shown in **Figure 4C**, the $ADN_{1.5}$ hydrogel was connected to LED beads by a 6V power supply. After cutting the $ADN_{1.5}$ hydrogel in half with a razor blade, the LED beads went out. After combining the two bifurcated parts together and repairing the dynamic cross-linking between the contact surfaces, the LED beads lit up again. The conductivity of the hydrogel after 1 h self-healing was 93% of the original hydrogel (**Figure 4D**). Due to the excellent self-repair ability of the hydrogel, the service life of the hydrogel as a flexible electronic device should be prolonged, leading to the great application advantages in flexible wearable strain sensors.

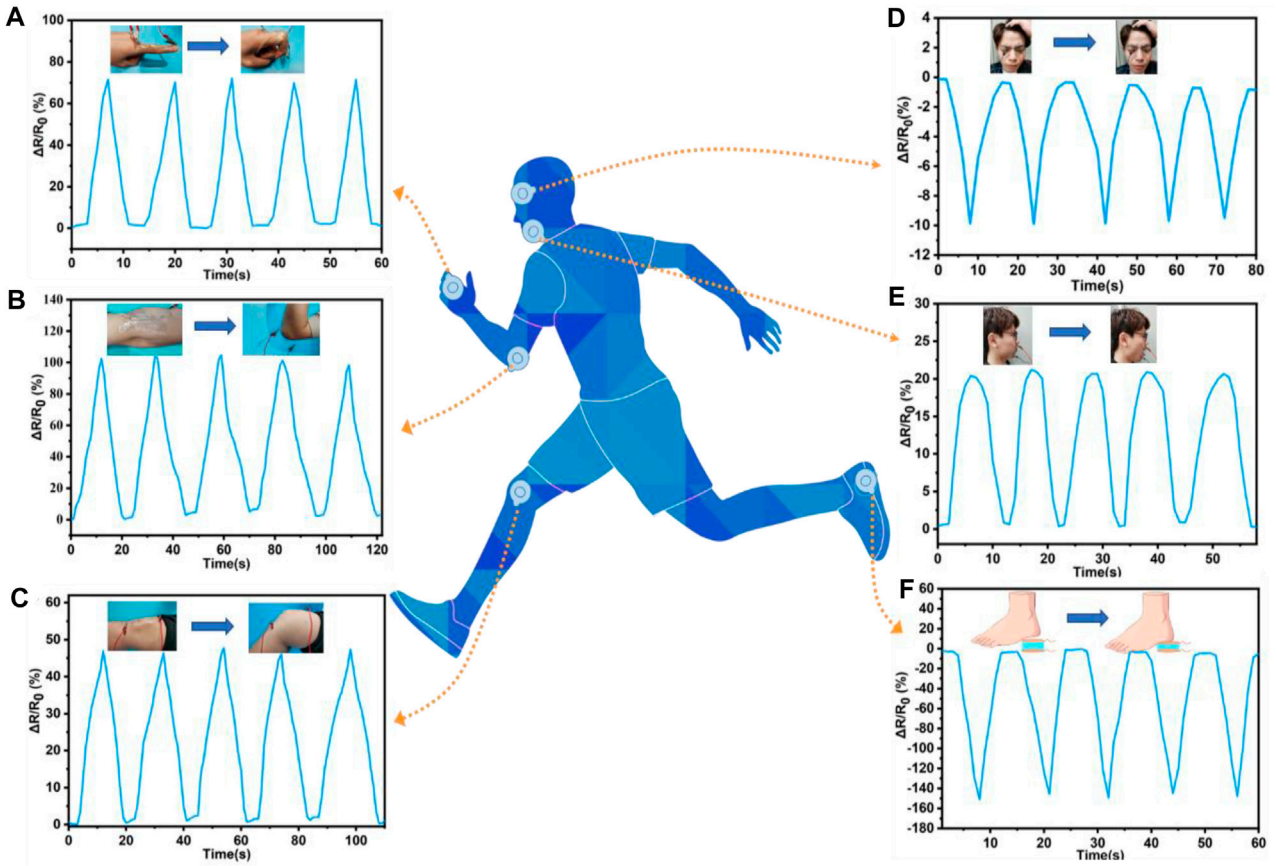

FIGURE 7 | The real-time monitoring of human motions with $ADN_{1.5}$ hydrogel-based strain sensors. The real-time monitoring of large-range human motions with finger **(A)**, elbow **(B)**, knee **(C)**. The real-time monitoring of tiny human motions: frown **(D)**, mouth movement **(E)**, and **(F)** foot planter pressure during locomotion.

Adhesive Properties of the Hydrogels

Mechanical compliance and durability are key factors for signal transmission of strain sensor, and conformation adhesion can adaptively overcome interfacial gaps and improve the sensitivity of signal acquisition (Choi et al., 2018). The $ADN_{1.5}$ hydrogel could adhere to different kinds of surfaces (such as porcine skin, PE, glass, etc.). The conformal adhesion of the $ADN_{1.5}$ hydrogel to porcine skin was shown in **Figure 5A**. The $ADN_{1.5}$ hydrogel adhered tightly to porcine skin under folding and twisting, making it difficult to peel off. The adhesion photographs and adhesion strength of the hydrogels on other substrates were shown in **Figures 5Bi-iii,C**, respectively. This adhesion was attributed to the high polarity of the zwitterionic polymer in the hydrogel (Asha et al., 2021; Yu and Wu, 2021). Both charged groups (cationic quaternary ammonium and anionic sulfonate) and polar groups (S=O) tend to interact with other charged or polar groups on the surface of most substrates via ion dipole and/or dipole-dipole interactions, resulting in a strong interfacial bonding (Kim et al., 2021). This inherent adhesive property enabled the ADN hydrogels to be applied in human-computer interaction, soft robotics and other fields in a fitting manner. In addition, the cyclic adhesion test of $ADN_{1.5}$ hydrogel on different substrates showed that the adhesion of the hydrogel remained stable after multiple use (**Figure 5D**). This multi-cycle adhesion made the ADN hydrogel an ideal material for building wearable strain sensors of easy use and economical.

Electronic Performance of the Hydrogel

The ADN hydrogel exhibited good electrical conductivity due to the introduction of the polyelectrolyte network. As shown in **Figure 6A**, compared with Alg hydrogel, the conductivity of ADN hydrogels was significantly improved. The conductivity of the composite hydrogel increased from 0.04 S/m to 0.25 S/m with the increase of NAS content from 1.0 wt% to 2.0 wt%. This might be due to the formation of more conductive pathways in the compound as the concentration of conductive ions increased. In order to study the variation in the resistance of the hydrogel with the tensile strain, the hydrogel was connected to the LCR meter to record the real-time resistance. The sensitivity of a strain sensor is expressed by the gauge factor (GF), which is calculated by the formula: $GF = (\Delta R/R_0)/\varepsilon$, where, $\Delta R = R - R_0$ (Chen et al., 2019; Xiong et al., 2020). Herein, R_0 and R are the original resistance without strain and the real-time resistance, respectively, and ε is the applied strain. The change in the resistance rate (ΔR/R0) of three stretch-release cycles under low strain (10, 30, and 50%) and high strain (100, 200, and 300%) were shown in **Figures 6B,C**,

respectively. It could be seen clearly that the resistance value of the hydrogel after three cyclic stretching (unstretched-stretched-unstretched) presented obvious and consistent cyclic change. As shown in **Figure 6D**, $\Delta R/R_0$ was linearly fitted to the strain and the GF of the $ADN_{1.5}$ hydrogel was calculated to be 3.21. Compared with most reported flexible wearable strain sensors, the ADN hydrogel had higher sensitivity and stability in a wide range of strain changes. The $ADN_{1.5}$ hydrogel-based strain sensor showed a stable response signal, when the strain was 100% (**Figure 6E**). The amplitude and waveform had tiny fluctuation after 100 consecutive loading and unloading cycles, proving the satisfactory stability and reliability of the strain sensor. The magnified signal during 1–10 cycles and 91–100 cycles were shown in **Figures 6F,G**, respectively.

Application in Human Motions Monitoring

The ADN hydrogel had the advantages of high sensitivity, fast response, wide sensing range, and good stability. Therefore, the wearable strain sensor based on the ADN hydrogel had a broad application prospect in human motion detection (Wang S. L. et al., 2022; Li et al., 2022). Herein, the $ADN_{1.5}$ hydrogel was made into a wearable strain sensor, which was attached to the volunteer's skin to monitor the movements of the human body from tiny deformations to large-scale motions in real-time. The ADN hydrogel-based strain sensor could accurately respond to full-range human motions, and it also had repeatable and stable signal output. In particular, the excellent optical transparency of the $ADN_{1.5}$ hydrogel gave the strain sensor an unobtrusive visual appearance and allowed precise targeting of specific positions for real-time monitoring of human movements. The large-scale movement monitoring curves of human fingers, elbows, and knees were shown in **Figure 7A–C**. In the case of finger bending, when the finger bending angle gradually increased from 0° to 90°, the change of relative resistance increased from 0 to 72.5%. As the fingers returned from the bending to the stretching, the relative resistance also returned to the initial state. A stable repetitive response was observed during the five periodic scaling processes. In addition to detecting large body movements, the strain sensors could also detect subtle body movements. As shown in **Figure 7D**, our hydrogel-based strain sensor could detect tiny muscle movements around the eyebrow. When the volunteer performed periodic frowns exercises, a distinct and relatively uniform pattern of resistance was observed, displaying a wide prospect for facial recognition. And a unique and relatively consistent pattern of resistance was observed when the volunteer performed the periodic "opening-closing" movement (**Figure 7E**). In addition, a circular hydrogel disc was sandwiched between the sheet electrodes and placed directly under the heel to detect load during motion (**Figure 7F**). A steady repetitive response was observed during five periodic foot-up-and-down cycles. This application of the ADN hydrogel was feasible because of its excellent compressive strength, low mechanical hysteresis and electrical conductivity. With the unique design, the ADN hydrogel-based sensor could be used for plantar pressure measurements, and it also had great application potential in sports injury prevention, sports biomechanics, footwear design and research, and so on.

CONCLUSION

In this study, we described a conductive double network hydrogel by introducing charge-rich polymorphic ions into the natural polysaccharide network. The ADN hydrogel exhibited remarkable stretchability, outstanding toughness, unique optical transmittance, self-healing, and general adhesion. In addition, we also designed a wearable strain sensor based on this ADN hydrogel. And the feasibility of monitoring human motions or analyzing human mental state based on signal acquisition of large joint flexion (such as finger, elbow, and knee) and local muscle movement (such as eyebrow and mouth) was demonstrated. Therefore, the highly stretchable, self-healing, and adhesive ADN hydrogel would be a promising material in aspects of human-machine interfaces, wearable monitoring systems and medical applications.

DATA AVAILABILITY STATEMENT

The original contributions presented in the study are included in the article/**Supplementary Material**, further inquiries can be directed to the corresponding author/s.

ETHICS STATEMENT

The studies involving human participants were reviewed and approved by the Human Experimental Ethics Committee of Fujian Normal University (Approve No.20200039). The patients/participants provided their written informed consent to participate in this study.

AUTHOR CONTRIBUTIONS

QF, XX, and YY conceived and supervised the project. KC carried out most experiments and wrote the manuscript. ML, YH, FW, PL, CL, and QD analysed the data and revised the manuscript. All authors discussed the results and revised the manuscript.

FUNDING

This work was supported by the National Natural Science Foundation of China (31900963); the Fundamental Research Funds for the Central Universities (2021CDJQY-017), the Natural Science Foundation of Chongqing (cstc2021jcyj-cxttX0002); Fujian Provincial Health and Education Project for Tackling the Key Research (2019-WJ-22), Natural Science Foundation of Fujian Province (2020J02033), Fuzhou Science and Technology Project (2020-PT-138).

SUPPLEMENTARY MATERIAL

The Supplementary Material for this article can be found online at: https://www.frontiersin.org/articles/10.3389/fbioe.2022.846401/full#supplementary-material

REFERENCES

Ahmed, M. K., Menazea, A. A., and Abdelghany, A. M. (2020). Blend Biopolymeric Nanofibrous Scaffolds of Cellulose Acetate/ε-Polycaprolactone Containing Metallic Nanoparticles Prepared by Laser Ablation for Wound Disinfection Applications. *Int. J. Biol. Macromolecules* 155, 636–644. doi:10.1016/j.ijbiomac.2020.03.257

Akay, S., Heils, R., Trieu, H. K., Smirnova, I., and Yesil-Celiktas, O. (2017). An Injectable Alginate-Based Hydrogel for Microfluidic Applications. *Carbohydr. Polym.* 161, 228–234. doi:10.1016/j.carbpol.2017.01.004

Asha, A. B., Chen, Y., and Narain, R. (2021). Bioinspired Dopamine and Zwitterionic Polymers for Non-fouling Surface Engineering. *Chem. Soc. Rev.* 50, 11668–11683. doi:10.1039/d1cs00658d

Chen, C. R., Qin, H., Cong, H. P., and Yu, S. H. (2019). A Highly Stretchable and Real-Time Healable Supercapacitor. *Adv. Mater.* 31, 1900573. doi:10.1002/adma.201900573

Chen, G., Hu, O., Lu, J., Gu, J., Chen, K., Huang, J., et al. (2021a). Highly Flexible and Adhesive Poly(vinyl Alcohol)/poly(acrylic Amide-Co-2-Acrylamido-2-Methylpropane Sulfonic Acid)/glycerin Hydrogel Electrolyte for Stretchable and Resumable Supercapacitor. *Chem. Eng. J.* 425, 131505. doi:10.1016/j.cej.2021.131505

Chen, Z., Chen, Y., Hedenqvist, M. S., Chen, C., Cai, C., Li, H., et al. (2021b). Multifunctional Conductive Hydrogels and Their Applications as Smart Wearable Devices. *J. Mater. Chem. B* 9, 2561–2583. doi:10.1039/D0TB02929G

Chimene, D., Kaunas, R., and Gaharwar, A. K. (2020). Hydrogel Bioink Reinforcement for Additive Manufacturing: A Focused Review of Emerging Strategies. *Adv. Mater.* 32, 1902026. doi:10.1002/adma.201902026

Choi, S., Han, S. I., Jung, D., Hwang, H. J., Lim, C., Bae, S., et al. (2018). Highly Conductive, Stretchable and Biocompatible Ag-Au Core-Sheath Nanowire Composite for Wearable and Implantable Bioelectronics. *Nat. Nanotech* 13, 1048–1056. doi:10.1038/s41565-018-0226-8

Dai, W., Sun, M., Leng, X., Hu, X., and Ao, Y. (2020). Recent Progress in 3D Printing of Elastic and High-Strength Hydrogels for the Treatment of Osteochondral and Cartilage Diseases. *Front. Bioeng. Biotechnol.* 8, 604814. doi:10.3389/fbioe.2020.604814

Deng, P., Yao, L., Chen, J., Tang, Z., and Zhou, J. (2022). Chitosan-based Hydrogels with Injectable, Self-Healing and Antibacterial Properties for Wound Healing. *Carbohydr. Polym.* 276, 118718. doi:10.1016/j.carbpol.2021.118718

Ding, H., Xu, S., Wang, J., Fan, Z., Huang, Z., Wu, H., et al. (2022). A Conductive, Antibacterial, and Antifouling Hydrogel Based on Zwitterion. *J. Appl. Polym. Sci.* 139, 51648. doi:10.1002/app.51648

El-Atab, N., Mishra, R. B., Al-Modaf, F., Joharji, L., Alsharif, A. A., Alamoudi, H., et al. (2020). Soft Actuators for Soft Robotic Applications: A Review. *Adv. Intell. Syst.* 2, 2000128. doi:10.1002/aisy.202000128

Fan, H., Wang, J., and Jin, Z. (2018). Tough, Swelling-Resistant, Self-Healing, and Adhesive Dual-Cross-Linked Hydrogels Based on Polymer-Tannic Acid Multiple Hydrogen Bonds. *Macromolecules* 51, 1696–1705. doi:10.1021/acs.macromol.7b02653

Feng, E., Li, J., Zheng, G., Li, X., Wei, J., Wu, Z., et al. (2022). Mechanically Toughened Conductive Hydrogels with Shape Memory Behavior toward Self-Healable, Multi-Environmental Tolerant and Bidirectional Sensors. *Chem. Eng. J.* 432, 134406. doi:10.1016/j.cej.2021.134406

He, F., You, X., Gong, H., Yang, Y., Bai, T., Wang, W., et al. (2020). Stretchable, Biocompatible, and Multifunctional Silk Fibroin-Based Hydrogels toward Wearable Strain/Pressure Sensors and Triboelectric Nanogenerators. *ACS Appl. Mater. Interfaces* 12, 6442–6450. doi:10.1021/acsami.9b19721

Huang, S., Wan, Y., Ming, X., Zhou, J., Zhou, M., Chen, H., et al. (2021). Adhering Low Surface Energy Materials without Surface Pretreatment via Ion-Dipole Interactions. *ACS Appl. Mater. Inter.* 13, 41112–41119. doi:10.1021/acsami.1c11822

Ilčíková, M., Tkáč, J., and Kasák, P. (2015). Switchable Materials Containing Polyzwitterion Moieties. *Polymers* 7, 2344–2370. doi:10.3390/polym7111518

Jin, R., Xu, J., Duan, L., and Gao, G. (2021). Chitosan-driven Skin-Attachable Hydrogel Sensors toward Human Motion and Physiological Signal Monitoring. *Carbohydr. Polym.* 268, 118240. doi:10.1016/j.carbpol.2021.118240

Kim, J. S., Choi, J., Ki, C. S., and Lee, K. H. (2021). 3D Silk Fiber Construct Embedded Dual-Layer PEG Hydrogel for Articular Cartilage Repair - *In Vitro* Assessment. *Front. Bioeng. Biotechnol.* 9, 653509. doi:10.3389/fbioe.2021.653509

Kim, J. W., Kim, S., Jeong, Y. R., Kim, J., Kim, D. S., Keum, K., et al. (2022). Self-healing Strain-Responsive Electrochromic Display Based on a Multiple Crosslinked Network Hydrogel. *Chem. Eng. J.* 430, 132685. doi:10.1016/j.cej.2021.132685

Kim, M. S., Kim, J. W., Yun, J., Jeong, Y. R., Jin, S. W., Lee, G., et al. (2020). A Rationally Designed Flexible Self-Healing System with a High Performance Supercapacitor for Powering an Integrated Multifunctional Sensor. *Appl. Surf. Sci.* 515, 146018. doi:10.1016/j.apsusc.2020.146018

Li, S., Cao, P., Li, F., Asghar, W., Wu, Y., Xiao, H., et al. (2022). Self-powered Stretchable Strain Sensors for Motion Monitoring and Wireless Control. *Nano Energy* 92, 106754. doi:10.1016/j.nanoen.2021.106754

Li, W., Jian, X., Zou, Y., Wu, L., Huang, H., Li, H., et al. (2021a). The Fabrication of a Gellan Gum-Based Hydrogel Loaded with Magnesium Ions for the Synergistic Promotion of Skin Wound Healing. *Front. Bioeng. Biotechnol.* 9, 709679. doi:10.3389/fbioe.2021.709679

Li, X., He, L., Li, Y., Chao, M., Li, M., Wan, P., et al. (2021b). Healable, Degradable, and Conductive MXene Nanocomposite Hydrogel for Multifunctional Epidermal Sensors. *ACS Nano* 15, 7765–7773. doi:10.1021/acsnano.1c01751

Lin, F., Wang, Z., Shen, Y., Tang, L., Zhang, P., Wang, Y., et al. (2019). Natural Skin-Inspired Versatile Cellulose Biomimetic Hydrogels. *J. Mater. Chem. A* 7, 26442–26455. doi:10.1039/C9TA10502F

Ling, Q., Ke, T., Liu, W., Ren, Z., Zhao, L., and Gu, H. (2021). Tough, Repeatedly Adhesive, Cyclic Compression-Stable, and Conductive Dual-Network Hydrogel Sensors for Human Health Monitoring. *Ind. Eng. Chem. Res.* 60, 18373–18383. doi:10.1021/acs.iecr.1c03358

Liu, B., Zhao, Y., Zhu, T., Gao, S., Ye, K., Zhou, F., et al. (2020). Biphasic Double-Network Hydrogel with Compartmentalized Loading of Bioactive Glass for Osteochondral Defect Repair. *Front. Bioeng. Biotechnol.* 8, 752. doi:10.3389/fbioe.2020.00752

Liu, C., Qiu, S., Du, P., Zhao, H., and Wang, L. (2018). An Ionic Liquid-Graphene Oxide Hybrid Nanomaterial: Synthesis and Anticorrosive Applications. *Nanoscale* 10, 8115–8124. doi:10.1039/c8nr01890a

Liu, Z., Zhang, T., Yang, M., Gao, W., Wu, S., Wang, K., et al. (2021). Hydrogel Pressure Distribution Sensors Based on an Imaging Strategy and Machine Learning. *ACS Appl. Electron. Mater.* 3, 3599–3609. doi:10.1021/acsaelm.1c00488

Luo, C., Huang, M., and Liu, H. (2021). A Highly Resilient and Ultra-sensitive Hydrogel for Wearable Sensors. *J. Appl. Polym. Sci*, 51925. doi:10.1002/app.51925

Ma, W., Cao, W., Lu, T., Jiang, Z., Xiong, R., Samal, S. K., et al. (2021). Healable, Adhesive, and Conductive Nanocomposite Hydrogels with Ultrastretchability for Flexible Sensors. *ACS Appl. Mater. Inter.* 13, 58048–58058. doi:10.1021/acsami.1c20271

Mirzaei, A., Turczel, G., Nagyházi, M., Farkas, V., Balla, Á., Dang Vu, H., et al. (2021). Cyclative MCRs of Azines and Azinium Salts. *Eur. J. Org. Chem.* 2021, 326–356. doi:10.1002/ejoc.202001048

Nam, J., Byun, E., Shim, H., Kim, E., Islam, S., Park, M., et al. (2020). A Hydrogel-Based Ultrasonic Backscattering Wireless Biochemical Sensing. *Front. Bioeng. Biotechnol.* 8, 596370. doi:10.3389/fbioe.2020.596370

Pei, Z., Yu, Z., Li, M., Bai, L., Wang, W., Chen, H., et al. (2021). Self-Healing and Toughness Cellulose Nanocrystals Nanocomposite Hydrogels for Strain-Sensitive Wearable Flexible Sensor. *Int. J. Biol. Macromol.* 179, 324–332. doi:10.1016/j.ijbiomac.2021.03.023

Peng, W., Han, L., Gao, Y., Gong, Z., Lu, T., Xu, X., et al. (2022). Flexible Organohydrogel Ionic Skin with Ultra-low Temperature Freezing Resistance and Ultra-durable Moisture Retention. *J. Colloid Interf. Sci.* 608, 396–404. doi:10.1016/j.jcis.2021.09.125

Qin, Z., Sun, X., Yu, Q., Zhang, H., Wu, X., Yao, M., et al. (2020). Carbon Nanotubes/Hydrophobically Associated Hydrogels as Ultrastretchable, Highly Sensitive, Stable Strain, and Pressure Sensors. *ACS Appl. Mater. Inter.* 12, 4944–4953. doi:10.1021/acsami.9b21659

Qu, B., Li, J., Xiao, H., He, B., and Qian, L. (2016). Facile Preparation and Characterization of Sodium Alginate/Graphite Conductive Composite Hydrogel. *Polym. Compos.* 37, 3050–3056. doi:10.1002/pc.23502

Shen, J., Guo, Y., Zuo, S., Shi, F., Jiang, J., and Chu, J. (2021). A Bioinspired Porous-Designed Hydrogel@polyurethane Sponge Piezoresistive Sensor for Human-Machine Interfacing. *Nanoscale* 13, 19155–19164. doi:10.1039/D1NR05017F

Sun, H., Zhao, Y., Jiao, S., Wang, C., Jia, Y., Dai, K., et al. (2021). Environment Tolerant Conductive Nanocomposite Organohydrogels as Flexible Strain Sensors and Power Sources for Sustainable Electronics. *Adv. Funct. Mater.* 31, 2101696. doi:10.1002/adfm.202101696

Sun, T. L., Kurokawa, T., Kuroda, S., Ihsan, A. B., Akasaki, T., Sato, K., et al. (2013). Physical Hydrogels Composed of Polyampholytes Demonstrate High Toughness and Viscoelasticity. *Nat. Mater* 12, 932–937. doi:10.1038/NMAT3713

Wang, S. L., Xu, X., Han, Z., Li, H., Wang, Q., and Yao, B. (2022a). Highly Stretchable Liquid-Metal Based Strain Sensor with High Sensitivity for Human Activity Monitoring. *Mater. Lett.* 308, 131277. doi:10.1016/j.matlet.2021.131277

Wang, T., Wang, J., Li, Z., Yue, M., Qing, X., Zhang, P., et al. (2022b). PVA/SA/MXene Dual-network Conductive Hydrogel for Wearable Sensor to Monitor Human Motions. *J. Appl. Polym. Sci.* 139, 51627. doi:10.1002/app.51627

Wen, N., Jiang, B., Wang, X., Shang, Z., Jiang, D., Zhang, L., et al. (2020). Overview of Polyvinyl Alcohol Nanocomposite Hydrogels for Electro-Skin, Actuator, Supercapacitor and Fuel Cell. *Chem. Rec.* 20, 773–792. doi:10.1002/tcr.202000001

Wu, L., Li, L., Qu, M., Wang, H., and Bin, Y. (2020). Mussel-Inspired Self-Adhesive, Antidrying, and Antifreezing Poly(acrylic acid)/Bentonite/Polydopamine Hybrid Glycerol-Hydrogel and the Sensing Application. *ACS Appl. Polym. Mater.* 2, 3094–3106. doi:10.1021/acsapm.0c00264

Xiong, Y., Shen, Y., Tian, L., Hu, Y., Zhu, P., Sun, R., et al. (2020). A Flexible, Ultra-highly Sensitive and Stable Capacitive Pressure Sensor with Convex Microarrays for Motion and Health Monitoring. *Nano Energy* 70, 104436. doi:10.1016/j.nanoen.2019.104436

Xu, Y., Lin, Z., Rajavel, K., Zhao, T., Zhu, P., Hu, Y., et al. (2022). Tailorable, Lightweight and Superelastic Liquid Metal Monoliths for Multifunctional Electromagnetic Interference Shielding. *Nano-micro Lett.* 14, 29. doi:10.1007/s40820-021-00766-5

Xue, B., Gu, J., Li, L., Yu, W., Yin, S., Qin, M., et al. (2021). Hydrogel tapes for Fault-Tolerant strong Wet Adhesion. *Nat. Commun.* 12, 7156. doi:10.1038/s41467-021-27529-5

Yang, X., Ren, Y., Liu, H., Huo, C., and Li, L. (2021). Differences in the Physicochemical, Digestion and Microstructural Characteristics of Soy Protein Gel Acidified with Lactic Acid Bacteria, Glucono-δ-Lactone and Organic Acid. *Int. J. Biol. Macromolecules* 185, 462–470. doi:10.1016/j.ijbiomac.2021.06.071

Yang, Y., Su, Y., Zhu, X., Ye, D., Chen, R., and Liao, Q. (2022a). Flexible Enzymatic Biofuel Cell Based on 1, 4-naphthoquinone/MWCNT-Modified Bio-Anode and Polyvinyl Alcohol Hydrogel Electrolyte. *Biosens. Bioelectron.* 198, 113833. doi:10.1016/j.bios.2021.113833

Yang, Y., Zhou, M., Peng, J., Wang, X., Liu, Y., Wang, W., et al. (2022b). Robust, Anti-freezing and Conductive Bonding of Chitosan-Based Double-Network Hydrogels for Stable-Performance Flexible Electronic. *Carbohydr. Polym.* 276, 118753. doi:10.1016/j.carbpol.2021.118753

Yao, Q., Liu, Y., Pan, Y., Li, Y., Xu, L., Zhong, Y., et al. (2022). Long-term Induction of Endogenous BMPs Growth Factor from Antibacterial Dual Network Hydrogels for Fast Large Bone Defect Repair. *J. Colloid Interf. Sci.* 607, 1500–1515. doi:10.1016/j.jcis.2021.09.089

Yu, Y., Zhao, X., and Ye, L. (2021). A New Mussel-Inspired Highly Self-Adhesive & Conductive Poly (Vinyl Alcohol)-Based Hydrogel for Wearable Sensors. *Appl. Surf. Sci.* 562, 150162. doi:10.1016/j.apsusc.2021.150162

Yu, Z., and Wu, P. (2021). Water-Resistant Ionogel Electrode with Tailorable Mechanical Properties for Aquatic Ambulatory Physiological Signal Monitoring. *Adv. Funct. Mater.* 31, 2107226. doi:10.1002/adfm.202107226

Zeng, J., Dong, L., Sha, W., Wei, L., and Guo, X. (2020). Highly Stretchable, Compressible and Arbitrarily Deformable All-Hydrogel Soft Supercapacitors. *Chemical Engineering Journal* 383, 123098. doi:10.1016/j.cej.2019.123098

Zhang, J., Liu, E., Hao, S., Yang, X., Li, T., Lou, C., et al. (2022). 3D Printable, Ultra-stretchable, Self-Healable, and Self-Adhesive Dual Cross-Linked Nanocomposite Ionogels as Ultra-durable Strain Sensors for Motion Detection and Wearable Human-Machine Interface. *Chem. Eng. J.* 431, 133949. doi:10.1016/j.cej.2021.133949

Zhang, Y., Tao, Y., Wang, K., Zhao, S., Zhu, J., and Cheng, H. (2021). Two Kinds of Polyaniline Fiber Photo Sensor with Interdigital Electrode and Flexible Hydrogel. *J. Appl. Polym. Sci.* 138, 50628. doi:10.1002/app.50628

Zhao, H., Wang, Z., Li, Y., and Yang, M. (2022). Single-sided and Integrated Polyaniline/Poly(vinylidene Fluoride) Flexible Membrane with Micro/nanostructures as Breathable, Nontoxic and Fast Response Wearable Humidity Sensor. *J. Colloid Interf. Sci.* 607, 367–377. doi:10.1016/j.jcis.2021.08.214

Zhao, X., Xia, Y., Zhang, X., Lin, X., and Wang, L. (2019a). Design of Mechanically strong and Tough Alginate Hydrogels Based on a Soft-Brittle Transition. *Int. J. Biol. Macromolecules* 139, 850–857. doi:10.1016/j.ijbiomac.2019.08.057

Zhao, Y., Li, Z., Song, S., Yang, K., Liu, H., Yang, Z., et al. (2019b). Skin-Inspired Antibacterial Conductive Hydrogels for Epidermal Sensors and Diabetic Foot Wound Dressings. *Adv. Funct. Mater.* 29, 1901474. doi:10.1002/adfm.201901474

Zhou, Y., Fei, X., Tian, J., Xu, L., and Li, Y. (2022). A Ionic Liquid Enhanced Conductive Hydrogel for Strain Sensing Applications. *J. Colloid Interf. Sci.* 606, 192–203. doi:10.1016/j.jcis.2021.07.158

Zhou, Y., Wan, C., Yang, Y., Yang, H., Wang, S., Dai, Z., et al. (2019). Highly Stretchable, Elastic, and Ionic Conductive Hydrogel for Artificial Soft Electronics. *Adv. Funct. Mater.* 29, 1806220. doi:10.1002/adfm.201806220

Zhu, H., Hu, X., Liu, B., Chen, Z., and Qu, S. (2021). 3D Printing of Conductive Hydrogel-Elastomer Hybrids for Stretchable Electronics. *ACS Appl. Mater. Inter.* 13, 59243–59251. doi:10.1021/acsami.1c17526

Conflict of Interest: The authors declare that the research was conducted in the absence of any commercial or financial relationships that could be construed as a potential conflict of interest.

Publisher's Note: All claims expressed in this article are solely those of the authors and do not necessarily represent those of their affiliated organizations, or those of the publisher, the editors and the reviewers. Any product that may be evaluated in this article, or claim that may be made by its manufacturer, is not guaranteed or endorsed by the publisher.

frontiers in Bioengineering and Biotechnology

ORIGINAL RESEARCH
published: 11 February 2022
doi: 10.3389/fbioe.2022.837750

Resilient and Self-Healing Hyaluronic Acid/Chitosan Hydrogel With Ion Conductivity, Low Water Loss, and Freeze-Tolerance for Flexible and Wearable Strain Sensor

Yunping Hu[1†], Nannan Liu[2†], Kai Chen[1], Mingxiang Liu[1], Feng Wang[1], Pei Liu[1], Yiyuan Zhang[2], Tao Zhang[2] and Xiufeng Xiao[1*]*

[1]Fujian Provincial Key Laboratory of Advanced Materials Oriented Chemical Engineering, College of Chemistry and Materials Science, Fujian Normal University, Fuzhou, China, [2]Fuzhou Second Hospital of Xiamen University, Xiamen University, Fuzhou, China

OPEN ACCESS

Edited by:
Kunyu Zhang,
Johns Hopkins University,
United States

Reviewed by:
Peng Zhao,
Chongqing University, China
Jianhao Wang,
Changzhou University, China

***Correspondence:**
Tao Zhang
james155@foxmail.com
Xiufeng Xiao
xfxiao@fjnu.edu.cn

[†]*These authors have contributed equally to this work*

Specialty section:
This article was submitted to Biomaterials, a section of the journal Frontiers in Bioengineering and Biotechnology

Received: *17 December 2021*
Accepted: *17 January 2022*
Published: *11 February 2022*

Citation:
Hu Y, Liu N, Chen K, Liu M, Wang F, Liu P, Zhang Y, Zhang T and Xiao X (2022) Resilient and Self-Healing Hyaluronic Acid/Chitosan Hydrogel With Ion Conductivity, Low Water Loss, and Freeze-Tolerance for Flexible and Wearable Strain Sensor. Front. Bioeng. Biotechnol. 10:837750. doi: 10.3389/fbioe.2022.837750

Conductive hydrogel is a vital candidate for the fabrication of flexible and wearable electric sensors due to its good designability and biocompatibility. These well-designed conductive hydrogel–based flexible strain sensors show great potential in human motion monitoring, artificial skin, brain computer interface (BCI), and so on. However, easy drying and freezing of conductive hydrogels with high water content greatly limited their further application. Herein, we proposed a natural polymer-based conductive hydrogel with excellent mechanical property, low water loss, and freeze-tolerance. The main hydrogel network was formed by the Schiff base reaction between the hydrazide-grafted hyaluronic acid and the oxidized chitosan, and the added KCl worked as the conductive filler. The reversible crosslinking in the prepared hydrogel resulted in its resilience and self-healing feature. At the same time, the synthetic effect of KCl and glycerol endowed our hydrogel with outstanding anti-freezing property, while glycerol also endowed this hydrogel with anti-drying property. When this hydrogel was assembled as a flexible strain sensor, it showed good sensitivity (GF = 2.64), durability, and stability even under cold condition (–37°C).

Keywords: hydrogel, self-healing, ionic conductivity, anti-freezing, anti-drying, flexible strain sensor

INTRODUCTION

Hydrogels with a water-rich polymer network structure are very similar to the native tissues of humans (Fergg et al., 2001; Sanchez et al., 2005). In recent years, due to their flexibility, biocompatibility, and designability, hydrogels are widely utilized in various areas, such as tissue engineering (Lee and Mooney, 2001; Khademhosseini and Langer, 2007), wearable devices (Fergg et al., 2001; Yuk et al., 2019; Cui et al., 2021), and flexible electrodes (Na et al., 2019; Zhang W. et al., 2020; Fu et al., 2020). Among these applications, wearable devices, as a new research field, have attracted more and more attention (Billinghurst and Starner, 1999; Seneviratne et al., 2017; Chong et al., 2019). The development of wearable devices provides great convenience for human motion monitoring and human–machine interaction (Liao et al., 2017; Xia et al., 2019; Xu et al., 2019). The hydrogel-based flexible strain sensor was the most commonly used wearable devices, especially for

human motion monitoring. First, endowing hydrogels with high conductivity is the foundation for hydrogels working as strain sensors. There are two main solutions: utilization of conductive polymers, such as polyaniline (Guo et al., 2015; Yan et al., 2015) and polypyrrole (Brahim et al., 2002; Shi et al., 2014), and introduction of conductive fillers into hydrogels, such as metal nanoparticles (Guo et al., 2003; Gao et al., 2016), MXene nanosheet (Zhang Y.-Z. et al., 2020, 2021), ionic liquid (Teo et al., 2019), and inorganic salt (Urbonaite et al., 2015; Sui et al., 2021). Various studies have reported that the addition of inorganic salts, such as LiCl, NaCl, KCl, and $ZnCl_2$, into the hydrogel systems could bestow the hydrogel with satisfactory ion conductivity (Li et al., 2017, Li et al., 2019, Li et al., 2021; Jiang et al., 2018; Hou et al., 2019). This method is simple, efficient, and economic, showing great potential for conductive hydrogel design and fabrication. On the other hand, the high water content of hydrogels also leads to a serious defect, that is, most hydrogels undergo inevitable freezing when the condition temperature falls below 0°C, the water freezing point (Jing et al., 2013; Bacelar et al., 2016; Mohammadzadeh Pakdel and Peighambardoust, 2018). The hydrogel will become fragile and inelastic at low temperature, which greatly limited the use scenarios of conductive hydrogel as a flexible and wearable strain sensor. Therefore, researchers are deeply aware of the urgency of the development of anti-freezing conductive hydrogels (Tang et al., 2020; Wei et al., 2020; Jian et al., 2021). Actually, freezing point depression is a common phenomenon in nature. For example, seawater still can retain its liquid state at subzero temperature because of the existence of salt. Salt is widely applied as the inhibitor for water freezing in our life, similar to preventing the ice covering of road. Therefore, mixing salt into hydrogels is a simple and convenient strategy to endow hydrogels with conductivity and freeze-tolerance simultaneously (Zhao et al., 2006; Kim T. G. et al., 2008; Jiang et al., 2019; Xu et al., 2021).

Herein, inspired by this mechanism, we designed a natural polymer-based conductive hydrogel with excellent stretchability, self-healing, and anti-freezing property. We choose hyaluronic acid (HA) and chitosan (CS) as the main backbone polymer for our conductive hydrogels due to their good biocompatibility, wide sourcing, and cheap cost (Madihally and Matthew, 1999; Di Martino et al., 2005; Kim I.-Y. et al., 2008, 2011; Burdick and Prestwich, 2011). In order to form reliable crosslinking between HA and chitosan, we first modified HA with hydrazide groups (HA-ADH) and CS with aldehyde groups (OCS). Based on the mild and quick Schiff base reaction between the hydrazide group and the aldehyde group (Cegłowski and Schroeder, 2015; Meher et al., 2018; Xu et al., 2022), the main network of the hydrogel could be rapidly prepared through one-step mixing-injection, while KCl was introduced into this hydrogel system to play the role of conductive and anti-freezing filler. At the same time, we also added glycerol into our hydrogel system which could not only further improve the freeze-tolerance of the hydrogel but also endowed the hydrogel with anti-drying property. This prepared hydrogel named HC-KG hydrogel showed satisfactory mechanical resilience and self-healing property driven by the reversible hydrazone crosslinking, ionic crosslinking, and hydrogen bond–based crosslinking inside the hydrogel. Moreover, our following exploratory experiments showed that this HC-KG hydrogel exhibited repeatable resistance variation responding to various human motions even in the cold when it was applied as a flexible and wearable strain sensor. Therefore, we believe that the exploring of this novel HC-KG hydrogel could further expand the application scenario of conductive hydrogel as a flexible and wearable strain sensor, especially in dry or cold environments.

MATERIALS AND METHODS

Materials

Hyaluronic acid (HA) was purchased from Shandong Focusfreda Biotech Co., Ltd, China. Chitosan (CS), adipic acid dihydrazide, potassium chloride (KCl), glycerol, sodium periodate, ethylene glycol, and N-(3-dimethylaminopropyl)-N′-ethylcarbodiimide hydrochloride (EDC) were purchased from Shanghai Macklin Biochemical Co., Ltd, China. 1-Hydroxybenzotriazole anhydrous (HOBT, 98%) was purchased from J&K. 2-(4-morpholino) ethanesulfonic acid (MES) was brought from Sigma-Aldrich Life Science. All reagents were used as received. Deionized water (DI water) was used for all experiments.

Preparation of HA-ADH

HA (Mw = 70 kDa) was dissolved in 100 ml MES buffer (PH = 6.5) with the concentration of 1 wt% completely. Then, 2.5 g EDC and 1.78 g HOBT were added into the HA solution carefully. After reaction of 1 h, 9 g ADH was added for another reaction of 24 h. Then, the final solution was dialyzed against DI water (molecular weight cutoff (MWCO) = 14 kDa) for 3 days, and the final product was obtained by freeze-drying at −80°C for 72 h.

Preparation of OCS

Chitosan (MW = 3 kDa) was completely dissolved in 400 ml glacial acetic acid aqueous solution with a concentration of 0.5 wt %. Then, 2.65 g sodium periodate ($NaIO_4$) was added, and the mixed solution was stirred in the dark at 25°C for 12 h. The final solution was dialyzed against DI water (molecular weight cutoff (MWCO) = 14 kDa) for 3 days, and the final product was obtained by freeze-drying at −80°C for 72 h.

FT-IR Analysis

The successful modification of HA and chitosan was characterized by the FT-IR test using a Bruker Tensor 27 FT-IR spectrometer (ATR-FT-IR, Thermo Fisher Scientific-Nicolet IS5, US). Freeze-dried samples were pressed with KBr and scanned from 4,000 to 500 cm^{-1}.

Preparation of HC Series Hydrogel

Before hydrogel preparation, OCS and HA-ADH solution were prepared with a concentration of 3 and 4%, respectively. Then, the HC series hydrogels were *in situ* formed by mixed injection with HA-ADH and OCS solution. In order to introduce conductive and anti-freeze properties to the HC hydrogel, we added glycerol and KCl to the HC hydrogel. In order to

differentiate these HC hydrogels, we abbreviate the HC hydrogel with KCl as HC-K hydrogel, HC hydrogel with glycerol as HC-G hydrogel, and HC hydrogel with both KCl and glycerol as HC-KG hydrogel.

Rheological Property Test

The rheological properties of the hydrogels were tested at room temperature using a rheometer (Ares G2, TA, and US) with an 8-mm diameter parallel plate and 1-mm gap. Time sweep was performed at fixed frequency of 6 rad/s and strain of 1%. As for the frequency sweep, the strain was fixed at 1%, and the frequency ranged from 0.5 to 500 rad/s. Strain sweep was performed at a fixed frequency of 6 rad/s and a strain range from 1 to 1,000%, and dynamic strain sweeps were performed at a strain range of 1–1,000%. (G′), and loss modulus (G″) of the four hydrogels was measured during the strain sweep.

Mechanical Test

The mechanical properties of hydrogels were determined by using the universal material testing machine (LR5KPlus, Lloyd, United Kingdom)). For the compression test, a cylindrical hydrogel 12 mm in diameter and 10 mm in height was compressed at a rate of 100 mm/min. In the continuous loading–unloading test, the rate was set at 300 mm/min. The compressive elastic modulus was calculated from the slope of the initial linear region of the stress–strain curve.

Self-Repair Performance Test

The two pentagram-shaped HC-KG hydrogels were dyed yellow and blue with methyl orange and methylene blue, respectively, and cut into two pieces, and then the two cut hydrogel samples of different colors were closely laminated together and transferred into a well-sealed self-sealing bag at 37°C for 5 min to test the self-healing performance of HC-KG hydrogels.

Electrical Measurement of Hydrogel

The resistivity of HC, HC-K, HC-G, and HC-KG hydrogels was measured with a digital four-probe tester (Suzhou lattice). The resistance changes of four groups of gel hydrogels were measured by an LCR meter (Changzhou, China). A copper wire is inserted into each end of the hydrogel and then connected it to a TH LCR meter to record the resistance change of the hydrogel in real time. In addition, the resistance change of HC-K and HC-KG hydrogel was measured between −25 and 10°C.

Fabrication and Testing of the Flexible Sensor

To fabricate the strain sensor, the hydrogel was cut into cylindrical specimens with a diameter of 0.9 cm and a length of 3 cm. Then, the hydrogel sample was assembled into a strain sensor with two layers of conductive copper sheets tightly fixed with copper wires at both ends of the hydrogel sample. The hydrogel was sandwiched between two PU film tapes. To monitor the human motion, the sensor was mounted directly on the skin of the volunteer, and the electrical signal of the strain sensor was recorded in real time using an LCR tester. The simultaneous resistance changes of the gel biosensor under different human motion were obtained by the following equation

$$\frac{\Delta R}{R_0} = \frac{R - R_0}{R_0}.$$

The resistance change ratio (%) was calculated by the following equation, where R_0 and R are the resistance of the hydrogel when no strain is applied and the resistance of the hydrogel after strain is applied, respectively.

The gauge factor is usually used to characterize the sensitivity of a strain sensor and it defined as

$$GF = \left(\frac{R - R_0}{R_0}\right) \Big/ \left(\frac{L - L_0}{L_0}\right),$$

where R_0 and L_0 are the initial resistance and length of the sensor, respectively, and R and L are the real-time resistance and length of the sensor, respectively.

Anti-Drying Experiments

The hydrogels were formed into 9-mm diameter cylinders with a volume of 500 μl as test samples and weighed for initial mass. Then, the hydrogel sample was completely exposed to room temperature, and the weight change was recorded according to the time gradient. The residual mass ratio (RMR) was calculated by the following equation:

$$RMR = \frac{W_S}{W_0} \times 100\%,$$

where RMR is the residual mass ratio, and W_S and W_0 are the weight of the hydrogel after water loss and the initial weight of the hydrogel, respectively.

DSC Test

DSC is the study of the heat flow rate versus temperature of a sample and a reference sample by controlling the variation of temperature. We used a differential calorimetry scanner (Mettler Toledo DSC-1, Switzerland) to characterize the hydrogel samples. The samples were encapsulated in a sealed crucible for testing, and an empty disk was used as an inert reference. The differential calorimetry scanner was operated at a nitrogen flow rate of 50 μl/min, and experimental data were recorded at a rate of 1 Hz. Our measurement range is −70–25°C, so the hydrogel samples are first equilibrated at 25°C and then cooled to −70°C at a rate of 5°C/min.

RESULTS AND DISCUSSION

Synthesis and Characterization of HC-KG Hydrogels

Before the preparation of our well-designed HC-KG hydrogel, we first synthesized the hydrazide-grafted HA (HA-ADH) (**Figure 1A**) and oxidized chitosan (OCS) (**Figure 1B**). The Fourier infrared spectrum in **Supplementary Figure S1** proved the successful synthesis of these two polymers. The mixed system of KCl/glycerol/water was used as the solvent for HA-ADH and OCS. Then, our conductive and anti-

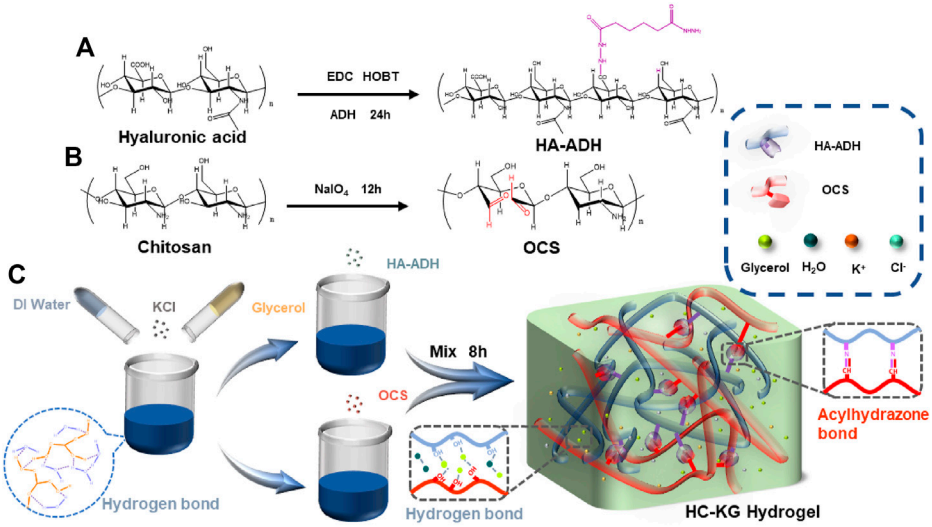

FIGURE 1 | Strategies for the fabrication of the stretchable, self-healing, conductive, and anti-freezing HC-KG hydrogel. The synthesis route of **(A)** HA-ADH and **(B)** OCS **(C)** of the preparation steps and the network structure of the HC-KG hydrogel.

freezing hydrogel, HC-KG hydrogel, was formed by a one-step mixing-injection between the prepared HA-ADH solution and OCS solution with equal volume (**Figure 1C**), **Supplementary Figure S2**; **Supplementary Table S1** showed that the addition of KCl prolonged gelation time greatly. We speculated that this might be because of the anti-ionization effect (Yang et al., 2020). In detail, K^+ and Cl^- would form reversible ionic crosslinks with negatively charged HA-ADH and positively charged OCS, which led to the intertangling of the HA-ADH, and OCS polymer chain, respectively. Therefore, the steric hindrance of the interaction between HA-ADH and OCS increased.

Mechanical properties of the HC-KG hydrogel

We first investigate the mechanical properties of this series hydrogel to investigate the effect of KCl and glycerol on the formation of the hydrogel network. The rheological time sweep results (**Figure 2A**) demonstrated that the addition of KCl could slightly improve the storage modulus of the hydrogel. We speculated that it was because that K^+ and Cl^- produced by the ionization of KCl helped form extra ionic crosslinking with the negative HA-ADH backbone and the positive OCS backbone, respectively. In addition, glycerol also could improve the storage modulus of the hydrogel. It might be contributed to the newly formed hydrogen bond–based crosslinking among the glycerol and the main backbone of the hydrogel. The further strain sweep results (**Figure 2B**) also proved our abovementioned speculation. It was clear that the addition of both KCl and glycerol increased the broken strain of the hydrogel. The following time sweep under alternative low/high strain showed the shear thinning property of the HC-KG hydrogel (**Figure 2C**). In detail, the HC-KG hydrogel would switch to "Sol" state and recover to "Gel" state. This procedure could be repeated many times, and the modulus recovery reached 100% every time. This phenomenon was just because all the crosslinking inside the HC-KG hydrogel network were reversible, including the dynamic hydrazone crosslinking between HA-ADH and OCS; ionic crosslinking between K^+ and HA-ADH; Cl^- and OCS; and hydrogen bonds among glycerol, HA-ADH, and OCS, and these reversible crosslinking could be untied under high shear fore and reformed after the disappearance of the high shear force. Moreover, the abovementioned reversible crosslinking was also the basis of the self-healing property of the HC-KG hydrogel. As shown in **Figure 2D**; **Supplementary Video S1**, two individual pentagram-shaped hydrogels, a blue and an orange one, could be reorganized to a new pentagram-shaped hydrogel after being cut. It was based on the re-forming of the reversible crosslinking between the exposed cross-sections. The HC-KG hydrogel also showed excellent compressive and tensile properties. **Figure 2E** showed that the HC-KG hydrogel had good resilience even under large-scale compression. The quantified compressive strain–stress curve showed that the addition of KCl and glycerol decreased Young's modulus while increasing the broken strain (**Figure 2F**). The reason for weakening of Young's modulus was because the formation of ionic crosslinking introduced by KCl and hydrogen bond introduced by glycerol hindered the formation of the hydrazone crosslinking, and these ionic crosslinking and hydrogen bond were weaker than the hydrazone crosslinking. At the same time, the formation of the weaker ionic crosslinking and hydrogen bond was beneficial to energy diffusion during the compression, therefore increasing the broken strain of the hydrogel. The excellent fatigue resistance was evidently validated by the following cyclic compression test, which showed that the nearly identical repeated strain–stress curves the small hysteresis

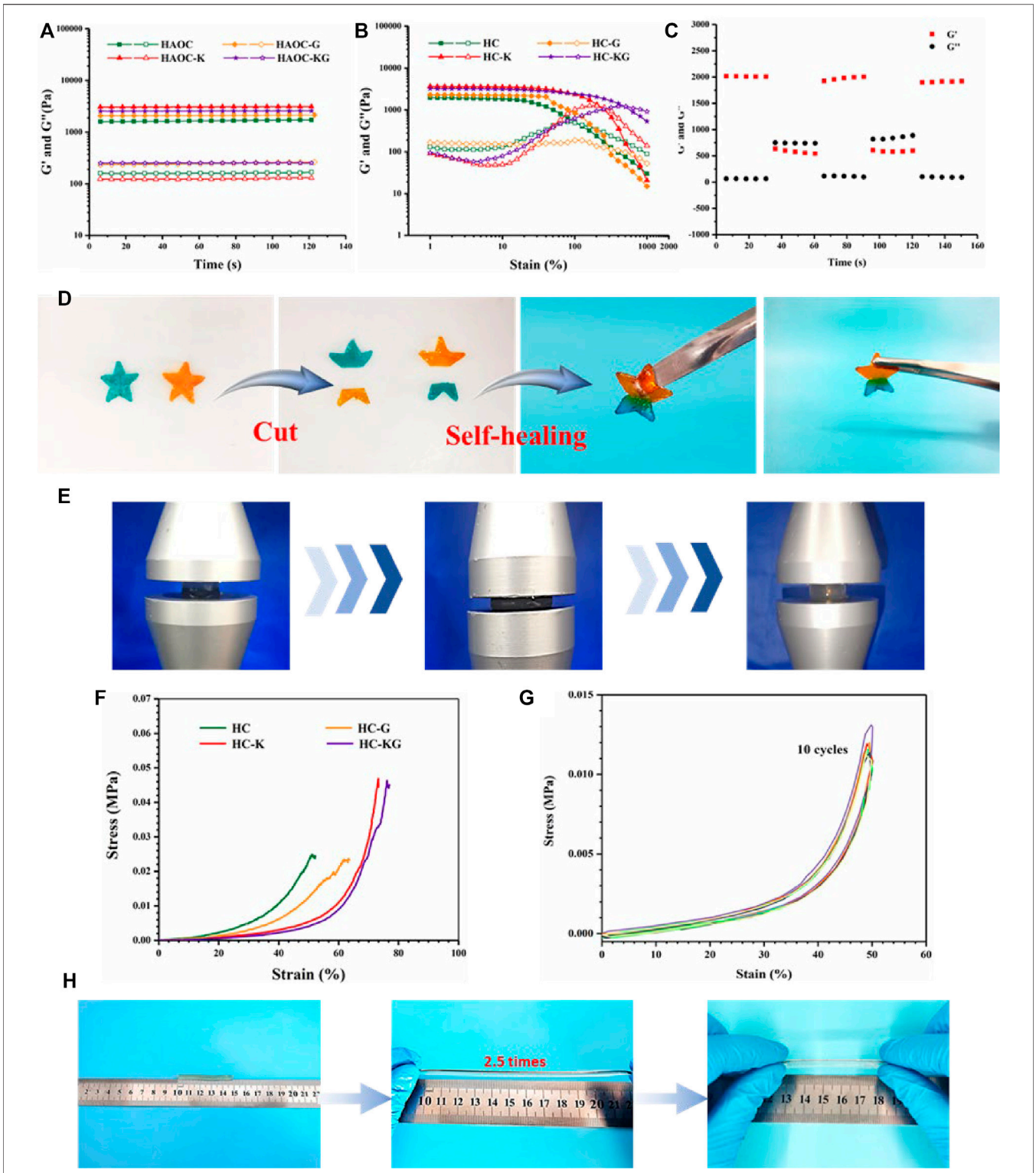

FIGURE 2 | Mechanical properties of the series hydrogel based on HA-ADH and OCS. Rheological time sweep **(A)** and strain sweep **(B)** of HC, HC-K, HC-G, and HC-KG hydrogels. **(C)** Rheological time sweep under alternative switching of low and high strain of the HC-KG hydrogel. **(D)** Quick self-healing property of the HC-KG hydrogel. **(E)** Compression process of the HC-KG hydrogel. **(F)** Compressive strain–stress curve of HC, HC-K, HC-G, and HC-KG hydrogel. **(G)** Cyclic compressive test of the HC-KG hydrogel. **(H)** Stretchability of the HC-KG hydrogel.

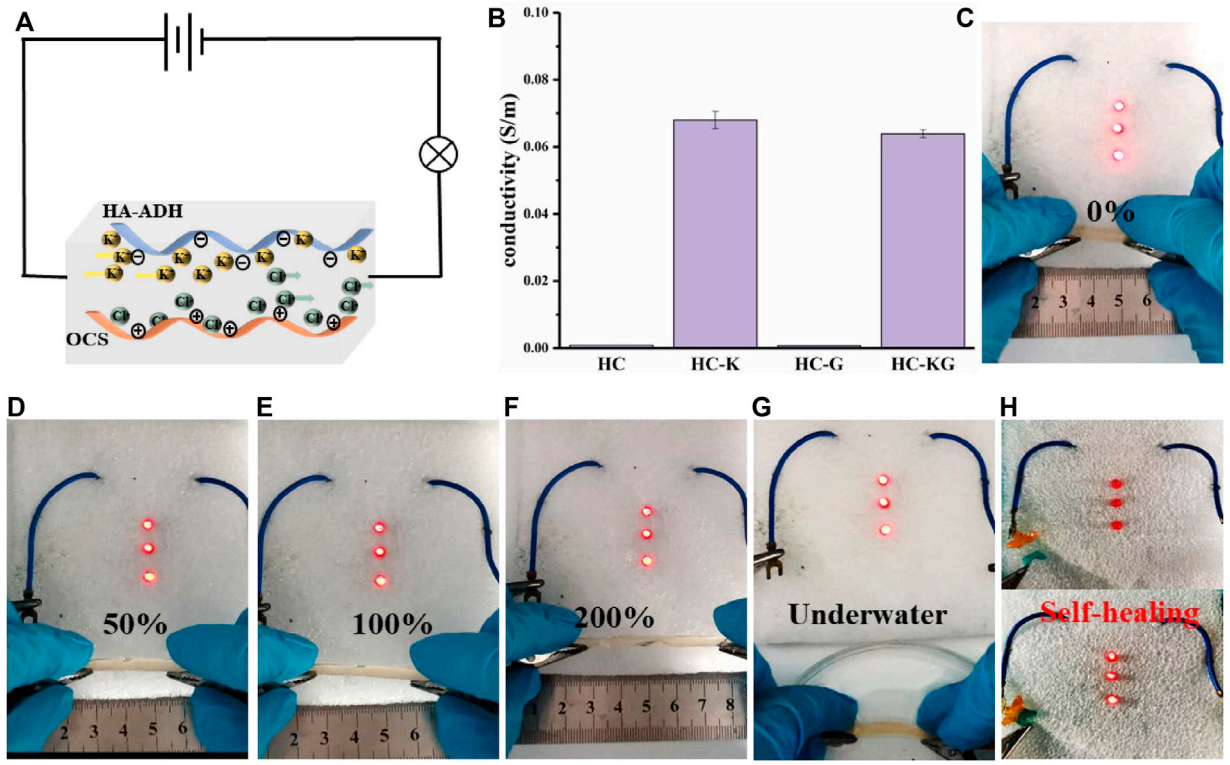

FIGURE 3 | Conductive properties of the series hydrogel based on HA-ADH and OCS. **(A)** Directional movement of ions in hydrogels under electrification. **(B)** Quantitative conductivity of HC, HC-K, HC-G, and HC-KG hydrogel. The HC-KG hydrogel could be applied as a flexible electric wire to lighten the LEDs under different elongation of 0% **(C)**, 50% **(D)**, 100% **(E)**, and 200% **(F)**. **(G)** HC-KG hydrogel also could be applied as a flexible electric wire under water condition. **(H)** HC-KG hydrogel still exhibited good conductivity after its self-healing.

loop (**Figure 2G**). The HC-KG hydrogel also showed good stretchability as proven by **Figure 2H**.

Conductive Properties of the HC-KG Hydrogel

As a strong electrolyte, KCl could fully electrolyze sufficient K^+ and Cl^- after being added into the hydrogel network, thus endowing the HC-K and HC-KG hydrogel with good conductivity, which was strongly proven by **Figure 3A**. It is also revealed that glycerol had negligible effect on the conductivity introduced by KCl. The conductivity of our target HC-KG hydrogel reached around 0.0638 S/m, which was enough for a flexible strain sensor. We then utilized a long cylindrical HC-KG hydrogel as a flexible electric wire to form a closed circuit to lighten the LEDs. Through the comparison from **Figures 3B–F**, we could easily find that the brightness of the LEDs decreased gradually with smooth elongation of the HC-KG hydrogel. As an excellent hydrogel strain sensor, HC-KG has good sensitivity with a gauge factor (GF) of 2.64 (**Supplementary Figure S3**). It indicated the sensitive resistance changing of the HC-KG hydrogel depending on the elongation change, which was fundamental for application of the HC-KG hydrogel as a flexible strain sensor. Furthermore, the HC-KG hydrogel still possessed good conductivity under water condition (**Figure 3G**), which demonstrated that the application scenario of our HC-KG hydrogel could be expanded to various water environments. Another exciting thing is that the self-healed HC-KG hydrogel still showed satisfactory conductivity (**Figure 3H**). It implied that the HC-KG hydrogel had the ability to resist various kinds of damage when applied as a flexible strain sensor.

Therefore, we then systematically tested the performance of the HC-KG hydrogel as a flexible and wearable strain sensor. As shown in **Figures 4A–C**, our HC–KG hydrogel was able to identify the large human motion, including the bending of finger, elbow, and knee. Moreover, taking finger bending as an example, the HC-KG hydrogel could even distinguish different angles of human motion obviously (**Figure 4D**). Our HC-KG hydrogel could also be competent for the detection of human micromotions, such as the closing and opening of mouth (**Figure 4E**). In particular, swallowing with different intensity also could be clearly separated by analyzing the curve shape of the relative resistance change (**Figure 4F**). All of these demonstrated enough sensitivity of our HC-KG hydrogel as the flexible and wearable strain sensor. We monitored the relative resistance change of the HC–KG hydrogel under the cyclic tensile state of 0–20%. The result

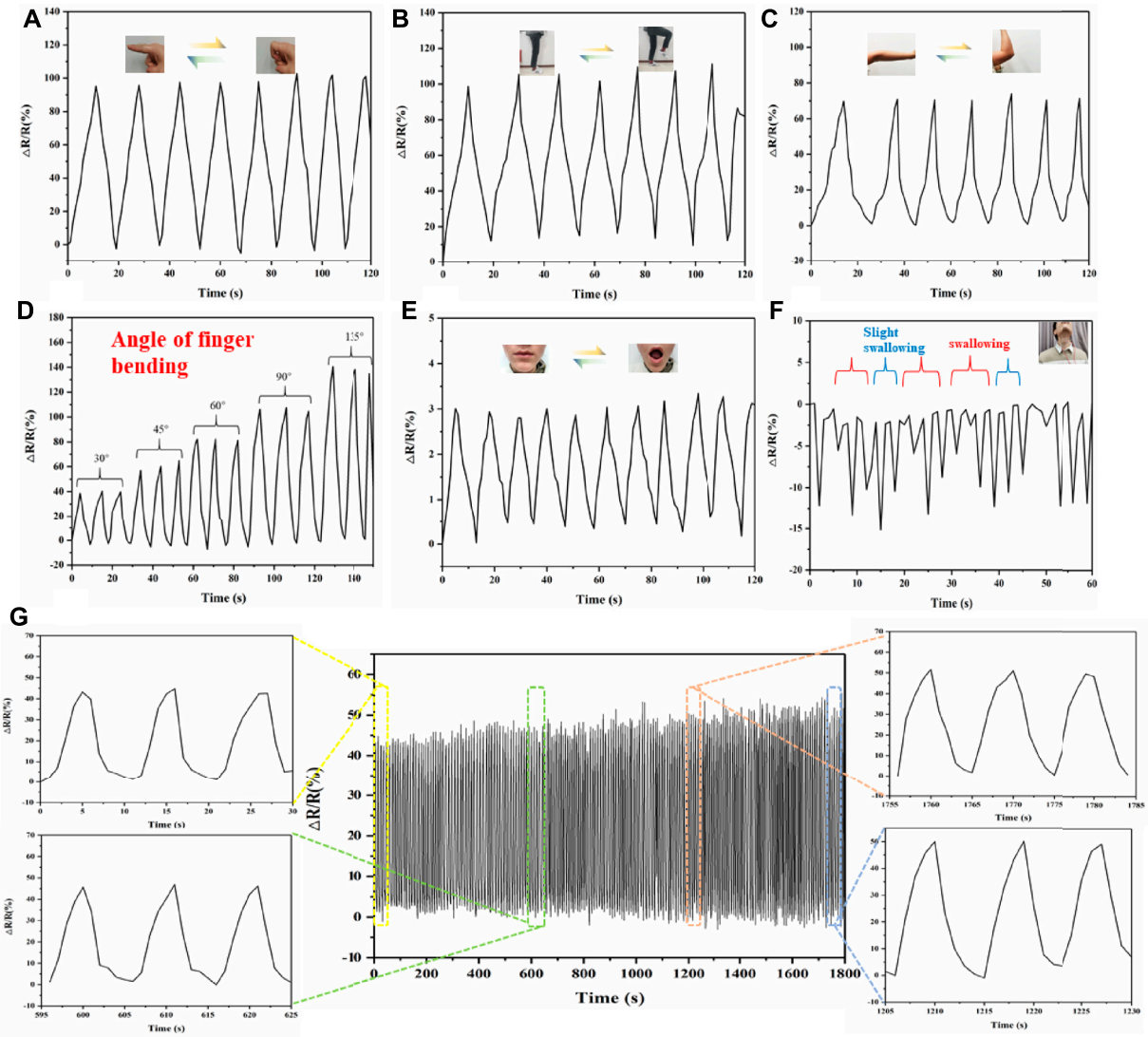

FIGURE 4 | Application of HC-KG hydrogel as a flexible strain sensor to detect various human motions. Real-time monitoring of large human motions, such as the bending of finger **(A)**, elbow **(B)**, and knee **(C)**. **(D)** HC-KG hydrogel showed different relative resistance change for finger bending at different angles. Real-time monitoring of human micromotions, such as the opening and closing of mouth **(E)** and swallowing with different intensity **(F)**. **(G)** Relative resistance change of the HC-KG hydrogel–based strain sensor under cyclic tensile from 0 to 20% for 30 min.

(**Figure 4G**) showed that the relative resistance change in every cycle was similar. It strongly confirmed the credible durability and stability of our HC-KG hydrogel, both of which were vital for a satisfactory flexible strain sensor.

The Anti-Drying and Anti-Freezing Properties of the HC-KG Hydrogel

The high water content of hydrogels also had limited the application of the conductive hydrogel–based flexible strain sensor, which mainly included the following two aspects: 1) The loss of water content of the hydrogel-based sensor led to the instability of their conductivity; 2) The freezing of water inside the hydrogel-based sensor rendered them unable to work at temperatures below 0°C. Our HC-KG hydrogel could solve the abovementioned two problems simultaneously based on the addition of KCl and glycerol. As shown in **Figure 5A**, hydrogel groups with glycerol (HC-G and HC-KG) could maintain stable water content greater than 60%, while hydrogel groups without glycerol (HC and HC-K) quickly dried up. Actually, the high water loss of the HC-K hydrogel greatly affected its conductivity. Furthermore, the conductivity of HC, HC-K, HC-G, and HC-KG gels was investigated as a function of temperature (**Figure 5B**). The results showed that the conductivity of HC-KG hydrogels during this process was almost all in the range of 0.63 S/m. While the HC-K hydrogels were more affected by temperature, the conductivity of HC-K hydrogels was almost 0 S/m

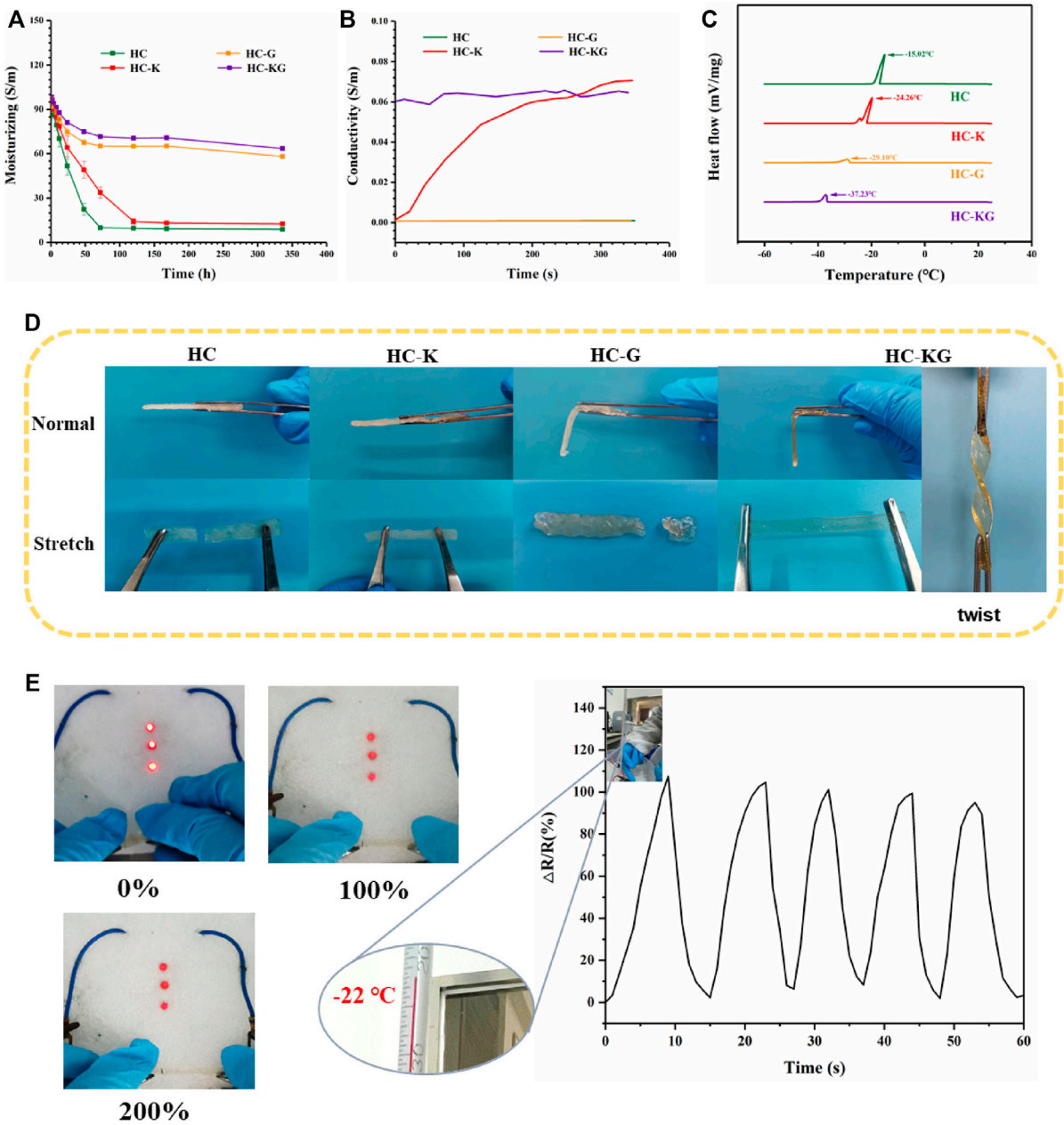

FIGURE 5 | Anti-drying and anti-freezing property of the HC-KG hydrogel. **(A)** Water content changing of HC, HC-K, HC-G, and HC-KG hydrogel under natural condition. **(B)** Conductivity as a function of time after transferring HC, HC-K, HC-G and HC-KG gel from a −26°C refrigerator to a 25°C environment. **(C)** DSC curves of these four kinds of HA-ADH- and OCS-based hydrogel. **(D)** Flexibility comparison of HC-K and HC-KG hydrogel under −26°C. **(E)** Conductivity of the HC-KG hydrogel with different elongation under −26°C. (**F**) HC-KG hydrogel worked as the flexible strain sensor under −20°C.

in the frozen state and then gradually increased to about 0.65 S/m with the increase of temperature. From the differential scanning calorimetry (DSC) results (**Figure 5C**), we found that the both KCl and glycerol acted as anti-freezing filler when added into the hydrogel system. Among these four groups, the HC-KG hydrogel had the lowest anti-freezing temperature, which reached −37°C based on the synergistic effect of KCl and glycerol. The following **Figure 5D**; **Supplementary Video S2** showed the freeze-tolerance of our HC-KG hydrogel intuitively. At a temperature of −26°C, the HC-KG hydrogel still showed transparency and flexibility. It even could be twisted easily without any damage. The anti-freezing property made our HC-KG hydrogel still suitable to be used as a strain sensor under cold conditions, which was proven by the brightness decrease of LEDs responding to the increase of HC-KG hydrogel elongation under −26°C (**Figure 5E**). But, the HC-K hydrogel does not conduct electricity at low temperatures to brighten the bulbs (**Supplementary**

Figure S4). We also tried to use this HC-KG hydrogel as a wearable strain sensor to monitor the human motion under cold condition. Taking the monitoring of finger bending as the test model, the HC-KG hydrogel–based wearable strain sensor exhibited good sensitivity (**Figure 5F**).

CONCLUSION

Collectively, the fabrication of our designed HC-KG hydrogel was convenient with low cost and simple process. The biocompatibility of the HC-KG hydrogel was guaranteed by selecting hyaluronic acid, chitosan, KCl, and glycerol as the main raw material. By modifying hyaluronic acid with hydrazide and chitosan with aldehyde, the main network of the HC-KG hydrogel was generated by the reversible dynamic chemical hydrazone crosslinking, which was the product of the Schiff base reaction between hydrazide groups of HA-ADH and aldehyde groups of OCS. Then, the addition of KCl and glycerol would introduce extra ionic crosslinking and hydrogen bond–based crosslinking to the HC-KG hydrogel, and these weak reversible crosslinking bestowed the hydrogel with the ability to withstand great deformation. These reversible crosslinking endowed our HC-KG hydrogel with outstanding self-healing property. Moreover, the HC-KG hydrogel showed good elasticity and fatigue resistance under cyclic deformation. The satisfactory conductivity of the HC-KG hydrogel was contributed by KCl, which was the basis for it to be utilized as the strain sensor. At the same time, the addition of KCl also helped the HC-KG hydrogel resist low temperature condition. Of course, glycerol also contributed greatly to the freeze-tolerance of the HC-KG hydrogel. Based on the synthetic effect of KCl and glycerol, the HC-KG hydrogel even could work at −37°C. Furthermore, glycerol endowed the HC-KG hydrogel with anti-drying property, which guaranteed the unchanged electric property of this hydrogel when it was exposed to outside environment for long time. All the abovementioned characterizations promised sensitivity, durability, and stability of the HC-KG hydrogel during its application as a flexible and wearable strain sensor. Besides, the anti-drying and anti-freezing property expended the application scenarios and working time of the HC-KG hydrogel. In short, this HC-KG hydrogel could be a promising competitor for flexible and wearable strain sensor manufacture, and this study could provide ideas for the following development of flexible and wearable electric sensors.

DATA AVAILABILITY STATEMENT

The original contributions presented in the study are included in the article/**Supplementary Material**; further inquiries can be directed to the corresponding authors.

AUTHOR CONTRIBUTIONS

YH and NL developed the hydrogels and performed the rheology and electrical measurements. KC synthesized the chemical components of the hydrogels. ML designed the self-repair performance. FW and PL designed the test mechanical properties and electrical conductivity at low temperatures. TZ and XX supervised the project and shared equal senior contributions. YH wrote the manuscript and prepared figures. YZ, and XX reviewed the manuscript. All authors commented on the manuscript.

FUNDING

The authors are grateful to the Health-Education Joint Research Project of Fujian Province (2019-WJ-22); the Education Scientific Research Project of Youth Teacher in the Education Department of Fujian Province (JT180490, JT180492); Fuzhou Science and Technology Project (2020-PT-138); the Natural Science Foundation of Fujian Province (No. 2020J011194); and the Project of Innovation Platform for Fuzhou Health and Family Planning Commission (No. 2020-S-wp2).

SUPPLEMENTARY MATERIAL

The Supplementary Material for this article can be found online at: https://www.frontiersin.org/articles/10.3389/fbioe.2022.837750/full#supplementary-material

REFERENCES

Bacelar, A. H., Silva-Correia, J., Oliveira, J. M., and Reis, R. L. (2016). Recent Progress in Gellan Gum Hydrogels provided by Functionalization Strategies. *J. Mater. Chem. B* 4, 6164–6174. doi:10.1039/C6TB01488G

Billinghurst, M., and Starner, T. (1999). Wearable Devices: New Ways to Manage Information. *Computer* 32, 57–64. doi:10.1109/2.738305

Brahim, S., Narinesingh, D., and Guiseppi-Elie, A. (2002). Polypyrrole-hydrogel Composites for the Construction of Clinically Important Biosensors. *Biosens. Bioelectron.* 17, 53–59. doi:10.1016/S0956-5663(01)00262-7

Burdick, J. A., and Prestwich, G. D. (2011). Hyaluronic Acid Hydrogels for Biomedical Applications. *Adv. Mater.* 23, H41–H56. doi:10.1002/adma.201003963

Cegłowski, M., and Schroeder, G. (2015). Preparation of Porous Resin with Schiff Base Chelating Groups for Removal of Heavy Metal Ions from Aqueous Solutions. *Chem. Eng. J.* 263, 402–411. doi:10.1016/j.cej.2014.11.047

Chong, Y.-W., Ismail, W., Ko, K., and Lee, C.-Y. (2019). Energy Harvesting for Wearable Devices: A Review. *IEEE Sensors J.* 19, 9047–9062. doi:10.1109/JSEN.2019.2925638

Cui, C., Fu, Q., Meng, L., Hao, S., Dai, R., and Yang, J. (2021). Recent Progress in Natural Biopolymers Conductive Hydrogels for Flexible Wearable Sensors and Energy Devices: Materials, Structures, and Performance. *ACS Appl. Bio Mater.* 4, 85–121. doi:10.1021/acsabm.0c00807

Di Martino, A., Sittinger, M., and Risbud, M. V. (2005). Chitosan: A Versatile Biopolymer for Orthopaedic Tissue-Engineering. *Biomaterials* 26, 5983–5990. doi:10.1016/j.biomaterials.2005.03.016

Fergg, F., Keil, F. J., and Quader, H. (2001). Investigations of the Microscopic Structure of Poly(vinyl Alcohol) Hydrogels by Confocal Laser Scanning Microscopy. *Colloid Polym. Sci.* 279, 61–67. doi:10.1007/s003960000398

Fu, F., Wang, J., Zeng, H., and Yu, J. (2020). Functional Conductive Hydrogels for Bioelectronics. *ACS Mater. Lett.* 2, 1287–1301. doi:10.1021/acsmaterialslett.0c00309

Gao, Y., Song, J., Li, S., Elowsky, C., Zhou, Y., Ducharme, S., et al. (2016). Hydrogel Microphones for Stealthy Underwater Listening. *Nat. Commun.* 7, 12316. doi:10.1038/ncomms12316

Guo, H., He, W., Lu, Y., and Zhang, X. (2015). Self-crosslinked Polyaniline Hydrogel Electrodes for Electrochemical Energy Storage. *Carbon* 92, 133–141. doi:10.1016/j.carbon.2015.03.062

Guo, H., Hu, J.-S., Liang, H.-P., Wan, L.-J., and Bai, C.-L. (2003). Highly Dispersed Metal Nanoparticles in Porous Anodic Alumina Films Prepared by a Breathing Process of Polyacrylamide Hydrogel. *Chem. Mater.* 15, 4332–4336. doi:10.1021/cm0343397

Hou, W., Sheng, N., Zhang, X., Luan, Z., Qi, P., Lin, M., et al. (2019). Design of Injectable Agar/NaCl/Polyacrylamide Ionic Hydrogels for High Performance Strain Sensors. *Carbohydrate Polymers* 211, 322–328. doi:10.1016/j.carbpol.2019.01.094

Jian, Y., Handschuh-Wang, S., Zhang, J., Lu, W., Zhou, X., and Chen, T. (2021). Biomimetic Anti-freezing Polymeric Hydrogels: Keeping Soft-Wet Materials Active in Cold Environments. *Mater. Horiz.* 8, 351–369. doi:10.1039/D0MH01029D

Jiang, X., Xiang, N., Zhang, H., Sun, Y., Lin, Z., and Hou, L. (2018). Preparation and Characterization of Poly(Vinyl Alcohol)/Sodium Alginate Hydrogel With High Toughness and Electric Conductivity. *Polymer* 186, 377–383. doi:10.1016/j.carbpol.2018.01.061

Jiang, L. B., Su, D. H., Ding, S. L., Zhang, Q. C., Li, Z. F., Chen, F. C., et al. (2019). Salt-Assisted Toughening of Protein Hydrogel with Controlled Degradation for Bone Regeneration. *Adv. Funct. Mater.* 29, 1901314. doi:10.1002/adfm.201901314

Jing, G., Wang, L., Yu, H., Amer, W. A., and Zhang, L. (2013). Recent Progress on Study of Hybrid Hydrogels for Water Treatment. *Colloids Surf. A: Physicochemical Eng. Aspects* 416, 86–94. doi:10.1016/j.colsurfa.2012.09.043

Khademhosseini, A., and Langer, R. (2007). Microengineered Hydrogels for Tissue Engineering. *Biomaterials* 28, 5087–5092. doi:10.1016/j.biomaterials.2007.07.021

Kim, I.-Y., Seo, S.-J., Moon, H.-S., Yoo, M.-K., Park, I.-Y., Kim, B.-C., et al. (2008a). Chitosan and its Derivatives for Tissue Engineering Applications. *Biotechnol. Adv.* 26, 1–21. doi:10.1016/j.biotechadv.2007.07.009

Kim, I. L., Mauck, R. L., and Burdick, J. A. (2011). Hydrogel Design for Cartilage Tissue Engineering: A Case Study with Hyaluronic Acid. *Biomaterials* 32, 8771–8782. doi:10.1016/j.biomaterials.2011.08.073

Kim, T. G., Chung, H. J., and Park, T. G. (2008b). Macroporous and Nanofibrous Hyaluronic Acid/collagen Hybrid Scaffold Fabricated by Concurrent Electrospinning and Deposition/leaching of Salt Particles. *Acta Biomater.* 4, 1611–1619. doi:10.1016/j.actbio.2008.06.008

Lee, K. Y., and Mooney, D. J. (2001). Hydrogels for Tissue Engineering. *Chem. Rev.* 101, 1869–1880. doi:10.1021/cr000108x

Li, H., Lv, T., Li, N., Yao, Y., Liu, K., and Chen, T. (2017). Ultraflexible and Tailorable All-Solid-State Supercapacitors Using Polyacrylamide-Based Hydrogel Electrolyte With High Ionic Conductivity. *Nanoscale* 9, 18474–18481. doi:10.1039/C7NR07424G

Li, J., Wei, H., Peng, Y., Geng, L., Zhu, L., Cao, X.-Y., et al. (2019). A Multifunctional Self-Healing G-PyB/KCl Hydrogel: Smart Conductive, Rapid Room-Temperature Phase-Selective Gelation, and Ultrasensitive Detection of Alpha-Fetoprotein. *Chemical Communications* 55, 7922–7925. doi:10.1039/C9CC02770J

Li, G., Li, C., Li, G., Yu, D., Song, Z., Wang, H., et al. (2021). Development of Conductive Hydrogels for Fabricating Flexible Strain Sensors. *Small*, 2101518. doi:10.1002/smll.202101518

Liao, M., Wan, P., Wen, J., Gong, M., Wu, X., Wang, Y., et al. (2017). Wearable, Healable, and Adhesive Epidermal Sensors Assembled from Mussel-Inspired Conductive Hybrid Hydrogel Framework. *Adv. Funct. Mater.* 27, 1703852. doi:10.1002/adfm.201703852

Madihally, S. V., and Matthew, H. W. T. (1999). Porous Chitosan Scaffolds for Tissue Engineering. *Biomaterials* 20, 1133–1142. doi:10.1016/S0142-9612(99)00011-3

Meher, N., Panda, S., Kumar, S., and Iyer, P. K. (2018). Aldehyde Group Driven Aggregation-Induced Enhanced Emission in Naphthalimides and its Application for Ultradetection of Hydrazine on Multiple Platforms. *Chem. Sci.* 9, 3978–3985. doi:10.1039/C8SC00643A

Mohammadzadeh Pakdel, P., and Peighambardoust, S. J. (2018). Review on Recent Progress in Chitosan-Based Hydrogels for Wastewater Treatment Application. *Carbohydr. Polym.* 201, 264–279. doi:10.1016/j.carbpol.2018.08.070

Na, R., Liu, Y., Lu, N., Zhang, S., Liu, F., and Wang, G. (2019). Mechanically Robust Hydrophobic Association Hydrogel Electrolyte with Efficient Ionic Transport for Flexible Supercapacitors. *Chem. Eng. J.* 374, 738–747. doi:10.1016/j.cej.2019.06.004

Sanchez, C., Arribart, H., and Giraud Guille, M. M. (2005). Biomimetism and Bioinspiration as Tools for the Design of Innovative Materials and Systems. *Nat. Mater* 4, 277–288. doi:10.1038/nmat1339

Seneviratne, S., Hu, Y., Nguyen, T., Lan, G., Khalifa, S., Thilakarathna, K., et al. (2017). A Survey of Wearable Devices and Challenges. *IEEE Commun. Surv. Tutorials* 19, 2573–2620. doi:10.1109/COMST.2017.2731979

Shi, Y., Pan, L., Liu, B., Wang, Y., Cui, Y., Bao, Z., et al. (2014). Nanostructured Conductive Polypyrrole Hydrogels as High-Performance, Flexible Supercapacitor Electrodes. *J. Mater. Chem. A.* 2, 6086–6091. doi:10.1039/C4TA00484A

Sui, X., Guo, H., Cai, C., Li, Q., Wen, C., Zhang, X., et al. (2021). Ionic Conductive Hydrogels with Long-Lasting Antifreezing, Water Retention and Self-Regeneration Abilities. *Chem. Eng. J.* 419, 129478. doi:10.1016/j.cej.2021.129478

Tang, L., Wu, S., Qu, J., Gong, L., and Tang, J. (2020). A Review of Conductive Hydrogel Used in Flexible Strain Sensor. *Materials* 13, 3947. doi:10.3390/ma13183947

Teo, M. Y., RaviChandran, N., Kim, N., Kee, S., Stuart, L., Aw, K. C., et al. (2019). Direct Patterning of Highly Conductive PEDOT:PSS/Ionic Liquid Hydrogel via Microreactive Inkjet Printing. *ACS Appl. Mater. Inter.* 11, 37069–37076. doi:10.1021/acsami.9b12069

Urbonaite, S., Poux, T., and Novák, P. (2015). Progress towards Commercially Viable Li-S Battery Cells. *Adv. Energ. Mater.* 5, 1500118. doi:10.1002/aenm.201500118

Wei, P., Chen, T., Chen, G., Liu, H., Mugaanire, I. T., Hou, K., et al. (2020). Conductive Self-Healing Nanocomposite Hydrogel Skin Sensors with Antifreezing and Thermoresponsive Properties. *ACS Appl. Mater. Inter.* 12, 3068–3079. doi:10.1021/acsami.9b20254

Xia, S., Song, S., Jia, F., and Gao, G. (2019). A Flexible, Adhesive and Self-Healable Hydrogel-Based Wearable Strain Sensor for Human Motion and Physiological Signal Monitoring. *J. Mater. Chem. B* 7, 4638–4648. doi:10.1039/C9TB01039D

Xu, G., Guo, N., Zhang, Q., Wang, T., Song, P., and Xia, L. (2022). An Ultrasensitive Surface-Enhanced Raman Scattering Sensor for the Detection of Hydrazine via the Schiff Base Reaction. *J. Hazard. Mater.* 424, 127303. doi:10.1016/j.jhazmat.2021.127303

Xu, J., Wang, G., Wu, Y., Ren, X., and Gao, G. (2019). Ultrastretchable Wearable Strain and Pressure Sensors Based on Adhesive, Tough, and Self-Healing Hydrogels for Human Motion Monitoring. *ACS Appl. Mater. Inter.* 11, 25613–25623. doi:10.1021/acsami.9b08369

Xu, S., Yan, Y., Zhao, Y., Qiu, X., Zhuang, D., Liu, H., et al. (2021). Spinnable Adhesive Functional-Hydrogel Fibers for Sensing and Perception Applications. *J. Mater. Chem. C* 9, 5554–5564. doi:10.1039/D1TC00151E

Yan, B., Chen, Z., Cai, L., Chen, Z., Fu, J., and Xu, Q. (2015). Fabrication of Polyaniline Hydrogel: Synthesis, Characterization and Adsorption of Methylene Blue. *Appl. Surf. Sci.* 356, 39–47. doi:10.1016/j.apsusc.2015.08.024

Yang, J., Shen, M., Wu, T., Luo, Y., Li, M., Wen, H., et al. (2020). Role of Salt Ions and Molecular Weights on the Formation of Mesona Chinensis Polysaccharide-Chitosan Polyelectrolyte Complex Hydrogel. *Food Chem.* 333, 127493. doi:10.1016/j.foodchem.2020.127493

Yuk, H., Lu, B., and Zhao, X. (2019). Hydrogel Bioelectronics. *Chem. Soc. Rev.* 48, 1642–1667. doi:10.1039/C8CS00595H

Zhang, W., Ma, J., Zhang, W., Zhang, P., He, W., Chen, J., et al. (2020a). A Multidimensional Nanostructural Design towards Electrochemically Stable and Mechanically strong Hydrogel Electrodes. *Nanoscale* 12, 6637–6643. doi:10.1039/D0NR01414A

Zhang, Y.-Z., El-Demellawi, J. K. J., Jiang, Q., Ge, G., Liang, H., Lee, K., et al. (2020b). MXene Hydrogels: Fundamentals and Applications. *Chem. Soc. Rev.* 49, 7229–7251. doi:10.1039/D0CS00022A

Zhang, Y., Gong, M., and Wan, P. (2021). MXene Hydrogel for Wearable Electronics. *Matter* 4, 2655–2658. doi:10.1016/j.matt.2021.06.041

Zhao, Y., Kang, J., and Tan, T. (2006). Salt-, pH- and Temperature-Responsive Semi-interpenetrating Polymer Network Hydrogel Based on Poly(aspartic Acid) and Poly(acrylic Acid). *Polymer* 47, 7702–7710. doi:10.1016/j.polymer.2006.08.056

Conflict of Interest: The authors declare that the research was conducted in the absence of any commercial or financial relationships that could be construed as a potential conflict of interest.

Publisher's Note: All claims expressed in this article are solely those of the authors and do not necessarily represent those of their affiliated organizations, or those of the publisher, the editors, and the reviewers. Any product that may be evaluated in this article, or claim that may be made by its manufacturer, is not guaranteed or endorsed by the publisher.

frontiers in Bioengineering and Biotechnology

REVIEW
published: 24 March 2022
doi: 10.3389/fbioe.2022.845779

A Review of Nanotechnology for Treating Dysfunctional Placenta

Huabo Jiang[1†], Li Li[2†], Dan Zhu[1†], Xinyao Zhou[1], Yongsheng Yu[3], Qian Zhou[3]* and Luming Sun[1]**

[1]Shanghai Key Laboratory of Maternal Fetal Medicine, Department of Fetal Medicine and Prenatal Diagnosis Center, Shanghai First Maternity and Infant Hospital, School of Medicine, Tongji University, Shanghai, China, [2]Reproductive Medicine Center, Shuguang Hospital Affiliated to Shanghai University of Traditional Chinese Medicine, Shanghai, China, [3]Clinical and Translational Research Center, Shanghai First Maternity and Infant Hospital, School of Medicine, Tongji University, Shanghai, China*

The placenta plays a significant role during pregnancy. Placental dysfunction contributes to major obstetric complications, such as fetal growth restriction and preeclampsia. Currently, there is no effective treatment for placental dysfunction in the perinatal period, and prophylaxis is often delivered too late, at which point the disease manifestation cannot be prevented. However, with recent integration of nanoscience and medicine to perform elaborate experiments on the human placenta, it is expected that novel and efficient nanotherapies will be developed to resolve the challenge of managing placental dysfunction. The advent of nanomedicine has enabled the safe and targeted delivery of drugs using nanoparticles. These smart nanoparticles can load the necessary therapeutic substances that specifically target the placenta, such as drugs, targeting molecules, and ligands. Packaging multifunctional molecules into specific delivery systems with high targeting ability, diagnosis, and treatment has emerged as a novel theragnostic (both therapeutic and diagnostic) approach. In this review, the authors discuss recent advances in nanotechnology for placental dysfunction treatment. In particular, the authors highlight potential candidate nanoparticle-loaded molecules that target the placenta to improve utero-placental blood flow, and reduce reactive oxygen species and oxidative stress. The authors intend to provide basic insight and understanding of placental dysfunction, potential delivery targets, and recent research on placenta-targeted nanoparticle delivery systems for the potential treatment of placental dysfunction. The authors hope that this review will sensitize the reader for continued exploration of novel nanomedicines.

Keywords: placental dysfunction, nanoparticles, nanotechnology, pregnancy, targeted therapeutic delivery

OPEN ACCESS

Edited by:
Liqiang Wang,
Shanghai Jiao Tong University, China

Reviewed by:
Gloria Bora Kim,
University of Pennsylvania, United States
Lei Li,
Shandong Provincial Hospital, China

****Correspondence:***
Yongsheng Yu
yongshengyu@tongji.edu.cn
Qian Zhou
shzhouqian@126.com
Luming Sun
luming_sun@163.com

[†]These authors have contributed equally to this work and share first authorship

Specialty section:
This article was submitted to Biomaterials, a section of the journal Frontiers in Bioengineering and Biotechnology

Received: *30 December 2021*
Accepted: *01 March 2022*
Published: *24 March 2022*

Citation:
Jiang H, Li L, Zhu D, Zhou X, Yu Y, Zhou Q and Sun L (2022) A Review of Nanotechnology for Treating Dysfunctional Placenta. Front. Bioeng. Biotechnol. 10:845779. doi: 10.3389/fbioe.2022.845779

INTRODUCTION

The placenta is a highly specialized transient organ during pregnancy. Placental dysfunction has been shown to be strongly associated with major obstetric diseases, such as fetal growth restriction (FGR), preeclampsia (PE), preterm premature membrane rupture, preterm labor, late spontaneous abortion, and placental abruption (Brosens et al., 2011). Although significant progress has been made in preventing the disease, current obstetric interventions in clinical obstetric practice are limited for management of the disease, after it has set in (Chappell and David, 2016). The interventions in current practice deal mostly with maternal symptoms or terminating pregnancy when maternal condition deteriorates. According to recent studies, the world population is growing by

TABLE 1 | Clinical categories and characteristics of pre-eclampsia and foetal growth restriction.

➢ Pre-eclampsia
➢ classically, new-onset hypertension, ≥20 weeks' gestation in association with:
➢ i. Proteinuria - ≥ 300 mg per day or protein/creatinine ratio ≥30 mg/mmol (0.3 mg/mg)
➢ ii. Other maternal organ dysfunction including:
➢ Acute kidney injury
➢ Liver involvement
➢ Neurological complications
➢ Haematological complications
➢ iii. Uteroplacental dysfunction
Intrauterine Growth Retardation
➢ Early FGR:
➢ In absence of congenital anomalies
➢ GA < 32 weeks
➢ AC/EFW <3rd centile or UA-AEDF; or AC/EFW <10th centile combined with UtA-PI > 95th centile and/or UA-PI > 95th centile
➢ Late FGR:
➢ In absence of congenital anomalies
➢ GA≥ 32 weeks
➢ AC/EFW <3rd centile Or at least two out of three of the following:
➢ 1. AC/EFW <10th centile
➢ 2. AC/EFW crossing centiles >2 quartiles on growth centiles[a]
➢ 3. CPR <5th centile or UA-PI > 95th centile

[a]*Growth centiles are non-customized centiles. BP, systolic blood pressure; AC, fetal abdominal circumference; AEDF, absent end-diastolic flow; CPR, cerebroplacental ratio; EFW, estimated foetal weight; GA, gestational age; PI, pulsatility index; UA, umbilical artery; UtA, uterine artery.*

approximately 80 million people each year, most of whom may experience maternal and neonatal disorders. Over 90% of pregnant women take at least one medication during their perinatal period, either over-the-counter or prescribed. Approximately 10% of pregnant women need medical prescriptions due to serious obstetric complications (Mitchell et al., 2011). The embryo is exceptionally sensitive and systemic toxicity of therapeutic agents may endanger the health of the mother and cause side effects to the fetus. This explains why only a limited number of therapeutic agents are applied for obstetric complications. Therefore, it is important to explore effective therapeutic drugs, seeking a balance between minimizing harmful effects on the fetal compartment and maximizing the dose to mothers.

Nanotechnology is the engineering of structures at the molecular level, often <100 nm in size (Kim et al., 2010). The field is expanding exponentially and is particularly designed to combine therapeutic drugs and deliver them to the targeted organs under controllable conditions, maximizing efficacy while minimizing off-target effects of drugs. In recent years, nanostructures have been widely used to prevent and treat diseases and are expected to become a substantial approach that assists in overcoming the limitations of various diseases. However, advances in targeted nanomedicine in the area of placental dysfunction-related diseases are still in their infancy (Kannan and Kannan, 2017). With rapid development and altered metabolism during gestation, the fetus is more sensitive to external toxic agents and represents one of the most vulnerable subgroups compared with adults. Therefore, fetal safety should be one of the utmost priorities when designing therapeutic approaches for placental dysfunction.

There is increasing interest in these novel treatments, as they improve the phenotype of placental dysfunction, including PE and FGR, where they could be used as therapeutic tools during pregnancy. This review focuses on the application of nanostructures and the advances and safety concerns of nanomedicine therapy for maternal and fetal health in placental dysfunction-related diseases. It also focuses on the use of nanoparticles as vectors that mediate the delivery of medicine to the placenta, and potential interventional targets that may have therapeutic effects in the future.

PATHOPHYSIOLOGY AND CLINICAL CHARACTERISTICS OF PE AND FETAL GROWTH RESTRICTION

PE is a series of maternal hypertensive disorders that affect 5–7% of all pregnancies and remains the major cause of death during the perinatal period worldwide, with >70,000 maternal and 500,000 fetal deaths every year (Rana et al., 2019). The clinical categories and characteristics of PE and FGR are shown in **Table 1**.

FGR is defined as a condition in which the fetus does not reach its genetic growth potential. The diagnostic criterion for FGR is an ultrasound-estimated fetal weight (EFW) below the 10th percentile of a specific gestational age (GA). It affects about 3–7% of all pregnancies, has significant short-term and long-term complications, and may adversely affect the quality of life of the fetus (Sharma et al., 2016). According to additional fetal biometric parameters, such as biparietal diameter, head circumference, femur length, and abdominal circumference (AC), FGR can be divided into two categories: symmetrical and asymmetrical. Furthermore, the severity of FGR is determined by EFW (**Table 1**).

The placenta is mainly composed of mesenchymal cells, trophoblasts, and microvascular endothelial cells. The chorionic membrane is the main functional component of the human placenta. It is composed of fetal capillaries surrounded by multiple trophoblasts (Baker et al., 1993). Trophoblasts are divided into the following three types: progenitor villous cytotrophoblasts (CTBs), extravillous cytotrophoblasts (EVTs), and syncytiotrophoblasts (STBs), which migrate from the villi and invade the maternal decidua. Different trophoblasts play different roles in placental development and function. As progenitor cells of the placenta, CTBs either differentiate to form anchor cell columns, which are responsible for attaching the fetus to the uterine wall, or fuse together to form multinucleated STBs (Genbacev and Miller, 2000). This is due to the further invasiveness of CTBs at the distal end of the cell column where EVTs are formed. These EVTs invade the uterine spiral arteries and convert these blood vessels into a low-resistance state that can transport a large volume of blood to the villus space (Pijnenborg et al., 2006), allowing nutrition, oxygen, maternal-fetal signaling molecules, and drugs to be

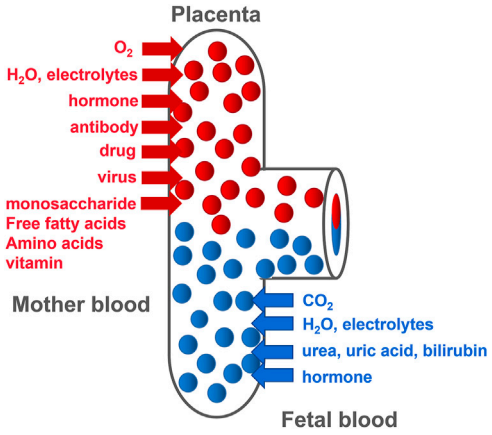

FIGURE 1 | Diagram of material exchange between mother and fetus.

transported by STB (**Figure 1**). CTBs fail to deeply invade the uterine wall, causing shallow placentation and incomplete remodeling of the spiral arteries. Inadequate spiral arteriolar remodeling induces insufficient placental perfusion, leading to placental ischemia and maternal syndrome of PE and FGR.

PE and FGR have similar pathophysiological processes and pathogenic factors; both involve uterine placental hypoperfusion, vascular endothelial dysfunction, and abnormal placental invasion (Tal et al., 2010). In normal pregnancy, after forming EVT cells, they invade the spiral arteries such that both the smooth muscle and endothelium of the vessels are eroded (Jauniaux et al., 2018). The pathophysiological process of placental dysfunction in PE, FGR (and other major obstetric syndromes) is mainly abnormal physiological transformation of the endometrial spiral artery, leading to shallow placental implantation and reduced placental blood perfusion (Brosens et al., 2011). PE is a systemic vascular disease, and the basic pathological changes include systemic arteriole spasm, vascular endothelial cell damage, and peroxidative remodeling. Among these, vascular endothelial cell damage can explain various clinical manifestations of the mother, such as hypertension, proteinuria, and edema. One of the main mechanisms underlying the pathophysiology of PE is that placental factors cause maternal vascular endothelial dysfunction, and an increase in placental anti-angiogenic factors is a crucial part of the pathogenesis. Compared with healthy pregnant women, patients with PE have less angiogenesis in the placenta, and the corresponding placental perfusion is reduced, which is consistent with the severity of hypertension (Brosens et al., 2011). At present, there are differing opinions on the pathogenesis of PE. It is generally believed that the PE is caused by a combination of placental, immune, inflammatory, and genetic factors, individually or simultaneously. Despite breakthroughs in our understanding of the etiology of PE, the pathophysiology that triggers the disease remains unclear. Most researchers consider PE to be a two-stage development process, a theory first proposed by Redman (Redman, 1992). The first stage (pre-clinical and symptomless) comprises poor placentation, which is caused by insufficient invasion of cytotrophoblast cells. When cytotrophoblast cells cannot invade the uterine spiral artery normally, the consequence is dysfunctional perfusion of the placenta with oxidative and hemodynamic stress. Excessive antiangiogenic and proinflammatory factors are released into the maternal circulation by the damaged placenta. The second is the clinical expression of the disease stage, when placental factors enter the maternal blood circulatory system, leading to a maternal systemic inflammatory response and systemic vascular endothelial damage, as well as the consequences of placental ischemia. The syndrome is mainly ascribed to diffuse maternal endothelial dysfunction, and the principal clinical manifestations are hypertension and new proteinuria. As the placenta is a unique organ during pregnancy, many pregnancy complications are related to placental structure and dysfunction.

The most common pathological change in FGR is damage to the placental villi. Failure to transform the branches of the placental spiral artery restricts the flow of maternal blood to the villus space, and continuous ischemic and perfusion damages the developing placental villi. Compared with normal pregnancy, the volume and surface area of the fetal FGR placenta decreases significantly, placental thickness increases, the blood vessels in the villi decrease or disappear, the lumen narrows or even becomes occluded, and the percentage of villi, capillaries, and surface area of the villi are all reduced (Erlandsson et al., 2021). Through experiments in guinea pigs, Canas et al. found that FGR is associated with a heterogeneous pro-constrictive vascular remodeling that sets in during pathologic pregnancy to sustain fetal blood redistribution (Cañas et al., 2017). Therefore, FGR not only increases the risk of intrauterine death and related diseases but also affects the growth rate and incidence of cardiovascular disease after birth. In short, the morphology of the FGR placenta is grossly abnormal. This is prominently manifested as the reduction of the surface area and volume of the villi blood vessels, resulting in insufficient placental blood flow, reduced material exchange area, placental hypoxia, malnutrition, and pathological changes around the villi. This results in compression of normal placental tissues, further exacerbating the condition. Abnormal placental morphology eventually leads to placental dysfunction, which adversely affects the fetus in the perinatal period and poses hidden dangers to the health of the fetus after birth.

Studies have found that hypoxia and/or ischemia-reperfusion causes the release of free radicals and inflammatory mediators. This causes cellular stress in STB cells (placental epithelium), resulting in excessive release of numerous factors, leading to exaggerated inflammation, endothelial cell proliferation, and survival defects (Powe et al., 2011). Studies have found that the balance between soluble fms-like tyrosine kinase 1 (sFlt1) and PIGF is of particular clinical importance (Burton et al., 2019; Ives et al., 2020). Excess release of sFlt1 and sENG isolate circulating PIGF and vascular endothelial growth factor (VEGF), thus reducing their bioavailability and subsequently the maternal plasma concentration of these hormones (Cindrova-Davies et al., 2011). This article

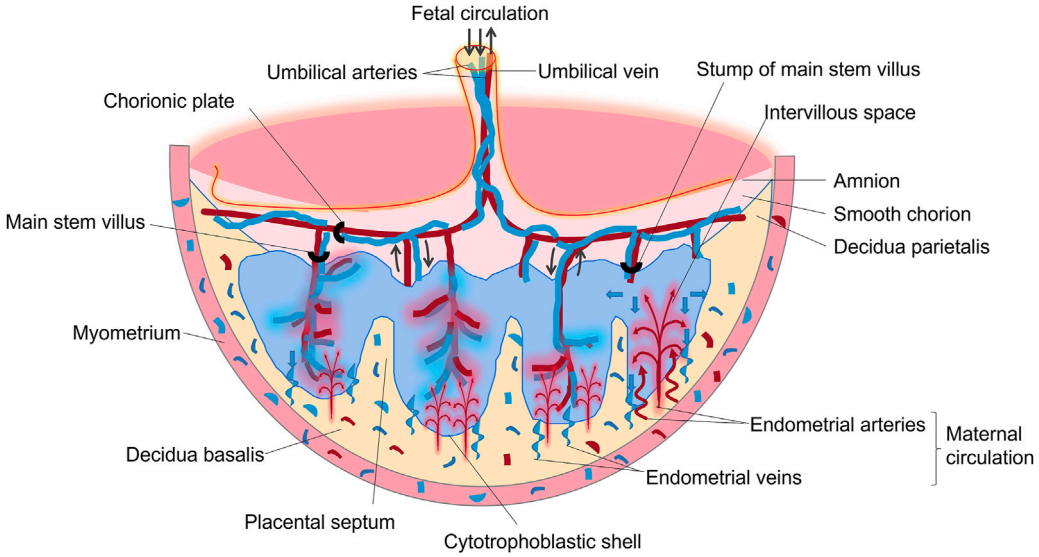

FIGURE 2 | Schematic drawing of a transverse section through a full-term placenta.

reviews the pathophysiology of PE and FGR, and proposes several possible therapeutic targets for the treatment of placental dysfunction.

OVERVIEW OF CLINICAL THERAPIES

Currently, there is no effective clinical therapy for placental conditions resulting in FGR or PE. Physicians often only administer symptomatic treatment or counsel the patient for early induction with premature delivery based on fetal or maternal conditions, which results in a high cost of neonatal intensive care and poor perinatal outcomes (Carr et al., 2017; Morton et al., 2017). Owing to an incomplete understanding of the underlying mechanisms of placental dysfunction in FGR and PE, therapeutic advances have been partially impaired. Current pharmacological treatments have significant similarities between PE and FGR, such as fetal monitoring, perinatal blood pressure control and monitoring, prenatal aspirin therapy, betamethasone for patients aged <34 weeks to mature fetal lung, parenteral magnesium sulfate to protect the brain tissue, preconception counseling, and careful follow-up of postpartum blood pressure. Timely pregnancy termination remains the only definitive treatment. (ACOG, 2013; ACOG, 2019)

PLACENTAL DEVELOPMENT

The placenta is an important, complex, and special organ between the mother and fetus. It is a critical organ for material exchange, nutrient metabolism, hormone secretion, and protection of the fetus from invasion by microorganisms. The placenta is indispensable for maintaining the normal processes of pregnancy and fetal development. It is composed of the fetal part (villous chorion) and maternal part (decidua), as shown in **Figure 2**. During pregnancy, the number of villi in contact with the decidua basalis increases rapidly, branching repeatedly, and is called the villous chorion. The placenta is divided by the decidua basalis into independent functional vascular units called cotyledons, which are villous tree-like structures consisting of villous stroma, fetal capillary endothelium, and trophoblast layer. The trophoblast layer is composed of syncytiotrophoblasts, which are derived from the bottom layer of replicating monocytes, called cytotrophoblasts. The trophoblast serves as the placental barrier and is located in the outer layer of the villus tree, which is immersed in maternal blood. As gestation progresses, the number of cytotrophoblasts decreases, resulting in a thinner layer near the end of term.

Approximately 5 days after conception, the embryo is called a blastocyst and contains 50–100 cells. As the blastocyst invades deep into the parenchyma layer of the endometrium, reestablishment of imprinting is underway. Trophoblasts are the outermost cell type of the placenta and are directly exposed to the maternal environment before and after implantation. Precursor monocyte trophoblast cells fuse to form multinucleated syncytial trophoblast cells or acquire a migrating phenotype to become EVTs.

Interactions between the blastocyst and uterine cells trigger the expression of numerous genes in the trophectoderm (Aplin and Ruane, 2017; Ruane et al., 2017) and initiate the development of primary invasive syncytial masses. A cytotrophoblast layer appears on the trophoblast plate. Placental villi appear on day 18 after conception. At this stage, several mononuclear trophoblasts escape from the placenta and begin to invade the maternal interstitium (**Figure 3**).

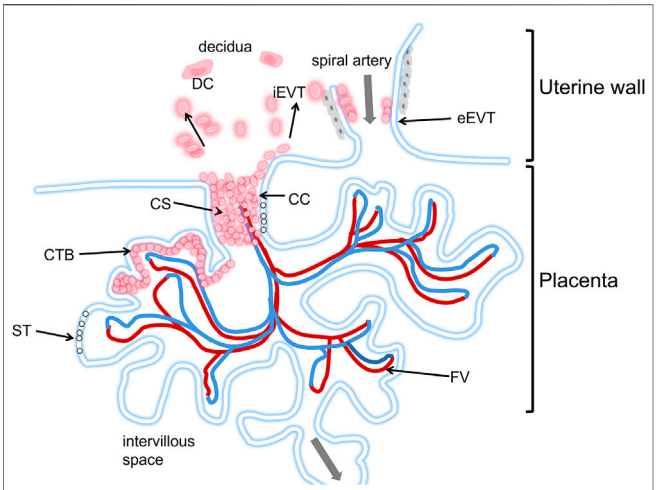

FIGURE 3 | Schematic diagram of the human placental implantation site. The placenta is in the lower part of the picture, Located in the villi space above the uterine wall, and adjacent to a uterine spiral artery. The maternal blood first immersed in the ST layer, and directly below the ST layer is the CTB layer. The blood flows to the fetus through the umbilical cord (see gray arrow). iEVTs are depicted breaking through the CS and invading through the decidua. iEVTs, Invasive interstitial extravillous cytotrophoblasts; ST, Syncytiotrophoblast; CTB, cytotrophoblast; CC, cell column; CS, cytotrophoblast shell; DC, decidual cell; FV, fetal vasculature.

In addition to being affected by the development of the placenta itself, circulating maternal substances may also have an impact on placental development. Nutritional ingredients can be transported by trophoblasts to the coelomic cavity and then to the yolk sac. The yolk sac, in turn, transports the metabolism to the embryonic intestine. This pathway is the main nutritional pathway before the formation of placental hemoglobin interface at 11 weeks. However, the specific mechanism of fetal growth defects caused by the lack of histotrophic support for the embryo remains to be explored.

POTENTIAL DELIVERY TARGETS

The placenta plays several key roles, including, but not limited to, the delivery of oxygen and nutrients to the fetus and the production of hormones and signals needed to support pregnancy (Lager and Powell, 2012; Napso et al., 2018). The characteristics of placental microvascular endothelial cells are similar to those of trophoblast cells (Troja et al., 2014). This similarity makes cell specificity particularly important, effectively avoiding the off-target effects of nanotherapy or other clinical treatments. Some studies have identified PLAC1 and CyP19a as genes with trophoblast-specific promoters (Rawn and Cross, 2008; Fant et al., 2010). They found that nanoparticles loaded with insulin-like growth factor 1 (IGF-1) molecules could effectively target human trophoblast cell lines. Nanoparticles are nanosized materials (diameter between 1 and 100 nm) that can load multiple drugs or agents. Because of their high surface-area-to-volume ratio and other properties, they can achieve high targeted drug or agent densities. Nanoparticles can also carry the drug within and controlled-release to increase the local drug concentration when tied to the targets. Nanoparticles are divided into different types based on structural differences, including polymeric nanocarriers, polymer conjugates, dendrimers, carbon nanotubes, gold nanocarriers, and lipid-based carriers, such as liposomes and micelles (**Figure 4**).

These nanoparticles have been used in various applications such as targeted drug delivery, imaging, apoptosis detection, tumor photothermal ablation, and sentinel lymph node localization. Due to the specificity of pregnancy, the application of nanomaterials is strictly limited. In addition to the types of materials, the size of nanomaterials also needs to be carefully designed because the size greatly affects their clearance, cellular uptake, and blood circulation time. For example, nanoparticles >5 nm in size can be quickly cleared by the kidneys. However, nanoparticles between 10 and 100 nm stay longer in circulation and exhibit higher cellular uptake. The type of surface charge also affects nanoparticle absorption (Nel et al., 2009; Blanco et al., 2015). Opsonization can enhance the recognition of NPs by the mononuclear phagocytic system, thereby promoting their uptake in the liver rather than reaching the expected target location. Therefore, to deliver therapeutic agents to targeted placental sites, it is necessary to control the hepatic clearance rate of nanomedicines to develop targeted therapies for the treatment of obstetric complications. Stealth agents, such as polyethylene glycol, can be used to encapsulate nanoparticles to prevent them from binding to blood proteins and have been shown to extend their blood circulation time (Gref et al., 1994; Suk et al., 2016). The safety and distribution of nanoparticles in the placenta are the main problems associated with the clinical use of nanomedicine in pregnancy-related diseases. The lack of knowledge on the transplacental pathways, targeting mechanisms, and their interaction with the placental membranes of NPs further limits the implementation of nanodrugs during pregnancy. In addition, the characteristics of nanoparticles targeting the placenta are not only affected by the physicochemical properties of nanoparticles but also depend on placental maturation and gestational age (Yang et al., 2012). A complete understanding of the placental characteristics facilitates the design of highly targeted nanomaterials and is conducive to the treatment of pregnancy-related diseases. Furthermore, because placental properties vary with pathological conditions, it is necessary to carefully assess the impact of these conditions (Saunders, 2009; Dimasuay et al., 2016). The tunability of nanomedicine has great potential to overcome biological obstacles in targeted drug delivery systems and for the clinical development of nanomedicine to treat maternal and perinatal complications.

Placental pathological conditions affect the interaction between the placenta and nanoparticles and alter gestational age (Mihaly and Morgan, 1983; Wang et al., 2010). Wang (Wang et al., 2010) examined the uptake of drugs at different gestational weeks and found that 63Ni uptake, retention, and transport in the placenta showed a dose-dependent increase. In

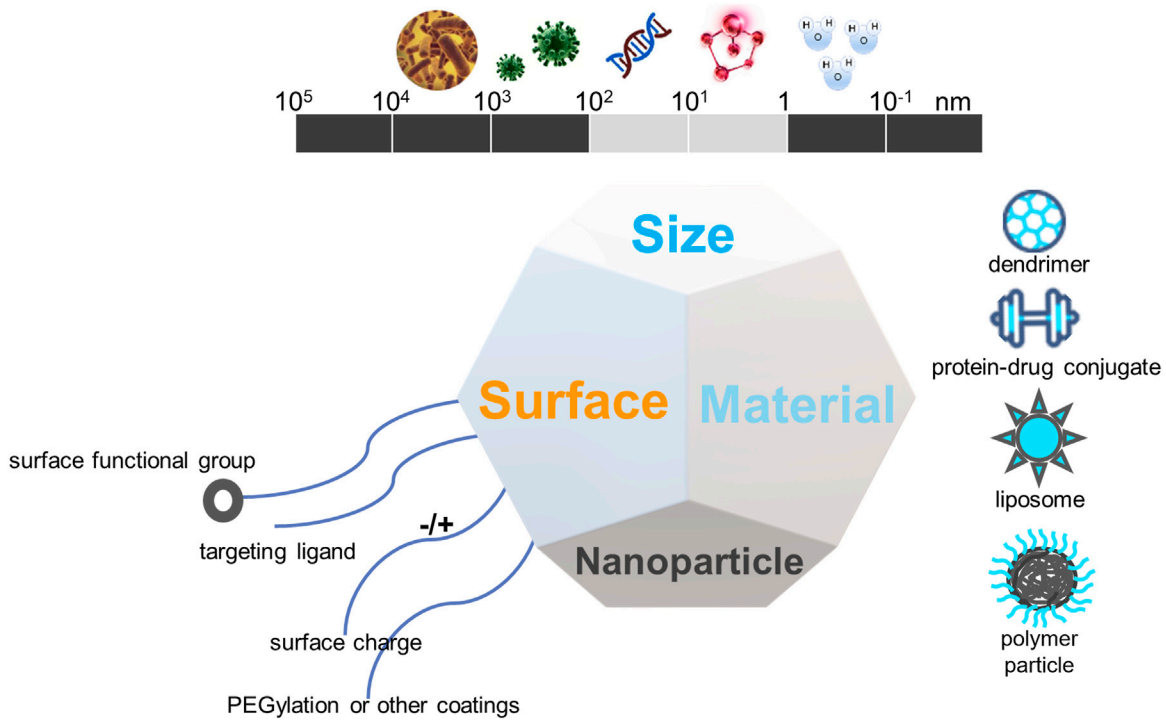

FIGURE 4 | The biophysiochemical properties of nanomaterials for drug delivery in placental dysfunction.

another study, McIntyre et al. assessed the effects of pathology on the delivery of important amino acids through the placenta and showed reduced delivery of glutamate and glutamine through the placenta in FGR models (McIntyre et al., 2020). As the delivery is limited, the influence of gestational age on nanoparticle targeting efficiency to placenta needs to be further discussed in the future. Since the placenta is immersed in the maternal blood, its main function is to absorb and exchange substances and is thus considered an excellent therapeutic target for dysfunctional placenta treatment. To achieve this specificity, the factors that influence the binding of particles to the placenta need to be recognized and studied. The physicochemical properties of the drug determine its rate of transfer across the placenta, including polarity, molecular weight, size, and lipid solubility (Syme et al., 2004; Evseenko et al., 2006). Most small-molecule drugs (<600 Da) pass through the placenta, mainly via passive diffusion, and are hence subject to placental blood perfusion. Some large proteins such as transthyretin and IgG tend to interact with specific receptors of the syncytial membrane and can be transcytosed across trophoblastic cells into the fetal part (Malek et al., 1995). Contrarily, micromolecules such as nanoparticles typically enter the placenta via other mechanisms, predominantly pinocytosis/endocytosis and phagocytosis (Hillaireau and Couvreur, 2009). Nanoparticles and other macromolecules are absorbed into the placenta, mainly via endocytosis, pinocytosis, and phagocytosis (Conner and Schmid, 2003). However, few studies have been published on the topic of nanoparticles crossing the placenta, and we do not yet fully understand the transplacental absorption and exchange mechanisms of all nanoparticles. Some studies have shown that trophoblasts can absorb polymeric nanoparticles via dynamin-mediated endocytosis. This result supports the ability of NPs to enter the placenta through endocytosis (Bajoria and Contractor, 1997; Menezes et al., 2011).

Systemic small-molecule therapy lacks specificity to the pathological site and can pass through the placenta and reach the fetus, causing adverse effects (Syme et al., 2004). For example, indomethacin is one of the most commonly used tocolytic agents in the clinical treatment of preterm birth because it can easily enter fetal circulation and can also cause side effects, such as intraventricular hemorrhage (Hammers et al., 2015), constriction of the fetal ductus arteriosus (Vermillion et al., 1997; Suarez et al., 2002), and necrotizing enterocolitis (Major et al., 1994; Sood et al., 2011). Targeted delivery aimed at disease-associated cells in the placenta can now open new avenues for developing targeted therapies to address perinatal health. The application of nanotechnology can ensure the delivery of therapeutic drugs to specific cells, thereby preventing harmful side effects in the mother or fetus. Because NPs can be modified to target specific cell populations, nanoloaded drugs can optimize their biodistribution, thereby reducing their side effects. In conclusion, it is vital to select specific targets based on their unique placental structure.

Studies have compared the difference between placental development and cancer, suggesting that the establishment of the placenta may represent controlled cancer (Fidler, 2003;

Ferretti et al., 2007; Holtan et al., 2009). Evidence suggests that placental development is similar to genetic and epigenetic regulation of cancer (Lorincz and Schübeler, 2017; Smith et al., 2017). In tumors, p32 has been identified as the main cell surface receptor for the peptide CGKRK (Fogal et al., 2008; Agemy et al., 2013); the same molecule has been shown to be highly expressed in the STB, underlying CTB, vascular endothelium, and villous stroma in the first trimester and term placenta. The expression of p32 was significantly reduced in FGR placentas, suggesting that p32 is important for the proliferation of CTB, as well as the process of FGR (Matos et al., 2014). Calreticulin, a calcium-binding protein in the endoplasmic reticulum (Waisman et al., 1985), plays a significant role in the proliferation, migration, and extracellular matrix degradation of cancer cells (Chiang et al., 2013). The same Calreticulin is overexpressed in PE placental tissues (Shi et al., 2012) and can selectively bind to the synthetic peptide KLGFFKR (Burns et al., 1994). a_v integrins are receptors for the homing sequence of iRGD in tumor cells (Sugahara et al., 2009), and act as adhesion molecules to mediate cell signaling and extracellular matrix attachment. The a_v integrin is continuously expressed in the mouse placenta throughout pregnancy (Sutherland et al., 1993). Studies have found that integrin a_vb_3 is expressed on the surface of the human placenta (Vanderpuye et al., 1991; Zhou et al., 1997). King et al. further developed nanoparticles packaged with FAM-iRGD, which could selectively deliver insulin-like growth factor 2 (IGF-2) to the mouse placenta in a mouse model of FGR. In summary, specific and highly expressed proteins or ligands in the placenta have the potential to be targets for the development of new drugs to treat placental dysfunctions.

NANOPARTICLES

Nanomedicine is the application of nanotechnology for the treatment, prevention, monitoring, and control of biological diseases, and has been widely applied in the field of oncology (Peer et al., 2007). The clinical therapeutic effect of nanomaterials also requires precise targets (receptors and/or cells), which can be specifically identified by nanoparticles and are suitable for the delivery system to improve the efficacy of the original drug and minimize side effects. Some of these precise targets include proteins, macrophages, dendritic cells, endothelial cells, and tumor cells (**Table 2**). When NPs contact and break down their targets, the drug is released to assert its therapeutic function. There are many types of nanomaterials and nanocarriers used for drug transfer with the aim of treating diseases, including liposomes, dendrimers, micelles, polymeric micelles, polymeric nanoparticles, and metallic nanoparticles (Adekiya et al., 2020; Pritchard et al., 2021). In summary, nanomaterials may provide novel treatment options for obstetric medical conditions. A few of these are discussed in the following section, focusing mainly on the three types of nanoparticles applied in the fields of obstetrics and gynecology (**Figure 4**).

Liposomes

Liposomal nanoparticles are a subgroup of lipid-based nanoparticles, which are spherical organic engineered vesicles whose central aqueous core is surrounded by a lipid bilayer and can effectively encapsulate macromolecules as well as DNA and siRNA inside the aqueous cores or in lipid membranes, similar to cell membranes. This means that liposomes have better drug distribution and lower systemic toxicity (Park, 2002). These properties make them the most versatile nanocarriers (Bamrungsap et al., 2012; Majzoub and Ewert, 2016; Zylberberg and Matosevic, 2016). Nanoparticles are usually composed of phospholipids and can form unilamellar and multilamellar liposome structures, allowing the transport and delivery of lipophilic, hydrophilic, and hydrophobic drugs and can expand their use by capturing lipophilic and hydrophilic compounds in the same system (Sarfraz et al., 2018). Their stability *in vivo* and *in vitro* can be altered during the synthesis process according to their potential application, which is affected by the nanoparticle size, lipid composition, surface modification, surface charge, and number of lamellae (Sercombe et al., 2015; Fenton et al., 2018; Sedighi et al., 2019). Because liposomes can be rapidly absorbed by the reticuloendothelial system, they are usually surface-modified to enhance delivery and extend their circulation. By conjugating with antibodies or peptides to target nanoparticle therapeutic delivery, it significantly lowers the required therapeutic dose compared to systemic administration. In addition, this conjugation also reduces side effects, and increases tissue targeting specificity. Such conjugation has allowed nanoparticles to be used clinically by loading chemotherapeutic drugs, such as cytarabine and daunorubicin, in treating cancers (Lowis et al., 2006; Khalin et al., 2014; Fonseca-Santos et al., 2015).

Polymeric Nanoparticles

Polymeric nanoparticles are solid-phase colloidal systems composed of biocompatible and biodegradable polymers, with the additional advantage of the ability to load drugs and proteins without chemical alteration. They can be synthesized from natural, synthetic materials, monomers, or prefabricated polymers (Le and Chen, 2018; Zhang et al., 2019; Brown et al., 2020; He et al., 2020; Zhang et al., 2020), resulting in various structures and functions; these may include dissolving, wrapping, encapsulating, or adsorbing drugs into the polymer matrix, followed by controlled release at the target site. Owing to their simple formulation parameters, they can be formulated to enable precise control of multiple nanoparticle features (Volpatti et al., 2020). These characteristics enable polymeric nanoparticles to deliver various payloads, including hydrophilic and hydrophobic compounds, small molecules, and bio-macromolecules, making polymeric nanoparticles an ideal vehicle for co-delivery applications (Xu et al., 2013; Afsharzadeh et al., 2018; Caldorera-Moore et al., 2019; Jose, 2019; Knight et al., 2019; Strand et al., 2019; Zhang et al., 2020). The most common forms of polymeric nanoparticles are nanocapsules and nanospheres. The former is a cavity surrounded by a polymer film or shell, and the latter is a solid matrix system. Within these two categories,

TABLE 2 | Characteristics of nanoparticles that would be beneficial in treating placental dysfunction.

➢Targeting ability
➢ Target to the mother, placenta or fetus selectively
➢ Reduce risks to the fetus and mother
➢ Increasing efficacy and/or bioavailability of drugs
➢ Lower concentration
➢ Reduce the required dose
➢ Reduce the potential adverse side effects
➢ Modified easily according to the intention
➢ Prevent drug degradation and avoid recognition by the immune systems
➢ Prolong half-life
➢ Target delivery of drugs to the placenta
➢ Encapsulate unstable or insoluble therapeutic agents
➢ Nanoscale properties
➢ Large surface area to volume ratio
➢ Capable to load, carry and deliver drugs
➢ Can be modified and designed to delivery drug through a specific route in the placenta during pregnancy
➢ Reduce dosing of drugs and limit the adverse side effects that the mother or fetus is exposed to

nanoparticles are further divided into polymersomes, dendrimers, and micelles, according to their shapes. Polymersomes have a structure similar to that of liposomes, but are usually composed of synthetic polymer amphiphiles, including poly (lactic acid)-based copolymers, which are difficult to biodegrade and limit their wide clinical application. However, some polymers, including polymer-mediated delivery of chemotherapeutics, are currently used in clinical practice (Rosen et al., 2003; Sabbatini et al., 2004; Duncan, 2006; Etrych et al., 2011) and PEGylated interferon (IFN)-a-2a for hepatitis C (Glue et al., 2000).

Dendrimers

Dendrimers, are morphologically complex three-dimensional hyperbranched polymers prepared by divergence or polymerization of branched monomers. Dendrimers consist of three regions: a core in the center, inner branches (dendrons), and exterior surface functional groups, each of which is called a generation (G). In the controlled synthesis process, different variables (size, molecular weight, and number of surface groups) gradually increased with increasing G number. For the most familiar poly (amidoamine) (PAMAM) dendrimers, the G0 type has a molecular weight and 1.5 nm diameter, whereas the G7 type has a mass molecular weight of 116,493 and 8.1 nm diameter (Esfand and Tomalia, 2001). Active functional groups enable biomolecules to conjugate to the surface, whereas drugs and DNA/RNA can be encapsulated in the interior. Their size, mass, shape, and surface chemistry can be highly modified and easily customized, making their pharmacokinetics more predictable and controllable (Lee et al., 2005). Similar to liposomes, both are rich in cavities and have a spherical shape with a hydrophobic core and hydrophilic periphery, making them a unique carrier for siRNA delivery (Svenson and Tomalia, 2005; Bawarski et al., 2008). Numerous studies have shown that the active functional groups that exist on the exterior of dendrimers can bind biomolecules or contrast agents to the surface, whereas drugs can be encapsulated in the interior. However, drugs can also be loaded onto the external branching surface of dendrimers, resulting in an extremely high load capacity (Svenson and Tomalia, 2005). Dendrimers can load many kinds of substances but are most commonly used to deliver small molecules and nucleic acids (Xu et al., 2014; Mendes et al., 2017). Several products based on dendrimers are currently being tested in clinical trials. These include theragnostic (therapeutic and diagnostic) agents, molecules used in transfection, contrast agents, topical gels, and charged polymers, such as PAMAM and polyethyleneimine (PEI) (Menjoge et al., 2010a; Kannan et al., 2014; Xu et al., 2014). Although there are currently no dendrimer drugs available for clinical use, they have great potential for clinical translation. Specifically, its utilization can target the delivery of chemotherapeutic drugs, improve the oral route of administration, and enhance intracellular drug delivery (Menjoge et al., 2010a; Myc et al., 2010; Najlah and Demanuele, 2006; Najlah et al., 2007; Wolinsky and Grinstaff, 2008).

NANOMEDICINE FOR THE TREATMENT OF PLACENTAL DYSFUNCTION

In nanomedicine, the development of promising NPs for biomedical applications requires many physical, chemical, biological, and functional properties. The key factor is size. The size and conformation of nanoparticles together determine their trajectory dynamics, which is decisive for nanodrug formulations. Other factors that should be considered include the surface charge of the nanoparticles, encapsulation ability, high drug-loading efficiency, long circulating half-life, minimal systemic toxicity, selective localization, high adhesion in the placental environment, and enhanced internalization and imaging of the placenta through endocytosis. The sustained and controlled release of drugs is an important factor for precise targeted drug delivery of nanodrugs. These characteristics are of great significance for the application of NPs in the diagnosis and treatment of diseases related to placental dysfunction. Most of the aforementioned nanodelivery systems rely on enhanced penetration and retention effects of targeted drug delivery. However, owing to the lack of knowledge regarding highly expressed targets and ligands, the application of nanomedicine in placental dysfunction is limited. In the past few decades, significant progress has been made in understanding the pathophysiology of placental dysfunction and its molecular mechanisms (**Table 3**). These studies have laid a solid foundation for nanodrug-targeted therapies. As placental dysfunction can lead to many pregnancy complications, the treatment of placental dysfunction can benefit the fetus, thus improving long-term health (Ganguly et al., 2020) (**Figure 5**). Next, we review the therapeutic options for enhancing placental function, as well as improving the subsequent state of hypoxia and oxidative stress. We also review targets including

TABLE 3 | Targeted drug delivery systems and human *ex vivo* placenta perfusion model to investigate placenta-NP interactions.

Treatment	Putative mode of action	Test system (s)	Dosing regime	Main outcomes of treatment (compared to appropriate control)	References
CSA targeting PEG-PLA NPs containing siNrf2 and sisFlt-1	inhibit the expression of Nrf2 and sFlt-1 synchronously	PAH model mice	1 mg/kg in T-NPsiNrf2 & sisFTL1 group; 2 mg/kg in T-NPsiNrf2 and T-NPsisFTL1 groups; IV	Decreased circulating Nrf2 and sFlt-1 *in vivo*, and improved pregnancy outcomes	Li et al., (2020a)
PAMAM dendrimer-SiRNA	significantly decreased sFlt1 secretion	HTR-8/SVneo; PE model mice	0.3 mg/kg sFlt1 siRNA at an N/P ratio of 10:1; IV	Decreased circulating sFlt-1 *in vivo*, and improved pregnancy outcomes	Yu et al., (2017)
Tumor homing peptide coated liposomes containing IGF-2	selectively deliver IGF-2 to mouse placenta	placenta-specific P0 knockout mice (P0 mice)	~ 0.3 mg/kg; IV	Increased mean placental weight and improved fetal weight distribution in healthy and FGR mice respectively	King and Ndifon, (2016)
Peptide coated liposomes containing SE175	significant relaxation of mouse uterine arteries and human placental arteries	endothelial nitric oxide synthase knockout (eNOS−/−) mice	0.44 mg/kg; IV	Increased fetal weight and improved placental efficiency	Cureton et al., (2017)
PEGylated AuNPs	transplacental transfer of nanoparticles in perfused human placenta	human placenta	2.0×10^{9}–7.9×10^{11} NPs/ml	AuNPs detected in placental tissue; mainly ST and CT layer, not in endothelium of fetal capillaries	Myllynen et al., (2008)
PEGylated AuNPs; Carboxylated AuNPs	different surface modifications (PEGylated versus carboxylated) are taken up and cross the human placental barrier	in a static human *in vitro* co-culture placenta model and the dynamic human *ex vivo* placental perfusion model	25 μg/ml	AuNPs mostly found attached to/in the outer ST layer; PEGylated AuNPs penetrated deeper into the tissue	Aengenheister et al., (2018)
PEGylated AgNPs; Carboxylated AgNPs	AgNPs are taken up and cross the human placenta	in the human *ex vivo* placenta perfusion model	PEGylated AgNPs (2–15 nm; 40 μg/ml) & carboxylated AgNPs	Mass concentration of Ag fraction that accumulated in the placenta	Vidmar et al., (2018)
Fluorescently labeled nonfunctionalized, carboxylated or amine-modified polystyrene beads	the transfer of polystyrene nanoparticles across the human placenta	human placenta	25 μg/ml	Fluorescent amine-modified particles found in the ST and the villous mesenchyme	Grafmueller et al., (2015)
Liposome encapsulated carboxyfluorescein	the low molecular-weight, hydrophilic and polar molecule carboxyfluorescein has been determined across the perfused human term placenta	human term placenta	20 nM	Small (15.2 ± 1.6%) Large (3.0 ± 0.4%) Multilamellar (1.3 ± 0.3%) of initial dose	Bajoria and Contractor, (1997)

trophoblasts, placental-specific affinity peptides, and placental growth factor pathways, and targeting placental delivery of miRNA, DNA, mRNA, and siRNA therapies.

Targeting affinity-based peptides was initially applied in the treatment of tumors to deliver therapeutic agents to tumors and related vascular systems (Ruoslahti et al., 2010). As stated in the study, some cell surface antigens are expressed in tumors but absent from healthy tissues. These antigens can bind to circulating ligands, including antibodies and peptides. Therefore, the injection of ligands to which drugs or genes are attached can target the therapeutic agent to be delivered to tumors rather than to normal cells. As previously discussed, placenta and solid tumors have many commonalities, such as rapid cell proliferation, production of growth factors and cytokines, and evasion of immune surveillance. Furthermore, the migration and invasion of placental trophoblast cells in the uterine spiral artery are similar to the invasion and metastasis of cancer cells.

Therefore, to provide a method for drug/gene-specific delivery to the placenta, King and Ndifon, (2016) linked the tumor-homing peptide sequence CGKRK or iRGD to the antigen specifically expressed on the surface of the placenta and bound it to the liposome; specifically, an immunochemistry assay revealed that the peptides could selectively target the segments of endovascular trophoblast lining remodeled arteries and the endothelium of established spiral arteries. The CGKRK-coated peptide also accumulated in the STB layer, but not in the CTB layer, during early gestation and in term human placental

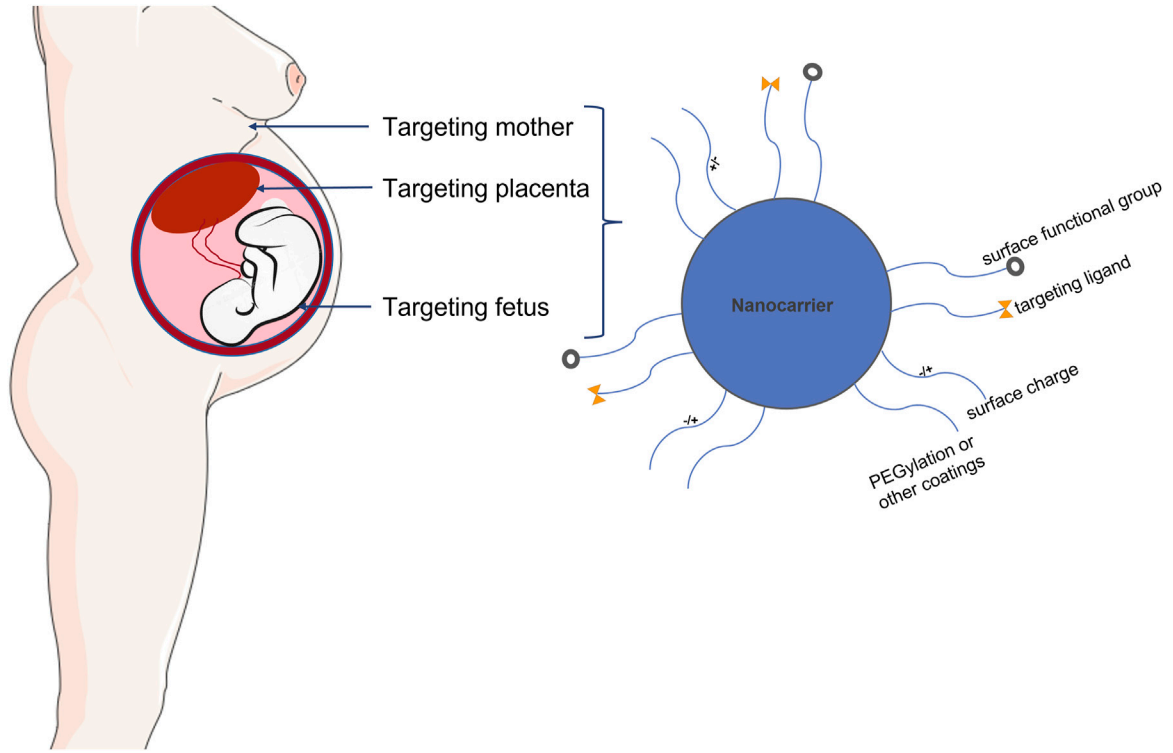

FIGURE 5 | Schematic illustration demonstrating placental targeted drug delivery and nanoparticles applied in pregnancy. Nanoparticle mediated controlled drug and gene delivery specifically targeted to placenta may provide novel avenues for treating placental dysfunction without potential side effects.

explants. In addition, it was found that the tumor-homing peptides CGKRK and iRGD could selectively bind to the human and mouse placenta and did not affect the normal development of the fetus. Liposome nanoparticles coated with these tumor-homing peptides were used as placental targeting ligands and accumulated in the mouse placenta after intravenous injection in pregnant mice. iRGD-coated nanoparticles delivered IGF-2 to the mouse placenta, significantly promoting placental growth in healthy wild-type mice. The average weights of FGR model P0 fetuses is 69% of wild-type birth weight in late gestation (Constancia et al., 2002). Targeted delivery of IGF-2 liposomes effectively increased fetal weight of P0 fetuses (83% wild-type weight), demonstrating the effectiveness of targeted delivery of drugs to the placenta and providing a new method of placental-specific treatment.

Subsequently, the same team further studied another targeting peptide, CNKGLRNK, which specifically binds the vasodilator 2-[[4-[(nitrox)methyl]benzoyl] thio]-benzoic acid methyl ester (SE175) to the placental tissue, as mentioned above. Nitric oxide is packaged to act as a vasodilator and enhance uterine placental perfusion. *In vitro* studies have shown that myography can relax placental blood vessels in both mice and humans. In in vivo studies, intravenous injection of liposomes coated with CNKGLRNK peptide to which the vasodilator SE175 was attached neither promoted placental nor increased fetal weight growth in healthy wild-type mice; however, in a mouse model (nitric oxide synthase knockout mice-eNOS−/−) of FGR, fetuses had a mean weight 13% lower than that of C57BL/6J mice; targeted delivery of SE175 increased mean fetal weight (4%) compared with the control group. In addition to weight gain, the team also found that spiral artery diameter was larger, and the expressions of placental oxidative stress markers, COX-1, COX-2, and 4-hydroxynonenal, were reduced in the placenta (Cureton et al., 2017). Another study (Cureton et al., 2017) showed that the use of specific vascular-targeting peptides to selectively deliver vasodilators to the uterine placental vasculature may provide a promising treatment for FGR caused by impaired uterine placental perfusion.

Other studies have found that microRNAs (miRNAs) affect the growth of the human placenta and fetus (Kang et al., 2015), and that the expression of miRNAs changes in pregnancy complications, including PE and FGR. Therefore, Beards et al. (2017) used a similar peptide-based strategy to study whether targeted placental delivery of miR-675 or miR-145 inhibitor conjugates can relieve these respective miRNA inhibitory effects on the proliferation of the human CTB layer *in vitro* and the growth of the mouse placenta. Therefore, liposomes coated with the peptide CCGKRK were linked to miR-675 or miR-145 inhibitor peptide nucleic acid (PNA) conjugates and injected intravenously into mice or added to human villous placental explants during the first trimester or term pregnancy. Compared with the control group, pregnant mice injected with miR-675 inhibitor or miR-145 inhibitor PNA had increased fetal and placental weights and significantly

increased proliferation of CTB, but neither the experimental group nor the control group exerted any effect on litter size or fetal absorption.

These studies have successfully exploited several placental homing peptide-packaged nanoparticles that provide a novel platform as potential therapeutic targets for placental dysfunction. In addition, researchers have also found that other peptides, such as the placental chondroitin sulfate A binding peptide (plCSA) packaged with nanoparticles, can selectively target the trophoblast layer (Zhang et al., 2019). Zhang et al. (2018) showed that plCSA nanoparticles specifically bound to trophoblast cells in mouse and human placental tissue *in vitro*, but not to the fetus, maternal, placental junctional zone, or decidua tissues. Additionally, plCSA NPs were injected intravenously into mice from 6.5 to 14.5 days of pregnancy, and it was found that plCSA NPs containing methotrexate significantly inhibited placental growth and induced apoptosis in the placenta but did not have side effects in maternal tissues. In the control group, animals treated with MTX alone showed severe damage to their maternal tissues, especially the liver and kidneys. In summary, these studies indicated that NPs decorated with a plCSA-binding peptide can be used as a novel placenta-specific therapeutic delivery platform.

Other promising approaches to enhance placental function based on peptide homing include DNA, mRNA, and siRNA therapies to correct the expression of genes that are important in the development of the placenta. IGF1 and IGF2 are critical for achieving appropriate development of the fetal placenta and fetus throughout gestation. Thus, they have been considered as potential targets for intrauterine growth restriction (FGR), which has been a source of interest for many researchers. Jones et al. (2013) demonstrated that overexpression of IGF1 in the placenta improves placental glucose transport in a model of human trophoblasts, thus correcting fetal weight deficits in a mouse model of FGR, and further elaborated the underlying mechanisms of the above effect by enhancing the expression of amino acid transporters (Jones et al., 2014). Abd Ellah et al. (2015) subsequently used a nanostructure delivery system, diblock copolymer (pHPMA-b-pDMAEMA), conjugated with the IGF-1 gene and trophoblast-specific gene promoters of Cyp19a or PLAC1 in a mouse model of FGR and trophoblast cell lines. They found that the offspring weights of experimental group had 20% higher than those in the control group, indicating that the complexes were effective in rescuing fetal growth in a mouse model of the FGR phenotype and significantly increased the expression of placental IGF-1, compared to the same complexes with empty plasmids that do not encode IGF-1. Moreover, Wilson et al. (2020) showed that nanoparticles complexed with IGF-1 and PLAC1 promoters maintained normal fetal growth in an FGR mouse model and in the human placental syncytium. However, it remains to be determined whether it is possible to achieve placental targeting of IGF-1 through the peripheral administration of placental homing peptide-decorated nanoparticles.

As described previously, in most cases of PE and FGR caused by placental dysfunction, the main pathophysiological process is abnormal invasion of the placenta into the uterine wall, which can lead to poor placental perfusion and subsequent hypoxia. Hypoxia in the placenta is assumed to cause STB stress, thus reducing nutrient transport, which, in turn, is a source of antiangiogenic factors for the fetus, such as sFlt1. sFlt1 is an angiogenesis-related factor and current studies have confirmed that it is a clinically specific biomarker for the prevention and diagnosis of PE. Gene therapy has shown great potential in placental dysfunction as demonstrated by Turanov et al. who showed that siRNAs-sFlt1 could effectively reduce circulating and placental levels of sFlt1. This led to alleviation of clinical symptoms, and improvement in pregnancy outcomes in a pregnant mouse model and baboon model of PE, respectively. Gene therapy combined with nanotechnology to regulate sFlt1 expression has been explored as a promising treatment for PE. Yu et al. (2017) found that siRNA-sFlt1-PAMAM dendrimer complexes significantly reduced the secretion of sFlt1, greatly attenuated the symptoms of PE, and improved pregnancy outcomes in a PE mouse model.

Because nanoparticles targeting CSA can specifically deliver drugs to the placenta, Li et al. (2020b) generated carboxyl-polyethylene glycol-poly (D, L-lactide; PEG-PLA) NPs, a new siRNA delivery system, using double-emulsion methods. They complexed placental CSA binding peptide (P-CSA-BP) and PEG-PLA nanoparticles to create a novel delivery system of siRNA-sFlt1 that can specifically target trophoblasts. Their results illustrated a significant decrease in sFlt1 mRNA in the placenta and sFlt1 protein in the serum without any maternal or fetal toxic effects on the utility of T-NPsisFlt1 nanoparticles. The same research group used placenta-targeted PEG-PLA NPs (T-NPNrf2, T-NPNrf2, and sFlt1) to simultaneously downregulate both Nrf2 and sFlt1 in the placenta, and their results showed that inactivation of sFlt1 and Nrf2 alleviated the symptoms of PE and improved pregnancy outcomes. These results suggest that inactivation of sFlt1 and Nrf2 may provide a new therapeutic strategy for PE (Li et al., 2020a).

siRNA by themselves are usually unstable in the bloodstream, thus limited in their ability to reach target tissues and cells. However, when encapsulated by nanoparticles, siRNA complexes have better stability and are easily internalized by the CTB, which minimizes potential side effects to the mother and fetus. Valero et al. (2017) previously confirmed using two *ex vivo* human models, a dual-perfused placenta and suspended villous explants that their liposomes exhibit great potential for the delivery of placental drugs. This was attributed to the fact that they were able to target delivery to the placenta without interfering with fetal circulation. They then applied three different charged states to liposomal formulations to deliver negatively charged siRNA, and the results showed that siRNA complexes were more biocompatible and better internalized by human primary villous CTBs, with a minimized toxicity effect (Valero et al., 2018). Their work highlights that liposome were designed to be used in conjunction with siRNAs and could provide a novel and promising approach to gene therapy in pregnant patients with placental dysfunction-related diseases.

Chronic placental dysfunction also leads to a state of oxidative stress, and accumulating evidence suggests that developing

embryos are extremely sensitive to reactive oxygen species (ROS) and oxidative stress during the organogenesis stage. Vafaei-Pour et al. (2018) found protective effects of ceria nanoparticles, showing that the treatment of nanoceria significantly inhibited oxidative stress and pathological changes in embryos. Therefore, systematic administration of antioxidant therapy can attenuate pregnancy complications. Phillips and Scott, (2017) investigated the maternal injection of a non-targeted c-PGA-Phe polymeric nanoparticle-bound antioxidant mitochondrial antioxidant (MitoQ) *in vitro* and *in vivo*. In a hypoxic pregnant rat model, exposure to hypoxia resulted in decreased birth weight. MitoQ combined with nanoparticles (concentrated in the CTB) rescued 60% of the deficit and reduced oxidative stress in the placenta but did not affect the weight of the placenta or fetus. More importantly, nanoparticle complexes were not detected in fetal thoracic, abdominal, or brain tissues. These results demonstrate that antioxidant therapy is a promising candidate for the treatment of placental dysfunction. Targeted delivery of hemoglobin (Hb) via liposomes (hemoglobin vesicles) was also developed as an artificial oxygen carrier for the treatment of fetal hypoxia, and using a model of pregnant rats, they found that there were no adverse effects on fetal development and the pregnant mother, but studies have found that there is the deposition of liposomes in the fetus. This safety study of Hb vesicles during pregnancy may contribute to a novel clinical treatment for placental dysfunction caused by fetal hypoxia. However, the possible clinical effects of liposome deposition require further investigation.

Infection is also one of the causative factors of FGR. Genital infections, both bacterial and viral infections, required urgent treatment during pregnancy. A study evaluated the transplacental kinetics biodistribution and transfer of PAMAM dendrimers and conjugates *ex vivo* across the human placenta model and found that the maternal side placental perfusate was 18-fold higher than the fetal side, indicating that the PAMAM dendrimers exhibited a low transplacental rate (Menjoge et al., 2011). Another study used an *ex vivo* model to evaluate the same PAMAM dendrimers for intravaginal application to treat the ascending genital infections in pregnant women. The results showed that the dendrimers exhibited a low transplacental rate (<3%) compared with almost 50% in the control group (Menjoge et al., 2010b). These results demonstrate that the use of dendrimers in combination with drugs can effectively prevent them from crossing human fetal membranes when administered intravaginally, and thus may provide a new way to selectively deliver therapeutic drugs to the mother, thereby reducing fetal exposure risks. Collectively, the studies outlined above clearly demonstrate the opportunity to exploit novel targeting NPs to deliver therapeutics to the placenta and provide platforms for the development of placenta-specific therapeutics, including gene delivery.

DISCUSSION

As discussed in this review, nanotechnology presents an exciting opportunity to improve many aspects of our lives and is believed to hold immense potential for treating placental dysfunction, reducing the risks to the mother and fetus. There is an urgent need for novel treatments of placental dysfunction-related diseases. Nanoparticles targeted to the placenta may offer noninvasive options for treating placental dysfunction-related diseases, such as PE and FGR. Specifically, the targeted delivery of therapeutic molecules to the dysfunctional placenta may provide opportunities to treat serious obstetric complications. This review highlights the application of nanotechnology, and the advances and safety concerns of nanomedicine therapy for maternal and fetal health in the phenotype of placental dysfunction. However, it is essential that any associated risks be fully assessed before the field develops too far. Fundamental to developing a comprehensive understanding of the risks of nanoparticles in this area is the evaluation of interaction of NPs with biological barriers, which dictate access to the whole organism and specific organs. Recent advances in targeted delivery strategies have stimulated our interest and broadened our horizons. Hence, our research team aimed to prepare nanodrugs specifically targeting the placenta to provide potential treatments for placental dysfunction.

In summary, the following scientific issues must be resolved in the field of nanoparticle research: 1) Optimal nanoparticle design. To achieve their diagnostic and therapeutic functions, nanoparticles must first be able to break through the physiological and cellular barriers; therefore, they must reach the target tissue and cells at a certain concentration, thus improving the therapeutic effect and reducing side effects on the mother and fetus. Achieving this targeted delivery process through the optimization and innovative structural design of nanoparticles and further increasing the cumulative dose in the placenta are important challenges for future research. 2) Nanoparticles have a complex relationship between structure and function. In addition, they may come in different material characteristics (size, shape, charge, and composition), and may exhibit different physiological environments, that may present different toxicological results in diseases. Thus, it is difficult to approve nanoformulations. To promote the application of NPs, the safety and effectiveness of clinical requirements must be coordinated with the complexity of NPs to promote the development of standard methods for the characterization and preparation of nanomaterials.

AUTHOR CONTRIBUTIONS

YY, QZ, and LS are the corresponding authors who initiated the project, made suggestions, and revised the article. HJ, LL, DZ, and XZ searched the database and wrote and finalized the manuscript. All authors reviewed and commented on the manuscript.

FUNDING

This work was supported by grants from the National Natural Science Foundation of China (Nos. 82071656, 81902622, and 81771659), Science and Technology Commission of Shanghai Municipality (No. 21Y11907500), and the Shanghai "Science and Technology Innovation Action Plan" Hong Kong, Macao, and Taiwan Science and Technology Cooperation Project (20430760100).

REFERENCES

Abd Ellah, N., Taylor, L., Troja, W., Owens, K., Ayres, N., Pauletti, G., et al. (2015). Development of Non-viral, Trophoblast-specific Gene Delivery for Placental Therapy. *PLoS One* 10, e0140879. doi:10.1371/journal.pone.0140879

Adekiya, T. A., Kondiah, P. P. D., Choonara, Y. E., Kumar, P., and Pillay, V. (2020). A Review of Nanotechnology for Targeted Anti-schistosomal Therapy. *Front. Bioeng. Biotechnol.* 8, 32. doi:10.3389/fbioe.2020.00032

Aengenheister, L., Dietrich, D., Sadeghpour, A., Manser, P., Diener, L., Wichser, A., et al. (2018). Gold Nanoparticle Distribution in Advanced *In Vitro* and *Ex Vivo* Human Placental Barrier Models. *J. Nanobiotechnol* 16, 79. doi:10.1186/s12951-018-0406-6

Afsharzadeh, M., Hashemi, M., Mokhtarzadeh, A., Abnous, K., and Ramezani, M. (2018). Recent Advances in Co-delivery Systems Based on Polymeric Nanoparticle for Cancer Treatment. *Artif. Cell Nanomedicine, Biotechnol.* 46, 1095–1110. doi:10.1080/21691401.2017.1376675

Agemy, L., Kotamraju, V. R., Friedmann-Morvinski, D., Sharma, S., Sugahara, K. N., and Ruoslahti, E. (2013). Proapoptotic Peptide-Mediated Cancer Therapy Targeted to Cell Surface P32. *Mol. Ther.* 21, 2195–2204. doi:10.1038/mt.2013.191

American College of Obstetricians and Gynecologists practice bulletin no (2019). 202 Summary: Gestational Hypertension and Preeclampsia. *Obstet. Gynecol.* 133, 211–214. doi:10.1097/AOG.0000000000003019

American College of Obstetricians and Gynecologists (2013). Task Force on Hypertension in Pregnancy. Hypertension in Pregnancy. Report of the American College of Obstetricians and Gynecologists' Task Force on Hypertension in Pregnancy. *Obstet. Gynecol.* 122, 1122–1131. doi:10.1097/01.AOG.0000437382.03963.88

Aplin, J. D., and Ruane, P. T. (2017). Embryo-epithelium Interactions during Implantation at a Glance. *J. Cell Sci* 130, 15–22. doi:10.1242/jcs.175943

Bajoria, R., and Contractor, S. F. (2011). Effect of the Size of Liposomes on the Transfer and Uptake of Carboxyfluorescein by the Perfused Human Term Placenta. *J. Pharm. Pharmacol.* 49, 675–681. doi:10.1111/j.2042-7158.1997.tb06091.x

Baker, J., Liu, J.-P., Robertson, E. J., and Efstratiadis, A. (1993). Role of Insulin-like Growth Factors in Embryonic and Postnatal Growth. *Cell* 75, 73–82. doi:10.1016/s0092-8674(05)80085-6

Bamrungsap, S., Zhao, Z., Chen, T., Wang, L., Li, C., Fu, T., et al. (2012). Nanotechnology in Therapeutics: a Focus on Nanoparticles as a Drug Delivery System. *Nanomedicine* 7, 1253–1271. doi:10.2217/nnm.12.87

Bawarski, W. E., Chidlowsky, E., Bharali, D. J., and Mousa, S. A. (2008). Emerging Nanopharmaceuticals. *Nanomedicine: Nanotechnology, Biol. Med.* 4, 273–282. doi:10.1016/j.nano.2008.06.002

Beards, F., Jones, L. E., Charnock, J., Forbes, K., and Harris, L. K. (2017). Placental Homing Peptide-microRNA Inhibitor Conjugates for Targeted Enhancement of Intrinsic Placental Growth Signaling. *Theranostics* 7, 2940–2955. doi:10.7150/thno.18845

Blanco, E., Shen, H., and Ferrari, M. (2015). Principles of Nanoparticle Design for Overcoming Biological Barriers to Drug Delivery. *Nat. Biotechnol.* 33, 941–951. doi:10.1038/nbt.3330

Brosens, I., Pijnenborg, R., Vercruysse, L., and Romero, R. (2011). The "Great Obstetrical Syndromes" Are Associated with Disorders of Deep Placentation. *Am. J. Obstet. Gynecol.* 204, 193–201. doi:10.1016/j.ajog.2010.08.009

Brown, S. B., Wang, L., Jungels, R. R., and Sharma, B. (2020). Effects of Cartilage-Targeting Moieties on Nanoparticle Biodistribution in Healthy and Osteoarthritic Joints. *Acta Biomater.* 101, 469–483. doi:10.1016/j.actbio.2019.10.003

Burns, K., Duggan, B., Atkinson, E. A., Famulski, K. S., Nemer, M., Bleackley, R. C., et al. (1994). Modulation of Gene Expression by Calreticulin Binding to the Glucocorticoid Receptor. *Nature* 367, 476–480. doi:10.1038/367476a0

Burton, G. J., Redman, C. W., Roberts, J. M., and Moffett, A. (2019). Pre-eclampsia: Pathophysiology and Clinical Implications. *Bmj* 366, l2381. doi:10.1136/bmj.l2381

Caldorera-Moore, M., Vela Ramirez, J. E., and Peppas, N. A. (2019). Transport and Delivery of Interferon-α through Epithelial Tight Junctions via pH-Responsive Poly(methacrylic Acid-Grafted-Ethylene Glycol) Nanoparticles. *J. Drug Target.* 27, 582–589. doi:10.1080/1061186x.2018.1547732

Cañas, D., Herrera, E. A., García-Herrera, C., Celentano, D., and Krause, B. J. (2017). Fetal Growth Restriction Induces Heterogeneous Effects on Vascular Biomechanical and Functional Properties in Guinea Pigs (*Cavia porcellus*). *Front. Physiol.* 8, 144. doi:10.3389/fphys.2017.00144

Carr, H., Cnattingius, S., Granath, F., Ludvigsson, J. F., and Edstedt Bonamy, A.-K. (2017). Preterm Birth and Risk of Heart Failure up to Early Adulthood. *J. Am. Coll. Cardiol.* 69, 2634–2642. doi:10.1016/j.jacc.2017.03.572

Chappell, L. C., and David, A. L. (2016). Improving the Pipeline for Developing and Testing Pharmacological Treatments in Pregnancy. *Plos Med.* 13, e1002161. doi:10.1371/journal.pmed.1002161

Chiang, W.-F., Hwang, T.-Z., Hour, T.-C., Wang, L.-H., Chiu, C.-C., Chen, H.-R., et al. (2013). Calreticulin, an Endoplasmic Reticulum-Resident Protein, Is Highly Expressed and Essential for Cell Proliferation and Migration in Oral Squamous Cell Carcinoma. *Oral Oncol.* 49, 534–541. doi:10.1016/j.oraloncology.2013.01.003

Cindrova-Davies, T., Sanders, D. A., Burton, G. J., and Charnock-Jones, D. S. (2011). Soluble FLT1 Sensitizes Endothelial Cells to Inflammatory Cytokines by Antagonizing VEGF Receptor-Mediated Signalling. *Cardiovasc. Res.* 89, 671–679. doi:10.1093/cvr/cvq346

Conner, S. D., and Schmid, S. L. (2003). Regulated Portals of Entry into the Cell. *Nature* 422, 37–44. doi:10.1038/nature01451

Cureton, N., Korotkova, I., Baker, B., Greenwood, S., Wareing, M., Kotamraju, V. R., et al. (2017). Selective Targeting of a Novel Vasodilator to the Uterine Vasculature to Treat Impaired Uteroplacental Perfusion in Pregnancy. *Theranostics* 7, 3715–3731. doi:10.7150/thno.19678

Dimasuay, K. G., Boeuf, P., Powell, T. L., and Jansson, T. (2016). Placental Responses to Changes in the Maternal Environment Determine Fetal Growth. *Front. Physiol.* 7, 12. doi:10.3389/fphys.2016.00012

Duncan, R. (2006). Polymer Conjugates as Anticancer Nanomedicines. *Nat. Rev. Cancer* 6, 688–701. doi:10.1038/nrc1958

Erlandsson, L., Masoumi, Z., Hansson, L. R., and Hansson, S. R. (2021). The Roles of Free Iron, Heme, Haemoglobin, and the Scavenger Proteins Haemopexin and Alpha-1-microglobulin in Preeclampsia and Fetal Growth Restriction. *J. Intern. Med.* 290, 952–968. doi:10.1111/joim.13349

Esfand, R., and Tomalia, D. A. (2001). Poly(amidoamine) (PAMAM) Dendrimers: from Biomimicry to Drug Delivery and Biomedical Applications. *Drug Discov. Today* 6, 427–436. doi:10.1016/s1359-6446(01)01757-3

Etrych, T., Kovář, L., Strohalm, J., Chytil, P., Říhová, B., and Ulbrich, K. (2011). Biodegradable star HPMA Polymer-Drug Conjugates: Biodegradability, Distribution and Anti-tumor Efficacy. *J. Controlled Release* 154, 241–248. doi:10.1016/j.jconrel.2011.06.015

Evseenko, D., Paxton, J. W., and Keelan, J. A. (2006). Active Transport across the Human Placenta: Impact on Drug Efficacy and Toxicity. *Expert Opin. Drug Metab. Toxicol.* 2, 51–69. doi:10.1517/17425255.2.1.51

Fant, M., Farina, A., Nagaraja, R., and Schlessinger, D. (2010). PLAC1 (Placenta-specific 1): a Novel, X-Linked Gene with Roles in Reproductive and Cancer Biology. *Prenat. Diagn.* 30, 497–502. doi:10.1002/pd.2506

Fenton, O. S., Olafson, K. N., Pillai, P. S., Mitchell, M. J., and Langer, R. (2018). Advances in Biomaterials for Drug Delivery. *Adv. Mater.* 30, 1705328. doi:10.1002/adma.201705328

Ferretti, C., Bruni, L., Dangles-Marie, V., Pecking, A. P., and Bellet, D. (2007). Molecular Circuits Shared by Placental and Cancer Cells, and Their Implications in the Proliferative, Invasive and Migratory Capacities of Trophoblasts. *Hum. Reprod. Update* 13, 121–141. doi:10.1093/humupd/dml048

Fidler, I. J. (2003). The Pathogenesis of Cancer Metastasis: the 'seed and Soil' Hypothesis Revisited. *Nat. Rev. Cancer* 3, 453–458. doi:10.1038/nrc1098

Fogal, V., Zhang, L., Krajewski, S., and Ruoslahti, E. (2008). Mitochondrial/cell-surface Protein p32/gC1qR as a Molecular Target in Tumor Cells and Tumor Stroma. *Cancer Res.* 68, 7210–7218. doi:10.1158/0008-5472.can-07-6752

Fonseca-Santos, B., Chorilli, M., and Palmira Daflon Gremião, M. (2015). Nanotechnology-based Drug Delivery Systems for the Treatment of Alzheimer's Disease. *Ijn* 10, 4981–5003. doi:10.2147/ijn.s87148

Ganguly, E., Hula, N., Spaans, F., Cooke, C.-L. M., and Davidge, S. T. (2020). Placenta-targeted Treatment Strategies: An Opportunity to Impact Fetal Development and Improve Offspring Health Later in Life. *Pharmacol. Res.* 157, 104836. doi:10.1016/j.phrs.2020.104836

Genbacev, O., and Miller, R. K. (2000). Post-implantation Differentiation and Proliferation of Cytotrophoblast Cells: *In Vitro* Models-A Review. *Placenta* 21 (Suppl. A), S45–S49. doi:10.1053/plac.1999.0523

Glue, P., Fang, J. W., Rouzier-Panis, R., Raffanel, C., Sabo, R., Gupta, S. K., et al. (2000). Pegylated Interferon-A2b: Pharmacokinetics, Pharmacodynamics, Safety, and Preliminary Efficacy Data. *Clin. Pharmacol. Ther.* 68, 556–567. doi:10.1067/mcp.2000.110973

Grafmueller, S., Manser, P., Diener, L., Diener, P.-A., Maeder-Althaus, X., Maurizi, L., et al. (2015). Bidirectional Transfer Study of Polystyrene Nanoparticles across the Placental Barrier in an *Ex Vivo* Human Placental Perfusion Model. *Environ. Health Perspect.* 123, 1280–1286. doi:10.1289/ehp.1409271

Gref, R., Minamitake, Y., Peracchia, M. T., Trubetskoy, V., Torchilin, V., and Langer, R. (1994). Biodegradable Long-Circulating Polymeric Nanospheres. *Science* 263, 1600–1603. doi:10.1126/science.8128245

Hammers, A. L., Sanchez-Ramos, L., and Kaunitz, A. M. (2015). Antenatal Exposure to Indomethacin Increases the Risk of Severe Intraventricular Hemorrhage, Necrotizing Enterocolitis, and Periventricular Leukomalacia: a Systematic Review with Metaanalysis. *Am. J. Obstet. Gynecol.* 212, e1–505. doi:10.1016/j.ajog.2014.10.1091

He, C., Yue, H., Xu, L., Liu, Y., Song, Y., Tang, C., et al. (2020). siRNA Release Kinetics from Polymeric Nanoparticles Correlate with RNAi Efficiency and Inflammation Therapy via Oral Delivery. *Acta Biomater.* 103, 213–222. doi:10.1016/j.actbio.2019.12.005

Hillaireau, H., and Couvreur, P. (2009). Nanocarriers' Entry into the Cell: Relevance to Drug Delivery. *Cell. Mol. Life Sci.* 66, 2873–2896. Epub 2009 Jun 5. doi:10.1007/s00018-009-0053-z

Holtan, S. G., Creedon, D. J., Haluska, P., and Markovic, S. N. (2009). Cancer and Pregnancy: Parallels in Growth, Invasion, and Immune Modulation and Implications for Cancer Therapeutic Agents. *Mayo Clinic Proc.* 84, 985–1000. doi:10.1016/s0025-6196(11)60669-110.4065/84.11.985

Ives, C. W., Sinkey, R., Rajapreyar, I., Tita, A. T. N., and Oparil, S. (2020). Preeclampsia-Pathophysiology and Clinical Presentations. *J. Am. Coll. Cardiol.* 76, 1690–1702. doi:10.1016/j.jacc.2020.08.014

Jauniaux, E., Collins, S., and Burton, G. J. (2018). Placenta Accreta Spectrum: Pathophysiology and Evidence-Based Anatomy for Prenatal Ultrasound Imaging. *Am. J. Obstet. Gynecol.* 218, 75–87. doi:10.1016/j.ajog.2017.05.067

Jones, H., Crombleholme, T., and Habli, M. (2014). Regulation of Amino Acid Transporters by Adenoviral-Mediated Human Insulin-like Growth Factor-1 in a Mouse Model of Placental Insufficiency *In Vivo* and the Human Trophoblast Line BeWo *In Vitro*. *Placenta* 35, 132–138. doi:10.1016/j.placenta.2013.11.012

Jones, H. N., Crombleholme, T., and Habli, M. (2013). Adenoviral-mediated Placental Gene Transfer of IGF-1 Corrects Placental Insufficiency via Enhanced Placental Glucose Transport Mechanisms. *PLoS One* 8, e74632. doi:10.1371/journal.pone.0074632

Jose, S. (2019). Transferrin-Conjugated Docetaxel-PLGA Nanoparticles for Tumor Targeting: Influence on MCF-7 Cell Cycle. *Polymers* 11, 1905. doi:10.3390/polym11111905

Kang, Y.-J., Lees, M., Matthews, L. C., Kimber, S. J., Forbes, K., and Aplin, J. D. (2015). MiR-145 Suppresses Embryo-Epithelial Juxtacrine Communication at Implantation by Modulating Maternal IGF1R. *J. Cell Sci* 128, 804–814. doi:10.1242/jcs.164004

Kannan, R. M., and Kannan, S. (2017). Emerging Nanomedicine Approaches in Obstetrics. *Am. J. Obstet. Gynecol.* 216, 201–203. doi:10.1016/j.ajog.2017.01.038

Kannan, R. M., Nance, E., Kannan, S., and Tomalia, D. A. (2014). Emerging Concepts in Dendrimer-Based Nanomedicine: from Design Principles to Clinical Applications. *J. Intern. Med.* 276, 579–617. doi:10.1111/joim.12280

Khalin, I., Alyautdin, R., Ismail, N. M., Haron, M. H., and Kuznetsov, D. (2014). Nanoscale Drug Delivery Systems and the Blood–Brain Barrier. *Ijn* 9, 795–811. doi:10.2147/ijn.s52236

Kim, B. Y. S., Rutka, J. T., and Chan, W. C. W. (2010). Nanomedicine. *N. Engl. J. Med.* 363, 2434–2443. doi:10.1056/NEJMra0912273

King, A., Ndifon, C., Lui, S., Widdows, K., Kotamraju, V. R., Agemy, L., et al. (2016). Tumor-homing Peptides as Tools for Targeted Delivery of Payloads to the Placenta. *Sci. Adv.* 2, e1600349. doi:10.1126/sciadv.1600349

Knight, F. C., Gilchuk, P., Kumar, A., Becker, K. W., Sevimli, S., Jacobson, M. E., et al. (2019). Mucosal Immunization with a pH-Responsive Nanoparticle Vaccine Induces Protective CD8+ Lung-Resident Memory T Cells. *ACS Nano* 13, 10939–10960. doi:10.1021/acsnano.9b00326

Lager, S., and Powell, T. L. (2012). Regulation of Nutrient Transport across the Placenta. *J. Pregnancy* 2012, 1–14. doi:10.1155/2012/179827

Le, Z., Chen, Y., Han, H., Tian, H., Zhao, P., Yang, C., et al. (2018). Hydrogen-Bonded Tannic Acid-Based Anticancer Nanoparticle for Enhancement of Oral Chemotherapy. *ACS Appl. Mater. Inter.* 10, 42186–42197. doi:10.1021/acsami.8b18979

Lee, C. C., MacKay, J. A., Fréchet, J. M. J., and Szoka, F. C. (2005). Designing Dendrimers for Biological Applications. *Nat. Biotechnol.* 23, 1517–1526. doi:10.1038/nbt1171

Li, L., Li, H., Xue, J., Chen, P., Zhou, Q., and Zhang, C. (2020a). Nanoparticle-Mediated Simultaneous Downregulation of Placental Nrf2 and sFlt1 Improves Maternal and Fetal Outcomes in a Preeclampsia Mouse Model. *ACS Biomater. Sci. Eng.* 6, 5866–5873. doi:10.1021/acsbiomaterials.0c00826

Li, L., Yang, H., Chen, P., Xin, T., Zhou, Q., Wei, D., et al. (2020b). Trophoblast-Targeted Nanomedicine Modulates Placental sFLT1 for Preeclampsia Treatment. *Front. Bioeng. Biotechnol.* 8, 64. doi:10.3389/fbioe.2020.00064

Lorincz, M. C., and Schübeler, D. (2017). Evidence for Converging DNA Methylation Pathways in Placenta and Cancer. *Developmental Cell* 43, 257–258. doi:10.1016/j.devcel.2017.10.009

Lowis, S., Lewis, I., Lewis, I., Elsworth, A., Weston, C., Doz, F., et al. (2006). A Phase I Study of Intravenous Liposomal Daunorubicin (DaunoXome) in Paediatric Patients with Relapsed or Resistant Solid Tumours. *Br. J. Cancer* 95, 571–580. doi:10.1038/sj.bjc.6603288

Major, C. A., Lewis, D. F., Harding, J. A., Porto, M. A., and Garite, T. J. (1994). Tocolysis with Indomethacin Increases the Incidence of Necrotizing Enterocolitis in the Low-Birth-Weight Neonate. *Am. J. Obstet. Gynecol.* 170, 102–106. doi:10.1016/s0002-9378(94)70392-2

Majzoub, R. N., Ewert, K. K., and Safinya, C. R. (2016). Cationic Liposome-Nucleic Acid Nanoparticle Assemblies with Applications in Gene Delivery and Gene Silencing. *Phil. Trans. R. Soc. A.* 374, 20150129. doi:10.1098/rsta.2015.0129

Malek, A., Sager, R., Zakher, A., and Schneider, H. (1995). Transport of Immunoglobulin G and its Subclasses across the In Vitro-perfused Human Placenta. *Am. J. Obstet. Gynecol.* 173, 760–767. doi:10.1016/0002-9378(95)90336-4

Matos, P., Horn, J. A., Beards, F., Lui, S., Desforges, M., and Harris, L. K. (2014). A Role for the Mitochondrial-Associated Protein P32 in Regulation of Trophoblast Proliferation. *Mol. Hum. Reprod.* 20, 745–755. doi:10.1093/molehr/gau039

McIntyre, K. R., Vincent, K. M. M., Hayward, C. E., Li, X., Sibley, C. P., Desforges, M., et al. (2020). Human Placental Uptake of Glutamine and Glutamate Is Reduced in Fetal Growth Restriction. *Sci. Rep.* 10, 16197. doi:10.1038/s41598-020-72930-7

Menezes, V., Malek, A., and A. Keelan, J. (2011). Nanoparticulate Drug Delivery in Pregnancy: Placental Passage and Fetal Exposure. *Cpb* 12, 731–742. doi:10.2174/138920111795471010

Menjoge, A. R., Kannan, R. M., and Tomalia, D. A. (2010a). Dendrimer-based Drug and Imaging Conjugates: Design Considerations for Nanomedical Applications. *Drug Discov. Today* 15, 171–185. doi:10.1016/j.drudis.2010.01.009

Menjoge, A. R., Navath, R. S., Asad, A., Kannan, S., Kim, C. J., Romero, R., et al. (2010b). Transport and Biodistribution of Dendrimers across Human Fetal Membranes: Implications for Intravaginal Administration of Dendrimer-Drug Conjugates. *Biomaterials* 31, 5007–5021. doi:10.1016/j.biomaterials.2010.02.075

Menjoge, A. R., Rinderknecht, A. L., Navath, R. S., Faridnia, M., Kim, C. J., Romero, R., et al. (2011). Transfer of PAMAM Dendrimers across Human Placenta: Prospects of its Use as Drug Carrier during Pregnancy. *J. Controlled Release* 150, 326–338. doi:10.1016/j.jconrel.2010.11.023

Mihaly, G. W., and Morgan, D. J. (1983). Placental Drug Transfer: Effects of Gestational Age and Species. *Pharmacol. Ther.* 23, 253–266. doi:10.1016/0163-7258(83)90015-3

Mitchell, A. A., Gilboa, S. M., Werler, M. M., Kelley, K. E., Louik, C., and Hernández-Díaz, S. (2011). Medication Use during Pregnancy, with Particular Focus on Prescription Drugs: 1976-2008. *Am. J. Obstet. Gynecol.* 205, e1–51. doi:10.1016/j.ajog.2011.02.029

Morton, P. D., Ishibashi, N., and Jonas, R. A. (2017). Neurodevelopmental Abnormalities and Congenital Heart Disease. *Circ. Res.* 120, 960–977. doi:10.1161/circresaha.116.309048

Myc, A., Kukowska-Latallo, J., Cao, P., Swanson, B., Battista, J., Dunham, T., et al. (2010). Targeting the Efficacy of a Dendrimer-Based Nanotherapeutic in Heterogeneous Xenograft Tumors *In Vivo*. *Anticancer Drugs* 21, 186–192. doi:10.1097/CAD.0b013e328334560f

Myllynen, P. K., Loughran, M. J., Howard, C. V., Sormunen, R., Walsh, A. A., and Vähäkangas, K. H. (2008). Kinetics of Gold Nanoparticles in the Human Placenta. *Reprod. Toxicol.* 26, 130–137. doi:10.1016/j.reprotox.2008.06.008

Najlah, M., and Demanuele, A. (2006). Crossing Cellular Barriers Using Dendrimer Nanotechnologies. *Curr. Opin. Pharmacol.* 6, 522–527. doi:10.1016/j.coph.2006.05.004

Najlah, M., Freeman, S., Attwood, D., and D'Emanuele, A. (2007). *In Vitro* evaluation of Dendrimer Prodrugs for Oral Drug Delivery. *Int. J. Pharmaceutics* 336, 183–190. doi:10.1016/j.ijpharm.2006.11.047

Napso, T., Yong, H. E. J., Lopez-Tello, J., and Sferruzzi-Perri, A. N. (2018). The Role of Placental Hormones in Mediating Maternal Adaptations to Support Pregnancy and Lactation. *Front. Physiol.* 9, 1091. doi:10.3389/fphys.2018.01091

Nel, A. E., Mädler, L., Velegol, D., Xia, T., Hoek, E. M. V., Somasundaran, P., et al. (2009). Understanding Biophysicochemical Interactions at the Nano-Bio Interface. *Nat. Mater* 8, 543–557. doi:10.1038/nmat2442

Palmerston Mendes, L., Pan, J., and Torchilin, V. (2017). Dendrimers as Nanocarriers for Nucleic Acid and Drug Delivery in Cancer Therapy. *Molecules* 22, 1401. doi:10.3390/molecules22091401

Park, J. W. (2002). Liposome-based Drug Delivery in Breast Cancer Treatment. *Breast Cancer Res.* 4, 95–99. doi:10.1186/bcr432

Peer, D., Karp, J. M., Hong, S., Farokhzad, O. C., Margalit, R., and Langer, R. (2007). Nanocarriers as an Emerging Platform for Cancer Therapy. *Nat. Nanotech* 2, 751–760. doi:10.1038/nnano.2007.387

Phillips, T. J., Scott, H., Menassa, D. A., Bignell, A. L., Sood, A., Morton, J. S., et al. (2017). Treating the Placenta to Prevent Adverse Effects of Gestational Hypoxia on Fetal Brain Development. *Sci. Rep.* 7, 9079. doi:10.1038/s41598-017-06300-1

Pijnenborg, R., Vercruysse, L., and Hanssens, M. (2006). The Uterine Spiral Arteries in Human Pregnancy: Facts and Controversies. *Placenta* 27, 939–958. doi:10.1016/j.placenta.2005.12.006

Powe, C. E., Levine, R. J., and Karumanchi, S. A. (2011). Preeclampsia, a Disease of the Maternal Endothelium. *Circulation* 123, 2856–2869. doi:10.1161/circulationaha.109.853127

Pritchard, N., Kaitu'u-Lino, T. u., Harris, L., Tong, S., and Hannan, N. (2021). Nanoparticles in Pregnancy: the Next Frontier in Reproductive Therapeutics. *Hum. Reprod. Update* 27, 280–304. doi:10.1093/humupd/dmaa049

Rana, S., Lemoine, E., Granger, J. P., and Karumanchi, S. A. (2019). Preeclampsia. *Circ. Res.* 124, 1094–1112. doi:10.1161/circresaha.118.313276

Rawn, S. M., and Cross, J. C. (2008). The Evolution, Regulation, and Function of Placenta-specific Genes. *Annu. Rev. Cell Dev. Biol.* 24, 159–181. doi:10.1146/annurev.cellbio.24.110707.175418

Redman, C. W. G. (1992). 10 Immunological Aspects of Pre-eclampsia. *Baillière's Clin. Obstet. Gynaecol.* 6, 601–615. doi:10.1016/s0950-3552(05)80012-4

Rosen, O., Müller, H. J., Gökbuget, N., Langer, W., Peter, N., Schwartz, S., et al. (2003). Pegylated Asparaginase in Combination with High-Dose Methotrexate for Consolidation in Adult Acute Lymphoblastic Leukaemia in First Remission: a Pilot Study. *Br. J. Haematol.* 123, 836–841. doi:10.1046/j.1365-2141.2003.04707.x

Ruane, P. T., Berneau, S. C., Koeck, R., Watts, J., Kimber, S. J., Brison, D. R., et al. (2017). Apposition to Endometrial Epithelial Cells Activates Mouse Blastocysts for Implantation. *Mol. Hum. Reprod.* 23, 617–627. doi:10.1093/molehr/gax043

Ruoslahti, E., Bhatia, S. N., and Sailor, M. J. (2010). Targeting of Drugs and Nanoparticles to Tumors. *J. Cell Biol* 188, 759–768. doi:10.1083/jcb.200910104

Sabbatini, P., Aghajanian, C., Dizon, D., Anderson, S., Dupont, J., Brown, J. V., et al. (2004). Phase II Study of CT-2103 in Patients with Recurrent Epithelial Ovarian, Fallopian Tube, or Primary Peritoneal Carcinoma. *Jco* 22, 4523–4531. doi:10.1200/jco.2004.12.043

Sarfraz, M., Afzal, A., Yang, T., Gai, Y., Raza, S., Khan, M., et al. (2018). Development of Dual Drug Loaded Nanosized Liposomal Formulation by A Reengineered Ethanolic Injection Method and its Pre-clinical Pharmacokinetic Studies. *Pharmaceutics* 10, 151. doi:10.3390/pharmaceutics10030151

Saunders, M. (2009). Transplacental Transport of Nanomaterials. *WIREs: Nanmed Nanobiotech* 1, 671–684. doi:10.1002/wnan.53

Sedighi, M., Sieber, S., Rahimi, F., Shahbazi, M.-A., Rezayan, A. H., Huwyler, J., et al. (2019). Rapid Optimization of Liposome Characteristics Using a Combined Microfluidics and Design-Of-experiment Approach. *Drug Deliv. Transl. Res.* 9, 404–413. doi:10.1007/s13346-018-0587-4

Sercombe, L., Veerati, T., Moheimani, F., Wu, S. Y., Sood, A. K., and Hua, S. (2015). Advances and Challenges of Liposome Assisted Drug Delivery. *Front. Pharmacol.* 6, 286. doi:10.3389/fphar.2015.00286

Sharma, D., Shastri, S., and Sharma, P. (2016). Intrauterine Growth Restriction: Antenatal and Postnatal Aspects. *Clin. Med. Insights Pediatr.* 10, CMPed.S40070–83. doi:10.4137/CMPed.S40070

Shi, Z., Hou, W., Hua, X., Zhang, X., Liu, X., Wang, X., et al. (2012). Overexpression of Calreticulin in Pre-eclamptic Placentas: Effect on Apoptosis, Cell Invasion and Severity of Pre-eclampsia. *Cell Biochem Biophys* 63, 183–189. doi:10.1007/s12013-012-9350-5

Smith, Z. D., Shi, J., Gu, H., Donaghey, J., Clement, K., Cacchiarelli, D., et al. (2017). Epigenetic Restriction of Extraembryonic Lineages Mirrors the Somatic Transition to Cancer. *Nature* 549, 543–547. doi:10.1038/nature23891

Sood, B. G., Lulic-Botica, M., Holzhausen, K. A., Pruder, S., Kellogg, H., Salari, V., et al. (2011). The Risk of Necrotizing Enterocolitis after Indomethacin Tocolysis. *Pediatrics* 128, e54–e62. doi:10.1542/peds.2011-0265

Strand, M. S., Krasnick, B. A., Pan, H., Zhang, X., Bi, Y., Brooks, C., et al. (2019). Precision Delivery of RAS-Inhibiting siRNA to KRAS Driven Cancer via Peptide-Based Nanoparticles. *Oncotarget* 10, 4761–4775. doi:10.18632/oncotarget.27109

Suarez, V. R., Thompson, L. L., Jain, V., Olson, G. L., Hankins, G. D. V., Belfort, M. A., et al. (2002). The Effect of In Utero Exposure to Indomethacin on the Need for Surgical Closure of a Patent Ductus Arteriosus in the Neonate. *Am. J. Obstet. Gynecol.* 187, 886–888. doi:10.1067/mob.2002.127464

Sugahara, K. N., Teesalu, T., Karmali, P. P., Kotamraju, V. R., Agemy, L., Girard, O. M., et al. (2009). Tissue-penetrating Delivery of Compounds and Nanoparticles into Tumors. *Cancer Cell* 16, 510–520. doi:10.1016/j.ccr.2009.10.013

Suk, J. S., Xu, Q., Kim, N., Hanes, J., and Ensign, L. M. (2016). PEGylation as a Strategy for Improving Nanoparticle-Based Drug and Gene Delivery. *Adv. Drug Deliv. Rev.* 99, 28–51. doi:10.1016/j.addr.2015.09.012

Sutherland, A. E., Calarco, P. G., and Damsky, C. H. (1993). Developmental Regulation of Integrin Expression at the Time of Implantation in the Mouse Embryo. *Development* 119, 1175–1186. doi:10.1242/dev.119.4.1175

Svenson, S., and Tomalia, D. (2005). Dendrimers in Biomedical Applications-Reflections on the Field. *Adv. Drug Deliv. Rev.* 57, 2106–2129. doi:10.1016/j.addr.2005.09.018

Syme, M. R., Paxton, J. W., and Keelan, J. A. (2004). Drug Transfer and Metabolism by the Human Placenta. *Clin. Pharmacokinet.* 43, 487–514. doi:10.2165/00003088-200443080-00001

Tal, R., Shaish, A., Barshack, I., Polak-Charcon, S., Afek, A., Volkov, A., et al. (2010). Effects of Hypoxia-Inducible Factor-1α Overexpression in Pregnant Mice. *Am. J. Pathol.* 177, 2950–2962. doi:10.2353/ajpath.2010.090800

Troja, W., Kil, K., Klanke, C., and Jones, H. N. (2014). Interaction between Human Placental Microvascular Endothelial Cells and a Model of Human Trophoblasts: Effects on Growth Cycle and Angiogenic Profile. *Physiol. Rep.* 2, e00244. doi:10.1002/phy2.244

Vafaei-Pour, Z., Shokrzadeh, M., Jahani, M., and Shaki, F. (2018). Embryo-Protective Effects of Cerium Oxide Nanoparticles against Gestational Diabetes in Mice. *Iran J. Pharm. Res.* 17, 964–975.

Valero, L., Alhareth, K., Espinoza Romero, J., Viricel, W., Leblond, J., Chissey, A., et al. (2018). Liposomes as Gene Delivery Vectors for Human Placental Cells. *Molecules* 23, 1085. doi:10.3390/molecules23051085

Valero, L., Alhareth, K., Gil, S., Simasotchi, C., Roques, C., Scherman, D., et al. (2017). Assessment of Dually Labelled PEGylated Liposomes Transplacental Passage and Placental Penetration Using a Combination of Two Ex-Vivo Human Models: the Dually Perfused Placenta and the Suspended Villous Explants. *Int. J. Pharmaceutics* 532, 729–737. doi:10.1016/j.ijpharm.2017.07.076

Vanderpuye, O. A., Labarrere, C. A., and McIntyre, J. A. (1991). A Vitronectin-Receptor-Related Molecule in Human Placental brush Border Membranes. *Biochem. J.* 280 (Pt 1), 9–17. doi:10.1042/bj2800009

Vermillion, S. T., Scardo, J. A., Lashus, A. G., and Wiles, H. B. (1997). The Effect of Indomethacin Tocolysis on Fetal Ductus Arteriosus Constriction with Advancing Gestational Age. *Am. J. Obstet. Gynecol.* 177, 256–261. discussion 259-61. doi:10.1016/s0002-9378(97)70184-4

Vidmar, J., Loeschner, K., Correia, M., Larsen, E. H., Manser, P., Wichser, A., et al. (2018). Translocation of Silver Nanoparticles in Theex Vivohuman Placenta Perfusion Model Characterized by Single Particle ICP-MS. *Nanoscale* 10, 11980–11991. doi:10.1039/c8nr02096e

Volpatti, L. R., Matranga, M. A., Cortinas, A. B., Delcassian, D., Daniel, K. B., Langer, R., et al. (2020). Glucose-Responsive Nanoparticles for Rapid and Extended Self-Regulated Insulin Delivery. *ACS Nano* 14, 488–497. doi:10.1021/acsnano.9b06395

Waisman, D. M., Salimath, B. P., and Anderson, M. J. (1985). Isolation and Characterization of CAB-63, a Novel Calcium-Binding Protein. *J. Biol. Chem.* 260, 1652–1660. doi:10.1016/s0021-9258(18)89644-2

Wang, X.-W., Gu, J.-Y., Li, Z., Song, Y.-F., Wu, W.-S., and Hou, Y.-P. (2010). Gestational Age and Dose Influence on Placental Transfer of 63Ni in Rats. *Placenta* 31, 305–311. doi:10.1016/j10.1016/j.placenta.2010.01.015

Wilson, R. L., Owens, K., Sumser, E. K., Fry, M. V., Stephens, K. K., Chuecos, M., et al. (2020). Nanoparticle Mediated Increased Insulin-like Growth Factor 1 Expression Enhances Human Placenta Syncytium Function. *Placenta* 93, 1–7. doi:10.1016/j.placenta.2020.02.006

Wolinsky, J., and Grinstaff, M. (2008). Therapeutic and Diagnostic Applications of Dendrimers for Cancer Treatment☆. *Adv. Drug Deliv. Rev.* 60, 1037–1055. doi:10.1016/j.addr.2008.02.012

Xu, J., Luft, J. C., Yi, X., Tian, S., Owens, G., Wang, J., et al. (2013). RNA Replicon Delivery via Lipid-Complexed PRINT Protein Particles. *Mol. Pharmaceutics* 10, 3366–3374. doi:10.1021/mp400190z

Xu, L., Zhang, H., and Wu, Y. (2014). Dendrimer Advances for the central Nervous System Delivery of Therapeutics. *ACS Chem. Neurosci.* 5, 2–13. doi:10.1021/cn400182z

Yang, H., Sun, C., Fan, Z., Tian, X., Yan, L., Du, L., et al. (2012). Effects of Gestational Age and Surface Modification on Materno-Fetal Transfer of Nanoparticles in Murine Pregnancy. *Sci. Rep.* 2, 847. doi:10.1038/srep00847

Yu, J., Jia, J., Guo, X., Chen, R., and Feng, L. (2017). Modulating Circulating sFlt1 in an Animal Model of Preeclampsia Using PAMAM Nanoparticles for siRNA Delivery. *Placenta* 58, 1–8. doi:10.1016/j.placenta.2017.07.360

Zhang, B., Tan, L., Yu, Y., Wang, B., Chen, Z., Han, J., et al. (2018). Placenta-specific Drug Delivery by Trophoblast-Targeted Nanoparticles in Mice. *Theranostics* 8, 2765–2781. doi:10.7150/thno.22904

Zhang, C.-x., Cheng, Y., Liu, D.-z., Liu, M., Cui, H., Zhang, B.-l., et al. (2019). Mitochondria-targeted Cyclosporin A Delivery System to Treat Myocardial Ischemia Reperfusion Injury of Rats. *J. Nanobiotechnol* 17, 18. doi:10.1186/s12951-019-0451-9

Zhang, L., Beatty, A., Lu, L., Abdalrahman, A., Makris, T. M., Wang, G., et al. (2020). Microfluidic-assisted Polymer-Protein Assembly to Fabricate Homogeneous Functionalnanoparticles. *Mater. Sci. Eng. C* 111, 110768. doi:10.1016/j.msec.2020.110768

Zhou, Y., Fisher, S. J., Janatpour, M., Genbacev, O., Dejana, E., Wheelock, M., et al. (1997). Human Cytotrophoblasts Adopt a Vascular Phenotype as They Differentiate. A Strategy for Successful Endovascular Invasion? *J. Clin. Invest.* 99, 2139–2151. doi:10.1172/jci119387

Zylberberg, C., and Matosevic, S. (2016). Pharmaceutical Liposomal Drug Delivery: a Review of New Delivery Systems and a Look at the Regulatory Landscape. *Drug Deliv.* 23, 3319–3329. doi:10.1080/10717544.2016.1177136

Conflict of Interest: The authors declare that the research was conducted in the absence of any commercial or financial relationships that could be construed as a potential conflict of interest.

Publisher's Note: All claims expressed in this article are solely those of the authors and do not necessarily represent those of their affiliated organizations, or those of the publisher, the editors, and the reviewers. Any product that may be evaluated in this article, or claim that may be made by its manufacturer, is not guaranteed or endorsed by the publisher.

frontiers | Frontiers in Bioengineering and Biotechnology

ORIGINAL RESEARCH
published: 06 April 2022
doi: 10.3389/fbioe.2022.874827

Preparation and Evaluation of Liposomes and Niosomes Containing Total Ginsenosides for Anti-Photoaging Therapy

Yuanyuan Jin[1†], Da Liu[1†], Zhen Lu[2], Lubing Yang[3], Jiangli Chen[1], Xuyan Zhou[1], Zhidong Qiu[1] and Ye Jin[1]**

[1]School of Pharmacy, Changchun University of Chinese Medicine, Changchun, China, [2]School of Environment and Quality Testing, Chongqing Chemical Industry Vocational College, Chongqing, China, [3]Department of Pharmacy, The Third Affiliated Hospital of Changchun University of Chinese Medicine, Changchun, China

OPEN ACCESS

Edited by:
Yongsheng Yu,
Tongji University, China

Reviewed by:
Guanyu Chen,
Sun Yat-sen University, China
Zhong-Ji Qian,
Guangdong Ocean University, China
Lesheng Teng,
Jilin University, China

***Correspondence:**
Zhidong Qiu
qzdcczy@163.com
Ye Jin
jy_ccucm@163.com

[†]These authors have contributed equally to this work

Specialty section:
This article was submitted to Biomaterials, a section of the journal Frontiers in Bioengineering and Biotechnology

Received: 13 February 2022
Accepted: 14 March 2022
Published: 06 April 2022

Citation:
Jin Y, Liu D, Lu Z, Yang L, Chen J, Zhou X, Qiu Z and Jin Y (2022) Preparation and Evaluation of Liposomes and Niosomes Containing Total Ginsenosides for Anti-Photoaging Therapy. Front. Bioeng. Biotechnol. 10:874827. doi: 10.3389/fbioe.2022.874827

Ginsenosides are the principal bioactive compounds of ginseng. Total ginsenosides (GS) contain a variety of saponin monomers, which have potent anti-photoaging activity and improve the skin barrier function. To enhance the efficiency of GS transdermal absorption, GS liposomes (GSLs) and GS niosomes (GSNs) were formulated as delivery vehicles. Based on the clarified and optimized formulation process, GSL and GSN were prepared. The structure, cumulative transmittance, skin retention, total transmittance, and bioactivity of GSLs and GSNs were characterized. GSL and GSN were shown to inhibit lipid peroxidation and increase the contents of superoxide dismutase (SOD) and glutathione peroxidase (GSH-Px) in human keratinocytes (HaCaTs). In addition, HaCAT cell migration, proliferation, and GS cellular uptake were significantly increased. The therapeutic effects of GSL and GSN were also evaluated in a rat model of photoaging. Histopathological changes were assessed in rat skin treated with GSL, GSN, or GS by hematoxylin–eosin (H&E) and aldehyde fuchsine staining. Malondialdehyde (MDA), SOD, GSH-Px, matrix metalloproteinases (MMPs), interleukin-6 (IL-6), interleukin-1β (IL-1β), and tumor necrosis factor-α (TNF-α) expression levels were determined. Results indicated that the optimal formulation of GSL used soybean lecithin (SPC) as the phospholipid, with a lipid–drug ratio of 1:0.4 and a phospholipid–cholesterol ratio of 1:3.5. The optimal temperature for the preparation process of GSN by ethanol injection was 65°C, with a ratio of the organic phase to aqueous phase of 1:9. It was demonstrated that the cumulative release rate, skin retention rate, and total transmission rate of GSL-7 at 24 h were higher than those of GSN-4 and GS. GSL-7 significantly inhibited skin lipid peroxidation caused by ultraviolet (UV) radiation. In addition, GSL-7 reduced the contents of MMPs and inflammatory cytokines in skin tissue. In conclusion, GSL-7 may reduce skin aging caused by UV radiation and contribute to skin tissue repair.

Keywords: liposomes, niosomes, total ginsenosides, transdermal delivery, photoaging

INTRODUCTION

As the body's first line of defense, the skin protects the body from external damage (Shin et al., 2021). There are generally two forms of skin aging: natural aging and photoaging (Bhattacharya et al., 2019). UV radiation is a major factor in the acceleration of both forms of skin aging by causing excessive reactive oxygen species (ROS) production (Chung 2003; Ho et al., 2005; Wolf et al., 2020). ROS can upregulate heterodimer-activated protein 1 (AP-1), which is composed of c-Fos and c-Jun proteins, by activating mitogen-activated protein kinase (MAPK), which induces the synthesis of matrix-degrading enzymes such as matrix metalloproteinase 1 (MMP-1) and matrix metalloproteinase 3 (MMP-3) (Lee et al., 2020; Mu et al., 2021; Wan et al., 2021). MMPs degrade collagen and elastin in the extracellular matrix *in vivo*. MMP-1 breaks down intact type I and III fibrillar collagen, ultimately leading to progressive senescence of fibroblasts (Rui-Zhen et al., 2004; Zhang and Tian, 2007; Zhou et al., 2021). Additionally, MMP-1 upregulates the expression of IL-6, IL-1β, and TNF-α by activating nuclear factor-κB (NF-κB), which can lead to the inflammatory infiltration of neutrophils and further production of ROS (Xiao et al., 2016; Ighodaro and Akinloye, 2018). Numerous studies have shown that natural antioxidants such as pinus densiflora (Jung et al., 2014), grape seed (Filip et al., 2013), and hawthorn (Liu S. et al., 2018) can inhibit UV radiation-induced skin photoaging by blocking MAPK and NF-κB signaling (Lu et al., 2017).

GS are the main pharmacologically active components of ginseng. More than 40 saponin monomers have been identified, of which Rb1, Rb2, Rb3, Rk3, Rg1, Re, and Rf account for approximately 70% of the GS (Ratan et al., 2021). GS have been shown to repair UV-induced skin cell damage (Jiao et al., 2021). The predominant cause of DNA damage caused by UV radiation is the formation of cyclobutane pyrimidine dimer (CPD) (Liu et al., 2021). GS significantly reduce the expression of CPD by inducing damage-specific DNA-binding protein 2 (Um et al., 2017). In addition, GS inhibit the apoptosis of damaged cells and subsequently upregulate the cellular repair cycle by modulating the expression of JNK and p53 (Bai et al., 2018). UV radiation also increases the expression of ROS and NO in skin cells, leading to DNA strand breaks, purine or pyrimidine oxidation, and lipid peroxidation (Yong et al., 2008; Salama et al., 2018). GS reduce UV-induced ROS and NO production. In addition, they may protect keratinocytes from UVB damage (Park et al., 2009). Oh et al. (2014); Oh et al. (2015); Oh et al. (2016); and Yang et al. (2020) demonstrated that GS Rb1, Rb3, and Rh2 inhibit the expression of UV-induced ROS and MMP expression. GS Rk3 may also decrease MDA expression and increase SOD and GSH-Px expression. Taken together, these results suggest that GS may have anti-photoaging properties in the skin (Nah, 2014; Zhang et al., 2014; Wan et al., 2021). However, the development and utilization of GS is limited by their low bioavailability, poor lipophilicity, and limited transdermal absorption. The most common methods of improving drug bioavailability include extending the skin surface residence time and increasing skin permeability. Selecting the appropriate dosage form may also present an effective approach to overcome these issues (Xu et al., 2003; Kang et al., 2009).

Liposomes are microvesicles composed of one or more lipid bilayers that can be used as drug delivery systems (Mao et al., 2015). Hydrophilic drugs can be embedded in the hydrophilic central region, and lipophilic drugs can be embedded in the lipid bilayers (Raj et al., 2018). Liposomes can be used for the targeted and controlled release of drugs (Rideau et al., 2018). The membrane structure of liposomes is biocompatible with the lipids in the cuticle of the skin, meaning that liposomes can enter cells or adsorb to the outer layer of target cells (Bozzuto and Molinari, 2015). Liposomes can also be metabolized and degraded by the body's metabolic enzymes, thereby reducing the risk of adverse drug reactions (Rideau et al., 2018). Thus, liposomes are often used as carriers for transdermal drug delivery to increase solubility, prevent degradation by enzymes, and prolong the release time (Gautam and Prajapati, 2012; Ahmed et al., 2019; Lu et al., 2020). Niosomes are closed bilayer structures composed of non-ionic surfactants (Gomaa et al., 2014; Vitorino et al., 2014). They have a biofilm structure similar to liposomes (Gurrapu et al., 2012; Moghassemi et al., 2015; Seleci et al., 2016; Chen et al., 2019). Because of the presence of non-ionic surfactants, niosomes have a higher stability than liposomes when stored (Abaee and Madadlou, 2016; Bi et al., 2019). Non-ionic surfactants can also enhance the transdermal absorption efficiency of drugs (Jacob et al., 2017; Barani et al., 2020; Farmoudeh et al., 2020).

TABLE 1 | Formulation optimization of GSL.

Sample	Phospholipid species	Lipid–drug ratio (n/n)	Phospholipid–cholesterol ratio (n/n)
GSL-1	SPC	1/0.2	1/2.5
GSL-2	Egg-PC	1/0.2	1/2.5
GSL-3	HSPC	1/0.2	1/2.5
GSL-4	DPPC	1/0.2	1/2.5
GSL-5	SPC	1/0.4	1/2.5
GSL-6	SPC	1/0.5	1/2.5
GSL-7	SPC	1/0.4	1/3.5
GSL-8	SPC	1/0.4	1/4.0
GSL-9	SPC	1/0.4	1/4.5

GSL, total ginsenoside liposome.

TABLE 2 | Formulation optimization of GSN.

Sample	Heating temperature (°C)	Organic phase–water phase ratio (%)
GSN-1	60	10
GSN-2	60	15
GSN-3	60	20
GSN-4	65	10
GSN-5	65	15
GSN-6	65	20
GSN-7	70	10
GSN-8	70	15
GSN-9	70	20

GSN, total ginsenoside niosome.

To explore the application of these vehicles for GS delivery, GS were embedded in liposomes and niosomes. The effects of liposomes and niosomes on the percutaneous administration of GS were evaluated using an optimized formulation process, measuring the effects of several parameters on transdermal absorption efficiency, such as particle size, ζ-potential, and encapsulation efficiency (EE%). The effects of GSL and GSN on HaCaT cells were investigated by cell proliferation, wound healing, and uptake assays. Furthermore, the therapeutic effects of GSL and GSN on rat skin photoaging were evaluated by determining the expression levels of MDA, SOD, GSH-Px, MMPs, and inflammatory cytokines in rat skin.

MATERIALS AND METHODS

Materials

GS, mannitol, fluorescein isothiocyanate (FITC), octadecylaminetech (ODA), and cholesterol were all purchased from Shanghai Yuanye Biological Co., LTD. (Shanghai, China). SPC, egg phosphatidylcholine (Egg-PC), hydrogenated soybean lecithin (HSPC), and two palmitoyl phosphatidylcholine (DPPC) were obtained from YiWeiTa Pharmaceutical Technology Co., LTD. (Shanghai, China). SOD, GSH-Px, MDA, and the bicinchoninic acid (BCA) kit were all purchased from Nanjing Jiancheng Institute of Biological Engineering, (Nanjing, China). Dicetaceumphosphate (DCP) was from Sigma-Aldrich (Shanghai, China). All enzyme-linked immunosorbent assay (ELISA) kits used in this experiment were from Jiangsu MEIMIAN Co., Ltd. (Jiangsu, China). The animals were purchased from Changchun Yisi Experimental Animal Technology Co., Ltd. (Certificate No.: SCXK (JI) -2019-0003). Other reagents were all of the analytical grade. DMEM was from Gibco (Grand Island, New York, United States). The phosphate-buffered solution (PBS), fetal bovine serum (FBS), and penicillin–streptomycin solution were obtained from Hyclone (Logan, UT, United States). The cell counting kit-8 (CCK-8) was obtained from Wuhan Boshide Biological Engineering Co. Ltd. (Wuhan, China). The HaCaT cell was from BeNa Culture Collection (Suzhou, China).

Preparation of GSL and GSN

The GSL was prepared by the ethanol injection method. Firstly, phospholipids, GS, and cholesterol were dissolved in anhydrous ethanol at a certain molar ration to form a mixture. Then, the lipid solution was slowly injected into the PBS under stirring at a volume ratio of 1/9. GSL suspension was thus obtained and anhydrous ethanol was removed by rotary evaporation. In these experiments, the formulation of GSLs was optimized by changing different prepared parameters including phospholipid species, lipid-drug ratio, and phospholipid to cholesterol ratio. The optimized parameters of GSL are shown in **Table 1**. To improve stability, the GSL suspension was freeze-dried to obtain GSL freeze-dried powder. 0.1 g of lyophilized protectant (mannitol) was added to 10 ml of GSL. After mixing, it was pre-frozen at −80°C and freeze-dried for 48 h to obtain GSL freeze-dried powder.

The preparation method of GSN was similar to that of GSL. Firstly, 79 mg of span-80, 396 mg of tween-80, 190.90 mg of cholesterol, and 10.09 mg of DCP were dissolved in a certain volume of anhydrous ethanol by ultrasonication. Then, the aforementioned mixture was mixed with GS. The GSN suspension was thus obtained and anhydrous ethanol was removed by rotary evaporation. The process parameters for GSN are shown in **Table 2**. The GSN was prepared by controlling the heating temperature and the organic phase to water phase ratio. The freeze-drying method of GSN freeze-dried powder was similar to GSL freeze-dried powder.

Characterization of GSL and GSN

In this experiment, the particle size, dispersion, and ζ-potential of GSL and GSN were determined by dynamic light scattering (DLS, Nano-ZS ZEN3600, Malvern, United Kingdom). The structure of GSL and GSN was measured by using a transmission electron microscope (TEM) at a 3-kV accelerating voltage (Japan, HITACHI H-7650). A differential scanning calorimeter (DSC, Germany, METTLER TOLEDO, DSC3) was used to evaluate the interaction between the total ginsenosides and membrane materials.

In addition to these, the concentration of GS was determined by high-performance liquid chromatography (HPLC, America, Agilent, LC-1260). The EE% of both GSL and GSN was determined by an ultracentrifugation method. The freshly prepared GSL-7 and GSN-4 were centrifuged at 4,000 rpm for 30 min and the supernatant was separated from the particles. The latter, when subtracted from the GS amount, gave the entrapped GS. The absorption wavelength of GS is 203 nm. 1.3 ml/min of acetonitrile and 0.1% of phosphate water were used as the mobile phase. The EE% of GSL and GSN were evaluated by HPLC and calculated by the following equation:

$$EE\ (\%) = 1 - W1/W2 \times 100\%, \quad (1)$$

where the content of free GS is W1 and the total content of GS in GSL or GSN is W2.

TABLE 3 | Encapsulation efficiency of GSL and GSN.

Sample	Encapsulation efficiency (%)	Sample	Encapsulation efficiency (%)
GSL-1	45.50 ± 1.07	GSN-1	28.79 ± 1.50
GSL-2	40.74 ± 1.10	GSN-2	39.14 ± 1.58
GSL-3	36.89 ± 1.23	GSN-3	50.89 ± 0.40
GSL-4	34.90 ± 1.53	GSN-4	56.50 ± 0.66
GSL-5	55.45 ± 0.93	GSN-5	50.56 ± 0.92
GSL-6	51.32 ± 1.54	GSN-6	56.52 ± 0.78
GSL-7	62.43 ± 2.25	GSN-7	43.52 ± 1.05
GSL-8	53.45 ± 1.12	GSN-8	34.10 ± 1.13
GSL-9	45.95 ± 0.45	GSN-9	52.86 ± 0.30

Transdermal Absorption of GSL and GSN

In this study, the Franz diffusion pool method was used to evaluate the transdermal absorption (Bi et al., 2019). The animal experiments were approved by the Institutional Animal Care and Use Committee of Changchun University of Chinese Medicine, the animal ethical review number is 20190130. SD rats were fed freely for 24 h according to clean standards. Before the transdermal absorption experiment, the rats were euthanized with pentobarbital sodium. A piece of rat abdomen skin was harvested without hair, then after removing the skin moisture with filter paper, the skin was placed between a receiving pool and supply pool, and then PBS (pH 7.2) solution was used as the receiving medium and placed in the receiving pool. One ml of GS, GSL, and GSN solution with the same content of GS (200 mg) was added into the supply pool. The temperature was controlled at 37°C and the speed was set as 300 r/min. Then, 1 ml of GS, GSL, or GSN solution was removed from the receiving pools at 6, 8, 12, 24, and 48 h. Then replaced equivalent fresh liquid was added into the receiving pool. The concentration of GS was measured by HPLC.

The residual GS on the skin surface was cleaned, the skin was cut into pieces, and was then homogenized with saline at 800 rpm for 30 min. The supernatant solution was added into 5 ml methanol with a vortex for 30 s. The aforementioned solution was processed by a 0.22-μm membrane. Finally, the transdermal absorption efficiency of GS, GSL, or GSN was calculated by the following equation:

$$Q = \left[\sum_{i=1}^{n-1} Ci * V + Cn * V0\right] \Big/ S, \quad (2)$$

where Q: the transdermal absorption efficiency of GS. Cn: concentration of GS at the nth hour. Ci: concentration of GS at the ith hour. V0: volume of the accept pool. V: volume of the sampling. S: diffusion area (2.23 cm^2).

The Proliferation and Uptake of GSL and GSN on HaCaT Cells

HaCaT cells were cultured in DMEM supplemented with 10% FBS and 1% penicillin–streptomycin solution at 5% CO_2 and 37°C.

Cell Viability

The cell viability was measured by a CCK-8 assay. Briefly, HaCaT cells (5×10^3 cells/well) were cultured in 96-well plates and incubated for 24 h at 37°C. After that, different concentrations of the GS (0, 5, 10, 20, 40, 60, 80, 100, and 200 μg/ml) were added into each well for another 24-h incubation. Ten μl of the CCK-8 solution was added to each well at 10% dilution. The cells were then incubated for 1 h, and the mean optical density (OD) was measured at 450 nm using a microplate reader. All experiments were performed in triplicate. The percentage of cell viability was calculated according to the following formula:

$$\text{Percentage of cell viability} = \frac{\text{OD treatment group}}{\text{OD control group}} \times 100\%. \quad (3)$$

GS, GSL-7, and GSN-4 on the Oxidation of HaCaT Cells

HaCaT cells with a density of 5×10^3 cells/well were inoculated in 96-well plates and cultured overnight. Then, different concentrations (10, 20, and 40 μg/ml) of GS or GSL-7 and GSN-4 with a drug loading of 20 μg/ml were added in 96-well plates and incubated for 24 h. Subsequently, the solution in the 96-well plates was removed, and the cells were washed three times with PBS. After that, the MDA, SOD, and GSH-Px were tested by a plate reader (SER33270-1236, Molecular Devices, United States).

Cellular Uptake Quantitative Analysis

Preparation of GSL-7-FITC and GSN-4-FITC

GSL-7 and GSN-4 were stained with FITC to study the HaCaT cell uptake. Firstly, 20 mg of ODA and 28 mg of FITC were dissolved in 6 ml of anhydrous ethanol and stirred in the dark for 24 h. Then, 10 times the amount of water was added, filtered through a microporous membrane, and dried at room temperature in the dark to obtain ODA-FITC. GSL-7-FITC was prepared by the ethanol injection method. Firstly, phospholipids, GS, cholesterol, and 10 mg of ODA-FITC were dissolved in anhydrous ethanol at a certain molar ration to form a mixture. Then, the lipid solution was slowly injected into PBS (pH 7.4) under stirring at a volume ratio of 1/9. GSL-7-FITC was thus obtained and the anhydrous ethanol was removed by rotary evaporation. Free ODA-FITC was removed by ultrafiltration. The preparation process needs to be protected from light throughout the process. GSN-4-FITC was prepared by the same method.

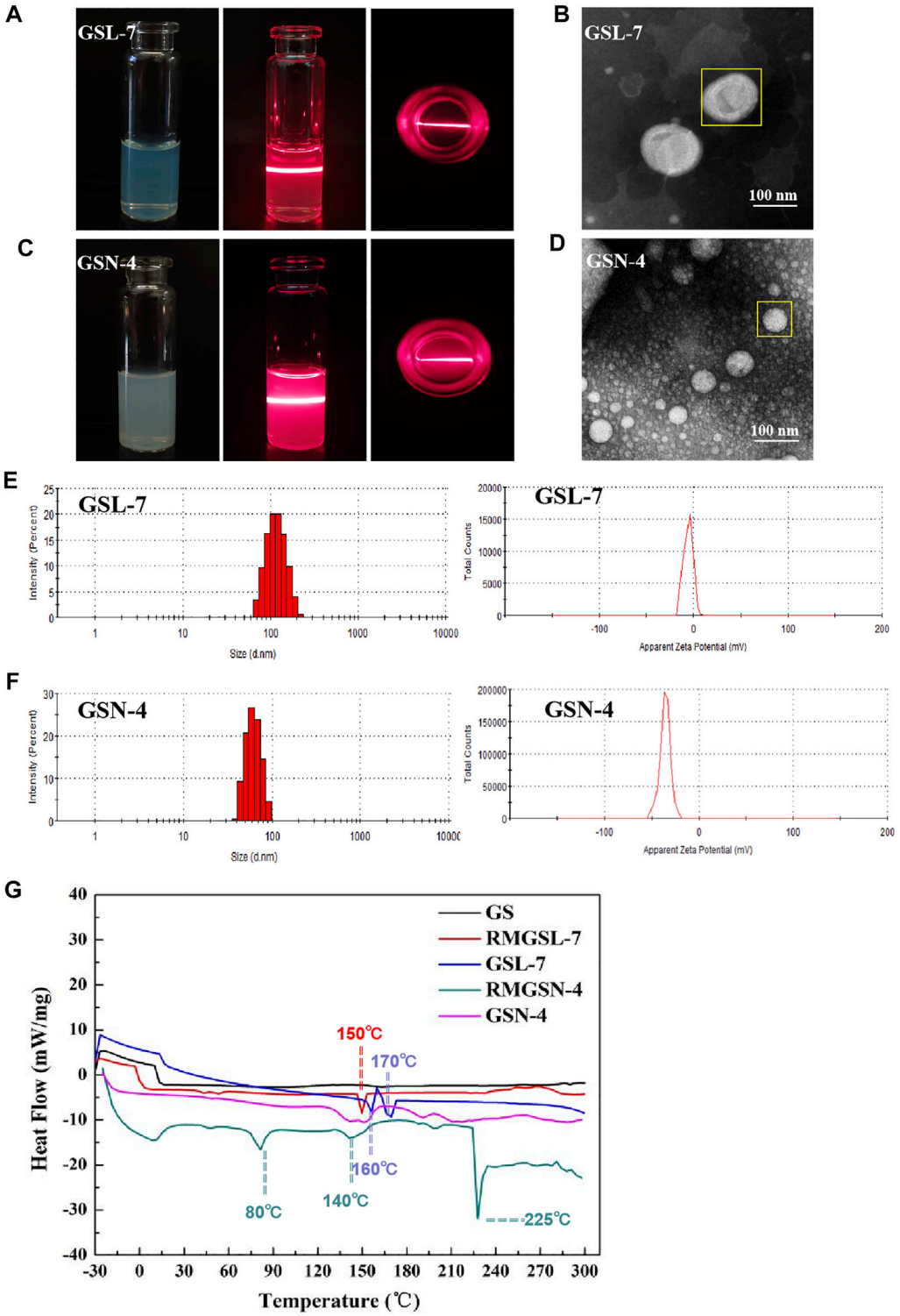

FIGURE 1 | Characterization evaluation of GSL-7and GSN-4. **(A)** Appearance and Tyndall effect of GSL-7; **(B)** TEM images of GSL-7. Scale bar: 100 nm; **(C)** Appearance and Tyndall Effect of GSN-4; **(D)** TEM images of GSN-4. Scale bar: 100 nm; **(E)** Size distribution and ξ-potential of GSL-7; **(F)** Size distribution and ξ-potential of GSN-4. **(G)** DSC curves of GSL-7 and GSN-4. Data are presented as $N = 3$. Abbreviations: GSL-7, total ginsenosides liposomes; GSN-4, total ginsenosides niosomes; RMGSL-7, a raw material mixture of prepared total ginsenosides liposomes; RMGSN-4, a raw material mixture of prepared total ginsenosides niosomes.

TABLE 4 | Cumulative transmittance, retention, and total transmittance of GS in the skin.

Time (h)	Accumulative release rate (%)			Skin retention rate (%)			Total skin transmittance (%)		
	GS	GSL-7	GSN-4	GS	GSL-7	GSN-4	GS	GSL-7	GSN-4
6	0.12 ± 0.01	21.43 ± 0.91	9.05 ± 1.83	0.46 ± 0.07	26.74 ± 2.68	16.78 ± 0.06	0.58 ± 0.06	48.17 ± 2.08	25.83 ± 2.40
8	0.19 ± 0.01	23.52 ± 2.33	11.31 ± 0.93	0.57 ± 0.01	30.92 ± 1.04	18.37 ± 0.50	0.76 ± 0.01	54.44 ± 1.34	29.68 ± 0.48
12	0.35 ± 0.02	29.40 ± 1.69	14.13 ± 0.79	0.85 ± 0.01	44.49 ± 0.95	31.98 ± 1.97	1.20 ± 0.01	73.89 ± 2.36	46.11 ± 1.17
24	0.72 ± 0.03	33.30 ± 2.29	26.15 ± 1.03	0.99 ± 0.01	52.16 ± 1.35	42.67 ± 1.90	1.72 ± 0.03	85.46 ± 3.64	68.82 ± 0.86
48	0.79 ± 0.05	34.21 ± 1.80	27.78 ± 0.89	1.02 ± 0.05	53.63 ± 0.49	43.21 ± 1.29	1.81 ± 0.05	87.84 ± 1.77	70.99 ± 0.39

GSL-7, total ginsenoside liposome-7; GSN-4, total ginsenoside niosome-4.

Cellular Uptake of GSL-7 and GSN-4

The HaCaT cells (5×10^4 cells per well) were seeded in confocal dishes and incubated for 24 h. The medium solution containing GSL-7, GSN-4, GSL-7-FITC, and GSN-4-FITC (the concentration of ODA-FITC in each group was 1 μg/ml) was added and incubated for 1 h, washed with PBS three times, added 400 μl DAPI dye solution, incubated at 37°C for 10 min, discarded the solution, washed three times with PBS, and then observed and recorded under a confocal microscope (ZEISS, Germany).

The HaCaT cells were seeded in six-well plates at a density of 2×10^5 cells per well and incubated for 24 h. The medium solution containing GSL-7, GSN-4, GSL-7-FITC, and GSN-4-FITC (the concentration of ODA-FITC in each group was 1 μg/ml) was added and incubated for 1 h and washed with PBS three times. After trypsinization, the cells were resuspended in PBS, and the fluorescence intensity of FITC in each group was detected by flow cytometry (Beckman Cytoflex, United States).

Wound Healing and Cell Proliferation Assay

The HaCaT cells were seeded in a six-well plate at a density of 5×10^5 cells/well and were adhered overnight. Subsequently, a 10-μl pipette tip was utilized to produce uniform scratches. Then, serum-free DMEM was added with the same concentration (20 μg/ml) of GS, GSL-7, and GSN-4, and incubated with the cells for another 24 h. The migration profile was recorded by using an inverted fluorescence microscope and the widths of the scratches were measured by the ImageJ software (NIH, United States).

$$\text{Healing rate\%} = \frac{\text{0 h wound area} - \text{24 h wound area}}{\text{0 h wound area}} \times 100\%. \quad (4)$$

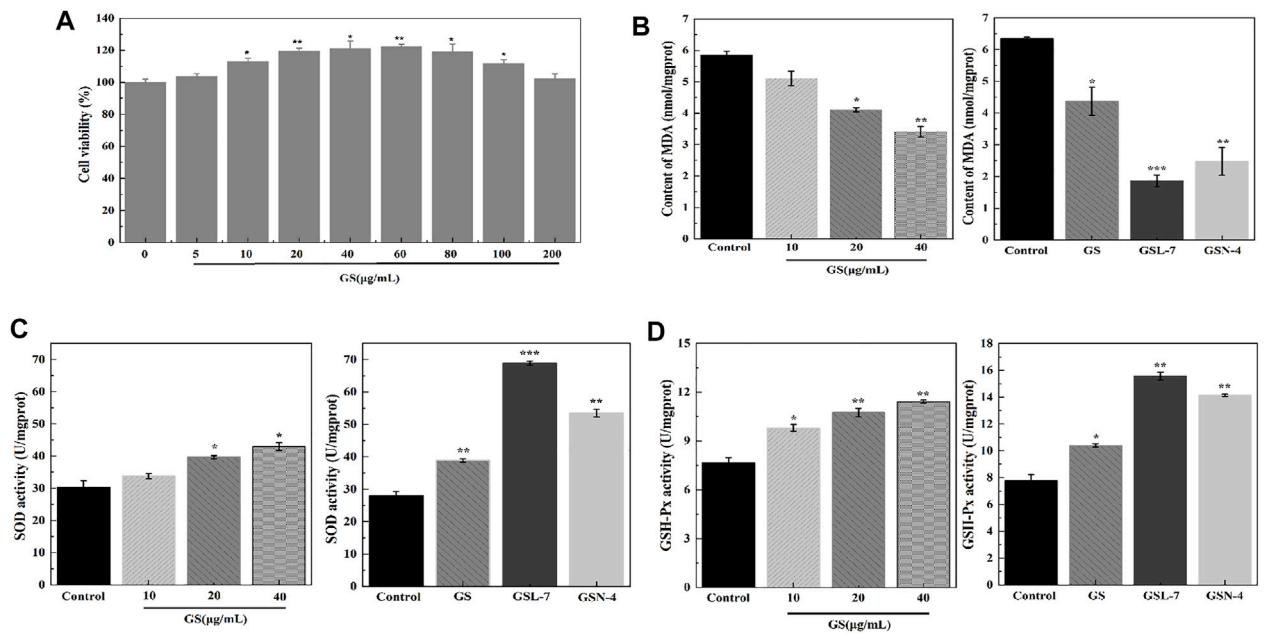

FIGURE 2 | GS, GSL, and GSN enhanced viability and anti-oxidative effects of HaCaT cells. **(A)** CCK-8 assay of GS ($n = 3$). **(B)** Effects of GS, GSL, and GSN on MDA content of HaCaT cells. **(C)** Effects of GS, GSL, and GSN on SOD content of HaCaT cells. **(D)** Effects of GS, GSL, and GSN on GSH-Px content of HaCaT cells. ***$p < 0.001$, GSL-7 group or GSN-4 vs control group, **$p < 0.01$, GSL-7 group or GSN-4 vs control group, *$p < 0.05$, GSL-7 group or GSN-4 group vs control group; Data are presented as $N = 3$, * represent significant difference between control group and treatment group. Abbreviations: GSL-7, total ginsenoside liposomes; GSN-4, total ginsenoside niosomes.

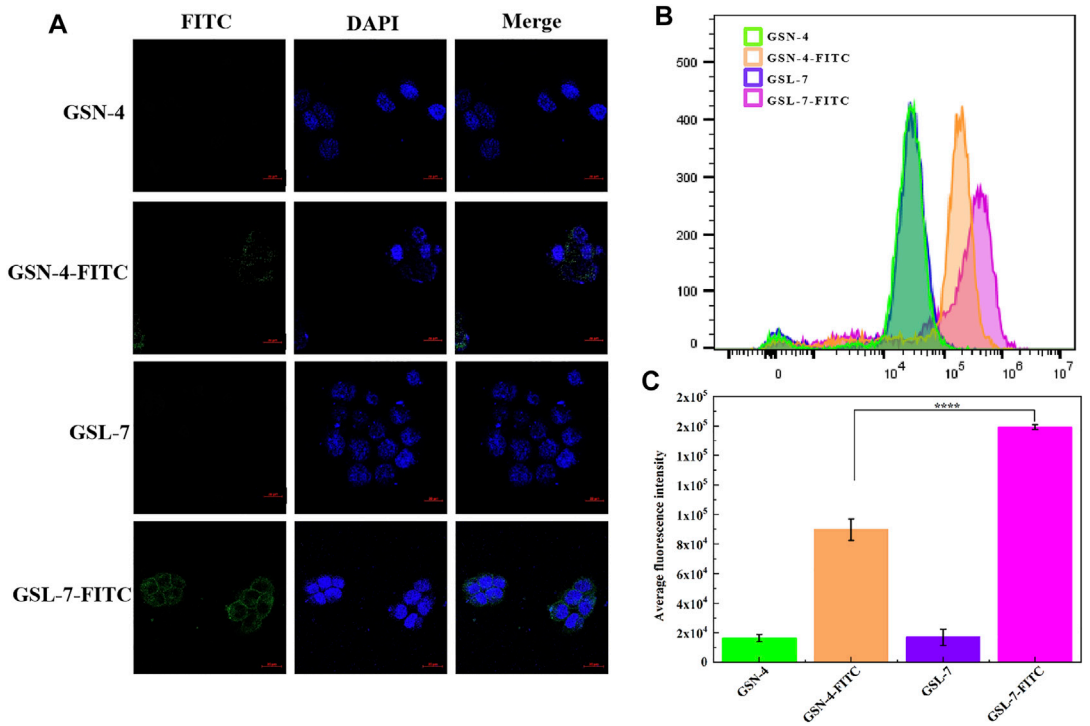

FIGURE 3 | *In vitro* evaluation of GS, GSL, and GSN in the promotion of cellular uptake. **(A)** HaCaT cell marker immunofluorescence staining by confocal laser scanning microscopy. Scale bar: 20 μm **(B)** Detection of FITC fluorescence intensity in different administration groups by flow cytometry **(C)** Quantitative analysis ($n = 3$). ****$p \leq 0.0001$, GSL-7-FITC group vs GSN-4-FITC group, * represents significant difference between control group and treatment group. Data are presented as $N = 3$. Abbreviations: GSL-7, total ginsenosides liposomes; GSN-4, total ginsenosides niosomes; GSL-7-FITC, GSL-7 link with FITC fluorescent markers; GSN-4-FITC, GSN-4 link with FITC fluorescent markers.

Proliferation of HaCaT Cells

The HaCaT cells were inoculated in a 12-well plate at a density of 5×10^4 cells/well and cultured overnight. Then, the same concentration (20 μg/ml) of GS, GSL, and GSN was added, and incubated with the cells for another five days. Every other day count and a microscope (EVOS, United States) were used to record the images.

GSL and GSN for Repairing Photoaging

Skin photoaging refers to long-term skin damage caused by UV radiation. GS effectively improve the situation. GS liposomes and niosomes were prepared to enhance the skin retention and improve the curative effect. Firstly, SD female rats were divided into five groups and each group included eight rats. The groups were recorded as follows: control group (shaving, no irradiation and treatment), model group (shaving and irradiation, no treatment), GS group, GSL group, and GSN group (GS, GSL, and GSN: shaving, irradiation, and treatment).

Before the experiment, the rats were firstly fed normally for seven days and fed freely for 24 h. Then, the back hair of the rats was shaved and the area was about 3 cm × 3 cm. Ultraviolet (UVA + UVB) irradiation was used to irradiate the naked back skin of the rats to establish the photoaging model (Rui-Zhen et al., 2004).

Except for the control group, the shaved rats were put into the self-made UV-lamp box and the fixed irradiation distance was 20 cm for ultraviolet (UVA + UVB) irradiation. The irradiated time was 20 min/day in the first week, 40 min/day in the second week, and 60 min/day in the third week. The photoaging model was successfully established when the skin on the back of the rats was dry, peeling, and even developed local ulceration. After modeling, the other three groups were given the same concentration (500 μg/ml) and the same dosage (0.5 ml/day) of GS, GSL, and GSN for treatment, except the control group and model group. The GS, GSL, or GSN was evenly applied on the skin of the affected area on the back of the rats and the skin of the rats in each group was observed after 10 days of continuous administration (Filip et al., 2013; Liu S. et al., 2018)

Five groups of rats were sacrificed after anesthesia to harvest the exposed target skin, the skin was fixed by 4% paraformaldehyde, and embedded in paraffin. Finally, the skin tissues were stained by the H&E and aldehyde fuchsin staining methods to analyze the histology of epidermis, dermis, collagen fibers, and elastic fibers (Gurrapu et al., 2012).

In addition, the effects of GSL-7 and GSN-4 on MDA, SOD, GSH-Px activities, MMPs content, IL-6, IL-1β, and TNF-α ontent were also measured using an ELISA kit in accordance with the manufacturer's protocol by a plate reader (SER33270-1236, Molecular Devices, United States).

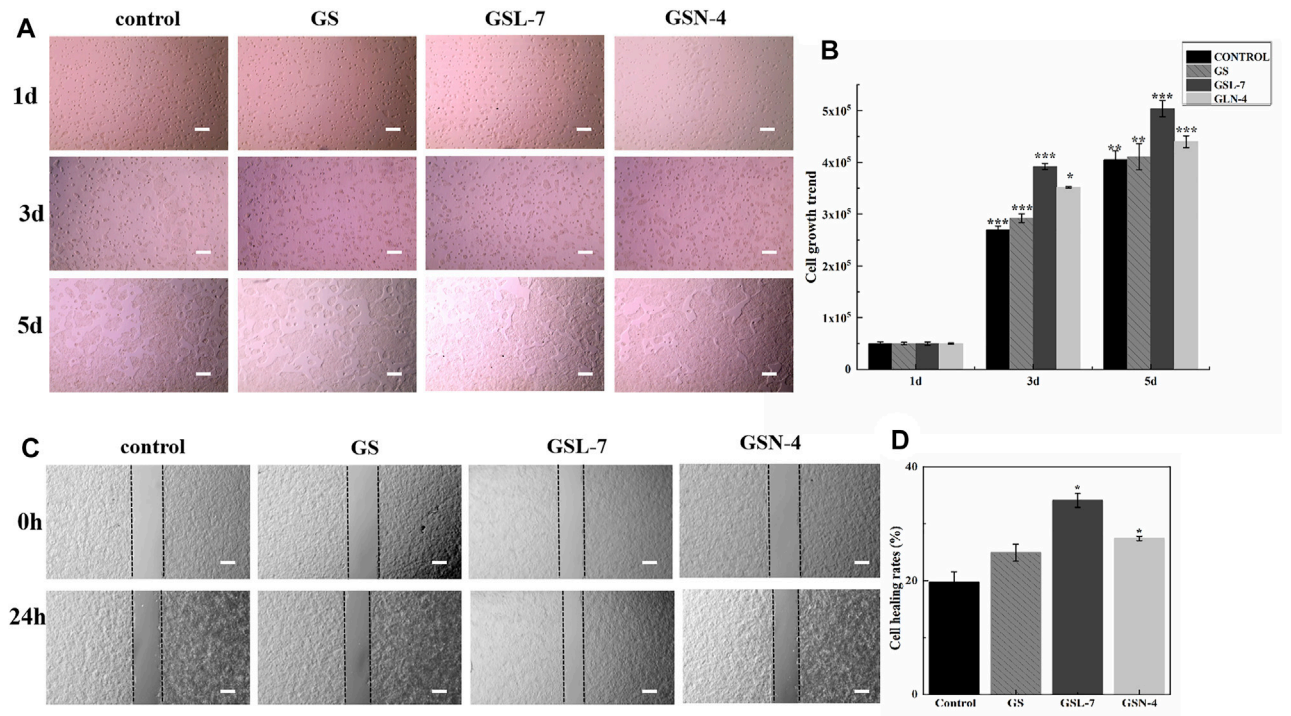

FIGURE 4 | *In vitro* evaluation of GS, GSL-7, and GSN-4 in the proliferation of HaCaT cells. **(A)** HaCaT cell growth diagram. Scale bar: 200 μm. **(B)** HaCaT cell growth trend. **(C)** GS, GSL-7, and GSN-4 promotion the migration of HaCaT cells by wounding healing assay. Scale bar: 200 μm. **(D)** Quantitative analysis. $^{*}p < 0.05$, $^{**}p \leq 0.01$, $^{***}p \leq 0.001$, GSL-7 group or GSN-4 group vs control group. * represents significant difference between control group and treatment group. Data are presented as $N = 3$. Abbreviations: GSL-7, total ginsenoside liposomes; GSN-4, total ginsenoside niosomes.

Statistical Analysis

Comparisons of two or multiple groups were analyzed by using *t*-tests (Mann–Whitney test), $p < 0.05$ indicated a significant difference and $p < 0.001$ indicated a highly significant difference. The results were expressed as mean ± standard deviation.

RESULTS AND DISCUSSION

Preparation of GSL and GSN

EE% is a key parameter of GSL and GSN quality. To prepare GSL and GSN with high EE%, the formulation process was optimized by changing the temperature and the ratios of the organic phase to aqueous phase, drug to phospholipid, and phospholipid to cholesterol. It can be observed from **Tables 1**, **3** that when preparing GSL, the phospholipid species influenced the EE% of GSL. The EE% of GSL was highest when the phospholipid used was SPC. The EE% of GSL was highest at an optimal lipid-drug ratio. When the ratio of phospholipid to cholesterol was increased to 1:3.5, the EE% of GSL was 62.43%. As the amount of lipids affects the drug-loading capacity, drugs beyond the upper limit cannot be loaded. Cholesterol can improve the fluidity of the lipid membrane and improve the EE%, but excessive cholesterol content will lead to the decrease of EE% and drug leakage. Therefore, the optimal parameters for preparing GSL used SPC as the phospholipid, with a lipid-drug ratio of 1:0.4 and a phospholipid to cholesterol ratio of 1:3.5. The sample was recorded as GSL-7. For preparing GSN, it can be seen from **Tables 2**, **3** that the EE% of GSN increased at first and then decreased with increasing temperature. When the heating temperature was 65°C, the EE% of GSN was the highest (56.50%). Similarly, the EE% of GSN was initially higher and then decreased with an increasing ratio of the organic phase to aqueous phase, which may compete with the drug for packing space within the bilayer and limit the assembly of the drug into the vesicle. Similar results have also been observed in other studies (Gomaa et al., 2014; Vitorino et al., 2014). When the ratio of the organic phase to aqueous phase was 10%, the EE% of GSN was 56.50%. Therefore, the optimal preparation process of GSN was as follows: the temperature was 65°C and the ratio of the organic phase to aqueous phase was 10%. The sample was recorded as GSN-4.

Characterization of GSL-7 and GSN-4

Morphology, Particle Size, and ξ-potential of GSL-7 and GSN-4

As shown in **Figures 1A, C**, the appearance of GSL-7 and GSN-4 was a clear and uniform liquid. When a beam of infrared light was passed through GSL-7 and GSN-4, the Tyndall effect was observed, indicating that GSL-7 and GSN-4 were polymer colloidal solutions (Liu Q. et al., 2018). The microstructure of GSL-7 and GSN-4 was determined by TEM. GSL-7 and GSN-4 both exhibited spherical shapes and uniform sizes (**Figures 1B, D**). The diameter of GSL-7 was ~100.0 nm and the diameter of GSN-4 was ~60.0 nm.

The particle size and ξ-potential of GSL-7 and GSN-4 were determined by DLS (**Figures 1E,F**). The particle size of GSL-7 was 110.0 ± 3.5 nm, the polydispersity index (PDI) was 0.056 ± 0.009, and the ξ-potential was −5.7 ± 0.5 mV. The particle size of GSN-4 was 60.93 ± 0.17 nm, the PDI was 0.086 ± 0.016, and the ξ-potential was −35.5 ± 1.8 mV. The particle size was consistent with the TEM data, and GSL had a larger particle size and a more uniform particle-size distribution than GSN-4.

Differential Scanning Calorimeter (DSC) of GSL-7 and GSN-4

DSC analyses were performed to determine whether the GSL-7 or GSN-4 could be successfully prepared, and to understand the nature and physical state of the GS, liposomes, and niosomes (**Figure 1G**). Compared with GS and the raw material mixture of GSL-7 (RMGSL-7), there was a marked endothermic peak shift at 150°C and the emergence of a new endothermic peak at 160 and 170°C for GSL-7. It can be inferred that GS and the raw materials of the prepared GSL-7 are not simply physically mixed, but interact, and that GS is embedded in the double-layer structure of phospholipids. Similarly, the raw material mixture of GSN-4 (RMGSN-4) had noticeable endothermic peaks at 80, 140, and 225°C, indicating that there was an interaction between GS and the raw materials. These endothermic peaks were not present in the DSC curves of GSN-4, demonstrating that a chemical interaction had not occurred between the GS and the niosomal system, and the GSN-4 was successfully prepared.

Transdermal Absorption of GSL-7 and GSN-4

The cumulative transmittance, skin retention rate, and total transmittance of GS, GSL-7, and GSN-4 were measured. The results are shown in **Table 4**. It can be observed that a minimal

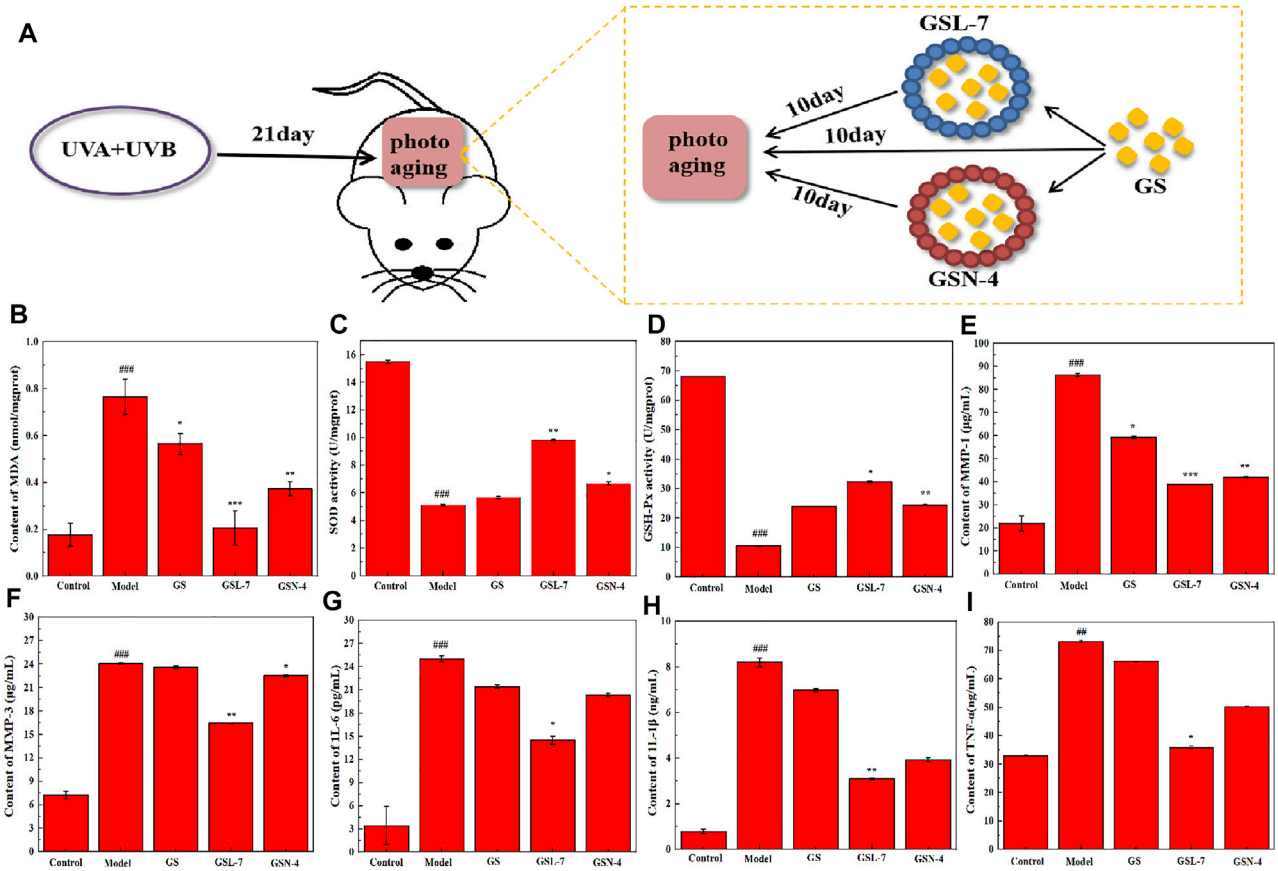

FIGURE 5 | Biological effects of GSL and GSN on the skin. **(A)** Schematic representations of repair photoaging. **(B)** Effects of GSL-7 and GSN-4 on MDA content in rat skin tissues. **(C)** Effects of GSL-7 and GSN-4 on SOD content in rat skin tissues. **(D)** Effects of GSL-7 and GSN-4 on GSH-Px content in rat skin tissues. **(E)** Effects of GSL-7 and GSN-4 on MMP-1 content in rat skin tissues. **(F)** Effects of GSL-7 and GSN-4 on MMP-3 content in rat skin tissues. **(G)** Effects of GSL-7 and GSN-4 on IL-6 content in rat skin tissues. **(H)** Effects of GSL-7 and GSN-4 on IL-1β content in rat skin tissues. **(I)** Effects of GSL-7 and GSN-4 on TNF-α content in rat skin tissues. $^{***}p < 0.001$, $^{***}p < 0.01$, model group vs Control group; $^{***}p < 0.001$, GSL-7 group or GSN-4 vs model group, $^{**}p < 0.01$, GSL-7 group or GSN-4 vs model group, $^{*}p < 0.05$, GSL-7 group or GSN-4 group vs model group; $^{**}p < 0.01$, GSL-7 group vs model group, $^{*}p < 0.05$, GSN-4 group vs control group; $^{*}p \leq 0.05$, $^{**}p \leq 0.01$, $^{***}p \leq 0.001$, $^{****}p \leq 0.0001$ represents significant difference, # represents significant difference between model group and control group, * represents significant difference between model group and treatment group. Data are presented as $N = 8$. Abbreviations: GSL-7, total ginsenoside liposomes; GSN-4, total ginsenoside niosomes.

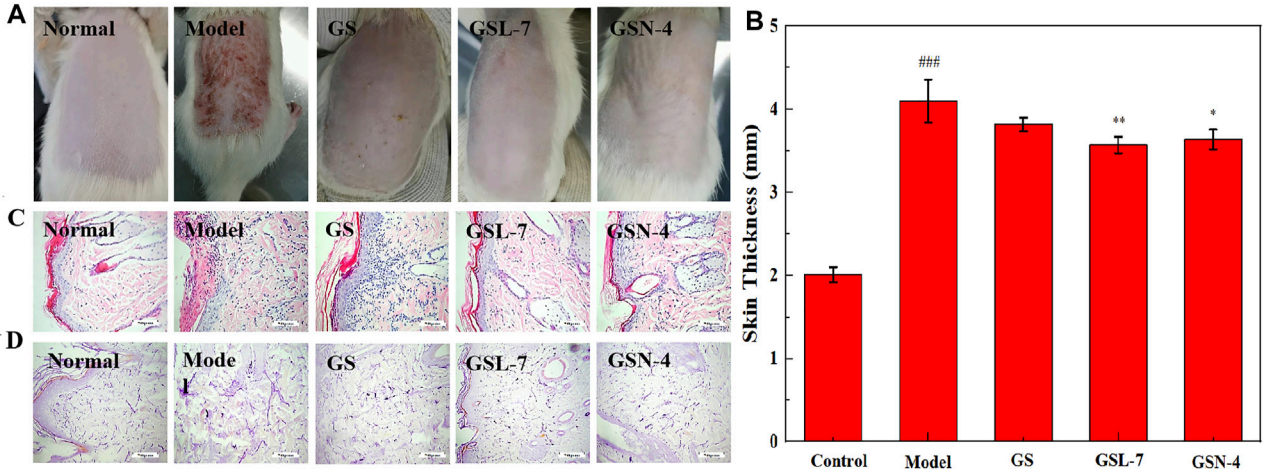

FIGURE 6 | Skin appearance of rats of repair photoaging. **(A)** Skin appearance of rats after 10 days of administration; **(B)** Change of skin thickness, control group, **(C)** Histology of skin by H&E staining of the skin tissue section (×200); **(D)** Histology of skin by aldehyde fuchsine stain of the skin tissue section (×200). Data are presented as $N = 8$, $^{**}p < 0.01$, GSL-7 group vs model group, $^{*}p < 0.05$, GSN-4 group vs control group; $^{\#\#\#}p < 0.001$, model group vs control group; $^{*}p \leq 0.05$, $^{**}p \leq 0.01$, $^{***}p \leq 0.001$, $^{****}p \leq 0.0001$ represents significant difference, # represents significant difference between model group and control group, * represents significant difference between model group and treatment group. Abbreviations: GSL-7, total ginsenoside liposomes; GSN-4, total ginsenoside niosomes.

amount of GS was detected within 48 h. The cumulative release rate, skin retention rate, and total penetration rate of GSL-7 at 48 h were higher than those of GSN-4, at 6.43, 10.42, and 16.85%, respectively. Both GSL-7 and GSN-4 improved the skin penetration rate of GS, but the effects of GSL-7 were more pronounced, with more than 85% of GS penetrating the skin barrier within 24 h. GSL-7 tended to be absorbed by the skin, which might be because of the structure and carrier material of GSL-7. These properties may improve the effect of GSL-7 on skin anti-photoaging.

GSL and GSN for the Proliferation and Uptake of HaCaT Cells

GS, GSL, and GSN Enhanced the Viability and Antioxidative Potential of HaCaT Cells

The concentration of GS was determined to evaluate the biocompatibility of GS. The analysis results show that the cell viability of the GS group was significantly higher than that of the control group (**Figure 2A**). As GS concentration increased, the cell viability initially increased before decreasing. The cell viability reached 119.57 ± 1.72%, 121.23 ± 4.51%, and 122.47 ± 1.34% with GS concentrations of 20, 40, and 60 μg/ml, respectively, indicating that GS had good biosafety. Therefore, 20, 40, and 60 μg/ml were determined as the administered concentrations for subsequent cell experiments.

To further understand the molecular mechanisms associated with the beneficial effects of GS, oxidative stress levels and endogenous antioxidant enzyme activity were measured in the HaCaT cells. MDA, SOD, and GSH-Px activity was determined using ELISA kits. Compared with the control group, the MDA expression was decreased at all GS doses (20, 40, 60 μg/ml). At the 20 μg/ml GS dose, the MDA content was significantly decreased in the GSL ($^{***}p < 0.001$) and GSN ($^{**}p < 0.01$) groups compared with the controls. SOD and GSH-Px activities were significantly increased in the GSL ($^{***}p < 0.001$) and GSN ($^{**}p < 0.01$) groups compared with the controls, particularly in the GSL-7 group.

During cell growth, intrinsic antioxidant systems emerge to reduce the levels of ROS and improve cell survival (Ighodaro and Akinloye, 2018). Among them, GSH-Px is known to catalyze the reduction of hydrogen peroxide and other peroxides, while SOD can catalytically reduce O_2 to hydrogen peroxide. The results of the present study showed that GS, GSL-7, and GSN-4 upregulated SOD and GSH expression, and downregulated the levels of MDA *in vivo*.

Cellular Uptake Quantitative Analysis

Cellular uptake is a key step in facilitating intracellular delivery. An analysis showed that GSL-7 and GSN-4 had no self-luminescence, whereas GSL-7-FITC and GSN-4-FITC had green fluorescence (**Figure 3A**). Compared with GSN-4-FITC, the GSL-7-FITC group had stronger fluorescence. The uptake of the GSL-7-FITC group was quantitatively analyzed by flow cytometry, as shown in **Figure 3B**. The results were consistent with those observed under the fluorescent microscope. The fluorescent intensity of the GSL-7-FITC group was 2.2-folder higher than the GSN-4-FITC group (**Figure 3C**), indicating that the liposome structure may aid HaCaT cell uptake.

Proliferation of HaCaT Cells

To investigate whether GS, GSL-7, and GSN-4 affected the proliferation of HaCaT cells, differences in cell growth between the GS, GSL-7, and GSN-4 groups and controls were analyzed. The HaCaT cells were counted every other day and recorded by a microscope. The results are shown in **Figure 4A**. On the first day, the cells in each group began to anchor to the plate surface. On the third day, cell proliferation of the GS, GSL-7,

and GSN-4 groups was noticeably higher than the control group. A quantitative analysis indicated that compared with the 5×10^4 HaCaT cells present at the time of inoculation, cell proliferation increased 5-fold, 5.8-fold, 7.8-fold, and 7.0-fold in the control, GS, GSL-7, and GSN-4 groups, respectively. On the fifth day, cell proliferation was higher in the GSL-7 and GSN-7 groups compared with the GS and control groups; the cell proliferation increased 8-fold, 8.2-fold, 10.0-fold, and 8.8-fold in the control, GS, GSL-7, and GSN-4 groups, respectively. These trends suggest that liposomes and niosomes may enhance the proliferative effect of GS on HaCaT cells. The proliferation trend of the cells in the control group was in line with previously reported results (Wilson 2014).

A wounding healing assay was performed to assess the influence of the GS, GSL, and GSN on the migration properties of HaCaT cells *in vitro*. Changes in the scratch width of each group were observed for 24 h to assess HaCaT-cell migration (**Figures 4C,D**). GS, GSL-7, and GSN-4 all promoted the HaCaT-cell migration. However, GSL-7 induced the surrounding HaCaT cells to crawl toward the center of the scratch, almost filling the gap within 24 h, showing the smallest scratch width in all treatment groups (GS, GSL-7, and GSN-4 groups) (**Figure 4C**) with a healing rate of 34.12 ± 1.22% ($p < 0.05$) (**Figure 4D**).

Repair of Photoaging by GSL-7 and GSN-4

Effects of GSL-7 and GSN-4 on MDA, SOD, and GSH-Px Expression

The schematic diagram of the rat skin photoaging modeling and repair process is shown in **Figure 5A**. An ELISA kit was used to determine the content of MDA in a skin tissue homogenate of rats in each group. MDA is the primary product of lipid peroxidation and can be used to measure the degree of skin anti-photoaging under oxidation. The results are shown in **Figure 5B**. Compared with the control group, MDA expression in the skin tissue of the model group was significantly increased ($p < 0.01$), indicating that UV radiation may cause skin lipid peroxidation and excessive MDA production. After treatment, the MDA expression was decreased in all the treatment groups (GS, GSL-7, and GSN-4). Furthermore, the decrease in the MDA expression was most pronounced in the GSL-7 group when compared with controls ($p < 0.01$). The expression of SOD and GSH-Px in the rat skin tissue homogenate was determined by using an ELISA kit. The expression of SOD and GSH-Px in the skin tissue also reflects the ability of the skin to resist oxidation and photoaging. The results are shown in **Figures 5C, D**. Compared with the control group, the activities of SOD and GSH-Px were significantly decreased in the model group ($p < 0.001$). The oxidative balance between the skin cells was also impaired. Compared with the model group, the SOD and GSH-Px expression was significantly increased in the GSN-4 ($p < 0.05$) and GSL-7 groups ($p < 0.01$). Therefore, it may be concluded that GS reduced UV radiation-induced skin-lipid peroxidation. GSL-7 and GSN-4 improved the transdermal efficiency and the percutaneous absorption of GS. According to the aforementioned experimental results, GSL-7 appears to have significant advantages over GSN-4 and a better therapeutic effect.

Effect of GSL-7 and GSN-4 on MMP Content

It has been shown that MMP-1 can degrade collagen Ⅰ and collagen Ⅲ. Moreover, MMP-3 can degrade collagen and elastin in a synergistic way, leading to collagen and elastin rupture (Lee et al., 2020; Wan et al., 2021). Therefore, MMP-1 and MMP-3 expression was measured in the rat skin tissue homogenate using ELISA kits (**Figures 5E, F**). Compared with the control group, MMP-1 and MMP-3 expression significantly increased in the model group. MMP-1 and MMP-3 expression decreased in all treatment groups, with the GSL-7 group showing the most prominent decrease ($p < 0.01$).

Effect of GSL and GSN on IL-6, IL-1β, and TNF-α Content

A cascade of reactions is triggered after UV exposure, with ROS triggering inducing the release of IL-6, IL-1β, and TNF-α (Zhou et al., 2021). ELISA kits were used to determine IL-6, IL-1β, and TNF-α expression in the rat skin tissue homogenate. The results are shown in **Figures 5G–I**. Compared with the control group, the expression of IL-1β, IL-6, and TNF-α was significantly increased in the model group ($p < 0.001$, $p < 0.001$, and $p < 0.01$, respectively). Compared with the model group, IL-6, IL-1β, and TNF-α were decreased in all the treatment groups, with the most marked decrease shown in the GSL-7 group.

In conclusion, GS can reduce the inflammatory factor expression in skin tissue following UV radiation. GSL-7 was more efficient than GSN-4 or GS in promoting GS absorption across the skin barrier.

Skin Appearance of Rats of Repair Photoaging

Clinically, photodamaged skin is characterized by the loss of elasticity, increased roughness and dryness, irregular pigmentation, and deep wrinkling (Bi et al., 2019). The results are presented in **Figure 6**. It can be seen from **Figure 6A** that the phenomena of rough skin, wrinkles, and abnormal thickness of the skin were all improved in the GS, GSL-7, and GSN-4 groups. The improvements were most pronounced in the GSL-7 group; the degree of rough skin was reduced and hair began to regenerate at the modeling site. Changes in the skin thickness of the rats in each group after treatment are shown in **Figure 6B**. Compared with the control group, the skin thickness in the model group was significantly increased ($p < 0.001$). On the contrary, compared with the model group, the skin thickness was decreased after the treatment, with the most marked effects observed in the GSL-7 group ($p < 0.05$). GS, GSL-7, and GSN-4 groups all received an acceptable therapeutic effect. GSL-7 had a therapeutic effect on photoaging.

Morphological changes in the rat skin were further analyzed by H&E staining and aldehyde fuchsin staining. The results are shown in **Figures 6C, D**. In the control group, the thickness of the epidermis was normal and the head of the epidermis and dermal papilla could be seen. In the model group, the stratum corneum was obviously thickened, the junction of epidermis and dermis was flattened, some epidermis in the damaged area was missing, and dermal papilla was rare or not present. After the treatment, signs of improvement were visible. In the GSL-7 group, the skin epidermis thickness was thin and close to normal, with a small

amount of inflammatory cell infiltration at the junction of the epidermis and dermis.

Aldehyde fuchsin staining is predominantly used to visualize elastic fibers in the skin tissue and can be used to assess the elasticity of the skin. In the control group, the elastic fibers showed a relatively clear reticular structure with long and thin fibers, and an orderly arrangement and density (**Figure 6D**). In the model group, the arrangement of elastic fibers was visibly irregular. The reticular structure was not presented and there were many fractures, clusters, and accumulation. The treatment groups showed different degrees of improvement. The improvement was most evident in the GSL-7 group: accumulation and clustering had not occurred, and there was a clear network structure, with an orderly arrangement and consistent density.

CONCLUSION

In this study, GSL and GSN were prepared and their skin anti-photoaging ability was assessed. The optimized GSL and GSN were characterized according to particle size, potential, EE%, drug transdermal release efficiency, and other parameters. The results showed that the particle size of GSL was smaller, more stable, and the EE% was higher than that of GSN. In the transdermal experiment, both GSL and GSN markedly improved the transdermal absorption efficiency of GS. The effect was more pronounced for GSL than the GS (48 h) and GSL-7 (48 h) groups, with a 48-fold total skin transmittance. In addition, equal doses of GS, GSN, and GSL showed that GSN and GSL effectively inhibited lipid peroxidation, and increased the SOD and GSH-Px expression in HaCaT cells. GSL and GSN also increased HaCaT cell proliferation, migration, and uptake *in vitro*. The expression of MMPs and inflammatory factors in the skin tissue was reduced by GSN and GSL, indicating that GS treatment—most notably with GSL—improved the ability of the skin to repair UV-induced skin tissue damage. In conclusion, GSN and GSL can be used as transdermal drug delivery vehicles of GS to enhance the anti-photoaging ability of GS in the skin. GSL may have significant potential as an effective treatment for skin photoaging, and further studies into its anti-inflammatory effects are required.

DATA AVAILABILITY STATEMENT

The original contributions presented in the study are included in the article/Supplementary Material, further inquiries can be directed to the corresponding authors.

ETHICS STATEMENT

All animal experiments were approved by the Institutional Animal Care and Use Committee, Changchun University of Chinese Medicine (No. 20190130).

AUTHOR CONTRIBUTIONS

Conceptualization, DL and YJ*; data curation, ZL; formal analysis, LY; funding acquisition, ZQ*; investigation, JC; methodology, YJ ZL and LY; project administration, YJ, ZL and LY; resources, XZ; software, XZ; supervision, YJ* and ZQ*; validation, DL, YJ* and ZQ*; visualization, JC; writing—original draft, YJ; and writing—review and editing, YJ*. All authors have read and agreed to the published version of the manuscript.

FUNDING

This work was supported by the National Natural Science Foundation of China (82003985), Science and Technology Research Project of Jilin Provincial Department of Education (JJKH20210995KJ), and Jilin Science and Technology Development Plan Project (20210204013YY).

REFERENCES

Abaee, A., and Madadlou, A. (2016). Niosome-loaded Cold-Set Whey Protein Hydrogels. *Food Chem.* 196, 106–113. doi:10.1016/j.foodchem.2015.09.037

Ahmed, K. S., Shan, X., Mao, J., Qiu, L., and Chen, J. (2019). Derma Roller Microneedles-Mediated Transdermal Delivery of Doxorubicin and Celecoxib Co-loaded Liposomes for Enhancing the Anticancer Effect. *Mater. Sci. Eng. C* 99, 1448–1458. doi:10.1016/j.msec.2019.02.095

Bai, L., Gao, J., Wei, F., Zhao, J., Wang, D., and Wei, J. (2018). Therapeutic Potential of Ginsenosides as an Adjuvant Treatment for Diabetes. *Front. Pharmacol.* 9, 423. doi:10.3389/fphar.2018.00423

Barani, M., Mirzaei, M., Torkzadeh-Mahani, M., Lohrasbi-Nejad, A., and Nematollahi, M. (2020). A New Formulation of Hydrophobin-Coated Niosome as a Drug Carrier to Cancer Cells. *Mater. Sci. Eng. C, Mater. Biol. Appl.* 113, 110975. doi:10.1016/j.msec.2020.110975

Bhattacharya, N., Sato, W. J., Kelly, A., Ganguli-Indra, G., and Indra, A. K. (2019). Epidermal Lipids: Key Mediators of Atopic Dermatitis Pathogenesis. *Trends Mol. Med.* 25, 551–562. doi:10.1016/j.molmed.2019.04.001

Bi, Y., Xia, H., Li, L., Lee, R. J., Xie, J., Liu, Z., et al. (2019). Liposomal Vitamin D-3 as an Anti-aging Agent for the Skin. *Pharmaceutics* 11, 311. doi:10.3390/pharmaceutics11070311

Bozzuto, G., and Molinari, A. (2015). Liposomes as Nanomedical Devices. *Int. J. Nanomedicine* 10, 975–999. doi:10.2147/ijn.S68861

Chen, S., Hanning, S., Falconer, J., Locke, M., and Wen, J. (2019). Recent Advances in Non-ionic Surfactant Vesicles (Niosomes): Fabrication, Characterization, Pharmaceutical and Cosmetic Applications. *Eur. J. Pharmaceutics Biopharmaceutics* 144, 18–39. doi:10.1016/j.ejpb.2019.08.015

Chung, J. H. (2003). Photoaging in Asians. *Photodermatol. Photoimmunology Photomed.* 19, 109–121. doi:10.1034/j.1600-0781.2003.00027.x

Farmoudeh, A., Akbari, J., Saeedi, M., Ghasemi, M., Asemi, N., and Nokhodchi, A. (2020). Methylene Blue-Loaded Niosome: Preparation, Physicochemical Characterization, and In Vivo Wound Healing Assessment. *Drug Deliv. translational Res.* 10, 1428–1441. doi:10.1007/s13346-020-00715-6

Filip, G. A., Postescu, I. D., Bolfa, P., Catoi, C., Muresan, A., and Clichici, S. (2013). Inhibition of UVB-Induced Skin Phototoxicity by a Grape Seed Extract as Modulator of Nitrosative Stress, ERK/NF-kB Signaling Pathway and Apoptosis,

in SKH-1 miceSKH-1 Mice. *Food Chem. Toxicol.* 57, 296–306. doi:10.1016/j.fct.2013.03.031

Gautam, A., and Prajapati, S. K. (2012). A Novel Approach for Transdermal Drug Delivery as a Liposomes Their Progress and Limitations: A Review. *Int. J. Pharm. Res. Scholars* 1, 697–722. doi:10.1016/S0165-1889(96)00003-6

Gomaa, Y. A., Garland, M. J., Mcinnes, F. J., Donnelly, R. F., and El-Khordagui, L. K. (2014). Microneedle/nanoencapsulation-mediated Transdermal Delivery: Mechanistic Insights. *Eur. J. Pharm. Biopharm.* 86, 145–155. doi:10.1016/j.ejpb.2013.01.026

Gurrapu, A., Jukanti, R., Bobbala, S. R., Kanuganti, S., and Jeevana, J. B. (2012). Improved Oral Delivery of Valsartan from Maltodextrin Based Proniosome Powders. *Adv. Powder Technol.* 23, 583–590. doi:10.1016/j.apt.2011.06.005

Ho, J. N., Lee, Y. H., Park, J. S., Jun, W. J., Kim, H. K., Hong, B. S., et al. (2005). Protective Effects of Aucubin Isolated from Eucommia Ulmoides against UVB-Induced Oxidative Stress in Human Skin Fibroblasts. *Biol. Pharm. Bull.* 28, 1244–1248. doi:10.1248/bpb.28.1244

Ighodaro, O. M., and Akinloye, O. A. (2018). First Line Defence Antioxidants-Superoxide Dismutase (SOD), Catalase (CAT) and Glutathione Peroxidase (GPX): Their Fundamental Role in the Entire Antioxidant Defence Grid. *Alexandria J. Med.* 54, 287–293. doi:10.1016/j.ajme.2017.09.001

Jacob, S., Nair, A., and Al-Dhubiab, B. (2017). Preparation and Evaluation of Niosome Gel Containing Acyclovir for Enhanced Dermal Deposition. *J. Liposome Res.* 27, 283–292. doi:10.1080/08982104.2016.1224897

Jiao, L., Li, J., Liu, F., Wang, J., Jiang, P., Li, B., et al. (2021). Characterisation, Chain Conformation and Antifatigue Effect of Steamed Ginseng Polysaccharides with Different Molecular Weight. *Front. Pharmacol.* 12, 712836. doi:10.3389/fphar.2021.712836

Jung, H.-Y., Shin, J.-C., Park, S.-M., Kim, N.-R., Kwak, W., and Choi, B.-H. (2014). Pinus Densiflora Extract Protects Human Skin Fibroblasts against UVB-Induced Photoaging by Inhibiting the Expression of MMPs and Increasing Type I Procollagen Expression. *Toxicol. Rep.* 1, 658–666. doi:10.1016/j.toxrep.2014.08.010

Kang, T. H., Park, H. M., Kim, Y.-B., Kim, H., Kim, N., Do, J.-H., et al. (2009). Effects of Red Ginseng Extract on UVB Irradiation-Induced Skin Aging in Hairless Mice. *J. Ethnopharmacology* 123, 446–451. doi:10.1016/j.jep.2009.03.022

Lee, E. H., Park, H. J., Kim, H. H., Jung, H. Y., Kang, I. K., and Cho, Y. J. (2021). Isolated Isoquercitrin from Green ball Apple Peel Inhibits Photoaging in CCD-986Sk Fibroblasts Cells via Modulation of the MMPs Signaling. *J. Cosmet. Dermatol.* 20, 2932–2939. doi:10.1111/jocd.13903

Lee, Y. J., Kim, H. Y., Kang, K. S., Lee, J. G., Yokozawa, T., and Park, J. H. (2008). The Chemical and Hydroxyl Radical Scavenging Activity Changes of Ginsenoside-Rb1 by Heat Processing. *Bioorg. Med. Chem. Lett.* 18, 4515–4520. doi:10.1016/j.bmcl.2008.07.056

Liu, Q., Kim, S. B., Jo, Y. H., Ahn, J. H., Turk, A., Kim, D. E., et al. (2021). Curcubinoyl Flavonoids from Wild Ginseng Adventitious Root Cultures. *Sci. Rep.* 11, 12212. doi:10.1038/s41598-021-91850-8

Liu, Q., Wang, H., Li, G., Liu, M., Ding, J., Huang, X., et al. (2018). A Photocleavable Low Molecular Weight Hydrogel for Light-Triggered Drug Delivery. *Chin. Chem. Lett.* 30, 485–488. doi:10.1016/j.cclet.2018.06.009

Liu, S., You, L., Zhao, Y., and Chang, X. (2018). Hawthorn Polyphenol Extract Inhibits UVB-Induced Skin Photoaging by Regulating MMP Expression and Type I Procollagen Production in Mice. *J. Agric. Food Chem.* 66, 8537–8546. doi:10.1021/acs.jafc.8b02785

Lu, J., Hou, H., Fan, Y., Yang, T., and Li, B. (2017). Identification of MMP-1 Inhibitory Peptides from Cod Skin Gelatin Hydrolysates and the Inhibition Mechanism by MAPK Signaling Pathway. *J. Funct. Foods* 33, 251–260. doi:10.1016/j.jff.2017.03.049

Lu, Z., Wang, X., Zhang, T., Zhang, L., Yang, J., Li, Y., et al. (2020). Cationic and Temperature-Sensitive Liposomes Loaded with Eugenol for the Application to Silk. *Chin. Chem. Lett.* 31, 3139–3142. doi:10.1016/j.cclet.2020.07.013

Mao, Y., Ji, H., Zheng, D., Mu, B., Tang, J., Gao, Y., et al. (2015). Application of Novel Liposomes in Transdermal Drug Delivery System. *China Pharmacist* 12, 2141–2144. doi:10.3969/j.issn.1008-049X.2015.12.044

Moghassemi, S., Parnian, E., Hakamivala, A., Darzianiazizi, M., Vardanjani, M. M., Kashanian, S., et al. (2015). Uptake and Transport of Insulin across Intestinal Membrane Model Using Trimethyl Chitosan Coated Insulin Niosomes. *Mater. Sci. Eng. C Mater. Biol. Appl.* 46, 333–340. doi:10.1016/j.msec.2014.10.070

Mu, J., Ma, H., Chen, H., Zhang, X., and Ye, M. (2021). Luteolin Prevents UVB-Induced Skin Photoaging Damage by Modulating SIRT3/ROS/MAPK Signaling: An In Vitro and In Vivo Studies. *Front. Pharmacol.* 12, 728261. doi:10.3389/fphar.2021.728261

Nah, S.-Y. (2014). Ginseng Ginsenoside Pharmacology in the Nervous System: Involvement in the Regulation of Ion Channels and Receptors. *Front. Physiol.* 5, 98. doi:10.3389/fphys.2014.00098

Oh, S.-J., Lee, S., Choi, W.-Y., and Lim, C.-J. (2014). Skin Anti-photoaging Properties of Ginsenoside Rh2 Epimers in UV-B-Irradiated Human Keratinocyte Cells. *J. Biosci.* 39, 673–682. doi:10.1007/s12038-014-9460-x

Oh, S.-J., Oh, Y., Ryu, I. W., Kim, K., and Lim, C.-J. (2016). Protective Properties of Ginsenoside Rb3 against UV-B Radiation-Induced Oxidative Stress in HaCaT Keratinocytes. *Biosci. Biotechnol. Biochem.* 80, 95–103. doi:10.1080/09168451.2015.1075862

Oh, S. J., Kim, K., and Lim, C. J. (2015). Protective Properties of Ginsenoside Rb1 against UV-B Radiation-Induced Oxidative Stress in Human Dermal Keratinocytes. *Pharmazie* 70, 381–387. doi:10.1691/ph.2015.4884

Park, B.-J., Lim, Y.-S., Lee, H.-J., Eum, W.-S., Park, J.-S., Han, K.-H., et al. (2009). Anti-oxidative Effects of Phellinus Linteus and Red Ginseng Extracts on Oxidative Stress-Induced DNA Damage. *Bmb Rep.* 42, 500–505. doi:10.5483/BMBRep.2009.42.8.500

Raj, R., Raj, P. M., and Ram, A. (2018). Nanosized Ethanol Based Malleable Liposomes of Cytarabine to Accentuate Transdermal Delivery: Formulation Optimization, in Vitroskin Permeation Andin Vivobioavailability. *Artif. Cell nanomedicine, Biotechnol.* 46, 951–963. doi:10.1080/21691401.2018.1473414

Ratan, Z. A., Haidere, M. F., Hong, Y. H., Park, S. H., Lee, J.-O., Lee, J., et al. (2021). Pharmacological Potential of Ginseng and its Major Component Ginsenosides. *J. ginseng Res.* 45, 199–210. doi:10.1016/j.jgr.2020.02.004

Rideau, E., Dimova, R., Schwille, P., Wurm, F. R., and Landfester, K. (2018). Liposomes and Polymersomes: a Comparative Review towards Cell Mimicking. *Chem. Soc. Rev.* 47, 8572–8610. doi:10.1039/c8cs00162f

Rui-Zhen, L. I., Yang, Q. J., and Chen, Y. R. (2004). Study of Determination of Superoxide Dismutase(SOD) Activation and Application. *J. Qiongzhou Univ.*, 11, 38–40. doi:10.3969/j.issn.1008-6722.2004.05.011

Salama, S. A., Arab, H. H., Omar, H. A., Gad, H. S., Abd-Allah, G. M., Maghrabi, I. A., et al. (2018). L-carnitine Mitigates UVA-Induced Skin Tissue Injury in Rats through Downregulation of Oxidative Stress, P38/c-Fos Signaling, and the Proinflammatory Cytokines. *Chemico-Biological Interactions* 285, 40–47. doi:10.1016/j.cbi.2018.02.034

Seleci, D. A., Seleci, M., Walter, J. G., Stahl, F., and Scheper, T. (2016). Niosomes as Nanoparticular Drug Carriers: Fundamentals and Recent Applications. *J. Nanomater.* 2016, 7372306. doi:10.1155/2016/7372306

Shin, J., Park, J., Che, D., Kang, H., Cho, B., Lim, Y., et al. (2021). Protective Effects of Halophyte Complex Extract against UVB-induced Damage in Human Keratinocytes and the Skin of Hairless Mice. *Exp. Ther. Med.* 22, 628. doi:10.3892/etm.2021.10114

Um, Y., Lee, Y., Kim, S.-C., Jeong, Y.-J., Kim, G.-S., Choi, D.-W., et al. (2017). Expression Analysis of Ginsenoside Biosynthesis-Related Genes in Methyl Jasmonate-Treated Adventitious Roots of Panax Ginseng via DNA Microarray Analysis. *Hortic. Environ. Biotechnol.* 58, 376–383. doi:10.1007/s13580-017-0041-4

Vitorino, C., Almeida, A., Sousa, J., Lamarche, I., Gobin, P., Marchand, S., et al. (2014). Passive and Active Strategies for Transdermal Delivery Using Co-encapsulating Nanostructured Lipid Carriers: In Vitro vs. In Vivo Studies. *Eur. J. Pharm. Biopharm.* 86, 133–144. doi:10.1016/j.ejpb.2013.12.004

Wan, S., Liu, Y., Shi, J., Fan, D., and Li, B. (2021). Anti-Photoaging and Anti-inflammatory Effects of Ginsenoside Rk3 during Exposure to UV Irradiation. *Front. Pharmacol.* 12, 716248. doi:10.3389/fphar.2021.716248

Wilson, V. G. (2014). Growth and Differentiation of HaCaT Keratinocytes. *Methods Mol. Biol.* 1195, 33–41. doi:10.1007/7651_2013_42

Wolf, S. T., Kenney, L. E., and Kenney, W. L. (2020). Ultraviolet Radiation Exposure, Risk, and Protection in Military and Outdoor Athletes. *Curr. Sports Med. Rep.* 19, 137–141. doi:10.1249/jsr.0000000000000702

Xiao, G., Chen, D., Xiao, H., Wei, J., Sun, J., Xu, G., et al. (2016). Bioinformatics Analysis of Human Glutathione Peroxidase. *J. Beihua University (Natural Science)* 17, 750–755. doi:10.11713/j.issn.1009-4822.2016.06.010

Xu, Q. F., Fang, X. L., and Chen, D. F. (2003). Pharmacokinetics and Bioavailability of Ginsenoside Rb1 and Rg1 from Panax Notoginseng in Rats. *J. Ethnopharmacology* 84, 187–192. doi:10.1016/s0378-8741(02)00317-3

Yang, Q., Qian, L., and Zhang, S. (2020). Ginsenoside Rh1 Alleviates HK-2 Apoptosis by Inhibiting ROS and the JNK/p53 Pathways. *Evidence-Based Complement. Altern. Med.* 2020, 1–8. doi:10.1155/2020/3401067

Zhang, K. S., and Tian, H. L. (2007). Research and Function of Catalase in Organism. *Food Sci. Techn.* 1, 8–10. doi:10.3969/j.issn.1005-9989.2007.01.003

Zhang, Y.-C., Li, G., Jiang, C., Yang, B., Yang, H.-J., Xu, H.-Y., et al. (2014). Tissue-Specific Distribution of Ginsenosides in Different Aged Ginseng and Antioxidant Activity of Ginseng Leaf. *Molecules* 19, 17381–17399. doi:10.3390/molecules191117381

Zhou, X., Du, H.-H., Long, X., Pan, Y., Hu, J., Yu, J., et al. (2021). β-Nicotinamide Mononucleotide (NMN) Administrated by Intraperitoneal Injection Mediates Protection against UVB-Induced Skin Damage in Mice. *J. Inflamm. Res.* 14, 5165–5182. doi:10.2147/jir.S327329

Conflict of Interest: The authors declare that the research was conducted in the absence of any commercial or financial relationships that could be construed as a potential conflict of interest.

Publisher's Note: All claims expressed in this article are solely those of the authors and do not necessarily represent those of their affiliated organizations, or those of the publisher, the editors, and the reviewers. Any product that may be evaluated in this article, or claim that may be made by its manufacturer, is not guaranteed or endorsed by the publisher.

frontiers | Frontiers in Bioengineering and Biotechnology

ORIGINAL RESEARCH
published: 27 April 2022
doi: 10.3389/fbioe.2022.865059

Multifunctional Arabinoxylan-*functionalized*-Graphene Oxide Based Composite Hydrogel for Skin Tissue Engineering

Muhammad Umar Aslam Khan[1,2]*, *Saiful Izwan Abd Razak*[1,3], *Anwarul Hassan*[4,5], *Saima Qureshi*[6], *Goran M. Stojanović*[6] and *Ihsan-Ul-Haq*[7]

[1]BioInspired Device and Tissue Engineering Research Group, School of Biomedical Engineering and Health Sciences, Faculty of Engineering, Universiti Teknologi Malaysia, Johor Bahru, Malaysia, [2]Nanosciences and Nanotechnology Department, National Centre for Physics, Quaid-i-Azam University, Islamabad, Pakistan, [3]Centre for Advanced Composite Materials, Universiti Teknologi Malaysia, Johor Bahru, Malaysia, [4]Department of Mechanical and Industrial Engineering, Qatar University, Doha, Qatar, [5]Biomedical Research Center, Qatar University, Doha, Qatar, [6]Faculty of Technical Sciences, University of Novi Sad, Novi Sad, Serbia, [7]Department of Pharmacy, Quaid-i-Azam University, Islamabad, Pakistan

OPEN ACCESS

Edited by:
Kunyu Zhang,
Johns Hopkins University,
United States

Reviewed by:
Mohammad Taghi Khorasani,
Iran Polymer and Petrochemical Institute, Iran
Yi-Chen Ethan Li,
Feng Chia University, Taiwan
Cheng Hu,
Sichuan University, China

***Correspondence:**
Muhammad Umar Aslam Khan
umar007khan@gmail.com

Specialty section:
This article was submitted to Biomaterials, a section of the journal Frontiers in Bioengineering and Biotechnology

Received: *29 January 2022*
Accepted: *21 March 2022*
Published: *27 April 2022*

Citation:
Khan MUA, Razak SIA, Hassan A, Qureshi S, Stojanović GM, Ihsan-Ul-Haq (2022) Multifunctional Arabinoxylan-functionalized-Graphene Oxide Based Composite Hydrogel for Skin Tissue Engineering. Front. Bioeng. Biotechnol. 10:865059. doi: 10.3389/fbioe.2022.865059

Wound healing is an important physiological process involving a series of cellular and molecular developments. A multifunctional hydrogel that prevents infection and promotes wound healing has great significance for wound healing applications in biomedical engineering. We have functionalized arabinoxylan and graphene oxide (GO) using the hydrothermal method, through cross-linking GO-arabinoxylan and polyvinyl alcohol (PVA) with tetraethyl orthosilicate (TEOS) to get multifunctional composite hydrogels. These composite hydrogels were characterized by FTIR, SEM, water contact angle, and mechanical testing to determine structural, morphological, wetting, and mechanical behavior, respectively. Swelling and biodegradation were also conducted in different media. The enhanced antibacterial activities were observed against different bacterial strains (*E. coli*, *S. aureus*, and *P. aeruginosa*); anticancer activities and biocompatibility assays were found effective against *U-87* and *MC3T3-E1* cell lines due to the synergic effect of hydrogels. *In vivo* activities were conducted using a mouse full-thickness skin model, and accelerated wound healing was found without any major inflammation within 7 days with improved vascularization. From the results, these composite hydrogels might be potential wound dressing materials for biomedical applications.

Keywords: antibacterial, anticancer, composite hydrogels, hemocompatibility, skin wound healing, tissue engineering

INTRODUCTION

The skin, the largest organ of the body and the first line of defense, has different morphological and structural characteristics. The skin serves to protect the internal organs of the body from external influences. The skin cells regenerate wounds due to their natural healing capacity, but it must be done quickly and appropriately for skin wounds (Yadav et al., 2019; Li et al., 2020). Traditional dressings such as bandages, gauze, and sutures have several drawbacks when it comes to wound healing. An ideal wound dressing should promote fast wound healing, remove exudate, provide wetting and gaseous exchange, have adequate mechanical strength, promote growth factors, and protect the

wound from microbes and environmental stresses. It must be non-cytotoxic and biodegradable (Liang et al., 2021; Huang et al., 2022). The wound dressing made of cotton gauze does not hydrate the wound and can harm the wound's regenerative cells when removed. To develop a multifunctional wound dressing, different materials have been used, which are prepared using advanced technologies in various ways (Dong and Guo, 2021). Multifunctional composite hydrogels are ideal wound dressing materials because of their multifunctional properties. The advanced composite hydrogels can control body fluid, moist environment, accelerate healing, reduce inflammation, and hinder bacterial growth by being biocompatible (Yin et al., 2022). Composite hydrogels are multifunctional biomaterials made up of a variety of natural and synthetic polymers as well as fillers. Polyvinyl alcohol (PVA) is a well-known synthetic polymer that has been widely used in wound healing because of its good mechanical properties and biocompatibility. It has poor antimicrobial characteristics, which limits its use as a wound-healing agent (Jia et al., 2018; Kalantari et al., 2020). However, due to its multifunctional behavior, its composite form may achieve desired antibacterial activities and play a significant role in wound healing. Polysaccharides (alginate, arabinoxylan, guar gum, chitosan, and hyaluronic acid) can also be modified into various forms, such as films and foams. The only disadvantage is poor mechanical stability, which can be overcome by incorporating physical or chemical cross-links into hybrid or composite hydrogels (Zhong et al., 2021). Arabinoxylan (ARX) is a biopolymer and a type of polysaccharide and hemicellulose with xylose backbone and arabinose side chains. It is a major fibrous component of several cereal grains and the second most abundant biopolymer in plants after cellulose. Some of the physiological benefits include fecal bulking, cholesterol reduction, glycemic regularity, prebiotic activity, and immune modulation (Khan et al., 2021a; Aslam Khan et al., 2021). Its inherent physicochemical properties, such as water retention, increased viscosity, and gelatinization, make it a versatile material with many different applications in the medical, food, and pharmaceutical industries (Al-Arjan et al., 2020; Khan et al., 2020). Graphene oxide is a reduced form of naturally occurring graphite made up of a single layer of carbon with honeycomb-like networking and sp^2 hybridization. Due to its biocompatibility and physicochemical properties, it has recently attracted interest in biomedical applications including biosensors, tissue engineering, wound healing, cancer therapy, and drug delivery systems (Khan et al., 2021b; Umar Aslam Khan et al., 2021). It is well known for dissolving kidney stones and has antibacterial and antitussive properties. Pan et al. have reported the synthesis of PVA/GO-based hydrogel for skin healing applications and found enhanced mechanical, self-healing, and super stretchable properties (Pan et al., 2020).

In this study, we present the development of composite hydrogels: the GO-functionalized arabinoxylan was cross-linked with PVA *via* TEOS (cross-linker) using a simple blending method to develop readily available economical composite hydrogel. According to the best of our knowledge, these formulations have never been reported in the open literature. The structural, morphological, mechanical, and wetting analyses were investigated by FTIR, SEM, UTM, and water contact angle, respectively. Swelling and biodegradation were carried out to determine physicochemical properties. The antibacterial and anticancer activities, and biocompatibility of composite hydrogel were found effective against bacteria, *U-87* and *MC3T3-E1*. *In vivo*, a wound-healing mouse model was employed to investigate healing. These composite hydrogels have the potential to heal skin wounds and would be a potential biomaterial for wound dressings.

MATERIALS AND METHODS

Materials

Graphite powder, TEOS, PBS solution, HCl, H_2SO_4, absolute ethanol, glacial acetic acid, nutrient broth, and nutrient agar were purchased from Sigma Aldrich, Malaysia. These chemicals were analytically graded and used without any purification.

Preosteoblast (*MC3T3-E1*) cell lines and alpha-MEM (α-MEM) were supplied by ATCC and Hyclone Laboratories Inc., respectively. Fetal bovine serum (FBS) and L-glutamine penicillin/streptomycin were purchased from ThermoFisher Scientific. Male albino mice (BALB/c) weighing 23–25 g (aged 5–7 weeks) were supplied by the National Institute of Health. Approval from the Animal Ethical Committee was obtained to carry out experiments on mice.

Methods

Extraction of Arabinoxylan From Ispaghula Seed Husk

The Ispaghula seed husk was obtained from a local market in Johor Bahru, Malaysia, as a by-product. Iqbal et al. used a well-known method to extract arabinoxylan from the husk of Ispaghula seed (Saghir et al., 2008). The dust and stones from 50 g of seed husk were removed and dispersed in 500 ml of deionized water for 24 h. The pH of the swollen mixture was then raised to 12 by slowly adding a 2.5% solution of sodium hydroxide (NaOH). The husk was separated from the gel by vacuum filtration, and the filtrate was coagulated at pH 3 by adding acetic acid dropwise. The coagulated gel was washed with deionized water to remove acetic acid and freeze-dried to get dried powder of ARX.

Hydrogel Fabrication

Arabinoxylan was functionalized with GO *via* the hydrothermal method. ARX (2 g) and GO (0.03 mg) were added to the autoclave and kept in an oven at 50°C overnight to get the composite gel, and the proposed schematic is shown in **Scheme 1A**. The composite gel was dispersed into 25 ml deionized water and stirred with PVA (0.3 g), which is dissolved in 10 ml deionized water at 80°C, for 1 h at 55°C. Different concentrations of TEOS (100, 150, 200, and 250 μL) were dissolved into 5 ml ethanol and added dropwise into the whorl loop of the mixture as a cross-linker. The polymeric mixture was homogenized for 1 h at the same temperature. Then, potassium persulfate (0.2 g) was dissolved in deionized water and added dropwise to the polymeric mixture and allowed

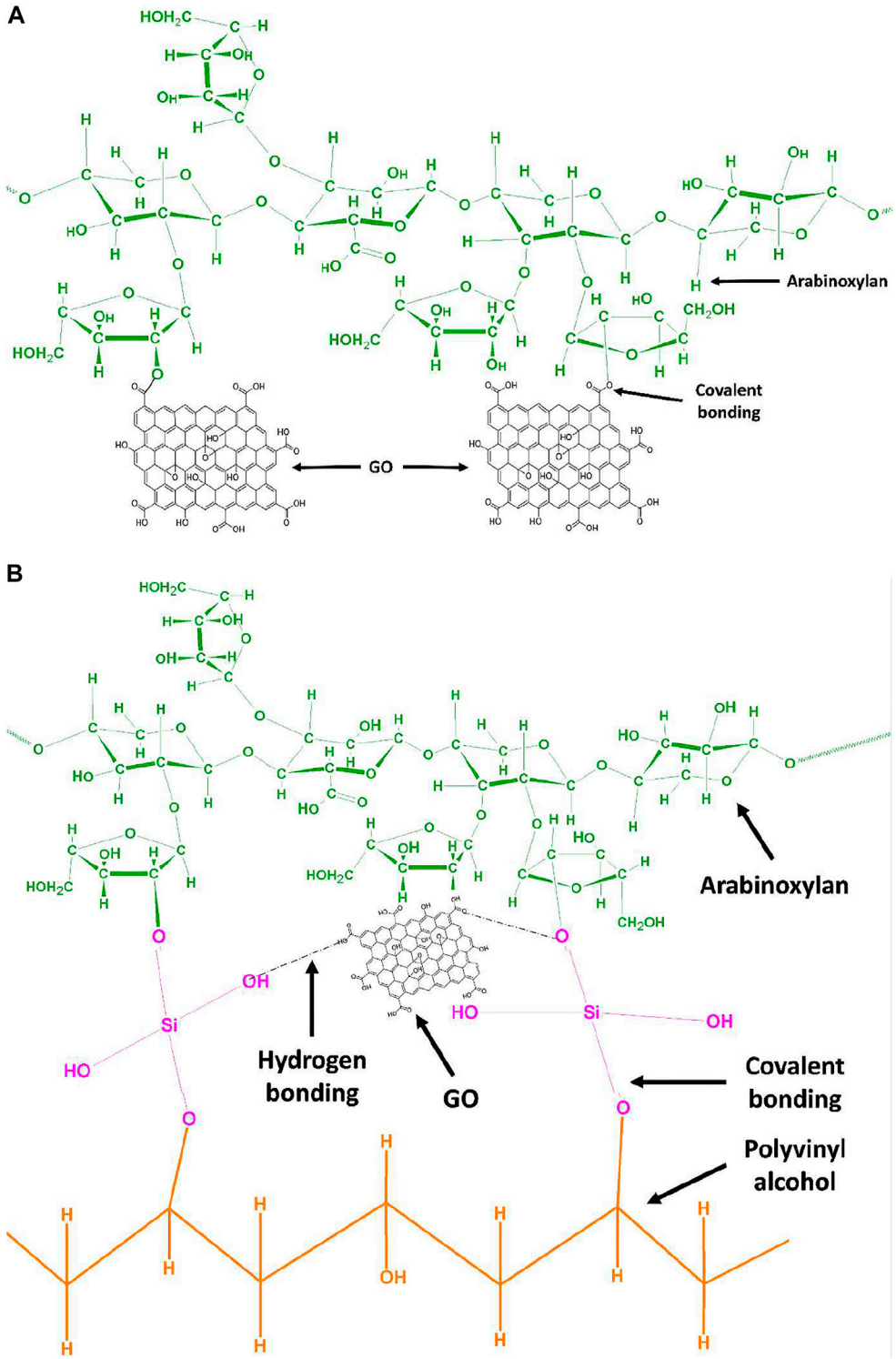

SCHEME 1 | (A) Proposed chemical mechanism of GO functionalized arabinoxylan *via* covalent bond interaction by hydrothermal method. **(B)** Proposed chemical mechanism of GO functionalized arabinoxylan and polyvinyl alcohol *via* TEOS cross-linker.

to stir for 3 h at 55°C for successful cross-linking. After 3 h, the mixture was poured into Petri plates and dried in the oven at 50°C overnight. Different codes were assigned after different concentrations of TEOS AGP-1 (100 ml), AGP-2 (150 ml), AGP-3 (200 ml), and AGP-4 (250 ml). The proposed reaction cross-linked composite hydrogel is shown in **Scheme 1B**.

Characterizations

The structural and functional group identification of composite hydrogels was analyzed by Fourier-transform infrared spectroscopy (Nicolet 5,700, Waltham, MA, United States). The range was 4,000–400 cm^{-1} with 150 scans. The surface morphology of the composite hydrogel was observed by a scanning electron microscope (JEOL-JSM 5410 LV) with an accelerating 10 kV voltage. The well-dried film of composite hydrogels was gold-supported before analysis. The wetting analysis of the composite hydrogel was performed using a water contact angle system (JY-82, Dingsheng, Chengde, China) to investigate the hydrophilicity and hydrophobicity. The mechanical testing of composite hydrogels was conducted by tensile tests, and hydrogel samples were shaped into strips. The tensile testing (length 55 mm, width 15 mm, and thickness 2 mm) and tests were conducted with 10 mm/min speed by ASTM D638 (Standard, 2003).

Gel Fraction

Weighing small pieces of composite hydrogels was used to conduct the gel fraction analysis. These small composite hydrogel pieces were submerged in deionized water for 12 h at room temperature. These hydrogel samples were then taken out and dried in an oven at 40 °C until they reached a consistent weight (**Eq. 3**).

$$Gel\,fraction\,(\%) = \frac{M'}{M^o}, \tag{1}$$

where M^o is the oven-dried hydrogel weight and M' is the initial hydrogel weight.

Swelling and Biodegradation

At 37°C, the pH sensitivity of composite hydrogels was tested in an aqueous and PBS medium at various pH (1–13). All composite hydrogel samples were cut into squares and properly weighed at 50 mg as an initial weight (W_i). After soaking in various conditions, the hydrogel samples were removed, and surface water was removed with a tissue paper before being weighed as the final weight (W_f). **Eq. 2** was used to calculate the swelling behavior.

$$Swelling\,(\%) = \frac{W_f - W_i}{W_i} \times 100 \tag{2}$$

At pH 7.4, 37°C, in PBS media, *in vitro* biodegradation of well-dried composite hydrogels was investigated. All hydrogel samples were carefully cut into squares with a 50 mg weight and placed in PBS media to see how much weight was lost over time. **Eq. 3** was used to calculate the biodegradation of the hydrogel samples.

$$Weight\,loss\,(\%) = \frac{W_i - W_t}{W_i} \times 100 \tag{3}$$

where W_i = initial weight, W_f = final weight, and W_t = weight at time "*t*."

In Vitro Assay

Antibacterial Activities

The antibacterial potential of the composite hydrogels was determined using the disc diffusion method. In the disk diffusion method, nutrient broth, nutrient agar, and all the apparatus used for the assay were first autoclaved to avoid any additional bacterial growth. The bacterial strains were refreshed by using 2 loop-full of bacteria in nutrient broth in test tubes and incubated for 24 h. The nutrient agar was poured into the Petri dish and allowed to settle. The bacterial strains were spread over nutrient agar using a glass rod. Then 75 μL hydrogel samples was placed by micropipette, and the Petri dishes were incubated for 12 h. The antibacterial behavior was recorded in terms of zone inhibition.

Hemocompatibility Assay

A hemocompatibility assay was carried out to find the compatibility of the hydrogel polymer with the blood. Hydrogels were assayed at different concentrations ranging from 500 to 100 ug with 5–10% solution of blood cells in PBS. After getting the blood, it was immediately mixed in EDTA solution to prevent the clotting of blood; 500 ul of blood was taken in each Eppendorf and centrifuged at 14,000 rpm for 15 min. Blood cells settled down, and serum was discarded. Blood cells were washed with PBS by adding 1 ml of phosphate buffer saline in this Eppendorf and centrifuged for 15 min. The supernatant was discarded, and the process was repeated 3 times. Isolated red blood cells were then mixed into PBS solution to make a 5% solution of red blood cells. Different concentrations of hydrogel were placed in each Eppendorf followed by the addition of 500 ul of RBC solution. It was then incubated at 37°C for 30 min, then centrifuged again at 14000 rpm for 10 min, 200 ul of supernatant was then collected in 96-well plates, and absorption was measured at 541 nm wavelength.

Cytotoxicity and Cell Proliferation

The cytocompatibility and cell proliferation of composite hydrogels with different concentrations have been studied against Uppsala (*U87*) and mouse pre-osteoblast (*MC3T3-E1*) cell lines at different intervals of time (24, 48, and 72 h). The well plates were coated with gelatin (0.1%), which is taken as a positive control. These plates were incubated under standard *in vitro* conditions. Cytotoxicity was conducted using the Neutral Red assay as reported by Repetto (Repetto et al., 2008). The optical density was recorded by absorbance at 540 and 550 nm *via* a microplate reader for *MC3T3-E1* and *U87*, respectively. The cell viability was calculated by **Eq. 3**.

$$Cell\,vaibility = \frac{OD_s}{OD_c} \times 100 \tag{4}$$

where OD_s is the sample optical density and OD_c is the controlled optical density.

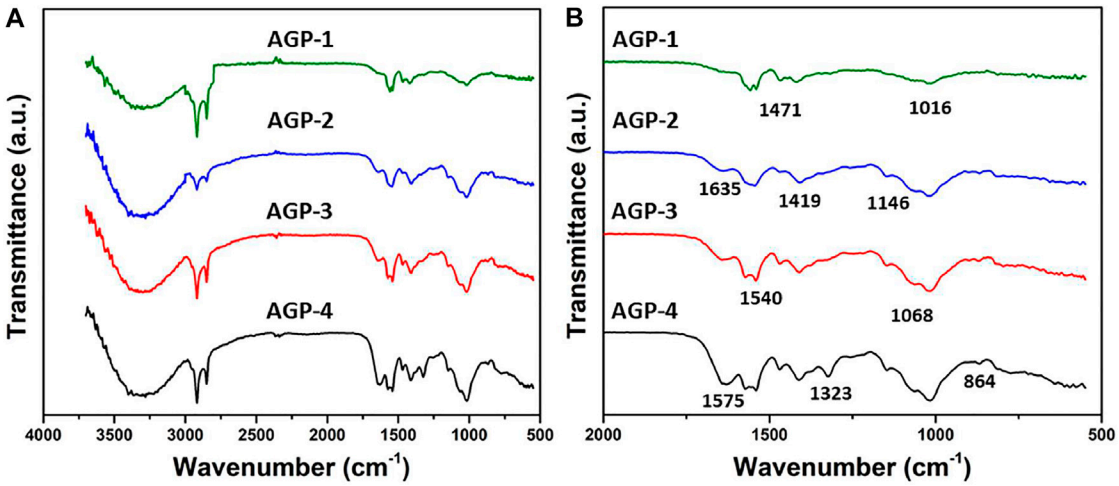

FIGURE 1 | FTIR spectrum of composite hydrogels.

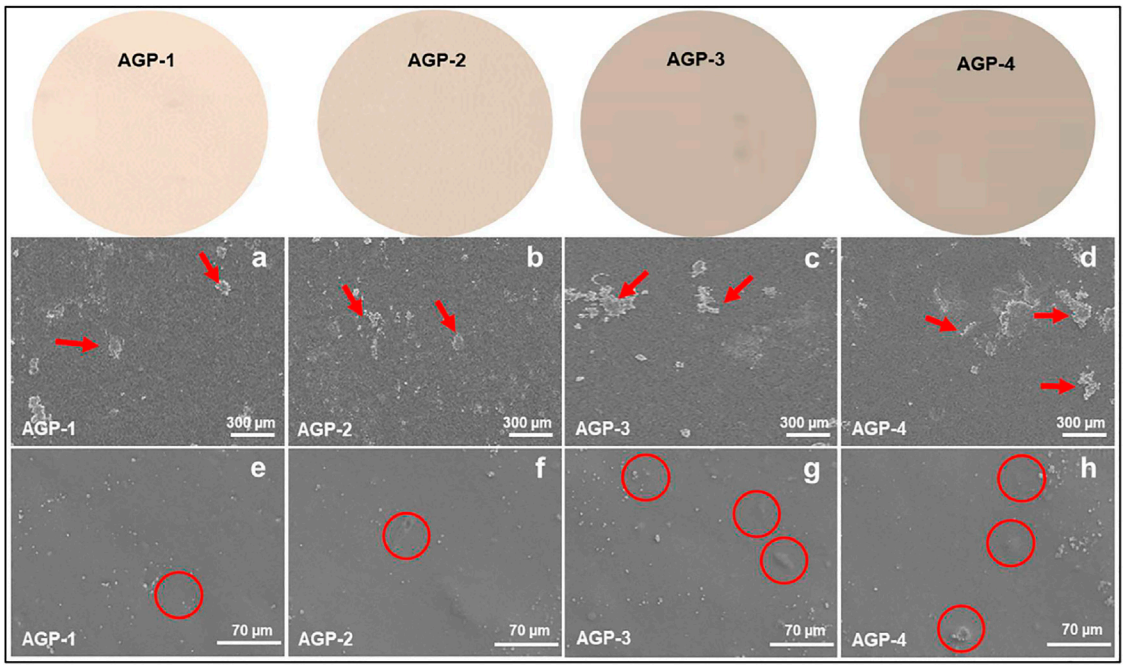

FIGURE 2 | Surface morphology of composite hydrogels at different scales (300 and 70 μm): red arrows indicate GO flakes and red circles indicate embedded GO particles.

In Vivo Wound Contraction

Mice were kept in the animal facility of the Department of Pharmacy, Quaid-i-Azam University, and acclimatized for 1 week in standard environmental conditions. After ensuring that the mice are acclimatized to the environment and are of standard weight, 60 μl of tramadol (25 mg/kg) was orally fed to the mice using a feeding tube and syringe. Hair was removed from the dorsum side of the mice (3 cm down from the neck and between the shoulder blades) by a clipper. Hair removing cream was applied lightly for no longer than 2 min. After 2 min, depilatory cream and fur were removed by using wetted gauze. Mice were placed in a jar for just 5 s, containing cotton wetted with chloroform to give them anesthesia. After cleaning the skin, they were disinfected with 70% alcohol. The skin was lifted from the dorsal side at the midline with the help of the index finger and thumb cranially and caudally. The mice were then placed in a lateral position, and two-layer skin was removed with the help of a sharp biopsy punch to make an excisional wound of 6 mm in

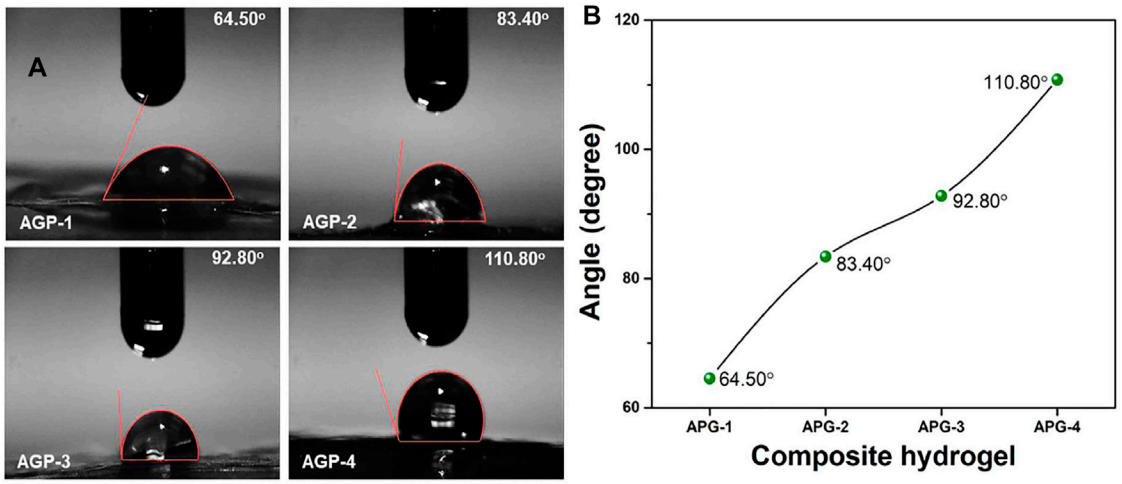

FIGURE 3 | Wetting behavior of composite hydrogels at ambient.

diameter. After excision, the mice were placed in a warm area to maintain their body temperature and observed until they recovered from anesthesia. When it gets normal, mice were transferred into their cage. Wound size was measured on alternate days by using a Vernier caliper, and percent wound closure was measured.

Statistical Analysis

The obtained data were statistically analyzed by statistical software (IBM, SPSS Statistics 21); standard error (S.E.) in the figures was represented as Y-error bars. The two-way ANOVA has been used with *post hoc* multiple comparisons ($*p < 0.05$, $**p < 0.01$, and $***p < 0.001$ size of sample, n = 3).

RESULTS AND DISCUSSION

FTIR Analysis

The FTIR spectrum of composite hydrogels with different formulations of composite hydrogels is shown in **Figure 1**. The broadband peak at 3,750–3,200 cm^{-1} is due to inter/intra hydrogen bonding. It confirms the hydrogen bond of composite hydrogels between arabinoxylan and PVA/GO (Aslam Khan et al., 2021). The stretching bands that were observed at 2,918–2,848 cm^{-1} are attributed to the aliphatic saturated C–H bond. It has different transmittance that is increased with an increased degree of cross-linking. The peak positions at 1,635 and 1,575 cm^{-1} indicate the presence of –C═O stretching band and C═C functional group of graphene oxide. The pyranose ring and saccharine structure peaks were observed at 864 and 1,146 cm^{-1}, respectively, which are fundamental peaks of arabinoxylan (Adorinni et al., 2021; Khan et al., 2021c). The stretching band 1,110–1,000 cm^{-1} is due to the presence of TEOS (cross-linker) and it confirms the presence of –Si–O–C and –Si–O–Si functional groups. The increasing transmittance intensities of the stretching band 1,110–1,000 cm^{-1} confirm the increasing amount of TEOS (Fan et al., 2021). Hence, the functional groups and variable transmittance confirm the successful development of a different formulation of composite hydrogels.

Morphological Analysis

The surface morphology of the generated hydrogel was examined using scanning electron microscopy as shown in **Figure 2**. The morphology of the hydrogels was investigated at various scales. According to the morphological analysis, the hydrogel's surface morphology is tight, thick, rough, and wavy. It possesses high toughness and dense cross-linking because of the enhanced TEOS amount. It also has a wrinkled, rough lamellar shape, which could be attributed to the presence of GO. This surface is rougher than typical, which helps to increase the surface area. By boosting ion transport and polymer chain mobility, it will improve the self-healing ability of hydrogels (Khan et al., 2021d; Zhao et al., 2022). It was also observed that increasing TEOS amount caused GO to cause more GO clustering at 300 μm as presented with red arrows. However, nano-GO and embedded GO flakes can also be observed in red circles. Hence, the rough surface morphology helps cell adherence and proliferation, while the close packing is formed due to the increasing cross-linker amount that retains its structure after containing substantial biofluids.

Wetting

One of the most significant features of all biomaterials is surface wettability because it depicts the true structure and chemical surface properties. Many features of therapeutic drugs, such as biocompatibility, adhesion, lubricity, selective absorption, and controlled release, are determined by wetting (Khan et al., 2021e). Soft hydrogels, which are made primarily of water and a hydrophilic polymeric network, are naturally hydrophilic. Because of their hydrophilic nature, they have a low water contact angle with their surfaces. The wetting behavior changed from hydrophilic to hydrophobic as the cross-linker quantity was increased, owing to increased and close packing that

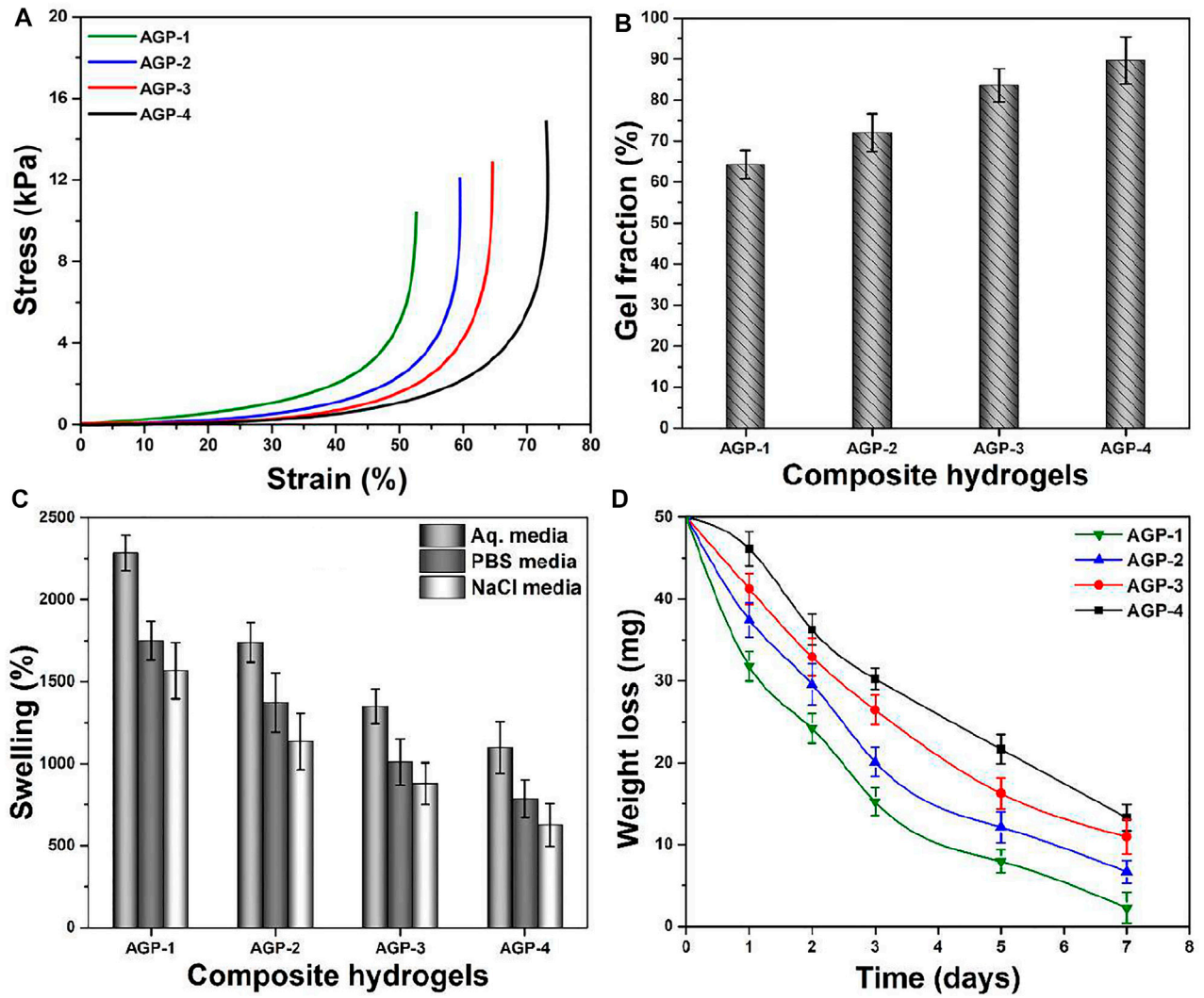

FIGURE 4 | (A) Mechanical testing, **(B)** gel fraction (%), **(C)** swelling in different media (aqueous, PBS solution, and NaCl solution), and **(D)** biodegradation in PBS media of composite hydrogels.

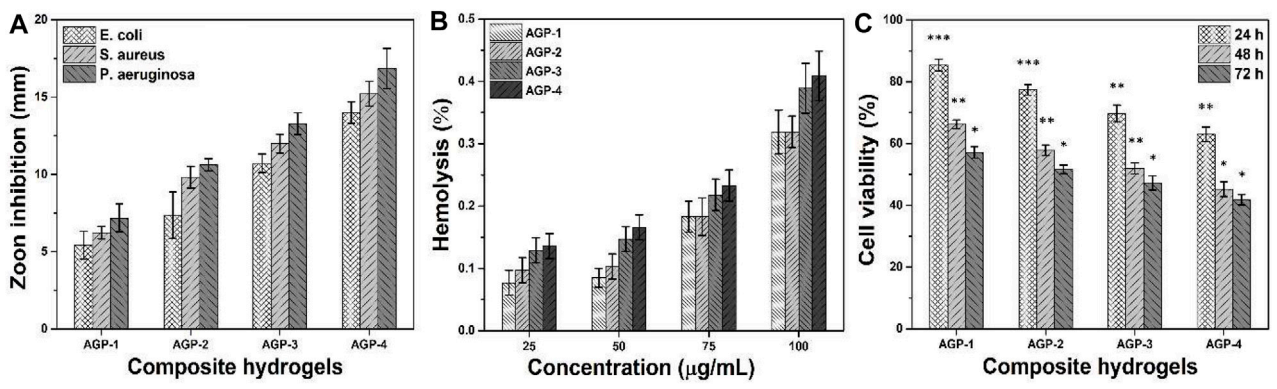

FIGURE 5 | Bioactivities of composite hydrogels were conducted to determine their biological behavior for different activities: **(A)** antibacterial activity against (Gram-positive and Gram-negative) bacterial strains, **(B)** hemocompatibility, and **(C)** anticancer activity. $*p < 0.05$, $**p < 0.001$, and $**p < 0.0001$.

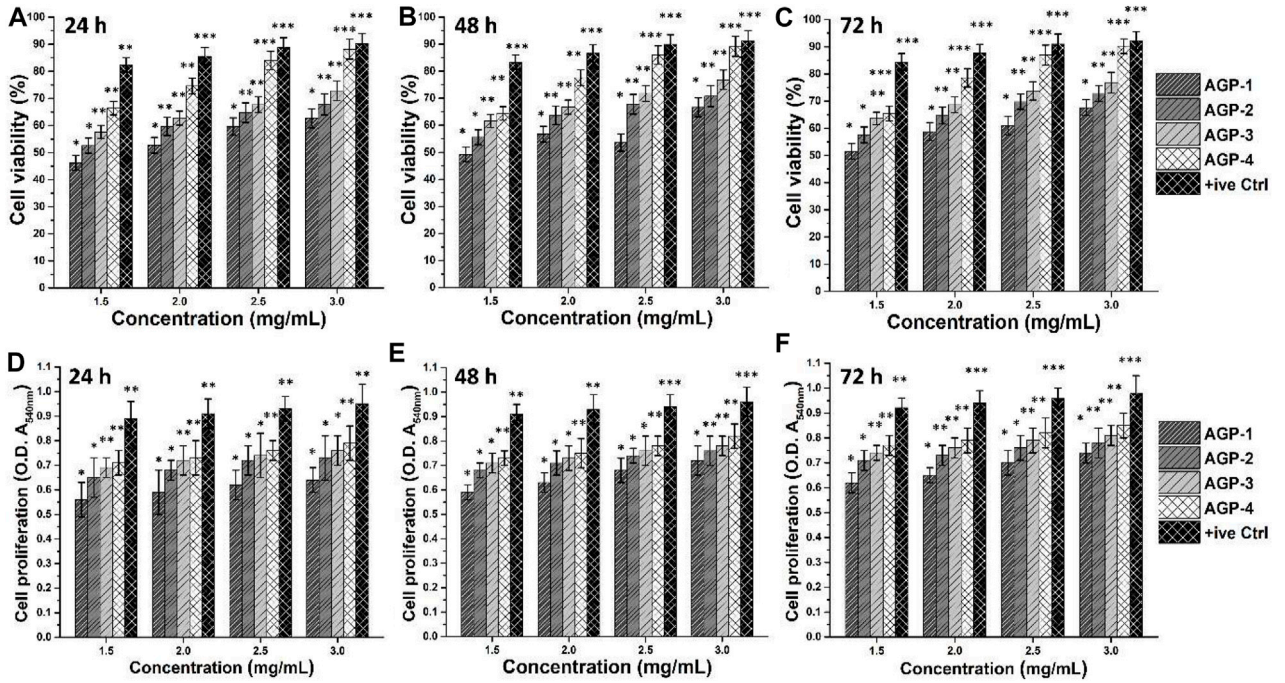

FIGURE 6 | Biocompatibility assays were performed against different concentrations of composite hydrogels to determine the bioactive behavior. The biocompatible behavior was studied by cell viability **(A–C)** and cell proliferation **(D–F)** using *MC3T3-E1* cell lines. Gelatin (0.1%) is taken as a positive control. $*p < 0.05$, $**p < 0.001$, and $**p < 0.0001$.

changed surface characteristics. Because of the dense packing and higher cross-linking, there is less hydrogen bonding available to create functional groups (Sala et al., 2021). As a result, the hydrogel sample (AGP-1) was found to have the highest hydrophilicity (64.50°) with minimal cross-linking and the highest hydrophobicity (AGP-4) with maximal cross-linking (110.80°) as presented in **Figure 3**. The required properties of the hydrogel can be attained by adjusting the cross-linking degree. As a result, we created hydrogels with varying degrees of cross-linking to provide distinct formulations with varying physicochemical properties to address various wound healing applications in various wound environments.

Mechanical Testing and Gel Fraction

The mechanical behavior of composite hydrogel was analyzed by stress–strain curves as shown in **Figure 4A**; it presents the substantial improvement in mechanical strength by increasing the cross-linking degree (from AGP-1 to AGP-4). The structural and mechanical properties of composite hydrogels were investigated by changing the amount of TEOS to obtain different formulations for wound healing applications. The mechanical behavior will aid in determining structural integrity and cross-linker (TEOS) quantity optimization. After absorbing wound exudate, the composite hydrogel swells during application. An ideal hydrogel material with optimized cross-linking will preserve structural integrity without dissolving or breaking, allowing it to absorb the maximum amount of biofluid and thereby guard against bacterial attack (Lin et al., 2021). The mechanical strength of composite hydrogels can be optimized by cross-linker amount. The elastic modulus of samples AGP-2 to AGP-4 is in the range of the elastic modulus of skin. The cross-linking degree increased by increasing the TEOS amount that will allow consistent adhesion when the composite hydrogel is removed from the skin. The mechanically stable composite hydrogels with bioactive properties could be excellent wound dressings for skin wound healing applications. The cross-linking degree is governed by the gel fraction, and the gel fraction percentage of the composite hydrogels has been calculated as shown in **Figure 4B**. It can be noticed that hydrogel sample AGP-1 has the lowest gel fraction percentage (64.25%) and hydrogel sample AGP-4 has the highest gel fraction percentage (89.67%). The increasing gel fraction % is attributable to an increase in the amount of cross-linker used to bind the polymeric chains together, or to a higher degree of cross-linking. As a result, increased cross-linking promotes covalent bonding, which improves the gel fraction (%) and may facilitate the physicochemical interaction between the functionalized polymer and the cross-linker.

Swelling and Biodegradation Analysis

When the hydrogel comes into contact with the wound, it absorbs the exudate and begins to swell, which protects against bacterial infection. As demonstrated in **Figure 4C**, the swelling hydrogel was performed in different media with a

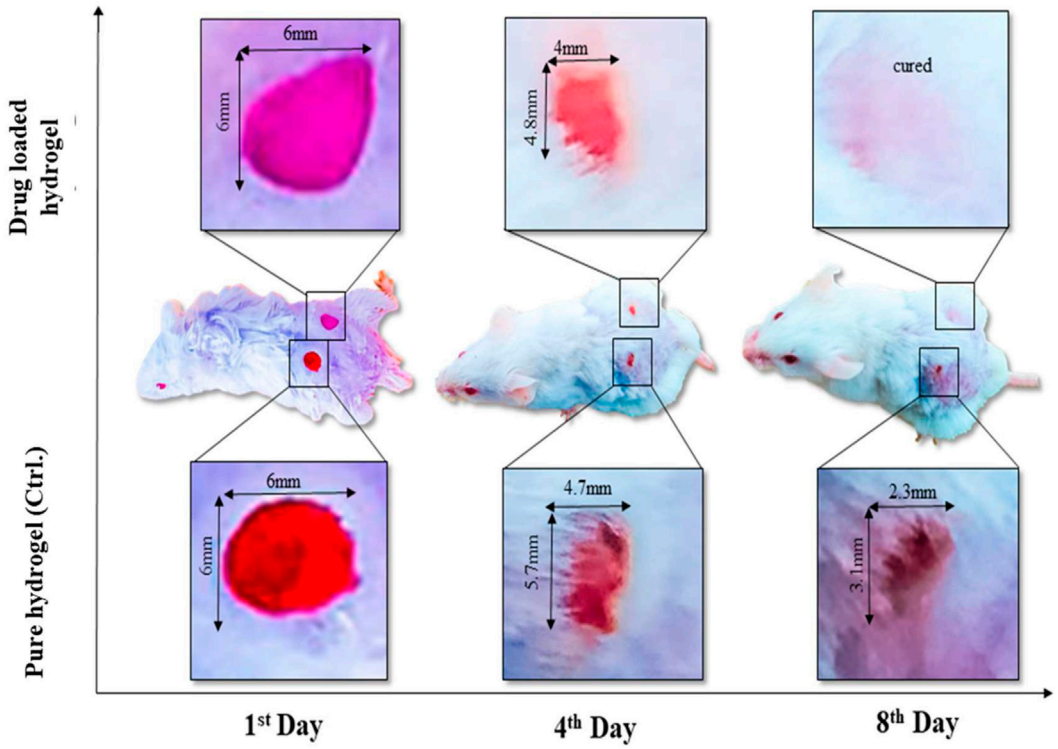

FIGURE 7 | *In vivo* assay (animal model) has presented the wound healing by using a single dose of plan composite hydrogel (control sample) to compare with drug-loaded composite hydrogel.

pH of 7.4 at 37°C. Composite hydrogels swelled the most in aqueous media, the least in PBS media, and the least in NaCl (electrolyte) media, according to the findings. The highest swelling in aqueous media may be attributed to the deionized nature of the media, while PBS and NaCl media show less swelling due to ion deposition, which may limit hydrogel porosity and prevent additional solution uptake. It was also discovered that AGP-1 has the most swelling and AGP-4 has the least swelling, which could be attributed to the increasing degree of cross-linking. Because AGP-1 has the least cross-linking, it has more open spaces to retain more solutions than AGP-4, which has fewer broad spaces accessible. After absorbing a significant volume of biofluids, biodegradation is an important occurrence for hydrogels because it allows for the prolonged release of therapeutic agents. As shown in **Figure 4D**, the biodegradation of composite hydrogel in PBS media at 37°C was determined. The least degraded AGP-4 was discovered, while the most degraded AGP-1 was observed. It could be related to varying levels of cross-linking. As a result, the degree of cross-linking can be used to maximize the biodegradation of composite hydrogels. However, because GO has a large surface area and multiple distinct oxygen-based functional groups, it cannot be ignored in the swelling and biodegradation of composite hydrogels. It conducts cross-linking behavior by interacting with the polymeric matrix of hydrogels in a variety of ways, including weak van Der Waal's forces of attraction and hydrogen bonding (Khan et al., 2021a; Khan et al., 2021f). Swelling and biodegradation can thus be regulated by adjusting the TEOS concentration to achieve the optimal formulation for the environment because we sometimes require distinct swelling that is not destroyed to keep the wound moist. These composite hydrogel degrees can be used in a variety of wound healing applications in a variety of environments to moisten the wound by absorbing biofluids and speed wound healing. After absorbing biofluid or wound exudate, these composite hydrogels would maintain a moisture environment with controlled biodegradation.

In Vitro Assay

Antibacterial Activities

The antimicrobial properties of any biomaterial are very important in medical applications to provide a biocompatible and protective environment. We have conducted antibacterial activities against Gram-positive and Gram-negative severe infection-causing pathogens, that is, *P. arginase*, *S. aureus*, and *E. coli*, as shown in **Figure 5A**. The antibacterial activities were presented in terms of zone inhibition. It was observed that increasing cross-linking caused increased antibacterial activities as AGP-1 presented

least and AGP-4 maximum. It may be due to the optimized degree of cross-linking that tailored physicochemical properties of the composite hydrogels that interact with pathogens differently. The role of GO cannot be denied; the sharp edges of GO may rupture the bacterial membrane to hinder its activity and replication (Liang et al., 2021; Duan et al., 2022; Kailasa et al., 2022). The polymeric part of the composite hydrogel may interact with the bacterial membrane due to different functional groups and transfer its electrostatic charge. It may interact with bacterial DNA and take over the charge for further replication (Khan et al., 2021f). The synergically composite hydrogels exhibit antibacterial activities for further bacterial replication and growth. Hence, the synergic effect of the composite hydrogel may protect the wound from severe pathogens for proper and quick wound healing.

Hemocompatibility Assay

The hemocompatibility of all samples of composite hydrogels has been conducted against healthy human blood, as shown in **Figure 5B**. A hemocompatibility assay was used to determine the hydrogel polymer's blood compatibility. Biocompatibility is usually the most significant factor because the materials are used in living beings. The hydrogels aid to speed up the healing process by coming into direct contact with cells and tissues during wound healing. They should not be hemotoxic as a result. According to hemocompatibility data, hydrogel formulations did not tear the membrane of red blood cells, and the cells remained intact. These samples have a hemolysis rate of less than 1%, making them the most blood compatible. It can be seen that these composite hydrogels have different hemocompatibility behavior with different concentrations. Increasing concentration can cause more hemolysis, but the rate is less than 1%. Possibly, the caused hemolysis is due to the GO-sharp edges that may rupture membranes of red blood cells (Duan et al., 2022). Hence, it is confirmed from the results that our composite hydrogels are hemocompatible. These may not cause any serious hemolysis during topical application for skin wound care and treatment.

Anticancer Activities

The anticancer activities of composite hydrogels against U87 have been studied at different time intervals (24, 48, and 72 h), as can be seen in **Figure 5C**. It is worth mentioning that increasing cell incubation time and TEOS amount caused more anticancer activities. Composite polymeric system (ARX-*f*-GO) and TEOS may have a synergetic effect on the U87 cell lines, as GO has sharp edges and ruptures cell membrane to cause cell death. Sample AGP-4 has maximum cell death or less cell viability; however, AGP-1 has more cell viability or less cell death. The polymeric part of the composite hydrogel may take control for further cell proliferation (Ou et al., 2017). Moreover, the longer contact time may also cause cell death to have better anticancer activities (Kumari et al., 2010). It is also observed that initially, the composite hydrogel did not exhibit any prominent anticancer activities. But later, they became more toxic toward U87 cell lines and performed better anticancer activities (Santhosh et al., 2017). This behavior may be due to the optimum amount of polymeric, TEOS, and GO that interact differently with U87 cell lines. These composite hydrogels might be considered potential biomaterials for anticancer applications.

Cell Viability and Proliferation

Figure 6 shows the vitality and proliferation of *MC3T3-E1* cell lines *in vitro* when exposed to various concentrations of composite hydrogels. Cell survival and proliferation have been demonstrated in these composite hydrogels. Furthermore, it has been demonstrated that when concentration and duration increase, cell viability and proliferation also increase. It could be related to the interaction time of *MC3T3-E1* cell lines with composite hydrogels. It is possible that boosting TEOS and optimizing GO quantity provides the required functionality to assist cell adhesion, which promotes cell viability and proliferation (Hu et al., 2021). The GO has an electroconductive response, and the right amount of GO in a composite hydrogel's polymeric matrix can produce electroconductive behavior. Since GO contains numerous oxygen-based functional groups, H-bonding aids cell adhesion to hydrogels. GO also has a larger surface area and a variety of functions that may improve cell survival and proliferation by facilitating cell adhesion (Yang et al., 2021). APG-4 >APG-3>APG-2>APG-1 was the order of cell viability and optical density behavior of *MC3T3-E1* cells on the hydrogel scaffold. These findings suggest that raising TEOS and optimizing GO concentrations enhance cell adhesion and proliferation while avoiding cytotoxicity.

Wound Contraction

A wound is a disruption in the continuity of the normal anatomy of the skin. Modern methods of wound healing have advantages over traditional methods. Polysaccharide hydrogel polymers have reduced mechanical strength. Hydrogel polymer composite cross-linked with graphene oxide has tissue regenerative and antimicrobial activity. Hydrogel polymers have their wound healing activity, and when cross-linked, it increases their mechanical strength, and when combined with the drug, it reduces the healing time of the wound. The area of the wound was measured using a scale, and wound closure was noted on days 1, 2, 4, 6, and 8 as shown in **Figure 7**. Wound contraction of mice showed that hydrogels showed a noteworthy wound healing process, but bergenin-loaded hydrogel had a more significant effect in the wound healing process and helped in the prompt healing process as compared to using hydrogel alone.

CONCLUSION

We have reported novel formulations of composite hydrogels with enhanced antibacterial, biodegradable, and bioactivity properties. Arabinoxylan was functionalized with GO *via* the

hydrothermal method and cross-linked with PVA using different TEOS amounts to optimize the properties of the hydrogel. FTIR confirms the successful cross-linking, and rough surface morphology was observed by SEM. The wetting behavior was shifted from hydrophilic to hydrophobic by increasing the TEOS amount, while mechanical properties and biodegradation also increased. The multifunctional behavior of GO has tuned the composite hydrogel to have synergic effects on antibacterial, cell viability, and proliferation. It was also found that increasing TEOS amount also enhances cell adherence and proliferation due to increased structural orientation and integrity. The wound healing was observed within 7 days with loading a potential wound-healing drug and plan hydrogel. Amazing wound healing was observed with a single dose of hydrogels loaded on the first day. Therefore, from the results, it is concluded that the composite hydrogel can be a promising biomaterial for healing without any prominent inflammation within a week.

DATA AVAILABILITY STATEMENT

The raw data supporting the conclusion of this article will be made available by the authors, without undue reservation.

ETHICS STATEMENT

The animal study was reviewed and approved by the Ethics Committee under UTM/2016/KHAIRUL NADWA/28-JAN./729-FEB-2016-JAN-2019.

AUTHOR CONTRIBUTIONS

Conceptualization, MK; data curation, MK and SQ; formal analysis, MK; funding acquisition, MK, SR, and GS; investigation, AH, SR, and GS; methodology, MK and SQ; project administration, SR and AH; resources, SR, I-U-H, and AH; software, MK; supervision, MK, SR, and AH; validation, MK, SR, I-U-H, and GS; visualization, MK; writing—original draft, MK; writing—review and editing, MK and GS.

FUNDING

This research was made possible through the Qatar National Research Foundation Grant NPRP12S-0310-190276 and European Union's Horizon 2020 research and innovation program under grant agreement No. 951747. All statements made herein are the sole responsibility of the authors.

REFERENCES

Adorinni, S., Rozhin, P., and Marchesan, S. (2021). Smart Hydrogels Meet Carbon Nanomaterials for New Frontiers in Medicine. *Biomedicines* 9 (5), 570. doi:10.3390/biomedicines9050570

Al-Arjan, W. S., Aslam Khan, M. U., Nazir, S., Abd Razak, S. I., and Abdul Kadir, M. R. (2020). Development of Arabinoxylan-Reinforced Apple Pectin/Graphene Oxide/Nano-Hydroxyapatite Based Nanocomposite Scaffolds with Controlled Release of Drug for Bone Tissue Engineering: *In-Vitro* Evaluation of Biocompatibility and Cytotoxicity against MC3T3-E1. *Coatings* 10 (11), 1120. doi:10.3390/coatings10111120

Aslam Khan, M. U., Haider, A., Abd Razak, S. I., Abdul Kadir, M. R., Haider, S., Shah, S. A., et al. (2021). Arabinoxylan/graphene-oxide/nHAp-NPs/PVA Bionano Composite Scaffolds for Fractured Bone Healing. *J. Tissue Eng. Regen. Med.* 15 (4), 322–335. doi:10.1002/term.3168

Dong, R., and Guo, B. (2021). Smart Wound Dressings for Wound Healing. *Nano Today* 41, 101290. doi:10.1016/j.nantod.2021.101290

Duan, S., Wu, R., Xiong, Y.-H., Ren, H.-M., Lei, C., Zhao, Y.-Q., et al. (2022). Multifunctional Antimicrobial Materials: From Rational Design to Biomedical Applications. *Prog. Mater. Sci.* 125, 100887. doi:10.1016/j.pmatsci.2021.100887

Fan, Z., Wei, Y., Yin, Z., Huang, H., Liao, X., Sun, L., et al. (2021). Near-Infrared Light-Triggered Unfolding Microneedle Patch for Minimally Invasive Treatment of Myocardial Ischemia. *ACS Appl. Mater. Inter.* 13 (34), 40278–40289. doi:10.1021/acsami.1c09658

Hu, C., Yang, Y., Lin, Y., Wang, L., Ma, R., Zhang, Y., et al. (2021). GO-based Antibacterial Composites: Application and Design Strategies. *Adv. Drug Deliv. Rev.* 178, 113967. doi:10.1016/j.addr.2021.113967

Huang, Y., Bai, L., Yang, Y., Yin, Z., and Guo, B. (2022). Biodegradable Gelatin/silver Nanoparticle Composite Cryogel with Excellent Antibacterial and Antibiofilm Activity and Hemostasis for Pseudomonas Aeruginosa-Infected Burn Wound Healing. *J. Colloid Interf. Sci.* 608, 2278–2289. doi:10.1016/j.jcis.2021.10.131

Jia, Y.-G., Jin, J., Liu, S., Ren, L., Luo, J., and Zhu, X. X. (2018). Self-Healing Hydrogels of Low Molecular Weight Poly(vinyl Alcohol) Assembled by Host-Guest Recognition. *Biomacromolecules* 19 (2), 626–632. doi:10.1021/acs.biomac.7b01707

Kailasa, S. K., Joshi, D. J., Kateshiya, M. R., Koduru, J. R., and Malek, N. I. (2022). Review on the Biomedical and Sensing Applications of Nanomaterial-Incorporated Hydrogels. *Mater. Today Chem.* 23, 100746. doi:10.1016/j.mtchem.2021.100746

Kalantari, K., Mostafavi, E., Saleh, B., Soltantabar, P., and Webster, T. J. (2020). Chitosan/PVA Hydrogels Incorporated with green Synthesized Cerium Oxide Nanoparticles for Wound Healing Applications. *Eur. Polym. J.* 134, 109853. doi:10.1016/j.eurpolymj.2020.109853

Khan, M. U. A., Abd Razak, S. I., Mehboob, H., Abdul Kadir, M. R., Anand, T. J. S., Inam, F., et al. (2021). Synthesis and Characterization of Silver-Coated Polymeric Scaffolds for Bone Tissue Engineering: Antibacterial and *In Vitro* Evaluation of Cytotoxicity and Biocompatibility. *ACS omega* 6 (6), 4335–4346. doi:10.1021/acsomega.0c05596

Khan, M. U. A., Haider, S., Raza, M. A., Shah, S. A., Razak, S. I. A., Kadir, M. R. A., et al. (2021). Smart and pH-Sensitive rGO/Arabinoxylan/chitosan Composite for Wound Dressing: *In-Vitro* Drug Delivery, Antibacterial Activity, and Biological Activities. *Int. J. Biol. Macromolecules* 192, 820–831. doi:10.1016/j.ijbiomac.2021.10.033

Khan, M. U. A., Haider, S., Shah, S. A., Razak, S. I. A., Hassan, S. A., Kadir, M. R. A., et al. (2020). Arabinoxylan-co-AA/HAp/TiO2 Nanocomposite Scaffold a Potential Material for Bone Tissue Engineering: An *In Vitro* Study. *Int. J. Biol. macromolecules* 151, 584–594. doi:10.1016/j.ijbiomac.2020.02.142

Khan, M. U. A., Iqbal, I., Ansari, M. N. M., Razak, S. I. A., Raza, M. A., Sajjad, A., et al. (2021). Development of Antibacterial, Degradable and pH-Responsive Chitosan/Guar Gum/Polyvinyl Alcohol Blended Hydrogels for Wound Dressing. *Molecules* 26 (19), 5937. doi:10.3390/molecules26195937

Khan, M. U. A., Razak, S. I. A., Ansari, M. N. M., Zulkifli, R. M., Ahmad Zawawi, N., and Arshad, M. (2021). Development of Biodegradable Bio-Based Composite for Bone Tissue Engineering: Synthesis, Characterization and *In Vitro* Biocompatible Evaluation. *Polymers* 13 (21), 3611. doi:10.3390/polym13213611

Khan, M. U. A., Razaq, S. I. A., Mehboob, H., Rehman, S., Al-Arjan, W. S., and Amin, R. (2021). Antibacterial and Hemocompatible pH-Responsive Hydrogel

for Skin Wound Healing Application: *In Vitro* Drug Release. *Polymers* 13 (21), 3703. doi:10.3390/polym13213703

Khan, M. U. A., Yaqoob, Z., Ansari, M. N. M., Razak, S. I. A., Raza, M. A., Sajjad, A., et al. (2021). Chitosan/Poly Vinyl Alcohol/Graphene Oxide Based pH-Responsive Composite Hydrogel Films: Drug Release, Antimicrobial and Cell Viability Studies. *Polymers* 13 (18), 3124. doi:10.3390/polym13183124

Kumari, A., Yadav, S. K., and Yadav, S. C. (2010). Biodegradable Polymeric Nanoparticles Based Drug Delivery Systems. *Colloids Surf. B: biointerfaces* 75 (1), 1–18. doi:10.1016/j.colsurfb.2009.09.001

Li, M., Liang, Y., He, J., Zhang, H., and Guo, B. (2020). Two-pronged Strategy of Biomechanically Active and Biochemically Multifunctional Hydrogel Wound Dressing to Accelerate Wound Closure and Wound Healing. *Chem. Mater.* 32 (23), 9937–9953. doi:10.1021/acs.chemmater.0c02823

Liang, Y., He, J., and Guo, B. (2021). Functional Hydrogels as Wound Dressing to Enhance Wound Healing. *ACS nano* 15 (8), 12687–12722. doi:10.1021/acsnano.1c04206

Lin, X., Wang, X., Zeng, L., Wu, Z. L., Guo, H., and Hourdet, D. (2021). Stimuli-Responsive Toughening of Hydrogels. *Chem. Mater.* 33 (19), 7633–7656. doi:10.1021/acs.chemmater.1c01019

Ou, L., Lin, S., Song, B., Liu, J., Lai, R., and Shao, L. (2017). The Mechanisms of Graphene-Based Materials-Induced Programmed Cell Death: a Review of Apoptosis, Autophagy, and Programmed Necrosis. *Ijn* Vol. 12, 6633–6646. doi:10.2147/ijn.s140526

Pan, X., Wang, Q., He, P., Liu, K., Ni, Y., Chen, L., et al. (2020). A Bionic Tactile Plastic Hydrogel-Based Electronic Skin Constructed by a Nerve-like Nanonetwork Combining Stretchable, Compliant, and Self-Healing Properties. *Chem. Eng. J.* 379, 122271. doi:10.1016/j.cej.2019.122271

Repetto, G., Del Peso, A., and Zurita, J. L. (2008). Neutral Red Uptake Assay for the Estimation of Cell Viability/cytotoxicity. *Nat. Protoc.* 3 (7), 1125–1131. doi:10.1038/nprot.2008.75

Saghir, S., Iqbal, M. S., Hussain, M. A., Koschella, A., and Heinze, T. (2008). Structure Characterization and Carboxymethylation of Arabinoxylan Isolated from Ispaghula (Plantago Ovata) Seed Husk. *Carbohydr. Polym.* 74 (2), 309–317. doi:10.1016/j.carbpol.2008.02.019

Sala, R. L., Venâncio, T., and Camargo, E. R. (2021). Probing the Structural Dynamics of the Coil-Globule Transition of Thermosensitive Nanocomposite Hydrogels. *Langmuir* 37 (4), 1531–1541. doi:10.1021/acs.langmuir.0c03079

Santhosh, K., Modak, M. D., and Paik, P. (2017). Graphene Oxide for Biomedical Applications. *J. Nanomed. Res.* 5 (6), 1–6.

Umar Aslam Khan, M., Haider, S., Haider, A., Izwan Abd Razak, S., Rafiq Abdul Kadir, M., Shah, S. A., et al. (2021). Development of Porous, Antibacterial and Biocompatible GO/n-HAp/bacterial Cellulose/β-Glucan Biocomposite Scaffold for Bone Tissue Engineering. *Arabian J. Chem.* 14 (2), 102924. doi:10.1016/j.arabjc.2020.102924

Yadav, N., Parveen, S., Chakravarty, S., and Banerjee, M. (2019). "Skin Anatomy and Morphology," in *Skin Aging & Cancer*. Editors A. Dwivedi, N. Agarwal, L. Ray, and A. K. Tripathi (Berlin/Heidelberg, Germany: Springer), 1–10.

Yang, Y., Cheng, Y., Peng, S., Xu, L., He, C., Qi, F., et al. (2021). Microstructure Evolution and Texture Tailoring of Reduced Graphene Oxide Reinforced Zn Scaffold. *Bioactive Mater.* 6 (5), 1230–1241. doi:10.1016/j.bioactmat.2020.10.017

Yin, C., Han, X., Lu, Q., Qi, X., Guo, C., and Wu, X. (2022). Rhein Incorporated Silk Fibroin Hydrogels with Antibacterial and Anti-inflammatory Efficacy to Promote Healing of Bacteria-Infected Burn Wounds. *Int. J. Biol. Macromolecules* 201, 14–19. doi:10.1016/j.ijbiomac.2021.12.156

Zhao, R., Jiang, L., Zhang, P., Li, D., Guo, Z., and Hu, L. (2022). Graphene Oxide-Based Composite Organohydrogels with High Strength and Low Temperature Resistance for Strain Sensors. *Soft Matter*. 18, 1201–1208. doi:10.1039/d1sm01655e

Zhong, Y., Seidi, F., Li, C., Wan, Z., Jin, Y., Song, J., et al. (2021). Antimicrobial/Biocompatible Hydrogels Dual-Reinforced by Cellulose as Ultrastretchable and Rapid Self-Healing Wound Dressing. *Biomacromolecules* 22 (4), 1654–1663. doi:10.1021/acs.biomac.1c00086

Conflict of Interest: The authors declare that the research was conducted in the absence of any commercial or financial relationships that could be construed as a potential conflict of interest.

Publisher's Note: All claims expressed in this article are solely those of the authors and do not necessarily represent those of their affiliated organizations, or those of the publisher, the editors, and the reviewers. Any product that may be evaluated in this article, or claim that may be made by its manufacturer, is not guaranteed or endorsed by the publisher.

frontiers | Frontiers in Bioengineering and Biotechnology

MINI REVIEW
published: 02 May 2022
doi: 10.3389/fbioe.2022.894667

Applications of Chitosan and its Derivatives in Skin and Soft Tissue Diseases

Yidan Xia[1†], Dongxu Wang[2†], Da Liu[3], Jiayang Su[1], Ye Jin[3], Duo Wang[1], Beibei Han[1], Ziping Jiang[1] and Bin Liu[1*]*

[1]Department of Hand and Foot Surgery, The First Hospital of Jilin University, Changchun, China, [2]Laboratory Animal Center, College of Animal Science, Jilin University, Changchun, China, [3]Department of Pharmacy, Changchun University of Chinese Medicine, Changchun, China

Chitosan and its derivatives are bioactive molecules that have recently been used in various fields, especially in the medical field. The antibacterial, antitumor, and immunomodulatory properties of chitosan have been extensively studied. Chitosan can be used as a drug-delivery carrier in the form of hydrogels, sponges, microspheres, nanoparticles, and thin films to treat diseases, especially those of the skin and soft tissue such as injuries and lesions of the skin, muscles, blood vessels, and nerves. Chitosan can prevent and also treat soft tissue diseases by exerting diverse biological effects such as antibacterial, antitumor, antioxidant, and tissue regeneration effects. Owing to its antitumor properties, chitosan can be used as a targeted therapy to treat soft tissue tumors. Moreover, owing to its antibacterial and antioxidant properties, chitosan can be used in the prevention and treatment of soft tissue infections. Chitosan can stop the bleeding of open wounds by promoting platelet agglutination. It can also promote the regeneration of soft tissues such as the skin, muscles, and nerves. Drug-delivery carriers containing chitosan can be used as wound dressings to promote wound healing. This review summarizes the structure and biological characteristics of chitosan and its derivatives. The recent breakthroughs and future trends of chitosan and its derivatives in therapeutic effects and drug delivery functions including anti-infection, promotion of wound healing, tissue regeneration and anticancer on soft tissue diseases are elaborated.

Keywords: chitosan, soft tissue disease, biological property, drug-delivery carrier, regenerative medicine

OPEN ACCESS

Edited by:
Yongsheng Yu,
Tongji University, China

Reviewed by:
Guangqi Song,
Fudan University, China
Guanyu Chen,
Sun Yat-sen University, China

****Correspondence:***
Ziping Jiang
waterjzp@jlu.edu.cn
Bin Liu
l_bin@jlu.edu.cn

[†]These authors have contributed equally to this work

Specialty section:
This article was submitted to Biomaterials, a section of the journal Frontiers in Bioengineering and Biotechnology

Received: *12 March 2022*
Accepted: *18 April 2022*
Published: *02 May 2022*

Citation:
Xia Y, Wang D, Liu D, Su J, Jin Y, Wang D, Han B, Jiang Z and Liu B (2022) Applications of Chitosan and its Derivatives in Skin and Soft Tissue Diseases. Front. Bioeng. Biotechnol. 10:894667. doi: 10.3389/fbioe.2022.894667

1 INTRODUCTION

Chitosan is a naturally occurring, newly identified cationic polysaccharide, which is a deacetylation product derived from chitin (Wang W. et al., 2020). Chitosan has been widely used in the medical field as a wound dressing because of its appreciable antibacterial activity (Matica et al., 2019). However, chitosan is poorly soluble and unstable in water; thus several chitosan derivatives have been developed (Shahid Ul and Butola, 2019). These derivatives were obtained by chemical modifications, which retained the effective biological properties of the parent chitosan while improving its physical and chemical properties (Ardean et al., 2021). Chitosan and its derivatives have been processed into hydrogels, sponges, microspheres, nanoparticles, and thin films for use as medical materials. These are widely used to treat different diseases, especially those of the skin and soft tissues, owing to the diverse properties of these compounds (Ma et al., 2017; Zhang N. et al., 2020; El Kadib, 2020; Hou et al., 2020; He et al., 2021).

Skin and soft tissue diseases include trauma, infections, and tumors of the skin, subcutaneous tissue, and fascia (Endo et al., 2019; Peetermans et al., 2020). Trauma to the skin, muscles, blood vessels, and nerves can be treated with chitosan and its derivatives as they promote wound healing (Guo et al., 2019; Alven and Aderibigbe, 2020; Rao F. et al., 2020; Zhao et al., 2021). Given that soft tissue infections such as those of the skin and subcutaneous tissues are caused by bacteria or fungi, chitosan and its derivatives can be used as dressings to treat infected wounds (Matica et al., 2019; Watkins and David, 2021). Soft tissue sarcomas are the most common malignancies of fat tissue, fascia, muscles, lymph nodes, and blood vessels, which always lead to a poor prognosis due to their insidious onset and rapid metastasis to distant organs. Chitosan and its derivatives exert antitumor activities and can, therefore, be potentially used in drug-delivery systems for the treatment of sarcoma (Maleki Dana et al., 2021). Besides, chitosan-based nanoparticles, sponges, films, hydrogels, and scaffolds have been used for soft tissue injury treatment (Oryan and Sahvieh, 2017; Hemmingsen et al., 2021; Rashki et al., 2021; Sun et al., 2021). Although chitosan and its derivatives have broad application prospects in the skin and soft tissue diseases, there is still a lack of review on this aspect. This review summarizes the sources, structures, biological characteristics, and different forms of drug carriers of chitosan and its derivatives. It also discusses the recent breakthroughs in the application of chitosan and its derivatives in preventing and treating trauma, infection, and tumor of skin and soft tissues.

2 PREPARATION OF CHITOSAN AND ITS DERIVATIVES

Chitin is mainly obtained from the corneum of crustaceans, such as shrimp and crab shells, which are purified by chemical and biological extraction to remove protein and precipitate calcium carbonate (Younes and Rinaudo, 2015). Chemically, chitosan consists of 2-amino-2-deoxy-D-glycopyranose units linked by β (1→4) glycosidic bonds and is obtained by the chemical and enzymatic deacetylation of chitin (**Supplementary Figure S1**) (Santos et al., 2020). The unique structure of chitosan makes it insoluble in water and most organic solvents, limiting its scope of applications (Muxika et al., 2017). Chitosan has been chemically and biologically modified by acylation, carboxylation, alkylation, and quaternization to improve its solubility and prepare derivatives for comprehensive applications.

The biocompatibility and anticoagulation effects of N-acylated chitosan have been significantly improved over the years and can be used as a sustained-release drug in a clinical setting (Wang W. et al., 2020). A previous study confirmed that the antibacterial activity of water-soluble N-alkylated disaccharide chitosan derivatives against *Escherichia coli* and *Staphylococcus aureus* was significantly higher than natural chitosan at pH 7.0 (Yang et al., 2005). Carboxymethyl chitosan can affect its solubility in water across different pH by affecting the degree of carboxymethylation, thus prolonging the reaction time of the drug-delivery system (Shariatinia, 2018). Therefore, modifying chitosan through quaternization could significantly improve its water solubility, antibacterial effects, mucosal adhesion, and permeability, which are beneficial for designing medical dressings and drug carriers (Freitas et al., 2020). Chitosan and its derivatives exert antibacterial, antioxidant, and anticancer effects *in vivo* as drug carriers, highlighting their potential application in clinical diseases.

3 BIOLOGICAL CHARACTERISTICS OF CHITOSAN AND ITS DERIVATIVES

3.1 Antibacterial Activity

The amino group in the chitosan structure can be converted to a positively charged ammonium ion, which confers cationic properties to chitosan (Fakhri et al., 2020). The cell walls of Gram-positive bacteria are mainly composed of teichoic acid, which is negatively charged and can react with chitosan via electrostatic interactions, leading to the destruction of the bacterial cell wall, loss of cellular function, and ultimately cell death (Abd El-Hack et al., 2020). The ammonium ions in chitosan interact with the anions of lipopolysaccharides present on the outer membrane of Gram-negative bacteria, leading to a bacteriostatic effect (Ardean et al., 2021). Additionally, chitosan can cross bacterial cell membranes and interfere with the transcription and translation of genetic material, thus affecting the normal cellular function (**Figure 1A**) (Verlee et al., 2017). The antibacterial performance of chitosan against *Staphylococcus epidermidis* significantly increased when the compound was functionalized with catechol, as demonstrated by a decrease in the minimum inhibitory concentration of the polymer (Amato et al., 2018). The antibacterial properties of chitosan when formulated as hydrogels, films, sponge wound dressings make it a good wound-treatment material for the prevention and treatment of infections. A novel lignin-chitosan-PVA composite hydrogel designed as a wound dressing shows good adsorption capacity and bacteriostatic effects (Zhang Y. et al., 2019). Chitosan films containing glycerin as a strengthening agent can be used as a wound dressing to inhibit bacterial infections (Ma et al., 2017). The composite sponge prepared using hydroxybutyl chitosan and chitosan combined the hydrophilic properties of hydroxybutyl chitosan and the antibacterial properties of chitosan, highlighting its potential as a wound dressing (Hu S. et al., 2018). The successful use of these preparations in treating skin and soft tissue infections is indicative of the antibacterial effects of chitosan.

3.2 Antioxidant Activity

The body maintains an oxidation balance under normal physiological conditions. When the antioxidant capacity is not adequate to combat the sudden increase in free radicals, the surplus free radicals lead to cell injury, metabolic disorders of the cellular macromolecules, and the occurrence of skin and soft tissue diseases (Sztretye et al., 2019). The antioxidant properties of chitosan are attributed to the amino and hydroxyl groups in its molecular chain, which can effectively scavenge excessive free radicals in the human body (Muthu et al., 2021). The antioxidant

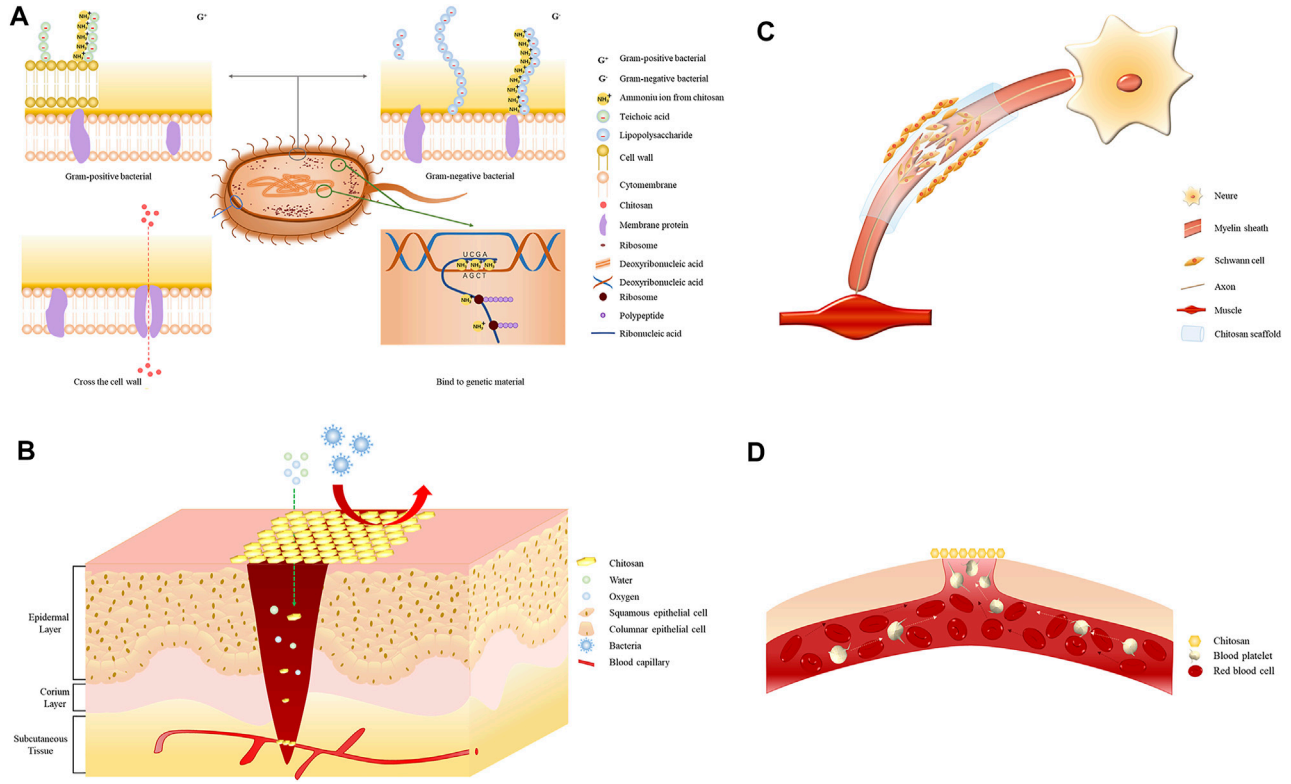

FIGURE 1 | (A) Electrostatic interaction of the positively charged ammonium ion with the negatively charged teichoic acid in Gram-positive bacteria. The positively charged ammonium ion interacts electrostatically with the negatively charged phospholipid molecule in Gram-negative bacteria. Chitosan molecules enter through protein channels on the bacterial membrane and interfere with physiological functions. Electrostatic interaction of the positively charged ammonium ion with the negatively charged nucleic acid group. **(B)** Chitosan wound dressings allow the permeation of oxygen and water to keep the wound moist while preventing bacterial contamination and wound infection. **(C)** Chitosan promotes nerve regeneration by promoting Schwann cell proliferation. **(D)** Chitosan promotes erythrocyte aggregation and platelet adhesion.

activity of chitosan mainly depends on its relative molecular weight and the level of acetylation (Abd El-Hack et al., 2020; Cabañas-Romero et al., 2020). Chitosan shows a greater ability in scavenging free radicals having relatively low molecular weights and higher levels of acetylation (Negm et al., 2020). Chitosan derivatives obtained by chemical modification can improve the antioxidant capacity of polymers and increase their application over a range of fields (Hao et al., 2021). Chitosan composite films prepared with ascorbate have stronger DPPH radical–scavenging ability and improved ability in resisting ultraviolet-visible light and visible light (Tan et al., 2020). Chitosan derivatives containing Schiff's base and a quaternary ammonium salt exhibit stronger antioxidant capability than chitosan due to the presence of hydroxyl and halogen groups (Wei et al., 2019). Novel chitosan derivatives containing sulfur salts have DPPH-, hydroxyl-, and superoxide radical-scavenging capacities of higher than 90%, without any associated cytotoxicity (Sun et al., 2020). Chitosan nanoparticles synthesized by doxorubicin can significantly enhance the scavenging ability of free radicals and reduce the cell viability of liver, stomach, lung, and breast cancer cells, which can be used as a potential drug carrier for tumors (Mi et al., 2021). The antioxidant capacity of chitosan can be regulated by adjusting its molecular weight, acetylation level, and the extent of chemical modification, thereby conferring tremendous application prospects in medical cosmetology and the treatment of soft tissue diseases and tumors.

3.3 Anticancer Activity

Cancer is one of the most challenging conditions to cure, with surgical resection being the most efficient and effective management technique. The development of targeted drugs provides new ideas to treat cancer; however, several drugs have poor bioavailability, low selectivity, and poor stability in tumor tissues (Kandra and Kalangi, 2015). Chitosan derivatives incorporated into the nano drug-delivery systems have emerged as one of the most advanced delivery systems in the biomedical field. This technology is associated with minimum systemic toxicity and maximum cytotoxicity to the tumors and cancer cells and is the most promising targeted therapy in cancer (Verlee et al., 2017). Chitosan can directly inhibit the growth of tumor cells, induce cell necrosis and apoptosis, and enhance immunity to achieve its antitumor effect (Yu et al., 2022). The chitosan-based nanoparticles could selectively permeate cancer cells and precisely exert their effects by continuously releasing the loaded drugs while maintaining drug stability (Kamath and Sunil, 2017). N, O-carboxymethyl chitosan/multialdehyde Guar hydrogels can

continuously release antitumor drug doxorubicin and possess injectable and self-healing biological properties (Pandit et al., 2021). A novel amphiphilic chitosan micelle reported to protect 75% of an anticancer drug from hydrolysis is now being used as a promising drug-delivery system (Almeida et al., 2020). The chitosan- and saline-based nanoparticles are used to deliver the pro-oxidant drug piperlongumine to prostate cancer cells due to their prostate cancer cells killing properties (Choi et al., 2019). The antitumor properties of chitosan make it a potential antitumor drug carrier for treating melanoma and sarcoma of skin and soft tissues.

3.4 Immunomodulatory Effects

Chitosan and its derivatives can stimulate phagocytes, induce natural killer cells to secrete cytokines, and activate immune-regulatory responses (Moran et al., 2018). The hydrolysate of chitosan can increase the phagocytic activity of macrophages and promote the proliferation of splenocytes and Payer's patch lymphocytes, thereby exerting unique immunomodulatory properties (Chang et al., 2019). Polymers containing chitosan can promote the polarization of primary bone marrow–derived macrophages to anti-inflammatory activity carrying macrophages (Papadimitriou et al., 2017). Acidified chitosan can provide an immune microenvironment for osteogenic differentiation by promoting crosstalk between the immune cells and stem cells to induce angiogenesis and bone regeneration (Shu et al., 2018). Hydrogels containing chitosan can promote the wound healing capacity of the skin of diabetic rats by downregulating the pro-inflammatory factors like tumor necrosis factor-α and interleukin (IL)-1β (Chen et al., 2021). Chitosan oligosaccharides can promote the phagocytic activity of RAW264.7 cells, produce reactive oxygen species, release pro-inflammatory factors through the NF-KB pathway, and significantly enhance the immunomodulatory effect (Deng et al., 2020). Chitosan can induce and regulate immune cells by altering the microenvironment of the immune system to achieve therapeutic effects by regulating immune function in the skin and soft tissues.

4 DRUG CARRIERS PREPARED USING CHITOSAN AND ITS DERIVATIVES

Chitosan has been used to synthesize several drug carriers for drug-delivery systems, such as nanoparticles, films, sponges, hydrogels, and scaffolds. The design of these carriers is based on the biological properties of chitosan and its derivatives. Some of these carriers are currently used in a clinical setting (**Supplementary Figure S2**).

4.1 Nanoparticles

In recent years, nanomaterials have gained increasing attention in the biomedical field (Zhang E. et al., 2019). Chitosan nanoparticles retain the biological properties of chitosan while improving the stability of the loaded drugs and controlling the drug-release rate (Rizeq et al., 2019). There is evidence that chitosan nanoparticles loaded with anticancer drugs could be used to target malignant tumors, thereby prolonging the drug action duration, enhancing the anticancer effect, and reducing toxicity (Assa et al., 2017). Chitosan nanoparticles are safe, biodegradable, and easy to form DNA or protein complexes for use as a potential gene delivery system (Bowman and Leong, 2006). Chitosan-coated silica nanoparticles have been shown to induce a strong immune response *in vivo* and can be used for oral delivery of protein vaccine (Wu et al., 2021). Chitosan nanoparticles retain the biocompatibility and biodegradability of chitosan, which is a valuable property and a promising therapeutic approach in targeted therapy when used in combination with anticancer drugs.

4.2 Film

The chitosan-based films possess good permeability, a large surface area, and unique antibacterial properties, thus making them a potential alternative to artificial skin and an important material for wound dressings (Vivcharenko et al., 2020). The surface hydrophobicity, permeability, and sensitivity of gamma ray–irradiated chitosan films can be increased without significant changes in the original chemical structure (Salari et al., 2021). Introducing montmorillonite-copper chloride into chitosan films can increase their tensile strength and elongation at break and also confer higher antibacterial activity against foodborne pathogens, further highlighting their use as a wound dressing to combat infections (Nouri et al., 2018). Additionally, chitosan films containing human epidermal growth factors can protect against enzymatic hydrolysis and endocytosis and significantly accelerate the rate of wound healing in mice (Umar et al., 2021). These antibacterial properties and regenerative effects of chitosan make it a suitable material for wound dressing.

4.3 Sponges

The porous structure, biocompatibility, and liquid-absorption properties of the chitosan sponge make it a suitable biomaterial for hemostasis (Zhang K. et al., 2020). Chitosan composite sponges can absorb water in the blood and increase blood viscosity. Moreover, they are non-toxic and biodegradable, hold antibacterial drugs, and promote blood coagulation in wounds (Hu S. et al., 2018). Chitosan composite sponges rich in andrographolide possess a large pore size and expansion rate and can effectively promote wound healing and reduce scar formation when used as a wound care material (Sanad and Abdel-Bar, 2017). Chitosan sponge provides a moist environment, allows gas exchange and blocks out microorganisms, suitable for burn wound dressing to keep away from contamination and dehydration (Jayakumar et al., 2011). Chitosan sponges have been widely used as hemostatic materials due to their porous structure and wound dressings promoting wound healing when loaded with drugs (Matica et al., 2019).

4.4 Hydrogels

Hydrogels are hydrophilic polymers with high water content and good biocompatibility. They can be loaded with chitosan and used as wound dressings to keep the wound moist and to continuously absorb exudates (Song et al., 2021). Chitosan

hydrogels loaded with metal ions can improve the imbalance in metal ions that cause delayed wound healing. Moreover, they inhibit infections and accelerate healing by regulating the expression of inflammatory factors and macrophages polarization (Xiao et al., 2021). An imbalance in metal ions can also lead to scar growth. Modulating the cation in chitosan hydrogel or adding aloe gel can lead to effective scar inhibition (Zhang N. et al., 2020). Chitosan hydrogels can also be used as hemostatic dressings. Thermal-responsive chitosan/DOPA hydrogels improve the adhesion and show a good hemostatic effect in rats (Shou et al., 2020). Chitosan sponges are often used as a hemostatic material. Hydrogels are commonly used as antibacterial dressings because their hydrophilicity and absorbability can suitably isolate infections from foreign substances and keep the wound moist.

4.5 Scaffolds

Tissue engineering is a research hotspot in regenerative medicine. Functional scaffolds composed of natural polymers have been widely used in surgical reconstruction (Rodríguez-Vázquez et al., 2015). Collagen/chitosan scaffolds made using 3D printing technology show remarkable therapeutic effects *in vivo* with complete spinal cord transection, and significantly improve sensory and motor recovery (Sun et al., 2019). Chitosan scaffolds surrounded by microcellulose arranged with twisted polylactic acid can simulate the extracellular matrix of tendons, provide structural support for tendon regeneration, and facilitate tendon-cell attachment and proliferation (Nivedhitha Sundaram et al., 2019). Composite chitosan-gelatin scaffold with a double-tubular structure having large internal pores and nonporous outer layers simulate blood vessels and significantly promote the proliferation of human dermal fibroblasts after being inoculated, and can be used for angiogenesis reconstruction (Badhe et al., 2017). Nano-scaffolds made of chitosan, sulfonated chitosan, polycaprolactone, and phosphoric acid can enhance the activity and adhesion of osteoblasts, making them excellent materials for bone tissue regeneration (Ghaee et al., 2017). Chitosan scaffolds have plastic structure and the ability to promote adhesion and proliferation of tissue cells, improving soft tissue and bone tissue regeneration.

5 APPLICATIONS OF CHITOSAN AND ITS DERIVATIVES TO TREAT SOFT TISSUE DISEASES

5.1 Promotion of Wound Healing

Soft tissue injury refers to laceration and contusion of the skin, subcutaneous tissue, and muscle caused by an external force, bleeding, and local swelling. Wound healing depends on the nature and degree of tissue defects, whereas age, nutritional status, and underlying diseases are systemic factors affecting wound healing (Wilkinson and Hardman, 2020). Promoting wound healing and reducing scar formation are urgent medical problems to be solved for patients with wounds and defects in body function. The antibacterial properties of chitosan and its ability to promote tissue regeneration have increased its usage in wound dressings combined with different materials, which have the overall effect of promoting wound healing (**Figure 1B**).

Impregnating chitosan hydrogels with silver nanoparticles can significantly improve antibacterial and antioxidant properties and enhance wound healing *in vivo* (Masood et al., 2019). The anti-biofilm formation ability of chitosan-immobilized ficin can inhibit *S. aureus* infections and promote the formation of smoother epithelial tissue (Baidamshina et al., 2020). Vaccinin-chitosan nanoparticles can promote vascular tissue production by upregulating IL-1β and PDGF-BB, thereby highlighting its potential in wound healing (Hou et al., 2020). The curcumin-loaded chitosan membranes can effectively inhibit bacterial pathogens in wounds by increasing the formation of fibrous connective tissue. Additionally, they have an obvious healing effect on wounds resulting from second-degree burns (Abbas et al., 2019). A study reports that macrophage dysfunction can lead to chronic inflammation and inhibit diabetic wound healing (Chen et al., 2021). Chitosan sulfate can improve macrophage function by inducing the polarization of M1 macrophages to M2 macrophages and promoting the production of anti-inflammatory factors, thus effectively promoting diabetic wound healing (Shen et al., 2020). Chitosan has antibacterial, antioxidant, and immunomodulatory effects that can prevent the infection of wounds and promote healing through soft tissue regeneration, making it a natural wound-dressing material.

5.2 Anti-Infective Effects in Skin and Soft Tissue

Soft tissue infection is an inflammatory condition caused by pathogenic bacteria that invade the skin and subcutaneous tissue. Elimination of necrotic tissue and pathogenic bacteria is the cornerstone of treatment in such infections (Burnham and Kollef, 2018). The effectiveness of different wound dressings in controlling and treating infection has been clearly demonstrated, highlighting their wide use in clinical practice (Simões et al., 2018). Chitosan is an effective carrier of anti-infective drugs due to its mucous membrane dependence and the ability to prolong drug activity by retarding the biodegradation rate (Rajitha et al., 2016). The inhibitory effects of antibacterial materials based on chitosan and its derivatives on different pathogens are listed in **Table 1**.

5.3 Promotion of Soft Tissue Regeneration

5.3.1 Skin Regeneration

Skin injuries or necrosis caused by crush, burn, or cut injuries are medical problems warranting urgent care. Common treatment methods include autogenous skin transplantation and free or pedicled skin-flap transplantation, which can cause problems, such as graft tissue necrosis, scar contracture, and poor cosmetic appearance (Przekora, 2020; Li et al., 2021). The tissue-repair function of chitosan provides a novel solution for skin reconstruction (Wei et al., 2022). Hydrogels synthesized from chitosan and cellulose can accelerate epithelial tissue formation on wounds and mimic skin structure, induce skin regeneration,

TABLE 1 | Antibacterial effect of chitosan and its derivatives on different microorganisms.

Polymer	Microbial	Ref
P-COOH-CS-PHMB	*E. coli*	Ng et al. (2020)
Boc-D-Phe-γ 4 -L-Phe-PEA/chitosan	*E. coli*	Malhotra et al. (2020)
CTs@Ag/Sep	*E. coli*	Li et al. (2020)
CS-MoS_2	*E. coli*	Cao et al. (2019)
Chitosan-sodium phytate nanoparticles	*E. coli*	Yang et al. (2017)
HBCS	*E. coli*	Li et al. (2019)
CS-MCA	*E. coli*	Luo et al. (2019)
CTS/C-Ag	*E. coli*	Hu et al. (2019)
CMCh-Zn	*E. coli*	Wang et al. (2020)
Chitosan-silver nanocomposite	*E. coli*	Raghavendra et al. (2016)
Chitosan/Alkynyl chitosan	*E. coli*	Ding et al. (2013)
PAN-chitosan	*E. coli*	Kim and Lee, (2014)
Chitosan/phosvitin	*E. coli*	Zhou et al. (2014)
CMCh/CuO	*E. coli*	Wahid et al. (2017)
O-CMCS	*E. coli*	He et al. (2016)
CT-TG/SiO_2	*E. coli*	Mallakpour and Abbasi, (2020)
Chitosan-silver nanoparticles	*E. coli*	Shahid Ul et al. (2019)
Chitosan-g-eugenol/zwitterionic copolymer	*E. coli*	Li et al. (2018)
N-phosphonium chitosan	*E. coli*	Guo et al. (2014)
CS-MnO_2	*E. coli*	Anwar, (2018)
3,6-O-[N-(2-aminoethyl)-acetamide-yl]-chitosan	*E. coli*	Yan et al. (2016)
Quaternary ammonium chitosan	*E. coli*	Min et al. (2020)
PVA-CS	*E. coli*	Liu et al. (2018)
O-acetyl-chitosan-N-2-hydroxypropyl trimethyl ammonium chloride	*E. coli*	Cai et al. (2015)
Carboxymethyl chitosan/ZnO	*E. coli*	Wahid et al. (2016)
β-chitosan	*E. coli*	Jung et al. (2014)
Carboxymethyl chitosan	*E. coli*	Olanipekun et al. (2021)
Chi-Ag NPs	*E. coli*	Senthilkumar et al. (2019)
Carboxymethyl chitosan-zinc supramolecular hydrogels	*E. coli*	Wahid et al. (2018)
Chitosan-g-poly acrylonitrile/silver nanocomposite	*E. coli*	Hebeish et al. (2014)
Quaternized carboxymethyl chitosan	*E. coli*	Yin et al. (2018)
CH-CL	*S. aureus*	Wang et al. (2021)
Boc-D-Phe-γ 4 -L-Phe-PEA/chitosan	*S. aureus*	Malhotra et al. (2020)
CTs@Ag/Sep	*S. aureus*	Li et al. (2020)
CS-MoS_2	*S. aureus*	Cao et al. (2019)
HBCS	*S. aureus*	Li et al. (2019)
CMCh-Zn	*S. aureus*	Wang et al. (2020)
Chitosan-silver nanocomposite films	*S. aureus*	Raghavendra et al. (2016)
N-quaternary chitosan	*S. aureus*	Ghazaie et al. (2019)
Chitosan/Alkynyl chitosan	*S. aureus*	Ding et al. (2013)
PAN-chitosan	*S. aureus*	Kim and Lee, (2014)
Chitosan/phosvitin	*S. aureus*	Zhou et al. (2014)
CMCh/CuO	*S. aureus*	Wahid et al. (2017)
O-CMCS	*S. aureus*	He et al. (2016)
CT-TG/SiO_2	*S. aureus*	Mallakpour and Abbasi, (2020)
Chitosan-silver nanoparticles	*S. aureus*	Shahid Ul et al. (2019)
Chitosan-g-eugenol/zwitterionic copolymer	*S. aureus*	Li et al. (2018)
N-phosphonium chitosan	*S. aureus*	Guo et al. (2014)
CS-MnO_2	*S. aureus*	Anwar, (2018)
CuS/PVACS	*S. aureus*	Wang and Fakhri, (2020)
3,6-O-[N-(2-aminoethyl)-acetamide-yl]-chitosan	*S. aureus*	Yan et al. (2016)
N, N, N-Trimethyl Chitosan	*S. aureus*	Sahariah et al. (2019)
Quaternary ammonium chitosan	*S. aureus*	Min et al. (2020)
PVA-CS	*S. aureus*	Liu et al. (2018)
Surface-quaternized chitosan particles	*S. aureus*	Wiarachai et al. (2012)
O-acetyl-chitosan-N-2-hydroxypropyl trimethyl ammonium chloride	*S. aureus*	Cai et al. (2015)
Carboxymethyl chitosan/ZnO	*S. aureus*	Wahid et al. (2016)
Chitosan-silver nanocomposites	*S. aureus*	Potara et al. (2011)
NAM-CMCS-ZnO	*S. aureus*	Rao et al. (2020)
MDAACS	*S. aureus*	Jou, (2011)
Chitosan-gold nanocomposites	*S. aureus*	Regiel-Futyra et al. (2015)
Carboxymethyl chitosan-zinc supramolecular hydrogels	*S. aureus*	Wahid et al. (2018)
Ferulic acid-grafted chitosan	*S. aureus*	Dasagrandhi et al. (2018)
Chitosan-g-poly acrylonitrile/silver nanocomposite	*S. aureus*	Hebeish et al. (2014)

(Continued on following page)

TABLE 1 | (*Continued*) Antibacterial effect of chitosan and its derivatives on different microorganisms.

Polymer	Microbial	Ref
Quaternized carboxymethyl chitosan	*S. aureus*	Yin et al. (2018)
Carboxymethyl chitosan	*Pseudomonas aeruginosa*	Olanipekun et al. (2021)
Boc-D-Phe-γ 4 -L-Phe-PEA/chitosan	*Pseudomonas aeruginosa*	Malhotra et al. (2020)
Chitosan-gold nanocomposites	*Pseudomonas aeruginosa*	Regiel-Futyra et al. (2015)
Ferulic acid-grafted chitosan	*Pseudomonas aeruginosa*	Dasagrandhi et al. (2018)
β-chitosan	*Listeria innocua*	Jung et al. (2014)
Ferulic acid-grafted chitosan	*Listeria innocua*	Dasagrandhi et al. (2018)
Carboxymethyl chitosan	*Klebsiella Pneumoniae*	Olanipekun et al. (2021)
MDAACS	*Klebsiella Pneumoniae*	Jou, (2011)
CTs@Ag/Sep	*Aspergillus niger*	Li et al. (2020)
Chitosan-glutaraldehyde	*Burkholderia cepacia*	Li et al. (2013)
PAN-chitosan	*Micrococcus luteus*	Kim and Lee, (2014)
CuS/PVACS	*Streptococcus pneumonia*	Wang and Fakhri, (2020)
Quaternary ammonium chitosan	*Botrytis cinerea*	Min et al. (2020)
CNPs	*N. gonorrhoeae*	Alqahtani et al. (2020)

and can be loaded with antibacterial agents to prevent wound infections (Alven and Aderibigbe, 2020). Lithium chloride–loaded chitosan hydrogels can significantly reduce wound inflammation, promote angiogenesis, and accelerate epithelial regeneration, thereby showing a potential dressing for skin regeneration (Yuan et al., 2020). Chitosan wound dressings containing exosomes derived from overexpressed miRNA-126 synovial mesenchymal stem cells can promote epithelium formation, angiogenesis, and collagen maturation in diabetic rats (Tao et al., 2017). Chitosan can promote skin regeneration by promoting angiogenesis and epithelium formation.

5.3.2 Tendon Regeneration

Tendons are one of the major components responsible for maintaining the movement of various joints in the body. Tendon rupture due to trauma can lead to irreversible impaired movement. The tendon structure simulated by poly (L-lactic acid) nanofibers can promote the regeneration of the broken flexor tendons and alginate gel, a novel natural biological scaffold suitable for tendon repair in the outer layer, and can prevent tendon adhesion (Deepthi et al., 2016). Asymmetric chitosan scaffolds have been developed to encapsulate rat tendon stem/progenitor cells and promote tendon regeneration (Chen et al., 2018). The polycaprolactone/chitosan nanofiber biocomposite prepared using the electrostatic spinning process can promote the adhesion and proliferation of human osteoblasts and be used for tendon and ligament regeneration (Wu et al., 2018). Biomaterials based on chitosan and its derivatives can promote tendon healing and prevent adhesion around tendons, which is beneficial for treating patients with tendon rupture.

5.3.3 Nerve Regeneration

Peripheral nerves are the nerves outside the brain and spinal cord. Damage to these nerves can lead to motor and sensory impairments. The biological materials with chitosan as the primary polymer are effective in nerve-injury repair. The related mechanisms are shown in **Figure 1C**. Chitosan nanofiber hydrogels prepared by electrospinning and mechanical stretching can stimulate brain-derived neurotrophic factor and vascular endothelial growth factor, promote Schwann cell proliferation, and secrete neurotrophic silver to repair sciatic nerve defects in the sciatic nerve–defect model of mice (Rao F. et al., 2020). Additionally, sciatic nerve defects in rats were repaired using a nerve catheter containing chitosan reinforced with chitosan membrane in the longitudinal direction, and the result was anastomosed with autologous nerve transplantation (Meyer et al., 2016). Heparin/chitosan scaffolds loaded with nerve growth factors through electrostatic interaction can significantly promote the morphological development of Schwann cells and exhibit good stability (Li et al., 2017). The effective proliferation of Schwann cells accelerates the rate of nerve regeneration. Chitosan derivatives can affect nerve regeneration through immunomodulatory effects. As a degradation product of chitosan, chitosan oligosaccharides can promote nerve regeneration by regulating the microenvironment of macrophages infiltrating around injured sciatic nerves (Zhao et al., 2017). Compared with traditional surgical repair techniques, chitosan and its derivatives are more coherent for soft tissues regeneration, with less damage, easier acquisition, and more satisfying outcomes.

5.4 Promotion of Coagulation

Bleeding due to trauma is a serious symptom that needs immediate attention during surgical emergencies. Chitosan can promote coagulation by enhancing red blood cell agglutination and platelet adhesion and is a potential hemostatic material (**Figure 1D**) (Hu Z. et al., 2018). Composite sponges containing alginate/carboxymethyl chitosan/kangfuxin are biodegradable materials that accelerate blood clotting and promote wound closure (He et al., 2021). Carboxymethyl chitosan sponges grafted with marine collagen peptides can promote coagulation both *in vivo* and *in vitro* through the synergistic effect of the collagen peptide and carboxymethyl chitosan (Cheng et al., 2020). Chitosan/diatom-biosilica aerogels are associated with large

surface areas and excellent water absorption capabilities and hence, show the shortest clotting time and the lowest amount of blood loss in a hemorrhage model of rats (Li J. et al., 2020). Chitosan/cellulose composite sponges with LiOH/KOH/urea solvent in the shell show better clotting ability, antibacterial effect, and good absorbability than traditional gauze and gelatin sponges (Fan et al., 2020). Different chitosan materials exhibit varying absorbability and coagulation-promoting effects and serve as convenient and effective hemostatic materials to arrest acute bleeding of the skin and soft tissues.

5.5 Targeted Therapy for Soft Tissue Malignancy

Soft tissue malignancy or sarcomas are tumors that originated from the mesenchymal tissue and mainly occur in the muscles, ligaments, periosteum, fat, and other sites. The efficacy of chitosan in drug-delivery systems for the targeted therapy of malignant tumors in sarcoma has been well documented (Tan et al., 2010). Methylglyoxal-conjugated chitosan nanoparticles can enhance the anticancer effect of methylglyoxal alone in tumor-bearing mice and protect it from enzymatic degradation *in vivo* by upregulating cytokines and surface receptors of macrophages (Chakrabarti et al., 2014; Pal et al., 2015). Thus, the immunomodulatory effects of macrophages should be activated to achieve the antitumor effect. Low-molecular-weight chitosan obtained through enzymolysis can increase the natural killing activity of tumor-bearing intestinal intraepithelial lymphocytes in mice and inhibit tumor growth by activating their intestinal immune function (Maeda and Kimura, 2004), suggesting that chitosan can achieve antitumor effects by regulating the immune system. Additionally, chitosan can reduce gastrointestinal tract injury caused by adriamycin in sarcoma-180–bearing mice without affecting the tumor-inhibition effect (Kimura et al., 2001). Chitosan can be used to prevent weight loss and spleen weight loss caused by cisplatin in tumor-bearing mice without reducing the antitumor activity of the drug (Kimura et al., 2000). Therefore, chitosan can be considered to alleviate the toxic and side effects of chemotherapy in individuals with sarcoma. Chitosan can increase the anticancer effect of drugs, reduce damage to the body, and achieve antitumor effects through immune regulation when used as a targeted drug carrier. These factors highlight its usage as a curative material in treating soft tissue tumors.

6 DISCUSSION

Chitosan and its derivatives exhibit good biocompatibility. They are biodegradable, nontoxic, and also exert antibacterial, antioxidant, antitumor, and immunomodulatory effects. Chitosan can be used to synthesize different types of drug carriers based on the intended use, as it plays a significant role in soft tissue diseases treatment (**Supplementary Table S1**) (Wang W. et al., 2020). Chitosan nanoparticles can improve drug stability while retaining the biological properties of chitosan, thereby rendering them suitable as carriers of targeted drugs (Aibani et al., 2021). Chitosan nanoparticles are associated with fewer drug-loading and biological distribution limitations compared with lipid-based nanoparticles. Moreover, chitosan nanoparticles are nontoxic and not radioactive as inorganic nanoparticles (Dadfar et al., 2019; Alphandéry, 2020; Plucinski et al., 2021). Chitosan films can be made into antibacterial dressings to enhance the antibacterial effect of chitosan (Rashki et al., 2021). Skin irritation or local side effects are rare due to the biodegradability and biocompatibility of chitosan. Thus, the incidence of contact dermatitis is lesser with the use of chitosan than with the use of traditional antibacterial agents (Homaeigohar and Boccaccini, 2020; Zheng et al., 2020). Chitosan sponges possess good absorbability and a porous structure and are not associated with immunogenicity and virality compared with other thrombin- and fibrin-based products (Yu and Zhong, 2021). Chitosan sponges are degraded *in vivo* after exerting their hemostatic role; these sponges are less toxic and exhibit fewer side effects than mineral hemostatic materials (Hickman et al., 2018). Chitosan hydrogels have a high-water content, which can keep wounds moist and prevent secondary damage caused by traditional gauze while changing dressings (Thapa et al., 2020). The drug-loaded chitosan hydrogels can slowly release drugs and prevent tissue damage caused by the burst effect due to sudden drug release (Teixeira et al., 2021). The ductility and absorbability of chitosan hydrogels render them suitable for application to limb injuries and avoid sliding of the dressing and wound exposure caused by joint movement (Zhang A. et al., 2020). Chitosan scaffolds are important components in bone tissue engineering. They can be used to repair bone defects and carry mesenchymal stem cells for nerve and tendon regeneration, which is a major breakthrough in regenerative medicine (Cofano et al., 2019; Zhang L. et al., 2019; Vijayavenkataraman, 2020; Russo et al., 2022). Compared with other drug carriers, chitosan and its derivatives could be a potential approach for preventing and treating of skin and soft tissue diseases.

Bacterial resistance limits the systemic effects of antibiotics and is one of the major factors delaying the healing of chronic infections of the skin and soft tissues (Theuretzbacher et al., 2020). Chitosan can directly interact with bacteria at the site of infection to exert antibacterial effects and eradicate the infection at the site (Jyoti et al., 2020). Chitosan can regulate the immune microenvironment of the body, activate immune cells, and exert anti-infective effects by enhancing immunity (Moran et al., 2018). Compared with silver nanoparticles, chitosan exhibits better antibacterial properties while promoting tissue regeneration (Tang and Zheng, 2018), making it more suitable as an antibacterial agent to treat skin and soft tissue infections. For bleeding caused by skin and soft tissue trauma, compression or tourniquet is often used to stop bleeding. However, this method has limited hemostatic effect and is easy to form thrombus and hematoma (Weiskopf, 2009). Chitosan and its derivatives can stop bleeding by inducing erythrocyte agglutination and platelet adhesion, thereby accelerating blood coagulation and promoting wound healing (He et al., 2021). However, there is little evidence on whether chitosan hemostatic material can induce thrombosis. At present, soft tissue sarcomas treatment relies on surgery. For patients who cannot suffer from surgery, radiotherapy and chemotherapy become the first choices (Hoefkens et al., 2016). Chitosan and its derivatives can carry anti-tumor drugs to achieve a targeted treatment of soft tissue sarcoma, which can increase the anti-tumor efficiency of drugs and reduce the toxicity and side effects (Kimura et al., 2000). The role of chitosan in

bone tissue engineering has been widely studied, but there is little evidence of the skin and soft tissue regeneration (Ghaee et al., 2017). Therefore, studies should pay more attention to the chitosan regeneration on the skin and soft tissue, especially peripheral nerves, as nerves take a long time to regenerate and are more prone to secondary rupture.

In conclusion, as a natural polymer, chitosan and its derivatives have been isolated from a wide range of sources. The advantages include ease of preparation and good biological characteristics, which are useful attributes in the prevention and treatment of soft tissue diseases.

AUTHOR CONTRIBUTIONS

YX and DOW wrote the manuscript. DL, JS, YJ, DUW, BH, ZJ and BL collected the references and prepared figures. All authors reviewed the manuscript.

FUNDING

This research was financially supported by the National Natural Science Foundation of China (Grant Nos. 52022095, 82071391, 51973216, 51873207, and 51833010), the Provincial Health Special Project of Jilin Province (Grant Nos. JLSCZD 2019-002 and JLSWSRCZX 2020-095), the Science and Technology Development Program of Jilin Province (Grant No. 20200404182YY), the Youth Innovation Promotion Association of Chinese Academy of Sciences (Grant No. 2019230), and Natural science Foundation of the Jilin province (Grant No. 20210101310JC).

SUPPLEMENTARY MATERIAL

The Supplementary Material for this article can be found online at: https://www.frontiersin.org/articles/10.3389/fbioe.2022.894667/full#supplementary-material

REFERENCES

Abbas, M., Hussain, T., Arshad, M., Ansari, A. R., Irshad, A., Nisar, J., et al. (2019). Wound Healing Potential of Curcumin Cross-Linked Chitosan/Polyvinyl Alcohol. *Int. J. Biol. Macromol.* 140, 871–876. doi:10.1016/j.ijbiomac.2019.08.153

Abd El-Hack, M. E., El-Saadony, M. T., Shafi, M. E., Zabermawi, N. M., Arif, M., Batiha, G. E., et al. (2020). Antimicrobial and Antioxidant Properties of Chitosan and its Derivatives and Their Applications: A Review. *Int. J. Biol. Macromol.* 164, 2726–2744. doi:10.1016/j.ijbiomac.2020.08.153

Aibani, N., Rai, R., Patel, P., Cuddihy, G., and Wasan, E. K. (2021). Chitosan Nanoparticles at the Biological Interface: Implications for Drug Delivery. *Pharmaceutics* 13 (10), 1686. doi:10.3390/pharmaceutics13101686

Almeida, A., Araújo, M., Novoa-Carballal, R., Andrade, F., Gonçalves, H., Reis, R. L., et al. (2020). Novel Amphiphilic Chitosan Micelles as Carriers for Hydrophobic Anticancer Drugs. *Mater. Sci. Eng. C* 112, 110920. doi:10.1016/j.msec.2020.110920

Alphandéry, E. (2020). Natural Metallic Nanoparticles for Application in Nano-Oncology. *Int. J. Mol. Sci.* 21 (12), 4412. doi:10.3390/ijms21124412

Alqahtani, F., Aleanizy, F., El Tahir, E., Alhabib, H., Alsaif, R., Shazly, G., et al. (2020). Antibacterial Activity of Chitosan Nanoparticles against Pathogenic N. Gonorrhoea. *Int. J. Nanomedicine* 15, 7877–7887. doi:10.2147/ijn.s272736

Alven, S., and Aderibigbe, B. A. (2020). Chitosan and Cellulose-Based Hydrogels for Wound Management. *Int. J. Mol. Sci.* 21 (24), 9656. doi:10.3390/ijms21249656

Amato, A., Migneco, L. M., Martinelli, A., Pietrelli, L., Piozzi, A., and Francolini, I. (2018). Antimicrobial Activity of Catechol Functionalized-Chitosan Versus Staphylococcus Epidermidis. *Carbohydr. Polym.* 179, 273–281. doi:10.1016/j.carbpol.2017.09.073

Anwar, Y. (2018). Antibacterial and Lead Ions Adsorption Characteristics of Chitosan-Manganese Dioxide Bionanocomposite. *Int. J. Biol. Macromol.* 111, 1140–1145. doi:10.1016/j.ijbiomac.2018.01.096

Ardean, C., Davidescu, C. M., Nemeş, N. S., Negrea, A., Ciopec, M., Duteanu, N., et al. (2021). Factors Influencing the Antibacterial Activity of Chitosan and Chitosan Modified by Functionalization. *Int. J. Mol. Sci.* 22 (14), 7449. doi:10.3390/ijms22147449

Assa, F., Jafarizadeh-Malmiri, H., Ajamein, H., Vaghari, H., Anarjan, N., Ahmadi, O., et al. (2017). Chitosan Magnetic Nanoparticles for Drug Delivery Systems. *Crit. Rev. Biotechnol.* 37 (4), 492–509. doi:10.1080/07388551.2016.1185389

Badhe, R. V., Bijukumar, D., Chejara, D. R., Mabrouk, M., Choonara, Y. E., Kumar, P., et al. (2017). A Composite Chitosan-Gelatin Bi-Layered, Biomimetic Macroporous Scaffold for Blood Vessel Tissue Engineering. *Carbohydr. Polym.* 157, 1215–1225. doi:10.1016/j.carbpol.2016.09.095

Baidamshina, D. R., Koroleva, V. A., Trizna, E. Y., Pankova, S. M., Agafonova, M. N., Chirkova, M. N., et al. (2020). Anti-biofilm and Wound-Healing Activity of Chitosan-Immobilized Ficin. *Int. J. Biol. Macromol.* 164, 4205–4217. doi:10.1016/j.ijbiomac.2020.09.030

Bowman, K., and Leong, K. W. (2006). Chitosan Nanoparticles for Oral Drug and Gene Delivery. *Int. J. Nanomedicine* 1 (2), 117–128. doi:10.2147/nano.2006.1.2.117

Burnham, J. P., and Kollef, M. H. (2018). Treatment of Severe Skin and Soft Tissue Infections: A Review. *Curr. Opin. Infect. Dis.* 31 (2), 113–119. doi:10.1097/qco.0000000000000431

Cabañas-Romero, L. V., Valls, C., Valenzuela, S. V., Roncero, M. B., Pastor, F. I. J., Diaz, P., et al. (2020). Bacterial Cellulose-Chitosan Paper with Antimicrobial and Antioxidant Activities. *Biomacromolecules* 21 (4), 1568–1577. doi:10.1021/acs.biomac.0c00127

Cai, J., Dang, Q., Liu, C., Wang, T., Fan, B., Yan, J., et al. (2015). Preparation, Characterization and Antibacterial Activity of O -Acetyl-Chitosan- N -2-hydroxypropyl Trimethyl Ammonium Chloride. *Int. J. Biol. Macromol.* 80, 8–15. doi:10.1016/j.ijbiomac.2015.05.061

Cao, W., Yue, L., and Wang, Z. (2019). High Antibacterial Activity of Chitosan - Molybdenum Disulfide Nanocomposite. *Carbohydr. Polym.* 215, 226–234. doi:10.1016/j.carbpol.2019.03.085

Chakrabarti, A., Talukdar, D., Pal, A., and Ray, M. (2014). Immunomodulation of Macrophages by Methylglyoxal Conjugated with Chitosan Nanoparticles against Sarcoma-180 Tumor in Mice. *Cell. Immunol.* 287 (1), 27–35. doi:10.1016/j.cellimm.2013.11.006

Chang, S.-H., Wu, G.-J., Wu, C.-H., Huang, C.-H., and Tsai, G.-J. (2019). Oral Administration with Chitosan Hydrolytic Products Modulates Mitogen-Induced and Antigen-Specific Immune Responses in BALB/c Mice. *Int. J. Biol. Macromol.* 131, 158–166. doi:10.1016/j.ijbiomac.2019.02.068

Chen, E., Yang, L., Ye, C., Zhang, W., Ran, J., Xue, D., et al. (2018). An Asymmetric Chitosan Scaffold for Tendon Tissue Engineering: *In Vitro* and *In Vivo* Evaluation with Rat Tendon Stem/Progenitor Cells. *Acta Biomater.* 73, 377–387. doi:10.1016/j.actbio.2018.04.027

Chen, T.-Y., Wen, T.-K., Dai, N.-T., and Hsu, S.-H. (2021). Cryogel/Hydrogel Biomaterials and Acupuncture Combined to Promote Diabetic Skin Wound Healing through Immunomodulation. *Biomaterials* 269, 120608. doi:10.1016/j.biomaterials.2020.120608

Cheng, Y., Lu, S., Hu, Z., Zhang, B., Li, S., and Hong, P. (2020). Marine Collagen Peptide Grafted Carboxymethyl Chitosan: Optimization Preparation and Coagulation Evaluation. *Int. J. Biol. Macromol.* 164, 3953–3964. doi:10.1016/j.ijbiomac.2020.09.006

Choi, D. G., Venkatesan, J., and Shim, M. S. (2019). Selective Anticancer Therapy Using Pro-Oxidant Drug-Loaded Chitosan-Fucoidan Nanoparticles. *Int. J. Mol. Sci.* 20 (13), 3220. doi:10.3390/ijms20133220

Cofano, F., Boido, M., Monticelli, M., Zenga, F., Ducati, A., Vercelli, A., et al. (2019). Mesenchymal Stem Cells for Spinal Cord Injury: Current Options,

Limitations, and Future of Cell Therapy. *Int. J. Mol. Sci.* 20 (11), 2698. doi:10.3390/ijms20112698

Dadfar, S. M., Roemhild, K., Drude, N. I., von Stillfried, S., Knüchel, R., Kiessling, F., et al. (2019). Iron Oxide Nanoparticles: Diagnostic, Therapeutic and Theranostic Applications. *Adv. Drug Deliv. Rev.* 138, 302–325. doi:10.1016/j.addr.2019.01.005

Dasagrandhi, C., Park, S., Jung, W. K., and Kim, Y. M. (2018). Antibacterial and Biofilm Modulating Potential of Ferulic Acid-Grafted Chitosan against Human Pathogenic Bacteria. *Int. J. Mol. Sci.* 19 (8), 2157. doi:10.3390/ijms19082157

Deepthi, S., Nivedhitha Sundaram, M., Deepti Kadavan, J., and Jayakumar, R. (2016). Layered Chitosan-Collagen Hydrogel/Aligned PLLA Nanofiber Construct for Flexor Tendon Regeneration. *Carbohydr. Polym.* 153, 492–500. doi:10.1016/j.carbpol.2016.07.124

Deng, J. J., Li, Z. Q., Mo, Z. Q., Xu, S., Mao, H. H., Shi, D., et al. (2020). Immunomodulatory Effects of N-Acetyl Chitooligosaccharides on RAW264.7 Macrophages. *Mar. Drugs* 18 (8), 421. doi:10.3390/md18080421

Ding, F., Nie, Z., Deng, H., Xiao, L., Du, Y., and Shi, X. (2013). Antibacterial Hydrogel Coating by Electrophoretic Co-Deposition of Chitosan/Alkynyl Chitosan. *Carbohydr. Polym.* 98 (2), 1547–1552. doi:10.1016/j.carbpol.2013.07.042

El Kadib, A. (2020). Green and Functional Aerogels by Macromolecular and Textural Engineering of Chitosan Microspheres. *Chem. Rec.* 20 (8), 753–772. doi:10.1002/tcr.201900089

Endo, M., Setsu, N., Fujiwara, T., Ishii, T., Nakagawa, M., Yahiro, K., et al. (2019). Diagnosis and Management of Subcutaneous Soft Tissue Sarcoma. *Curr. Treat. Options Oncol.* 20 (7), 54. doi:10.1007/s11864-019-0656-z

Fakhri, E., Eslami, H., Maroufi, P., Pakdel, F., Taghizadeh, S., Ganbarov, K., et al. (2020). Chitosan Biomaterials Application in Dentistry. *Int. J. Biol. Macromol.* 162, 956–974. doi:10.1016/j.ijbiomac.2020.06.211

Fan, X., Li, Y., Li, N., Wan, G., Ali, M. A., and Tang, K. (2020). Rapid Hemostatic Chitosan/Cellulose Composite Sponge by Alkali/urea Method for Massive Haemorrhage. *Int. J. Biol. Macromol.* 164, 2769–2778. doi:10.1016/j.ijbiomac.2020.07.312

Freitas, E. D., Moura, C. F., Jr., Kerwald, J., and Beppu, M. M. (2020). An Overview of Current Knowledge on the Properties, Synthesis and Applications of Quaternary Chitosan Derivatives. *Polym. (Basel)* 12 (12), 2878. doi:10.3390/polym12122878

Ghaee, A., Nourmohammadi, J., and Danesh, P. (2017). Novel Chitosan-Sulfonated Chitosan-Polycaprolactone-Calcium Phosphate Nanocomposite Scaffold. *Carbohydr. Polym.* 157, 695–703. doi:10.1016/j.carbpol.2016.10.023

Ghazaie, M., Ghiaci, M., Soleimanian-Zad, S., and Behzadi-Teshnizi, S. (2019). Preparing Natural Biocomposites of N-Quaternary Chitosan with Antibacterial Activity to Reduce Consumption of Antibacterial Drugs. *J. Hazard. Mater.* 371, 224–232. doi:10.1016/j.jhazmat.2019.03.003

Guo, A., Wang, F., Lin, W., Xu, X., Tang, T., Shen, Y., et al. (2014). Evaluation of Antibacterial Activity of N-Phosphonium Chitosan as a Novel Polymeric Antibacterial Agent. *Int. J. Biol. Macromol.* 67, 163–171. doi:10.1016/j.ijbiomac.2014.03.024

Guo, B., Qu, J., Zhao, X., and Zhang, M. (2019). Degradable Conductive Self-Healing Hydrogels Based on Dextran-Graft-Tetraaniline and N-Carboxyethyl Chitosan as Injectable Carriers for Myoblast Cell Therapy and Muscle Regeneration. *Acta Biomater.* 84, 180–193. doi:10.1016/j.actbio.2018.12.008

Hao, W., Li, K., Ma, Y., Li, R., Xing, R., Yu, H., et al. (2021). Preparation and Antioxidant Activity of Chitosan Dimers with Different Sequences. *Mar. Drugs* 19 (7), 366. doi:10.3390/md19070366

He, G., Chen, X., Yin, Y., Cai, W., Ke, W., Kong, Y., et al. (2016). Preparation and Antibacterial Properties of O-Carboxymethyl Chitosan/Lincomycin Hydrogels. *J. Biomater. Sci. Polym. Ed.* 27 (4), 370–384. doi:10.1080/09205063.2015.1132616

He, Y., Zhao, W., Dong, Z., Ji, Y., Li, M., Hao, Y., et al. (2021). A Biodegradable Antibacterial Alginate/Carboxymethyl Chitosan/Kangfuxin Sponges for Promoting Blood Coagulation and Full-Thickness Wound Healing. *Int. J. Biol. Macromol.* 167, 182–192. doi:10.1016/j.ijbiomac.2020.11.168

Hebeish, A. A., Ramadan, M. A., Montaser, A. S., and Farag, A. M. (2014). Preparation, Characterization and Antibacterial Activity of Chitosan-G-Poly Acrylonitrile/Silver Nanocomposite. *Int. J. Biol. Macromol.* 68, 178–184. doi:10.1016/j.ijbiomac.2014.04.028

Hemmingsen, L. M., Julin, K., Ahsan, L., Basnet, P., Johannessen, M., and Skalko-Basnet, N. (2021). Chitosomes-In-Chitosan Hydrogel for Acute Skin Injuries: Prevention and Infection Control. *Mar. Drugs* 19 (5), 269. doi:10.3390/md19050269

Hickman, D. A., Pawlowski, C. L., Sekhon, U. D. S., Marks, J., and Gupta, A. S. (2018). Biomaterials and Advanced Technologies for Hemostatic Management of Bleeding. *Adv. Mater* 30 (4), 1700859. doi:10.1002/adma.201700859

Hoefkens, F., Dehandschutter, C., Somville, J., Meijnders, P., and Van Gestel, D. (2016). Soft Tissue Sarcoma of the Extremities: Pending Questions on Surgery and Radiotherapy. *Radiat. Oncol.* 11 (1), 136. doi:10.1186/s13014-016-0668-9

Homaeigohar, S., and Boccaccini, A. R. (2020). Antibacterial Biohybrid Nanofibers for Wound Dressings. *Acta Biomater.* 107, 25–49. doi:10.1016/j.actbio.2020.02.022

Hou, B., Qi, M., Sun, J., Ai, M., Ma, X., Cai, W., et al. (2020). Preparation, Characterization and Wound Healing Effect of Vaccarin-Chitosan Nanoparticles. *Int. J. Biol. Macromol.* 165 (Pt B), 3169–3179. doi:10.1016/j.ijbiomac.2020.10.182

Hu, S., Bi, S., Yan, D., Zhou, Z., Sun, G., Cheng, X., et al. (2018). Preparation of Composite Hydroxybutyl Chitosan Sponge and its Role in Promoting Wound Healing. *Carbohydr. Polym.* 184, 154–163. doi:10.1016/j.carbpol.2017.12.033

Hu, Z., Zhang, D. Y., Lu, S. T., Li, P. W., and Li, S. D. (2018). Chitosan-Based Composite Materials for Prospective Hemostatic Applications. *Mar. Drugs* 16 (8), 273. doi:10.3390/md16080273

Hu, Z., Zhang, L., Zhong, L., Zhou, Y., Xue, J., and Li, Y. (2019). Preparation of an Antibacterial Chitosan-Coated Biochar-Nanosilver Composite for Drinking Water Purification. *Carbohydr. Polym.* 219, 290–297. doi:10.1016/j.carbpol.2019.05.017

Jayakumar, R., Prabaharan, M., Sudheesh Kumar, P. T., Nair, S. V., and Tamura, H. (2011). Biomaterials Based on Chitin and Chitosan in Wound Dressing Applications. *Biotechnol. Adv.* 29 (3), 322–337. doi:10.1016/j.biotechadv.2011.01.005

Jou, C.-H. (2011). Antibacterial Activity and Cytocompatibility of Chitosan-N-Hydroxy-2,3-Propyl-N Methyl-N,N-Diallylammonium Methyl Sulfate. *Colloids Surfaces B Biointerfaces* 88 (1), 448–454. doi:10.1016/j.colsurfb.2011.07.028

Jung, J., Cavender, G., and Zhao, Y. (2014). The Contribution of Acidulant to the Antibacterial Activity of Acid Soluble α- and β-Chitosan Solutions and Their Films. *Appl. Microbiol. Biotechnol.* 98 (1), 425–435. doi:10.1007/s00253-013-5334-7

Jyoti, K., Malik, G., Chaudhary, M., Sharma, M., Goswami, M., Katare, O. P., et al. (2020). Chitosan and Phospholipid Assisted Topical Fusidic Acid Drug Delivery in Burn Wound: Strategies to Conquer Pharmaceutical and Clinical Challenges, Opportunities and Future Panorama. *Int. J. Biol. Macromol.* 161, 325–335. doi:10.1016/j.ijbiomac.2020.05.230

Kamath, P. R., and Sunil, D. (2017). Nano-Chitosan Particles in Anticancer Drug Delivery: An Up-To-Date Review. *Mini Rev. Med. Chem.* 17 (15), 1457–1487. doi:10.2174/1389557517666170228105731

Kandra, P., and Kalangi, H. P. J. (2015). Current Understanding of Synergistic Interplay of Chitosan Nanoparticles and Anticancer Drugs: Merits and Challenges. *Appl. Microbiol. Biotechnol.* 99 (5), 2055–2064. doi:10.1007/s00253-015-6384-9

Kim, S. S., and Lee, J. (2014). Antibacterial Activity of Polyacrylonitrile-Chitosan Electrospun Nanofibers. *Carbohydr. Polym.* 102, 231–237. doi:10.1016/j.carbpol.2013.11.028

Kimura, Y., Onoyama, M., Sera, T., and Okuda, H. (2000). Antitumour Activity and Side Effects of Combined Treatment with Chitosan and Cisplatin in Sarcoma 180-Bearing Mice. *J. Pharm. Pharmacol.* 52 (7), 883–890. doi:10.1211/0022357001774570

Kimura, Y., Sawai, N., and Okuda, H. (2001). Antitumour Activity and Adverse Reactions of Combined Treatment with Chitosan and Doxorubicin in Tumour-Bearing Mice. *J. Pharm. Pharmacol.* 53 (10), 1373–1378. doi:10.1211/0022357011777873

Li, B., Shan, C.-L., Zhou, Q., Fang, Y., Wang, Y.-L., Xu, F., et al. (2013). Synthesis, Characterization, and Antibacterial Activity of Cross-Linked Chitosan-Glutaraldehyde. *Mar. Drugs* 11 (5), 1534–1552. doi:10.3390/md11051534

Li, D., Gao, X., Huang, X., Liu, P., Xiong, W., Wu, S., et al. (2020). Preparation of Organic-Inorganic Chitosan@silver/Aepiolite Composites with High Synergistic Antibacterial Activity and Stability. *Carbohydr. Polym.* 249, 116858. doi:10.1016/j.carbpol.2020.116858

Li, G., Xiao, Q., Zhang, L., Zhao, Y., and Yang, Y. (2017). Nerve Growth Factor Loaded Heparin/chitosan Scaffolds for Accelerating Peripheral Nerve Regeneration. *Carbohydr. Polym.* 171, 39–49. doi:10.1016/j.carbpol.2017.05.006

Li, J., Sun, X., Zhang, K., Yang, G., Mu, Y., Su, C., et al. (2020). Chitosan/Diatom-Biosilica Aerogel with Controlled Porous Structure for Rapid Hemostasis. *Adv. Healthc. Mater* 9 (21), e2000951. doi:10.1002/adhm.202000951

Li, J., Wu, X., Shi, Q., Li, C., and Chen, X. (2019). Effects of Hydroxybutyl Chitosan on Improving Immunocompetence and Antibacterial Activities. *Mater. Sci. Eng. C* 105, 110086. doi:10.1016/j.msec.2019.110086

Li, Y., Jiang, Q.-l., Van der Merwe, L., Lou, D.-h., and Lin, C. (2021). Preclinical Efficacy of Stem Cell Therapy for Skin Flap: A Systematic Review and Meta-Analysis. *Stem Cell Res. Ther.* 12 (1), 28. doi:10.1186/s13287-020-02103-w

Li, Z., Hu, W., Zhao, Y., Ren, L., and Yuan, X. (2018). Integrated Antibacterial and Antifouling Surfaces via Cross-Linking Chitosan- G -eugenol/Zwitterionic Copolymer on Electrospun Membranes. *Colloids Surfaces B Biointerfaces* 169, 151–159. doi:10.1016/j.colsurfb.2018.04.056

Liu, Y., Wang, S., and Lan, W. (2018). Fabrication of Antibacterial Chitosan-PVA Blended Film Using Electrospray Technique for Food Packaging Applications. *Int. J. Biol. Macromol.* 107 (Pt A), 848–854. doi:10.1016/j.ijbiomac.2017.09.044

Luo, Q., Han, Q., Wang, Y., Zhang, H., Fei, Z., and Wang, Y. (2019). The Thiolated Chitosan: Synthesis, Gelling and Antibacterial Capability. *Int. J. Biol. Macromol.* 139, 521–530. doi:10.1016/j.ijbiomac.2019.08.001

Ma, Y., Xin, L., Tan, H., Fan, M., Li, J., Jia, Y., et al. (2017). Chitosan Membrane Dressings Toughened by Glycerol to Load Antibacterial Drugs for Wound Healing. *Mater. Sci. Eng. C* 81, 522–531. doi:10.1016/j.msec.2017.08.052

Maeda, Y., and Kimura, Y. (2004). Antitumor Effects of Various Low-Molecular-Weight Chitosans Are Due to Increased Natural Killer Activity of Intestinal Intraepithelial Lymphocytes in Sarcoma 180-bearing Mice. *J. Nutr.* 134 (4), 945–950. doi:10.1093/jn/134.4.945

Maleki Dana, P., Hallajzadeh, J., Asemi, Z., Mansournia, M. A., and Yousefi, B. (2021). Chitosan Applications in Studying and Managing Osteosarcoma. *Int. J. Biol. Macromol.* 169, 321–329. doi:10.1016/j.ijbiomac.2020.12.058

Malhotra, K., Shankar, S., Chauhan, N., Rai, R., and Singh, Y. (2020). Design, Characterization, and Evaluation of Antibacterial Gels, Boc-D-Phe-γ4-L-Phe-PEA/Chitosan and Boc-L-Phe-γ4-L-Phe-PEA/Chitosan, for Biomaterial-Related Infections. *Mater. Sci. Eng. C* 110, 110648. doi:10.1016/j.msec.2020.110648

Mallakpour, S., and Abbasi, M. (2020). Hydroxyapatite Mineralization on Chitosan-Tragacanth Gum/silica@silver Nanocomposites and Their Antibacterial Activity Evaluation. *Int. J. Biol. Macromol.* 151, 909–923. doi:10.1016/j.ijbiomac.2020.02.167

Masood, N., Ahmed, R., Tariq, M., Ahmed, Z., Masoud, M. S., Ali, I., et al. (2019). Silver Nanoparticle Impregnated Chitosan-PEG Hydrogel Enhances Wound Healing in Diabetes Induced Rabbits. *Int. J. Pharm.* 559, 23–36. doi:10.1016/j.ijpharm.2019.01.019

Matica, M. A., Aachmann, F. L., Tøndervik, A., Sletta, H., and Ostafe, V. (2019). Chitosan as a Wound Dressing Starting Material: Antimicrobial Properties and Mode of Action. *Int. J. Mol. Sci.* 20 (23), 5889. doi:10.3390/ijms20235889

Meyer, C., Stenberg, L., Gonzalez-Perez, F., Wrobel, S., Ronchi, G., Udina, E., et al. (2016). Chitosan-Film Enhanced Chitosan Nerve Guides for Long-Distance Regeneration of Peripheral Nerves. *Biomaterials* 76, 33–51. doi:10.1016/j.biomaterials.2015.10.040

Mi, Y., Chen, Y., Gu, G., Miao, Q., Tan, W., Li, Q., et al. (2021). New Synthetic Adriamycin-Incorporated Chitosan Nanoparticles with Enhanced Antioxidant, Antitumor Activities and pH-Sensitive Drug Release. *Carbohydr. Polym.* 273, 118623. doi:10.1016/j.carbpol.2021.118623

Min, T., Zhu, Z., Sun, X., Yuan, Z., Zha, J., and Wen, Y. (2020). Highly Efficient Antifogging and Antibacterial Food Packaging Film Fabricated by Novel Quaternary Ammonium Chitosan Composite. *Food Chem.* 308, 125682. doi:10.1016/j.foodchem.2019.125682

Moran, H. B. T., Turley, J. L., Andersson, M., and Lavelle, E. C. (2018). Immunomodulatory Properties of Chitosan Polymers. *Biomaterials* 184, 1–9. doi:10.1016/j.biomaterials.2018.08.054

Muthu, M., Gopal, J., Chun, S., Devadoss, A. J. P., Hasan, N., and Sivanesan, I. (2021). Crustacean Waste-Derived Chitosan: Antioxidant Properties and Future Perspective. *Antioxidants (Basel)* 10 (2), 228. doi:10.3390/antiox10020228

Muxika, A., Etxabide, A., Uranga, J., Guerrero, P., and de la Caba, K. (2017). Chitosan as a Bioactive Polymer: Processing, Properties and Applications. *Int. J. Biol. Macromol.* 105 (Pt 2), 1358–1368. doi:10.1016/j.ijbiomac.2017.07.087

Negm, N. A., Kana, M. T. H. A., Abubshait, S. A., and Betiha, M. A. (2020). Effectuality of Chitosan Biopolymer and its Derivatives during Antioxidant Applications. *Int. J. Biol. Macromol.* 164, 1342–1369. doi:10.1016/j.ijbiomac.2020.07.197

Ng, I.-S., Ooi, C. W., Liu, B.-L., Peng, C.-T., Chiu, C.-Y., and Chang, Y.-K. (2020). Antibacterial Efficacy of Chitosan- and Poly(Hexamethylene Biguanide)-Immobilized Nanofiber Membrane. *Int. J. Biol. Macromol.* 154, 844–854. doi:10.1016/j.ijbiomac.2020.03.127

Nivedhitha Sundaram, M., Deepthi, S., Mony, U., Shalumon, K. T., Chen, J.-P., and Jayakumar, R. (2019). Chitosan Hydrogel Scaffold Reinforced with Twisted Poly(l Lactic Acid) Aligned Microfibrous Bundle to Mimic Tendon Extracellular Matrix. *Int. J. Biol. Macromol.* 122, 37–44. doi:10.1016/j.ijbiomac.2018.10.151

Nouri, A., Yaraki, M. T., Ghorbanpour, M., Agarwal, S., and Gupta, V. K. (2018). Enhanced Antibacterial Effect of Chitosan Film Using Montmorillonite/CuO Nanocomposite. *Int. J. Biol. Macromol.* 109, 1219–1231. doi:10.1016/j.ijbiomac.2017.11.119

Olanipekun, E. O., Ayodele, O., Olatunde, O. C., and Olusegun, S. J. (2021). Comparative Studies of Chitosan and Carboxymethyl Chitosan Doped with Nickel and Copper: Characterization and Antibacterial Potential. *Int. J. Biol. Macromol.* 183, 1971–1977. doi:10.1016/j.ijbiomac.2021.05.162

Oryan, A., and Sahvieh, S. (2017). Effectiveness of Chitosan Scaffold in Skin, Bone and Cartilage Healing. *Int. J. Biol. Macromol.* 104 (Pt A), 1003–1011. doi:10.1016/j.ijbiomac.2017.06.124

Pal, A., Talukdar, D., Roy, A., Ray, S., Mallick, A., Mandal, C., et al. (2015). Nanofabrication of Methylglyoxal with Chitosan Biopolymer: A Potential Tool for Enhancement of its Anticancer Effect. *Int. J. Nanomedicine* 10, 3499–3518. doi:10.2147/IJN.S78284

Pandit, A. H., Nisar, S., Imtiyaz, K., Nadeem, M., Mazumdar, N., Rizvi, M. M. A., et al. (2021). Injectable, Self-Healing, and Biocompatible N,O-Carboxymethyl Chitosan/Multialdehyde Guar Gum Hydrogels for Sustained Anticancer Drug Delivery. *Biomacromolecules* 22 (9), 3731–3745. doi:10.1021/acs.biomac.1c00537

Papadimitriou, L., Kaliva, M., Vamvakaki, M., and Chatzinikolaidou, M. (2017). Immunomodulatory Potential of Chitosan-Graft-Poly(ε-Caprolactone) Copolymers toward the Polarization of Bone-Marrow-Derived Macrophages. *ACS Biomater. Sci. Eng.* 3 (7), 1341–1349. doi:10.1021/acsbiomaterials.6b00440

Peetermans, M., de Prost, N., Eckmann, C., Norrby-Teglund, A., Skrede, S., and De Waele, J. J. (2020). Necrotizing Skin and Soft-Tissue Infections in the Intensive Care Unit. *Clin. Microbiol. Infect.* 26 (1), 8–17. doi:10.1016/j.cmi.2019.06.031

Plucinski, A., Lyu, Z., and Schmidt, B. V. K. J. (2021). Polysaccharide Nanoparticles: From Fabrication to Applications. *J. Mat. Chem. B* 9 (35), 7030–7062. doi:10.1039/d1tb00628b

Potara, M., Jakab, E., Damert, A., Popescu, O., Canpean, V., and Astilean, S. (2011). Synergistic Antibacterial Activity of Chitosan-Silver Nanocomposites on *Staphylococcus A*. *Nanotechnology* 22 (13), 135101. doi:10.1088/0957-4484/22/13/135101

Przekora, A. (2020). A Concise Review on Tissue Engineered Artificial Skin Grafts for Chronic Wound Treatment: Can We Reconstruct Functional Skin Tissue *In Vitro*? *Cells* 9 (7), 1622. doi:10.3390/cells9071622

Raghavendra, G. M., Jung, J., Kim, D., and Seo, J. (2016). Microwave Assisted Antibacterial Chitosan-Silver Nanocomposite Films. *Int. J. Biol. Macromol.* 84, 281–288. doi:10.1016/j.ijbiomac.2015.12.026

Rajitha, P., Gopinath, D., Biswas, R., Sabitha, M., and Jayakumar, R. (2016). Chitosan Nanoparticles in Drug Therapy of Infectious and Inflammatory Diseases. *Expert Opin. Drug Deliv.* 13 (8), 1177–1194. doi:10.1080/17425247.2016.1178232

Rao, F., Wang, Y., Zhang, D., Lu, C., Cao, Z., Sui, J., et al. (2020). Aligned Chitosan Nanofiber Hydrogel Grafted with Peptides Mimicking Bioactive Brain-Derived Neurotrophic Factor and Vascular Endothelial Growth Factor Repair Long-Distance Sciatic Nerve Defects in Rats. *Theranostics* 10 (4), 1590–1603. doi:10.7150/thno.36272

Rao, K. M., Suneetha, M., Park, G. T., Babu, A. G., and Han, S. S. (2020). Hemostatic, Biocompatible, and Antibacterial Non-Animal Fungal Mushroom-Based Carboxymethyl Chitosan-ZnO Nanocomposite for Wound-Healing Applications. *Int. J. Biol. Macromol.* 155, 71–80. doi:10.1016/j.ijbiomac.2020.03.170

Rashki, S., Asgarpour, K., Tarrahimofrad, H., Hashemipour, M., Ebrahimi, M. S., Fathizadeh, H., et al. (2021). Chitosan-Based Nanoparticles against Bacterial Infections. *Carbohydr. Polym.* 251, 117108. doi:10.1016/j.carbpol.2020.117108

Regiel-Futyra, A., Kus-Liśkiewicz, M., Sebastian, V., Irusta, S., Arruebo, M., Stochel, G., et al. (2015). Development of Noncytotoxic Chitosan-Gold Nanocomposites as Efficient Antibacterial Materials. *ACS Appl. Mat. Interfaces* 7 (2), 1087–1099. doi:10.1021/am508094e

Rizeq, B. R., Younes, N. N., Rasool, K., and Nasrallah, G. K. (2019). Synthesis, Bioapplications, and Toxicity Evaluation of Chitosan-Based Nanoparticles. *Int. J. Mol. Sci.* 20 (22), 5776. doi:10.3390/ijms20225776

Rodríguez-Vázquez, M., Vega-Ruiz, B., Ramos-Zúñiga, R., Saldaña-Koppel, D. A., and Quiñones-Olvera, L. F. (2015). Chitosan and its Potential Use as a Scaffold for Tissue Engineering in Regenerative Medicine. *Biomed. Res. Int.* 2015, 821279. doi:10.1155/2015/821279

Russo, V., El Khatib, M., Prencipe, G., Cerveró-Varona, A., Citeroni, M. R., Mauro, A., et al. (2022). Scaffold-Mediated Immunoengineering as Innovative Strategy for Tendon Regeneration. *Cells* 11 (2), 266. doi:10.3390/cells11020266

Sahariah, P., Cibor, D., Zielińska, D., Hjálmarsdóttir, M. Á., Stawski, D., and Másson, M. (2019). The Effect of Molecular Weight on the Antibacterial Activity of N,N,N-Trimethyl Chitosan (TMC). *Int. J. Mol. Sci.* 20 (7), 1743. doi:10.3390/ijms20071743

Salari, M., Sowti Khiabani, M., Rezaei Mokarram, R., Ghanbarzadeh, B., and Samadi Kafil, H. (2021). Use of Gamma Irradiation Technology for Modification of Bacterial Cellulose Nanocrystals/Chitosan Nanocomposite Film. *Carbohydr. Polym.* 253, 117144. doi:10.1016/j.carbpol.2020.117144

Sanad, R. A.-B., and Abdel-Bar, H. M. (2017). Chitosan-Hyaluronic Acid Composite Sponge Scaffold Enriched with Andrographolide-Loaded Lipid Nanoparticles for Enhanced Wound Healing. *Carbohydr. Polym.* 173, 441–450. doi:10.1016/j.carbpol.2017.05.098

Santos, V. P., Marques, N. S. S., Maia, P. C. S. V., Lima, M. A. B., Franco, L. O., and Campos-Takaki, G. M. (2020). Seafood Waste as Attractive Source of Chitin and Chitosan Production and Their Applications. *Int. J. Mol. Sci.* 21 (12), 4290. doi:10.3390/ijms21124290

Senthilkumar, P., Yaswant, G., Kavitha, S., Chandramohan, E., Kowsalya, G., Vijay, R., et al. (2019). Preparation and Characterization of Hybrid Chitosan-Silver Nanoparticles (Chi-Ag NPs); A Potential Antibacterial Agent. *Int. J. Biol. Macromol.* 141, 290–298. doi:10.1016/j.ijbiomac.2019.08.234

Shahid Ul, I., and Butola, B. S. (2019). Recent Advances in Chitosan Polysaccharide and its Derivatives in Antimicrobial Modification of Textile Materials. *Int. J. Biol. Macromol.* 121, 905–912. doi:10.1016/j.ijbiomac.2018.10.102

Shahid Ul, I., Butola, B. S., and Verma, D. (2019). Facile Synthesis of Chitosan-Silver Nanoparticles onto Linen for Antibacterial Activity and Free-Radical Scavenging Textiles. *Int. J. Biol. Macromol.* 133, 1134–1141. doi:10.1016/j.ijbiomac.2019.04.186

Shariatinia, Z. (2018). Carboxymethyl Chitosan: Properties and Biomedical Applications. *Int. J. Biol. Macromol.* 120 (Pt B), 1406–1419. doi:10.1016/j.ijbiomac.2018.09.131

Shen, T., Dai, K., Yu, Y., Wang, J., and Liu, C. (2020). Sulfated Chitosan Rescues Dysfunctional Macrophages and Accelerates Wound Healing in Diabetic Mice. *Acta Biomater.* 117, 192–203. doi:10.1016/j.actbio.2020.09.035

Shou, Y., Zhang, J., Yan, S., Xia, P., Xu, P., Li, G., et al. (2020). Thermoresponsive Chitosan/DOPA-Based Hydrogel as an Injectable Therapy Approach for Tissue-Adhesion and Hemostasis. *ACS Biomater. Sci. Eng.* 6 (6), 3619–3629. doi:10.1021/acsbiomaterials.0c00545

Shu, Y., Yu, Y., Zhang, S., Wang, J., Xiao, Y., and Liu, C. (2018). The Immunomodulatory Role of Sulfated Chitosan in BMP-2-Mediated Bone Regeneration. *Biomater. Sci.* 6 (9), 2496–2507. doi:10.1039/c8bm00701b

Simões, D., Miguel, S. P., Ribeiro, M. P., Coutinho, P., Mendonça, A. G., and Correia, I. J. (2018). Recent Advances on Antimicrobial Wound Dressing: A Review. *Eur. J. Pharm. Biopharm.* 127, 130–141. doi:10.1016/j.ejpb.2018.02.022

Song, F., Kong, Y., Shao, C., Cheng, Y., Lu, J., Tao, Y., et al. (2021). Chitosan-Based Multifunctional Flexible Hemostatic Bio-Hydrogel. *Acta Biomater.* 136, 170–183. doi:10.1016/j.actbio.2021.09.056

Sun, X., Li, J., Shao, K., Su, C., Bi, S., Mu, Y., et al. (2021). A Composite Sponge Based on Alkylated Chitosan and Diatom-Biosilica for Rapid Hemostasis. *Int. J. Biol. Macromol.* 182, 2097–2107. doi:10.1016/j.ijbiomac.2021.05.123

Sun, X., Zhang, J., Mi, Y., Chen, Y., Tan, W., Li, Q., et al. (2020). Synthesis, Characterization, and the Antioxidant Activity of the Acetylated Chitosan Derivatives Containing Sulfonium Salts. *Int. J. Biol. Macromol.* 152, 349–358. doi:10.1016/j.ijbiomac.2020.02.177

Sun, Y., Yang, C., Zhu, X., Wang, J. J., Liu, X. Y., Yang, X. P., et al. (2019). 3D Printing Collagen/Chitosan Scaffold Ameliorated Axon Regeneration and Neurological Recovery after Spinal Cord Injury. *J. Biomed. Mat. Res.* 107 (9), 1898–1908. doi:10.1002/jbm.a.36675

Sztretye, M., Dienes, B., Gönczi, M., Czirják, T., Csernoch, L., Dux, L., et al. (2019). Astaxanthin: A Potential Mitochondrial-Targeted Antioxidant Treatment in Diseases and with Aging. *Oxid. Med. Cell Longev.* 2019, 3849692. doi:10.1155/2019/3849692

Tan, M. L., Friedhuber, A. M., Dunstan, D. E., Choong, P. F. M., and Dass, C. R. (2010). The Performance of Doxorubicin Encapsulated in Chitosan-Dextran Sulphate Microparticles in an Osteosarcoma Model. *Biomaterials* 31 (3), 541–551. doi:10.1016/j.biomaterials.2009.09.069

Tan, W., Zhang, J., Zhao, X., Li, Q., Dong, F., and Guo, Z. (2020). Preparation and Physicochemical Properties of Antioxidant Chitosan Ascorbate/methylcellulose Composite Films. *Int. J. Biol. Macromol.* 146, 53–61. doi:10.1016/j.ijbiomac.2019.12.044

Tang, S., and Zheng, J. (2018). Antibacterial Activity of Silver Nanoparticles: Structural Effects. *Adv. Healthc. Mater* 7 (13), e1701503. doi:10.1002/adhm.201701503

Tao, S.-C., Guo, S.-C., Li, M., Ke, Q.-F., Guo, Y.-P., and Zhang, C.-Q. (2017). Chitosan Wound Dressings Incorporating Exosomes Derived from MicroRNA-126-Overexpressing Synovium Mesenchymal Stem Cells Provide Sustained Release of Exosomes and Heal Full-Thickness Skin Defects in a Diabetic Rat Model. *Stem Cells Transl. Med.* 6 (3), 736–747. doi:10.5966/sctm.2016-0275

Teixeira, M. O., Antunes, J. C., and Felgueiras, H. P. (2021). Recent Advances in Fiber-Hydrogel Composites for Wound Healing and Drug Delivery Systems. *Antibiot. (Basel)* 10 (3), 248. doi:10.3390/antibiotics10030248

Thapa, R. K., Diep, D. B., and Tønnesen, H. H. (2020). Topical Antimicrobial Peptide Formulations for Wound Healing: Current Developments and Future Prospects. *Acta Biomater.* 103, 52–67. doi:10.1016/j.actbio.2019.12.025

Theuretzbacher, U., Outterson, K., Engel, A., and Karlén, A. (2020). The Global Preclinical Antibacterial Pipeline. *Nat. Rev. Microbiol.* 18 (5), 275–285. doi:10.1038/s41579-019-0288-0

Umar, A. K., Sriwidodo, S., Maksum, I. P., and Wathoni, N. (2021). Film-Forming Spray of Water-Soluble Chitosan Containing Liposome-Coated Human Epidermal Growth Factor for Wound Healing. *Molecules* 26 (17), 5326. doi:10.3390/molecules26175326

Verlee, A., Mincke, S., and Stevens, C. V. (2017). Recent Developments in Antibacterial and Antifungal Chitosan and its Derivatives. *Carbohydr. Polym.* 164, 268–283. doi:10.1016/j.carbpol.2017.02.001

Vijayavenkataraman, S. (2020). Nerve Guide Conduits for Peripheral Nerve Injury Repair: A Review on Design, Materials and Fabrication Methods. *Acta Biomater.* 106, 54–69. doi:10.1016/j.actbio.2020.02.003

Vivcharenko, V., Benko, A., Palka, K., Wojcik, M., and Przekora, A. (2020). Elastic and Biodegradable Chitosan/Agarose Film Revealing Slightly Acidic pH for Potential Applications in Regenerative Medicine as Artificial Skin Graft. *Int. J. Biol. Macromol.* 164, 172–183. doi:10.1016/j.ijbiomac.2020.07.099

Wahid, F., Wang, H.-S., Lu, Y.-S., Zhong, C., and Chu, L.-Q. (2017). Preparation, Characterization and Antibacterial Applications of Carboxymethyl Chitosan/CuO Nanocomposite Hydrogels. *Int. J. Biol. Macromol.* 101, 690–695. doi:10.1016/j.ijbiomac.2017.03.132

Wahid, F., Yin, J.-J., Xue, D.-D., Xue, H., Lu, Y.-S., Zhong, C., et al. (2016). Synthesis and Characterization of Antibacterial Carboxymethyl Chitosan/ZnO Nanocomposite Hydrogels. *Int. J. Biol. Macromol.* 88, 273–279. doi:10.1016/j.ijbiomac.2016.03.044

Wahid, F., Zhou, Y.-N., Wang, H.-S., Wan, T., Zhong, C., and Chu, L.-Q. (2018). Injectable Self-Healing Carboxymethyl Chitosan-Zinc Supramolecular Hydrogels and Their Antibacterial Activity. *Int. J. Biol. Macromol.* 114, 1233–1239. doi:10.1016/j.ijbiomac.2018.04.025

Wang, G., and Fakhri, A. (2020). Preparation of CuS/polyvinyl Alcohol-Chitosan Nanocomposites with Photocatalysis Activity and Antibacterial Behavior against G+/G- Bacteria. *Int. J. Biol. Macromol.* 155, 36–41. doi:10.1016/j.ijbiomac.2020.03.077

Wang, W., Meng, Q., Li, Q., Liu, J., Zhou, M., Jin, Z., et al. (2020). Chitosan Derivatives and Their Application in Biomedicine. *Int. J. Mol. Sci.* 21 (2), 487. doi:10.3390/ijms21020487

Wang, X., Cheng, F., Wang, X., Feng, T., Xia, S., and Zhang, X. (2021). Chitosan Decoration Improves the Rapid and Long-Term Antibacterial Activities of Cinnamaldehyde-Loaded Liposomes. *Int. J. Biol. Macromol.* 168, 59–66. doi:10.1016/j.ijbiomac.2020.12.003

Wang, Y.-L., Zhou, Y.-N., Li, X.-Y., Huang, J., Wahid, F., Zhong, C., et al. (2020). Continuous Production of Antibacterial Carboxymethyl Chitosan-Zinc Supramolecular Hydrogel Fiber Using a Double-Syringe Injection Device. *Int. J. Biol. Macromol.* 156, 252–261. doi:10.1016/j.ijbiomac.2020.04.073

Watkins, R. R., and David, M. Z. (2021). Approach to the Patient with a Skin and Soft Tissue Infection. *Infect. Dis. Clin. N. Am.* 35 (1), 1–48. doi:10.1016/j.idc.2020.10.011

Wei, L., Tan, J., Li, L., Wang, H., Liu, S., Chen, J., et al. (2022). Chitosan/Alginate Hydrogel Dressing Loaded FGF/VE-Cadherin to Accelerate Full-Thickness Skin Regeneration and More Normal Skin Repairs. *Int. J. Mol. Sci.* 23 (3), 1249. doi:10.3390/ijms23031249

Wei, L., Tan, W., Wang, G., Li, Q., Dong, F., and Guo, Z. (2019). The Antioxidant and Antifungal Activity of Chitosan Derivatives Bearing Schiff Bases and Quaternary Ammonium Salts. *Carbohydr. Polym.* 226, 115256. doi:10.1016/j.carbpol.2019.115256

Weiskopf, R. B. (2009). Hemostasis in Trauma. *Transfusion* 49 (Suppl. 5), 237S–9S. doi:10.1111/j.1537-2995.2008.01985.x

Wiarachai, O., Thongchul, N., Kiatkamjornwong, S., and Hoven, V. P. (2012). Surface-Quaternized Chitosan Particles as an Alternative and Effective Organic Antibacterial Material. *Colloids Surfaces B Biointerfaces* 92, 121–129. doi:10.1016/j.colsurfb.2011.11.034

Wilkinson, H. N., and Hardman, M. J. (2020). Wound Healing: Cellular Mechanisms and Pathological Outcomes. *Open Biol.* 10 (9), 200223. doi:10.1098/rsob.200223

Wu, G., Deng, X., Song, J., and Chen, F. (2018). Enhanced Biological Properties of Biomimetic Apatite Fabricated Polycaprolactone/Chitosan Nanofibrous Bio-Composite for Tendon and Ligament Regeneration. *J. Photochem. Photobiol. B Biol.* 178, 27–32. doi:10.1016/j.jphotobiol.2017.10.011

Wu, X., Farooq, M. A., Li, T., Geng, T., Kutoka, P. T., and Wang, B. (2021). Cationic Chitosan-Modified Silica Nanoparticles for Oral Delivery of Protein Vaccine. *J. Biomed. Mater Res.* 109 (11), 2111–2119. doi:10.1002/jbm.a.37198

Xiao, J., Zhou, Y., Ye, M., An, Y., Wang, K., Wu, Q., et al. (2021). Freeze-Thawing Chitosan/Ions Hydrogel Coated Gauzes Releasing Multiple Metal Ions on Demand for Improved Infected Wound Healing. *Adv. Healthc. Mater* 10 (6), e2001591. doi:10.1002/adhm.202001591

Yan, F., Dang, Q., Liu, C., Yan, J., Wang, T., Fan, B., et al. (2016). 3,6-O-[N-(2-Aminoethyl)-Acetamide-yl]-Chitosan Exerts Antibacterial Activity by a Membrane Damage Mechanism. *Carbohydr. Polym.* 149, 102–111. doi:10.1016/j.carbpol.2016.04.098

Yang, J., Lu, H., Li, M., Liu, J., Zhang, S., Xiong, L., et al. (2017). Development of Chitosan-Sodium Phytate Nanoparticles as a Potent Antibacterial Agent. *Carbohydr. Polym.* 178, 311–321. doi:10.1016/j.carbpol.2017.09.053

Yang, T.-C., Chou, C.-C., and Li, C.-F. (2005). Antibacterial Activity of N-Alkylated Disaccharide Chitosan Derivatives. *Int. J. Food Microbiol.* 97 (3), 237–245. doi:10.1016/s0168-1605(03)00083-7

Yin, M., Lin, X., Ren, T., Li, Z., Ren, X., and Huang, T.-S. (2018). Cytocompatible Quaternized Carboxymethyl Chitosan/poly(vinyl Alcohol) Blend Film Loaded Copper for Antibacterial Application. *Int. J. Biol. Macromol.* 120 (Pt A), 992–998. doi:10.1016/j.ijbiomac.2018.08.105

Younes, I., and Rinaudo, M. (2015). Chitin and Chitosan Preparation from Marine Sources. Structure, Properties and Applications. *Mar. Drugs* 13 (3), 1133–1174. doi:10.3390/md13031133

Yu, D., Feng, J., You, H., Zhou, S., Bai, Y., He, J., et al. (2022). The Microstructure, Antibacterial and Antitumor Activities of Chitosan Oligosaccharides and Derivatives. *Mar. Drugs* 20 (1), 69. doi:10.3390/md20010069

Yu, P., and Zhong, W. (2021). Hemostatic Materials in Wound Care. *Burns Trauma* 9, tkab019. doi:10.1093/burnst/tkab019

Yuan, J., Hou, Q., Chen, D., Zhong, L., Dai, X., Zhu, Z., et al. (2020). Chitosan/LiCl Composite Scaffolds Promote Skin Regeneration in Full-Thickness Loss. *Sci. China Life Sci.* 63 (4), 552–562. doi:10.1007/s11427-018-9389-6

Zhang, Y., Jiang, M., Zhang, Y., Cao, Q., Wang, X., Han, Y., , et al.Sun, G., Li, Y., Zhou, J. (2019). Novel Llignin-Cchitosan-PVA Ccomposite Hhydrogel for Wwound Ddressing. *Mater.ials Sci.ence and Eng.ineering: C* 104, 110002. doi:10.1016/j.msec.2019.110002

Zhang, E., Xing, R., Liu, S., Qin, Y., Li, K., and Li, P. (2019). Advances in Cchitosan-Bbased Nnanoparticles for Ooncotherapy. *Carbohydr.ate Polym.ers* 222, 115004. doi:10.1016/j.carbpol.2019.115004

Zhang, L., Yang, G., Johnson, B. N., and Jia, X. (2019). Three-dimensional (3D) Pprinted Sscaffold and Mmaterial Sselection for Bbone Rrepair. *Acta Biomater.ialia* 84, 16–33. doi:10.1016/j.actbio.2018.11.039

Zhang, N., Gao, T., Wang, Y., Liu, J., Zhang, J., Yao, R., , et al.Wu, F. (2020). Modulating Ccationicity of Cchitosan Hhydrogel to Pprevent Hhypertrophic Sscar Fformation during Wwound Hhealing. *Int.ernational J.ournal of Biol.ogical Macromol.ecules* 154, 835–843. doi:10.1016/j.ijbiomac.2020.03.161

Zhang, K., Li, J., Wang, Y., Mu, Y., Sun, X., Su, C., , et al.Dong, Y., Pang, J., Huang, L., Chen, X., Feng, C. (2020). Hydroxybutyl Cchitosan/diatom-Bbiosilica Ccomposite Ssponge for Hhemorrhage Ccontrol. *Carbohydr.ate Polym.ers* 236, 116051. doi:10.1016/j.carbpol.2020.116051

Zhang, A., Liu, Y., Qin, D., Sun, M., Wang, T., and Chen, X. (2020). Research Sstatus of Sself-Hhealing Hhydrogel for Wwound Mmanagement: A Rreview. *Int.ernational J.ournal of Biol.ogical Macromol.ecules* 164, 2108–2123. doi:10.1016/j.ijbiomac.2020.08.109

Zhao, Y., Wang, Y., Gong, J., Yang, L., Niu, C., Ni, X., , et al.Wang, Y., Peng, S., Gu, X., Sun, C., Yang, Y. (2017). Chitosan Ddegradation Pproducts Ffacilitate Pperipheral Nnerve Rregeneration by Iimproving Mmacrophage-Cconstructed Mmicroenvironments. *Biomaterials* 134, 64–77. doi:10.1016/j.biomaterials.2017.02.026

Zhao, Y., Hao, J., Chen, Z., Li, M., Ren, J., and Fu, X. (2021). Blood-clotting Mmodel and Ssimulation Aanalysis of Ppolyvinyl Aalcohol-Cchitosan Ccomposite Hhemostatic Mmaterials. *J. Mat.Mater. Chem. B* 9 (27), 5465–5475. doi:10.1039/d1tb00159k

Zheng, L., Li, S., Luo, J., and Wang, X. (2020). Latest Advances on Bacterial Cellulose-Based Antibacterial Materials as Wound Dressings. *Front. Bioeng. Biotechnol.* 8, 593768. doi:10.3389/fbioe.2020.593768

Zhou, B., Hu, Y., Li, J., and Li, B. (2014). Chitosan/phosvitin Aantibacterial Ffilms Ffabricated via Llayer-Bby-Llayer Ddeposition. *Int.ernational J.ournal of Biol.ogical Macromol.ecules* 64, 402–408. doi:10.1016/j.ijbiomac.2013.12.016

Conflict of Interest: The authors declare that the research was conducted in the absence of any commercial or financial relationships that could be construed as a potential conflict of interest.

Publisher's Note: All claims expressed in this article are solely those of the authors and do not necessarily represent those of their affiliated organizations, or those of the publisher, the editors and the reviewers. Any product that may be evaluated in this article, or claim that may be made by its manufacturer, is not guaranteed or endorsed by the publisher.

frontiers | Frontiers in Materials

REVIEW
published: 04 July 2022
doi: 10.3389/fmats.2022.942957

Applications of Hydrogels in Premature Ovarian Failure and Intrauterine Adhesion

Donghai Zhang[1], *Chuanfeng Ding*[1], *Tao Duan*[2]* *and Qian Zhou*[3]*

[1]Clinical and Translational Research Center, School of Medicine, Shanghai First Maternity and Infant Hospital, Tongji University, Shanghai, China, [2]Department of Obstetrics, School of Medicine, Shanghai First Maternity and Infant Hospital, Tongji University, Shanghai, China, [3]Department of Reproductive Immunology, School of Medicine, Shanghai First Maternity and Infant Hospital, Tongji University, Shanghai, China

Premature ovarian failure (POF) and intrauterine adhesion (IUA) that easily lead to reduced fertility in premenopausal women are two difficult diseases to treat in obstetrics and gynecology. Hormone therapy, *in vitro* fertilization and surgical treatments do not completely restore fertility. The advent of hydrogels offers new hope for the treatment of POF and IUA. Hydrogels are noncytotoxic and biodegradable, and do not cause immune rejection or inflammatory reactions. Drug delivery and stem cell delivery are the main application forms. Hydrogels are a local drug delivery reservoir, and the control of drug release is achieved by changing the physicochemical properties. The porous properties and stable three-dimensional structure of hydrogels support stem cell growth and functions. In addition, hydrogels are promising biomaterials for increasing the success rate of ovarian tissue transplantation. Hydrogel-based *in vitro* three-dimensional culture of follicles drives the development of artificial ovaries. Hydrogels form a barrier at the site of injury and have antibacterial, antiadhesive and antistenosis properties for IUA treatment. In this review, we evaluate the physicochemical properties of hydrogels, and focus on the latest applications of hydrogels in POF and IUA. We also found the limitations on clinical application of hydrogel and provide future prospects. Artificial ovary as the future of hydrogel in POF is worth studying, and 3D bioprinting may help the mass production of hydrogels.

Keywords: hydrogel, premature ovarian failure, intrauterine adhesion, mesenchymal stem cells, artificial ovary

OPEN ACCESS

Edited by:
Boguang Yang,
The Chinese University of Hong Kong, China

Reviewed by:
Sayan Ganguly,
Bar-Ilan University, Israel
Wei Kang,
Dalian University of Technology, China

***Correspondence:**
Tao Duan
tduan@yahoo.com
Qian Zhou
shzhouqian@126.com

Specialty section:
This article was submitted to Biomaterials, a section of the journal Frontiers in Materials

Received: *13 May 2022*
Accepted: *31 May 2022*
Published: *04 July 2022*

Citation:
Zhang D, Ding C, Duan T and Zhou Q (2022) Applications of Hydrogels in Premature Ovarian Failure and Intrauterine Adhesion. Front. Mater. 9:942957. doi: 10.3389/fmats.2022.942957

INTRODUCTION

In obstetrics and gynecology, both premature ovarian failure (POF) and intrauterine adhesion (IUA) are difficult diseases that often cause infertility in premenopausal women. POF is defined as a primary ovarian defect characterized by premature follicular depletion or impaired folliculogenesis before the age of 40 years (Beck-Peccoz and Persani, 2006). Known causes of POF mainly include autoimmune diseases, chromosomal abnormalities, radiation and chemotherapy for tumors, infections, and surgical injuries, these causes are difficult to avoid (Goswami and Conway, 2005). POF patients experience early menopause and are susceptible to cardiovascular disease, type 2 diabetes and osteoporosis, and this susceptibility may be related to a decrease in estrogen (Wu et al., 2014). Hormone replacement therapy (HRT) replenishes ovarian hormone deficiencies and improves menopausal syndrome, but may increase the risk of breast cancer and stroke (Sullivan et al.,

2016). A low pregnancy rate (5%–10%) is the biggest problem for POF patients (van Kasteren and Schoemaker, 1999). HRT and gonadotropin-releasing hormone agonists are not effective in restoring fertility (Demeestere et al., 2016; Ishizuka et al., 2021). *In vitro* fertilization (IVF) may allow POF patients to have healthy children, but the success rate is low especially after the age of 35 (Ishizuka et al., 2021).

IUA is defined as adhesion in uterine cavity resulting from endometrial damage, characterized by amenorrhea, infertility, pregnancy loss and abnormal placentation (Dreisler and Kjer, 2019). IUA is mainly due to surgical operations in the uterine cavity, and extensive fibrosis of the uterine cavity leads to failure of decidualization and embryo implantation (Hou et al., 2019). Transcervical resection of adhesion (TCRA) is a standardized treatment that loosens adhesion and improves fertility. TCRA itself is also an intrauterine surgical operation, adhesion in the uterine cavity can be removed by TCRA, but there is also a risk of damage to the endometrium caused by the operation of TCRA, and the risk of re-adhesion after surgery is difficult to minimize (March 2011). The recurrence rate of severe IUA patients even exceeds 60% after TCRA (Capella-Allouc et al., 1999). The clinical pregnancy rate of IUA patients does not exceed 20% after TCRA (20%) (Wang Z. et al., 2021), transdermal estrogen treatment (16.67%) (Chi et al., 2018) and IVF (15.3%) (Mao et al., 2020).

Hydrogels are a cross-linked form of hydrophilic polymers (Tibbitt and Anseth, 2009). The structure and composition of hydrogels are similar to those of the extracellular matrix; thus, hydrogels show great potential for biological and medical applications (Slaughter et al., 2009). Hydrogel-based treatments have emerged in many diseases, including bone injury, skin injury, kidney diseases, heart failure, etc (Mohapatra et al., 2021). Hydrogels have been extensively studied in skin injury. To date, at least 43 clinical trials have reported that hydrogel dressings increased the cure rate of skin injury and relieved pain, and in these trials no adverse effects were found (Zhang et al., 2019). The safety and efficacy in the treatment of skin injury has driven the application of hydrogels in other diseases. The application of hydrogels in other diseases is still at the stage of animal experiment. In animal experiment the therapeutic effects and safety of hydrogels have been exhibited. Both drug-loaded and stem cell-loaded hydrogels promoted the regeneration of bone tissue (Hasani-Sadrabadi et al., 2020; Zuo et al., 2022). IL-10-loaded hydrogels reduced the fibrosis of chronic kidney disease (Rodell et al., 2015), and mitigated the local and systemic inflammation of acute kidney injury (Soranno et al., 2016). After myocardial infarction, necrotic cardiomyocytes are replaced by fibroblasts, resulting in impaired electrical signal conduction. Conductive hydrogels effectively improved electrical signal transmission and protected ventricular function (Bao et al., 2017; Zhang, C et al., 2020).

In obstetrics and gynecology, the main application of hydrogel is in the treatment of POF and IUA. Hydrogels have been studied for ovarian tissue transplantation and artificial ovary, and the three-dimensional structure of hydrogels provides support for follicle growth and morphology maintenance, making ovarian tissue and follicle autologous transplantation possible (Shikanov et al., 2009; Yoon et al., 2021). The application of hydrogels in IUA is mainly focused on drug delivery and stem cell delivery therapy (Mettler et al., 2008; Xue et al., 2019). Hydrogels are capable of controlling drug release and extending stem cell retention (Zhang S. et al., 2017; Huang et al., 2022). In this review, we discuss the physicochemical properties of hydrogels and the latest applications of hydrogels in POF and IUA. Applications of hydrogels in POF and IUA were studied mainly in animal models, and hydrogels have shown therapeutic effects in animal models, but we still have a long way to go for clinical application; hence, we discuss the limiting factors that hinder clinical application and we highlight the future prospects for the applications of hydrogels.

PHYSICOCHEMICAL PROPERTIES

Swelling is a phenomenon whereby the volume of hydrogels rapidly increases after they absorb a solvent. The dried hydrogels were immersed in phosphate buffer solution (PBS) (Qi et al., 2020), medium (Qi et al., 2020), double-distilled water (DDW) (Zheng et al., 2021) or deionized water (Sutthasupa et al., 2021) according to different experimental designs. Then swollen hydrogels were removed from the solvent at a certain time, and weighed after gently blotting water on the surface. The swelling ratio (SR) was calculated by the following equation: $SR=(W_s-W_i)/W_i\times100$ (W_i: the weight of initial dried hydrogel; W_s: the weight of swollen hydrogels) (Qi et al., 2020; Sutthasupa et al., 2021; Zheng et al., 2021). SR is associated with the hydroxyl groups, hydrophilic groups and carboxyl groups (Lv et al., 2021), and the pH and ionic strength of solutions also affect the SR (Ganguly et al., 2017). The swelling property confers a swollen three-dimensional (3D) structure resembling the extracellular matrix in which cells physiologically live; therefore, researchers increasingly regard hydrogels as novel cell culture media (Jackson et al., 2009; Xu et al., 2009; West et al., 2007a). Traditional 2D culture achieve the survival of follicles *in vitro*, but cannot maintain the normal morphology of follicles (Desai et al., 2012; Choi et al., 2013), the 3D structure of the swollen hydrogels maintains the normal morphology of the follicles *in vitro*. Hydrogels are promisingly applied to treat IUA, because hydrogels are not easily expelled due to the strong adhesion to uterine walls (Zhang, W et al., 2020; Yang et al., 2020), and the stable 3D structure due to swelling prevents adjacent uterine walls from directly contacting (Mettler et al., 2008; Wang, Z. et al., 2021).

Rheology, which is defined by Eugene Bingham, is the study of the flow and deformation of materials under applied forces (Dawn and Kumari., 2018; Wilson, 2018). The rheology of hydrogels is measured by a rheometer. The storage modulus (G') and the loss modulus (G'') parameters are always used, the storage modulus (G') reflects viscous behavior and loss modulus (G'') reflects elastic behavior (Müller et al., 2011; Zheng et al., 2021). The viscous behavior facilitates the injection of the hydrogel from the syringe into the uterine cavity and adhesion to the uterine cavity; moreover, the elastic behavior facilitates the retention of the hydrogel in the uterine cavity (Xu HL. et al.,

2017). Hydrogels that exhibit more viscous behavior under large frequency and exhibit more elastic behavior under low frequency are appropriately applied to IUA (Müller et al., 2011). Thermosensitive hydrogels exhibit more viscous behavior at 4°C. After the hydrogels are injected into the uterine cavity, the temperature increases gradually and reaches the gelation temperature, and hydrogels exhibit more elastic behavior (Xu HL. et al., 2017).

Biocompatibility is the ability of biomaterials to perform without adverse host responses in their application (Naahidi et al., 2013). Sterility is a prerequisite for clinical applications, and the assurance of no introduced pathogens is imperative after hydrogels are implanted. Hydrogels are sterilized by high pressure steam, 75% ethanol and UV light according to their physicochemical properties (Müller et al., 2011; Zheng et al., 2021). Some hydrogels, such as antibacterial electroactive self-healing hydrogels, have antibacterial and antioxidant properties in their own composition, but aseptic operation is also necessary in the preparation process (Zhao X. et al., 2017). Cell-loaded hydrogels are applied to treat diseases; however, encapsulated cells may lead to host immune rejection. MHC molecules are the critical bridge for the recognition of allogeneic cells through host lymphocytes; therefore, host immune rejection can be examined by detecting the expression of MHC molecules (Yuan et al., 2011). In addition, the one-way mixed lymphocyte reactions (MLR) assay can also detect host immune rejection (Yuan et al., 2010). The cytotoxicity of hydrogels to encapsulated cells and host cells is not negligible, and the migration and viability of cells reflect whether hydrogels are cytotoxic to cells (Zhao X. et al., 2017; Cui et al., 2019). In addition, the growth of encapsulated cells requires the hydrogels to complete the exchange of oxygen, nutrients and metabolites (Slaughter et al., 2009). Many factors affect the biocompatibility of hydrogels; for natural hydrogels, natural sources may contain heavy metals, endotoxins, and polyphenolic compounds (Lee and Mooney, 2012), and the purification process (Kong et al., 2002), the structure and formulation of the biomaterials affect biocompatibility (Tabata et al., 1999).

Biodegradability provides space for cell growth and new tissue formation (Li et al., 2012). High-quality hydrogels require proper biodegradability, and the degradation products are not harmful to tissues and cells. Nondegradable biomaterials accumulate in the mononuclear phagocytic system and are difficult to excrete; this accumulation is permanent and may be potentially harmful to the body (Owens and Peppas, 2006). Natural hydrogels, such as chitosan, alginate, gelatin and heparin, are mainly derived from natural sources and are readily degraded by cells *in vivo* (Yamaguchi et al., 2007). The following factors affect hydrogel degradability: different crosslinking methods (Jeon et al., 2009), water content (Tabata et al., 1999) and the ratio of each component (Yu et al., 2010).

PREMATURE OVARIAN FAILURE

Premature ovarian failure (POF) is defined as amenorrhea due to ovarian hypofunction before the age of 40 years (Goswami and Conway, 2005). A wide range of causes lead to POF, including chemotherapy, autoimmune diseases, infection and genetic aberrations; however, most causes are not clear and known causes are difficult to avoid (Goswami and Conway, 2005). The most difficult problem of POF is the reduced fertility of premenopausal women; in addition, the dyspareunia due to decreased sexual function and frequent night sweats due to abnormal vasodilation also cause distress in patients (Schover, 2008). Hormone replacement therapy (HRT) is the main treatment strategy for POF, but hormone therapy may lead to an increased probability of breast cancer and stroke (Rossouw et al., 2002); moreover, HRT only relieves the uncomfortable symptoms of POF and cannot fully restore the function of the ovaries (Sullivan et al., 2016). *In vitro* oocyte maturation successfully restores fertility in POF patients, but these are case reports, and more statistical data are needed to confirm the efficiency of this technique (Grynberg et al., 2020; Lucie et al., 2021). The fertility rate after IVF is low, and the success rate is related to age and disease duration (Ishizuka et al., 2021); therefore, novel treatment strategies are urgently needed.

THE APPLICATION OF HYDROGELS IN POF

Hydrogels are introduced in POF treatment in the following four ways (shown in **Figure 1**). The first method is transplantation of ovarian tissues. POF may occur in cancer patients after radiation and chemotherapy, and the autologous transplantation of ovarian tissue that are frozen before radiation and chemotherapy improved the patient's menopausal symptoms (Fabbri et al., 2019); however, the patient's pregnancy rate is low. One report showed only seven pregnancies in 21 patients who received autologous transplantation (Jadoul et al., 2017), and fertility was not fully restored despite orthotopic transplantation of ovarian tissue (von Wolff et al., 2009). Hydrogel-coated ovarian tissue transplantation was superior to autologous transplantation alone in promoting follicular proliferation in animal models; however, there are no reports of fertility restoration due to the difficulty of achieving orthotopic transplantation in animal models. Tavana et al. (2016) encapsulated ovarian tissues in a hyaluronic acid (HA) hydrogel containing VEGF and fibroblast growth factor (bFGF), and the hydrogel promoted follicle proliferation and restoration of ovarian function and inhibited apoptosis after transplantation. Tanaka et al. (2018) wrapped human ovarian tissues in a gelatin hydrogel containing bFGF and transplanted them into immunodeficient mice, found that primordial and primary follicular density significantly increased. Ovarian tissue allotransplantation may be achieved by hydrogel encapsulation because hydrogel-encapsulated ovarian tissue transplantation did not cause follicle apoptosis or immune rejection. Gao et al. (2013) performed allotransplantation with fibrin hydrogels containing bFGF-coated ovarian tissues, and found that the number of apoptotic follicles was significantly reduced. Day et al. (2019) demonstrated that poly (ethylene-glycol) (PEG) hydrogel-coated ovarian tissue prevents allotransplantation immune rejection.

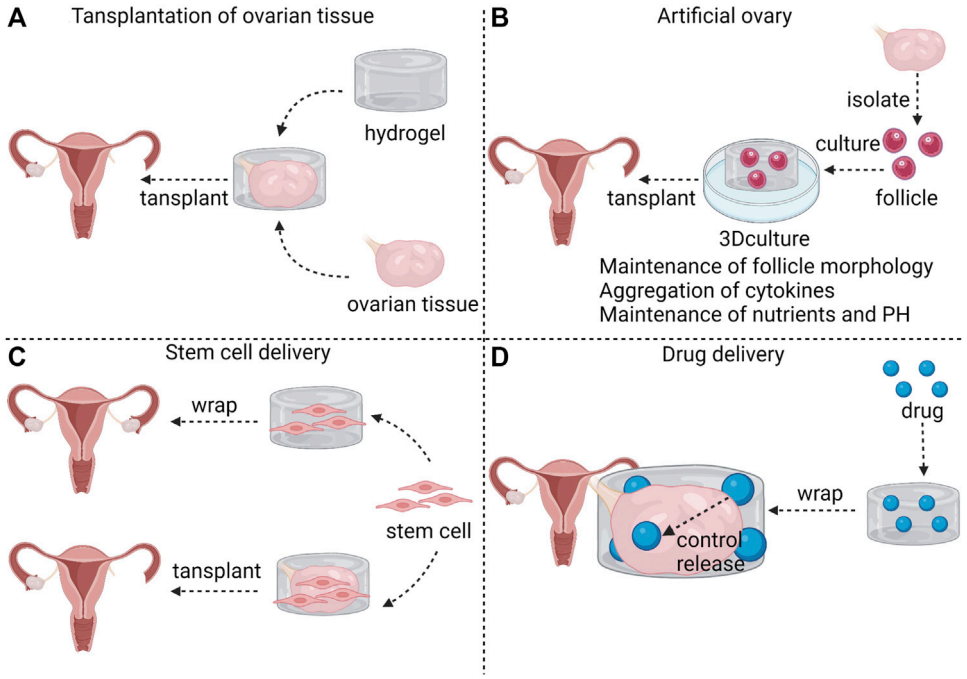

FIGURE 1 | The application of hydrogels in POF. Hydrogel can be used as a carrier for ovarian tissue transplantation **(A)**. Hydrogel 3D culture is characterized by maintenance of follicle morphology, aggregation of cytokines and maintenance of nutrients and PH; thus, hydrogel can be used as a material for artificial ovaries **(B)**. Stem cells can be encapsulated in hydrogel to wrap ovaries in POF patients to exert therapeutic effects; Stem cells can also be encapsulated in hydrogel along with ovarian tissues for ovarian transplantation **(C)**. Hydrogels surrounding ovaries control the rate of drug release **(D)**.

The second method of hydrogel application is artificial ovary. Artificial ovary mainly consists of isolated follicles and biocompatible and biodegradable biomaterials. Transplanting ovarian tissues is a major method through which to restore fertility in cancer patients, but tissue transplantation easily reintroduces tumor cells (Camboni et al., 2013). Follicular basal lamina does not have capillaries and nerves from the granulosa layer; thus, tumors metastasis to the follicles is not possible (Rodgers et al., 2003). Isolated follicles may be transplanted into patients instead of ovarian tissue, and the storage and culture of follicles *in vitro* is the foundation for artificial ovary feasibility (*See The Application of Hydrogels in Follicle Culture* for details). Studies have shown that the transplantation of artificial ovaries promotes the survival and maturation of follicles *in vivo* (Rios et al., 2018), improves local vascularization (Rajabzadeh et al., 2020), and restores hormones to a level at which the endometrium regenerates (Yoon et al., 2021).

The third method is stem cell delivery. Mesenchymal stem cells (MSCs) treatment in POF increased the number of follicles, restored plasma sex hormone levels (Zhang et al., 2021b), reduced ovarian inflammation and reduced granulosa cell apoptosis (Ling et al., 2017; Deng et al., 2021). Stem cells are mainly administered by caudal intraperitoneal injection or ovarian orthotopic injections (Zhang, Q et al., 2017; Woo et al., 2012). These traditional injection methods are associated with problems of low efficiency and growth restriction in target organs (Liu, S et al., 2016). Hydrogels enrich stem cells in the target organ and provide a suitable environment for the growth of stem cells. A study found that co-transplantation of fibrin-collagen hydrogel-coated MSCs and ovarian tissue increased the transplantation success rate (Mehdinia et al., 2020). Huang et al. (2021) embedded human amniotic epithelial cells (hAECs) in sodium alginate-bioglass (SA-BG) hydrogel and wrapped ovarian tissues with the hAECs-loaded hydrogel in POF mice. The SA-BG hydrogel not only enhanced the viability of hAECs in ovary, but also with the help of hAECs restored follicle development and enhanced angiogenesis in POF ovaries. To date, there are insufficient studies on the treatment of hydrogels combined with stem cells for POF; thus, whether this combination enhances efficacy for POF is worth investigating.

The fourth method is drug delivery. Hydrogels enrich drugs in the local tissue. This local delivery maintains the high concentration of drugs in the local tissue and reduces adverse effects (Bhattarai et al., 2010). Drugs are released from hydrogels in a controlled manner, avoiding burst release (Jiang et al., 2014). The long-term sustained release avoids multiple-dose regimens. Drug release is determined by molecular mass, degradation rate and affinity between drugs and hydrogels (Li and Guan., 2011). In addition, environment-stimulated release can also modulate the drug release. Temperature-responsive hydrogels are a good example, drug release is slow when the temperature is below the thermal transition temperature of the hydrogel. Once the temperature rises above the thermal transition temperature, the drug is released rapidly due to hydrogel contraction (Li and Guan, 2011). Electricity-response and magnetism-response hydrogels

control the "on" and "off" of drug release by applying and withdrawing electric and magnetic fields (Murdan 2003; Ganguly and Margel, 2021). Excessive activation of mammalian target of rapamycin (mTOR) induces POF (Reddy et al., 2008). Rapamycine, a mTOR inhibitor, prolongs ovarian lifespan (Dou et al., 2017), but mTOR inhibitors may have adverse effects on the immune system (Araki et al., 2009). Ala-Glu-Ala-Ala-Leu-Tyr- Lys-Asn-Leu-Leu-His-Ser-OH (Inh), a peptide sequence, competitively inhibits the autophosphorylation of receptor tyrosine kinases (RTKs), which are the upstream kinases of mTOR (Thömmes et al., 1999). Hydrogels are able to control the release and ensure the enrichment of Inh, and Shi et al. (2021) reported that the Inh embedded in hydrogels delayed ovarian aging.

THE APPLICATION OF HYDROGELS IN FOLLICLE CULTURE

Hydrogel-based *in vitro* three-dimensional (3D) culture is significantly superior to traditional two-dimensional (2D) culture, promoting the development of follicle science and advancing the emergence of artificial ovary. The advantages of 3D culture are shown in **Figure 1**. Traditional 2D culture fail to fully simulate the ovarian microenvironment for the following reasons: 1) The 3D structure of follicle cannot be easily maintained in 2D culture. Granulosa cells and theca cells attach to the dish surface and lose physiological morphology, and flat follicle disrupt intercellular communication (Desai et al., 2012; Choi et al., 2013); 2) Endogenous autocrine and paracrine factors are diluted, which affects cell development (West et al., 2007a); 3) Consumption of nutrients and accumulation of metabolites lead to pH fluctuations in the medium (Duval et al., 1992). Regular medium changes improve the culture environment, but increase the possibility of contamination and culture cost. The 3D structure of hydrogels simulates the native microenvironment and maintains follicle morphology. The follicular cavity, a closed and filled-fluid cavity, is an indicator of progressive follicular maturation. The normal morphology and expansion of the follicular cavity have been demonstrated in a fibrin-alginate hydrogel (Shikanov et al., 2009). The limited volume of the hydrogels slows down the escape of cellular secretions (West et al., 2007a), and the porous property of the hydrogels ensures the exchange of cellular secretions. The nutrients necessary for cell development can be encapsulated in a responsive polyurea hydrogel based on organic sol–gel chemistry, and the nutrients are constantly released to compensate for cellular consumption, thus maintaining a dynamic balance of nutrients. In addition, this hydrogel is able to simultaneously neutralize lactic acid and maintain pH (Skory et al., 2015).

Natural hydrogels are the most commonly used hydrogels for follicle culture. Alginate, mainly obtained from brown algae cell walls, is a linear water-soluble high swelling natural source. With the goal of facilitating better water solubility in cell culture and disease treatment, alginates are commonly converted into the form of monovalent salts, such as sodium alginates or calcium alginates (Kang et al., 2021). The concentration and stiffness of alginates influence follicle growth and development. *Min Xu. et al* isolated mouse follicles and demonstrated that 0.25% (w/v) and 0.5% (w/v) alginates promoted secondary follicle growth and follicular cavity expansion more rapidly than 1.0% (w/v) and 1.5% (w/v) alginates, and 0.25% (w/v) alginate was the optimal concentration given the high production of estradiol and mature oocytes (Xu et al., 2006). Alginates (0.3% w/v) are suitably applied in human follicle culture. More than half of the preantral follicles were viable and most of them were in a fast growing state in a 0.3% (w/v) alginate hydrogel (Yin et al., 2016); moreover, for primary and secondary follicles, steroid and peptide hormone secretion patterns similar to those observed *in vivo* were induced after the sequential addition of follicle-stimulating hormone (FSH), human chorionic gonadotrophin (hCG) and epidermal growth factor (EGF) (Skory et al., 2015). Erin R West. et al reduced the stiffness of alginate via radiation and chemical oxidation, and found that cell differentiation, steroid production and oocyte quality were superior when follicles were grown on low-stiffness alginates (West et al., 2007b). In addition to follicle culture, alginates are also applied in follicle cryopreservation. Vanacker et al. (2013) showed that human preantral follicles embedded in alginate hydrogel were successfully cryopreserved and that the viability of frozen follicles was comparable to that of fresh follicles in *in vitro* culture; moreover, ME_2SO was found to be superior to ethylene glycol for cryopreservation of follicles embedded in alginate hydrogel (Camboni et al., 2013). Jamalzaei et al. (2020) compared the effects of three hydrogels (hyaluronic acid-alginate hydrogel, alginate and fibrin-alginate hydrogel) in preantral follicles cultures and demonstrated that hyaluronic acid-alginates hydrogel has more advantages over the other two in terms of follicle-secreted estradiol levels and the expression of differentiation genes .

Collagen is abundant in ovarian tissues; thus, collagen hydrogels are biocompatible and biodegradable (Berkholtz et al., 2006). Anthony Atala. et al encapsulated follicles in collagen hydrogels from 1% to 7% (w/v) and demonstrated that follicles had the best viability in 5% collagen hydrogels and 17 β-estradiol levels remained increasing during 20-days culture; therefore, 5% may be the optimal concentration for follicle growth (Joo et al., 2016). Gelatin is derived from collagen, Laronda et al. (2017) found that the shape of pores in gelatin hydrogels affected the survival of the follicle. 3D printing can control the advancing angle to change the shape of the pores, and advancing angles of 30° and 60° were more favorable for follicle survival than 90°.

INTRAUTERINE ADHESION

Traumatic intrauterine adhesions were reported in 1894 (Fritsch, 1894). *Asherman* linked amenorrhea to IUA in 1948 by observing 29 patients, and in 1950 *Asherman* found that miscarriages and menstrual disorders also were caused by IUA (Asherman, 1950). Later, IUA with symptoms (e.g., amenorrhea, chronic pain, menstrual disorders) is called Asherman's syndrome. Although

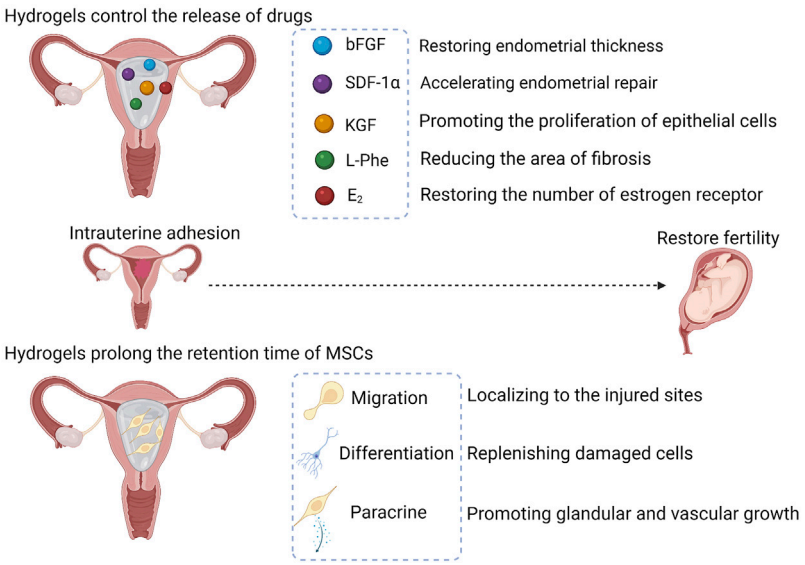

FIGURE 2 | The applications of hydrogels in IUA. The swollen hydrogels form a physical barrier to prevent adhesions. Hydrogels control the release of drugs in the uterine cavity, and drugs exert different therapeutic effects. Hydrogels prolong the retention time of MSCs in the uterus, giving MSCs the opportunity to exert its therapeutic effects. The therapeutic effects are dependent on migration, differentiation, and paracrine function of MSCs. MSCs, mesenchymal stem cells; bFGF, basic fibroblast growth factor; SDF-1α, stromal cell-derived factor-1α; KGF, Keratinocyte growth factor; L-Phe, L-Phenylalanine; E_2, β-estradiol.

some researchers agreed that Asherman's syndrome should be distinguished from asymptomatic IUA (Dreisler and Kjer, 2019), the Asherman's syndrome and IUA are interchangeable in the clinic. In addition to mechanical injuries (e.g., curettage, hysteroscopy), infection, genetic susceptibility and uterine malformation may also cause IUA (Yu et al., 2008). Histologically, fibrosis, which is not conducive to embryo implantation, occurs after the endometrium is damaged. Numerous fibroblasts replace endometrial mesenchymal cells, resulting in a decreased decidualization in response to hormonal stimulation (Hou et al., 2019). The demarcation between the functional and basal layers becomes unclear, and fibrotic endometrium is usually avascular and exhibits a reduced gland number (Foix et al., 1966).

Transcervical resection of adhesions (TCRA) is a primary choice for IUA (March 2011), but TCRA itself may cause damage to the uterine cavity and lead to re-adhesion; thus, adjuvant treatments are often used in conjunction with TCRA to prevent postoperative re-adhesion in clinical treatment. Oral administration of 9 mg/diet estrogen before TCRA and 10 mg/diet after TCRA improved pregnancy rates and menstrual cycles in patients with moderate or severe IUA (Liu AZ et al., 2016); however, estrogen therapy may increase the risk of cancer (Rossouw et al., 2002) and venous thrombosis (Bracamonte and Miller, 2001). Balloon dilatation after TCRA and early second-look hysteroscopy improved pregnancy outcomes (Sun et al., 2020), and the appropriate delay of balloon placement in the uterine cavity prevented re-adhesion but was not effective in severe IUA (Zhang et al., 2021a). The dilated balloon is a nonvariable sphere that is not able to be plasticized according to the shape of the uterine cavity, resulting in ineffective improvement of adhesions in the uterine horns (Sun et al., 2020). IVF after TCRA improved reproductive outcomes, but increased the miscarriage rate (Wang, Y et al., 2021).

THE APPLICATION OF HYDROGELS COMBINED WITH DRUGS IN IUA

Drug and cell delivery are two main hydrogel applications in IUA (shown in **Figure 2**). Hydrogels maintain the shape of the uterus after being introduced into the uterine cavity, and hydrogels cling more completely to the uterine wall compared with balloons, supporting every part of the uterus and effectively preventing re-adhesion. Natural hydrogels, such as collagen and chitosan, have the ability to carry drugs. Leukemia inhibitory factor (LIF) is increased at the site of injury and may be associated with tissue regeneration. LIF/collagen hydrogel restored uterine structure and function of uterine in rat models with full-thickness injury (Xue et al., 2019). Basic fibroblast growth factor (bFGF) plays an important role in wound repair and angiogenesis. The bFGF/collagen hydrogel partially restored endometrial thickness and fertility in IUA infertile patients in a clinical trial (Jiang et al., 2019). Chitosan is a nature polysaccharide, The chitosan-heparin hydrogel carries stromal cell-derived factor-1α (SDF-1α) and releases it at the site of injury, accelerating the repair of the damaged endothelium (Qi et al., 2020). The exact biocompatibility and biodegradability are advantages for natural hydrogels, but achieving controlled drug release is difficult. Synthetic hydrogels are capable of controlling drug release by changing the type and ratio of materials. Keratinocyte growth factor (KGF) is a factor associated with epithelial repair. The binding of KGF to thermosensitive heparin-poloxamer (HP) hydrogels prolonged the retention of KGF in the

uterus, and the KGF-HP hydrogel promoted the proliferation of epithelial cells (Xu HL et al., 2017). ε-polylysine (EPL) was added as a functional excipient to the HP hydrogel, and the release rate of KGF and the rheology of the hydrogel were easily changed by adjusting the concentration of EPL; moreover, angiogenesis was also significantly increased compared with the KGF-HP hydrogel group (Xu H et al., 2017). HP released β-estradiol (E_2) at a constant rate *in vivo*, resulting in a significantly longer retention time of E_2 in the uterine cavity compared to the E2 solution injection (Zhang S et al., 2017). The E_2-HP hydrogel effectively improved the fertility rate, and the effect may be due to the expression of kisspeptin through the MAPK p38 and ERK1/2 signaling pathways (Zhang S et al., 2020). Wang B et al. (2021) synthesized injectable poly (ethylene glycol)-b-poly (L-phenylalanine) (PEBP)/poly (ethylene glycol) (PEG) hydrogel according to the π−π accumulation effect, and the ratio of methoxy-poly (ethylene glycol)-amine (MeO-PEG-NH2) and L-phenylalanine N-carboxy anhydride (L-Phe-NCA) in PEBP affected the release of L-Phe. At a ratio of two to eight (feed mass ratio of MeO-PEG-NH2 via L-Phe NCA), most L-Phe was released; however, considering the extended retention time of the PEBP/PEG hydrogel in the uterus, a ratio of three to seven is considered more appropriate. The L-Phe released by the PEBP/PEG hydrogel effectively reduced the area of fibrosis in the damaged endothelium in a rat model . The release of E_2 in the injectable aloe/poloxamer (AP) hydrogel is independent of pH; thus, the E_2-AP hydrogel is suitable for administration in the presence of cervical mucus. The E_2-AP hydrogel restored the number of estrogen receptors and promoted endometrial regeneration (Yao et al., 2020).

THE APPLICATION OF HYDROGELS COMBINED WITH MSCS IN IUA

Hydrogels are a good three-dimensional medium to meet the growth needs of cells, allowing cells to be maintained at the site of injury for a long time. Proliferation and connectivity were not inhibited when cells were encapsulated in hydrogels (Sara et al., 2021; Kim Y et al., 2019), and hydrogels prolonged cell retention in the uterus compared with cell injection alone (Xiao et al., 2019). Therefore, the combination of hydrogels and MSCs is receiving increasing attention, and many animal and clinical trials have shown that the combination of both effectively treats IUA and restoresfertility.

Mesenchymal stem cells (MSCs) are capable of promoting the proliferation of glands and blood vessels, reducing the area of fibrosis and restoring fertility (Nagori et al., 2011; Santamaria et al., 2016; Wang et al., 2016; Zheng et al., 2020). This successful treatment stems from the low antigenicity, pleiotropic differentiation, strong migration, and paracrine signaling of MSCs. Low antigenicity is the key for clinical application, making allogeneic transplantation possible. MSCs express low levels of major histocompatibility complex class I (MHC I) molecules and hardly express major histocompatibility complex class II (MHC II) and costimulatory molecules (Kim K et al., 2019; Tsuchiya et al., 2019). A meta-analysis showed that allogeneic MSCs did not cause significant adverse effects (Lalu et al., 2012). Multidirectional differentiation is a characteristic of stem cells, and MSCs can be induced to differentiate into osteoblasts, chondrocytes, adipocytes and neurons *in vitro* (Ding et al., 2014; Yang et al., 2021). MSCs differentiate into epithelial and endothelial cells in the injured uterus, providing a cellular source for vascular and endometrial renewal (Shao et al., 2019; Zheng et al., 2020). MSCs are capable of accumulating in the injured uterus by tail vein injection or intraperitoneal injection in rats (Wang et al., 2016; Liu et al., 2018; Zheng et al., 2020), and migration allows MSCs to localize to the injured uterus for multidirectional differentiation and paracrine signaling.

Researchers believe that the repair function of MSCs is mainly derived from paracrine signaling (Bao and He, 2021; Zhou et al., 2022). MSCs secrete a variety of cytokines (e.g., VEGF-A, TGF-β1, FGF-2) to promote glandular and vascular growth and degradation of fibrous scars (Ding et al., 2014; Xin et al., 2019; Xu, L et al., 2017). Collagen increases the number of endometrial glands and endometrial thickness, reduces the area of fibrosis and improves pregnancy rates in a rat model (Ding et al., 2014; Liu et al., 2020). Compared with collagen alone, combining hUCMSCs more significantly increased the number of glands and reduced the area of fibrosis (Liu et al., 2020), and combining BMSCs was more effective in improving pregnancy rates, as well as in myometrium recovery and revascularization (Ding et al., 2014). These significant improvements may be due to the secretion of factors that promote vascular and glandular neogenesis by MSCs. Poly (glycerol sebacate) (PGS) restored soft tissue deformation without causing mechanical damage and porous PGS favored the attachment and growth of cells (Mi et al., 2017). Xiao et al. (2019) found that although no difference in pregnancy rates was observed between the PGS/BMSCs group and the collagen/BMSCs groups, higher concentrations of growth factors (e.g., bFGF, IGF-1, TGF-β1, VEGF) were detected in the endometrium treated with PGS/BMSCs than with collagen/BMSCs.

The beneficial effects of autologous stem cell therapy and hydrogel-encapsulated autologous cell therapy in clinical patients have been reported (shown in **Table 1**). Autologous cell therapy is effective in avoiding autoimmune system attacks, but the extraction of autologous cells is always invasive and difficult to extract in large quantities. hUCMSCs are derived from discarded umbilical cords and can be easily and abundantly extracted; Therefore, hUCMSCs are a potential alternative in allogeneic cell therapy. In clinical trials, synthetic hydrogels are rarely used in IUA treatment. researchers mostly chose natural hydrogels to encapsulate the cells, probably because the safety of synthetic hydrogels in clinical IUA treatment is still difficult to guarantee and ethical approval is difficult to pass. Future experiments on the application synthetic hydrogels in IUA should pay more attention to safety assessments.

LIMITATIONS AND FUTURE PROSPECTS

Artificial Ovary

The development of artificial ovary can be divided into three stages, cellular experiment stage, animal experiment stage, the

TABLE 1 | Clinical trials of stem cell therapy for IUA.

Type of cells	Hydrogel	Number of patients	Main results	References
Autologous BMSCs	No	1	Patient had an increase in endometrial thickness and restore fertility	Nagori et al. (2011)
Autologous MNCs	No	6	6 patients had a significant increase in endometrial thickness and 5 patients resumed normal menstrual cycles	Singh et al. (2014)
$CD133^+$ BMSCs	No	11	7 patients were successful to be pregnant and 1 healthy baby was born	Santamaria et al. (2016)
Autologous BMNCs	Collagen	10	5 patients achieved successful pregnancies and live births	Zhao et al., 2017
Allogeneic hUCMSCs	No	26	8 patients delivered healthy babies without placenta complications	Cao et al. (2018)

IUA, intrauterine adhesion; BMSCs, bone marrow stem cells; MNCs, mononuclear stem cells; hUCMSCs, human umbilical cord mesenchymal stem cells.

TABLE 2 | Animal experiments on artificial ovary.

Material	Follicle source	Grafting Location	Grafting time	Main results	References
Collagen	Mouse preantral follicles	Kidney capsule	12 days	Antral follicles; No ovulation; Blood vessels; Embryo (IVF)	Telfer et al. (1990)
Fibrin	Mouse primordial follicle	Ovarian bursa	3 weeks	Antral follicles; FSH level was restored	Smith et al. (2014)
Alginate	Mouse Preantral follicles	Peritoneal pocket	1 week	Antral follicles; Blood capillaries; Endothelial cells; No inflammation	Vanacker et al. (2014)
Fibrin; Fibrin-alginate; Fibrin-collagen; VEGF-fibrin	Mouse primordial and primary follicles	Ovarian bursa	20 weeks	Antral follicles; Ovulation; Offspring (VEGF-fibrin); The normalized follicle number was highest in fibrin group	Kniazeva et al. (2015)
PL-loaded fibrin	Mouse Preantral follicles	Subcutaneous pocket of neck	2 weeks	Antral follicles; blood vessels; The normalized follicle number was highest in 15% PL-loaded fibrin group	Rajabzadeh et al. (2015)
PEG-VS	Mouse primordial follicles	Ovarian bursa	60 days	Antral follicles; Blood vessels; HPG axis was restored	Kim et al. (2016)
Fibrin	Mouse Preantral follicles and ovarian stromal cells	Peritoneal pocket	1 week	Antral follicles	Chiti et al. (2016)
Fibrin; Fibrin-HA	human preantral follicles (Cryopreserved)	Peritoneal pocket	1 week	Antral follicles	Paulini et al. (2016)
Gelatin (3D print)	Mouse preantral follicles	Ovarian bursa	10 weeks	Antral follicles; Blood vessels; Ovulation; Offspring	Laronda et al. (2017)
Alginate	Mouse Preantral follicles	Ovarian bursa	1 week	Antral follicles; Embryo (IVF)	Rios et al. (2018)
15% PL-loaded Fibrin	Mouse Preantral Follicle (Cryopreserved)	Subcutaneous pocket of neck	2 weeks	Significantly decreased antral follicles in cryopreserved grafts compared to fresh grafts	Rajabzadeh et al. (2020)
PNIPAM-gelatin	Mouse theca and granulosa cells	Ischemia leg	8 weeks	Endometrium regeneration; Endocrine function was restored	Yoon et al. (2021)

IVF, in vitro *fertilization; FSH, follicle-stimulating hormone; VEGF, vascular endothelial growth factor; HA, hyaluronic acid; PL, platelet lysate; PEG-VS, poly(ethylene glycol) vinyl sulfone; HPG, hypothalamus–pituitary–gonad; PNIPAM, poly(N-isopropylacrylamide).*

clinical experiment stage. The current development is in the first two stages, and these two stages is not mature enough to support the development of the clinic stage. Follicle isolation and *in vitro* culture has been established. Hydrogel 3D culture is significantly better than traditional 2D culture (*See The Application of Hydrogels in Follicle Culture* for details), maintenance of follicular morphology has been achieved in hydrogel 3D culture; however, ovulation *in vitro* 3D culture was rarely reported. Preantral follicles can develop into antral follicles in artificial ovary, but ovulation and natural-mating offspring is unsatisfactory (see **Table 2**). Ovulation is the key to pregnancy. Successful ovulation is difficult to achieve without the help of other cells of the ovary (Ren et al., 2016). In the ovarian cortex, stromal cells, vascular endothelial cells and epithelial cells were the top 3 cell types (approximately 83%, 10%, and 5%, respectively) (Wagner et al., 2020). Artificial ovary was created mainly to ensure that cancer patients preserve fertility after radiotherapy. In order to avoid reintroduction of tumor cells, most previous studies only added follicles in the artificial ovary, and removed the stromal cells, vascular endothelial cells, and epithelial cells (see **Table 2**). To make the artificial environment of the follicles closer to the physiological environment and avoid reintroduction of tumor cells, adding allogeneic stromal cells, vascular endothelial cells, and epithelial cells to artificial ovary may be alternative. Hydrogels exhibited the ability to prevent allotransplantation immune rejection in ovarian tissue

transplantation (Day et al., 2019); thus, allogeneic transplantation of artificial ovary is not a pipe dream.

The presence of blood vessels in the graft is essential for the long-term survival of the artificial ovary. Neovascularization in artificial ovary has been reported (Telfer et al., 1990), adding pro-angiogenic factors to hydrogels is beneficial for neovascularization (Kniazeva et al., 2015; Rajabzadeh et al., 2015), but whether a complete blood circulation system can be developed is unclear due to short grafting time. How to prolong the degradation time is the problem to achieve long-term artificial ovary. Fibrin, collagen, gelatin, hyaluronic acid and alginate are common materials used to build artificial ovaries (see **Table 2**). Doxycycline, a matrix metalloproteinase (MMP) inhibitor, effectively prolonged the degradation of fibrin and collagen *in vivo* (Wassenaar et al., 2016). Integrating photocuring 3D bioprint and lyophilization techniques successfully decreased the degradation rate of gelatin and hyaluronic acid (Xia et al., 2018). Integrating alginate into N,O-18 carboxymethyl chitosan-aldehyde hyaluronic acid network significantly prolonged degradation time (Le et al., 2020). Collagen and alginate were added to fibrin hydrogel to slow down degradation, but these additions were detrimental to follicle survival and development (Kniazeva et al., 2015); thus, balancing hydrogel degradation and follicle survival is important in exploring long-term artificial ovaries.

Fresh follicles were used in majority of animal experiments, and cryopreserved follicles do not develop as well as fresh follicles in hydrogel (see **Table 2**). Cryopreserved follicles, however, are more readily available than fresh follicles in clinic; hence, how to build artificial ovary using cryopreserved follicles is worth studying. More research is needed on which hydrogel is best for follicle growth and development. Some additives may help cryopreserved follicle recovery. Cryopreservation has an inhibitory effect on the expression of estrogen receptor β (Depalo et al., 2009); thus, adding estrogen to hydrogels may help estrogen receptor recovery. FSH alleviated depletion of the resting follicle pool in cryopreserved ovary (von Schönfeldt et al., 2012); thus, Follicle stimulating hormone (FSH) is also a promising additive. Addressing the above problems may advance the development of artificial ovaries to the clinical stage.

3D Bioprinting in Hydrogel Synthesis

Although there are numerous studies of hydrogels in regenerative medicine, and most of them suggest good therapeutic effects, there are few hydrogel products on the market available for clinical applications. The biosafety of hydrogels in clinical applications cannot be fully guaranteed (Tonbul et al., 2014). In addition, hydrogels are synthesized in small batches at the pre-clinical stage, and to realize the clinical application of hydrogels, achieving large-batch production of high-quality hydrogels is an inevitable problem (Mandal et al., 2020).

3D bioprinting, which allows for controllable material structure through computer-controlled formation of continuous layers of material, has been used for the synthesis of cell-loaded hydrogels (Elkhoury et al., 2021). 3D bioprinting technology is developing rapidly. Compared with traditional inkjet 3D bioprinting, microextrusion 3D bioprinting is suitable for high viscosity materials and yields higher cell density (Billiet et al., 2014; Pedde et al., 2017). Stereolithography (SLA) 3D bioprinting has a higher resolution and higher speed, and cells are not damaged by external forces during the printing process, ensuring higher cell viability (Wang et al., 2018). 3D bioprinting enables mechanical controllability of the hydrogel synthesis process, a reduction in human errors and a more uniform distribution of cells in hydrogels; thus, 3D printing is a potential method for large-batch production of cell-loaded hydrogels and may advance the clinical application of hydrogels in POF and IUA therapy.

CONCLUSION

Suitable swelling and rheology as well as good biocompatibility and degradability are the key physicochemical properties of hydrogels for the application in POF and IUA treatment. Hydrogels are involved in POF treatment in four ways: transplantation of ovarian tissues, artificial ovary, stem cell delivery and drug delivery. 3D hydrogels mimic the physiological environment of the follicle and are more suitable for *in vitro* culture of follicles than the traditional 2D culture, providing a basis for the development of artificial ovaries. Hydrogels are involved in IUA treatment in two main ways: drug delivery and cell delivery. Hydrogels control the release of drugs and increase the retention time of drugs in the uterine cavity. MSCs themselves are capable of improving tissue repair through differentiation and paracrine secretion, and the therapeutic effect of MSCs combined with hydrogels may be more remarkable. The effect of hydrogels in POF and IUA treatment has been confirmed in many animal experiments, but there are still many stumbling blocks to the clinical application of hydrogels; thus, more safety evaluations and efficacy validations are needed.

AUTHOR CONTRIBUTIONS

DZ: literature search, manuscript writing. CD: manuscript editing and revise. QZ: manuscript revise and project supervision. TD: project supervision and final approval.

FUNDING

The National Natural Science Foundation of China (82071663).

REFERENCES

Araki, K., Turner, A. P., Shaffer, V. O., Gangappa, S., Keller, S. A., Bachmann, M. F., et al. (2009). mTOR Regulates Memory CD8 T-Cell Differentiation. *Nature* 460 (7251), 108–112. doi:10.1038/nature08155

Asherman, J. G. (1950). Traumatic Intra-uterine Adhesions. *BJOG:An Int. J. O&G* 57 (6), 892–896. doi:10.1111/j.1471-0528.1950.tb06053.x

Bao, C., and He, C. (2021). The Role and Therapeutic Potential of MSC-Derived Exosomes in Osteoarthritis. *Archives Biochem. Biophysics* 710, 109002. doi:10.1016/j.abb.2021.109002

Bao, R., Tan, B., Liang, S., Zhang, N., Wang, W., and Liu, W. (2017). A π-π Conjugation-Containing Soft and Conductive Injectable Polymer Hydrogel Highly Efficiently Rebuilds Cardiac Function after Myocardial Infarction. *Biomaterials* 122, 63–71. doi:10.1016/j.biomaterials.2017.01.012

Beck-Peccoz, P., and Persani, L. (2006). Premature Ovarian Failure. *Orphanet J. Rare Dis.* 1, 9. doi:10.1186/1750-1172-1-9

Berkholtz, C. B., Lai, B. E., Woodruff, T. K., and Shea, L. D. (2006). Distribution of Extracellular Matrix Proteins Type I Collagen, Type IV Collagen, Fibronectin, and Laminin in Mouse Folliculogenesis. *Histochem Cell Biol.* 126 (5), 583–592. doi:10.1007/s00418-006-0194-1

Bhattarai, N., Gunn, J., and Zhang, M. (2010). Chitosan-based Hydrogels for Controlled, Localized Drug Delivery. *Adv. Drug Deliv. Rev.* 62 (1), 83–99. doi:10.1016/j.addr.2009.07.019

Billiet, T., Gevaert, E., De Schryver, T., Cornelissen, M., and Dubruel, P. (2014). The 3D Printing of Gelatin Methacrylamide Cell-Laden Tissue-Engineered Constructs with High Cell Viability. *Biomaterials* 35 (1), 49–62. doi:10.1016/j.biomaterials.2013.09.078

Bracamonte, M. P., and Miller, V. M. (2001). Vascular Effects of Estrogens: Arterial Protection versus Venous Thrombotic Risk. *Trends Endocrinol. Metabolism* 12 (5), 204–209. doi:10.1016/s1043-2760(01)00406-4

Camboni, A., Van Langendonckt, A., Donnez, J., Vanacker, J., Dolmans, M. M., and Amorim, C. A. (2013). Alginate Beads as a Tool to Handle, Cryopreserve and Culture Isolated Human Primordial/primary Follicles. *Cryobiology* 67 (1), 64–69. doi:10.1016/j.cryobiol.2013.05.002

Cao, Y., Sun, H., Zhu, H., Zhu, X., Tang, X., Yan, G., et al. (2018). Allogeneic Cell Therapy Using Umbilical Cord MSCs on Collagen Scaffolds for Patients with Recurrent Uterine Adhesion: a Phase I Clinical Trial. *Stem Cell Res. Ther.* 9 (1), 192. doi:10.1186/s13287-018-0904-3

Capella-Allouc, S., Morsad, F., Rongières-Bertrand, C., Taylor, S., and Fernandez, H. (1999). Hysteroscopic Treatment of Severe Asherman's Syndrome and Subsequent Fertility. *Hum. Reprod.* 14 (5), 1230–1233. doi:10.1093/humrep/14.5.1230

Chi, Y., He, P., Lei, L., Lan, Y., Hu, J., Meng, Y., et al. (2018). Transdermal Estrogen Gel and Oral Aspirin Combination Therapy Improves Fertility Prognosis via the Promotion of Endometrial Receptivity in Moderate to Severe Intrauterine Adhesion. *Mol. Med. Rep.* 17 (5), 6337–6344. doi:10.3892/mmr.2018.8685

Chiti, M. C., Dolmans, M. M., Orellana, R., Soares, M., Paulini, F., Donnez, J., et al. (2016). Influence of Follicle Stage on Artificial Ovary Outcome Using Fibrin as a Matrix. *Hum. Reprod.* 31 (2), dev299–435. doi:10.1093/humrep/dev299

Choi, J. K., Agarwal, P., and He, X. (2013). *In Vitro* culture of Early Secondary Preantral Follicles in Hanging Drop of Ovarian Cell-Conditioned Medium to Obtain MII Oocytes from Outbred Deer Mice. *Tissue Eng. Part A* 19 (23-24), 2626–2637. doi:10.1089/ten.TEA.2013.0055

Cui, X., Lee, J. J. L., and Chen, W. N. (2019). Eco-friendly and Biodegradable Cellulose Hydrogels Produced from Low Cost Okara: towards Non-toxic Flexible Electronics. *Sci. Rep.* 9 (1), 18166. doi:10.1038/s41598-019-54638-5

Dawn, A., and Kumari, H. (2018). Low Molecular Weight Supramolecular Gels under Shear: Rheology as the Tool for Elucidating Structure-Function Correlation. *Chem. Eur. J.* 24 (4), 762–776. doi:10.1002/chem.201703374

Day, J. R., David, A., Barbosa, M. G. d. M., Brunette, M. A., Cascalho, M., and Shikanov, A. (2019). Encapsulation of Ovarian Allograft Precludes Immune Rejection and Promotes Restoration of Endocrine Function in Immune-Competent Ovariectomized Mice. *Sci. Rep.* 9 (1), 16614. doi:10.1038/s41598-019-53075-8

Demeestere, I., Brice, P., Peccatori, F. A., Kentos, A., Dupuis, J., Zachee, P., et al. (2016). No Evidence for the Benefit of Gonadotropin-Releasing Hormone Agonist in Preserving Ovarian Function and Fertility in Lymphoma Survivors Treated with Chemotherapy: Final Long-Term Report of a Prospective Randomized Trial. *J. Clin. Oncol.* 34 (22), 2568–2574. doi:10.1200/JCO.2015.65.8864

Deng, T., He, J., Yao, Q., Wu, L., Xue, L., Wu, M., et al. (2021). Human Umbilical Cord Mesenchymal Stem Cells Improve Ovarian Function in Chemotherapy-Induced Premature Ovarian Failure Mice through Inhibiting Apoptosis and Inflammation via a Paracrine Mechanism. *Reprod. Sci.* 28 (6), 1718–1732. doi:10.1007/s43032-021-00499-1

Depalo, R., Lorusso, F., Bettocchi, S., Selvaggi, L., Cavallini, A., Valentini, A. M., et al. (2009). Assessment of Estrogen Receptors and Apoptotic Factors in Cryopreserved Human Ovarian Cortex. *Syst. Biol. Reproductive Med.* 55 (5-6), 236–243. doi:10.3109/19396360903046761

Desai, N., Abdelhafez, F., Calabro, A., and Falcone, T. (2012). Three Dimensional Culture of Fresh and Vitrified Mouse Pre-antral Follicles in a Hyaluronan-Based Hydrogel: a Preliminary Investigation of a Novel Biomaterial for *In Vitro* Follicle Maturation. *Reprod. Biol. Endocrinol.* 10 (1), 29. doi:10.1186/1477-7827-10-29

Ding, L., Li, X. a., Sun, H., Su, J., Lin, N., Péault, B., et al. (2014). Transplantation of Bone Marrow Mesenchymal Stem Cells on Collagen Scaffolds for the Functional Regeneration of Injured Rat Uterus. *Biomaterials* 35 (18), 4888–4900. doi:10.1016/j.biomaterials.2014.02.046

Dou, X., Sun, Y., Li, J., Zhang, J., Hao, D., Liu, W., et al. (2017). Short-term Rapamycin Treatment Increases Ovarian Lifespan in Young and Middle-Aged Female Mice. *Aging Cell* 16 (4), 825–836. doi:10.1111/acel.12617

Dreisler, E., and Kjer, J. J. (2019). Asherman's Syndrome: Current Perspectives on Diagnosis and Management. *Int. J. Womens Health* 11, 191–198. doi:10.2147/IJWH.S165474

Duval, D., Demangel, C., Miossec, S., and Geahel, I. (1992). Role of Metabolic Waste Products in the Control of Cell Proliferation and Antibody Production by Mouse Hybridoma Cells. *Hybridoma* 11 (3), 311–322. doi:10.1089/hyb.1992.11.311

Elkhoury, K., Morsink, M., Sanchez-Gonzalez, L., Kahn, C., Tamayol, A., and Arab-Tehrany, E. (2021). Biofabrication of Natural Hydrogels for Cardiac, Neural, and Bone Tissue Engineering Applications. *Bioact. Mater.* 6 (11), 3904–3923. doi:10.1016/j.bioactmat.2021.03.040

Fabbri, R., Seracchioli, R., Vicenti, R., Paradisi, R., Rossi, S., De Meis, L., et al. (2019). Successful Achievement after Heterotopic Transplantations of Long-Term Stored Ovarian Tissue in Hodgkin's Lymphoma Survivor. *Gynecol. Endocrinol.* 35 (6), 470–472. doi:10.1080/09513590.2018.1549218

Foix, A., Bruno, R. O., Davison, T., and Lema, B. (1966). The Pathology of Postcurettage Intrauterine Adhesions. *Am. J. Obstetrics Gynecol.* 96 (7), 1027–1033. doi:10.1016/0002-9378(66)90452-2

Fritsch, H. (1894). Ein Fall von volligem Schwund der Gebarmutterhohle nach Auskratzung. *Zentralbl Gynaekol* 18, 1337–1342.

Ganguly, S., Maity, T., Mondal, S., Das, P., and Das, N. C. (2017). Starch Functionalized Biodegradable Semi-IPN as a pH-Tunable Controlled Release Platform for Memantine. *Int. J. Biol. Macromol.* 95, 185–198. doi:10.1016/j.ijbiomac.2016.11.055

Ganguly, S., and Margel, S. (2021). Design of Magnetic Hydrogels for Hyperthermia and Drug Delivery. *Polymers* 13 (23), 4259. doi:10.3390/polym13234259

Gao, J.-M., Yan, J., Li, R., Li, M., Yan, L.-Y., Wang, T.-R., et al. (2013). Improvement in the Quality of Heterotopic Allotransplanted Mouse Ovarian Tissues with Basic Fibroblast Growth Factor and Fibrin Hydrogel. *Hum. Reprod.* 28 (10), 2784–2793. doi:10.1093/humrep/det296

Goswami, D., and Conway, G. S. (2005). Premature Ovarian Failure. *Hum. Reprod. Update* 11 (4), 391–410. doi:10.1093/humupd/dmi012

Grynberg, M., Jacquesson, L., and Sifer, C. (2020). *In Vitro* maturation of Oocytes for Preserving Fertility in Autoimmune Premature Ovarian Insufficiency. *Fertil. Steril.* 114 (4), 848–853. doi:10.1016/j.fertnstert.2020.04.049

Hasani-Sadrabadi, M. M., Sarrion, P., Pouraghaei, S., Chau, Y., Ansari, S., Li, S., et al. (2020). An Engineered Cell-Laden Adhesive Hydrogel Promotes Craniofacial Bone Tissue Regeneration in Rats. *Sci. Transl. Med.* 12 (534), eaay6853. doi:10.1126/scitranslmed.aay6853

Hou, X., Liu, Y., Streuli, I., Dällenbach, P., Dubuisson, J., Ansaldi, Y., et al. (2019). Endometrial Regeneration in Asherman's Syndrome: Clinical and Translational Evidence of Stem Cell Therapies. *Curr. Stem Cell Res. Ther.* 14 (6), 454–459. doi:10.2174/1574888X14666190213100528

Huang, J., Zhang, W., Yu, J., Gou, Y., Liu, N., Wang, T., et al. (2022). Human Amniotic Mesenchymal Stem Cells Combined with PPCNg Facilitate Injured Endometrial Regeneration. *Stem Cell Res. Ther.* 13 (1), 17. doi:10.1186/s13287-021-02682-2

Huang, Y., Ma, Z., Kuang, X., Zhang, Q., Li, H., and Lai, D. (2021). Sodium Alginate-Bioglass-Encapsulated hAECs Restore Ovarian Function in Premature Ovarian Failure by Stimulating Angiogenic Factor Secretion. *Stem Cell Res. Ther.* 12 (1), 223. doi:10.1186/s13287-021-02280-2

Ishizuka, B., Furuya, M., Kimura, M., Kamioka, E., and Kawamura, K. (2021). Live Birth Rate in Patients with Premature Ovarian Insufficiency during Long-Term Follow-Up under Hormone Replacement with or without Ovarian Stimulation. *Front. Endocrinol.* 12, 795724. doi:10.3389/fendo.2021.795724

Jackson, K. S., Inoue, K., Davis, D. A., Hilliard, T. S., and Burdette, J. E. (2009). Three-dimensional Ovarian Organ Culture as a Tool to Study Normal Ovarian Surface Epithelial Wound Repair. *Endocrinology* 150 (8), 3921–3926. doi:10.1210/en.2008-1674

Jadoul, P., Guilmain, A., Squifflet, J., Luyckx, M., Votino, R., Wyns, C., et al. (2017). Efficacy of Ovarian Tissue Cryopreservation for Fertility Preservation: Lessons Learned from 545 Cases. *Hum. Reprod.* 32 (5), 1046–1054. doi:10.1093/humrep/dex040

Jamalzaei, P., Rezazadeh Valojerdi, M., Montazeri, L., and Baharvand, H. (2020). Applicability of Hyaluronic Acid-Alginate Hydrogel and Ovarian Cells for *In Vitro* Development of Mouse Preantral Follicles. *Cell J.* 22 (Suppl. 1), 49–60. doi:10.22074/cellj.2020.6925

Jeon, O., Bouhadir, K. H., Mansour, J. M., and Alsberg, E. (2009). Photocrosslinked Alginate Hydrogels with Tunable Biodegradation Rates and Mechanical Properties. *Biomaterials* 30 (14), 2724–2734. doi:10.1016/j.biomaterials.2009.01.034

Jiang, G., Sun, J., and Ding, F. (2014). PEG-g-chitosan Thermosensitive Hydrogel for Implant Drug Delivery: Cytotoxicity,in Vivodegradation and Drug Release. *J. Biomaterials Sci. Polym. Ed.* 25 (3), 241–256. doi:10.1080/09205063.2013.851542

Jiang, P., Tang, X., Wang, H., Dai, C., Su, J., Zhu, H., et al. (2019). Collagen-binding Basic Fibroblast Growth Factor Improves Functional Remodeling of Scarred Endometrium in Uterine Infertile Women: a Pilot Study. *Sci. China Life Sci.* 62 (12), 1617–1629. doi:10.1007/s11427-018-9520-2

Joo, S., Oh, S.-H., Sittadjody, S., Opara, E. C., Jackson, J. D., Lee, S. J., et al. (2016). The Effect of Collagen Hydrogel on 3D Culture of Ovarian Follicles. *Biomed. Mat.* 11 (6), 065009. doi:10.1088/1748-6041/11/6/065009

Kang, S.-M., Lee, J.-H., Huh, Y. S., and Takayama, S. (2021). Alginate Microencapsulation for Three-Dimensional *In Vitro* Cell Culture. *ACS Biomater. Sci. Eng.* 7 (7), 2864–2879. doi:10.1021/acsbiomaterials.0c00457

Kim, J., Perez, A. S., Claflin, J., David, A., Zhou, H., and Shikanov, A. (2016). Synthetic Hydrogel Supports the Function and Regeneration of Artificial Ovarian Tissue in Mice. *NPJ Regen. Med.* 1, 16010. doi:10.1038/npjregenmed.2016.10

Kim, K., Bou-Ghannam, S., Thorp, H., Grainger, D. W., and Okano, T. (2019). Human Mesenchymal Stem Cell Sheets in Xeno-free Media for Possible Allogenic Applications. *Sci. Rep.* 9 (1), 1–12. doi:10.1038/s41598-019-50430-7

Kim, Y. Y., Park, K.-H., Kim, Y. J., Kim, M. S., Liu, H. C., Rosenwaks, Z., et al. (2019). Synergistic Regenerative Effects of Functionalized Endometrial Stromal Cells with Hyaluronic Acid Hydrogel in a Murine Model of Uterine Damage. *Acta Biomater.* 89, 139–151. doi:10.1016/j.actbio.2019.03.032

Kniazeva, E., Hardy, A. N., Boukaidi, S. A., Woodruff, T. K., Jeruss, J. S., and Shea, L. D. (2015). Primordial Follicle Transplantation within Designer Biomaterial Grafts Produce Live Births in a Mouse Infertility Model. *Sci. Rep.* 5, 17709. doi:10.1038/srep17709

Kong, H.-J., Lee, K. Y., and Mooney, D. J. (2002). Decoupling the Dependence of Rheological/mechanical Properties of Hydrogels from Solids Concentration. *Polymer* 43 (23), 6239–6246. doi:10.1088/1748-605X/ac4d7b10.1016/s0032-3861(02)00559-1

Lalu, M. M., McIntyre, L., Pugliese, C., Fergusson, D., Winston, B. W., Marshall, J. C., et al. (2012). Safety of Cell Therapy with Mesenchymal Stromal Cells (SafeCell): A Systematic Review and Meta-Analysis of Clinical Trials. *PloS one* 7 (10), e47559. doi:10.1371/journal.pone.0047559

Laronda, M. M., Rutz, A. L., Xiao, S., Whelan, K. A., Duncan, F. E., Roth, E. W., et al. (2017). A Bioprosthetic Ovary Created Using 3D Printed Microporous Scaffolds Restores Ovarian Function in Sterilized Mice. *Nat. Commun.* 8, 15261. doi:10.1038/ncomms15261

Le, A. N. M., Nguyen, T. T., Ly, K. L., Luong, T. D., Ho, M. H., Minh-Phuong Tran, N., et al. (2020). Modulating Biodegradation and Biocompatibility of *In Situ* Crosslinked Hydrogel by the Integration of Alginate into N, O-Carboxylmethyl Chitosan–Aldehyde Hyaluronic Acid Network. *Polym. Degrad. Stab.* 180, 109270. doi:10.1016/j.polymdegradstab.2020.109270

Lee, K. Y., and Mooney, D. J. (2012). Alginate: Properties and Biomedical Applications. *Prog. Polym. Sci.* 37 (1), 106–126. doi:10.1016/j.progpolymsci.2011.06.003

Li, Y., Rodrigues, J., and Tomás, H. (2012). Injectable and Biodegradable Hydrogels: Gelation, Biodegradation and Biomedical Applications. *Chem. Soc. Rev.* 41 (6), 2193–2221. doi:10.1039/c1cs15203c

Li, Z., and Guan, J. (2011). Thermosensitive Hydrogels for Drug Delivery. *Expert Opin. Drug Deliv.* 8 (8), 991–1007. doi:10.1517/17425247.2011.581656

Ling, L., Feng, X., Wei, T., Wang, Y., Wang, Y., Zhang, W., et al. (2017). Effects of Low-Intensity Pulsed Ultrasound (LIPUS)-pretreated Human Amnion-Derived Mesenchymal Stem Cell (hAD-MSC) Transplantation on Primary Ovarian Insufficiency in Rats. *Stem Cell Res. Ther.* 8 (1), 283. doi:10.1186/s13287-017-0739-3

Liu Az, A. Z., Zhao, H. G., Gao, Y., Liu, M., and Guo, B. Z. (2016). Effectiveness of Estrogen Treatment before Transcervical Resection of Adhesions on Moderate and Severe Uterine Adhesion Patients. *Gynecol. Endocrinol.* 32 (9), 737–740. doi:10.3109/09513590.2016.1160375

Liu S, S., Zhou, J., Zhang, X., Liu, Y., Chen, J., Hu, B., et al. (2016). Strategies to Optimize Adult Stem Cell Therapy for Tissue Regeneration. *Int. J. Mol. Sci.* 17 (6), 982. doi:10.3390/ijms17060982

Liu, Y., Cai, J., Luo, X., Wen, H., and Luo, Y. (2020). Collagen Scaffold with Human Umbilical Cord Mesenchymal Stem Cells Remarkably Improves Intrauterine Adhesions in a Rat Model. *Gynecol. Obstet. Invest.* 85 (3), 267–276. doi:10.1159/000505691

Liu, Y., Tal, R., Pluchino, N., Mamillapalli, R., and Taylor, H. S. (2018). Systemic Administration of Bone Marrow-Derived Cells Leads to Better Uterine Engraftment Than Use of Uterine-Derived Cells or Local Injection. *J. Cell Mol. Med.* 22 (1), 67–76. doi:10.1111/jcmm.13294

Lucie, C.-D., Elisabeth, R., Chloé, D., Volcy, S., Claude, H., Clément, J., et al. (2021). Successful Live Birth after *In Vitro* Maturation Treatment in a Patient with Autoimmune Premature Ovarian Failure: a Case Report and Review of the Literature. *Gynecol. Endocrinol.* 37 (12), 1138–1142. doi:10.1080/09513590.2021.1928065

Lv, H., Wu, B., Song, J., Wu, W., Cai, W., and Xu, J. (2021). Hydrogel, a Novel Therapeutic and Delivery Strategy, in the Treatment of Intrauterine Adhesions. *J. Mater Chem. B* 9 (33), 6536–6552. doi:10.1039/d1tb01005k

Mandal, A., Clegg, J. R., Anselmo, A. C., and Mitragotri, S. (2020). Hydrogels in the Clinic. *Bioeng. Transl. Med.* 5 (2), e10158. doi:10.1002/btm2.10158

Mao, X., Tao, Y., Cai, R., Zhang, J., Gao, H., Chen, Q., et al. (2020). Cross-linked Hyaluronan Gel to Improve Pregnancy Rate of Women Patients with Moderate to Severe Intrauterine Adhesion Treated with IVF: a Randomized Controlled Trial. *Arch. Gynecol. Obstet.* 301 (1), 199–205. doi:10.1007/s00404-019-05368-6

March, C. M. (2011). Management of Asherman's Syndrome. *Reprod. Biomed. Online* 23 (1), 63–76. doi:10.1016/j.rbmo.2010.11.018

Mehdinia, Z., Ashrafi, M., Fathi, R., Taheri, P., and Valojerdi, M. R. (2020). Restoration of Estrous Cycles by Co-transplantation of Mouse Ovarian Tissue with MSCs. *Cell Tissue Res.* 381 (3), 509–525. doi:10.1007/s00441-020-03204-x

Mettler, L., Hucke, J., Bojahr, B., Tinneberg, H. R., Leyland, N., and Avelar, R. (2008). A Safety and Efficacy Study of a Resorbable Hydrogel for Reduction of Post-operative Adhesions Following Myomectomy. *Hum. Reprod.* 23 (5), 1093–1100. doi:10.1093/humrep/den080

Mi, H., Jing, X., Napiwocki, B. N., Hagerty, B. S., Chen, G., and Turng, L. (2017). Biocompatible, Degradable Thermoplastic Polyurethane Based on Polycaprolactone-Block-Polytetrahydrofuran-Block-Polycaprolactone Copolymers for Soft Tissue Engineering. *J. Mater Chem. B* 5 (22), 4137–4151. doi:10.1039/C7TB00419B

Mohapatra, S., Mirza, M. A., Hilles, A. R., Zakir, F., Gomes, A. C., Ansari, M. J., et al. (2021). Biomedical Application, Patent Repository, Clinical Trial and Regulatory Updates on Hydrogel: An Extensive Review. *Gels* 7 (4), 207. doi:10.3390/gels7040207

Müller, S. A., Weis, C., Odermatt, E. K., Knaebel, H. P., and Wente, M. N. (2011). A Hydrogel for Adhesion Prevention: Characterization and Efficacy Study in a Rabbit Uterus Model. *Eur. J. Obstet. Gynecol. Reprod. Biol.* 158 (1), 67–71. doi:10.1016/j.ejogrb.2010.11.008

Murdan, S. (2003). Electro-responsive Drug Delivery from Hydrogels. *J. Control Release* 92 (1-2), 1–17. doi:10.1016/s0168-3659(03)00303-1

Naahidi, S., Jafari, M., Edalat, F., Raymond, K., Khademhosseini, A., and Chen, P. (2013). Biocompatibility of Engineered Nanoparticles for Drug Delivery. *J. Control Release* 166 (2), 182–194. doi:10.1016/j.jconrel.2012.12.013

Nagori, C. B., Panchal, S. Y., and Patel, H. (2011). Endometrial Regeneration Using Autologous Adult Stem Cells Followed by Conception by *In Vitro* Fertilization in a Patient of Severe Asherman's Syndrome. *J. Hum. Reprod. Sci.* 4 (1), 43–48. doi:10.4103/0974-1208.82360

Owens, D. E., 3rd., and Peppas, N. A. (2006). Opsonization, Biodistribution, and Pharmacokinetics of Polymeric Nanoparticles. *Int. J. Pharm.* 307 (1), 93–102. doi:10.1016/j.ijpharm.2005.10.010

Paulini, F., Vilela, J. M., Chiti, M. C., Donnez, J., Jadoul, P., Dolmans, M. M., et al. (2016). Survival and Growth of Human Preantral Follicles after Cryopreservation of Ovarian Tissue, Follicle Isolation and Short-Term Xenografting. *Reprod. Biomed. Online* 33 (3), 425–432. doi:10.1016/j.rbmo.2016.05.003

Pedde, R. D., Mirani, B., Navaei, A., Styan, T., Wong, S., Mehrali, M., et al. (2017). Emerging Biofabrication Strategies for Engineering Complex Tissue Constructs. *Adv. Mater* 29 (19), 1606061. doi:10.1002/adma.201606061

Qi, W., Xu, L., Zhao, S., Zheng, J., Tian, Y., Qi, X., et al. (2020). Controlled Releasing of SDF-1α in Chitosan-Heparin Hydrogel for Endometrium Injury Healing in Rat Model. *Int. J. Biol. Macromol.* 143, 163–172. doi:10.1016/j.ijbiomac.2019.11.184

Rajabzadeh, A., Jahanpeyma, F., Talebi, A., Moradi, F., Hamidieh, A. A., and Eimani, H. (2020). Fibrin Scaffold Incorporating Platelet Lysate Enhance Follicle Survival and Angiogenesis in Cryopreserved Preantral Follicle Transplantation. *Galen. Med. J.* 9, e1558. doi:10.31661/gmj.v9i0.1558

Rajabzadeh, A. R., Eimani, H., Mohseni Koochesfahani, H., Shahvardi, A. H., and Fathi, R. (2015). Morphological Study of Isolated Ovarian Preantral Follicles Using Fibrin Gel Plus Platelet Lysate after Subcutaneous Transplantation. *Cell J.* 17 (1), 145–152. doi:10.22074/cellj.2015.521

Reddy, P., Liu, L., Adhikari, D., Jagarlamudi, K., Rajareddy, S., Shen, Y., et al. (2008). Oocyte-specific Deletion of Pten Causes Premature Activation of the Primordial Follicle Pool. *Science* 319 (5863), 611–613. doi:10.1126/science.1152257

Ren, Y. A., Liu, Z., Mullany, L. K., Fan, C. M., and Richards, J. S. (2016). Growth Arrest Specific-1 (GAS1) Is a C/EBP Target Gene that Functions in Ovulation and Corpus Luteum Formation in Mice. *Biol. Reprod.* 94 (2), 44. doi:10.1095/biolreprod.115.133058

Rios, P. D., Kniazeva, E., Lee, H. C., Xiao, S., Oakes, R. S., Saito, E., et al. (2018). Retrievable Hydrogels for Ovarian Follicle Transplantation and Oocyte Collection. *Biotechnol. Bioeng.* 115 (8), 2075–2086. doi:10.1002/bit.26721

Rodell, C. B., Rai, R., Faubel, S., Burdick, J. A., and Soranno, D. E. (2015). Local Immunotherapy via Delivery of Interleukin-10 and Transforming Growth Factor β Antagonist for Treatment of Chronic Kidney Disease. *J. Control Release* 206, 131–139. doi:10.1016/j.jconrel.2015.03.025

Rodgers, R. J., Irving-Rodgers, H. F., and Russell, D. L. (2003). Extracellular Matrix of the Developing Ovarian Follicle. *Reproduction* 126 (4), 415–424. doi:10.1530/rep.0.1260415

Rossouw, J. E., Anderson, G. L., Prentice, R. L., LaCroix, A. Z., Kooperberg, C., Stefanick, M. L., et al. (2002). Writing Group for the Women's Health Initiative Investigators. Risks and Benefits of Estrogen Plus Progestin in Healthy Postmenopausal Women: Principal Results from the Women's Health Initiative Randomized Controlled Trial. *JAMA* 288 (3), 321–333. doi:10.1001/jama.288.3.321

Santamaria, X., Cabanillas, S., Cervelló, I., Arbona, C., Raga, F., Ferro, J., et al. (2016). Autologous Cell Therapy with CD133+ Bone Marrow-Derived Stem Cells for Refractory Asherman's Syndrome and Endometrial Atrophy: a Pilot Cohort Study. *Hum. Reprod.* 31 (5), 1087–1096. doi:10.1093/humrep/dew042

Sara, L.-M., Hannes, C., Lucía, de M.-G, L., Amparo, F., Alfredo, T. N., Ana, D., et al. (2021). A Natural Xenogeneic Endometrial Extracellular Matrix Hydrogel toward Improving Current Human *In Vitro* Models and Future *In Vivo* Applications. *Front. Bioeng. Biotechnol.* 9, 639688. doi:10.3389/fbioe.2021.639688

Schover, L. R. (2008). Premature Ovarian Failure and its Consequences: Vasomotor Symptoms, Sexuality, and Fertility. *J. Clin. Oncol.* 26 (5), 753–758. doi:10.1200/JCO.2007.14.1655

Shao, X., Ai, G., Wang, L., Qin, J., Li, Y., Jiang, H., et al. (2019). Adipose-derived Stem Cells Transplantation Improves Endometrial Injury Repair. *Zygote* 27 (6), 367–374. doi:10.1017/S096719941900042X

Shi, Z., Li, X., Wei, M., Chen, P., Zhang, T., Ling, X., et al. (2021). Receptor Tyrosine Kinases-Instructed Release of its Inhibitor from Hydrogel to Delay Ovarian Aging. *Biomaterials* 269, 120536. doi:10.1016/j.biomaterials.2020.120536

Shikanov, A., Xu, M., Woodruff, T. K., and Shea, L. D. (2009). Interpenetrating Fibrin-Alginate Matrices for *In Vitro* Ovarian Follicle Development. *Biomaterials* 30 (29), 5476–5485. doi:10.1016/j.biomaterials.2009.06.054

Singh, N., Mohanty, S., Seth, T., Shankar, M., Bhaskaran, S., and Dharmendra, S. (2014). Autologous Stem Cell Transplantation in Refractory Asherman's Syndrome: A Novel Cell Based Therapy. *J. Hum. Reprod. Sci.* 7 (2), 93–98. doi:10.4103/0974-1208.138864

Skory, R. M., Xu, Y., Shea, L. D., and Woodruff, T. K. (2015). Engineering the Ovarian Cycle Using *In Vitro* Follicle Culture. *Hum. Reprod.* 30 (6), 1386–1395. doi:10.1093/humrep/dev052

Slaughter, B. V., Khurshid, S. S., Fisher, O. Z., Khademhosseini, A., and Peppas, N. A. (2009). Hydrogels in Regenerative Medicine. *Adv. Mater* 21 (32-33), 3307–3329. doi:10.1002/adma.200802106

Smith, R. M., Shikanov, A., Kniazeva, E., Ramadurai, D., Woodruff, T. K., and Shea, L. D. (2014). Fibrin-mediated Delivery of an Ovarian Follicle Pool in a Mouse Model of Infertility. *Tissue Eng. Part A* 20 (21-22), 3021–3030. doi:10.1089/ten.TEA.2013.0675

Soranno, D. E., Rodell, C. B., Altmann, C., Duplantis, J., Andres-Hernando, A., Burdick, J. A., et al. (2016). Delivery of Interleukin-10 via Injectable Hydrogels Improves Renal Outcomes and Reduces Systemic Inflammation Following Ischemic Acute Kidney Injury in Mice. *Am. J. Physiol. Ren. Physiol.* 311 (2), F362–F372. doi:10.1152/ajprenal.00579.2015

Sullivan, S. D., Sarrel, P. M., and Nelson, L. M. (2016). Hormone Replacement Therapy in Young Women with Primary Ovarian Insufficiency and Early Menopause. *Fertil. Steril.* 106 (7), 1588–1599. doi:10.1016/j.fertnstert.2016.09.046

Sun, J., Shi, C., Liang, Y., Niu, J., Guo, S., and Cheng, Z. (2020). Effects of Early Second-Look Hysteroscopy Combined with Intrauterine Balloon Dilatation on Reproductive Outcomes for Women with Intrauterine Adhesions. *Int. J. Gynaecol. Obstet.* 149 (2), 192–196. doi:10.1002/ijgo.13108

Sutthasupa, S., Padungkit, C., and Suriyong, S. (2021). Colorimetric Ammonia (NH3) Sensor Based on an Alginate-Methylcellulose Blend Hydrogel and the Potential Opportunity for the Development of a Minced Pork Spoilage Indicator. *Food Chem.* 362, 130151. doi:10.1016/j.foodchem.2021.130151

Tabata, Y., Nagano, A., and Ikada, Y. (1999). Biodegradation of Hydrogel Carrier Incorporating Fibroblast Growth Factor. *Tissue Eng.* 5 (2), 127–138. doi:10.1089/ten.1999.5.127

Tanaka, A., Nakamura, H., Tabata, Y., Fujimori, Y., Kumasawa, K., and Kimura, T. (2018). Effect of Sustained Release of Basic Fibroblast Growth Factor Using Biodegradable Gelatin Hydrogels on Frozen-Thawed Human Ovarian Tissue in a Xenograft Model. *J. Obstet. Gynaecol. Res.* 44 (10), 1947–1955. doi:10.1111/jog.13726

Tavana, S., Valojerdi, M. R., Azarnia, M., and Shahverdi, A. (2016). Restoration of Ovarian Tissue Function and Estrous Cycle in Rat after Autotransplantation Using Hyaluronic Acid Hydrogel Scaffold Containing VEGF and bFGF. *Growth factors.* 34 (3-4), 97–106. doi:10.1080/08977194.2016.1194835

Telfer, E., Torrance, C., and Gosden, R. G. (1990). Morphological Study of Cultured Preantral Ovarian Follicles of Mice after Transplantation under the Kidney Capsule. *J. Reprod. Fertil.* 89 (2), 565–571. doi:10.1530/jrf.0.0890565

Thömmes, K., Lennartsson, J., Carlberg, M., and Rönnstrand, L. (1999). Identification of Tyr-703 and Tyr-936 as the Primary Association Sites for Grb2 and Grb7 in the C-Kit/stem Cell Factor Receptor. *Biochem. J.* 341 (Pt 1Pt 1), 211–216.

Tibbitt, M. W., and Anseth, K. S. (2009). Hydrogels as Extracellular Matrix Mimics for 3D Cell Culture. *Biotechnol. Bioeng.* 103 (4), 655–663. doi:10.1002/bit.22361

Tonbul, M., Adas, M., Bekmezci, T., and Kara, A. D. (2014). Intra-articular Polyacrylamide Hydrogel Injections Are Not Innocent. *Case Rep. Orthop.* 2014, 150709. doi:10.1155/2014/150709

Tsuchiya, A., Takeuchi, S., Watanabe, T., Yoshida, T., Nojiri, S., Ogawa, M., et al. (2019). Mesenchymal Stem Cell Therapies for Liver Cirrhosis: MSCs as "conducting Cells" for Improvement of Liver Fibrosis and Regeneration. *Inflamm. Regen.* 39 (1), 1–6. doi:10.1186/s41232-019-0107-z

van Kasteren, Y. M., and Schoemaker, J. (1999). Premature Ovarian Failure: a Systematic Review on Therapeutic Interventions to Restore Ovarian Function and Achieve Pregnancy. *Hum. Reprod. Update* 5 (5), 483–492. doi:10.1093/humupd/5.5.483

Vanacker, J., Dolmans, M.-M., Luyckx, V., Donnez, J., and Amorim, C. A. (2014). First Transplantation of Isolated Murine Follicles in Alginate. *Regen. Med.* 9 (5), 609–619. doi:10.2217/rme.14.33

Vanacker, J., Luyckx, V., Amorim, C., Dolmans, M. M., Van Langendonckt, A., Donnez, J., et al. (2013). Should We Isolate Human Preantral Follicles before or after Cryopreservation of Ovarian Tissue? *Fertil. Steril.* 99 (5), 1363–1368. e2. doi:10.1016/j.fertnstert.2012.12.016

von Schönfeldt, V., Chandolia, R., Ochsenkühn, R., Nieschlag, E., Kiesel, L., and Sonntag, B. (2012). FSH Prevents Depletion of the Resting Follicle Pool by Promoting Follicular Number and Morphology in Fresh and Cryopreserved Primate Ovarian Tissues Following Xenografting. *Reprod. Biol. Endocrinol.* 10, 98. doi:10.1186/1477-7827-10-98

von Wolff, M., Donnez, J., Hovatta, O., Keros, V., Maltaris, T., Montag, M., et al. (2009). Cryopreservation and Autotransplantation of Human Ovarian Tissue Prior to Cytotoxic Therapy-Aa Technique in its Infancy but Already Successful in Fertility Preservation. *Eur. J. Cancer* 45 (9), 1547–1553. doi:10.1016/j.ejca.2009.01.029

Wagner, M., Yoshihara, M., Douagi, I., Damdimopoulos, A., Panula, S., Petropoulos, S., et al. (2020). Single-cell Analysis of Human Ovarian Cortex Identifies Distinct Cell Populations but No Oogonial Stem Cells. *Nat. Commun.* 11 (1), 1147. doi:10.1038/s41467-020-14936-3

Wang B, B., Feng, C., Dang, J., Zhu, Y., Yang, X., Zhang, T., et al. (2021). Preparation of Fibroblast Suppressive Poly(ethylene Glycol)-B-Poly(l-phenylalanine)/Poly(ethylene Glycol) Hydrogel and its Application in Intrauterine Fibrosis Prevention. *ACS Biomater. Sci. Eng.* 7 (1), 311–321. doi:10.1021/acsbiomaterials.0c01390

Wang, J., Ju, B., Pan, C., Gu, Y., Zhang, Y., Sun, L., et al. (2016). Application of Bone Marrow-Derived Mesenchymal Stem Cells in the Treatment of Intrauterine Adhesions in Rats. *Cell Physiol. Biochem.* 39 (4), 1553–1560. doi:10.1159/000447857

Wang Y, Y., Yao, Z., Zhao, H., Yue, C., Yu, Q., Zhang, Y., et al. (2021). Reproductive Outcomes of *In Vitro* Fertilization-Intracytoplasmic Sperm Injection after Transcervical Resection of Adhesions: A Retrospective Cohort Study. *J. Minim. Invasive Gynecol.* 28 (7), 1367–1374. doi:10.1016/j.jmig.2020.10.029

Wang, Z., Yang, M., Mao, L., Wang, X., Wang, S., Cui, G., et al. (2021). Efficacy and Safety of Autologous Platelet-Rich Fibrin for the Treatment of Infertility with Intrauterine Adhesions. *J. Obstet. Gynaecol. Res.* 47 (11), 3883–3894. doi:10.1111/jog.14964

Wang, Z., Kumar, H., Tian, Z., Jin, X., Holzman, J. F., Menard, F., et al. (2018). Visible Light Photoinitiation of Cell-Adhesive Gelatin Methacryloyl Hydrogels for Stereolithography 3D Bioprinting. *ACS Appl. Mater Interfaces* 10 (32), 26859–26869. doi:10.1021/acsami.8b06607

Wassenaar, J. W., Braden, R. L., Osborn, K. G., and Christman, K. L. (2016). Modulating *In Vivo* Degradation Rate of Injectable Extracellular Matrix Hydrogels. *J. Mater Chem. B* 4 (16), 2794–2802. doi:10.1039/C5TB02564H

West, E. R., Shea, L. D., and Woodruff, T. K. (2007a). Engineering the Follicle Microenvironment. *Semin. Reprod. Med.* 25 (4), 287–299. doi:10.1055/s-2007-980222

West, E. R., Xu, M., Woodruff, T. K., and Shea, L. D. (2007b). Physical Properties of Alginate Hydrogels and Their Effects on *In Vitro* Follicle Development. *Biomaterials* 28 (30), 4439–4448. doi:10.1016/j.biomaterials.2007.07.001

Wilson, D. I. (2018). What Is Rheology? *Eye (Lond).* 32 (2), 179–183. doi:10.1038/eye.2017.267

Woo, D. H., Kim, S. K., Lim, H. J., Heo, J., Park, H. S., Kang, G. Y., et al. (2012). Direct and Indirect Contribution of Human Embryonic Stem Cell-Derived Hepatocyte-like Cells to Liver Repair in Mice. *Gastroenterology* 142 (3), 602–611. doi:10.1053/j.gastro.2011.11.030

Wu, X., Cai, H., Kallianpur, A., Li, H., Yang, G., Gao, J., et al. (2014). Impact of Premature Ovarian Failure on Mortality and Morbidity Among Chinese Women. *PloS one* 9 (3), e89597. doi:10.1371/journal.pone.0089597

Xia, H., Zhao, D., Zhu, H., Hua, Y., Xiao, K., Xu, Y., et al. (2018). Lyophilized Scaffolds Fabricated from 3D-Printed Photocurable Natural Hydrogel for Cartilage Regeneration. *ACS Appl. Mater Interfaces* 10 (37), 31704–31715. doi:10.1021/acsami.8b10926

Xiao, B., Yang, W., Lei, D., Huang, J., Yin, Y., Zhu, Y., et al. (2019). PGS Scaffolds Promote the *In Vivo* Survival and Directional Differentiation of Bone Marrow Mesenchymal Stem Cells Restoring the Morphology and Function of Wounded Rat Uterus. *Adv. Healthc. Mater* 8 (5), e1801455. doi:10.1002/adhm.201801455

Xin, L., Lin, X., Pan, Y., Zheng, X., Shi, L., Zhang, Y., et al. (2019). A Collagen Scaffold Loaded with Human Umbilical Cord-Derived Mesenchymal Stem Cells Facilitates Endometrial Regeneration and Restores Fertility. *Acta Biomater.* 92, 160–171. doi:10.1016/j.actbio.2019.05.012

Xu H, H., Xu, J., Shen, B., Zhang, S., Jin, B., Zhu, Q., et al. (2017). Dual Regulations of Thermosensitive Heparin-Poloxamer Hydrogel Using ε-Polylysine: Bioadhesivity and Controlled KGF Release for Enhancing Wound Healing of Endometrial Injury. *ACS Appl. Mater Interfaces* 9 (35), 29580–29594. doi:10.1021/acsami.7b10211

Xu Hl, H. L., Xu, J., Zhang, S. S., Zhu, Q. Y., Jin, B. H., ZhuGe, D. L., et al. (2017). Temperature-sensitive Heparin-Modified Poloxamer Hydrogel with Affinity to KGF Facilitate the Morphologic and Functional Recovery of the Injured Rat Uterus. *Drug Deliv.* 24 (1), 867–881. doi:10.1080/10717544.2017.1333173

Xu L, L., Ding, L., Wang, L., Cao, Y., Zhu, H., Lu, J., et al. (2017). Umbilical Cord-Derived Mesenchymal Stem Cells on Scaffolds Facilitate Collagen Degradation via Upregulation of MMP-9 in Rat Uterine Scars. *Stem Cell Res. Ther.* 8 (1), 84. doi:10.1186/s13287-017-0535-0

Xu, M., Banc, A., Woodruff, T. K., and Shea, L. D. (2009). Secondary Follicle Growth and Oocyte Maturation by Culture in Alginate Hydrogel Following Cryopreservation of the Ovary or Individual Follicles. *Biotechnol. Bioeng.* 103 (2), 378–386. doi:10.1002/bit.22250

Xu, M., West, E., Shea, L. D., and Woodruff, T. K. (2006). Identification of a Stage-specific Permissive *In Vitro* Culture Environment for Follicle Growth and Oocyte Development. *Biol. Reprod.* 75 (6), 916–923. doi:10.1095/biolreprod.106.054833

Xue, B., Liu, D., Song, M., Zhao, G., Cao, Y., Yan, G., et al. (2019). Leukemia Inhibitory Factor Promotes the Regeneration of Rat Uterine Horns with Full-Thickness Injury. *Wound Repair Regen.* 27 (5), 477–487. doi:10.1111/wrr.12729

Yamaguchi, N., Zhang, L., Chae, B. S., Palla, C. S., Furst, E. M., and Kiick, K. L. (2007). Growth Factor Mediated Assembly of Cell Receptor-Responsive Hydrogels. *J. Am. Chem. Soc.* 129 (11), 3040–3041. doi:10.1021/ja0680358

Yang, J., Bai, R., Chen, B., and Suo, Z. (2020). Hydrogel Adhesion: A Supramolecular Synergy of Chemistry, Topology, and Mechanics. *Adv. Funct. Mater* 30 (2), 1901693. doi:10.1002/adfm.201901693

Yang, K., Xie, D., Lin, W., Xiang, P., and Peng, C. (2021). Adipose Mesenchymal Stem Cells and Gingival Mesenchymal Stem Cells Have a Comparable Effect in Endothelium Repair. *Exp. Ther. Med.* 22 (6), 1415. doi:10.3892/etm.2021.10851

Yao, Q., Zheng, Y. W., Lan, Q. H., Wang, L. F., Huang, Z. W., Chen, R., et al. (2020). Aloe/poloxamer Hydrogel as an Injectable β-estradiol Delivery Scaffold with Multi-Therapeutic Effects to Promote Endometrial Regeneration for Intrauterine Adhesion Treatment. *Eur. J. Pharm. Sci.* 148, 105316. doi:10.1016/j.ejps.2020.105316

Yin, H., Kristensen, S. G., Jiang, H., Rasmussen, A., and Andersen, C. Y. (2016). Survival and Growth of Isolated Pre-antral Follicles from Human Ovarian Medulla Tissue during Long-Term 3D Culture. *Hum. Reprod.* 31 (7), 1531–1539. doi:10.1093/humrep/dew049

Yoon, H. J., Lee, Y. J., Baek, S., Chung, Y. S., Kim, D. H., Lee, J. H., et al. (2021). Hormone Autocrination by Vascularized Hydrogel Delivery of Ovary Spheroids to Rescue Ovarian Dysfunctions. *Sci. Adv.* 7 (18), eabe8873. doi:10.1126/sciadv.abe8873

Yu, D., Wong, Y. M., Cheong, Y., Xia, E., and Li, T. C. (2008). Asherman Syndrome-Oone Century Later. *Fertil. Steril.* 89 (4), 759–779. doi:10.1016/j.fertnstert.2008.02.096

Yu, L., Zhang, Z., Zhang, H., and Ding, J. (2010). Biodegradability and Biocompatibility of Thermoreversible Hydrogels Formed from Mixing a Sol and a Precipitate of Block Copolymers in Water. *Biomacromolecules* 11 (8), 2169–2178. doi:10.1021/bm100549q

Yuan, T., Li, K., Guo, L., Fan, H., and Zhang, X. (2011). Modulation of Immunological Properties of Allogeneic Mesenchymal Stem Cells by Collagen Scaffolds in Cartilage Tissue Engineering. *J. Biomed. Mater Res. A* 98 (3), 332–341. doi:10.1002/jbm.a.33121

Yuan, T., Zhang, L., Feng, L., Fan, H., and Zhang, X. (2010). Chondrogenic Differentiation and Immunological Properties of Mesenchymal Stem Cells in Collagen Type I Hydrogel. *Biotechnol. Prog.* 26 (6), 1749–1758. doi:10.1002/btpr.484

Zhang C, C., Hsieh, M. H., Wu, S. Y., Li, S. H., Wu, J., Liu, S. M., et al. (2020). A Self-Doping Conductive Polymer Hydrogel that Can Restore Electrical Impulse Propagation at Myocardial Infarct to Prevent Cardiac Arrhythmia and Preserve Ventricular Function. *Biomaterials* 231, 119672. doi:10.1016/j.biomaterials.2019.119672

Zhang, L., Yin, H., Lei, X., Lau, J., Yuan, M., Wang, X., et al. (2019). A Systematic Review and Meta-Analysis of Clinical Effectiveness and Safety of Hydrogel Dressings in the Management of Skin Wounds. *Front. Bioeng. Biotechnol.* 7, 342. doi:10.3389/fbioe.2019.00342

Zhang Q, Q., Bu, S., Sun, J., Xu, M., Yao, X., He, K., et al. (2017). Paracrine Effects of Human Amniotic Epithelial Cells Protect against Chemotherapy-Induced Ovarian Damage. *Stem Cell Res. Ther.* 8 (1), 270. doi:10.1186/s13287-017-0721-0

Zhang, S., Xia, W., Xu, J., Xu, H., Lu, C., Zhao, Y., et al. (2017). Three-dimensional Structure Micelles of Heparin-Poloxamer Improve the Therapeutic Effect of 17β-Estradiol on Endometrial Regeneration for Intrauterine Adhesions in a Rat Model. *Int. J. Nanomedicine* 12, 5643–5657. doi:10.2147/IJN.S137237

Zhang S, S., Xu, X., Xiang, W., Zhang, H., Lin, H., Shen, L., et al. (2020). Using 17β-Estradiol Heparin-Poloxamer Thermosensitive Hydrogel to Enhance the Endometrial Regeneration and Functional Recovery of Intrauterine Adhesions in a Rat Model. *FASEB J.* 34 (1), 446–457. doi:10.1096/fj.201901603RR

Zhang W, W., Wang, R., Sun, Z., Zhu, X., Zhao, Q., Zhang, T., et al. (2020). Catechol-functionalized Hydrogels: Biomimetic Design, Adhesion Mechanism, and Biomedical Applications. *Chem. Soc. Rev.* 49 (2), 433–464. doi:10.1039/c9cs00285e

Zhang, X., Liu, W., Zhou, Y., Qiu, J., Sun, Y., Li, M., et al. (2021a). Comparison of Therapeutic Efficacy of Three Methods to Prevent Re-adhesion after Hysteroscopic Intrauterine Adhesion Separation: a Parallel, Randomized and Single-Center Trial. *Ann. Palliat. Med.* 10 (6), 6804–6823. doi:10.21037/apm-21-1296

Zhang, X., Zhang, L., Li, Y., Yin, Z., Feng, Y., and Ji, Y. (2021b). Human Umbilical Cord Mesenchymal Stem Cells (hUCMSCs) Promotes the Recovery of Ovarian Function in a Rat Model of Premature Ovarian Failure (POF). *Gynecol. Endocrinol.* 37 (4), 353–357. doi:10.1080/09513590.2021.1878133

Zhao G, G., Cao, Y., Zhu, X., Tang, X., Ding, L., Sun, H., et al. (2017). Transplantation of Collagen Scaffold with Autologous Bone Marrow Mononuclear Cells Promotes Functional Endometrium Reconstruction via Downregulating ΔNp63 Expression in Asherman's Syndrome. *Sci. China Life Sci.* 60 (4), 404–416. doi:10.1007/s11427-016-0328-y

Zhao X, X., Wu, H., Guo, B., Dong, R., Qiu, Y., and Ma, P. X. (2017). Antibacterial Anti-oxidant Electroactive Injectable Hydrogel as Self-Healing Wound Dressing with Hemostasis and Adhesiveness for Cutaneous Wound Healing. *Biomaterials* 122, 34–47. doi:10.1016/j.biomaterials.2017.01.011

Zheng, J., Zhang, J., Kong, D., Song, Y., Zhao, S., Qi, W., et al. (2020). Quantification of the CM-Dil-Labeled Human Umbilical Cord Mesenchymal Stem Cells Migrated to the Dual Injured Uterus in SD Rat. *Stem Cell Res. Ther.* 11 (1), 280. doi:10.1186/s13287-020-01806-4

Zheng, W., Hao, Y., Wang, D., Huang, H., Guo, F., Sun, Z., et al. (2021). Preparation of Triamcinolone Acetonide-Loaded Chitosan/fucoidan Hydrogel and its Potential Application as an Oral Mucosa Patch. *Carbohydr. Polym.* 272, 118493. doi:10.1016/j.carbpol.2021.118493

Zhou, Y., Wen, L. L., Li, Y. F., Wu, K. M., Duan, R. R., Yao, Y. B., et al. (2022). Exosomes Derived from Bone Marrow Mesenchymal Stem Cells Protect the Injured Spinal Cord by Inhibiting Pericyte Pyroptosis. *Neural Regen. Res.* 17 (1), 194–202. doi:10.4103/1673-5374.314323

Zuo, Y., Xiong, Q., Li, Q., Zhao, B., Xue, F., Shen, L., et al. (2022). Osteogenic Growth Peptide (OGP)-loaded Amphiphilic Peptide (NapFFY) Supramolecular Hydrogel Promotes Osteogenesis and Bone Tissue Reconstruction. *Int. J. Biol. Macromol.* 195, 558–564. doi:10.1016/j.ijbiomac.2021.12.028

Conflict of Interest: The authors declare that the research was conducted in the absence of any commercial or financial relationships that could be construed as a potential conflict of interest.

Publisher's Note: All claims expressed in this article are solely those of the authors and do not necessarily represent those of their affiliated organizations, or those of the publisher, the editors and the reviewers. Any product that may be evaluated in this article, or claim that may be made by its manufacturer, is not guaranteed or endorsed by the publisher.

frontiers | Frontiers in Bioengineering and Biotechnology

ORIGINAL RESEARCH
published: 04 July 2022
doi: 10.3389/fbioe.2022.914675

Biocompatibility and Efficacy of a Linearly Cross-Linked Sodium Hyaluronic Acid Hydrogel as a Retinal Patch in Rhegmatogenous Retinal Detachment Repairment

Chuanzhen Zheng[1†], *Hongwei Xi*[2†], *Dejia Wen*[1], *Yifeng Ke*[1], *Xiaomin Zhang*[1], *Xinjun Ren*[1*] *and Xiaorong Li*[1*]

[1]Tianjin Key Laboratory of Retinal Functions and Diseases, Tianjin International Joint Research and Development Centre of Ophthalmology and Vision Science, Eye Institute and School of Optometry, Tianjin Medical University Eye Hospital, Tianjin, China, [2]Qisheng Biological Preparation Co., Ltd., Shanghai, China

OPEN ACCESS

Edited by:
Yongsheng Yu,
Chinese Academy of Sciences (CAS), China

Reviewed by:
Ehab Elrayes,
Research Institute of Ophthalmology, Egypt
Di Huang,
Massachusetts Eye and Ear Infirmary and Harvard Medical School, United States

***Correspondence:**
Xinjun Ren
zlrxjrsy@126.com
Xiaorong Li
xiaorli@163.com

†These authors have contributed equally to this work

Specialty section:
This article was submitted to Biomaterials, a section of the journal Frontiers in Bioengineering and Biotechnology

Received: 07 April 2022
Accepted: 25 May 2022
Published: 04 July 2022

Citation:
Zheng C, Xi H, Wen D, Ke Y, Zhang X, Ren X and Li X (2022) Biocompatibility and Efficacy of a Linearly Cross-Linked Sodium Hyaluronic Acid Hydrogel as a Retinal Patch in Rhegmatogenous Retinal Detachment Repairment. Front. Bioeng. Biotechnol. 10:914675. doi: 10.3389/fbioe.2022.914675

To prevent the migration of retinal pigment epithelium (RPE) cells into the vitreous cavity through retinal breaks after the pars plana vitrectomy for the repair of rhegmatogenous retinal detachment (RRD), sealing retinal breaks with an appropriate material appears to be a logical approach. According to a review of ocular experiments or clinical trials, the procedure for covering retinal breaks with adhesives is complex. A commercially available cross-linked sodium hyaluronic acid (HA) hydrogel (Healaflow®) with the injectable property was demonstrated to be a perfect retinal patch in RRD clinical trials by our team. Based on the properties of Healaflow®, a linearly cross-linked sodium HA hydrogel (HA-engineered hydrogel) (Qisheng Biological Preparation Co. Ltd. Shanghai, China) with the injectable property was designed, whose cross-linker and cross-linking method was improved. The purpose of this study is to report the characteristics of an HA-engineered hydrogel using Healaflow® as a reference, and the biocompatibility and efficacy of the HA-engineered hydrogel as a retinal patch in the rabbit RRD model. The HA-engineered hydrogel exhibited similar dynamic viscosity and cohesiveness and G′ compared with Healaflow®. The G′ of the HA-engineered hydrogel varied from 80 to 160 Pa at 2% strain under 25°C, and remained constantly higher than G″ over the range of frequency from 0.1 to 10 Hz. In the animal experiment, clinical examinations, electroretinograms, and histology suggested no adverse effects of the HA-engineered hydrogel on retinal function and morphology, confirming its favorable biocompatibility. Simultaneously, our results demonstrated the efficacy of the HA-engineered hydrogel as a retinal patch in the RRD model of rabbit eyes, which can aid in the complete reattachment of the retina without the need for expansile gas or silicone oil endotamponade. The HA-engineered hydrogel could play the role of an ophthalmologic sealant due to its high viscosity and cohesiveness. This pilot study of a small series of RRD models with a short-term follow-up provides preliminary evidence to support the favorable biocompatibility and efficacy of the HA-engineered hydrogel as a promising retinal patch for sealing retinal breaks in retinal detachment repair. More cases and longer follow-up studies are needed to assess its safety and long-term effects.

Keywords: linearly cross-linked sodium hyaluronic acid hydrogel, rhegmatogenous retinal detachment, biocompatibility, efficacy, cohesiveness, viscosity

INTRODUCTION

The vitreous gel is a transparent ocular tissue located between the lens and the retina, composed of 98–99% water and a framework of collagen fibers and hyaluronic acid (HA). Aging leads to vitreous liquefaction and detachment of the vitreous from the retinal surface, which may induce retinal breaks. The liquefied vitreous can pass through these breaks and accumulate in the subretinal space between the neurosensory retina and the retinal pigment epithelium (RPE) leading to a rhegmatogenous retinal detachment (RRD) (**Figure 1**) (Feltgen and Walter, 2014; Lumi et al., 2015). Attachment of the retina is mandatory for its proper functioning. The principles for managing RRD include treating all retinal breaks and weakening or eliminating vitreous traction using one or more of the following surgical techniques: pneumatic retinopexy, scleral buckling, and pars plana vitrectomy (PPV) (Kuhn and Aylward, 2014). PPV involves surgical removal of the vitreous, thus releasing vitreoretinal traction, and subsequent filling of the vitreous cavity with long-lasting substitutes (expansile gas or silicon oil) to prevent the connection between the subretinal space and vitreous cavity through the break; moreover, laser photocoagulation is used to build chorioretinal adhesion around the retinal breaks, and the surface tension of vitreous substitutes keeps the neurosensory retina attached to the RPE until the chorioretinal adhesion becoming sufficiently strong to seal the retinal edge around the breaks; last, after the expansile gas has been absorbed in 2 weeks–2 months or the silicon oil has been removed by a second surgery (Wagenfeld et al., 2010; Chen et al., 2015; Kontos et al., 2017; Raczynska et al., 2018; Tetsumoto et al., 2020), the vitreous cavity is filled with aqueous humor produced by the eyeball itself, which has a refractive index approximately identical to natural vitreous (Popovic et al., 2022). With the advancement of the microinvasion system, PPV combined with expansile gas or silicon oil endotamponade is gaining popularity as a first-line procedure for the repair of RRD, but the first retinal reattachment rates range from 74 to 96.3% (Bourla et al., 2010; Oshima et al., 2010; Kobashi et al., 2014; Haugstad et al., 2017; Romano et al., 2017). Proliferative vitreoretinopathy (PVR) is the major cause of surgical failure in retinal detachment, in which RPE cells migrate to the vitreous cavity through retinal breaks (**Figure 1**) and undergo cellular proliferation and epithelial–mesenchymal transition (EMT), resulting in the formation of a proliferative membrane on the retinal surface, whose contraction property causes a tractional retinal detachment (Pastor et al., 2016). Hence, sealing retinal breaks with an appropriate material appears to be a logical approach to prevent migration, proliferation, and EMT of RPE cells, thereby preventing PVR.

Currently, there are two major categories of clinical adhesives: synthetic glues (such as cyanoacrylate, polyethylene glycol (PEG) derivatives, and HA derivatives) and biological glues (such as fibrin). However, as a retinal patch, each has its own set of limitations, such as potential ocular toxicity, difficulty in intraocular delivery, poor adhesive force, inflammatory response, and granulomatous tissue reaction. For these and other reasons, the use of glue in the treatment of retinal detachment has not yet become a standard procedure (Hoshi et al., 2015). Nevertheless, a commercially available cross-linked sodium HA hydrogel (Healaflow®) (Anteis S.A., Plan Les Ouates, Switzerland) has been shown to be an ideal retinal patch. Cellular experiments and animal studies have demonstrated its favorable biocompatibility, strong and durable adhesion (Barth et al., 2014; Barth et al., 2016; Barth et al., 2019). A clinical trial conducted by our team also confirmed its strong and durable adhesion, safety, and efficacy; ease of acquisition, preservation, and delivery to the retina; and simple procedure of covering retinal breaks (Ren et al., 2020). Based on the properties of Healaflow®, a linearly cross-linked sodium HA hydrogel (HA-engineered hydrogel) (Qisheng Biological Preparation Co. Ltd. Shanghai, China) was designed, in which both the cross-linker and cross-linking methods were improved. The HA-engineered hydrogel was developed using the patented technology, which utilizes the fluid characteristics of HA and guides the molecular structural rearrangement of cross-linked HA by providing a certain direction of stress (Wei et al., 2019). Compared with the most commercially available cross-linked HA products, this patented technology does not include fragmentation or the sieving process (Wongprasert et al., 2022), thus protecting the molecular structure's integrity and improving the resistance to gel degradation effectively (Wei et al., 2019). The resulting HA-engineered hydrogel was homogeneous and monophasic, showing oriented-arranged morphology. It

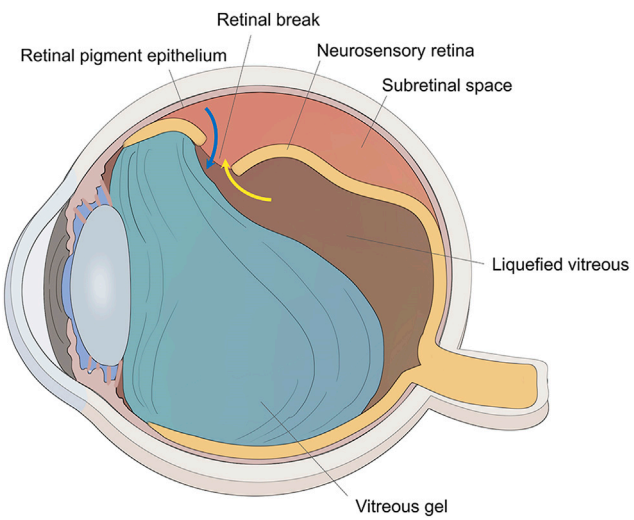

FIGURE 1 | The schematic diagram of RRD. The traction of vitreous gel onto the retina created the retinal break, and liquefied vitreous penetrated the subretinal space through the retinal break to induce retinal detachment (yellow arrow). Retinal pigment epithelial cells could migrate to the vitreous cavity through the retinal break (blue arrow).

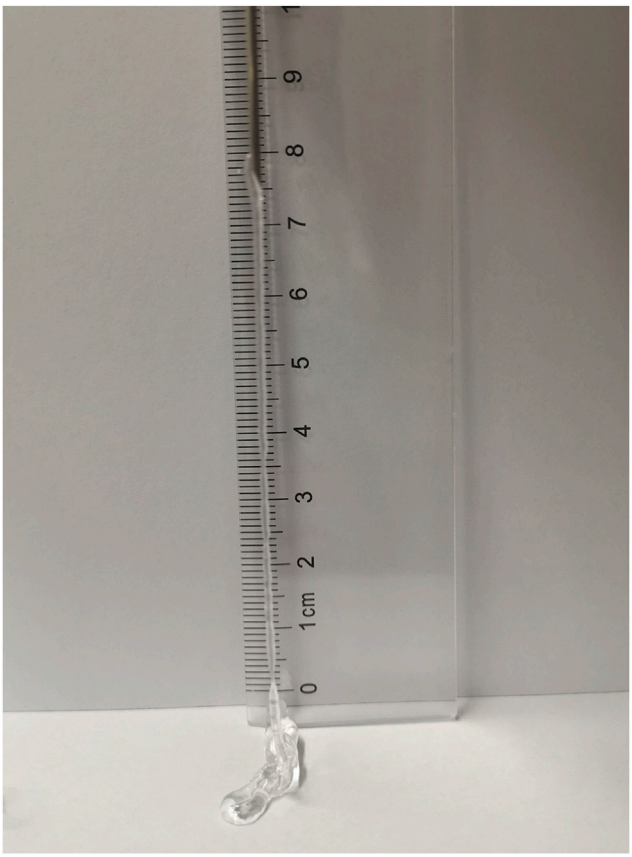

FIGURE 2 | The photograph of the HA-engineered hydrogel extruded from the syringes through an 18-gauge cannula.

possessed good viscoelasticity, injectability, and cohesion, which benefits *in vivo* tissue integration post-implantation (Tran et al., 2014). Different from Healaflow® which uses 1, 4-butanediol diglycidyl ether (BDDE) as the cross-linker, the HA-engineered hydrogel was cross-linked by divinylsulfone (DVS). Both BDDE and DVS are the well-acknowledged industry-standard cross-linkers of the market-leading cross-linked HA products, whose stability and metabolism have been studied in detail, and their long-term safety has been verified by numerous studies and clinical practice over the years (Pérez et al., 2021). The purpose of this study is to report the characteristics of the HA-engineered hydrogel using Healaflow® as a reference, and the biocompatibility and efficacy of the HA-engineered hydrogel as a retinal patch in the rabbit RRD model.

MATERIALS AND METHODS

HA-Engineered Hydrogel

The HA-engineered hydrogel is a commercially available transplant, a smooth and cohesive hydrogel manufactured by Shanghai Qisheng Biological Preparation Co., Ltd. (**Figure 2**). It is composed of balanced salt solution (BSS), phosphate and NaCl salts, and non-animal sodium HA (16 mg/ml) that has been linearly cross-linked with DVS. Whereas the concentration of HA is 22.5 mg/ml and the cross-linker is BDDE in Healaflow®. The improved process of linear cross-linking in the HA-engineered hydrogel makes the sodium HA molecules exhibit linear tropism that could prolong the structural integrity. The properties of the HA-engineered hydrogel are similar to those of Healaflow® (Barth et al., 2014). **Table 1** summarizes their physical and chemical properties.

TABLE 1 | Comparison of physicochemical properties between the HA-engineered hydrogel and Healaflow®.

Properties	HA-engineered hydrogel (Qisheng Biological Preparation Co. Ltd. Shanghai, China)	Healaflow® (Anteis S.A., Plan Les Ouates, Switzerland)
Cross-linker	DVS	BDDE
HA concentration	16 mg/ml	22.5 mg/ml
pH	7.3	7.0
Osmolarity	300 mOsm/kg	305 mOsm/kg
Specific gravity	1.01	1.03
Refractive index	1.341	1.341
Dynamic viscosity	252170 mPa·s	258000 mPa s

Table footer. HA, hyaluronic acid; DVS, divinyl sulfone; BDDE, 1, 4-butanediol diglycidyl ether

Comparison of Characteristics Between HA-Engineered Hydrogel and Healaflow®

Rheology

The rheological properties of HA-engineered hydrogel and Healaflow® were measured using a rheometer (Thermo Scientific HAAKE MARS III) equipped with a P35 TiL measuring geometry with a gap of 1 mm at 25°C. The applied strain was 2% and the frequency sweep was from 0.1 to 10 Hz. The storage modulus (G') and the loss modulus (G'') of the HA-engineered hydrogel were recorded.

Cohesiveness

We tested the cohesiveness of HA-engineered hydrogel and Healaflow® by two previously published methods. 1) The drop-weight method (Edsman et al., 2015). Three samples in each group were loaded into 1-ml glass syringes with an 18-gauge cannula and centrifugated to eliminate air bubbles. Then the samples were extruded using a mechanical testing instrument (GOTECH, China) at a constant speed. While the stress was stable, 10 drops of each sample were collected and weighed, and the average drop weight was calculated. 2) The stained hydrogel dispersion method (Edsman et al., 2015). The 1-ml gels were first stained with 30 μL of 1% toluidine blue solution between two syringes for 3 min. The gel with air removed by centrifugation was then filled into a 1-ml BD glass syringe (Becton, Dickinson and Company, Franklin Lakes, NJ, United States). Three 1000-ml beakers filled with 700 ml water were placed on a magnetic stirrer with a magnetic stirring bar at 170 revolutions per minute. The stained gel in the syringe was placed with the orifice 2 cm above the surface of the water and pushed out of the syringe at a speed of 400 mm/min with Zwick BTC-FR 2.5 TH.D09 (ZwickRoell, Ulm, Germany). Photographs were taken at 15, 75, and 90 s after the gel hit the surface. We also tested the cohesiveness of two other HA-based hydrogels, Matrifill® and Janlane®, which were cross-linked by DVS and BDDE, separately.

Animal Preparation

The left eyes of 24 pigmented rabbits (Dutch, weighing 2.0–3.0 kg) were tested in our study. The biocompatibility of retinal covering with the HA-engineered hydrogel was tested in 8 rabbits, and the efficacy of the HA-engineered hydrogel was tested in the remaining 16 rabbits, which were divided into two groups of 8 each: the RRD-hydrogel group and the RRD group. We certify that all applicable institutional and governmental regulations concerning the ethical use of animals were followed during this research. All procedures were performed in the left eyes of rabbits using sterile techniques. The rabbits were anesthetized with an intravenous injection of 5.0 ml midazolam (1 mg/ml) and an intramuscular injection of 1.0 ml xylazine hydrochloride (10 mg/ml). Topical anesthesia (0.4% oxybuprocaine hydrochloride drops) was also administered to the eyes. The pupils were dilated using tropicamide phenylephrine eye drops.

Biocompatibility of HA-Engineered Hydrogel Onto Retina

Vitrectomy and Application of HA-Engineered Hydrogel

The conjunctiva was prepared using a 5% povidone-iodine solution. Using three ports 1 mm from the corneoscleral limbus, 25-gauge PPV was performed in all study rabbits using a Constellation system (Alcon Laboratories, Inc., Fort Worth, TX, United States) by an experienced vitreoretinal surgeon (X.R.); one port was used for the infusion cannula, while the other two ports were used for the vitreous cutter and endoilluminator optical fiber. Sclerotomy was performed *via* biplanar entry using a trocar and cannula, initially tangential to the sclera and then perpendicular, to create a self-sealing incision. The lens was not removed. Core vitrectomy was performed under a surgical microscope with a fundus wide-angle viewing system (Volk Mini Quad XL; Volk Optical, Inc., Mentor, OH, United States), and posterior vitreous detachment (PVD) was created using triamcinolone acetonide. Fluid–air exchange was performed, and 0.1 ml HA-engineered hydrogel was applied with a 27-gauge needle through a trocar and cannula to cover the retina at 2 disc diameters (DD) below the optic disc. The microcannulas were removed after vitrectomy, and the sclerotized area was gently massaged with a cotton-tipped applicator to prevent leakage. The surgical eyes received eye drops containing antibiotics and dexamethasone for 1 week after surgery.

Clinical Examination

Slit lamp microscopy, indirect ophthalmoscopy, and iCare tonometer were used with the pupils dilated preoperatively, and at 1, 3, and 5 days; 1 and 2 weeks; and 1 month postoperatively. Intraocular pressure (IOP) was assessed using repeated measures analysis of variance.

Electroretinogram

Under general and topical anesthesia and with the pupils dilated, an electroretinogram (ERG) was recorded before and 1 month after the application of the HA-engineered hydrogel. Contact lens electrodes (ChongQing IRC Medical Equipment Co., Ltd., Chongqing, China) were placed on the corneas of both eyes; a needle electrode was attached to the occipital region at the midpoint of the two ears, and a ground electrode was attached to the tail. The ERG was recorded from both eyes simultaneously using an ERG recording system (RetiMINER-C; ChongQing IRC Medical Equipment Co., Ltd.). This apparatus combines a stimulus instrument, an amplifier, and a recorder. The frequency band ranges from 0.3 to 300 Hz. The luminance values of the stimuli were 0.01, 3.0, and 30 cds/m^2. The recording started with the weakest stimulus after 30 min of dark adaptation. No background light was applied. The light stimulus interval was 30 s, and three responses were averaged for each eye. Amplitude and implicit times were recorded for both eyes. The differences between the pre- and post-operation in the left eyes were analyzed.

Histology

The rabbits were killed with an overdose of pentobarbital 1 month after vitrectomy, and their eyes were enucleated for histological analysis. After enucleation, all eyes were fixed in 2% paraformaldehyde and 2.5% glutaraldehyde solution, dehydrated in a series of increasing alcohol concentrations, and embedded in paraffin. Sections cut at a thickness of 4 μm were stained with hematoxylin and eosin (H&E) and examined under a light microscope.

Immunofluorescence

Sections of samples embedded in paraffin were deparaffinized in a xylene ethanol series, placed in Tris-EDTA buffer for antigen retrieval (10 mM Tris, 1 mM EDTA, 0.05% Tween, pH = 9.0), and then blocked in 5% bovine serum albumin. Sections were immunostained for rhodopsin (rod photoreceptors) (Ab 5417; Abcam, United Kingdom; diluted 1:100). Detection of the primary antibodies was performed using fluorescein isothiocyanate (FITC)–conjugated goat anti-mouse IgG secondary antibody (F-2761; Thermo Fisher Scientific, United States; diluted 1:400). Nuclei were detected using 4′,6′-diamino-2-phenyl inodole (DAPI), which was included in the mounting solution (Solarbio; Beijing, China).

Efficacy of HA-Engineered Hydrogel as a Retinal Patch in RRD Repairment

RRD Model

Complete vitrectomy and PVD were performed as previously described, and a retinal break, approximately 1/2 DD in size, was created 2 DD inferior to the optic disc using the vitreous cutter. BSS was gently infused into the subretinal space through the retinal break to create a localized retinal detachment, which was approximately 2 DD in size. Fluid–air exchange was performed to reattach the retina. In the RRD-hydrogel group, the HA-engineered hydrogel was applied with a 25-gauge syringe through a trocar and cannula to completely cover the retinal break (**Figure 3**). The RRD group underwent the same procedures as the RRD-hydrogel group, except for the HA-engineered hydrogel application. The microcannulas were removed after vitrectomy, and the sclerotized area was gently massaged with a cotton-tipped applicator to prevent leakage. The surgical eyes received eye drops containing antibiotics and dexamethasone for 1 week after surgery.

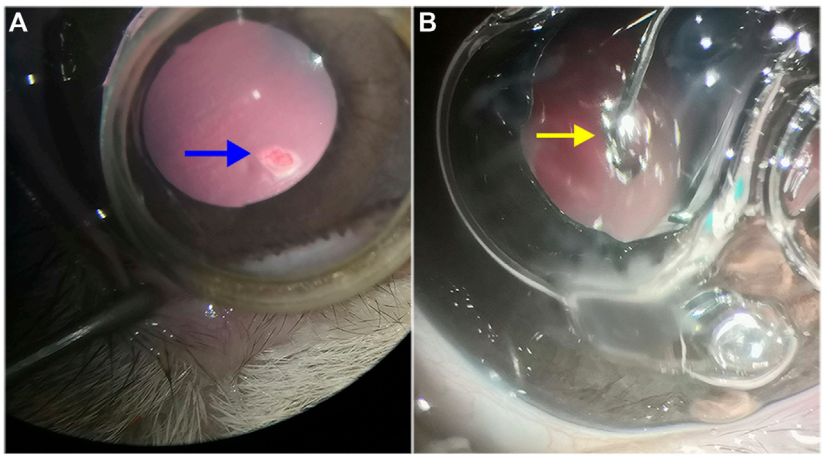

FIGURE 3 | Retinal detachment and HA-engineered hydrogel coverage. **(A)** After vitrectomy and PVD in the rabbit eye, the vitreous cutter was used to make a retinal break that was approximately 1/2 DD in size (blue arrow). The break was made 2 DD inferior to the optic disc. **(B)** The HA-engineered hydrogel (yellow arrow) was gently applied over the retinal break with a 25-gauge syringe through a trocar cannula in the RRD-hydrogel group.

Clinical Examination

Slit lamp microscopy, indirect ophthalmoscopy, and iCare tonometer were used with the pupils dilated preoperatively, and at 1 and 7 days, and 1 and 3 months postoperatively. B-mode ultrasound and fundus photography were used to evaluate the state of the retina in both groups before surgery and at 7 days and 1 and 3 months after surgery.

Statistical Analysis

Descriptive data were shown as mean ± standard deviation, and the difference between groups or pre- and post-operation was analyzed with paired *t*-tests or repeated measures analysis of variance. Qualitative data were presented as numbers and percentages, and were compared with the chi-square test (or Fischer's exact test if the criteria for the chi-square test were not fulfilled). $p < 0.05$ indicated that the difference was statistically significant.

RESULTS

The Physicochemical Properties of HA-Engineered Hydrogel Were Similar With Those of Healaflow®

Rheology

The HA-engineered hydrogel sealant and Healaflow® exhibited a higher G′ than G″ over a wide range of frequency from 0.1 to 10 Hz (**Figure 4A**), indicating that both the two hydrogels were gel-like rather than the sol-like in nature. The G' of the HA-engineered hydrogel varied from 80 to 160 Pa at 2% strain under 25°C, which was similar to that of Healaflow® (100–190 Pa). In addition, as shown in Table 1, the dynamic viscosity was 252,170 mPa s at 0.25 Hz under 25°C, which was similar to that of Healaflow® (258,000 mPa s).

Cohesiveness

As shown in **Figure 4B**, the stretched height of the HA-engineered hydrogel gel extruded from the syringe was about 4.5 cm, which was similar to that of the Healaflow® sample. The drop weight of the HA-engineered hydrogel was 0.038 ± 0.002 g, which was also similar to that of the Healaflow® sample (0.037 ± 0.004 g) (**Figure 4C**).

As shown in **Figure 4D**, both HA-engineered hydrogel and Healaflow® remained intact at the time point of 15 s, while dispersed into obvious small strips gradually afterward. By comparison, the Matrifill® and Janlane® samples dispersed quickly once stirred in the water, and scattered into barely visible particles (**Supplementary Figure S1**). The dispersion degree of HA-engineered hydrogel and Healaflow® was much lower than that of Matrifill® and Janlane®.

The aforementioned results indicated that the cohesiveness of the HA-engineered hydrogel was similar to that of Healaflow® and much higher than those of Matrifill® and Janlane®.

HA-Engineered Hydrogel Showed Favorable Biocompatibility With Retina

During the 1-month follow-up, no inflammatory reaction was observed in the eyes on which the HA-engineered hydrogel was applied to the retina. Slit lamp and indirect ophthalmoscopy examinations showed normal conjunctivae, corneas, aqueous humor, crystalline lenses, vitreous humor, and retinas at all time points. No cells or flares were observed in the anterior chamber or vitreous chamber. There was no significant change in IOP of the left eyes pre- and post-operation throughout the observation period (**Figure 5A** and **Supplementary Table S1**).

The ERGs of the left eyes before and 1 month after the operation showed the typical components of an ERG, an a-wave followed by a rapidly rising b-wave. **Figures 5B–F** and **Supplementary Table S2** show that there was no significant

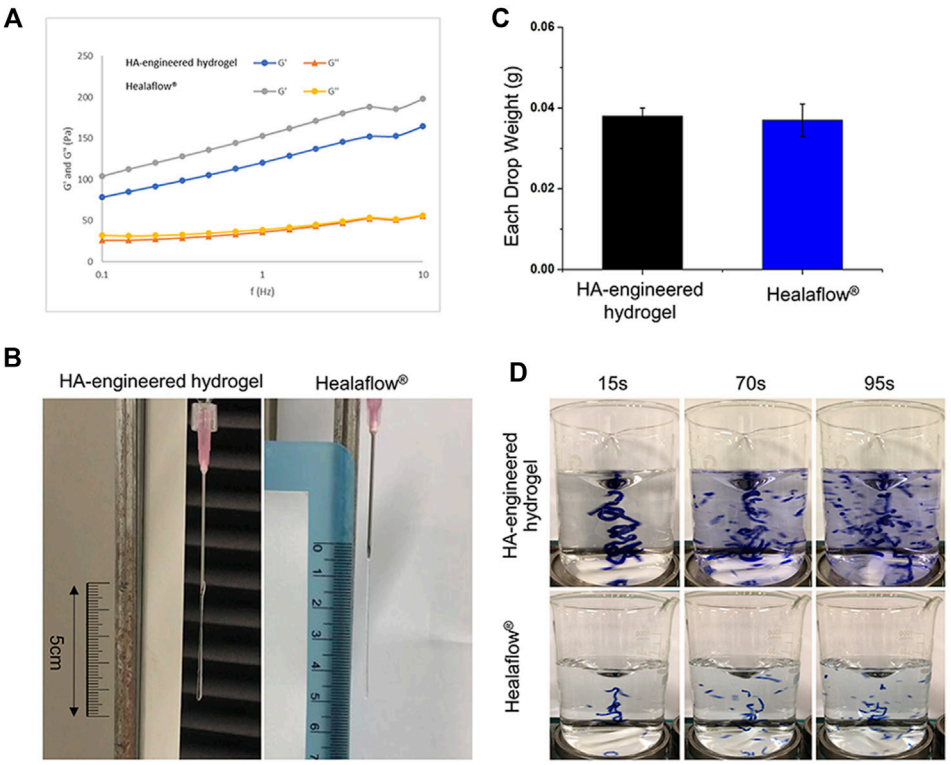

FIGURE 4 | Comparison of characteristics between HA-engineered hydrogel and Healaflow®. **(A)** G′ and G″ of HA-engineered hydrogel and Healaflow® at 2% strain over the frequency sweep from 0.1 to 10 Hz under 25°C. **(B,C)** Cohesiveness characterization of HA-engineered hydrogel and Healaflow® using the drop-weight method. **(B)** The photographs of HA-engineered hydrogel and Healaflow® when they were about to break. **(C)** The average drop weight of the collected HA-engineered hydrogel and Healaflow® hydrogels (n = 3). **(D)** Cohesiveness characterization of HA-engineered hydrogel and Healaflow® using the stained hydrogel dispersion method. The images were captured at the time point of 15, 75, and 90 s after the gel hit the surface.

difference in the pre- and postoperative implicit times and amplitudes of a-waves and b-waves of the ERGs at any stimulus intensity level on the left eyes.

Compared with a normal healthy right eye, H&E and immunofluorescence revealed no significant abnormality or inflammation in the left eye, such as the presence of inflammatory cells, epiretinal membrane, retinal edema, disorganization, or atrophic changes of the retinal layers (**Figure 6**).

HA-Engineered Hydrogel Significantly Improved the Retinal Reattachment Rates as Retinal Patch in RRD Repairment

There was a significant statistical difference in the retinal reattachment rates between the RRD-hydrogel and RRD groups (100 and 25%, respectively, $p = 0.007$, $\chi^2 = 9.6$); all retinas were reattached in the eight eyes of the RRD-hydrogel group, while the retina was reattached in two eyes and detached in six eyes in the RRD group throughout the 3-month follow-up. Fundus examination before surgery and typical fundus photography of retinal reattachment in the RRD-hydrogel group and B-mode ultrasound of retinal detachment in the RRD group are shown in **Figure 7**.

DISCUSSION

In this study, the HA-engineered hydrogel, a transparent, smooth, and cohesive ophthalmic hydrogel manufactured using a novel linearly cross-linking technology, showed not only its favorable biocompatibility during one-month follow-up, but also high viscosity and cohesiveness as the retinal patch in the RRD model of rabbit eyes during 3-month follow-up.

HA is a naturally occurring linear anionic polysaccharide, which has applications in diverse areas. In clinical ophthalmology, HA has been employed as an artificial tear ingredient for the treatment of dry eyes and a viscoelastic agent for cataract surgery. However, without further modification or functionalization, some inherent disadvantages, such as poor mechanical properties and restricted cell adhesion, have limited its wider application in its natural state. Implementing a cross-linking approach can compensate for these unsatisfactory shortcomings. Cross-linking is a stabilization process in polymer chemistry that results in a network structure depending on a multi-dimensional extension of a chain polymer. By cross-linking, HA is transformed into a gel-like substance that differs from its raw sol-like nature. Hydrogels are classified into two types

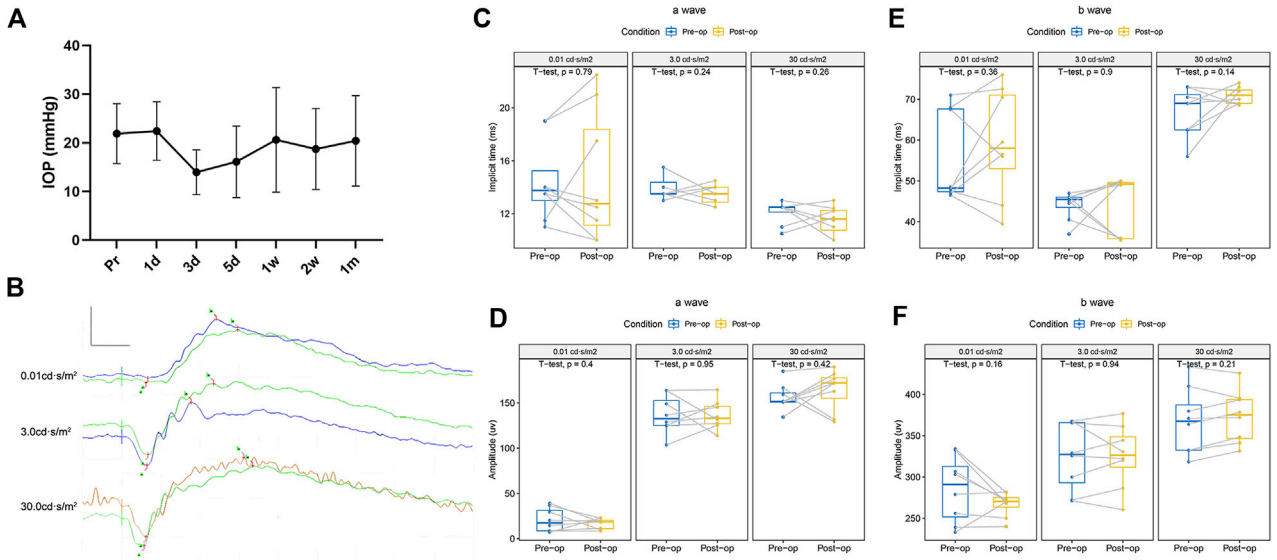

FIGURE 5 | Variation of IOP and function before and 1 month after the operation in the eye with HA-engineered hydrogel coverage. **(A)** The IOP fluctuated within 1 week after the operation and recovered spontaneously within 1 month, with no statistical difference. **(B)** A splicing ERG diagram of the left eye was recorded before (green line) and 1 month after the retina coverage with the HA-engineered hydrogel. Scale bar: 200 uv and 20 ms. **(C–F)** Left eyes' implicit time and amplitude of the a-wave and b-wave before and 1 month after the retina coverage with the HA-engineered hydrogel.

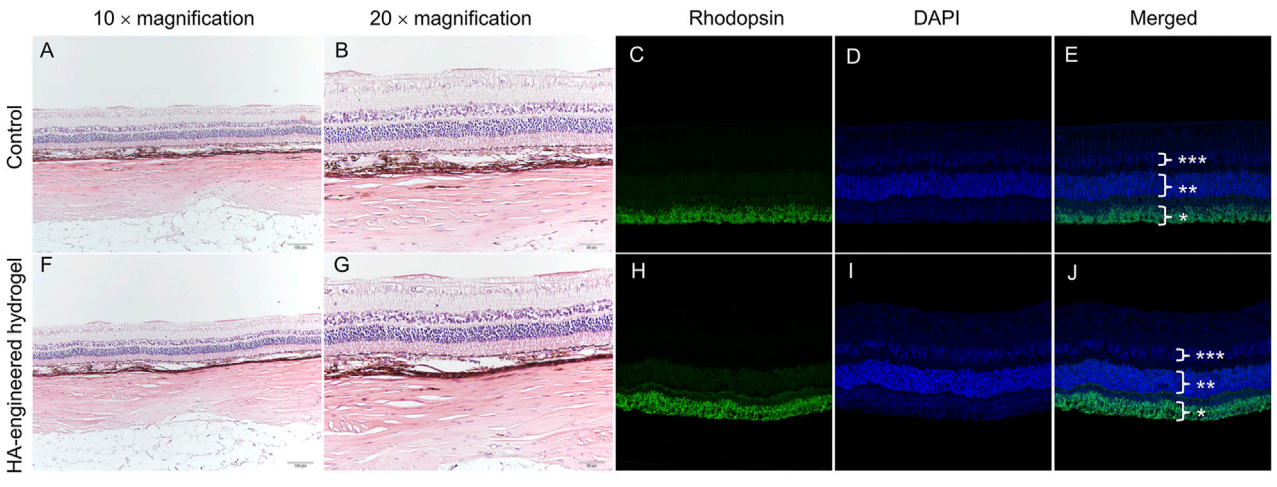

FIGURE 6 | Variation of morphology before and 1 month after the operation in the eye with HA-engineered hydrogel coverage. H&E staining images and immunostaining images of the normal retina **(A–E)** and the retina with HA-engineered hydrogel coverage **(F–J)**. The magnification of immunostaining images was 20 × *, rod photoreceptor layers. **, outer nuclear layer; ***, inner nuclear layer. The scale bar for the 10 × magnification was 100 um and that for the 20 × magnification was 50 um.

based on the type of cross-link junctions: physically cross-linked and chemically cross-linked. Physical cross-linking has high biocompatibility and is not toxic, but the junction is reversible *via* hydrogen bonds, hydrophobic interactions, and chain entanglements. On the other hand, chemical cross-linking has irreversible junctions, in which covalent bonds are present between different polymer chains, thus leading to excellent mechanical strength (Lu et al., 2018). The mechanical property, biological function, and degradation behaviors of the hydrogel are strongly dependent on the cross-linker concentration in the chemical cross-linking, for instance, **Figure 4D** and **Supplementary Figure S1** illustrate that the cohesiveness of the HA-engineered hydrogel is similar to that of Healaflow®, and much higher than those of Matrifill® and Janlane®, though both the cross-linkers are DVS in HA-engineered hydrogel and Matrifill®, while it is BDDE in both Healaflow® and Janlane®. But the cross-linker may induce cytotoxicity that the human body cannot tolerate when the

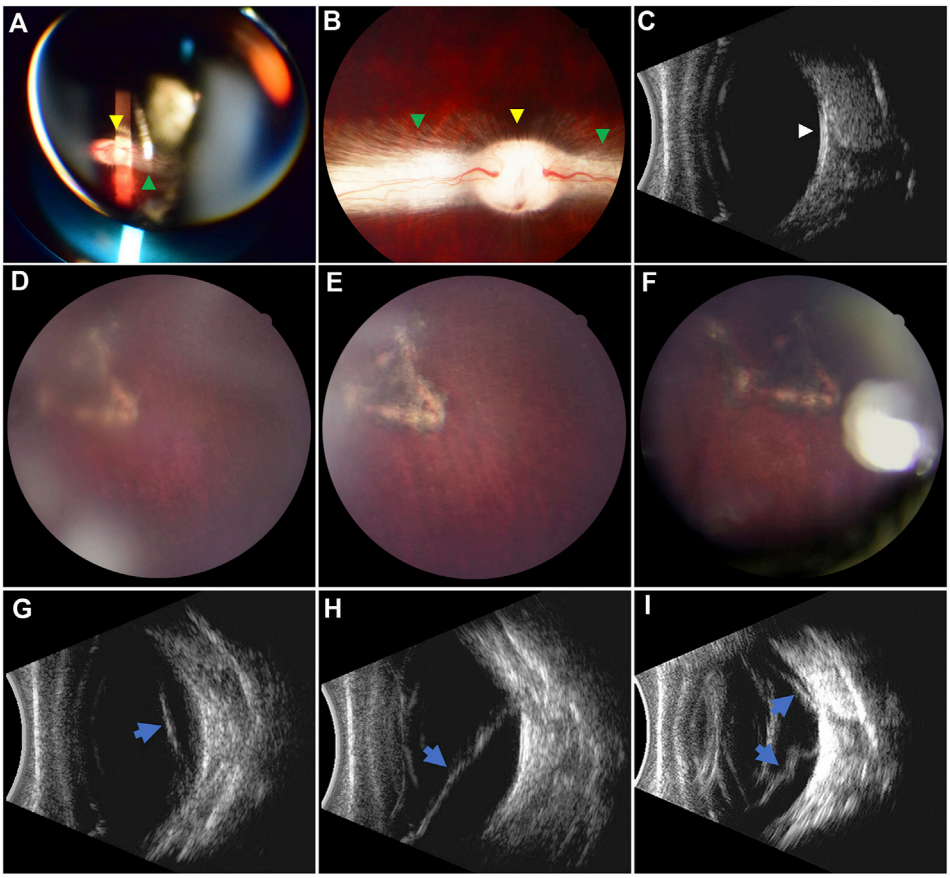

FIGURE 7 | Pre- and postoperative fundus examination. **(A–C)** Preoperative fundus examination *via* indirect ophthalmoscopy, fundus photography, and B-mode ultrasound, respectively. The optic disc (yellow arrowheads) and myelinated nerve fibers (green arrowheads) were well-marked. The vitreous cavity was clear, and the retina was attached (white arrowhead) in the ultrasound image. **(D–F)** Retinal reattachment in the RRD-hydrogel group at 7 days and 1 and 3 months after surgery, respectively. Pigmentation around the retinal break was apparent. **(G–I)** Retinal detachment (blue arrows) in the RRD group at 7 days and 1 and 3 months after surgery, respectively. The localized retinal detachment **(G)** extended **(H)** and gradually became stiff from a soft state over time **(I)**.

concentration is too high (Jeon et al., 2007; Lai, 2014). For example, cyanoacrylate is a synthetic gel that provides strong permanent adhesion and continuous seal in seconds in a vast number of experiments and general surgical trials (Guhan et al., 2018). However, localized but definite retinal toxicity in rabbit eyes 1 month after implantation was validated by histological examinations (Hida et al., 1988). Therefore, the evaluation of the biocompatibility of biomaterial is the most important prerequisite before clinical application.

An ideal retinal patch must have certain characteristics on the premise of favorable biocompatibility. First, it must remain firmly adhered and compliant to the retina long enough to allow the development of chorioretinal adhesion induced by classic retinopexy. Second, it should be biodegradable to avoid the need for a second surgical procedure to remove it. Finally, it must be delivered to the eye with minimal or no trauma *via* a simple procedure. The Bio-Alcamid® showed strong adverse effects on the retina in an *in vitro* study, preventing further effectiveness studies (Barth et al., 2014). PEG gel elicited reactions similar to the control retinas in the *in vitro* study. In the *in vivo* study, the PEG gel was not toxic to the eye, could successfully close the retinal breaks, and maintain retinal reattachment. However, the PEG sealant requires the illumination of a xenon arc lamp (450–500 nm, blue-green) for 40–60 s before it can polymerize to form a clear, flexible, and firmly adherent hydrogel (Hoshi et al., 2015; Hoshi et al., 2018). With further technological advancements, the PEG-derived polymer is now stored in powder form, and it needs to be mixed with methylcellulose for 150 s to polymerize before use (Hubschman et al., 2017). The procedure is more complex compared to the injectable properties of Healaflow® and our HA-engineered hydrogel. The commercially available bioresorbable translucent membrane Seprafilm®, composed of sodium HA and carboxymethylcellulose, presented favorable biocompatibility and powerful adhesion in the *in vitro* and *in vivo* studies and clinical trials. But the sclerotomy site needs to be expanded to 3 mm to deliver a 5 × 2 mm sheet of Seprafilm® onto the retina (Sueda et al., 2006; Teruya et al., 2009; Haruta et al., 2017). The biological glues, such as representative fibrine glue, are composed of separate glue A and glue B. Retinal breaks must be covered with glue A first, followed by a quick and precise mixture of glue B to form the membrane. Thus, there is a risk of glue migration to the

subretinal space due to the fluidity of the glue before membrane formation and the spherical shape of the eyeball(Kwon et al., 2019; Tyagi and Basu, 2019; Wang et al., 2020; Mamlouk et al., 2021). Healaflow® is a slow resorbable and self-degrading viscoelastic agent. In the *in vitro* investigation, it exhibited strong and lasting adhesion, and protection from culture-induced trauma; in the animal experiment, it did not negatively affect retinal morphology or function, indicating favorable biocompatibility; and in a clinical trial, it was found to be beneficial to patch retinal breaks with vitrectomy (Barth et al., 2014; Barth et al., 2016; Ren et al., 2020). According to the review of the current literature on ocular experiments or clinical trials, most adhesives have good biocompatibility and strong tissue adhesiveness, but the manipulation of delivery or covering retinal breaks is complex. The injectable gel property of Healaflow® presents obvious advantages.

Herein, our novel ophthalmic HA-engineered hydrogel is similar to Healaflow® in terms of pH, osmolarity, specific gravity, and refractive index (Table 1), suggesting that the HA-engineered hydrogel exhibits the basic physicochemical properties required as an ideal ophthalmic sealant. In comparison to other tissue adhesives, the HA-engineered hydrogel appears to be a better candidate for use as a retinal patch because its injectable property eliminates the need for expanded sclerotomies for delivery and additional procedures to mix or polymerize. Importantly, the HA-engineered hydrogel displays high dynamic viscosity and cohesiveness, which is similar to Healaflow® (**Figure 4**). The viscosity and cohesiveness are two curtail properties, which have a close relationship with the biocompatibility and efficacy of the hydrogel sealant. To prevent the migration of RPE cells into the vitreous cavity through retinal breaks, the sealant should possess a high viscosity to ensure its tight adhesion to the surrounded tissues of the breaks (Barth et al., 2016). According to our results, the dynamic viscosity of the HA-engineered hydrogel is similar to that of Healaflow® (252,170 mPa·s for the HA-engineered hydrogel and 258,000 mPa·s for Healaflow® at 0.25 Hz, respectively), both of which are significantly higher than that of PEG (700–1,400 mPa·s) in the previously published reports (Hoshi et al., 2015). Our group has previously verified that Healaflow® could remain adherent for at least 14 days in the culture flask filled with a balanced solution, and could effectively adhere to the retina in RRD patients (Ren et al., 2020). Based on the fact that HA-engineered hydrogel and Healaflow® share almost identical physical and chemical properties, it is assumed that the HA-engineered hydrogel sealant possesses sufficiently high viscosity to meet the need for break sealing. After sealing the breaks, a high cohesiveness keeps the sealant intact and not dissociating under the infiltration of aqueous humor after the sterile air was absorbed in a few days; thus, a prolonged retention time of the sealant and a better clinical effect could be achieved. Our results showed that the HA-engineered hydrogel exhibited similar cohesiveness as compared with Healaflow®, and much higher cohesiveness than Matrifill® and Janlane®. The discrepancy of cohesiveness was also reflected in the morphology of hydrogels, as the HA-engineered hydrogel and Healaflow® appeared to be smooth and homogeneous, while Matrifill® and Janlane® appeared to be firm and particulate. The high cohesiveness of the HA-engineered hydrogel contributed to a stable and prolonged retinal attachment during the 3-month follow-up period in the animal studies. In addition, the HA-engineered hydrogel exhibited a relatively higher G' (80–160 Pa at 2% strain under 25°C) than the native vitreous body (1–7 Pa), (Tram et al., 2020), indicating the ability of the HA-engineered hydrogel to rebound to its original shape when acted on by dynamic forces. The G' of the HA-engineered hydrogel was similar to that of Healaflow®, indicating similar resistance to deformation of the two gels.

In the development of any biomaterial, the evaluation of potential inflammatory or toxic responses *in vivo* is critical. The laser-induced chorioretinal adhesion takes about 3 weeks to be strong enough, according to the results of rabbit eyes (Smiddy and Hernandez, 1992), during which time the eyeball is relatively unstable. For instance, the cyanoacrylate tissue adhesive showed retinal toxicity 1 month after the implantation; however, no identifiable distant toxic effects or electrophysiologic changes were observed during the 6-month follow-up period (Hida et al., 1988). Consequently, many studies choose approximately 3 weeks after surgery as the cutoff to report the biocompatibility of tissue adhesives (Sueda et al., 2006; Teruya et al., 2009; Hoshi et al., 2015). In this study, our ERG records, H&E, and immunofluorescence one month after the operation suggested no adverse effects of the HA-engineered hydrogel on retinal function and morphology, confirming its favorable biocompatibility. Simultaneously, our results demonstrated the efficacy of the HA-engineered hydrogel as the retinal patch in the RRD model of rabbit eyes with a 3-month follow-up, which can aid in the complete reattachment of the retina without the need for expansile gas or silicone oil endotamponade. Sterile air as endotamponade combined with the HA-engineered hydrogel as the retinal patch avoids the adverse complications of long-acting gas and silicone oil, discomfort from the strict postoperative face-down position, and the long-term poor visual quality caused by the higher (silicone oil) or lower (long-acting gas) refractive index compared to the natural human vitreous (Hoshi et al., 2019). The IOP fluctuated significantly within 1 week after the operation and recovered spontaneously within 1 month in our study, with no statistical difference. Transient hypotony is a common phenomenon after 25-gauge vitrectomy (Bamonte et al., 2011); thus, the 25-gauge vitrectomy was assumed to be the main risk factor of transient postoperative hypotony in this study.

There are some limitations to this study. First, during the manipulation of the RRD model, the size of the retinal break was small, and the localized retinal detachment only lasted a few seconds; hence, there were few or no RPE cells migrating to the vitreous cavity, and the RRD model failed to fully mimic the pathological processes of human RRD. Second, unlike in human RRD, we did not use endolaser photocoagulation around the retinal break in the RRD model. It is unclear whether the HA-engineered hydrogel eliminates the need for laser retinopexy in clinical trials, despite animal experiments showing 100% retinal reattachment without laser retinopexy. Finally, the behavior of rabbits was uncontrollable during the recovery period.

In conclusion, the HA-engineered hydrogel could play the role of an ophthalmologic sealant *via* its high viscosity and cohesiveness. This pilot study of a small series of RRD models

with a short-term follow-up provides preliminary evidence to support the favorable biocompatibility and efficacy of the HA-engineered hydrogel as a promising retinal patch for sealing retinal breaks in retinal detachment repair. More cases and longer follow-up studies are needed to assess the safety and long-term effects of the HA-engineered hydrogel.

DATA AVAILABILITY STATEMENT

The original contributions presented in the study are included in the article/**Supplementary Material**; further inquiries can be directed to the corresponding authors.

ETHICS STATEMENT

The animal study was reviewed and approved by the Institutional Animal Care and Use Committee of Tianjin Medical University Eye Hospital.

AUTHOR CONTRIBUTIONS

XR and XL conceived the study and were in charge of overall direction and planning. CZ, HX, and DW performed the measurements; YK and XZ were involved in planning and supervising the work; and CZ, HX, and XR processed the experimental data and performed the analysis. CZ drafted the manuscript and designed the figures with help from HX. All authors discussed the results and commented on the manuscript.

FUNDING

This work was supported by the grants from the Fund for Less Developed Regions of the National Natural Science Foundation of China (82160202) and the Shanghai Sailing Program (21YF1432200).

ACKNOWLEDGMENTS

The authors wish to acknowledge Kejia Xu for providing professional painting services.

SUPPLEMENTARY MATERIAL

The Supplementary Material for this article can be found online at: https://www.frontiersin.org/articles/10.3389/fbioe.2022.914675/full#supplementary-material

REFERENCES

Bamonte, G., Mura, M., and Stevie Tan, H. (2011). Hypotony after 25-Gauge Vitrectomy. *Am. J. Ophthalmol.* 151 (1), 156–160. doi:10.1016/j.ajo.2010.06.042

Barth, H., Crafoord, S., Andréasson, S., and Ghosh, F. (2016). A Cross-Linked Hyaluronic Acid Hydrogel (Healaflow((R))) as a Novel Vitreous Substitute. *Graefes Arch. Clin. Exp. Ophthalmol.* 254 (4), 697–703. doi:10.1007/s00417-015-3256-z

Barth, H., Crafoord, S., Arnér, K., and Ghosh, F. (2019). Inflammatory Responses after Vitrectomy with Vitreous Substitutes in a Rabbit Model. *Graefes Arch. Clin. Exp. Ophthalmol.* 257 (4), 769–783. doi:10.1007/s00417-019-04242-0

Barth, H., Crafoord, S., O'Shea, T. M., Pritchard, C. D., Langer, R., and Ghosh, F. (2014). A New Model for *In Vitro* Testing of Vitreous Substitute Candidates. *Graefes Arch. Clin. Exp. Ophthalmol.* 252 (10), 1581–1592. doi:10.1007/s00417-014-2714-3

Bourla, D. H., Bor, E., Axer-Siegel, R., Mimouni, K., and Weinberger, D. (2010). Outcomes and Complications of Rhegmatogenous Retinal Detachment Repair with Selective Sutureless 25-Gauge Pars Plana Vitrectomy. *Am. J. Ophthalmol.* 149 (4), 630–634. doi:10.1016/j.ajo.2009.11.003

Chen, X., Yan, Y., Hong, L., and Zhu, L. (2015). A Comparison of Strict Face-Down Positioning with Adjustable Positioning after Pars Plana Vitrectomy and Gas Tamponade for Rhegmatogenous Retinal Detachment. *Retina* 35 (5), 892–898. doi:10.1097/iae.0000000000000413

Edsman, K. L., Wiebensjö, Å. M., Risberg, A. M., and Öhrlund, J. Å. (2015). Is There a Method that Can Measure Cohesivity? Cohesion by Sensory Evaluation Compared with Other Test Methods. *Dermatol Surg.* 41 (Suppl. 1), S365–S372. doi:10.1097/DSS.0000000000000550

Feltgen, N., and Walter, P. (2014). Rhegmatogenous Retinal Detachment-Aan Ophthalmologic Emergency. *Dtsch. Arztebl Int.* 111 (1-2), 12–21. doi:10.3238/arztebl.2014.0012

Guhan, S., Peng, S.-L., Janbatian, H., Saadeh, S., Greenstein, S., Al Bahrani, F., et al. (2018). Surgical Adhesives in Ophthalmology: History and Current Trends. *Br. J. Ophthalmol.* 102 (10), 1328–1335. doi:10.1136/bjophthalmol-2017-311643

Haruta, M., Arai, M., Sueda, J., Hirose, T., and Yamakawa, R. (2017). Patching Retinal Breaks with Seprafilm for Treating Retinal Detachments in Humans: 9 Years of Follow-Up. *Eye* 31 (5), 776–780. doi:10.1038/eye.2016.329

Haugstad, M., Moosmayer, S., and Bragadóttir, R. (2017). Primary Rhegmatogenous Retinal Detachment - Surgical Methods and Anatomical Outcome. *Acta Ophthalmol.* 95 (3), 247–251. doi:10.1111/aos.13295

Hida, T., Sheta, S. M., Proia, A. D., and McCuen, B. W., 2nd (1988). Retinal Toxicity of Cyanoacrylate Tissue Adhesive in the Rabbit. *Retina* 8 (2), 148–153. doi:10.1097/00006982-198808020-00013

Hoshi, S., Okamoto, F., Arai, M., Hirose, T., Sugiura, Y., Kaji, Y., et al. (2015). *In Vivo* and *In Vitro* Feasibility Studies of Intraocular Use of Polyethylene Glycol-Based Synthetic Sealant to Close Retinal Breaks in Porcine and Rabbit Eyes. *Invest. Ophthalmol. Vis. Sci.* 56 (8), 4705–4711. doi:10.1167/iovs.14-15349

Hoshi, S., Okamoto, F., Arai, M., Hirose, T., Sugiura, Y., Murakami, T., et al. (2018). Patching Retinal Breaks with Polyethylene Glycol-Based Synthetic Hydrogel Sealant for Retinal Detachment in Rabbits. *Exp. Eye Res.* 177, 117–121. doi:10.1016/j.exer.2018.08.004

Hoshi, S., Okamoto, F., Murakami, T., Sakai, T., Shinohara, Y., Fujii, T., et al. (2019). Ability of Nonswelling Polyethylene Glycol-Based Vitreous Hydrogel to Maintain Transparency in the Presence of Vitreous Hemorrhage. *Trans. Vis. Sci. Tech.* 8 (6), 33. doi:10.1167/tvst.8.6.33

Hubschman, J. P., Govetto, A., Farajzadeh, M., Sato, T., Askari, S., and Glasgow, B. (2017). Feasibility of a Polyethylene Glycol-Derived Polymer as Retinal Patch to Seal Retinal Breaks during Vitrectomy for Rhegmatogenous Retinal Detachment: A Prospective, *In Vivo* Pilot Study in a Porcine Model. *Clin. Exp. Ophthalmol.* 45 (7), 708–716. doi:10.1111/ceo.12942

Jeon, O., Song, S. J., Lee, K.-J., Park, M. H., Lee, S.-H., Hahn, S. K., et al. (2007). Mechanical Properties and Degradation Behaviors of Hyaluronic Acid Hydrogels Cross-Linked at Various Cross-Linking Densities. *Carbohydr. Polym.* 70 (3), 251–257. doi:10.1016/j.carbpol.2007.04.002

Kobashi, H., Takano, M., Yanagita, T., Shiratani, T., Wang, G., Hoshi, K., et al. (2014). Scleral Buckling and Pars Plana Vitrectomy for Rhegmatogenous Retinal Detachment: An Analysis of 542 Eyes. *Curr. Eye Res.* 39 (2), 204–211. doi:10.3109/02713683.2013.838270

Kontos, A., Tee, J., Stuart, A., Shalchi, Z., and Williamson, T. H. (2017). Duration of Intraocular Gases Following Vitreoretinal Surgery. *Graefes Arch. Clin. Exp. Ophthalmol.* 255 (2), 231–236. doi:10.1007/s00417-016-3438-3

Kuhn, F., and Aylward, B. (2014). Rhegmatogenous Retinal Detachment: A Reappraisal of its Pathophysiology and Treatment. *Ophthalmic Res.* 51 (1), 15–31. doi:10.1159/000355077

Kwon, J., Shin, S. H., Lee, S., Park, G., Park, Y., Lee, S. J., et al. (2019). The Effect of Fibrinogen/Thrombin-Coated Collagen Patch (TachoSil((R))) Application in Pancreaticojejunostomy for Prevention of Pancreatic Fistula after Pancreaticoduodenectomy: A Randomized Clinical Trial. *World J. Surg.* 43 (12), 3128–3137. doi:10.1007/s00268-019-05172-y

Lai, J.-Y. (2014). Relationship between Structure and Cytocompatibility of Divinyl Sulfone Cross-Linked Hyaluronic Acid. *Carbohydr. Polym.* 101, 203–212. doi:10.1016/j.carbpol.2013.09.060

Lu, L., Yuan, S., Wang, J., Shen, Y., Deng, S., Xie, L., et al. (2018). The Formation Mechanism of Hydrogels. *Curr. Stem Cell Res. Ther.* 13 (7), 490–496. doi:10.2174/1574888x12666170612102706

Lumi, X., Hawlina, M., Glavač, D., Facskó, A., Moe, M. C., Kaarniranta, K., et al. (2015). Ageing of the Vitreous: From Acute Onset Floaters and Flashes to Retinal Detachment. *Ageing Res. Rev.* 21, 71–77. doi:10.1016/j.arr.2015.03.006

Mamlouk, M. D., Shen, P. Y., Sedrak, M. F., and Dillon, W. P. (2021). CT-Guided Fibrin Glue Occlusion of Cerebrospinal Fluid-Venous Fistulas. *Radiology* 299 (2), 409–418. doi:10.1148/radiol.2021204231

Oshima, Y., Wakabayashi, T., Sato, T., Ohji, M., and Tano, Y. (2010). A 27-Gauge Instrument System for Transconjunctival Sutureless Microincision Vitrectomy Surgery. *Ophthalmology* 117 (1), 93–102. doi:10.1016/j.ophtha.2009.06.043

Pastor, J. C., Rojas, J., Pastor-Idoate, S., Di Lauro, S., Gonzalez-Buendia, L., and Delgado-Tirado, S. (2016). Proliferative Vitreoretinopathy: A New Concept of Disease Pathogenesis and Practical Consequences. *Prog. Retin. Eye Res.* 51, 125–155. doi:10.1016/j.preteyeres.2015.07.005

Pérez, L. A., Hernández, R., Alonso, J. M., Pérez-González, R., and Sáez-Martínez, V. (2021). Hyaluronic Acid Hydrogels Crosslinked in Physiological Conditions: Synthesis and Biomedical Applications. *Biomedicines* 9 (9), 1113. doi:10.3390/biomedicines9091113

Popovic, M. M., Muni, R. H., Nichani, P., and Kertes, P. J. (2022). Pars Plana Vitrectomy, Scleral Buckle, and Pneumatic Retinopexy for the Management of Rhegmatogenous Retinal Detachment: A Meta-Analysis. *Surv. Ophthalmol.* 67 (1), 184–196. doi:10.1016/j.survophthal.2021.05.008

Raczynska, D., Mitrosz, K., Raczynska, K., and Glasner, L. (2018). The Influence of Silicone Oil on the Ganglion Cell Complex after Pars Plana Vitrectomy for Rhegmatogenous Retinal Detachment. *Curr. Pharm. Des.* 24 (29), 3476–3493. doi:10.2174/1381612824666180813115438

Ren, X. J., Bu, S. C., Wu, D., Liu, B. S., Yang, F. H., Hu, B. J., et al. (2020). Patching Retinal Breaks with Healaflow in 27-Gauge Vitrectomy for the Treatment of Rhegmatogenous Retinal Detachment. *Retina* 40 (10), 1900–1908. doi:10.1097/iae.0000000000002701

Romano, M. R., Cennamo, G., Ferrara, M., Cennamo, M., and Cennamo, G. (2017). Twenty-Seven-Gauge Versus 25-Gauge Vitrectomy for Primary Rhegmatogenous Retinal Detachment. *Retina* 37 (4), 637–642. doi:10.1097/iae.0000000000001215

Smiddy, W. E., and Hernandez, E. (1992). Histopathologic Characteristics of Diode Laser-Induced Chorioretinal Adhesions for Experimental Retinal Detachment in Rabbit Eyes. *Arch. Ophthalmol.* 110 (11), 1630–1633. doi:10.1001/archopht.1992.01080230130037

Sueda, J., Sakuma, T., Nakamura, H., Usumoto, N., Okuno, T., Arai, M., et al. (2006). *In Vivo* and *In Vitro* Feasibility Studies of Intraocular Use of Seprafilm to Close Retinal Breaks in Bovine and Rabbit Eyes. *Invest. Ophthalmol. Vis. Sci.* 47 (3), 1142–1148. doi:10.1167/iovs.05-0931

Teruya, K., Sueda, J., Arai, M., Tsurumaru, N., Yamakawa, R., Hirata, A., et al. (2009). Patching Retinal Breaks with Seprafilm in Experimental Rhegmatogenous Retinal Detachment of Rabbit Eyes. *Eye* 23 (12), 2256–2259. doi:10.1038/eye.2008.403

Tetsumoto, A., Imai, H., Hayashida, M., Otsuka, K., Matsumiya, W., Miki, A., et al. (2020). The Comparison of the Surgical Outcome of 27-Gauge Pars Plana Vitrectomy for Primary Rhegmatogenous Retinal Detachment between Air and SF6 Gas Tamponade. *Eye* 34 (2), 299–306. doi:10.1038/s41433-019-0726-2

Tram, N. K., Jiang, P., Torres-Flores, T. C., Jacobs, K. M., Chandler, H. L., and Swindle-Reilly, K. E. (2020). A Hydrogel Vitreous Substitute that Releases Antioxidant. *Macromol. Biosci.* 20 (2), e1900305. doi:10.1002/mabi.201900305

Tran, C., Carraux, P., Micheels, P., Kaya, G., and Salomon, D. (2014). *In Vivo* bio-Integration of Three Hyaluronic Acid Fillers in Human Skin: A Histological Study. *Dermatology* 228 (1), 47–54. doi:10.1159/000354384

Tyagi, M., and Basu, S. (2019). Glue-Assisted Retinopexy for Rhegmatogenous Retinal Detachments (GuARD): A Novel Surgical Technique for Closing Retinal Breaks. *Indian J. Ophthalmol.* 67 (5), 677–680. doi:10.4103/ijo.IJO_1943_18

Wagenfeld, L., Zeitz, O., Skevas, C., and Richard, G. (2010). Long-Lasting Endotamponades in Vitreoretinal Surgery. *Ophthalmologica* 224 (5), 291–300. doi:10.1159/000298749

Wang, Q., Zhao, J., Xu, Q., Han, C., and Hou, B. (2020). Intraocular Application of Fibrin Glue as an Adjunct to Pars Plana Vitrectomy for Rhegmatogenous Retinal Detachment. *Retina* 40 (4), 718–724. doi:10.1097/iae.0000000000002584

Wei, C., Wang, X., and Jiang, L. (2019). Method for Rearranging the Structure of Crosslinked Sodium Hyaluronate Gel. C.N. Patent No 201910807020.2. State Intellectual Property Office of the People's Republic of China.

Wongprasert, P., Dreiss, C. A., and Murray, G. (2022). Evaluating Hyaluronic Acid Dermal Fillers: A Critique of Current Characterization Methods. *Dermatol Ther.*, e15453 [Epub ahead of print]. doi:10.1111/dth.15453

Conflict of Interest: HX was employed by the company Qisheng Biological Preparation Co., Ltd.

The remaining authors declare that the research was conducted in the absence of any commercial or financial relationships that could be construed as a potential conflict of interest.

Publisher's Note: All claims expressed in this article are solely those of the authors and do not necessarily represent those of their affiliated organizations, or those of the publisher, the editors, and the reviewers. Any product that may be evaluated in this article, or claim that may be made by its manufacturer, is not guaranteed or endorsed by the publisher.

frontiers | Frontiers in Bioengineering and Biotechnology

TYPE Mini Review
PUBLISHED 19 July 2022
DOI 10.3389/fbioe.2022.954699

OPEN ACCESS

EDITED BY
Yongsheng Yu,
Chinese Academy of Sciences, China

REVIEWED BY
Gajanan Arbade,
National Centre for Cell Science, India
Zhiwei Fang,
Johns Hopkins University, United States

*CORRESPONDENCE
Xiangjuan Li,
386501678@qq.com
Chengchen Guo,
guochengchen@westlake.edu.cn

†These authors have contributed equally to this work

SPECIALTY SECTION
This article was submitted to Biomaterials, a section of the journal Frontiers in Bioengineering and Biotechnology

RECEIVED 27 May 2022
ACCEPTED 29 June 2022
PUBLISHED 19 July 2022

CITATION
Chen M, Jiang R, Deng N, Zhao X, Li X and Guo C (2022), Natural polymer-based scaffolds for soft tissue repair. *Front. Bioeng. Biotechnol.* 10:954699. doi: 10.3389/fbioe.2022.954699

Natural polymer-based scaffolds for soft tissue repair

Meiwen Chen[1†], Rui Jiang[2†], Niping Deng[2], Xiumin Zhao[1], Xiangjuan Li[1*] and Chengchen Guo[2*]

[1]Hangzhou Women's Hospital, Hangzhou, Zhejiang, [2]School of Engineering, Westlake University, Hangzhou, Zhejiang

Soft tissues such as skin, muscle, and tendon are easily damaged due to injury from physical activity and pathological lesions. For soft tissue repair and regeneration, biomaterials are often used to build scaffolds with appropriate structures and tailored functionalities that can support cell growth and new tissue formation. Among all types of scaffolds, natural polymer-based scaffolds attract much attention due to their excellent biocompatibility and tunable mechanical properties. In this comprehensive mini-review, we summarize recent progress on natural polymer-based scaffolds for soft tissue repair, focusing on clinical translations and materials design. Furthermore, the limitations and challenges, such as unsatisfied mechanical properties and unfavorable biological responses, are discussed to advance the development of novel scaffolds for soft tissue repair and regeneration toward clinical translation.

KEYWORDS

soft tissue repair, natural polymers, scaffolds, clinical translation, materials processing

Introduction

Soft tissue injury is generally caused by traumatic or pathological lesions where muscle or connective tissues get damaged (Henriksen et al., 2017). Biomaterials are used to replace the impaired soft tissue or function as scaffolds to facilitate tissue regeneration to repair the damaged soft tissue (Keane and Badylak, 2014; Gaharwar et al., 2020). Though the direct replacement of the damaged soft tissue using inert implants or autologous grafts is still commonly applied in current clinical practices, some adverse effects exist, such as chronic pain and implant-related complications (Entekhabi et al., 2021; Liang et al., 2021; Rodrigues and Raz, 2022). In comparison, scaffolds in two-dimensional or three-dimensional forms can be used as templates for tissue regeneration. The cells can bind to the scaffolds and then proliferate and differentiate (Avolio et al., 2017; Turnbull et al., 2020; Abdollahiyan et al., 2021; Bianchi et al., 2021; Masson-Meyers and Tayebi, 2021). In addition, growth factors can be incorporated into the scaffolds to advance tissue regrowth and repair (Hormozi et al., 2017; Kakudo et al., 2020; González-Pérez et al., 2021). To meet the clinical needs, the scaffolds for soft tissue repair should have tissue-matching mechanical properties, excellent biocompatibility, and appropriate biodegradability. Both synthetic polymers and natural polymers have been used to fabricate scaffolds. The synthetic polymers include polylactic acid (PLA), polyglycolic

TABLE 1 Status of natural polymer-based scaffolds in clinical use/translation.

Trade name/Product name	Materials	Company/Institution	Applications	References
Chongshu ® composite hernia patch	Fibrinogen; poly (lactide-co-epsilon-caprolactone)	Shanghai Pine and Power Technology Co., LTD	Hernia repair	Gang et al., (2021)
Haiao ® oral repair membrane	Collagen	Yantai Zhenghai Biotechnology Co. LTD	Periodontal tissue repair	-
GenossDES™	Cobalt-chromium platform scaffolds containing sirolimus biodegradable polymers	Genoss Company Limited, Suwon, Korea	Coronary stent implantation	Lee and Park., (2020)
BEGO® collagen membrane	Collagen membrane	BEGO Implant Systems	Tissue engineering	Al-Maawi et al., (2019)
Mucograft	Collagen types I and III	Geistlich Pharma AG, Wolhusen, Switzerland	Gingival recession	Rokn et al., (2020)
Collagen Graft and Collagen Membrane	Collagen Membrane, Collagen Graf	Genoss Company Limited, Suwon, Korea	Cleft palate repair	Ha et al., (2020)
PACG-GelMA Hydrogels	Poly (N-acryloyl 2-glycine)/ methacrylated gelatin hydrogels	Tianjin Key Laboratory of Composite and Functional Materials	Osteochondral Regeneration	Gao et al., (2019)
PEG silk composite hydrogel	Silk	Research Institute of Agriculture and Life Sciences, Seoul National University, Seoul, South Korea	Articular cartilage repair	Kim et al., (2021)
Elastin-silk fibroin double raschel knitted vascular graft	Silk	Tokyo University of Agriculture and Technology, Fuchu, Japan	Artificial blood vessel	Tanaka et al., (2020)
Chondrotissue®	PGA, HA	Chondrotissue, BioTissue AG, Zurich, Switzerland)	Cartilage tissue engineering	Kanatlı et al., (2017)
IC scaffold	PLGA, COL	Tissue Engineering Research Center, AIST Kansai, Amagasaki Site	Cartilage tissue engineering	Eviana Putri et al., (2020)
C2C1H scaffold	PLA, COL, CH	BioMediTech, Institute of Biosciences and Medical Technology, Tampere, Finland	Cartilage tissue engineering	Haaparanta et al., (2014)
Chitosan-modified PLCL scaffold	PLCL, CH	Tissue Engineering Program, Life Sciences Institute, National University of Singapore, Singapore	Cartilage tissue formation	Yang et al., (2012)
CSMA/PECA/GO (S2) scaffold	CSMA, MPEG-PCL-AC (PECA), GO	State Key Laboratory of Biotherapy and Cancer Center, West China Hospital, Sichuan University	Cartilage tissue engineering	Liao et al., (2015)
Hyalofast®	Benzyl ester of hyaluronic acid	Anika Therapeutics Inc., Bedford, Massachusetts, United States	Osteochondral Injury	Bajuri et al., (2021)
ChondroGide®	Type I/III collagen	Geistlich Biomaterials, Wolhusen, Switzerland	Cartilage defects of the knee joint	Niemeyer et al., (2008)
Cartipatch®	Agarose and alginate	Tissue Bank of France, TBF, Lyon, France	Knee cartilage injury	Clavé et al., (2016)
Silk Voice®	Silk	Sofregen, United States	Wound healing	-
NOVOCART® 3D	Type I collagen, chondroitin sulfate	TETEC, Reutlingen, Germany	Isolated retro patellar cartilage defects	Kayaalp et al., (2021)

CH, chitosan; COL, collagen; CSMA, methacrylated chondroitin sulfate; HA, hyaluronic acid; PCL, polycaprolactone; PLA, polylactic acid; PLLA, poly (l-lactide); PGA, poly (glycolic acid); PLGA, polylactic-co-glycolic acid; ECM, extracellular matrix; PLCL, poly (l-lactide-co-ε-caprolactone); AC, acryloyl chloride; GO, graphene oxide.

acid (PGA), poly (lactic-co-glycolic acid) (PLGA), and poly-e-caprolactone (PCL), while the natural polymers include proteins and polysaccharides (Janoušková, 2018; Rao et al., 2018). Compared with synthetic polymers, natural polymers such as collagen, fibrin, silk protein, chitosan, and hyaluronic acid generally present better biocompatibility but limited processability (Naghieh et al., 2017; Caillol, 2020; Taghipour et al., 2020). With the rapid development of processing technology in recent years, more natural polymer-based scaffolds have been successfully fabricated and applied in biomedical applications. This mini-review summarizes the status of the natural polymer-based scaffold in clinical translation and the advanced processing techniques used for making scaffolds for soft tissue repair.

Current status of natural polymer-based scaffolds in clinical translations

Over the past decades, many natural polymer-based scaffolds for soft tissue repair have been developed for biomedical applications and some of them are commercially available. Table 1 summarizes the natural polymer-based scaffolds either commercially available or in clinical trials. These developed

scaffolds are primarily composed of fibrinogen, collagen, silk, and alginate. Through advanced processing, these materials can be fabricated into functional scaffolds for various applications, including wound repair, hernia repair, cartilage repair, and blood vessel grafting. In some cases, the repairing efficacy can be improved by incorporating bioactive materials such as growth factors and antibacterial agents in the scaffolds. In recent years, silk-based scaffolds have attracted much attention due to their excellent mechanical properties and biocompatibility (Zhao and Li, 2011; Zhou et al., 2018; Mao et al., 2021; Zhao et al., 2021).

Fabrication of natural polymer-based scaffolds

An ideal scaffold for soft tissue repair should meet the requirements for specific applications, including good biocompatibility, suitable mechanical properties, satisfied porosity, and controlled degradability. (Arbade et al., 2020) (Janoušková, 2018) The satisfied pore size for soft engineering is ~5–200 μM. (Janoušková, 2018) Regarding the mechanical properties, constructing scaffolds with matching mechanical properties to native soft tissues is very critical. Human tissues span a broad spectrum of mechanical properties, where stiffness of soft tissues typically ranges from 1 kPa (e.g., brain) to ~1 MPa (e.g., nerve and cartilage). (Guimarães et al., 2020) Over the past decades, numerous approaches have been developed for fabricating natural polymer-based scaffolds, such as electrospinning, freeze-drying, and 3D printing. In this section, we provide a general overview of these approaches and discuss their use in processing natural polymers into functional scaffolds.

Electrospinning

Electrospinning offers a convenient approach to fabricate fiber-based scaffolds for soft tissue repair. Nanofibers can be fabricated through electrospinning from polymer solutions under a high electrical field and further organized into porous nanofiber-based mats. When designing an ideal electrospun scaffold for soft tissue repair, some critical factors need to be considered. These factors include biocompatibility, mechanical properties, porosity, and the ability to regulate cellular behavior (Zhong et al., 2022). Many studies have been reported on fabrication of natural polymer-based scaffolds using electrospinning. Lee et al. fabricated electrospun nanofibrous gelatin sheets and investigated the influence of electron beam (e-beam) irradiation doses on the molecular weight, morphology, pore structure, and cell proliferation profiles of the sheets (Lee et al., 2017). In addition, electrospinning using a core-shell nozzle was employed to make collagen/polyvinylpyrrolidone (PVP) core-shell nanofibers where the collagen was encapsulated within a shell of PVP. The PVP shell was then washed away in a basic ethanol solution to yield anisotropic collagen nanofibers which mimics the structures of the native extracellular matrix (Wakuda et al., 2018). It is worth mentioning here that the structure of the nanofiber-based mats mimics the structure of the natural extracellular matrix, providing a biomimetic microenvironment for cells to proliferate and differentiate (Nie et al., 2020). Moreover, some strategies have been developed to enhance the physical properties and biofunctions of the scaffolds. These scaffolds have been widely used in several soft tissue engineering, such as skin, vascular tissue, cavernous nerve (CN) and cardiac tissues (Ehrmann, 2021). For instance, Uibo et al. demonstrated that the scaffold composed of salmon fibrinogen and chitosan could promote wound healing without any complications (Laidmäe et al., 2018). Jadbabaei et al. developed a novel approach to enhance the electrospinnability of sodium alginate and made alginate-PVA polymeric scaffolds for skin tissue engineering applications (Jadbabaei et al., 2021). Zhang et al. successfully fabricated silk-based scaffolds for cavernous nerve (CN) regeneration using coaxial electrospinning. The scaffolds with a core of RSF-VEGF and a shell of RSF-BDNF promoted the regeneration of cavernous nerves and were able to converse into nerve guidance conduit to facilitate nerve regeneration (Figure 1A) (Zhang et al., 2016). Recombinant spider silk protein (pNSR32) and gelatin (Gt) were also used to enhance the cytocompatibility of electrospun PCL scaffolds. The pNSR32/PCL/Gt composite scaffolds show potential for small-caliber vascular tissue engineering (Xiang et al., 2018). Wu et al. designed a scaffold for cardiac tissue regeneration to guide the orientation of the cells by mimicking the anisotropic cardiac structure (Wu Y. et al., 2017). The scaffold within a hydrogel shell was composed of aligned electrospun conductive nanofibers (NEYs-NET) which contained the polycaprolactone, silk fibroin, and carbon nanotubes. Cardiomyocytes (CMs) were aligned along the nanofibers on each layer of the 3D nanofibrous scaffold in the stable hydrogel environment (Figure 1B). Overall, the electrospinning technique allows researchers to fabricate ECM-mimic nanofibrous scaffolds with tunable fiber diameters, surface areas, porosity depending on different technique factors, such as solution viscosity and work voltage. Furthermore, electrospinning provides the feasibility for introducing and incorporating bioactive molecules for soft tissue repair and regeneration (Arbade et al., 2019).

Freeze-drying

Freeze-drying is an easy and eco-friendly method that can be readily used to fabricate 3D scaffolds with microporous structures. For fabrication of natural polymer-based scaffolds,

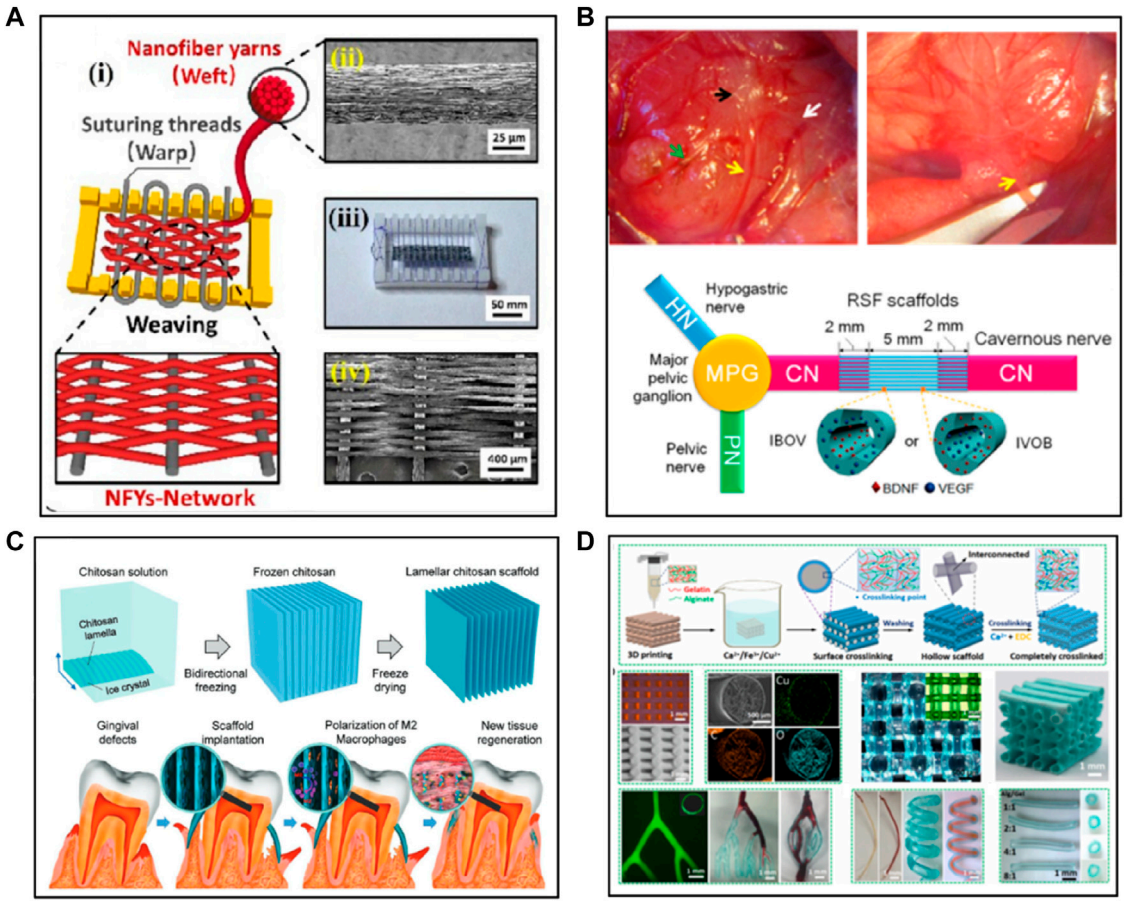

FIGURE 1
The fabrication of natural polymer-based scaffolds via various methods: **(A,B)** Electrospinning. **(C)** Freeze-drying and **(D)** 3D printing. The pictures got permissions from (Zhang et al., 2016), (Wu Y. et al., 2017), (Feng et al., 2021), (Luo et al., 2022), respectively.

natural polymers were first dissolved in water to obtain aqueous solutions, followed by freeze-drying. During freeze-drying, the water in the frozen sample undergoes sublimation under a high vacuum, leading to the scaffolds with porous structures. The pore size in the scaffolds depends on the type of natural polymers and the concentration of the solution. The porous structures generated via freeze-drying benefit the cells to attach, differentiate, proliferate, and mass transport. Indurkar et al. showed that the physical parameters of the scaffolds, such as surface roughness, porosity, interconnectivity, and contact angle influence the transport of nutrition and waste products (Indurkar et al., 2020). Furthermore, Afjoul et al. prepared alginate-gelatin scaffolds through freezing dry and revealed that the ratio of alginate to gelatin affects swelling, biodegradation, cell culture, and mechanical properties of the scaffolds. The optimized scaffolds showed good biocompatibility and satisfied outcomes of wound healing in rats (Afjoul et al., 2020). In another study, Chen et al. prepared a hybrid cobalt-doped alginate/waterborne polyurethane 3D porous scaffold with nano-topology of a "coral reef-like" rough surface via two-step freeze-drying (Chen et al., 2021). The "coral reef-like" rugged surface topology and bioactive cobalt dopant synergistically promote the neurite outgrowth and up-regulate the synaptophysin expression of neuron-like cells PC12 on the scaffold. In addition, two types of cellulose-derived materials, oxidized cellulose and carboxymethyl cellulose (CMC), were mixed with collagen to fabricate scaffolds through freeze drying. The prepared scaffolds showed good mechanical properties, hemostasis, and antibacterial properties (Kacvinská et al., 2022). Protein-based scaffolds have also been developed. For example, dual-crosslinked silk fibroin scaffolds with EGDE have been developed, where the researchers showed that an appropriate dosage of crosslinking agent was critical to achieve good mechanical properties, *in vivo* degradability, and mild immune responses in soft tissue engineering (Mao et al., 2021). The scaffold notably relieved the inflammatory response of microglial cells BV2 with the transformation from pro-inflammatory (M1) to anti-inflammatory (M2) phenotype.

Regarding better control of the structure, morphology, and density of scaffolds, Jiang et al. developed chitosan scaffolds with tunable microchannels by combining a 3D printing-assisted microfiber templates-leaching approach and a freeze-drying approach (Jiang et al., 2021). Moreover, Feng et al. fabricated a novel chitosan scaffold with lamellar structures by mimicking the layered structure of the attached gingiva using a bidirectional freeze-drying method (Feng et al., 2021). The bio-inspired lamellar chitosan scaffold (LCS) with ordered porous structure showed excellent mechanical properties, good cell-compatibility and could promote the vessel formation and gingival tissue regeneration *in vivo*. In addition, the LCS is found to be capable of inducing macrophage differentiation to M2 macrophages, which is thought to play an important role in tissue regeneration (Figure 1C). Also, the microstructure of the scaffolds could be controlled by optimizing the mold and freezing parameters for a certain application. Brougham et al. developed organ-specific collagen-based scaffolds geometries for tissue engineering applications, where the geometries of the scaffolds could be tailored by adjusting the mold patterns and freezing parameters (Brougham et al., 2017). In a brief summary, freeze-drying is a good method for natural polymer-based scaffold fabrication since it is easily applied to obtain porous structures without a high temperature or a washing step though the fabrication time is relatively long (Boffito et al., 2014).

3D printing

Three-dimensional (3D) printing is a technique that can be used to fabricate biomedical scaffolds in a controlled way (Pérez-Köhler et al., 2021). Compared with traditional thermal-based 3D printing, 3D bioprinting combines 3D printing with living cells or other non-living biological materials (e.g., growth factors, drugs) to construct scaffolds for tissue engineering and tissue regeneration. 3D bioprinting allows researchers to design 3D tissue-mimicking scaffolds which provide tailored cellular environments to facilitate the growth and proliferation of cells (Kim et al., 2016; Perez-Puyana et al., 2020). A broad range of natural polymer-based scaffolds have been fabricated using 3D bioprinting and some studies have been reported. Regarding the materials used for making the bioinks, a variety of materials have been used including collagen, gelatin, alginate, silk fibroin, and extra cellular matrix (ECM). For example, Jang et al. fabricated the artificial skin based on decellularized ECM derived from porcine skin via 3D bioprinting method (Jang et al., 2021). The 3D printed artificial skin exhibited rapid re-epithelialization and facilitate tissue regeneration on a mouse chimney wound model, showing great potential of clinical translation. In addition, alginate-based scaffolds with the features of high cell viability and low concentration alginate for potential nerve tissue engineering application were developed (Naghieh et al., 2019). Moreover, Tijore et al. developed a 3D bioprinting microchannel gelatin hydrogel that promoted human mesenchymal stem cells (hMSCs) myocardial commitment and supports native cardiomyocytes (CMs) contractile functionality (Tijore et al., 2018). Luo et al. used gelatin and alginate to fabricate scaffolds with microporous structures and interconnected microchannels using 3D bioprinting (Figure 1D) (Luo et al., 2022). The fabricated scaffold could support vascularization and growth of new tissues, promoting wound healing. Furthermore, Wang et al. fabricated a hybrid hydrogel system using a combination of decellularized extracellular matrix (dECM-G) and photo-crosslinkable gelatin methacrylate (GelMA) for nerve regeneration (Wang et al., 2022). The system showed good printability and structural fidelity for facilitating neurite growth and cell migration. Fabrication of scaffolds with designed microstructures to guide cell growth also attracts a lot of attention recently. Wu et al. precisely controlled architectures of micro-structured and stretchable chitosan hydrogels for guided cell growth (Wu Q. et al., 2017). The hybrid bioink prepared with gelatin, sodium alginate, and carbon nanotubes were used to fabricate cylindrical scaffolds through a combination of the vertical directional extrusion of printing nozzle and axial rotation of stepper motor module for blood vessel regeneration (Li et al., 2020).

Challenges and opportunities

Natural polymer-based scaffolds have been rapidly developed and applied in soft tissue repair in the past few decades. Some products are now commercially available and in clinical use. However, some limitations are associated with the current products, such as unsatisfied mechanical properties, uncontrolled degradability, and unfavorable immune response. Some critical points need to be considered when developing high-performance scaffolds that better meet clinical needs. Firstly, advanced processing approaches are required to achieve high-quality processing of natural polymers. For collagen-based materials, how to maintain their bioactivity during processing is a challenge. Secondly, rational materials design and advanced fabrication technologies are needed since the structures and properties of the scaffolds should be tailored for different applications. For instance, for treating pelvic organ prolapse, porous scaffolds with robust mechanical properties and controlled biodegradability are required. In some applications, an aligned scaffold is preferred to allow the cells to grow directionally. Moreover, enhancing the biocompatibility and mimicking the biological functions of the extracellular matrix should be considered. Integrins and cadherins can be grafted to the scaffolds since they are serving as adhesion molecules for migration and localization of cells. Furthermore, patient-oriented scaffold design with the

assistance of the 3D printing fabrication technique is of great potential to offer precise repair. Thirdly, scaffolds with bioresponsiveness or biofunctions are promising since such scaffolds allow better tissue repair control. For example, scaffolds with the incorporation of antibiotics can effectively prevent infections during the tissue regeneration process. In addition, growth factors can be incorporated into scaffolds to facilitate tissue repair. Lastly, a comprehensive understanding of the materials-cell interactions is needed to support the development of novel functional scaffolds. The fundamental research would lay a solid foundation for novel material designs, the development of advanced fabrication techniques, and clinical translations.

Author contributions

MC, RJ, ND, XZ, and XL wrote the manuscript; XL and CG conceived the idea of the study, supervised, and wrote the manuscript.

Funding

This work was supported by The National Health Commission of the People's Republic of China Research Fund (WKJ-ZJ-2215) and National Natural Science Foundation of China (No. 52103129).

Conflict of interest

The authors declare that the research was conducted in the absence of any commercial or financial relationships that could be construed as a potential conflict of interest.

Publisher's note

All claims expressed in this article are solely those of the authors and do not necessarily represent those of their affiliated organizations, or those of the publisher, the editors and the reviewers. Any product that may be evaluated in this article, or claim that may be made by its manufacturer, is not guaranteed or endorsed by the publisher.

Supplementary material

The Supplementary Material for this article can be found online at: https://www.frontiersin.org/articles/10.3389/fbioe.2022.954699/full#supplementary-material

References

Abdollahiyan, P., Oroojalian, F., and Mokhtarzadeh, A. (2021). The triad of nanotechnology, cell signalling, and scaffold implantation for the successful repair of damaged organs: An overview on soft-tissue engineering. *J. Control. Release* 332, 460–492. doi:10.1016/j.jconrel.2021.02.036

Afjoul, H., Shamloo, A., and Kamali, A. (2020). Freeze-gelled alginate/gelatin scaffolds for wound healing applications: An *in vitro*, *in vivo* study. *Mater. Sci. Eng. C* 113, 110957. doi:10.1016/j.msec.2020.110957

Al-Maawi, S., Herrera-Vizcaíno, C., Orlowska, A., Willershausen, I., Sader, R., Miron, R. J., et al. (2019). Biologization of collagen-based biomaterials using liquid-platelet-rich fibrin: New insights into clinically applicable tissue engineering. *Mater. (Basel)* 12 (23), 3993. doi:10.3390/ma12233993

Arbade, G. K., Kumar, V., Tripathi, V., Menon, A., Bose, S., Patro, T. U., et al. (2019). Emblica officinalis-loaded poly(ε-caprolactone) electrospun nanofiber scaffold as potential antibacterial and anticancer deployable patch. *New J. Chem.* 43 (19), 7427–7440. doi:10.1039/C9NJ01137D

Arbade, G. K., Srivastava, J., Tripathi, V., Lenka, N., and Patro, T. U. (2020). Enhancement of hydrophilicity, biocompatibility and biodegradability of poly(ε-caprolactone) electrospun nanofiber scaffolds using poly(ethylene glycol) and poly(L-lactide-co-ε-caprolactone-co-glycolide) as additives for soft tissue engineering. *J. Biomaterials Sci. Polym. Ed.* 31 (13), 1648–1670. doi:10.1080/09205063.2020.1769799

Avolio, E., Alvino, V. V., Ghorbel, M. T., and Campagnolo, P. (2017). Perivascular cells and tissue engineering: Current applications and untapped potential. *Pharmacol. Ther.* 171, 83–92. doi:10.1016/j.pharmthera.2016.11.002

Bajuri, M. Y., Sabri, S., Mazli, N., Sarifulnizam, F. A., and Mohd Apandi, H. (2021). Osteochondral injury of the talus treated with cell-free hyaluronic acid-based scaffold (Hyalofast®) - a reliable solution. *Cureus* 13 (9), e17928. doi:10.7759/cureus.17928

Bianchi, E., Ruggeri, M., Rossi, S., Vigani, B., Miele, D., Bonferoni, M. C., et al. (2021). Innovative strategies in tendon tissue engineering. *Pharmaceutics* 13 (1), 89. doi:10.3390/pharmaceutics13010089

Boffito, M., Sartori, S., and Ciardelli, G. (2014). Polymeric scaffolds for cardiac tissue engineering: Requirements and fabrication technologies. *Polym. Int.* 63 (1), 2–11. doi:10.1002/pi.4608

Brougham, C. M., Levingstone, T. J., Shen, N., Cooney, G. M., Jockenhoevel, S., Flanagan, T. C., et al. (2017). Freeze-drying as a novel biofabrication method for achieving a controlled microarchitecture within large, complex natural biomaterial scaffolds. *Adv. Healthc. Mat.* 6 (21), 1700598. doi:10.1002/adhm.201700598

Caillol, S. (2020). Special issue "natural polymers and biopolymers II. *Molecules* 26 (1), 112. doi:10.3390/molecules26010112

Chen, Y., Long, X., Lin, W., Du, B., Yin, H., Lan, W., et al. (2021). Bioactive 3D porous cobalt-doped alginate/waterborne polyurethane scaffolds with a coral reef-like rough surface for nerve tissue engineering application. *J. Mat. Chem. B* 9 (2), 322–335. doi:10.1039/d0tb02347g

Clavé, A., Potel, J. F., Servien, E., Neyret, P., Dubrana, F., Stindel, E., et al. (2016). Third-generation autologous chondrocyte implantation versus mosaicplasty for knee cartilage injury: 2-year randomized trial. *J. Orthop. Res.* 34 (4), 658–665. doi:10.1002/jor.23152

Ehrmann, A. (2021). Non-toxic crosslinking of electrospun gelatin nanofibers for tissue engineering and biomedicine-A review. *Polym. (Basel)* 13 (12), 1973. doi:10.3390/polym13121973

Entekhabi, E., Haghbin Nazarpak, M., Shafieian, M., Mohammadi, H., Firouzi, M., Hassannejad, Z., et al. (2021). Fabrication and *in vitro* evaluation of 3D composite scaffold based on collagen/hyaluronic acid sponge and electrospun polycaprolactone nanofibers for peripheral nerve regeneration. *J. Biomed. Mat. Res. A* 109 (3), 300–312. doi:10.1002/jbm.a.37023

Eviana Putri, N. R., Wang, X., Chen, Y., Li, X., Kawazoe, N., Chen, G., et al. (2020). Preparation of PLGA-collagen hybrid scaffolds with controlled pore structures for cartilage tissue engineering. *Prog. Nat. Sci. Mater. Int.* 30 (5), 642–650. doi:10.1016/j.pnsc.2020.07.003

Feng, Y., Gao, H. L., Wu, D., Weng, Y. T., Wang, Z. Y., Yu, S. H., et al. (2021). Biomimetic lamellar chitosan scaffold for soft gingival tissue regeneration. *Adv. Funct. Mat.* 31 (43), 2105348. doi:10.1002/adfm.202105348

Gaharwar, A. K., Singh, I., and Khademhosseini, A. (2020). Engineered biomaterials for *in situ* tissue regeneration. *Nat. Rev. Mat.* 5 (9), 686–705. doi:10.1038/s41578-020-0209-x

Gang, Y., Yansha, Q., Yan, L., Lu, W., and Hongbing, H. (2021). Preparation and characterization of polylactic acid-caprolactone/fibrinogen nanofiber based hernia mesh. *J. Text. Res.* 42 (01), 40–45. doi:10.13475/j.fzxb.20200301106

Gao, F., Xu, Z., Liang, Q., Li, H., Peng, L., Wu, M., et al. (2019). Osteochondral regeneration with 3D-printed biodegradable high-strength supramolecular polymer reinforced-gelatin hydrogel scaffolds. *Adv. Sci. (Weinh).* 6 (15), 1900867. doi:10.1002/advs.201900867

González-Pérez, F., Ibáñez-Fonseca, A., Alonso, M., and Rodríguez-Cabello, J. C. (2021). Combining tunable proteolytic sequences and a VEGF-mimetic peptide for the spatiotemporal control of angiogenesis within Elastin-Like Recombinamer scaffolds. *Acta Biomater.* 130, 149–160. doi:10.1016/j.actbio.2021.06.005

Ha, J. H., Jeong, Y., Koo, Y. T., Jeon, S., Chung, J., Kim, S., et al. (2020). Effect of collagen matrix on postoperative palatal fistula in cleft palate repair. *Sci. Rep.* 10 (1), 15236. doi:10.1038/s41598-020-72046-y

Haaparanta, A. M., Järvinen, E., Cengiz, I. F., Ellä, V., Kokkonen, H. T., Kiviranta, I., et al. (2014). Preparation and characterization of collagen/PLA, chitosan/PLA, and collagen/chitosan/PLA hybrid scaffolds for cartilage tissue engineering. *J. Mat. Sci. Mat. Med.* 25 (4), 1129–1136. doi:10.1007/s10856-013-5129-5

Henriksen, N. A., Jensen, K. K., and Jorgensen, L. N. (2017). "The biology of hernia formation," in *Textbook of hernia*. Editors W. W. Hope, W. S. Cobb, and G. L. Adrales (Cham: Springer International Publishing), 1–5. doi:10.1007/978-3-319-43045-4_1

Hormozi, M., Assaei, R., and Boroujeni, M. B. (2017). The effect of aloe vera on the expression of wound healing factors (TGFβ1 and bFGF) in mouse embryonic fibroblast cell: *In vitro* study. *Biomed. Pharmacother.* 88, 610–616. doi:10.1016/j.biopha.2017.01.095

Indurkar, A., Bangde, P., Gore, M., Agrawal, A. K., Jain, R., Dandekar, P., et al. (2020). Fabrication of guar gum-gelatin scaffold for soft tissue engineering. *Carbohydr. Polym. Technol. Appl.* 1, 100006. doi:10.1016/j.carpta.2020.100006

Jadbabaei, S., Kolahdoozan, M., Naeimi, F., and Ebadi-Dehaghani, H. (2021). Preparation and characterization of sodium alginate–PVA polymeric scaffolds by electrospinning method for skin tissue engineering applications. *RSC Adv.* 11 (49), 30674–30688. doi:10.1039/D1RA04176B

Jang, K. S., Park, S. J., Choi, J. J., Kim, H. N., Shim, K. M., Kim, M. J., et al. (2021). Therapeutic efficacy of artificial skin produced by 3D bioprinting. *Mater. (Basel)* 14 (18), 5177. doi:10.3390/ma14185177

Janoušková, O. (2018). Synthetic polymer scaffolds for soft tissue engineering. *Physiol. Res.* 67, S335–S348. doi:10.33549/physiolres.933983

Jiang, Z., Zhang, K., Du, L., Cheng, Z., Zhang, T., Ding, J., et al. (2021). Construction of chitosan scaffolds with controllable microchannel for tissue engineering and regenerative medicine. *Mater. Sci. Eng. C* 126, 112178. doi:10.1016/j.msec.2021.112178

Kacvinská, K., Trávničková, M., Vojtová, L., Poláček, P., Dorazilová, J., Kohoutek, M., et al. (2022). Porous cellulose-collagen scaffolds for soft tissue regeneration: Influence of cellulose derivatives on mechanical properties and compatibility with adipose-derived stem cells. *Res. Square).* doi:10.21203/rs.3.rs-1187939/v1

Kakudo, N., Morimoto, N., Ogawa, T., and Kusumoto, K. (2020). Effects of fibroblast growth factor-2 combined with a collagen/gelatin sponge for adipogenesis in the mouse subcutis. *Ann. Plast. Surg.* 84 (2), 216–221. doi:10.1097/sap.0000000000002046

Kanatlı, U., Eren, A., Eren, T. K., and Vural, A. (2017). Treatment of osteochondral lesions of the talus with cell-free polymer-based scaffold in single-step arthroscopic surgery. *Arthrosc. Tech.* 6 (5), e1727–e1734. doi:10.1016/j.eats.2017.06.043

Kayaalp, M. E., Cirdi, Y. U., Kopf, S., and Becker, R. (2021). Prone-positioned knee arthroscopy for isolated retropatellar cartilage defects with gel-type autologous chondrocyte implantation. *Oper. Orthop. Traumatol.* 33 (5), 436–444. doi:10.1007/s00064-021-00710-1

Keane, T. J., and Badylak, S. F. (2014). ""Biomaterials for tissue engineering applications," in *Seminars in pediatric surgery* (Elsevier), 112–118. doi:10.1053/j.sempedsurg.2014.06.010

Kim, J. E., Kim, S. H., and Jung, Y. (2016). Current status of three-dimensional printing inks for soft tissue regeneration. *Tissue Eng. Regen. Med.* 13 (6), 636–646. doi:10.1007/s13770-016-0125-8

Kim, J. S., Choi, J., Ki, C. S., and Lee, K. H. (2021). 3D silk fiber construct embedded dual-layer PEG hydrogel for articular cartilage repair - *in vitro* assessment. *Front. Bioeng. Biotechnol.* 9, 653509. doi:10.3389/fbioe.2021.653509

Kim, W. J., Yun, H.-S., and Kim, G. H. (2017). An innovative cell-laden α-TCP/collagen scaffold fabricated using a two-step printing process for potential application in regenerating hard tissues. *Sci. Rep.* 7 (1), 3181. doi:10.1038/s41598-017-03455-9

Laidmäe, I., Ērglis, K., Cēbers, A., Janmey, P. A., and Uibo, R. (2018). Salmon fibrinogen and chitosan scaffold for tissue engineering: *In vitro* and *in vivo* evaluation. *J. Mat. Sci. Mat. Med.* 29 (12), 182. doi:10.1007/s10856-018-6192-8

Lee, J. B., Ko, Y. G., Cho, D., Park, W. H., and Kwon, O. H. (2017). Modification and optimization of electrospun gelatin sheets by electron beam irradiation for soft tissue engineering. *Biomater. Res.* 21, 14. doi:10.1186/s40824-017-0100-z

Lee, J. H., and Park, J. H. (2020). Can genoss DES™ stand out in the crowd of stents? *Korean Circ. J.* 50 (4), 328. doi:10.4070/kcj.2020.0040

Li, L., Qin, S., Peng, J., Chen, A., Nie, Y., Liu, T., et al. (2020). Engineering gelatin-based alginate/carbon nanotubes blend bioink for direct 3D printing of vessel constructs. *Int. J. Biol. Macromol.* 145, 262–271. doi:10.1016/j.ijbiomac.2019.12.174

Liang, S., Chen, J., Zhang, Y., Ma, Y. D., Ma, C. C., Ye, Y., et al. (2021). Long-term mesh-related complications after total pelvic reconstruction surgery with tension-free transvaginal mesh. *Zhonghua Yi Xue Za Zhi* 101 (24), 1908–1914. doi:10.3760/cma.j.cn112137-20210306-00575

Liao, J., Qu, Y., Chu, B., Zhang, X., and Qian, Z. (2015). Biodegradable CSMA/PECA/graphene porous hybrid scaffold for cartilage tissue engineering. *Sci. Rep.* 5, 9879. doi:10.1038/srep09879

Luo, Y., Zhang, T., and Lin, X. (2022). 3D printed hydrogel scaffolds with macro pores and interconnected microchannel networks for tissue engineering vascularization. *Chem. Eng. J.* 430, 132926. doi:10.1016/j.cej.2021.132926

Mao, Z., Bi, X., Ye, F., Du, P., Shu, X., Sun, L., et al. (2021). The relationship between crosslinking structure and silk fibroin scaffold performance for soft tissue engineering. *Int. J. Biol. Macromol.* 182, 1268–1277. doi:10.1016/j.ijbiomac.2021.05.058

Masson-Meyers, D. S., and Tayebi, L. (2021). Vascularization strategies in tissue engineering approaches for soft tissue repair. *J. Tissue Eng. Regen. Med.* 15 (9), 747–762. doi:10.1002/term.3225

Naghieh, S., Foroozmehr, E., Badrossamay, M., and Kharaziha, M. (2017). Combinational processing of 3D printing and electrospinning of hierarchical poly(lactic acid)/gelatin-forsterite scaffolds as a biocomposite: Mechanical and biological assessment. *Mater. Des.* 133, 128–135. doi:10.1016/j.matdes.2017.07.051

Naghieh, S., Sarker, M. D., Abelseth, E., and Chen, X. (2019). Indirect 3D bioprinting and characterization of alginate scaffolds for potential nerve tissue engineering applications. *J. Mech. Behav. Biomed. Mat.* 93, 183–193. doi:10.1016/j.jmbbm.2019.02.014

Nie, K., Han, S., Yang, J., Sun, Q., Wang, X., Li, X., et al. (2020). Enzyme-crosslinked electrospun fibrous gelatin hydrogel for potential soft tissue engineering. *Polym. (Basel)* 12 (9), 1977. doi:10.3390/polym12091977

Niemeyer, P., Pestka, J. M., Kreuz, P. C., Erggelet, C., Schmal, H., Suedkamp, N. P., et al. (2008). Characteristic complications after autologous chondrocyte implantation for cartilage defects of the knee joint. *Am. J. Sports Med.* 36 (11), 2091–2099. doi:10.1177/0363546508322131

Parmaksiz, M., Elçin, A. E., and Elçin, Y. M. (2019). Decellularized bovine small intestinal submucosa-PCL/hydroxyapatite-based multilayer composite scaffold for hard tissue repair. *Mater. Sci. Eng. C* 94, 788–797. doi:10.1016/j.msec.2018.10.011

Pérez-Köhler, B., Benito-Martínez, S., Gómez-Gil, V., Rodríguez, M., Pascual, G., Bellón, J. M., et al. (2021). New insights into the application of 3D-printing technology in hernia repair. *Mater. (Basel)* 14 (22), 7092. doi:10.3390/ma14227092

Perez-Puyana, V., Jiménez-Rosado, M., Romero, A., and Guerrero, A. (2020). Polymer-based scaffolds for soft-tissue engineering. *Polym. (Basel)* 12 (7), 1566. doi:10.3390/polym12071566

Rao, S. H., Harini, B., Shadamarshan, R. P. K., Balagangadharan, K., and Selvamurugan, N. (2018). Natural and synthetic polymers/bioceramics/bioactive compounds-mediated cell signalling in bone tissue engineering. *Int. J. Biol. Macromol.* 110, 88–96. doi:10.1016/j.ijbiomac.2017.09.029

Rodrigues, P., and Raz, S. (2022). The burden of reoperations and timeline of problems in 1, 530 cases of mesh-related complications. *Urol. Int.* 106 (3), 235–242. doi:10.1159/000514389

Rokn, A., Zare, H., and Haddadi, P. (2020). Use of mucograft collagen Matrix(®) versus free gingival graft to augment keratinized tissue around teeth: A randomized controlled clinical trial. *Front. Dent.* 17 (5), 1–8. doi:10.18502/fid.v17i1.3965

Taghipour, Y. D., Hokmabad, V. R., Del Bakhshayesh, A. R., Asadi, N., Salehi, R., Nasrabadi, H. T., et al. (2020). The application of hydrogels based on natural polymers for tissue engineering. *Curr. Med. Chem.* 27 (16), 2658–2680. doi:10.2174/0929867326666190711103956

Tanaka, T., Abe, Y., Cheng, C. J., Tanaka, R., Naito, A., Asakura, T., et al. (2020). Development of small-diameter elastin-silk fibroin vascular grafts. *Front. Bioeng. Biotechnol.* 8, 622220. doi:10.3389/fbioe.2020.622220

Tijore, A., Irvine, S. A., Sarig, U., Mhaisalkar, P., Baisane, V., Venkatraman, S., et al. (2018). Contact guidance for cardiac tissue engineering using 3D bioprinted gelatin patterned hydrogel. *Biofabrication* 10 (2), 025003. doi:10.1088/1758-5090/aaa15d

Turnbull, G., Clarke, J., Picard, F., Zhang, W., Riches, P., Li, B., et al. (2020). 3D biofabrication for soft tissue and cartilage engineering. *Med. Eng. Phys.* 82, 13–39. doi:10.1016/j.medengphy.2020.06.003

Wakuda, Y., Nishimoto, S., Suye, S. I., and Fujita, S. (2018). Native collagen hydrogel nanofibres with anisotropic structure using core-shell electrospinning. *Sci. Rep.* 8 (1), 6248. doi:10.1038/s41598-018-24700-9

Wang, T., Han, Y., Wu, Z., Qiu, S., Rao, Z., Zhao, C., et al. (2022). Tissue-specific hydrogels for three-dimensional printing and potential application in peripheral nerve regeneration. *Tissue Eng. Part A* 28 (3-4), 161–174. doi:10.1089/ten.TEA.2021.0093

Wu, Q., Maire, M., Lerouge, S., Therriault, D., and Heuzey, M.-C. (2017a). 3D printing of microstructured and stretchable chitosan hydrogel for guided cell growth. *Adv. Biosyst.* 1 (6), 1700058. doi:10.1002/adbi.201700058

Wu, Y., Wang, L., Guo, B., and Ma, P. X. (2017b). Interwoven aligned conductive nanofiber yarn/hydrogel composite scaffolds for engineered 3D cardiac anisotropy. *ACS Nano* 11 (6), 5646–5659. doi:10.1021/acsnano.7b01062

Xiang, P., Wang, S. S., He, M., Han, Y. H., Zhou, Z. H., Chen, D. L., et al. (2018). The *in vitro* and *in vivo* biocompatibility evaluation of electrospun recombinant spider silk protein/PCL/gelatin for small caliber vascular tissue engineering scaffolds. *Colloids Surfaces B Biointerfaces* 163, 19–28. doi:10.1016/j.colsurfb.2017.12.020

Yang, Z., Wu, Y., Li, C., Zhang, T., Zou, Y., Hui, J. H. P., et al. (2012). Improved mesenchymal stem cells attachment and *in vitro* cartilage tissue formation on chitosan-modified poly(L-lactide-co-epsilon-caprolactone) scaffold. *Tissue Eng. Part A* 18 (3-4), 242–251. doi:10.1089/ten.TEA.2011.0315

Zhang, Y., Huang, J., Huang, L., Liu, Q., Shao, H., Hu, X., et al. (2016). Silk fibroin-based scaffolds with controlled delivery order of VEGF and BDNF for cavernous nerve regeneration. *ACS Biomater. Sci. Eng.* 2 (11), 2018–2025. doi:10.1021/acsbiomaterials.6b00436

Zhao, H., and Li, M. (2011). "Preparation of braided silk as a tubular tissue engineering scaffold," in *7th China international silk conference on inheritance and innovation - modern silk road* (STAFA-ZURICH: Trans Tech Publications Ltd), 95–99. doi:10.4028/www.scientific.net/AMR.175-176.95

Zhao, Y., Zhu, Z. S., Guan, J., and Wu, S. J. (2021). Processing, mechanical properties and bio-applications of silk fibroin-based high-strength hydrogels. *Acta Biomater.* 125, 57–71. doi:10.1016/j.actbio.2021.02.018

Zhong, H., Huang, J., Wu, J., and Du, J. (2022). Electrospinning nanofibers to 1D, 2D, and 3D scaffolds and their biomedical applications. *Nano Res.* 15 (2), 787–804. doi:10.1007/s12274-021-3593-7

Zhou, B. G., Zhou, Q., Wang, P., Yuan, J. G., Yu, Y. Y., Deng, C., et al. (2018). HRP-mediated graft polymerization of acrylic acid onto silk fibroins and *in situ* biomimetic mineralization. *J. Mat. Sci. Mat. Med.* 29 (6), 72. doi:10.1007/s10856-018-6084-y

frontiers | Frontiers in Bioengineering and Biotechnology

TYPE Review
PUBLISHED 22 July 2022
DOI 10.3389/fbioe.2022.970041

OPEN ACCESS

EDITED BY
Kunyu Zhang,
South China University of Technology, China

REVIEWED BY
Zhiwei Fang,
Johns Hopkins University, United States
Hani Nasser Abdelhamid,
Assiut University, Egypt

*CORRESPONDENCE
Dongxu Wang,
wang_dong_xu@jlu.edu.cn

†These authors have contributed equally to this work

SPECIALTY SECTION
This article was submitted to Biomaterials, a section of the journal Frontiers in Bioengineering and Biotechnology

RECEIVED 15 June 2022
ACCEPTED 04 July 2022
PUBLISHED 22 July 2022

CITATION
Yang Z, Liu W, Liu H, Li R, Chang L, Kan S, Hao M and Wang D (2022), The applications of polysaccharides in dentistry.
Front. Bioeng. Biotechnol. 10:970041.
doi: 10.3389/fbioe.2022.970041

The applications of polysaccharides in dentistry

Zhijing Yang[1,3†], Weiwei Liu[1,3†], Huimin Liu[1,3], Rong Li[2], Lu Chang[1,3], Shaoning Kan[1,3], Ming Hao[1,3] and Dongxu Wang[2*]

[1]Department of Oral and Maxillofacial Surgery, Hospital of Stomatology, Jilin University, Changchun, China, [2]Laboratory Animal Center, College of Animal Science, Jilin University, Changchun, China, [3]Jilin Provincial Key Laboratory of Tooth Development and Bone Remodeling, Hospital of Stomatology, Jilin University, Changchun, China

Polysaccharides are natural polymers widely present in animals, plants, and several microorganisms. Polysaccharides have remarkable properties, including easy extractions, degradability, and renewability, and have no apparent toxicity, making them ideal for biomedical applications. Moreover, polysaccharides are suitable for repairing oral tissue defects and treating oral diseases due to their excellent biocompatibility, biosafety, anti-inflammatory, and antibacterial properties. The oral cavity is a relatively complex environment vulnerable to numerous conditions, including soft tissue diseases, hard tissue disorders, and as well as soft and hard tissue diseases, all of which are complex to treat. In this article, we reviewed different structures of natural polysaccharides with high commercial values and their applications in treating various oral disease, such as drug delivery, tissue regeneration, material modification, and tissue repair.

KEYWORDS

natural polysaccharide, oral disease, tissue repair, tissue regeneration, biomaterials

Introduction

Oral diseases are a global public health concern, often affecting the aesthetics and diet of patients, and in some cases, they cause systematic diseases (P aradowska-Stolarz et al., 2021; Wong et al., 2019). Treating oral diseases require many biological materials. Dental caries treatment requires filling the dental pulp with resin (Malkondu et al., 2014), pulp capping agent (Kunert and Lukomska-Szymanska, 2020), and gutta percha (Del Fabbro et al., 2016). Also, denture restoration, impression, and dental implant materials are required for tooth loss treatment (Roumanas, 2009). Tissue-guided regeneration and defect repair materials are necessary for oral surgery (Frassica and Grunlan, 2020; Niu et al., 2021). Toothpaste, floss, and mouthwash are needed to prevent oral diseases (Zhang et al., 2021). The common materials used in dentistry include polymethylmethacrylate (PMMA), vulcanized rubber, celluloid, phenol-formaldehyde, and polyvinyl chloride (PVC) (P aradowska-Stolarz et al., 2021). Ideal dentistry materials should possess high biocompatibility as well as good biofunction and mechanical properties (Abdelhamid and Mathew, 2022). In stomatology, natural polysaccharides are used to modify materials repairing chewing organs, and improve oral health (Vergnes and Mazevet, 2020).

Polysaccharides are natural branched or non-branched polymers, usually composed of more than 10 monosaccharides joined together *via* glycosidic bonds (Yu et al., 2018).

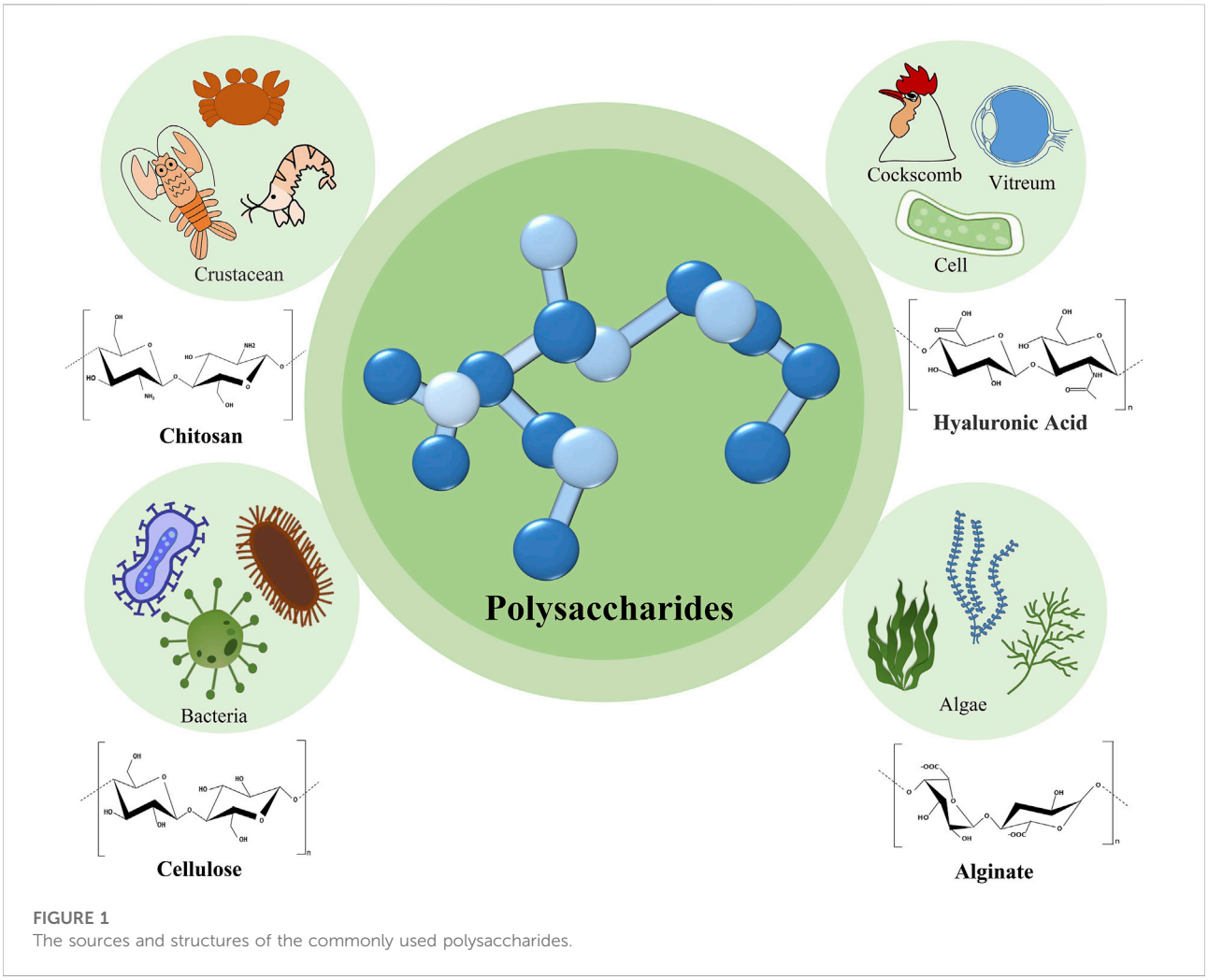

FIGURE 1
The sources and structures of the commonly used polysaccharides.

Polysaccharides are widely present in plants, microorganisms and animals. They possess anti-tumor, anti-oxidation, and anti-inflammatory properties, favouring their application in biomedicine (Silva et al., 2021). In recent years, natural polysaccharides and their derivatives have been widely used in packaging, food and pharmaceutical industries, and dentistry, given their sustainability, renewability, biodegradability, and non-toxicity. Also, the wide application of polysaccharides in the above-mentioned industries is attributed to their structural diversity (Torres et al., 2019). Materials used in the oral cavity are in direct contact with human tissue; thus, they should be biocompatible and non-toxic. Moreover, they should promote efficient healing of the mouth to perform its main functions, including chewing, breathing and talking (Whitters et al., 1999). In addition, given the role of the mouth on the facial outlook, the materials used in the oral cavity need special consideration. Previous reports have shown that natural polysaccharides have numerous advantages in treating oral diseases. In this review, we discussed several natural polysaccharides with high commercial values and their applications in treating different oral diseases.

Classification of polysaccharides

Polysaccharides can be broadly classified into homogeneous and heterogeneous polysaccharides. Homogeneous polysaccharides are derived from joining several monosaccharide molecules of the same kind, including starch, cellulose, and chitosan. Heterogeneous polysaccharides are derivatives of different monosaccharide molecules. The common heterogeneous polysaccharides include hyaluronic acid and chondroitin sulfate. Since they are naturally available, easy to obtain, non-toxic, cheap, biodegradable, and biocompatible, polysaccharides are suitable for the oral cavity environment (Prajapati et al., 2014). The most commonly used polysaccharides are shown in Figure 1.

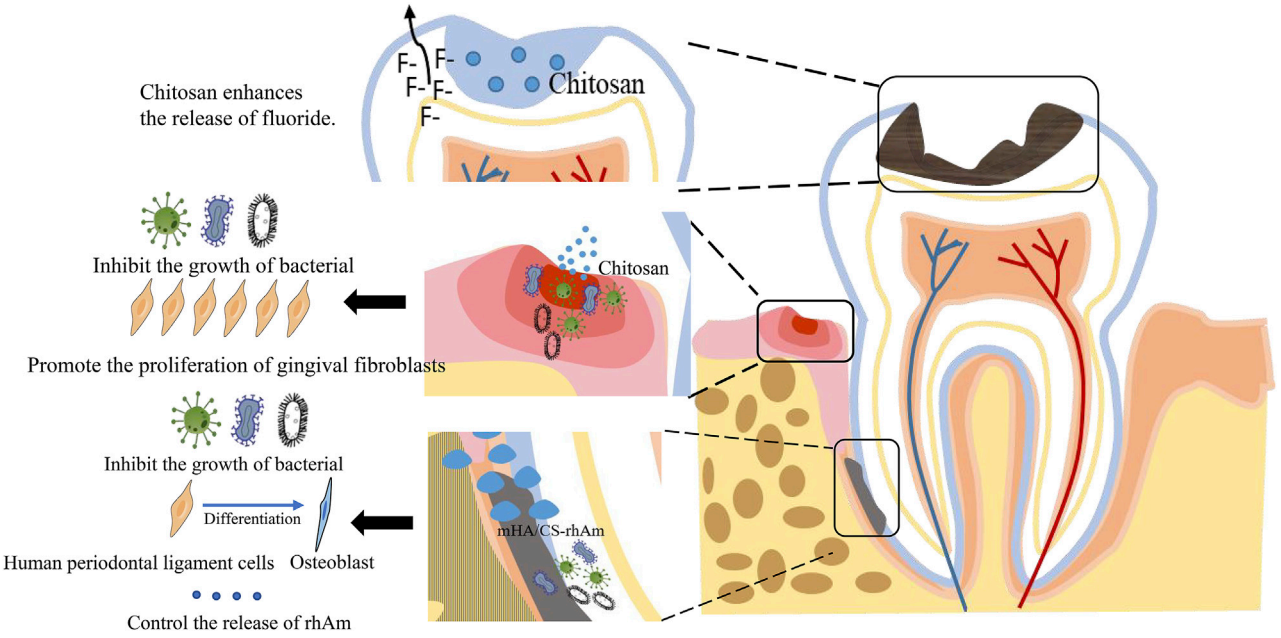

FIGURE 2
The applications of chitosan in dentistry.

Chitosan

Chitosan is a linear, semi-crystalline natural polysaccharide derived from chitin, readily available in crustaceans and fungal cell walls. The U.S. Food and Drug Administration (FDA) has approved chitosan for food and drug use (Wang et al., 2020). Chitosan contains random glucosamine (deacetylation unit) and N-acetylglucosamine (acetyl unit) units linked to the primary chain through *ß* (1–4) glycosidic bonds. Chitosan is positively charged due to the presence of the amino group (Abd El-Hack et al., 2020). The molecule has a straight-chain structure, and weighs between 10 and 1,000 kDa (Kou et al., 2021). Chitosan is widely utilized for antibacterial purposes (Muxika et al., 2017), drug release (Hudson and Margaritis, 2014), target therapy (Mushtaq et al., 2021; Narmani and Jafari, 2021), and drug delivery in stomatology (Ahsan et al., 2018). Studies have shown that it effectively inhibits the biofilm formation and the acid production capacity of *Streptococcus mutans*, the main causal agent of dental caries (Kawakita et al., 2019). Several delivery systems that carry drugs for anti-inflammatory purposes, tissue, and periodontitis treatment have been modeled around chitosan (Sah et al., 2019; Baranov et al., 2021). Chitosan has been used for modifying nanomaterials and hydrogel, and its derivatives for treating oral diseases have been gradually developed (Wang et al., 2020; Shivakumar et al., 2021) (Figure 2).

Cellulose

Cellulose is one of the most abundant biological polymers on Earth (Lynd et al., 2002). Plant cellulose is present in most green plants and algae. Bacterial cellulose is naturally secreted by several non-pathogenic bacteria, including *acetobacter*, agrobacterium, and rhizobium. Cellulose has a well-arranged three-dimensional fiber network, 3.0–3.5 μm thick (Klemm et al., 2005; Svensson et al., 2005). Compared with plant cellulose, bacterial cellulose, excluding lignin and hemicellulose, contains small fibers (100 times lower than plant cellulose) and has a highly crystalline structure. Heat, steam, ethylene oxide gas, and radiation will not destroy the inherent physicochemical properties and structural integrity of cellulose (de Oliveira Barud et al., 2020). The three-dimensional structure of cellulose is very similar to the extracellular matrix (ECM) of living tissues and, thus, suitable for preserving oxygen and nutrients, providing a favourable environment for the growth and proliferation of cells in stomatology (Halib et al., 2019). Moreover, cellulose can be used for tissue engineering as scaffolds and implants for wound healing, drug delivery, and dental materials (de Oliveira Barud et al., 2016; de Oliveira Barud et al., 2020; Klinthoopthamrong et al., 2020). Studies have shown that restorable BC could be used in GBR to improve bone generation. Moreover, the electron beam irradiation (EI) can sever the BC glucose bonds to increase biodegradation (An et al., 2017).

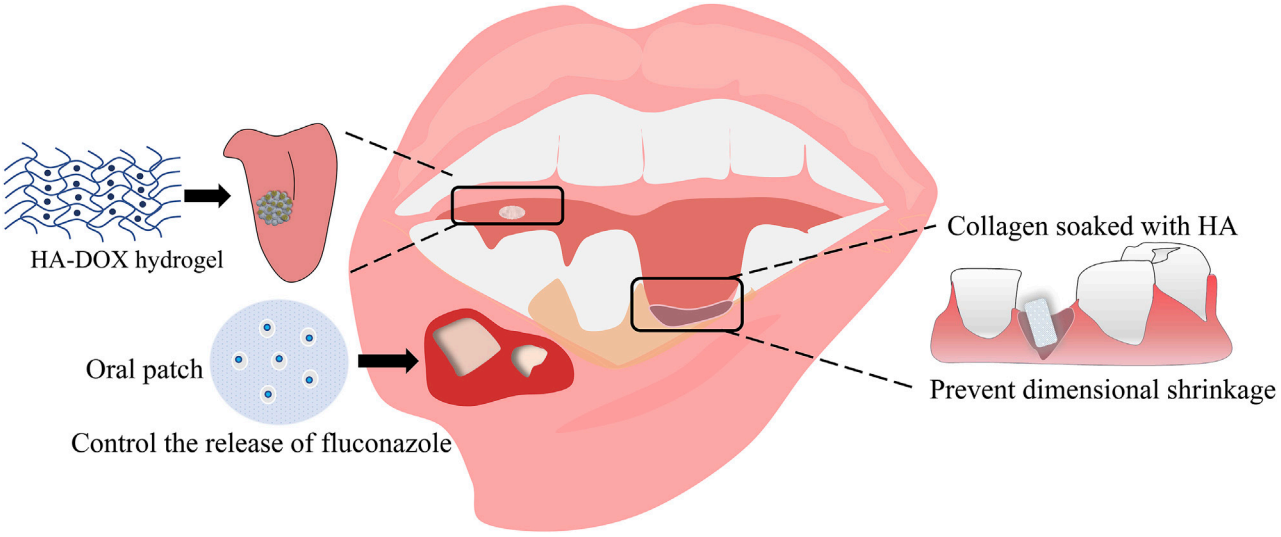

FIGURE 3
The applications of HA in dentistry.

Hyaluronic acid

Hyaluronic acid (HA) is a glycosaminoglycan composed of repeated N-acetyl D-glucosamine and D-glucuronic acid units (Marinho et al., 2021). It is the main skin extracellular matrix (ECM) component and participates in inflammatory responses, angiogenesis, and tissue regeneration. Given its anti-inflammatory property, HA is often used to treat oral ulcers (Graca et al., 2020). HA is also a good drug delivery system, given its mucosal adhesion and ease of chemical modification (Huang and Huang, 2018; Salari et al., 2021). Notably, a local administration strategy is preferred for treating oral diseases than systemic administration. HA does not affect other body organs and tissues when used for drug delivery. Moreover, the local treatment ensures better delivery of drugs to soft periodontal tissue, gingiva, periodontal ligament, and hard tissues, such as alveolar bone and cementum. Catechol (Cat)-modified chitosan/hyaluronic acid nanoparticles (NPs) is a newly developed system for delivering doxorubicin (DOX) to oral squamous cell carcinoma. It displays excellent adhesion to the oral mucosa and delivery of DOX to the target tissues in a sustained manner (Pornpitchanarong et al., 2020). HA has good biocompatibility, biodegradability, and hydrophilicity and can alleviate inflammatory pain. These desired biological properties promote the use of HA in the oral cavity (Figure 3).

Marine algae polysaccharides

Seaweed polysaccharides, including alginate, agar, carrageenan, galactan, fucoidan, urfan, and laver polysaccharides, are widely used in pharmaceutical industry (Rahmati et al., 2019; Beaumont et al., 2021). Marine algae polysaccharides possess numerous physical and chemical properties. These types of polysaccharides are soft and expansible (Bilal and Iqbal, 2019). Sodium alginate and agarose, widely used in treating oral diseases, are the common marine algae polysaccharides. Sodium alginate was included on the list of Pharmacopoeia products in the United States as early as 1938. Sodium alginate is a by-product of kelp or sargassum, ß-D-mannuronic acid (β-D-mannuronic, m), and *a*- L-guluronic acid (α-L-guluronic, g), joined together *via* the 1 → 4 linkages. The compound is stable, soluble, viscous, and safe, suitable for pharmaceutical use (Sanchez-Ballester et al., 2021). Furthermore, it contains numerous -COO- units that give it its polyanionic behavior in an aqueous solution, facilitating drug attachment and adhesion to the mucosal membrane (Amin and Boateng, 2022). Some studies have suggested that sodium alginate could treat recurrent aphthous ulcers. The compound can alleviate the pain and improve the persistence of a drug in the oral mucosa (Laffleur and Kuppers, 2019; Suharyani et al., 2021). In addition, alginate is mainly used for stomatology as an impression of oral materials (Cervino et al., 2018). Obtaining an oral model is an important step before orthodontics and prosthodontics treatment. Alginate impression materials have remarkable fluidity, resilience, plasticity, and high drug delivery accuracy, promoting their clinical use.

Agarose is a linear polymer polysaccharide extracted from kelp (Zucca et al., 2016), composed of alternating 1→3-linked ß-Dgalactopyranose and 1→4-linked 3,6 anhydro-α-

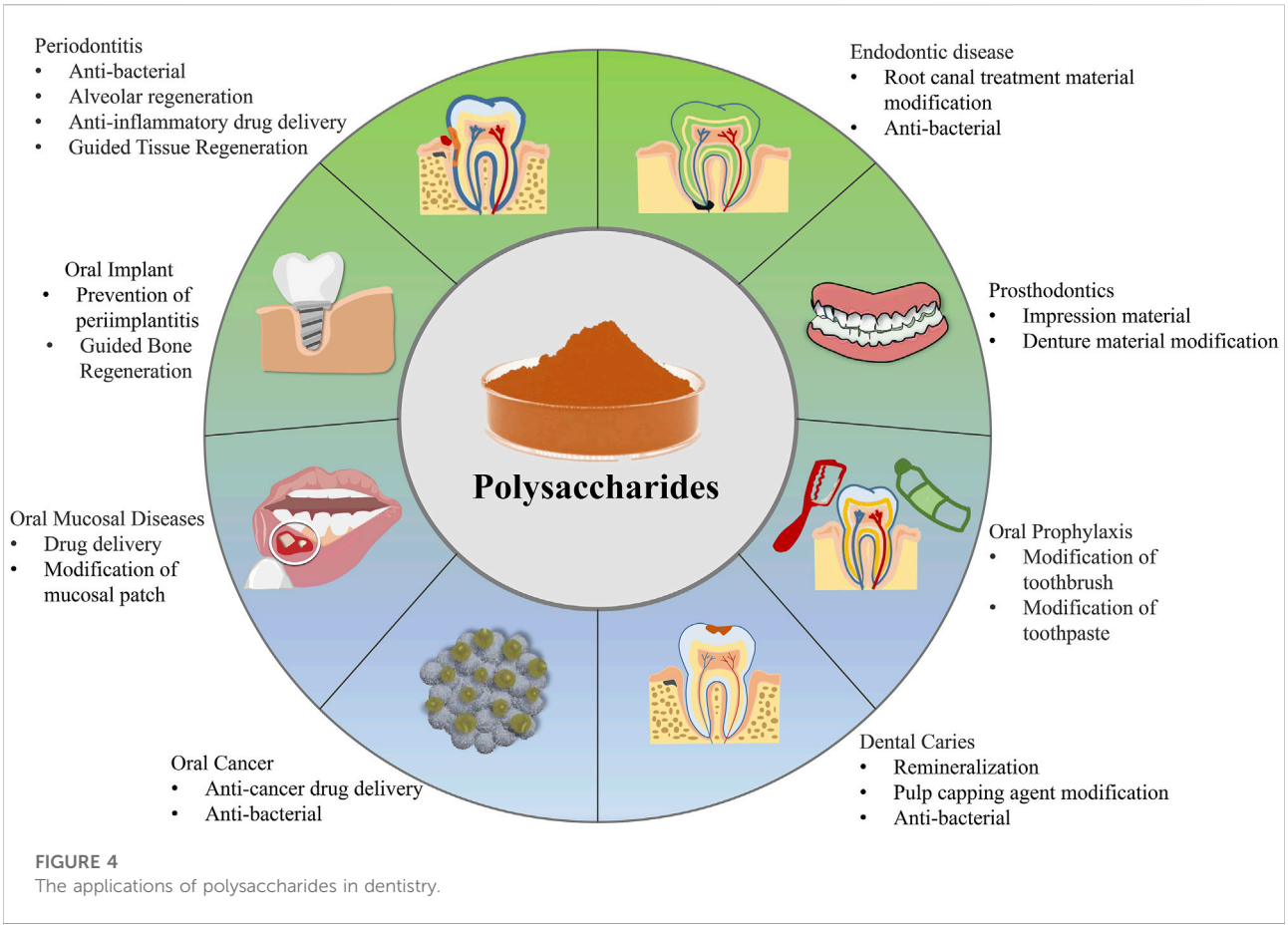

FIGURE 4
The applications of polysaccharides in dentistry.

L-galactopyranose units, designated as G and A residues, respectively (Trivedi et al., 2015). Agarose is a potential hydrogel for the controlled release of bioactive substances, given its good biocompatibility and natural biodegradability (Kim et al., 2019). In the oral cavity, agarose gel regulates the size and shape of hydroxyapatite crystals (Ling et al., 2019). A new biomimetic mineralization system containing agarose gel can induce a dense hydroxyapatite layer on the surface of demineralized dentin to block dentin tubules for dentin remineralization, a potentially new method for treating dentin hypersensitivity and dental caries (Ning et al., 2012). These two algal polysaccharides are highly biocompatible and have broad dental applications, including treating oral diseases.

Applications of natural polymers in stomatology

The oral cavity is located in the lower 1/3 of the maxillofacial region, starting from the lips. It has several sections, including the buccal, the inner lining of the cheeks, the pharynx at the back, the palate on the upper side, and the floor of the mouth on the lower side. Together, these parts form the cavitas oris propria (Tuominen and Rautava, 2021). Dental caries is an idiopathic disease of the oral cavity (Akintoye and Mupparapu, 2020). The teeth structure is different from that of bones and includes the enamel, dentin, pulp, and cementum. Enamel is the hardest tissue in the body that has neither blood vessels nor nerves and cannot regenerate. The dentin is softer than the enamel and can regenerate or repair itself to a certain degree. However, excessive teeth damage can create irreversible defects. If dental caries is not treated on time, the enamel is continually eaten up, causing bacteria infection in the pulp and periapical tissue. This eventually causes pulpitis, periapical periodontitis, jaw osteomyelitis, and other concurrent diseases, inducing severe pain and tissue damage. Moreover, dental caries not only destroy the integrity of the chewing organs but also affects the digestive function, seriously affecting an individual's overall health. Natural polysaccharides, which have antibacterial, drug delivery, and material modification capability with remarkable biocompatibility, are suitable for different dental functions to prevent oral diseases of soft and hard tissues or a combination of both (Figure 4).

Treatment of oral hard tissue diseases

Oral hard tissue diseases include dental caries, maxillofacial fractures, and bone defects (Melo et al., 2013). In dentistry, chitosan and alginate are used to improve the property of adhesive material. A combination of chitosan and triclosan supplemented with resin inhibits biofilm formation and improves the stability between dentin and adhesive interface, promoting long-term edge sealing (Machado et al., 2019). A mixture of chitosan and glass ionomer cement (GIC) can be another repair material that allows the slow-release of fluoride (Ibrahim et al., 2020). Chitosan reacts with the GIC to generate a compound with a better ion release rate, which is important for tooth structure (Mulder and Anderson-Small, 2019). Moreover, a formulation of type I collagen (Col), nanocrystalline hydroxyapatite (HAp), and alginate (Alg) is suitable for 3D printing of scaffolds with properties similar to those of natural dentin. The formulation effectively treats tooth sensitivity by blocking the dentin microtubules (Naseri et al., 2021). On the whole, polysaccharides could be modified to generate desired products suitable for treating hard tissue diseases in dentistry.

Treatment of oral soft tissue diseases

Diseases of the soft mouth tissues include pulpitis, periapical periodontitis, gingivitis, and other oral mucosal diseases. Infected dental pulp is very painful, significantly affecting the normal life of patients. The infection can spread to periapical tissues, causing periapical periodontitis. Gingivitis is an inflammation of teeth gums caused by accumulated dental plaque and some physical stimulation in the papillary. The disease can cause periodontitis and loss of the alveolar bone. Therefore, removing the root canal infection and dental plaque is important in treating oral soft tissue diseases. Given the unique anatomy, histology, and microbial environment of the oral cavity, materials for oral cavity uses should possess anti-bacterial properties, adhere on the oral cavity, be easy to apply, and should allow slow release of important molecules (Karolewicz, 2016; Timur et al., 2019). Natural polysaccharides can be modified to possess good adhesion, repair, and mechanical properties suitable for treating oral soft tissue diseases.

Chitosan inhibits the growth of *Porphyromonas gingivalis* and *Actinomyces aggregatum* and can modulate inflammation in human gingival fibroblasts by regulating the level of PGE2 through the JNK pathway. Chitosan is well tolerated by gingival fibroblasts and can stimulate cell proliferation via the ERK1/2 signaling pathway. Furthermore, the synergistic effect of chitosan and growth factors such as PDGF-BB stimulates the proliferation of gingival fibroblasts and inhibits the growth of *Porphyromonas gingivalis* and *Actinomyces aggregatum* (Silva et al., 2013). Bacterial cellulose fastens the solidification of diatomite and enhances the biological activity of the mineral. Moreover, it has good biocompatibility and promotes the proliferation and adhesion of mesenchymal stem cells (Voicu et al., 2017). In addition, it does not generate oxidative stress and is, therefore, an excellent material in endodontics. Compared with the ordinary absorbent paper tips, bacterial cellulose has a higher moisture absorption rate, expansion rate, tensile strength, and biocompatibility. Moreover, it is hard and causes no obvious allergic reactions (Yoshino et al., 2013). HA and platelet lysates' complex increase the metabolism of dental pulp mesenchymal stem cells and repair damaged dental pulp/dentin tissue by stimulating the deposition of mineralized matrix (Almeida et al., 2018; Schmidt et al., 2020). A combination of bacterial cellulose (BC) and photoactivated carbene-based biological adhesive (PDZ) forms a flexible film platform that can repair soft tissue in the ever-wet mouth environment. The shear strength and adhesion of the composite have been significantly improved, making it suitable for treating oral mucosal wounds (Singh et al., 2021). Therefore, polysaccharides can be used as antibacterial, root canal therapy materials and tissue treating oral patches, underlining the novel application prospects of these materials.

Treatment of a combination of oral soft and hard tissue diseases

Diseases involving soft and hard tissues in the mouth include cancer and periodontitis. Both diseases can cause lesions, gingival, buccal and lingual mucosa recession, and even alveolar bone and jaw bone loss. Gingival recession and the alveolar bone defect caused by periodontitis are irreversible and greatly affect a person's facial appearance. In serious cases, it causes tooth loss and facial deformity, affecting eating and talking. Therefore, periodontitis should be promptly treated. The periodontium repair involves using multiple materials to prevent further damage and restore bone and periodontal losses. Pure chitosan scaffolds promote the proliferation of cementoblasts (CB) and periodontal ligament cells (PDLCs), the alkaline phosphatase activity, and mineralization level. The CS scaffolds, combined with other polymer biomaterials and bioceramics, promote rapid periodontal regeneration (Lauritano et al., 2020). Mesoporous hydroxyapatite/chitosan (MHA/CS) composite scaffolds promote periodontal tissue regeneration, inhibit the growth of *Clostridium nucleatum* and *Porphyromonas gingivalis*, promote the differentiation of periodontal ligament stem cells into osteoblasts, and upregulate the ALP activity, and the expression of RUNX-2, OPN, and DLX-5 *in vitro*. Moreover, MHA/CS composite induces the cementum-like tissue formation *in vivo*, demonstrating its potential for periodontal tissue regeneration (Liao et al., 2020). Mice models with bone defects comparing bacterial cellulose and collagen biofilms regarding guided bone regeneration during periodontal tissue repair revealed that

bacterial cellulose biofilms only promote soft tissue repair in skulls but do not induce bone regeneration (Farnezi Bassi et al., 2020). However, hydrolyzed cellulose biofilm through strontium apatite modulates inflammation at the wound site and promotes the formation of connective tissue and the increase of calcium and magnesium, important elements that promote the bone generation and calcification (Luz et al., 2020). In general, the natural polysaccharides can effectively induce periodontal tissue regeneration, supporting periodontitis treatment.

Oral cancer is another disease of oral soft and hard tissues. Oral cancer is a life-threatening disease, whether local or metastatic. Natural polysaccharides have remarkable adhesion property, which is suitable for the wet oral environment. The polysaccharide sticks to the oral tissues, ensuring precise and sustained delivery of antibiotics. Combining bacterial cellulose, alginate, gelatin, and curcumin forms a multifunctional biopolymer film material that can release curcumin in saliva and has no obvious toxicity to human keratinocytes and human gingival fibroblasts. However, the biopolymer inhibits the growth of oral cancer cells and has good antibacterial activity against *Escherichia coli* and *Staphylococcus aureus* and, thus, is suitable for topical wound care and periodontitis and oral cancer treatment (Chiaoprakobkij et al., 2020). TQ/Ca-alg-PVA, a product of loading with calcium alginate and polyvinyl alcohol onto thymoquinone (TQ), inhibits early-stage oral cancer in 7,12-Dimethylbenz [a]anthracene (DMBA) painted hamster by downregulating the expression of NF-κB p50/p65, and PI3K/AKT/mTOR mRNA (Pu et al., 2021). In summary, natural polysaccharides can achieve precise treatment and reduce the drug resistance of oral cancer.

Oral care

Caries and periodontal disease, the most common disease in the oral cavity, is primarily prevented through oral hygiene. Mouthwash containing natural polysaccharides such as chitosan is a safe and effective natural product for reducing harmful oral microorganisms (Farias et al., 2019). Chitosan mouthwash has been proven safe, and its cytotoxicity is lower than that of commercial mouthwash, and effectively inhibits *Streptococcus* spp. *And Enterococcus spp*, preventing oral diseases (Costa et al., 2014). Paper-like nanofiber materials made from bacterial cellulose and chitosan inhibit the growth of bacteria and yeast, biofilm formation, and oxidation (Cabanas-Romero et al., 2020). Given that polysaccharides are biodegradable, they are environmentally friendly biomaterials. Chitosan-based toothpaste prevents tooth enamel erosion and wear. Toothpaste supplemented with chitosan and Sn^{2+} prevents corrosion and abrasion of teeth gums (Schluet er et al., 2014). In addition, chitosan-containing chewing gum reduces enamel demineralization and maintains bacteriostatic levels in saliva (Hayashi et al., 2007). Thus, the polysaccharides can be supplemented in the oral care products to prevent oral diseases.

Alveolar ridge preservation after tooth extraction remains an oral implant challenge. A mixture of DBBM-C and HA covered in a collagen membrane prevents dimensional shrinkage and increases bone formation after tooth extraction (Lee et al., 2021). Colonization of the bacteria is a major cause of implant failure (Jiang et al., 2020). Studies have shown that chitosan reduces colonization of *Fusobacterium nucleatum* on the implant surface, plaque biofilm formation, and decrease periimplantitis, increasing the success of implanting (Vaz et al., 2018). Therefore, chitosan is a remarkable antibacterial material that can improve the success of oral implants. Generally, the natural polysaccharide has good biocompatibility and is non-toxic and, thus, an attractive oral care material in stomatology.

Discussion

In recent years, natural polysaccharides extracted from animals, plants, and microorganisms have attracted the attention of researchers because of their good degradability, non-toxicity, and renewability (Zhao et al., 2020). At present, the antibacterial, anti-inflammatory, modifiable, tissue regeneration, and drug carrier potential of polysaccharides have been investigated (Cui et al., 2018; Serrano-Sevilla et al., 2019; Hou et al., 2020; Layek and Mandal, 2020; Zhai et al., 2020). Different polysaccharides are used for treating different oral diseases (Table 1). Natural polysaccharides have attracted greater attention than synthetic materials because they are biocompatible, biodegradable, and ecological.

Despite the advantages of natural polysaccharides in dentistry, these molecules have certain disadvantages in biomedical applications; 1) They have poor mechanical properties. The inferior adhesiveness and the short-term *in vivo* stability of natural polysaccharides limit their therapeutic efficacy (Kim et al., 2021). 2) The quality of polysaccharides is limited to their original material. The method of extraction and purification affects controlled the products' reliability (Luo et al., 2021). 3) Natural polysaccharides are highly moisture sensitive. They undergo hydrolysis during processing and are unstable in the oral cavity (Imre et al., 2019).

Natural polysaccharides are generated through natural processes. However, researches are needed to explore strategies for modifying the chemical structure of these molecules to broaden their biomedical applications. Moreover, the natural polysaccharides are made to the namomaterials (Georgouvelas et al., 2021), which might improve their inherent properties to enhance drug delivery efficacy (Ahmed and Aljaeid, 2016) and applied in wound healing (Yang et al., 2020). In future, natural material could be brought to clinical practice and their effect to environment should be valued. It is believed that advances in the development of biomaterials and

TABLE 1 The applications of polysaccharide in oral diseases.

Polysaccharides	Dental Specialties	Models	Biological Activity/Application	References
Chitosan dispersion	Dental caries	*In vitro*	Exert antimicrobial effect against mature S. mutans biofilms	Kawakita et al. (2019)
Bacterial cellulose	Bone regeneration	*In vivo* rat calvarial defect models	The BC biofilms exhibited significantly larger new bone area *in vivo*	Coelho et al. (2019)
Hyaluronic acid	Oral squamous cell carcinoma	*Ex vivo* porcine oral mucosal tissues	Deliver DOX to HN22 with a low IC50	Pornpitchanarong et al. (2020)
Hyaluronic acid	Oral candidiasis	*In vivo* sheep buccal mucosa	Hyaluronic acid hydrogel delivers a nanotransfersome with fluconazole entrapped, which exert enhanced antifungal efficacy	Alkhalidi et al. (2020)
Alginate	Recurrent aphthous stomatitis	*In vitro*	Adhesion time was improved and the AL. Ambroxol was controlled release	Laffleur and Kuppers (2019)
Alginate	Tooth sensitivity	*In vitro*	The 3D printing dentin mimics is of good cytocompability and could block the dentinal tubule effectively	Naseri et al. (2021)
Bacterial cellulose	Pulpitis	*In vivo* Sprague–Dawley rat	BC showed higher absorption and expansion than paper points, and maintained a high tensile strength even wet.	Yoshino et al. (2013)
Chitosan	Periodontitis	*In vitro*	Chitosan induces the proliferation of human gingival fibroblasts by activating of the ERK1/2 signaling pathway	Silva et al. (2013)
Agarose	Dentin hypersensitivity and dental caries	*In vitro*	Induced a layer of tightly packed hydroxyapatite on the surface of demineralized dentine and the dentinal tubules was occluded	Ning et al. (2012)
Chitosan	Mouthwash	*In vitro*	The chitosan mouthwash inhibits the streptococci and enterococci and cause no major reductions to the normal oral microflora viability	Costa et al. (2014)
Chitosan	Dental caries filling materials	*In vitro*	Triclosan-loaded chitosan showed antibacterial activity and induced dentin/adhesive interface stability	Machado et al. (2019)
Chitosan	Modify glass ionomer restorative cements	*In vitro*	Chitosan modifications increase the ion release of aluminium, sodium, silicon and strontium for materials	Mulder and Anderson-Small (2019)
Chitosan	The nano hydroxyapatite/chitosan composite scaffold for periodontal regeneration	*In vivo*	mHA/CS could promote periodontal regeneration	Liao et al. (2020)
Bacterial cellulose	The guided bone regeneration (GBR) membranes	BALB/c mice	Promoting soft tissue repair in rat skulls	Farnezi Bassi et al. (2020)
Bacterial cellulose	The guided bone regeneration (GBR) membranes	*In vivo*	Modulates inflammation, promotes the formation of connective tissue and the increase of calcium and magnesium	Luz et al. (2020)
Bacterial cellulose/ Alginate	Oral mucoadhesive patches for periodontitis or oral cancer treatment	Rats	Showing anticancer activity against oral cancer cells (CAL-27), but non-cytotoxicity to HaCaT and GF cells	Chiaoprakobkij et al. (2020)
Alginate	Oral cancer	*In vivo*	Inhibits early-stage oral cancer	Pu et al. (2021)
Chitosan	Mouthwash	Swiss albino mice	Antimicrobial effectiveness and toxicological safety	Farias et al. (2019)
Chitosan	Toothpaste	*In vitro* porcine mucosa	Chitosan enhanced the efficacy of the Sn^{2+}-containing toothpaste as an anti-erosive/anti-abrasive agent	Schlueter et al. (2014)
Chitosan	Chewing gum	*In vivo* hamster buccal	Chitosan-containing gum chewing has a better antibacterial effect and increases salivary secretion	Hayashi et al. (2007)
Hyaluronic Acid	Ridge preservation	*In vitro*	Prevents dimensional shrinkage and increases bone formation after tooth extraction	Lee et al. (2021)

molecular biology-related technologies will enhance the application of natural polysaccharides in stomatology.

Author Contributions

ZY and DW wrote the manuscript. ZY, HL, LC, RL, MH, SK, and WL collected the references and prepared figures. All authors reviewed the manuscript.

Funding

This work was supported by the Fundamental Research Funds of the Jilin Province, Department of Finance (Grant No. jcsz202189313), the Jilin Scientific and Technological Development Program (Grant Nos. 81602377), the Changchun Scientific and Technological Development Program (Grant Nos. 21ZY26), the Jilin Province Scientific and Technological Development Program (Grant Nos. 20200801077GH).

Conflict of interest

The authors declare that the research was conducted in the absence of any commercial or financial relationships that could be construed as a potential conflict of interest.

Publisher's note

All claims expressed in this article are solely those of the authors and do not necessarily represent those of their affiliated organizations, or those of the publisher, the editors and the reviewers. Any product that may be evaluated in this article, or claim that may be made by its manufacturer, is not guaranteed or endorsed by the publisher.

References

Abd El-Hack, M. E., El-Saadony, M. T., Shafi, M. E., Zabermawi, N. M., Arif, M., Batiha, G. E., et al. (2020). Antimicrobial and antioxidant properties of chitosan and its derivatives and their applications: a review. *Int. J. Biol. Macromol.* 164, 2726–2744. doi:10.1016/j.ijbiomac.2020.08.153

Abdelhamid, H. N., and Mathew, A. P. (2022). Cellulose-based nanomaterials advance biomedicine: a review. *Int. J. Mol. Sci.* 23, 5405. doi:10.3390/ijms23105405

Ahmed, T. A., and Aljaeid, B. M. (2016). Preparation, characterization, and potential application of chitosan, chitosan derivatives, and chitosan metal nanoparticles in pharmaceutical drug delivery. *Drug Des. devel. Ther.* 10, 483–507. doi:10.2147/DDDT.S99651

Ahsan, S. M., Thomas, M., Reddy, K. K., Sooraparaju, S. G., Asthana, A., and Bhatnagar, I. (2018). Chitosan as biomaterial in drug delivery and tissue engineering. *Int. J. Biol. Macromol.* 110, 97–109. doi:10.1016/j.ijbiomac.2017.08.140

Akintoye, S. O., and Mupparapu, M. (2020). Clinical evaluation and anatomic variation of the oral cavity. *Dermatol. Clin.* 38, 399–411. doi:10.1016/j.det.2020.05.001

Alkhalidi, H. M., Hosny, K. M., and Rizg, W. Y. (2020). Oral gel loaded by fluconazolesesame oil nanotransfersomes: Development, optimization, and assessment of antifungal activity. *Pharmaceutics* 13 (1). doi:10.3390/pharmaceutics13010027

Almeida, L. D. F., Babo, P. S., Silva, C. R., Rodrigues, M. T., Hebling, J., Reis, R. L., et al. (2018). Hyaluronic acid hydrogels incorporating platelet lysate enhance human pulp cell proliferation and differentiation. *J. Mat. Sci. Mat. Med.* 29, 88. doi:10.1007/s10856-018-6088-7

Amin, M. K., and Boateng, J. S. (2022). Enhancing stability and mucoadhesive properties of chitosan nanoparticles by surface modification with sodium alginate and polyethylene glycol for potential oral mucosa vaccine delivery. *Mar. Drugs* 20, 156. doi:10.3390/md20030156

An, S. J., Lee, S. H., Huh, J. B., Jeong, S., Park, J. S., Gwon, H. J., et al. (2017). Preparation and characterization of resorbable bacterial cellulose membranes treated by electron beam irradiation for guided bone regeneration. *Int. J. Mol. Sci.* 18, 2236. doi:10.3390/ijms18112236

Baranov, N., Popa, M., Atanase, L. I., and Ichim, D. L. (2021). Polysaccharide-based drug delivery systems for the treatment of periodontitis. *Molecules* 26, 2735. doi:10.3390/molecules26092735

Beaumont, M., Tran, R., Vera, G., Niedrist, D., Rousset, A., Pierre, R., et al. (2021). Hydrogel-forming algae polysaccharides: from seaweed to biomedical applications. *Biomacromolecules* 22, 1027–1052. doi:10.1021/acs.biomac.0c01406

Bilal, M., and Iqbal, H. M. N. (2019). Marine seaweed polysaccharides-based engineered cues for the modern biomedical sector. *Mar. Drugs* 18, 7. doi:10.3390/md18010007

Cabanas-Romero, L. V., Valls, C., Valenzuela, S. V., Roncero, M. B., Pastor, F. I. J., Diaz, P., et al. (2020). Bacterial cellulose-chitosan paper with antimicrobial and antioxidant activities. *Biomacromolecules* 21, 1568–1577. doi:10.1021/acs.biomac.0c00127

Cervino, G., Fiorillo, L., Herford, A., Laino, L., Troiano, G., Amoroso, G., et al. (2018). Alginate materials and dental impression technique: a current state of the art and application to dental practice. *Mar. Drugs* 17, 18. doi:10.3390/md17010018

Chiaoprakobkij, N., Suwanmajo, T., Sanchavanakit, N., and Phisalaphong, M. (2020). Curcumin-Loaded bacterial cellulose/alginate/gelatin as a multifunctional biopolymer composite film. *Molecules* 25, 3800. doi:10.3390/molecules25173800

Coelho, F., Cavicchioli, M., Specian, S. S., Scarel-Caminaga, R. M., Penteado, L. A., Medeiros, A. I., et al. (2019). Bacterial cellulose membrane functionalized with hydroxiapatite and anti-bone morphogenetic protein 2: A promising material for bone regeneration. *PLoS One* 14 (8), e0221286. doi:10.1371/journal.pone.0221286

Costa, E. M., Silva, S., Costa, M., Pereira, M., Campos, D., Odila, J., et al. (2014). Chitosan mouthwash: toxicity and *in vivo* validation. *Carbohydr. Polym.* 111, 385–392. doi:10.1016/j.carbpol.2014.04.046

Cui, X., Wang, S., Cao, H., Guo, H., Li, Y., Xu, F., et al. (2018). A review: the bioactivities and pharmacological applications of polygonatum sibiricum polysaccharides. *Molecules* 23, 1170. doi:10.3390/molecules23051170

de Oliveira Barud, H. G., da Silva, R. R., Borges, M. A. C., Castro, G. R., Ribeiro, S. J. L., and da Silva Barud, H. (2020). Bacterial nanocellulose in dentistry: perspectives and challenges. *Molecules* 26, 49. doi:10.3390/molecules26010049

de Oliveira Barud, H. G., da Silva, R. R., da Silva Barud, H., Tercjak, A., Gutierrez, J., Lustri, W. R., et al. (2016). A multipurpose natural and renewable polymer in medical applications: bacterial cellulose. *Carbohydr. Polym.* 153, 406–420. doi:10.1016/j.carbpol.2016.07.059

Del Fabbro, M., Corbella, S., Sequeira-Byron, P., Tsesis, I., Rosen, E., Lolato, A., et al. (2016). Endodontic procedures for retreatment of periapical lesions. *Cochrane Database Syst. Rev.* 10, CD005511. doi:10.1002/14651858.CD005511.pub3

Farias, J. M., Stamford, T. C. M., Resende, A. H. M., Aguiar, J. S., Rufino, R. D., Luna, J. M., et al. (2019). Mouthwash containing a biosurfactant and chitosan: an eco-sustainable option for the control of cariogenic microorganisms. *Int. J. Biol. Macromol.* 129, 853–860. doi:10.1016/j.ijbiomac.2019.02.090

Farnezi Bassi, A. P., Bizelli, V. F., Brasil, L. F. d. M., Pereira, J. C., Al-Sharani, H. M., Momesso, G. A. C., et al. (2020). Is the bacterial cellulose membrane feasible for osteopromotive property? *Membr. (Basel)* 10, 230. doi:10.3390/membranes10090230

Frassica, M. T., and Grunlan, M. A. (2020). Perspectives on synthetic materials to guide tissue regeneration for osteochondral defect repair. *ACS Biomater. Sci. Eng.* 6, 4324–4336. doi:10.1021/acsbiomaterials.0c00753

Georgouvelas, D., Abdelhamid, H. N., Li, J., Edlund, U., and Mathew, A. P. (2021). All-cellulose functional membranes for water treatment: adsorption of metal ions and catalytic decolorization of dyes. *Carbohydr. Polym.* 264, 118044. doi:10.1016/j.carbpol.2021.118044

Graca, M. F. P., Miguel, S. P., Cabral, C. S. D., and Correia, I. J. (2020). Hyaluronic acid-based wound dressings: a review. *Carbohydr. Polym.* 241, 116364. doi:10.1016/j.carbpol.2020.116364

Halib, N., Ahmad, I., Grassi, M., and Grassi, G. (2019). The remarkable three-dimensional network structure of bacterial cellulose for tissue engineering applications. *Int. J. Pharm. X.* 566, 631–640. doi:10.1016/j.ijpharm.2019.06.017

Hayashi, Y., Ohara, N., Ganno, T., Ishizaki, H., and Yanagiguchi, K. (2007). Chitosan-containing gum chewing accelerates antibacterial effect with an increase in salivary secretion. *J. Dent. (Shiraz).* 35, 871–874. doi:10.1016/j.jdent.2007.08.004

Hou, C., Chen, L., Yang, L., and Ji, X. (2020). An insight into anti-inflammatory effects of natural polysaccharides. *Int. J. Biol. Macromol.* 153, 248–255. doi:10.1016/j.ijbiomac.2020.02.315

Huang, G., and Huang, H. (2018). Application of hyaluronic acid as carriers in drug delivery. *Drug Deliv. (Lond).* 25, 766–772. doi:10.1080/10717544.2018.1450910

Hudson, D., and Margaritis, A. (2014). Biopolymer nanoparticle production for controlled release of biopharmaceuticals. *Crit. Rev. Biotechnol.* 34, 161–179. doi:10.3109/07388551.2012.743503

Ibrahim, M. S., Garcia, I. M., Kensara, A., Balhaddad, A. A., Collares, F. M., Williams, M. A., et al. (2020). How we are assessing the developing antibacterial resin-based dental materials? a scoping review. *J. Dent. (Shiraz).* 99, 103369. doi:10.1016/j.jdent.2020.103369

Imre, B., Garcia, L., Puglia, D., and Vilaplana, F. (2019). Reactive compatibilization of plant polysaccharides and biobased polymers: review on current strategies, expectations and reality. *Carbohydr. Polym.* 209, 20–37. doi:10.1016/j.carbpol.2018.12.082

Jiang, X., Yao, Y., Tang, W., Han, D., Zhang, L., Zhao, K., et al. (2020). Design of dental implants at materials level: an overview. *J. Biomed. Mat. Res. A* 108, 1634–1661. doi:10.1002/jbm.a.36931

Karolewicz, B. (2016). A review of polymers as multifunctional excipients in drug dosage form technology. *Saudi Pharm. J.* 24, 525–536. doi:10.1016/j.jsps.2015.02.025

Kawakita, E. R. H., Re, A. C. S., Peixoto, M. P. G., Ferreira, M. P., Ricomini-Filho, A. P., Freitas, O., et al. (2019). Effect of chitosan dispersion and microparticles on older Streptococcus mutans biofilms. *Molecules* 24, 1808. doi:10.3390/molecules24091808

Kim, C., Jeong, D., Kim, S., Kim, Y., and Jung, S. (2019). Cyclodextrin functionalized agarose gel with low gelling temperature for controlled drug delivery systems. *Carbohydr. Polym.* 222, 115011. doi:10.1016/j.carbpol.2019.115011

Kim, J., Kim, S., Son, D., and Shin, M. (2021). Phenol-hyaluronic acid conjugates: correlation of oxidative crosslinking pathway and adhesiveness. *Polym. (Basel)* 13, 3130. doi:10.3390/polym13183130

Klemm, D., Heublein, B., Fink, H. P., and Bohn, A. (2005). Cellulose: fascinating biopolymer and sustainable raw material. *Angew. Chem. Int. Ed.* 44, 3358–3393. doi:10.1002/anie.200460587

Klinthoopthamrong, N., Chaikiawkeaw, D., Phoolcharoen, W., Rattanapisit, K., Kaewpungsup, P., Pavasant, P., et al. (2020). Bacterial cellulose membrane conjugated with plant-derived osteopontin: preparation and its potential for bone tissue regeneration. *Int. J. Biol. Macromol.* 149, 51–59. doi:10.1016/j.ijbiomac.2020.01.158

Kou, S. G., Peters, L. M., and Mucalo, M. R. (2021). Chitosan: a review of sources and preparation methods. *Int. J. Biol. Macromol.* 169, 85–94. doi:10.1016/j.ijbiomac.2020.12.005

Kunert, M., and Lukomska-Szymanska, M. (2020). Bio-inductive materials in direct and indirect pulp capping-a review article. *Mater. (Basel)* 13, 1204. doi:10.3390/ma13051204

Laffleur, F., and Kuppers, P. (2019). Adhesive alginate for buccal delivery in aphthous stomatitis. *Carbohydr. Res.* 477, 51–57. doi:10.1016/j.carres.2019.03.009

Lauritano, D., Limongelli, L., Moreo, G., Favia, G., and Carinci, F. (2020). Nanomaterials for periodontal tissue engineering: chitosan-based scaffolds. A systematic review. *Nanomater. (Basel)* 10, 605. doi:10.3390/nano10040605

Layek, B., and Mandal, S. (2020). Natural polysaccharides for controlled delivery of oral therapeutics: a recent update. *Carbohydr. Polym.* 230, 115617. doi:10.1016/j.carbpol.2019.115617

Lee, J. B., Chu, S., Ben Amara, H., Song, H. Y., Son, M. J., Lee, J., et al. (2021). Effects of hyaluronic acid and deproteinized bovine bone mineral with 10% collagen for ridge preservation in compromised extraction sockets. *J. Periodontol.* 92, 1564–1575. doi:10.1002/JPER.20-0832

Liao, Y., Li, H., Shu, R., Chen, H., Zhao, L., Song, Z., et al. (2020). Mesoporous hydroxyapatite/chitosan loaded with recombinant-human amelogenin could enhance antibacterial effect and promote periodontal regeneration. *Front. Cell. Infect. Microbiol.* 10, 180. doi:10.3389/fcimb.2020.00180

Ling, Z., He, Y., Huang, H., Xie, X., Li, Q. l., and Cao, C. Y. (2019). Effects of oligopeptide simulating DMP-1/mineral trioxide aggregate/agarose hydrogel biomimetic mineralisation model for the treatment of dentine hypersensitivity. *J. Mat. Chem. B* 7, 5825–5833. doi:10.1039/c9tb01684h

Luo, M., Zhang, X., Wu, J., and Zhao, J. (2021). Modifications of polysaccharide-based biomaterials under structure-property relationship for biomedical applications. *Carbohydr. Polym.* 266, 118097. doi:10.1016/j.carbpol.2021.118097

Luz, E., das Chagas, B. S., de Almeida, N. T., de Fatima Borges, M., Andrade, F. K., Muniz, C. R., et al. (2020). Resorbable bacterial cellulose membranes with strontium release for guided bone regeneration. *Mater. Sci. Eng. C* 116, 111175. doi:10.1016/j.msec.2020.111175

Lynd, L. R., Weimer, P. J., van Zyl, W. H., and Pretorius, I. S. (2002). Microbial cellulose utilization: fundamentals and biotechnology. *Microbiol. Mol. Biol. Rev.* 66, 506–577. doi:10.1128/MMBR.66.3.506-577.2002

Machado, A. H. S., Garcia, I. M., Motta, A. S. D., Leitune, V. C. B., and Collares, F. M. (2019). Triclosan-loaded chitosan as antibacterial agent for adhesive resin. *J. Dent. (Shiraz).* 83, 33–39. doi:10.1016/j.jdent.2019.02.002

Malkondu, O., Karapinar Kazandag, M., and Kazazoglu, E. (2014). A review on biodentine, a contemporary dentine replacement and repair material. *Biomed. Res. Int.* 2014, 160951. doi:10.1155/2014/160951

Marinho, A., Nunes, C., and Reis, S. (2021). Hyaluronic acid: a key ingredient in the therapy of inflammation. *Biomolecules* 11, 1518. doi:10.3390/biom11101518

Melo, M. A., Guedes, S. F., Xu, H. H., and Rodrigues, L. K. (2013). Nanotechnology-based restorative materials for dental caries management. *Trends Biotechnol.* 31, 459–467. doi:10.1016/j.tibtech.2013.05.010

Mulder, R., and Anderson-Small, C. (2019). Ion release of chitosan and nanodiamond modified glass ionomer restorative cements. *Clin. Cosmet. Investig. Dent.* 11, 313–320. doi:10.2147/CCIDE.S220089

Mushtaq, A., Li, L., and Grondahl, L. (2021). Chitosan nanomedicine in cancer therapy: targeted delivery and cellular uptake. *Macromol. Biosci.* 21, e2100005. doi:10.1002/mabi.202100005

Muxika, A., Etxabide, A., Uranga, J., Guerrero, P., and de la Caba, K. (2017). Chitosan as a bioactive polymer: processing, properties and applications. *Int. J. Biol. Macromol.* 105, 1358–1368. doi:10.1016/j.ijbiomac.2017.07.087

Narmani, A., and Jafari, S. M. (2021). Chitosan-based nanodelivery systems for cancer therapy: recent advances. *Carbohydr. Polym.* 272, 118464. doi:10.1016/j.carbpol.2021.118464

Naseri, S., Cooke, M. E., Rosenzweig, D. H., and Tabrizian, M. (2021). 3D printed *in vitro* dentin model to investigate occlusive agents against tooth sensitivity. *Mater. (Basel)* 14, 7255. doi:10.3390/ma14237255

Ning, T. Y., Xu, X. H., Zhu, L. F., Zhu, X. P., Chu, C. H., Liu, L. K., et al. (2012). Biomimetic mineralization of dentin induced by agarose gel loaded with calcium phosphate. *J. Biomed. Mat. Res.* 100, 138–144. doi:10.1002/jbm.b.31931

Niu, X., Wang, L., Xu, M., Qin, M., Zhao, L., Wei, Y., et al. (2021). Electrospun polyamide-6/chitosan nanofibers reinforced nano-hydroxyapatite/polyamide-6 composite bilayered membranes for guided bone regeneration. *Carbohydr. Polym.* 260, 117769. doi:10.1016/j.carbpol.2021.117769

Paradowska-Stolarz, A., Wieckiewicz, M., Owczarek, A., and Wezgowiec, J. (2021). Natural polymers for the maintenance of oral health: review of recent advances and perspectives. *Int. J. Mol. Sci.* 22, 10337. doi:10.3390/ijms221910337

Pornpitchanarong, C., Rojanarata, T., Opanasopit, P., Ngawhirunpat, T., and Patrojanasophon, P. (2020). Catechol-modified chitosan/hyaluronic acid nanoparticles as a new avenue for local delivery of doxorubicin to oral cancer cells. *Colloids Surfaces B Biointerfaces* 196, 111279. doi:10.1016/j.colsurfb.2020.111279

Prajapati, V. D., Maheriya, P. M., Jani, G. K., and Solanki, H. K. (2014). Retracted: Carrageenan: a natural seaweed polysaccharide and its applications. *Carbohydr. Polym.* 105, 97–112. doi:10.1016/j.carbpol.2014.01.067

Pu, Y., Hu, S., Chen, Y., Zhang, Q., Xia, C., Deng, H., et al. (2021). Thymoquinone loaded calcium alginate and polyvinyl alcohol carrier inhibits the 7, 12-dimethylbenz[a]anthracene-induced hamster oral cancer via the down-regulation of PI3K/AKT/mTOR signaling pathways. *Environ. Toxicol.* 36, 339–351. doi:10.1002/tox.23040

Rahmati, M., Alipanahi, Z., and Mozafari, M. (2019). Emerging biomedical applications of algal polysaccharides. *Curr. Pharm. Des.* 25, 1335–1344. doi:10.2174/1381612825666190423160357

Roumanas, E. D. (2009). The social solution-denture esthetics, phonetics, and function. *J. Prosthodont.* 18, 112–115. doi:10.1111/j.1532-849X.2009.00440.x

Sah, A. K., Dewangan, M., and Suresh, P. K. (2019). Potential of chitosan-based carrier for periodontal drug delivery. *Colloids Surfaces B Biointerfaces* 178, 185–198. doi:10.1016/j.colsurfb.2019.02.044

Salari, N., Mansouri, K., Valipour, E., Abam, F., Jaymand, M., Rasoulpoor, S., et al. (2021). Hyaluronic acid-based drug nanocarriers as a novel drug delivery system for cancer chemotherapy: a systematic review. *DARU J. Pharm. Sci.* 29, 439–447. doi:10.1007/s40199-021-00416-6

Sanchez-Ballester, N. M., Bataille, B., and Soulairol, I. (2021). Sodium alginate and alginic acid as pharmaceutical excipients for tablet formulation: Structure-function relationship. *Carbohydr. Polym.* 270, 118399. doi:10.1016/j.carbpol.2021.118399

Schlueter, N., Klimek, J., and Ganss, C. (2014). Effect of a chitosan additive to a Sn2+-containing toothpaste on its anti-erosive/anti-abrasive efficacy--a controlled randomised *in situ* trial. *Clin. Oral Investig.* 18, 107–115. doi:10.1007/s00784-013-0941-3

Schmidt, J., Pilbauerova, N., Soukup, T., Suchankova-Kleplova, T., and Suchanek, J. (2020). Low molecular weight hyaluronic acid effect on dental pulp stem cells *in vitro*. *Biomolecules* 11, 22. doi:10.3390/biom11010022

Serrano-Sevilla, I., Artiga, A., Mitchell, S. G., De Matteis, L., and de la Fuente, J. M. (2019). Natural polysaccharides for siRNA delivery: nanocarriers based on chitosan, hyaluronic acid, and their derivatives. *Molecules* 24, 2570. doi:10.3390/molecules24142570

Shivakumar, P., Gupta, M. S., Jayakumar, R., and Gowda, D. V. (2021). Prospection of chitosan and its derivatives in wound healing: proof of patent analysis (2010-2020). *Int. J. Biol. Macromol.* 184, 701–712. doi:10.1016/j.ijbiomac.2021.06.086

Silva, A. C. Q., Silvestre, A. J. D., Vilela, C., and Freire, C. S. R. (2021). Natural polymers-based materials: a contribution to a greener future. *Molecules* 27, 94. doi:10.3390/molecules27010094

Silva, D., Arancibia, R., Tapia, C., Acuna-Rougier, C., Diaz-Dosque, M., Caceres, M., et al. (2013). Chitosan and platelet-derived growth factor synergistically stimulate cell proliferation in gingival fibroblasts. *J. Periodontal Res.* 48, 677–686. doi:10.1111/jre.12053

Singh, J., Tan, N. C., Mahadevaswamy, U. R., Chanchareonsook, N., Steele, T. W., and Lim, S. (2021). Bacterial cellulose adhesive composites for oral cavity applications. *Carbohydr. Polym.* 274, 118403. doi:10.1016/j.carbpol.2021.118403

Suharyani, I., Fouad Abdelwahab Mohammed, A., Muchtaridi, M., Wathoni, N., and Abdassah, M. (2021). Evolution of drug delivery systems for recurrent aphthous stomatitis. *Drug Des. devel. Ther.* 15, 4071–4089. doi:10.2147/DDDT.S328371

Svensson, A., Nicklasson, E., Harrah, T., Panilaitis, B., Kaplan, D., Brittberg, M., et al. (2005). Bacterial cellulose as a potential scaffold for tissue engineering of cartilage. *Biomaterials* 26, 419–431. doi:10.1016/j.biomaterials.2004.02.049

Timur, S. S., Yuksel, S., Akca, G., and Senel, S. (2019). Localized drug delivery with mono and bilayered mucoadhesive films and wafers for oral mucosal infections. *Int. J. Pharm. X.* 559, 102–112. doi:10.1016/j.ijpharm.2019.01.029

Torres, F. G., Troncoso, O. P., Pisani, A., Gatto, F., and Bardi, G. (2019). Natural polysaccharide nanomaterials: an overview of their immunological properties. *Int. J. Mol. Sci.* 20, 5092. doi:10.3390/ijms20205092

Trivedi, T. J., Bhattacharjya, D., Yu, J. S., and Kumar, A. (2015). Functionalized agarose self-healing ionogels suitable for supercapacitors. *ChemSusChem* 8, 3294–3303. doi:10.1002/cssc.201500648

Tuominen, H., and Rautava, J. (2021). Oral microbiota and cancer development. *Pathobiology* 88, 116–126. doi:10.1159/000510979

Vaz, J. M., Pezzoli, D., Chevallier, P., Campelo, C. S., Candiani, G., and Mantovani, D. (2018). Antibacterial coatings based on chitosan for pharmaceutical and biomedical applications. *Curr. Pharm. Des.* 24, 866–885. doi:10.2174/1381612824666180219143900

Vergnes, J. N., and Mazevet, M. (2020). Oral diseases: a global public health challenge. *Lancet* 395, 186. doi:10.1016/S0140-6736(19)33015-6

Voicu, G., Jinga, S. I., Drosu, B. G., and Busuioc, C. (2017). Improvement of silicate cement properties with bacterial cellulose powder addition for applications in dentistry. *Carbohydr. Polym.* 174, 160–170. doi:10.1016/j.carbpol.2017.06.062

Wang, W., Meng, Q., Li, Q., Liu, J., Zhou, M., Jin, Z., et al. (2020). Chitosan derivatives and their application in biomedicine. *Int. J. Mol. Sci.* 21, 487. doi:10.3390/ijms21020487

Whitters, C. J., Strang, R., Brown, D., Clarke, R., Curtis, R., Hatton, P., et al. (1999). Dental materials: 1997 literature review. *J. Dent. (Shiraz).* 27, 401–435. doi:10.1016/s0300-5712(99)00007-x

Wong, F. M. F., Ng, Y. T. Y., and Leung, W. K. (2019). Oral health and its associated factors among older institutionalized residents-a systematic review. *Int. J. Environ. Res. Public Health* 16, 4132. doi:10.3390/ijerph16214132

Yang, M., Ward, J., and Choy, K. L. (2020). Nature-inspired bacterial cellulose/methylglyoxal (BC/MGO) nanocomposite for broad-spectrum antimicrobial wound dressing. *Macromol. Biosci.* 20, e2000070. doi:10.1002/mabi.202000070

Yoshino, A., Tabuchi, M., Uo, M., Tatsumi, H., Hideshima, K., Kondo, S., et al. (2013). Applicability of bacterial cellulose as an alternative to paper points in endodontic treatment. *Acta Biomater.* 9, 6116–6122. doi:10.1016/j.actbio.2012.12.022

Yu, Y., Shen, M., Song, Q., and Xie, J. (2018). Biological activities and pharmaceutical applications of polysaccharide from natural resources: a review. *Carbohydr. Polym.* 183, 91–101. doi:10.1016/j.carbpol.2017.12.009

Zhai, P., Peng, X., Li, B., Liu, Y., Sun, H., and Li, X. (2020). The application of hyaluronic acid in bone regeneration. *Int. J. Biol. Macromol.* 151, 1224–1239. doi:10.1016/j.ijbiomac.2019.10.169

Zhang, C., Hui, D., Du, C., Sun, H., Peng, W., Pu, X., et al. (2021). Preparation and application of chitosan biomaterials in dentistry. *Int. J. Biol. Macromol.* 167, 1198–1210. doi:10.1016/j.ijbiomac.2020.11.073

Zhao, Y., Yan, B., Wang, Z., Li, M., and Zhao, W. (2020). Natural polysaccharides with immunomodulatory activities. *Mini Rev. Med. Chem.* 20, 96–106. doi:10.2174/1389557519666190913151632

Zucca, P., Fernandez-Lafuente, R., and Sanjust, E. (2016). Agarose and its derivatives as supports for enzyme immobilization. *Molecules* 21, 1577. doi:10.3390/molecules21111577

frontiers | Frontiers in Bioengineering and Biotechnology

TYPE Original Research
PUBLISHED 22 July 2022
DOI 10.3389/fbioe.2022.960310

OPEN ACCESS

EDITED BY
Kunyu Zhang,
South China University of Technology, China

REVIEWED BY
Jiacan Su,
Second Military Medical University, China
Jingfeng Li,
Zhongnan Hospital, Wuhan University, China

*CORRESPONDENCE
Guohui Liu,
liuguohui@hust.edu.cn
Wu Zhou,
2016XH0120@hust.edu.cn

†These authors have contributed equally to this work and share first authorship

SPECIALTY SECTION
This article was submitted to Biomaterials, a section of the journal Frontiers in Bioengineering and Biotechnology

RECEIVED 02 June 2022
ACCEPTED 29 June 2022
PUBLISHED 22 July 2022

CITATION
Xue H, Zhang Z, Liu M, Lin Z, Endo Y, Liu G, Mi B, Zhou W and Liu G (2022), Finite element analysis of different fixation methods of screws on absorbable plate for rib fractures. *Front. Bioeng. Biotechnol.* 10:960310. doi: 10.3389/fbioe.2022.960310

Finite element analysis of different fixation methods of screws on absorbable plate for rib fractures

Hang Xue[1†], Zhenhe Zhang[1†], Mengfei Liu[1†], Ze Lin[1], Yori Endo[2], Guodong Liu[3], Bobin Mi[1], Wu Zhou[1*] and Guohui Liu[1*]

[1]Department of Orthopedics, Union Hospital, Tongji Medical College, Huazhong University of Science and Technology, Wuhan, China, [2]Division of Plastic Surgery, Brigham and Women's Hospital, Harvard Medical School, Boston, MA, United States, [3]Medical Center of Trauma and War Injuries, Daping Hospital, Army Medical University, Chongqing, China

Multiple rib fractures caused by trauma are common injuries and the internal fixation methods of these injuries have been paid more and more attention by surgeons. Absorbable plates and screws are the effective way to treat rib fractures, but there are no reports on which type of screw fixation method is most effective. In this study, finite element analysis was used to study the effects of five different types of screw fixation methods on anterior rib, lateral rib and posterior rib. The finite element model of the ribs was reconstructed from CT images, and the internal pressure (40 kPa) and intercostal force (30 N) on the surfaces of the ribs were simulated accordingly. An intercostal force of 30 N was applied to the upper and lower surfaces of the ribs to simulate the effect of intercostal muscle force. The pressure of 40 kPa was applied to the inner surface of the ribs, and the normal direction was applied to the inner surface of the ribs. The positive direction was considered inspiratory pressure, and the negative direction was considered expiratory pressure. The results indicate the optimal type of screw fixation on the absorbable plate for rib fractures, and provide a basis and reference for clinical application.

KEYWORDS

finite element, biomechanical analysis, absorbable plate, rib fixation, fracture healing

Introduction

Rib fracture is a relatively common injury, and multiple rib fractures can disrupt normal life of the affected patients (Baiu and Spain, 2019; Coary et al., 2020). In addition, as the global population continues to age, the incidence of rib fractures has increased significantly. At present, a variety of techniques have been used for the surgical fixation of rib fractures with varying recovery effects (Leinicke et al., 2013). The development of absorbable bone plates has received great attention for the treatment of rib fractures and maintenance of normal respiratory functions in the affected patients (Hur et al., 2016; Oyamatsu et al., 2016). The main rib fixation methods include anterior plate, intramedullary fixation, U-shaped plate and absorbable bone plate (Pieracci et al.,

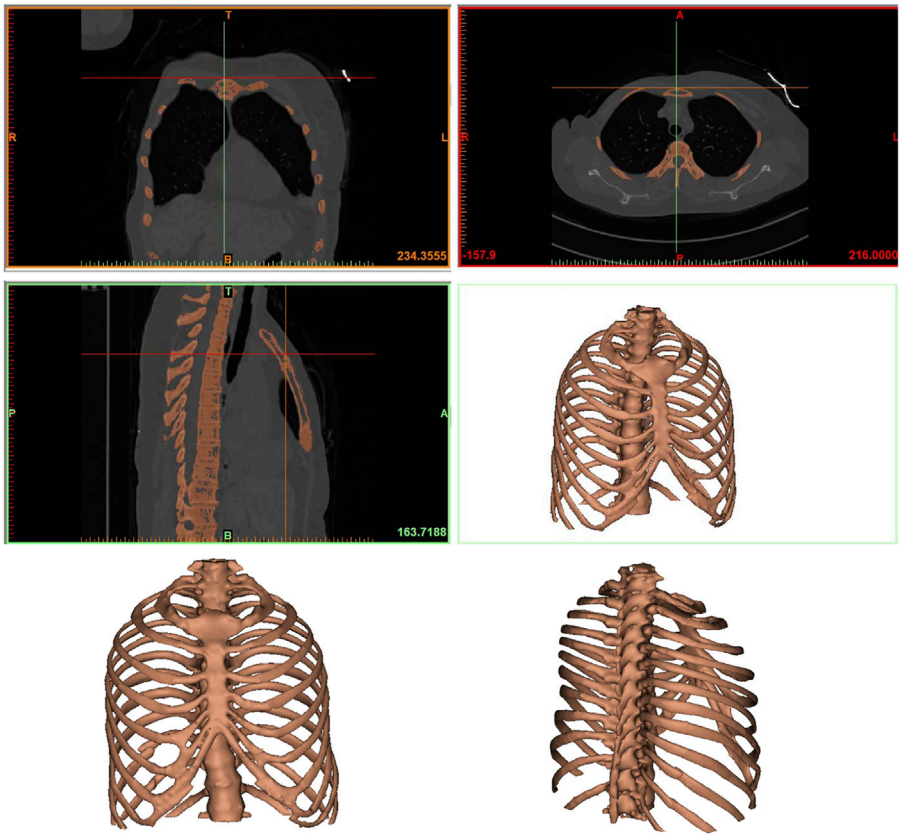

FIGURE 1
The finite element model of the rib. Anteroposterior and lateral thoracic models were reconstructed from CT data.

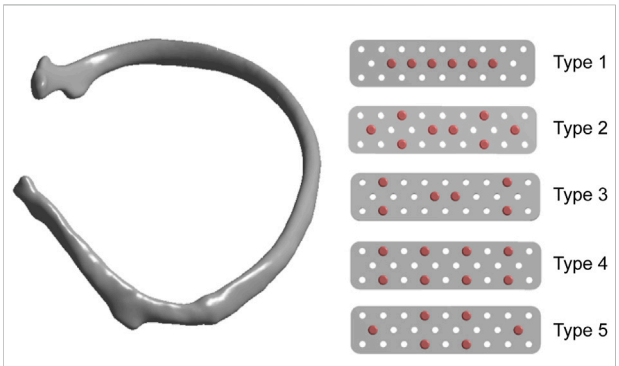

FIGURE 2
Five different screw fixation methods for the rib fractures with absorbable bone plates.

2017; Zhang et al., 2019). Nevertheless, the surgical fixation of rib fractures still needs further improvement. Some remain reluctant to surgically fix fractured ribs because of the poor results of internal fixation, the need for secondary removal, and the lack of strong evidence for this approach.

Biodegradable and absorbable bone plates have been used in a wide range of clinical applications, including cranial and maxillofacial fractures, metacarpal and phalanx fractures, ribs and ankle fractures (Chalidis et al., 2020). About 30% of fracture patients treated with traditional metal fixation experience serious complications, including nonunion, exposed plate, infection, and tendon rupture (Marasco et al., 2010). While metal implants help patients with early mobility, less strong implants may facilitate formation of more callus at the fracture site and improve the healing rates. Stress shielding is also a well-known complication of metal plate fixation, which can be mitigated by the use of a less rigid absorbable plate (Denard et al., 2018; Liverani et al., 2021). Similarly, the use of absorbable plates can reduce the risk of infection associated with traditional metal plate fixation. Several studies evaluating the use of absorbable plates and screws for surgical fixation of rib fractures in flail chest patients have shown that the technique is safe and effective (Nolasco-de la Rosa et al., 2015; Waseda et al., 2019). The slow absorption of absorbable

TABLE 1 Mechanical properties of physiological structures and internal fixation implants used to simulate finite element models.

Component/Materials	Elastic modulus (MPa)	Poisson ration
Cortical bone	9000	0.29
Cancellous bone	450	0.29
Cartilage	8	0.40
Absorbable plate/screw	5500	0.30

plates gradually transfers pressure to the bone, preventing osteoporosis at the fracture site and promoting fracture healing.

Although there are more and more studies on rib internal fixation, to our knowledge, no previous studies have been published on the effect of rib absorbable screw position on fixation. Previous rib models have incorporated some respiratory muscle mechanics, intercostal muscle movement, and fixation failures, but the optimal fixation type of rib fractures with screws on absorbable plates is yet to be examined. To date, there has been no study that simulates the effect of different screw fixation methods for rib fracture fixation using absorbable plates. Therefore, the purpose of this study was to establish a finite element model of the rib fracture and to analyze the optimal fixation position of the screws on the absorbable plate. These results will enable us to improve the internal fixation of rib fractures and provide a valuable reference for clinical work.

Materials and method

Clinical data and finite element modeling

A patient with a rib fracture sustained in a car accident underwent a CT examination and modeling after admission. In order to better characterize the injured site of the patient, Mimics software was used to reconstruct the thoracic rib model according to the CT data (Figure 1). A common fracture of the sixth rib was taken as an example to analyze the force of the anterior, lateral and posterior ribs fixed by absorbable plates and screws. Therefore, this part of the study involves construction of a computer finite element model that takes into account the geometry of ribs and plates, material properties and boundary conditions, as well as the respiratory muscle forces.

Firstly, the CT scan image was imported by selecting New Project Wizard on Mimics 20.0 software, and a model was initially generated. The pixels that affect the analysis and the bones that were not used in this analysis were then removed. Calculate 3D tool was used to build a 3D model for each layer, and a rib model was obtained and saved in STL format. Using the Geomagic Studio 2015 software, STL file saved in the previous step was opened and a ×4 mesh subdivision of the model polygon was performed to ensure that no serious deformation would occur during the model processing. The excess deformation features and sharp spikes were removed to obtain an accurate rib model. The precise surface module was used to detect the contour of the model, and the deformed or unreasonable contour was edited. The contour was added appropriately to generate regular surface pieces for the subsequent model processing. After the successful generation of surface slices, the surface slices were fitted, and the fitted surface model was derived into a general Step geometric model format. The Step geometric model file of the rib saved from Geomagic Studio 2015 software was opened with SolidWorks2017 software, and the geometric model was identified and surface was diagnosed according to the software, then the problematic surface was repaired, and the model was saved. The anterior, middle, and posterior fracture models of the ribs were established using a split command, while the ligament force area was cut to facilitate the subsequent loading.

Experimental conditions and biomechanical analysis

We set up five types of screw fixation methods on absorbable plates to analyze the stress (Figure 2). Referring to previous literature, in order to facilitate the simulation of real stress state on the ribs, the pressure of respiratory movement was set at 40 kPa, and the force of intercostal muscle was set at 30 N (Marasco et al., 2010; Kang et al., 2018). Establishment of the absorbable plate model: The bone plate and screw were established according to the model parameters (Table 1), and the plate and screw were assembled to the fracture area using the assembly command. After the assembly, the analysis model was saved and imported into ANSYS for finite element analysis. The geometric model was imported into ANSYS19.2, and isotropic material attribute parameters were established respectively, and related materials were assigned to each model. In order to ensure that accuracy of the calculation met the requirements of the analysis, the grid type and size were controlled, and the mesh type was set as the second-order tetrahedral mesh. After the mesh was set, the model was loaded and submitted for calculation according to the pressure and muscle force generated by human respiration.

Results

In this study, finite element analysis was used to simulate the screw distribution during the fixation of rib fracture with

10.3389/fbioe.2022.960310

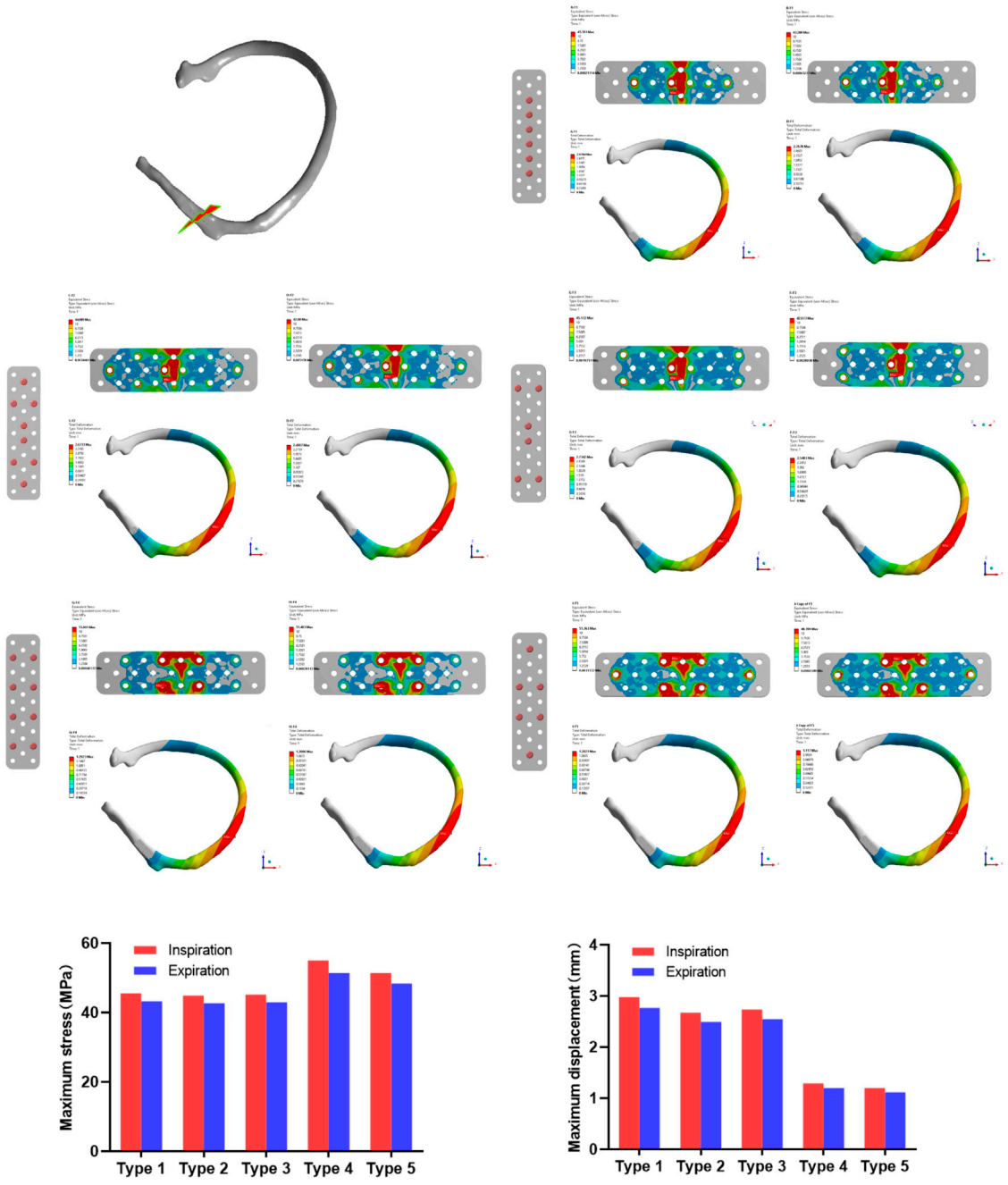

FIGURE 3
The maximum stress and displacement during inhalation and exhalation with anterior rib fracture in 5 different screw modes after plate fixation.

absorbable plate, and the optimal screw fixation form was determined to provide a reference for clinical application. In the analysis of the anterior rib fracture, as shown in Figure 3, the maximum stress of the absorbable plate on inhalation and exhalation with the first screw fixation was 45.593 MPa–43.288 MPa, and the maximum displacements during inhalation and exhalation were 2.9784 mm–2.7678 mm, respectively. In the second screw fixation method, the maximum stress of the absorbable bone plate on inspiration was 44.889 MPa and the maximum displacement was 2.6733 mm. During exhalation, the maximum stress of the absorbable bone plate was 42.68 MPa and the maximum displacement was 2.4907 mm. In the third screw fixation method, the maximum stress of the absorbable plate was 45.172 MPa and the maximum

10.3389/fbioe.2022.960310

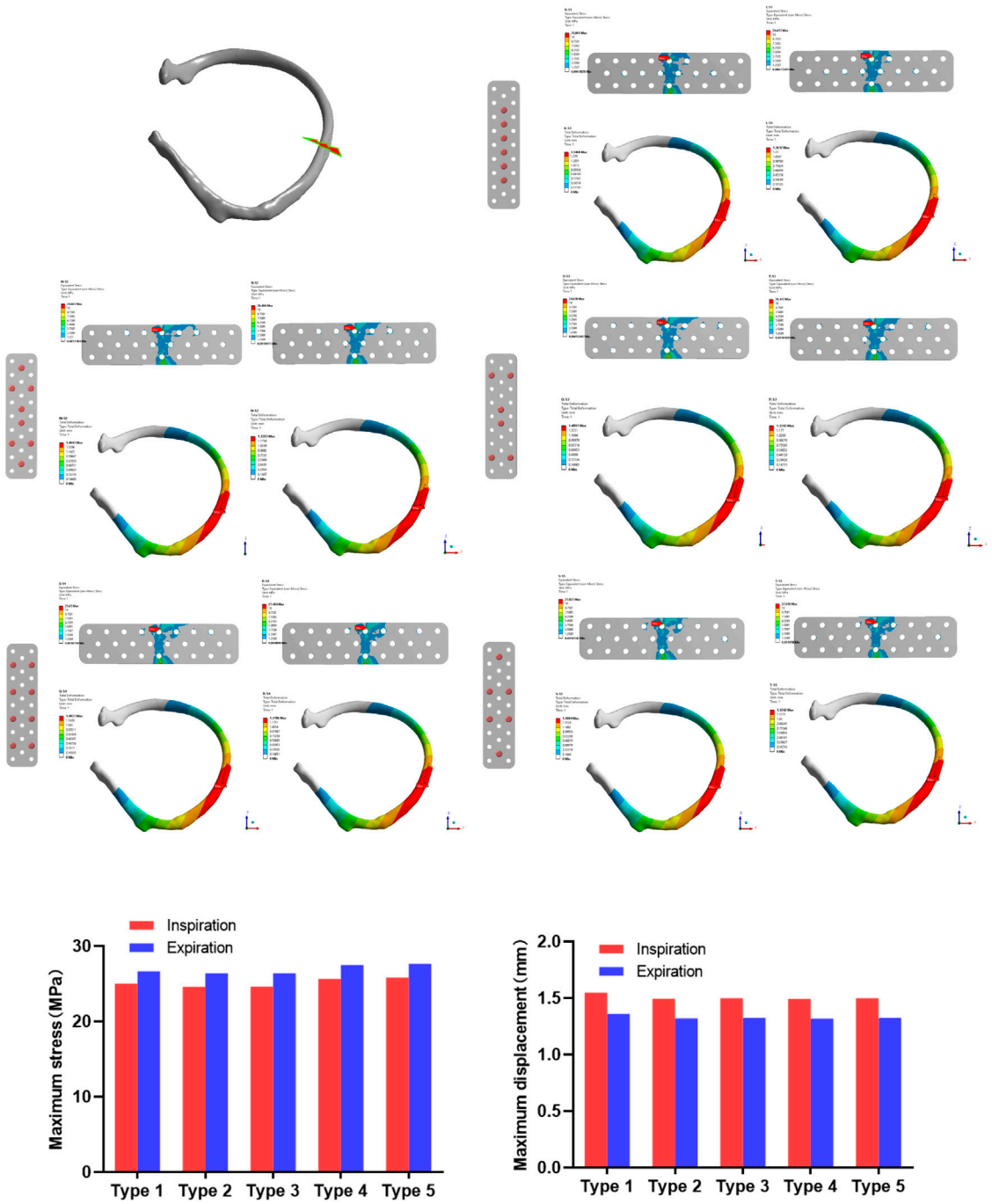

FIGURE 4
The maximum stress and displacement during inhalation and exhalation after the lateral rib fracture with different screw fixation methods.

displacement was 2.7342 mm on inhalation, while the maximum stress was 42.973 MPa and the maximum displacement was 2.5483 mm on exhalation. In the fourth screw fixation method, the maximum stress of the absorbable bone plate was 55.001 MPa on inhalation and 51.403 MPa on exhalation, and the corresponding maximum displacement of the absorbable plate on inhalation is 1.2923 mm and the maximum displacement on exhalation is 1.2006 mm. In the fifth screw fixation method, the maximum stress and maximum displacement of the absorbable plate on inhalation were 51.363 MPa and 1.2021mm, and the maximum stress and maximum displacement on exhalation were 48.399 MPa and 1.117 mm.

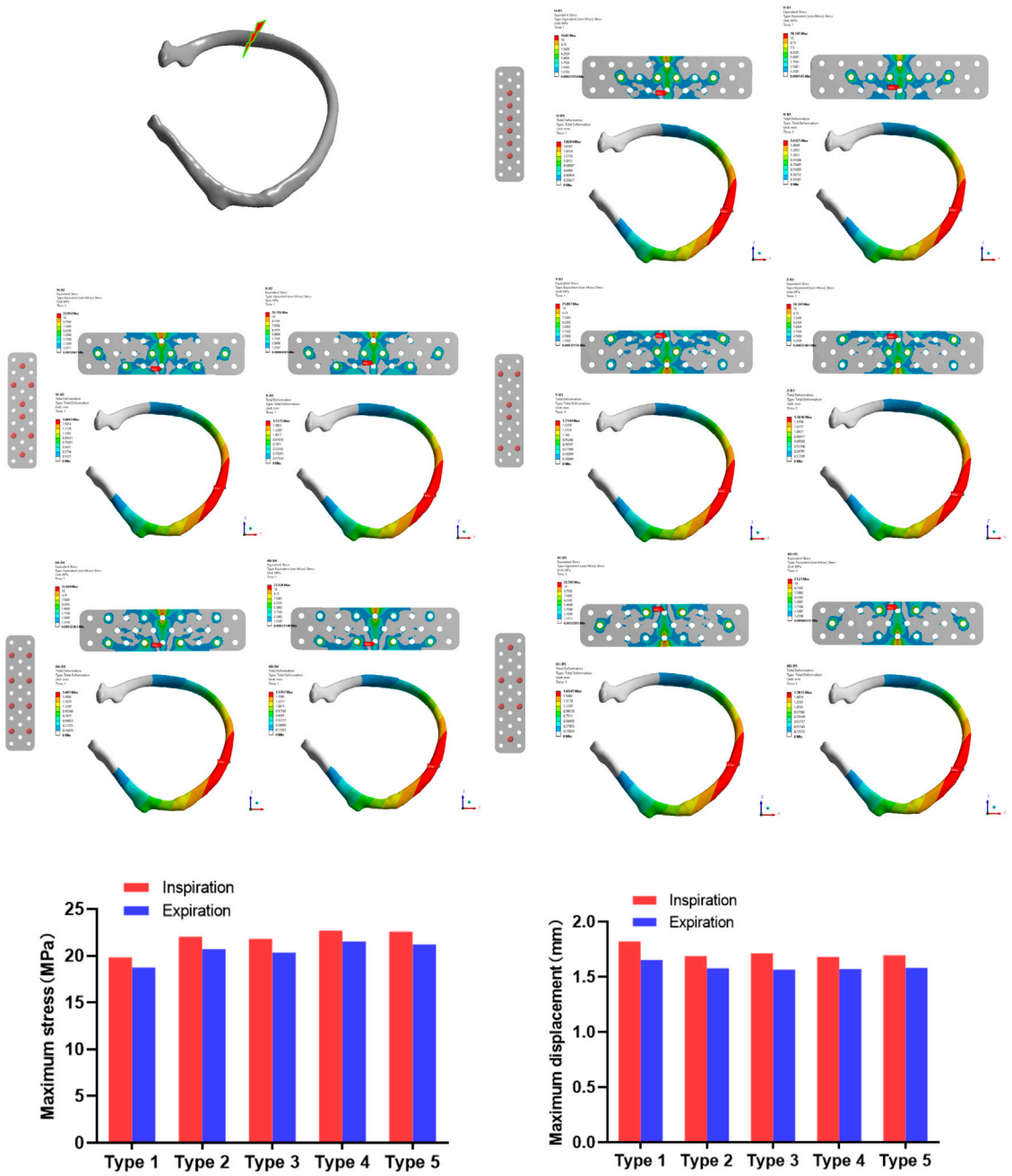

FIGURE 5
The maximum stress and displacement during inhalation and exhalation of the posterior rib fracture after the fixation with the absorbable plate and screws.

In the analysis of lateral rib fracture (Figure 4), the maximum inspiratory stress corresponding to 1-5 screw fixation methods was 25.005, 24.607, 24.638, 25.650, 25.825 MPa respectively. The maximum stress corresponding to expiratory stress was 26.657, 26.406, 26.412, 27.484, 27.656 MPa, respectively. In the analysis of displacement, the maximum displacements corresponding to the 1 to 5 screw fixation modes were 1.5468, 1.4947, 1.4997, 1.4927 and 1.4994 mm during inspiratory, and 1.3612, 1.3203, 1.3242, 1.3186 and 1.3242 mm, respectively during expiratory.

In the stress analysis of the rear rib fracture (Figure 5), the maximum stress of the absorbable bone plate upon inspiration in the 1-5 screw fixation modes was 19.82, 22.054, 21.807, 22.694, and 22.592 MPa. The maximum stress corresponding to exhalation is

18.741, 20.726, 20.341, 21.528, and 21.21 MPa respectively. In the analysis of the displacement of the rear rib fracture, the maximum displacements corresponding to the 1-5 screw fixation modes were 1.8204, 1.6893, 1.7144, 1.681 and 1.6945 mm during inspiration, and 1.6525, 1.5775, 1.5656, 1.5707 and 1.5815 mm respectively during expiration.

Discussion

The incidence of rib fractures is high, and patients with stable fractures can be treated conservatively with external fixation. In recent years, the treatment of multiple rib fractures has gradually shifted from conservative treatment to surgical internal fixation (Marasco et al., 2012). Early surgery can effectively restore the integrity of the thoracic structure, reduce respiratory energy consumption, accelerate the recovery of patients, and reduce complications (Shen et al., 2008). At the same time, the medical instruments for the fixation of rib fracture are constantly updated, from the early Kirschner wire, intramedullary nail, memory alloy bone graft to claw rib plate and absorbable bone plate, so that the operation is less complicated and the fixation effect is more optimized. The absorbable bone plate is expected to be an ideal rib fixation material because it does not require secondary removal and can eliminate stress masking (Väänänen et al., 2008; Al-Tamimi et al., 2020). Currently, although there are commercial absorbable bone plates for metacarpal, phalangeal, rib and ankle fractures, there is no unified standard for the fixation of screws on bone plates.

In this study, the rib fractures were divided into anterior, lateral and posterior ribs and absorbable plates were fixed according to the five different screw fixation methods described above. In the lateral rib fracture, the screw fixation methods of 1, 4, 5 showed greater stress on the fixed plate, while the 2 and 3 types of screw fixation showed less stress. Except for the displacement of the first fixation method being slightly larger, the displacement gaps of the other four types of screw fixation were not obvious. In the posterior rib fracture, the first type of screw fixation showed less stress, and the other four types of screw fixation showed no significant difference. In the analysis of displacement, the displacement of the first fixed model was more obvious than the other four modes, which was similar to the results of stress analysis.

Compared with the fracture of the lateral rib and the posterior rib, the anterior rib has a weaker structure because of the presence of cartilage, and the bone plate bears most of the force when stressed, so the stress of the anterior rib is relatively large (Holcombe et al., 2020). The analysis results showed that the displacement of the side ribs was relatively small, which may be because the ribs are curved and the structure is relatively stable in the middle of the arc when subjected to internal and external stresses, so the displacement of the lateral ribs fixed with absorbable plates is relatively small.

In summary, the conclusion is that the bone plate with anterior rib fracture has the largest stress, while the bone plates with 4 and 5 type screw fixation methods have the largest stress and the best fixation effect. The 1, 2 and 3 types of screw fixation have less stress, but the fixation effect is not adequate. Based on this, it can be inferred that the fixation effect of the fourth and fifth types of screw is better. Compared with the fourth type, the fifth type uses the least number of screws, so the optimal screw fixation form overall is the fifth type.

Conclusion

According to the method of finite element analysis evaluating different types of screw fixations of absorbable bone plate, anterior rib fracture fixation showed relatively higher stress values than lateral and posterior rib fractures, especially in the 4th and 5th types of screw fixation methods. Interestingly, 4 and 5 types of screw fixation methods displayed the least displacement for the largest stress value regardless of the type of rib fracture, and the best fixation effect when the stress of the absorbable bone plate was simulated. The fifth fixation method uses fewer screws and therefore can be considered the best fixation method among the five types examined.

Data availability statement

The original contributions presented in the study are included in the article/supplementary material, further inquiries can be directed to the corresponding authors.

Ethics statement

This study was approved by the Ethics Committee of the Wuhan Union Hospital, and written informed consent was obtained from all participants.

Author contributions

HX and ZZ designed the study and wrote the initial draft of this manuscript. ML and ZL performed the data collection and statistical analyses. YE searched and selected relevant studies. GL and BM put forward valuable opinions on the subject design. WZ and GL critically reviewed and approved the final manuscript. All authors read and approved the final manuscript.

Funding

This work was supported by the National Key Research and Development Program of China (2018YFB1105705), the Key

Research and Development Program of Hubei Province (2020BCB004).

Conflict of interest

The authors declare that the research was conducted in the absence of any commercial or financial relationships that could be construed as a potential conflict of interest.

Publisher's note

All claims expressed in this article are solely those of the authors and do not necessarily represent those of their affiliated organizations, or those of the publisher, the editors and the reviewers. Any product that may be evaluated in this article, or claim that may be made by its manufacturer, is not guaranteed or endorsed by the publisher.

Reference

Abdulaziz Al-Tamimi, A., Quental, C., Folgado, J., Peach, C., and Bartolo, P. (2020). Stress analysis in a bone fracture fixed with topology-optimised plates. *Biomech. Model. Mechanobiol.* 19 (2), 693–699. doi:10.1007/s10237-019-01240-3

Baiu, I., and Spain, D. (2019). Rib fractures. *Jama* 321 (18), 1836. doi:10.1001/jama.2019.2313

Chalidis, B., Kitridis, D., Savvidis, P., Papalois, A., and Givissis, P. (2020). Does the inion OTPS(TM) absorbable plating system induce higher foreign-body reaction than titanium implants? An experimental randomized comparative study in rabbits. *Biomed. Mat.* 15 (6), 065011. doi:10.1088/1748-605X/aba326

Coary, R., Skerritt, C., Carey, A., Rudd, S., and Shipway, D. (2020). New horizons in rib fracture management in the older adult. *Age Ageing* 49 (2), 161–167. doi:10.1093/ageing/afz157

Denard, P. J., Raiss, P., Gobezie, R., Edwards, T. B., and Lederman, E. (2018). Stress shielding of the humerus in press-fit anatomic shoulder arthroplasty: Review and recommendations for evaluation. *J. Shoulder Elb. Surg.* 27 (6), 1139–1147. doi:10.1016/j.jse.2017.12.020

Holcombe, S. A., Agnew, A. M., Derstine, B., and Wang, S. C. (2020). Comparing FE human body model rib geometry to population data. *Biomech. Model. Mechanobiol.* 19 (6), 2227–2239. doi:10.1007/s10237-020-01335-2

Hur, W., Park, M., Lee, J. Y., Kim, M. H., Lee, S. H., Park, C. G., et al. (2016). Bioabsorbable bone plates enabled with local, sustained delivery of alendronate for bone regeneration. *J. Control. Release* 222, 97–106. doi:10.1016/j.jconrel.2015.12.007

Kang, J., Wang, L., Yang, C., Wang, L., Yi, C., He, J., et al. (2018). Custom design and biomechanical analysis of 3D-printed PEEK rib prostheses. *Biomech. Model. Mechanobiol.* 17 (4), 1083–1092. doi:10.1007/s10237-018-1015-x

Leinicke, J. A., Elmore, L., Freeman, B. D., and Colditz, G. A. (2013). Operative management of rib fractures in the setting of flail chest: A systematic review and meta-analysis. *Ann. Surg.* 258 (6), 914–921. doi:10.1097/SLA.0b013e3182895bb0

Liverani, E., Rogati, G., Pagani, S., Brogini, S., Fortunato, A., Caravaggi, P., et al. (2021). Mechanical interaction between additive-manufactured metal lattice structures and bone in compression: Implications for stress shielding of orthopaedic implants. *J. Mech. Behav. Biomed. Mat.* 121, 104608. doi:10.1016/j.jmbbm.2021.104608

Marasco, S. F., Liovic, P., and Šutalo, I. D. (2012). Structural integrity of intramedullary rib fixation using a single bioresorbable screw. *J. Trauma Acute Care Surg.* 73 (3), 668–673. doi:10.1097/TA.0b013e3182569f75

Marasco, S. F., Sutalo, I. D., and Bui, A. V. (2010). Mode of failure of rib fixation with absorbable plates: A clinical and numerical modeling study. *J. Trauma* 68 (5), 1225–1233. doi:10.1097/TA.0b013e3181d27cab

Nolasco-de la Rosa, A. L., Mosiñoz-Montes, R., Matehuala-García, J., Román-Guzmán, E., Quero- Sandoval, F., Reyes-Miranda, A. L., et al. (2015). Unstable thorax fixation with bioabsorbable plates and screws. Presentation of some cases. *Cir. Cir.* 83 (1), 23–28. doi:10.1016/j.circir.2015.04.019

Oyamatsu, H., Ohata, N., and Narita, K. (2016). New technique for fixing rib fracture with bioabsorbable plate. *Asian cardiovasc. Thorac. Ann.* 24 (7), 736–738. doi:10.1177/0218492316650774

Pieracci, F. M., Majercik, S., Ali-Osman, F., Ang, D., Doben, A., Edwards, J. G., et al. (2017). Consensus statement: Surgical stabilization of rib fractures rib fracture colloquium clinical practice guidelines. *Injury* 48 (2), 307–321. doi:10.1016/j.injury.2016.11.026

Shen, W., Niu, Y., Mattrey, R. F., Fournier, A., Corbeil, J., Kono, Y., et al. (2008). Development and validation of subject-specific finite element models for blunt trauma study. *J. Biomech. Eng.* 130 (2), 021022. doi:10.1115/1.2898723

Väänänen, P., Koistinen, A., Nurmi, J., and Lappalainen, R. (2008). Biomechanical *in vitro* evaluation of the effect of cyclic loading on the postoperative fixation stability and degradation of a biodegradable ankle plate. *J. Orthop. Res.* 26 (11), 1485–1488. doi:10.1002/jor.20684

Waseda, R., Matsumoto, I., Tatsuzawa, Y., and Iwasaki, A. (2019). Successful surgical fixation using bio-absorbable plates for frail chest in a severe osteoporotic octogenarian. *Ann. Thorac. Cardiovasc. Surg.* 25 (6), 336–339. doi:10.5761/atcs.cr.17-00223

Zhang, Q., Song, L., Ning, S., Xie, H., Li, N., Wang, Y., et al. (2019). Recent advances in rib fracture fixation. *J. Thorac. Dis.* 11 (Suppl. 8), S1070–s1077. doi:10.21037/jtd.2019.04.99

frontiers | Frontiers in Materials

TYPE Original Research
PUBLISHED 03 August 2022
DOI 10.3389/fmats.2022.935096

OPEN ACCESS

EDITED BY
Boguang Yang,
The Chinese University of Hong Kong, China

REVIEWED BY
Jie Gao,
Second Military Medical University, China
Zhiwei Fang,
Johns Hopkins University, United States

*CORRESPONDENCE
Xiufeng Xiao,
xfxiao@fjnu.edu.cn
Yongqi Shan,
yongqishan@126.com

†These authors have contributed equally to this work

SPECIALTY SECTION
This article was submitted to Biomaterials, a section of the journal Frontiers in Materials

RECEIVED 03 May 2022
ACCEPTED 04 July 2022
PUBLISHED 03 August 2022

CITATION
Chen H, Liao R, Du Q, Li C, Xiao X and Shan Y (2022), Injectable hyaluronic acid/oxidized chitosan hydrogels with hypochlorous acid released for instant disinfection and antibacterial effects. *Front. Mater.* 9:935096. doi: 10.3389/fmats.2022.935096

Injectable hyaluronic acid/oxidized chitosan hydrogels with hypochlorous acid released for instant disinfection and antibacterial effects

Han Chen[1†], Ran Liao[2†], Qianqian Du[3], Cong Li[3], Xiufeng Xiao[4*] and Yongqi Shan[1*]

[1]Department of Pharmacy, Department of General Surgery, The General Hospital of Northern Theater Command, Shenyang, China, [2]Department of Urology, The Second Affiliated Hospital of Chengdu Medical College (China National Nuclear Corporation 416 Hospital), Chengdu, China, [3]Department of Biomaterial, College of Life Sciences, Mudanjiang Medical University, Mudanjiang, China, [4]College of Chemistry and Materials Science, Fujian Provincial Key Laboratory of Advanced Materials Oriented Chemical Engineering, Fujian Normal University, Fuzhou, China

Bacterial infections of wounds significantly increase the occurrence of complications, which have become a public health problem and pose a serious threat to human health. Therefore, an ideal wound dressing should not only possess suitable mechanical strength and a moist environment, but also instant disinfection and antibacterial properties. Owing to their high water content and permeability, hydrogels have great potential for the application in wound dressing. In this study, we developed an injectable hyaluronic acid (HA)/oxidized chitosan (OCS) hydrogel with good biocompatibility, self-healing, and tissue adhesive properties. Moreover, the slow release of micro hypochlorous acid (HClO), which is a common bactericide during hydrogel formation, can lead to instant disinfection; and the positive charge of OCS in this hydrogel can achieve a sustainable antibacterial effect. Thus, this hydrogel is a promising wound dressing material in clinical treatments.

KEYWORDS

hydrogel, injectable, hypochlorous acid, antibacterial effects, biocompatibility

Introduction

Bacteria are highly adaptable and ubiquitous in natural environments and bacterial infections of wounds are quite common in daily life (Li et al., 2018; Ahmed et al., 2020; Jamaledin et al., 2020). For instance, skin injuries caused by mechanical damage, undesirable temperatures, and chemicals are easily infected by bacteria when one fails to clean potentially infectious microbiological and necrotic tissues in time. Currently, various antibacterial strategies have been proposed, including photodynamic antimicrobial therapy (Hu et al., 2019; Chandna et al., 2020), hydrophilic antifouling coatings (Knowles et al., 2017; Tian et al., 2019), and metallic nanomaterials (Vimbela

et al., 2017; Rehman et al., 2018). However, the aforementioned strategies also have some limitations, such as the complex operation and release of harmful ions. Therefore, it is still a challenge to develop a convenient wound dressing material with effective antibacterial properties.

The process of wound healing provides the inspiration for antibacterial wound dressing design (Makvandi et al., 2019; Zhang et al., 2019). Wound healing, a complex process of natural restoration and tissue growth progression, involves the following four different phases: the coagulation and hemostasis phase, inflammatory phase, proliferation period, and maturation phase (Derakhshanfar et al., 2019; Abdollahi et al., 2021). These phases must occur in a proper sequence and penetrate each other in a well-connected cascade to create optimal wound healing. The pathological conditions of the wound and the type of dressing material significantly affect the progress of these phases. Inspired by the progress of moist wound healing, we envision hydrogels to be the ideal wound dressing material because of their three-dimensional (3D) polymer network structure, which is similar to an extracellular matrix (Smithmyer et al., 2014; Gaspar-Pintiliescu et al., 2019). Owing to their excellent biocompatibility, absorption capability, and biodegradability, natural polymers containing alginate (Aikawan et al., 2015; Emami et al., 2018; Zhang et al., 2018), collagen (Cho et al., 2017; Wakuda et al., 2018; Lin et al., 2019), chitosan (CS) (Wang et al., 2018; Shariatinia, 2019; Bagheri et al., 2021), and hyaluronic acid (HA) (Li et al., 2018; Zhu et al., 2018; Kim et al., 2019; Wolf and Kumar, 2019), derived from animals, plants, and microorganisms are widely used to prepare antibacterial hydrogels applied in wound dressings.

CS is the product of the *N*-deacetylation of chitin with widespread applications in biomaterials owing to its non-toxicity, ease of modification, and antibacterial activity. Its unique antibacterial effect is based on the abundant positively charged primary amine groups, garnering increasing attention from researchers in the design of CS-derived antibacterial biomaterials. Bagheri et al., designed and fabricated CS/polyethylene oxide (PEO) nanofibers conjugated with antibacterial silver and zinc oxide nanoparticles. These nanocomposites showed a good antioxidant effect and antibacterial activity against *S. aureus*, *E. coli*, and *P. aeruginosa* (Bagheri et al., 2021). For the application of CS, its poor water solubility is the main obstacle (Pellá et al., 2018). Fortunately, the oxidation of CS can solve this problem and simultaneously provide CS with a new reactivity. Another natural polymer, HA, is an acidic glycosaminoglycan consisting of *N*-acetyl-D-glucosamine and D-glucuronic acid units. Because HA has super water absorption and retention properties, HA has been applied in a wide range from cosmetic materials to bioengineering scaffolds (Litwiniuk et al., 2016; Park et al., 2019).

Recently, diverse injectable antibacterial hydrogels have been developed using various methods, such as physical crosslinking (hydrogen bond, hydrophobic interactions, and electrostatic interactions) (Shao et al., 2017; Deng et al., 2018; Liang et al., 2019; Wang J et al., 2020), and chemical crosslinking (Michael addition, Schiff-base reaction, and click reaction) (Jalalvandi et al., 2017; Huang et al., 2018; Du et al., 2019; Pupkaite et al., 2019; Pérez-Madrigal et al., 2020). The Schiff-base reaction has primarily garnered particular interest owing to its short gelling time and gentle gelling condition. Therefore, we designed and prepared this hydrogel, which is based on the Schiff-base reaction of oxidized chitosan (OCS) and hydrazine-modified HA (HA-ADH). Although hypochlorous acid (HClO) is an efficient antibacterial agent (Chen et al., 2016; Raval, et al., 2021), it is limited in application to clinical treatment owing to its instability. To address this issue, we utilized the reaction between calcium hypochlorite and salicylic acid to produce hypochlorous acid along with the formation of the hydrogel. During hydrogel formation, through the mixing of OCS and HA-ADH solutions, HClO is released simultaneously owing to the reaction between salicylic acid (SA) and calcium hypochlorite that are previously dissolved in the OCS and HA-ADH solutions, respectively.

In this article, we present a novel hydrogel system that can *in situ* gel on the surface of a wound to be used as an antibacterial wound dressing material. This new hydrogel dressing is able to achieve a desirable "instant disinfection and antibacterial" therapeutic effect. Moreover, this hydrogel shows good biocompatibility, mechanical, and tissue-adhesive properties. All these characterizations demonstrate that this hydrogel has great potential to be used as an antibacterial wound dressing material to accelerate wound healing.

Experimental

Materials

Chitosan (CS, molecular mass of ~50 kDa, deacetylation degree of 95%), sodium periodate ($NaIO_4$ ≥99.0%), N-(3-Dimethylaminopropyl)-N′-ethylcarbodiimide hydrochloride (EDC), sodium hydroxide (NaOH), agarose, methylene blue, methyl orange, and propidium iodide (PI) were purchased were purchased from Macklin and were used directly. Sodium hyaluronate (HA, molecular mass of 92000 Da) was purchased from Shandong Focuschem Biotech Co., Ltd. 1-Hydroxybenzotriazole (HOBt) and adipic acid dihydrazide (ADH) were purchased from J&K Chemical. PBS (pH = 7.4), fetal bovine serum (FBS), penicillin–streptomycin (PS) solution, Dulbecco's modified Eagle medium (DMEM) L-glutamine, and calcein AM were purchased from Gibco Co., Ltd. (Carlsbad, CA, Uniteed States).

Synthesis and characterization of OCS

For the synthesis of OCS, 2 g chitosan was first dissolved in 200 ml 0.5 wt% dilute glacial acetic acid aqueous solution. 1.325 g

sodium periodate ($NaIO_4$) was added into the mixture to oxide the chitosan polymer. The reaction was stirred for 24 h in the dark at room temperature. Subsequently, the mixture solution was dialyzed against deionized water (DI water) for 4 days to remove the unreacted small $NaIO_4$ molecule (14 kDa cutoff dialysis membrane). The obtained purified product was freeze-dried by a lyophilizer and stored at −20°C in the freezer. The OCS samples were analyzed by Fourier transform infrared (FT-IR) spectroscopy. In detail, the KBr pellet method was used in the range of 500–4,000 cm^{-1} at 25°C, recorded with a Nicolet 5700 spectrophotometer (Thermo Fisher Scientific Inc., MA).

Synthesis and characterization of HA-ADH

First, 2 g of HA (M = 920000 Da) was dissolved in 200 ml of the buffer solution (pH = 6.5). Afterward, 2.5 g EDC and 1.78 g HOBT were added into the HA solution and kept stirring at room temperature. After 1 h, 9 g adipic dihydrazide (ADH) was added into the mixture solution and the reaction was further stirred and kept for 24 h at room temperature to obtain the crude product. The product was purified against DI water for 4 days by a dialysis membrane (14 kDa cutoff dialysis membrane), and the product was lyophilized, and then stored at- 20°C in the freezer. The HA-ADH samples were also analyzed by Fourier transform infrared (FT-IR) spectroscopy with a similar protocol as that of OCS.

Preparation of injectable OCS/HA hydrogels

An injectability test was performed as described (Makvandi et al., 2019; Makvandi et al., 2021). In the first step, the HA-ADH solution and OCS solution was prepared separately by dissolving in PBS at different concentrations. Then, these two solutions were subsequently mixed at a volume ratio of 1:1 by using a double-barrel syringe. The hydrogels with different component concentrations were labeled as OCS_x/HA hydrogels meaning that the concentration of HA-ADH was fixed at 3% and the concentration of OCS was signed as y % (4%, 5%, 6%, and 7%).

Preparation of injectable OCS/HA-HClO hydrogels

Based on the preparation of the OCS/HA hydrogel, we further developed the OCS/HA-HClO hydrogel. Briefly, HA-ADH was dissolved in the PBS buffer with 125 mg/L of a $Ca(ClO)_2$ solution and OCS was dissolved in the PBS buffer of 2.5 mM salicylic acid (SA), respectively. Then, these two precursor solutions were added into the two independent cavities of the double-barrel syringe. Through the mixed injection of these prepared two solutions into models or in the surface of skin with the volume ratio of 1:1, a series of OCS/HA-HClO hydrogels was formed with the *in situ* gelation method.

Gelation time test of the OCS/HA hydrogels

The gelation time was measured by a tube-inversion method (Jommanee et al., 2018; Wang Y et al., 2020). Briefly, HA-ADH and OCS were separately dissolved in the PBS solution. These two kinds of solutions were mixed with a double-barrel syringe to obtain the HA/OCS hydrogels, and the gel time was denoted as the time when the hydrogels showed no ability to flow. The gel time of OCS/HA-HClO hydrogel was determined by a similar method.

Swelling ratio measurement of the OCS/HA hydrogels

To evaluated the swelling kinetics behavior of the OCS/HA hydrogels, all samples (100 μL, n = 5) were prepared in a PTFE mold (10 mm in diameter, 1 mm in height), respectively. All samples were immersed in 500 μl of the PBS buffer for 24 h at room temperature. Then, the hydrogels were removed from the PBS buffer and weighted at specific time intervals (0.5, 1, 3, 7, 12, and 24 h) after removing the liquid around the samples. This weight was marked as W_s. Hydrogels were subsequently freeze-dried to obtain the dry weight (W_d).

The following formulation is used to calculate the swelling ratio of hydrogels:

$$\text{Swelling ratio}\,(\%) = \frac{W_s - W_d}{W_d} \times 100\%.$$

Degradation properties' measurement of hydrogels

The degradation rate of hydrogels was also characterized. OCS_4/HA, OCS_5/HA, OCS_6/HA, and OCS_7/HA (100 μl, n = 5) were immersed in 1 ml of the PBS buffer for 12 h at room temperature to reach the swelling equilibrium. We marked this time point as 0 h and the weight of the hydrogel samples were recorded as W0. Then, these swelled hydrogel samples were immersed in 1 ml PBS buffer at 37°C for the degradation test. At specific time intervals (1, 4, 10h, 1d, 2d, 4d, and 7d), the hydrogel samples were weighed as W1. Therefore, the degradation remaining ratio was calculated as W1/W0 × 100%.2.9 Rheological test of hydrogels.

All rheological experiments were carried out on a TA Discovery DHR-2 rheometer equipped with a parallel plate with an 8 mm diameter and a 1 mm gap size at 25°C. Oscillation strain sweep was performed with fixed oscillation frequency 1 Hz and variable applied strain from 1 % to 1,000%.

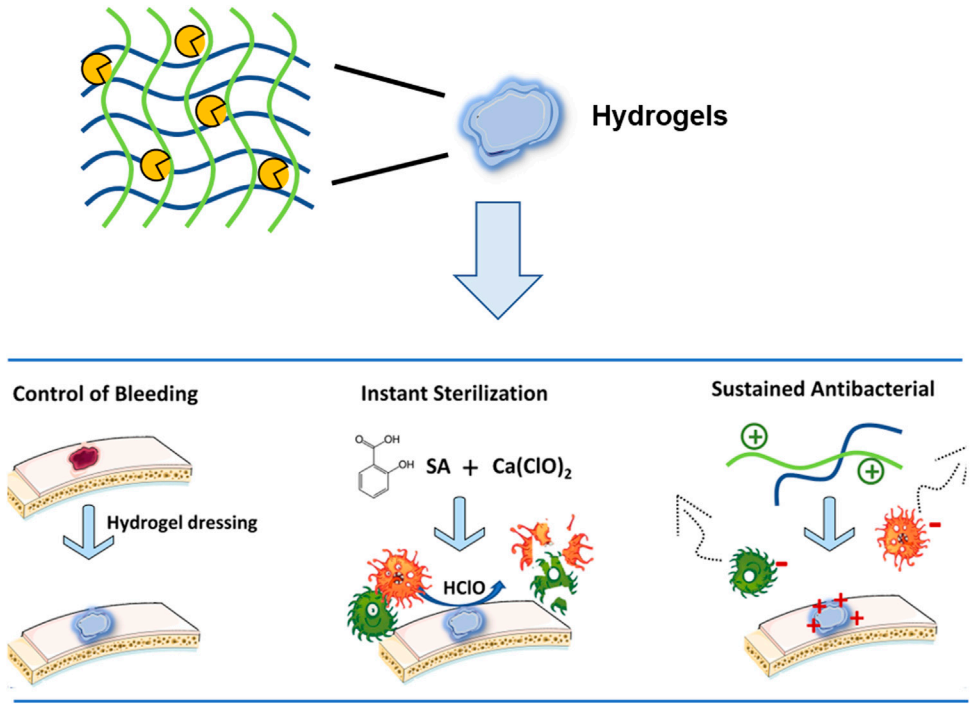

SCHEME 1
Scheme of the antibacterial activity of the OCS/HA-HClO hydrogel.

Alternating strain sweep was measured with a fixed oscillation frequency of 1 Hz and sequential strains with 1% (100 s) and 500% (100 s) for 3 cycles.

Self-healing, injectable, and tissue-adhesive properties' observation

The self-healing, injectable, and adhesion behaviors were measured by a macroscopic experiment. In detail, in order to test the self-healing performance of hydrogels, two triangular pieces (10 mm sides, 1 mm thickness) of a hydrogel were stained with methylene blue and methyl orange, respectively. These behaviors of hydrogels were monitored by digital photographs with specific time intervals. As for the injectable behavior test, the dyed hydrogel is directly injected into the PVC mold of the pentacle successively. Porcine skin was purchased to test the adhesive of the hydrogel, and the hydrogel was stained with methylene blue.

In Vitro antibacterial activity test of hydrogels

E. coli (Gram-negative) and *S. aureus* (Gram-positive) were used to assess the antibacterial activity of hydrogels. Antibacterial activity of the OCS/HA hydrogel and the OCS/HA-HClO hydrogel were evaluated *in vitro* by agar plate diffusion tests. During antibacterial activity tests, the OCS/HA hydrogel and the OCS/HA-HClO hydrogel were selected as the experimental groups. Then the as-prepared bacterial suspensions, which contained approximately 1×10^6 CFU ml^{-1}, were added into the following groups: 1) PBS buffer (990 μl); 2) agarose hydrogel coated 48-well plate; 3) OCS/HA hydrogel coated 48-well plate; 4) OCS/HA-HClO hydrogel coated 48-well plate; and 5) penicillin–streptomycin (PS) solution (990 μL). All samples were incubated at 37°C for 2 h, and the bacterial was re-suspended in 1 ml of PBS buffer. The diluent bacterial suspension solution (10^4 CFU ml^{-1}) was seeded onto the Luria-Bertani (LB) agar surface and then incubated for 24 h at 37°C. The samples were measured with macroscopic digital photographs.

In Vitro biocompatiblity test of hydrogels

In order to test the biocompatibility of our OCS/HA-HClO and OCS/HA-HClO hydrogels, we used 3T3 cells as the model cells. The OCS/HA and OCS/HA-HClO hydrogels (total volume for per hydrogel is 200 μl, $n = 4$) were formed in the bottom of 24-well plates, respectively. Then, 1 ml of a growth media containing 2×10^5 3T3 cells were added into the 24-well plate. After 2 d or 5 d of culture, the OCS/HA and OCS/HA-HClO hydrogels were taken out

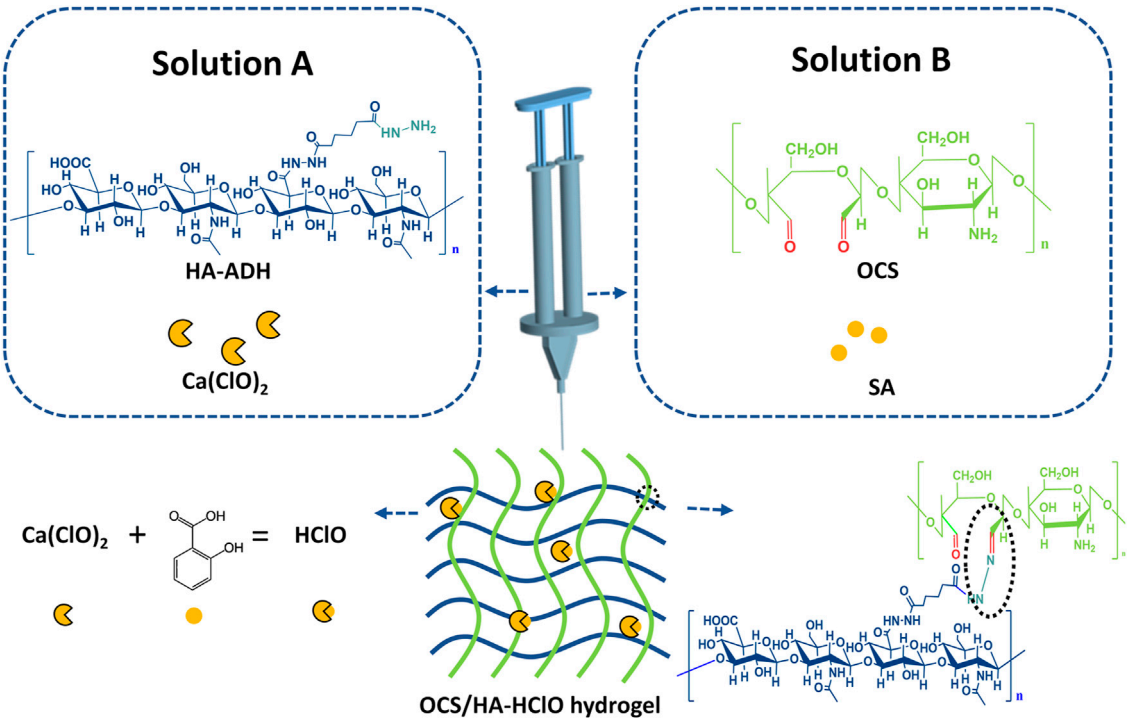

FIGURE 1
Fabrication of the OCS/HA-HClO hydrogel based on the reversible Schiff-based reaction.

from the 24-well plate to test the cell viability of 3T3 cells on the surface of the hydrogels by live/dead staining.

After 2 d or 5 d of culture as described previously, the cell viability assay was performed. The cells were cultured without hydrogels as the control group. 90 μl culture medium of each group was taken out and added into the 96-well plates. Then, 10 μl of a CCK-8 kit solution was added to each well and the plates were incubated at 37°C for about 2 h. Next, a microplate reader was used to measure the optical density (OD) at 450 nm. The survival rate of cells = (experimental group OD value—blank group OD value)/(control group OD value—blank group OD value).

Results and discussion

Fabrication of the OCS/HA-HClO hydrogels

In this study, we developed an injectable, self-healing, bioadhesive, and antibacterial hydrogel that is based on the natural polymer materials of CS and HA to overcome the challenge of covering irregular wounds and subsequently providing an antibacterial protection of the wounds (Scheme 1 and Figure 1).

The synthetic routes of HA-ADH and OCS are shown in Figures 2A,B. HA was conjugated with ADH in the presence of EDC and HOBT. CS reacted with $NaIO_4$ to form the OCS. The successful modification of natural HA and CS polymers was then characterized by Fourier transform infrared (FT-IR) spectroscopy. Compared with HA, the FT-IR spectra of the HA-ADH shows characteristic peaks at 1,130 cm^{-1} that are attributed to the hydrazide group, indicating that HA-ADH was successfully prepared (Figure 2C). In the FT-IR spectra of OCS, the clear peaks at 2,900 and 3,010 cm^{-1} indicate the satisfactory formation of the aldehyde groups in the OCS backbone (Figure 2D). Two types of precursor solutions were obtained by dissolving HA-ADH and OCS in $Ca(ClO)_2$ and SA solutions, respectively. Notably, the acidity of SA can improve the solubility of OCS. The prepared solution A (HA-ADH/$Ca(ClO)_2$ solution) and the solution B (OCS/SA solution) were separately sucked into two independent syringes. We used a tee cock valve to connect these two syringes and a 27G needle, and subsequently performed the mixing injection to form the OCS/HA-HClO hydrogel on the surface of the wound directly. This hydrogel is mildly but rapidly formed within minutes after mixing (Supplementary Figure S1 and Supplementary Table S1). As shown in Supplementary Figure S1, the gelation time decreases accompanied by the increase of the OCS concentration. The crosslinkings of the OCS/HA-HClO hydrogel are formed based on the spontaneous Schiff-base reaction of the aldehyde groups in OCS and the hydrazide

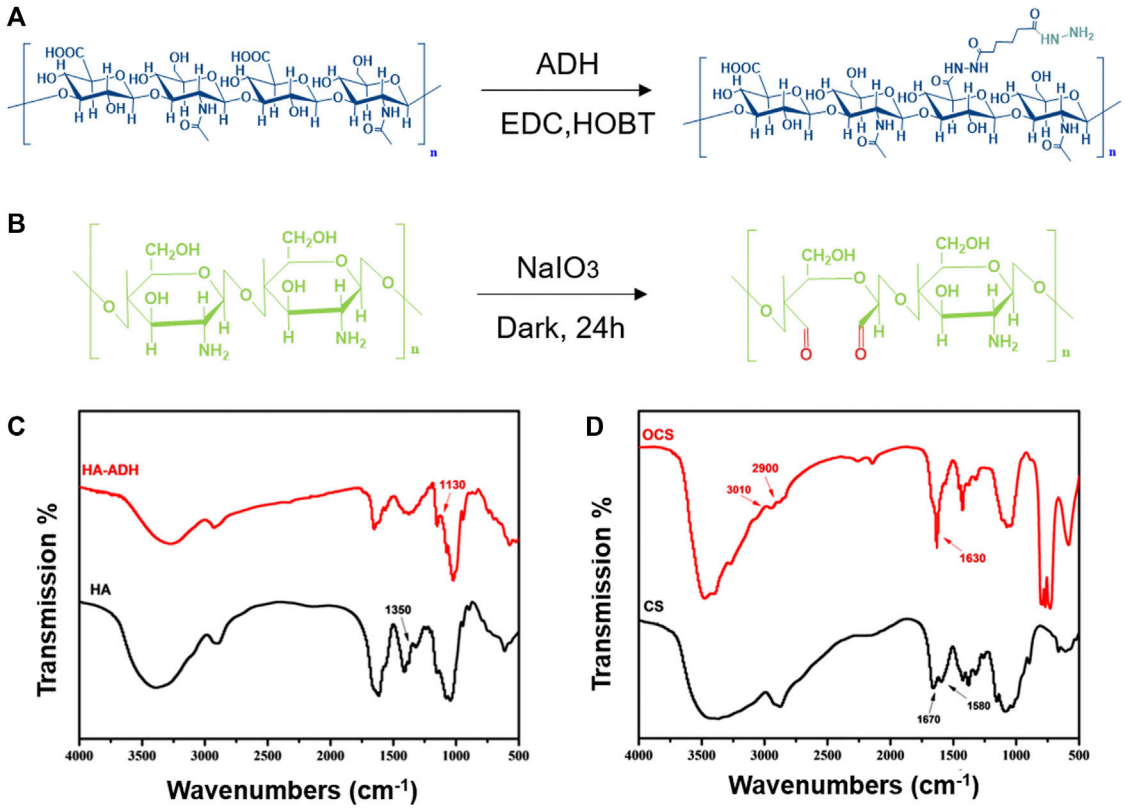

FIGURE 2
Fabrication and structural characterization of HA-ADH and OCS. The synthetic route of **(A)** HA-ADH and **(B)** OCS. FT-IR spectra of **(C)** HA, HA-ADH, **(D)** CS, and OCS.

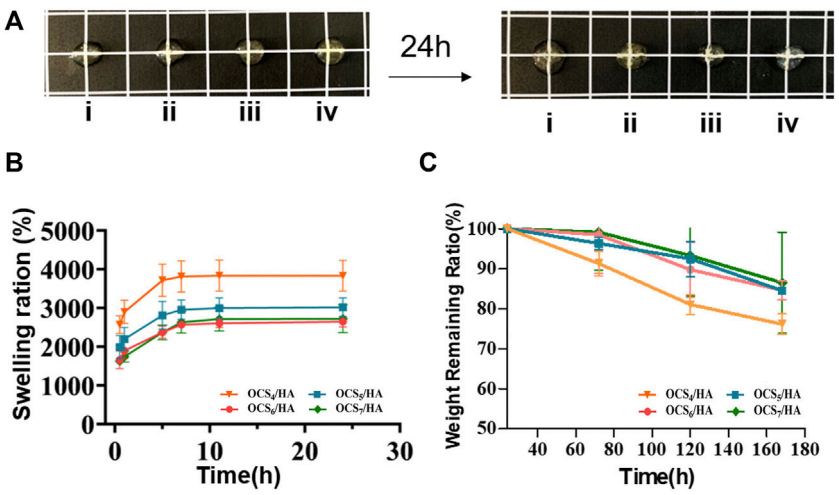

FIGURE 3
Swelling and degradation properties of the OCS/HA hydrogels with different OCS concentrations. **(A)** Photographic illustration of the OCS/HA hydrogels before and after reaching swelling equilibrium in a phosphate-buffered saline (PBS) buffer after 24 h: (i) OCS_4/HA, (ii) OCS_5/HA, (iii) OCS_6/HA, and (iv) OCS_7/HA. The square grid is 1 × 1 cm. **(B)** Swelling profiles of OCS/HA hydrogels over 24 h in PBS at 37°C. **(C)** Degradation ratio of the OCS/HA hydrogel in PBS at 37°C for 7 days *in vitro*.

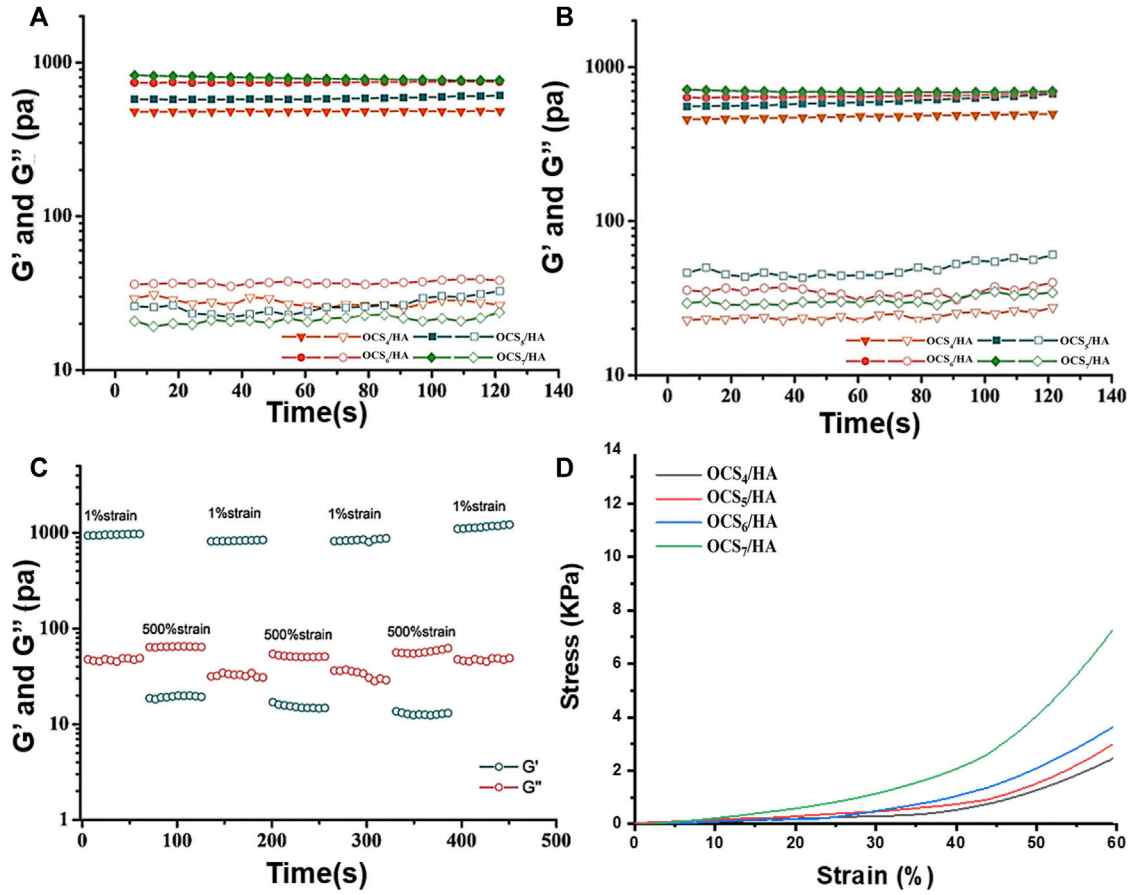

FIGURE 4
Rheological properties of the OCS/HA hydrogels. Time sweep measurements of the **(A)** OCS/HA hydrogel and the **(B)** OCS/HA-HClO hydrogel. **(C)** Alternating strain sweep of the OCS_7/HA-HClO hydrogel with a low strain at 1% and a high strain at 500%. **(D)** Compressive test of the OCS/HA hydrogel.

groups in HA-ADH. Simultaneously, the predissolved $Ca(ClO)_2$ in solution A and SA in solution B react with each other to release bactericide HClO (Scheme 1). The fresh HClO functions as an oxidizer to oxidate the protein on the surface of the bacteria to timely kill the bacteria in the wound. After the instant disinfection, the positive charges of the OCS/HA-HClO hydrogels from the protonated amino groups of OCS provide antibacterial protection for the wound. During gelation, some aldehyde groups of OCS also react with the amino groups of the wound tissue, such that the OCS/HA-HClO hydrogel can adhere to the wound tightly to offer all-around protection for the wound.

Swelling and degradation profiles of the OCS/HA hydrogels

Comparing the photographs of the OCS/HA hydrogels before and after immersing in the PBS buffer for 24 h, we discovered that the swelling ratio of the OCS/HA hydrogel decreases with increasing OCS concentration (Figure 3A). The swelling profile of this series of OCS/HA hydrogels in Figure 3B also indicates this phenomenon and further shows that when the OCS concentration is greater than 6%, the swelling ratio remains basically unchanged at 1.5 times of the hydrogels' original weights. All groups of the OCS/HA hydrogels reach the swelling equilibrium after soaking for 10 h in PBS, demonstrating the good water-absorbing quality of the OCS/HA hydrogels. Therefore, the OCS/HA hydrogel is able to absorb the exudate promptly and efficiently. Furthermore, the degradation behavior was determined in Figure 3C. The degradation rate of hydrogels decreases with the increase in the OCS concentration and reaches the maximum value when the OCS concentration exceeds 6%. The aforementioned results indicate that the changing trends of the swelling ratio and degradation speed are highly similar. This is because both the swelling and degradation behaviors are closely related to the

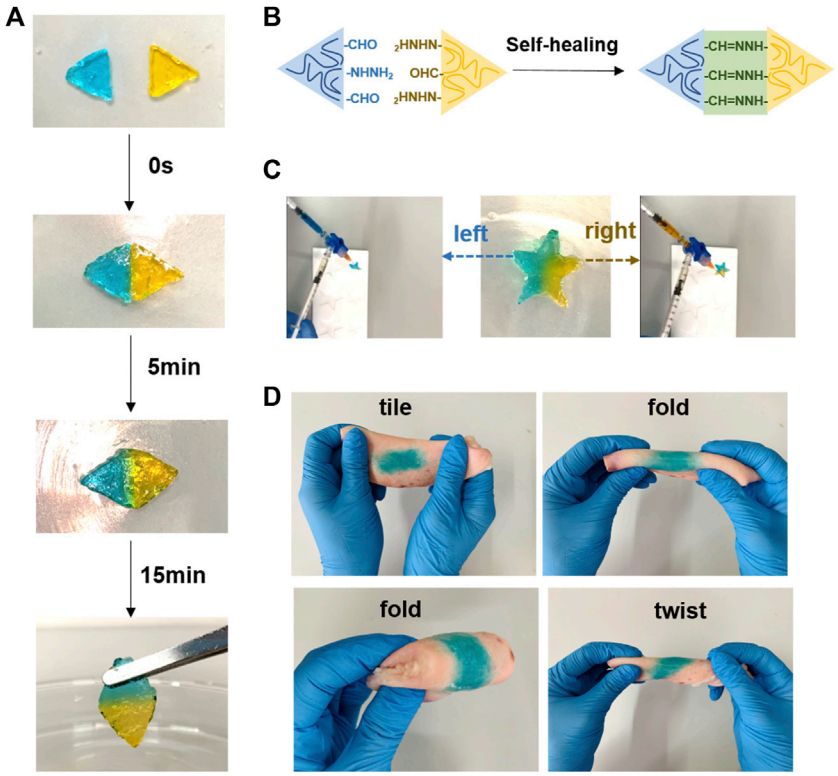

FIGURE 5
Self-healing, injection, and adhesion performance of the OCS/HA-HClO hydrogels. **(A)** Photo illustration of the self-healing process. **(B)** Schematic of self-healing of the OCS/HA-HClO hydrogels. Photo illustration of **(C)** injection and **(D)** adhesion of hydrogels.

crosslinking density of the hydrogel. A high crosslinking density implies a dense 3D hydrogel structure that prevents the permeation of water into the hydrogel and the degradation of the hydrogel framework. Therefore, these results illustrate that the crosslinking density of the OCS/HA hydrogel is improved through the increment in the OCS concentration and does not change after the OCS concentration reaches 6%. This is because the hydrazide group number of HA-ADH is more than the aldehyde group number of OCS in OCS_4/HA and OCS_5/HA groups, and the excess OCS can lead to the further formation of crosslinkings. When the OCS concentration was raised to 6%, all hydrazide groups of HA-ADH were utilized to form crosslinkings; thus, a further increment of OCS concentration did not affect the crosslinking density of the OCS/HA hydrogel.

Rheological properties of the OCS/HA and OCS/HA-HClO hydrogels

The time sweep results of OCS/HA in Figure 4A show that the storage modulus (G′) is higher than the loss modulus (G″) for all groups of the OCS/HA hydrogels, demonstrating the successful gelation of the OCS/HA hydrogels. It also proves that the increasing amount of OCS in the OCS/HA hydrogels leads to the increment of both G′ and G″ until the OCS concentration reaches 6% (Figure 4A). Therefore, the changing trend of the modulus is similar to those of the swelling and degradation ratios. This finding confirms our speculation that when the OCS concentration reaches 6%, all the hydrazide groups of HA-ADH are consumed to form the crosslinking inside the hydrogel; thus, increasing the OCS concentration to 7% no longer improves the modulus of the OCS/HA hydrogels. We subsequently performed the rheological time sweep test for the OCS/HA-HClO hydrogels. The results prove that the addition of SA and $Ca(ClO)_2$ has no negative effects on the formation of hydrogels (Figure 4B). Considering the swelling ratio, degradation rate, and rheological modulus results, we selected the OCS_7/HA-HClO hydrogel for all the subsequent tests. Accordingly, the redundant aldehyde groups of OCS can react with the amino groups of wound tissue to help the OCS/HA-HClO hydrogel adhere to wounds tightly.

Through the strain sweep of the OCS/HA-HClO hydrogel in Supplementary Figure S2, we observe that the intersection of G′ and G″ curves is approximately 200%, implying that the strain higher than 200% could break the large proportion of crosslinkings inside the OCS/HA-HClO hydrogels. Therefore,

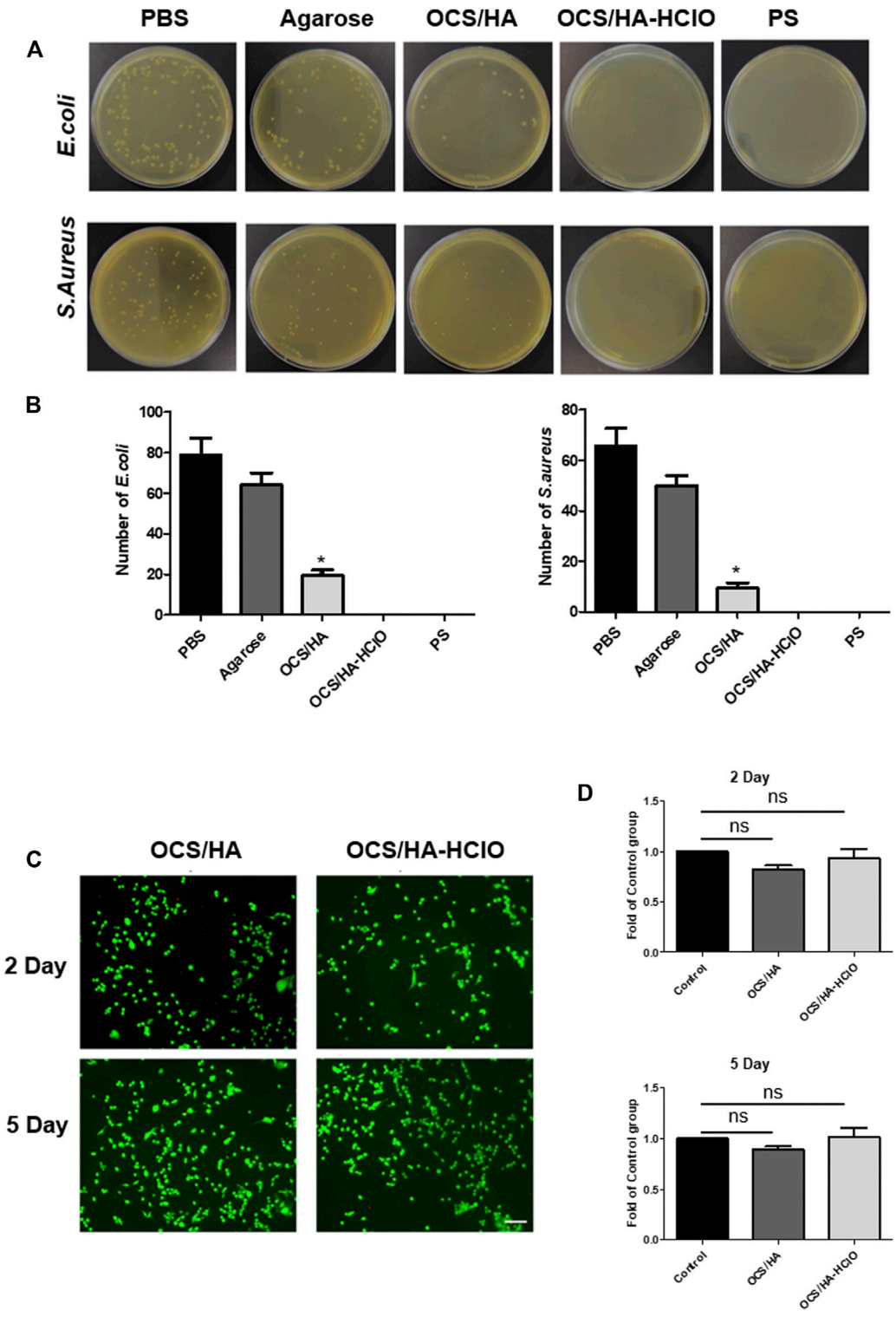

FIGURE 6
Antibacterial performance and biocompatibility of the OCS/HA and OCS/HA-HClO hydrogels. **(A)** Antibacterial performance of hydrogels against *E.coli* and *S.aureus*. **(B)** Quantitative data of A. In this experiment, the PBS group is the blank control; the Agarose group is the negative control; Penicillin-Streptomycin (PS) is the positive control. $p < 0.05$ **(C)** Live/dead staining of 3T3 cells on the surface of the OCS/HA and OCS/HA-HClO hydrogels after 2 d and 5 d of *in vitro* culture, respectively ($n = 4$, scale bar: 100 μm).**(D)** Anti-proliferation effect of the OCS/HA and OCS/HA-HClO hydrogels at 2 d and 5 d. ns: no significant, $p > 0.05$.

we selected 500% as the high train in the subsequent alternating straining sweep test. Figure 4C demonstrates that the OCS/HA-HClO hydrogel has a satisfactory "sol-gel" transition with cyclic changing of the high/low strain. The OCS/HA-HClO hydrogel is transferred to the "sol" state ($G'' > G'$) under the high shear strain and reverts to the original "Gel" state ($G' > G''$) owing to the reversible dynamic crosslinkings in the OCS/HA-HClO hydrogel. The compressive test (Figure 4D) also demonstrates the enhancement of the mechanical properties of the OCS/HA-HClO hydrogel with the increase of the OCS concentration. These strongly indicate that the OCS/HA-HClO hydrogel has a good injection and self-healing property, which is proved in our subsequent studies.

Self-healing, injection, and adhesion performance of the OCS/HA and OCS/HA-HClO hydrogels

The self-healing, injection, and tissue-adhesive properties of hydrogels play a critical role for its application in wound dressing. The photographs in Figure 5A show the injectable behavior of the OCS/HA-HClO hydrogel. The HA-ADH solution dyed using methylene blue is mixed and injected into the left half of the polytetrafluoroethylene (PTFE) mold with the OCS solution. Thereafter, the methylene orange-dyed HA-ADH solution is mixed and injected into the right half of the same mold with the OCS concentration. Finally, the OCS/HA-HClO hydrogel is removed from the PTFE mold and assumes the perfect pentacle shape. These results reveal that the OCS/HA-HClO hydrogel has the ability to match various wound shapes perfectly. Macroscopic photographic evidence of the self-healing behavior is presented in Figure 5B. The cylindrical hydrogel was cut to two semi-cylindrical ones after the compressive test. The compressive test was performed after 1 h of self-healing. As shown in Supplementary Figure S3, there is no significant difference between these two results, indicating the efficient self-healing property of the OCS/HA-HClO hydrogel. The injectability test was performed as described (Makvandi et al., 2019; Makvandi et al., 2021). Two triangle hydrogels, blue and orange, come into contact and become an integrated rhomboid hydrogel after 15 min. The color of the contact interface between these two hydrogels becomes light green, demonstrating the good coalescence between these two triangular hydrogels and indicating their excellent self-healing performance, which is attributed to the reversible dynamic Schiff-base reaction between the hydrazide group of HA-ADH and the aldehyde group of OCS (Figure 5C). Moreover, the OCS/HA-HClO hydrogels exhibit a strong tissue adhesion to wet pig skin, even under sustained folding and twisting (Figure 5D), indicating that after the OCS/HA-HClO hydrogel covers the wound it can adhere to the wound tightly to offer an all-round protection for the wound.

In Vitro antibacterial and biocompatibility of the OCS/HA-HClO hydrogels

Antibacterial resistance to antibiotics, e.g., Penicillin-Streptomycin (PS), has become a global healthcare problem. New strategies against the antibiotic-resistant are urgent to be developed. Numerous articles address the effects of HClO as a treatment for the pathogens and infection. HClO is an effective antimicrobial chemotherapeutic agent which is non-irritating and non-sensitizing due to its less cytotoxicity to eukaryotic cells. It can be generated by the body's immune system to fight invading microbes (Wang et al., 2007). HClO can oxidize the microbial amino acids containing amines and sulfurs, and then cleave to the microbial DNA after it is transformed into a hydroxyl radical (Baek et al., 2020). The *in vitro* antibacterial experiment indicates that the OCS/HA hydrogel has a clear antibacterial effect, which is because of the positive charge in the OCS backbone (Figures 6A,B). Notably, the OCS/HA-HClO hydrogel group reaches 100% bacterial mortality, which is at the same level as the antibiotics PS positive control group. These results demonstrate our assumption for this antibacterial hydrogel that the fresh release of HClO during the OCS/HA-HClO hydrogel formation is responsible for the instant disinfection, whereas the positive charges in the OCS/HA-HClO hydrogel are responsible for the antibacterial effect. We also tested the biocompatibility of the OCS/HA and OCS/HA-HClO hydrogels by using the 3T3 cells as the model cells. The live/dead results in Figure 6C show that the 3T3 cells on the surface of the OCS/HA and OCS/HA-HClO hydrogels remain largely viable with no significant differences to the positive group, indicating the good biocompatibility of the OCS/HA and OCS/HA-HClO hydrogels. Last, we examined the anti-proliferation effect of 3T3 cells with the OCS/HA and OCS/HA-HClO hydrogels or without hydrogel as the control. Compared with the control group, both the OCS/HA and OCS/HA-HClO hydrogel groups demonstrate no significantly suppressed proliferation of the 3T3 cells after 2 d and 5 d (Figure 6D). These results indicate the good biocompatibility of the OCS/HA and OCS/HA-HClO hydrogels.

Conclusion

In conclusion, we present an injectable, self-healing, and tissue adhesive hydrogel mainly based for the convenient and efficient Schiff-base reaction between HA-ADH and OCS. Moreover, during the *in situ* gelation, the HClO originated from the reaction between the predissolved SA and $Ca(ClO)_2$. The hydrogel possesses an outstanding instant sterilization capacity. Meanwhile, the hydrogel is capable of maintaining an antibacterial effect owing to positive charge of OCS. Based on these outstanding properties, the OCS/HA-HClO hydrogel can easily fill and cover the irregular wound, disinfect the wound promptly, and thereafter provide an all-around wound antibacterial protection consistently. This OCS/HA-HClO

hydrogel should be a promising material that can be used for clinical wound dressing.

Data availability statement

The original contributions presented in the study are included in the article/Supplementary Material; further inquiries can be directed to the corresponding authors.

Author contributions

HC and RL carried out the experiments. QD and CL analyzed the data. XX and YS wrote and revised the manuscript. All authors contributed and approved the submitted manuscript.

Funding

This work was supported by the Chengdu Science and Technology Bureau, China (grant no. 2021-YF05-00818-SN).

Conflict of interest

The authors declare that the research was conducted in the absence of any commercial or financial relationships that could be construed as a potential conflict of interest.

Publisher's note

All claims expressed in this article are solely those of the authors and do not necessarily represent those of their affiliated organizations, or those of the publisher, the editors, and the reviewers. Any product that may be evaluated in this article, or claim that may be made by its manufacturer, is not guaranteed or endorsed by the publisher.

Supplementary material

The Supplementary Material for this article can be found online at: https://www.frontiersin.org/articles/10.3389/fmats.2022.935096/full#supplementary-material

References

Abdollahi, Z., Zare, N. E., Salimi, F., Goudarzi, I., Tay, F., Makvandi, P., et al. (2021). Bioactive carboxymethyl starch-based hydrogels decorated with CuO nanoparticles: Antioxidant and antimicrobial properties and accelerated wound healing *in vivo*. *Int. J. Mol. Sci.* 22 (5), 2531. doi:10.3390/ijms22052531

Ahmed, J., Gultekinoglu, M., and Edirisinghe, M. (2020). Bacterial cellulose micro-nano fibres for wound healing applications. *Biotechnol. Adv.* 41, 107549. doi:10.1016/j.biotechadv.2020.107549

Aikawan, T., Ito, S., Shinohara, M., Kaneko, M., Kondo, T., Yuasa, M., et al. (2015). A drug formulation using an alginate hydrogel matrix for efficient oral delivery of the manganese porphyrin-based superoxide dismutase mimic. *Biomater. Sci.* 3 (6), 861–869. doi:10.1039/c5bm00056d

Baek, Y., Kim, J., Ahn, J., Jo, I., Ha, N. C., Ryu, S., et al. (2020). Structure and function of the hypochlorous acid-induced flavoprotein rcla from escherichia coli. *J. Biol. Chem.* 295, 3202–3212. doi:10.1074/jbc.RA119.011530

Bagheri, M., Validi, M., Gholipour, A., Makvandi, P., and Sharifi, E. (2021). Chitosan nanofiber biocomposites for potential wound healing applications: Antioxidant activity with synergic antibacterial effect. *Bioeng. Transl. Med.* 7, e10254. doi:10.1002/btm2.10254

Chandna, S., Thakur, N. S., Kaur, R., and Bhaumik, J. (2020). Lignin-bimetallic nanoconjugate doped pH-responsive hydrogels for laser-assisted antimicrobial photodynamic therapy. *Biomacromolecules* 21 (8), 3216–3230. doi:10.1021/acs.biomac.0c00695

Chen, C. J., Chen, C. C., and Ding, S. J. (2016). Effectiveness of hypochlorous acid to reduce the biofilms on titanium alloy surfaces *in vitro*. *Int. J. Mol. Sci.* 17 (7), 1161. doi:10.3390/ijms17071161

Cho, S. H., Noh, J. R., Cho, M. Y., Go, M. J., Kim, Y. H., Kang, E. S., et al. (2017). An injectable collagen/poly(γ-glutamic acid) hydrogel as a scaffold of stem cells and α-lipoic acid for enhanced protection against renal dysfunction. *Biomater. Sci.* 5 (2), 285–294. doi:10.1039/c6bm00711b

Deng, Y., Hussain, I., Kang, M., Li, K., Yao, F., Liu, S., et al. (2018). Self-recoverable and mechanical-reinforced hydrogel based on hydrophobic interaction with selfhealable and conductive properties. *Chem. Eng. J.* 353, 900–910. doi:10.1016/j.cej.2018.07.187

Derakhshanfar, A., Moayedi, J., Derakhshanfar, G., and Poostforoosh Fard, A. (2019). The role of Iranian medicinal plants in experimental surgical skin wound healing: An integrative review. *Iran. J. Basic Med. Sci.* 22 (6), 590–600. doi:10.22038/ijbms.2019.32963.7873

Du, S., Chen, X., Chen, X., Li, S., Yuan, G., Zhou, T., et al. (2019). Covalent chitosan-cellulose hydrogels via Schiff-Base reaction containing macromolecular microgels for pH-sensitive drug delivery and wound dressing. *Macromol. Chem. Phys.* 220 (23), 1900399. doi:10.1002/macp.201900399

Emami, Z., Ehsani, M., Zandi, M., and Foudazi, R. (2018). Controlling alginate oxidation conditions for making alginate-gelatin hydrogels. *Carbohydr. Polym.* 198, 509–517. doi:10.1016/j.carbpol.2018.06.080

Gaspar-Pintiliescu, A., Stanciuc, A. M., and Craciunescu, O. (2019). Natural composite dressings based on collagen, gelatin and plant bioactive compounds for wound healing: A review. *Int. J. Biol. Macromol.* 38, 854–865. doi:10.1016/j.ijbiomac.2019.07.155

Hu, C., Zhang, F., Kong, Q., Lu, Y., Zhang, B., Wu, C., et al. (2019). Synergistic chemical and photodynamic antimicrobial therapy for enhanced wound healing mediated by multifunctional light-responsive nanoparticles. *Biomacromolecules* 20 (12), 4581–4592. doi:10.1021/acs.biomac.9b01401

Huang, J., Guo, X., Yue, G., Hu, Q., and Wang, L. (2018). Boosting CH3OH production in electrocatalytic CO2 reduction over partially oxidized 5 nm cobalt nanoparticles dispersed on single-layer nitrogen-doped graphene. *ACS Appl. Mat. Interfaces* 10 (51), 44403–44414. doi:10.1021/acsami.8b14822

Jalalvandi, E., Hanton, L. R., and Moratti, S. C. (2017). Schiff-base based hydrogels as degradable platforms for hydrophobic drug delivery. *Eur. Polym. J.* 90, 13–24. doi:10.1016/j.eurpolymj.2017.03.003

Jamaledin, R., Yiu, C. K. Y., Zare, E. N., Niu, L. N., Vecchione, R., Chen, G., et al. (2020). Advances in antimicrobial microneedle patches for combating infections. *Adv. Mat.* 32 (33), e2002129. doi:10.1002/adma.202002129

Jommanee, N., Chanthad, C., and Manokruang, K. (2018). Preparation of injectable hydrogels from temperature and pH responsive grafted chitosan with tuned gelation temperature suitable for tumor acidic environment. *Carbohydr. Polym.* 198, 486–494. doi:10.1016/j.carbpol.2018.06.099

Kim, H., Shin, M., Han, S., Kwon, W., and Hahn, S. K. (2019). Hyaluronic acid derivatives for translational medicines. *Biomacromolecules* 20 (8), 2889–2903. doi:10.1021/acs.biomac.9b00564

Knowles, B. R., Wagner, P., Maclaughlin, S., Higgins, M. J., and Molino, P. J. (2017). Silica nanoparticles functionalized with zwitterionic sulfobetaine siloxane for application as a versatile antifouling coating system. *ACS Appl. Mat. Interfaces* 9 (22), 18584–18594. doi:10.1021/acsami.7b04840

Li, M., Liu, X., Tan, L., Cui, Z., Yang, X., Li, Z., et al. (2018). Noninvasive rapid bacteria-killing and acceleration of wound healing through photothermal/photodynamic/copper ion synergistic action of a hybrid hydrogel. *Biomater. Sci.* 6, 2110–2121. doi:10.1039/C8BM00499D

Liang, Y., Xue, J., Du, B., and Nie, J. (2019). Ultrastiff, tough, and healable ionic-hydrogen bond cross-linked hydrogels and their uses as building blocks to construct complex hydrogel structures. *ACS Appl. Mat. Interfaces* 11 (5), 5441–5454. doi:10.1021/acsami.8b20520

Lin, K., Zhang, D., Macedo, M. H., Cui, W., Sarmento, B., Shen, G., et al. (2019). Advanced collagen-based biomaterials for regenerative biomedicine. *Adv. Funct. Mat.* 29 (3), 1804943. doi:10.1002/adfm.201804943

Litwiniuk, M., Krejner, A., Speyrer, M. S., Gauto, A. R., and Grzela, T. (2016). Hyaluronic acid in inflammation and tissue regeneration. *Wounds*. 28 (3), 78–88.

Makvandi, P., Ali, G. W., Della Sala, F., Abdel-Fattah, W. I., and Borzacchiello, A. (2019). Biosynthesis and characterization of antibacterial thermosensitive hydrogels based on corn silk extract, hyaluronic acid and nanosilver for potential wound healing. *Carbohydr. Polym.* 223, 115023. doi:10.1016/j.carbpol.2019.115023

Makvandi, P., Ashrafizadeh, M., Ghomi, M., Najafi, M., Hossein, H. H. S., Zarrabi, A., et al. (2021). Injectable hyaluronic acid-based antibacterial hydrogel adorned with biogenically synthesized AgNPs-decorated multi-walled carbon nanotubes. *Prog. Biomater.* 10 (1), 77–89. doi:10.1007/s40204-021-00155-6

Park, S. H., Seo, J. Y., Park, J. Y., Ji, Y. B., Kim, K., Choi, H. S., et al. (2019). An injectable, click-crosslinked, cytomodulin-modified hyaluronic acid hydrogel for cartilage tissue engineering. *NPG Asia Mat.* 11 (1), 30. doi:10.1038/s41427-019-0130-1

Pellá, M. C. G., Lima-Tenório, M. K., Tenório-Neto, E. T., Guilherme, M. R., Muniz, E. C., Rubira, A. F., et al. (2018). Chitosan-based hydrogels: From preparation to biomedical applications. *Carbohydr. Polym.* 196, 233–245. doi:10.1016/j.carbpol.2018.05.033

Pérez-Madrigal, M. M., Shaw, J. E., Arno, M. C., Hoyland, J. A., Richardson, S. M., and Dove, A. P. (2020). Robust alginate/hyaluronic acid thiol-yne click-hydrogel scaffolds with superior mechanical performance and stability for load-bearing soft tissue engineering. *Biomater. Sci.* 8 (1), 405–412. doi:10.1039/c9bm01494b

Pupkaite, J., Rosenquist, J., Hilborn, J., and Samanta, A. (2019). Injectable shape-holding collagen hydrogel for cell encapsulation and delivery cross-linked using thiol-michael addition click reaction. *Biomacromolecules* 20 (9), 3475–3484. doi:10.1021/acs.biomac.9b00769

Raval, Y. S., Flurin, L., Mohamed, A., Greenwood-Quaintance, K. E., Beyenal, H., and Patel, R. (2021). *In vitro* activity of hydrogen peroxide and hypochlorous acid generated by electrochemical scaffolds against planktonic and biofilm bacteria. *Antimicrob. Agents Chemother.* 65 (5), AAC.01966-20. doi:10.1128/AAC.01966-20

Rehman, F. U., Jiang, H., Selke, M., and Wang, X. (2018). Mammalian cells: A unique scaffold for *in situ* biosynthesis of metallic nanomaterials and biomedical applications. *J. Mat. Chem. B* 6 (41), 6501–6514. doi:10.1039/c8tb01955j

Shao, C., Chang, H., Wang, M., Xu, F., and Yang, J. (2017). High-strength, tough, and self-healing nanocomposite physical hydrogels based on the synergistic effects of dynamic hydrogen bond and dual coordination bonds. *ACS Appl. Mat. Interfaces* 9 (34), 28305–28318. doi:10.1021/acsami.7b09614

Shariatinia, Z. (2019). Pharmaceutical applications of chitosan. *Adv. Colloid Interface Sci.* 263, 131–194. doi:10.1016/j.cis.2018.11.008

Smithmyer, M. E., Sawicki, L. A., and Kloxin, A. M. (2014). Hydrogel scaffolds as *in vitro* models to study fibroblast activation in wound healing and disease. *Biomater. Sci.* 2 (5), 634–650. doi:10.1039/C3BM60319A

Tian, S., Jiang, D., Pu, J., Sun, X., Li, Z., Wu, B., et al. (2019). A new hybrid silicone-based antifouling coating with nanocomposite hydrogel for durable antifouling properties. *Chem. Eng. J.* 370, 1–9. doi:10.1016/j.cej.2019.03.185

Vimbela, G. V., Ngo, S. M., Fraze, C., Yang, L., and Stout, D. A. (2017). Antibacterial properties and toxicity from metallic nanomaterials. *Int. J. Nanomedicine* 12, 3941–3965. doi:10.2147/IJN.S134526

Wakuda, Y., Nishimoto, S., Suye, S. I., and Fujita, S. (2018). Native collagen hydrogel nanofibres with anisotropic structure using core-shell electrospinning. *Sci. Rep.* 8 (1), 6248. doi:10.1038/s41598-018-24700-9

Wang, L., Bassiri, M., Najafi, R., Najafi, K., Yang, J., Khosrovi, B., et al. (2007). Hypochlorous acid as a potential wound care agent. Part I. Stabilized hypochlorous acid: A component of the inorganic armamentarium of innate immunity. *J. Burns Wounds* 6, 65.

Wang, H., Qian, J., and Ding, F. (2018). Emerging chitosan-based films for food packaging applications. *J. Agric. Food Chem.* 66 (2), 395–413. doi:10.1021/acs.jafc.7b04528

Wang, J., Wang, L., Wu, C., Pei, X., Cong, Y., Zhang, R., et al. (2020). Antibacterial zwitterionic polyelectrolyte hydrogel adhesives with adhesion strength mediated by electrostatic mismatch. *ACS Appl. Mat. Interfaces* 12 (41), 46816–46826. doi:10.1021/acsami.0c14959

Wang, Y., Xie, R., Li, Q., Dai, F., Lan, G., Shang, S., et al. (2020). A self-adapting hydrogel based on chitosan/oxidized konjac glucomannan/AgNPs for repairing irregular wounds. *Biomater. Sci.* 8 (7), 1910–1922. doi:10.1039/c9bm01635j

Wolf, K. J., and Kumar, S. (2019). Hyaluronic acid: Incorporating the bio into the material. *ACS Biomater. Sci. Eng.* 5 (8), 3753–3765. doi:10.1021/acsbiomaterials.8b01268

Zhang, X., Zhao, G., Cao, Y., Haider, Z., Wang, M., Fu, J., et al. (2018). Magnetothermal heating facilitates the cryogenic recovery of stem cell-laden alginate-Fe_3O_4 nanocomposite hydrogels. *Biomater. Sci.* 6 (12), 3139–3151. doi:10.1039/c8bm01004h

Zhang, S., Ou, Q., Xin, P., Yuan, Q., Wang, Y., Wu, J., et al. (2019). Polydopamine/puerarin nanoparticle-incorporated hybrid hydrogels for enhanced wound healing. *Biomater. Sci.* 7 (10), 4230–4236. doi:10.1039/c9bm00991d

Zhu, Q., Jiang, M., Liu, Q., Yan, S., Feng, L., Lan, Y., et al. (2018). Enhanced healing activity of burn wound infection by a dextran-HA hydrogel enriched with sanguinarine. *Biomater. Sci.* 6 (9), 2472–2486. doi:10.1039/c8bm00478a

frontiers | Frontiers in Bioengineering and Biotechnology

TYPE Review
PUBLISHED 23 September 2022
DOI 10.3389/fbioe.2022.973301

OPEN ACCESS

EDITED BY
Qian Feng,
Chongqing University, China

REVIEWED BY
Guicai Li,
Nantong University, China
Chengchen Guo,
Westlake University, China
Chengbin Xue,
Affiliated Hospital of Nantong University, China

*CORRESPONDENCE
Peng Lei,
peng.lei@scu.edu.cn
Yue Zhuo,
18686691176@163.com

†These authors have contributed equally to this work

SPECIALTY SECTION
This article was submitted to Biomaterials, a section of the journal Frontiers in Bioengineering and Biotechnology

RECEIVED 20 June 2022
ACCEPTED 19 August 2022
PUBLISHED 23 September 2022

CITATION
Li X, Zhang X, Hao M, Wang D, Jiang Z, Sun L, Gao Y, Jin Y, Lei P and Zhuo Y (2022), The application of collagen in the repair of peripheral nerve defect. *Front. Bioeng. Biotechnol.* 10:973301. doi: 10.3389/fbioe.2022.973301

The application of collagen in the repair of peripheral nerve defect

Xiaolan Li[1†], Xiang Zhang[1†], Ming Hao[2,3†], Dongxu Wang[4†], Ziping Jiang[5], Liqun Sun[6], Yongjian Gao[7], Ye Jin[8], Peng Lei[1*] and Yue Zhuo[2*]

[1]Department of Neurology and State Key Laboratory of Biotherapy, West China Hospital, Sichuan University, Chengdu, China, [2]School of Acupuncture-Moxi Bustion and Tuina, Changchun University of Chinese Medicine, Changchun, China, [3]Department of Oral and Maxillofacial Surgery, School and Hospital of Stomatology, Jilin University, Changchun, China, [4]Laboratory Animal Center, College of Animal Science, Jilin University, Changchun, China, [5]Department of Hand and Foot Surgery, The First Hospital of Jilin University, Changchun, China, [6]Department of Pediatrics, First Hospital of Jilin University, Changchun, China, [7]Department of Gastrointestinal Colorectal and Anal Surgery, China-Japan Union Hospital of Jilin University, Changchun, China, [8]Department of Pharmacy, Changchun University of Chinese Medicine, Changchun, China

Collagen is a natural polymer expressed in the extracellular matrix of the peripheral nervous system. It has become increasingly crucial in peripheral nerve reconstruction as it was involved in regulating Schwann cell behaviors, maintaining peripheral nerve functions during peripheral nerve development, and being strongly upregulated after nerve injury to promote peripheral nerve regeneration. Moreover, its biological properties, such as low immunogenicity, excellent biocompatibility, and biodegradability make it a suitable biomaterial for peripheral nerve repair. Collagen provides a suitable microenvironment to support Schwann cells' growth, proliferation, and migration, thereby improving the regeneration and functional recovery of peripheral nerves. This review aims to summarize the characteristics of collagen as a biomaterial, analyze its role in peripheral nerve regeneration, and provide a detailed overview of the recent advances concerning the optimization of collagen nerve conduits in terms of physical properties and structure, as well as the application of the combination with the bioactive component in peripheral nerve regeneration.

KEYWORDS

collagen, peripheral nerve injuries, peripheral nerve repair, nerve regeneration, nerve conduit

1 Introduction

Peripheral nerve injury (PNI) is a commonly encountered clinical issue with varying severity worldwide, reported in approximately 2.8% of all trauma patients (Noble et al., 1998). Despite relatively low incidence, the frequency of PNI is increasing worldwide and creating a severe economic burden (Grinsell and Keating, 2014). PNI is usually caused by direct mechanical trauma (Jiang et al., 2020a). Patients with peripheral neuropathy typically have severe motor or sensory deficits, innervation regions dysfunction, and neuropathic pain due to the destruction of the peripheral nerve plexus, nerve trunk, or its branches (Li et al., 2014; Sullivan et al., 2016).

Repairing severe PNI has always been one of the most challenging clinical practices in neurosurgery (Faroni et al., 2015). Large nerve defects are often difficult to recover due to the extremely slow process of axon regeneration (Holmquist et al., 1993). Currently, autologous nerve transplantation (ANT) remains the most efficacious microsurgical approach for repairing long peripheral nerve gaps (Ladak et al., 2011; Bassilios Habre et al., 2018; Choi et al., 2018). However, the application of ANT is plagued by damage to the donor site and limited donors (Nectow et al., 2012). Moreover, more than half of patients treated with ANT have failed to achieve successful recovery (Ruijs et al., 2005). Artificial nerve conduits, as an alternative to ANT, can act to connect the proximal and distal ends of the nerve defect, providing physical and biological guidance for axonal regeneration (Zhang et al., 2020). Various materials with excellent biocompatibility and biodegradability have been explored to prepare artificial nerve conduits, such as natural and synthetic biodegradable polymers (Boni et al., 2018).

Collagen is a natural polymer approved for clinical use as a nerve conduit (Boni et al., 2018). It is the main fibrous structural protein widely expressed throughout all organs and tissues and is therefore readily available (Karsdal et al., 2017). Further, collagen is known to exhibit low immunogenic properties and offers a porous structure, good biocompatibility, and biodegradability (Dong and Lv, 2016). Advanced understanding of these properties makes this natural polymer a novel biomaterial that can mimic the physiological property of nervous tissue and is widely used in peripheral nerve repair.

Previous preclinical and clinical studies have investigated the therapeutic effects of collagen-based nerve conduits on nerve regeneration (Okamoto et al., 2010; Cao et al., 2013; Lu et al., 2015). Functionalized collagen nerve conduits further enhanced nerve regeneration and functional recovery through improved physical properties, structural optimization, and incorporation of various bioactive components (Pereira Lopes et al., 2006; Yao et al., 2010a; Fujimaki et al., 2017). Collagen nerve conduits filled with growth factors-loaded collagen filaments have been successfully used to repair 35-mm nerve defects in large animal models (Cui et al., 2014; Yao et al., 2018), suggesting the potential applicability of collagen nerve conduits in bridging critical-sized defects in peripheral nerves. Given the breakthrough in peripheral nerve repair, this review summarizes the characteristics of collagen and its role in peripheral nerve regeneration, focusing on the research progress in using collagen as a nerve conduit biomaterial to repair peripheral nerve defects.

2 Characteristics of collagen as a biomaterial

2.1 The structure of collagen

As the most abundant protein in mammals, collagen constitutes approximately 30% of total protein mass (Ricard-Blum, 2011). To date, 40 collagen genes have been identified to encode 29 collagen molecules, from collagen types I to XXIX (Sorushanova et al., 2019), which can be divided into fibril-forming collagens, fibril-associated collagens, network-forming collagens, anchoring fibrils, transmembrane collagens, basement membrane collagens and others with unique functions (Gelse et al., 2003). Among them, type I collagen is the major fibril-forming collagen in tissues and organs, and its wide range of sources makes it in great demand in tissue engineering. The collagen molecule consists of a triple-helical region and two non-helical regions at either end of the helix. The three left-handed α-chains are woven together around a central axis into a triple helix of procollagen. The amino acid sequence Gly-X-Y is the predominant repeating peptide triplets in trimeric collagen. As the minor amino acid, glycine residue is located in the center of the triple helix during the α chain assembly, while other bulky amino acid residues occupy the outer positions. The X and Y positions are usually occupied by proline and hydroxyproline, respectively (Gelse et al., 2003) (Figure 1). To stabilize the structure of the triple helix in collagen molecules, two hydrogen bonds per triplet are formed: one hydrogen bond is formed between the N-H group of Gly and the hydroxyl group of the adjacent chain X residue, another is an intramolecular hydrogen bond formed by hydroxyproline residues (Sorushanova et al., 2019). The non-collagenous domains flanking the central helical part are also essential collagen components in cross-linking and fibril formation (Koopmans et al., 2009). The triple helix structure of collagen prevents hydrolysis by most proteases and increases the stability of the collagen structure (Chung et al., 2004).

In addition, fibril-forming collagens can self-assemble into a fibril structure. The C- and N-propeptides of procollagen must be cleaved off by special enzymatic hydrolysis to initiate spontaneous assembly (Holmes et al., 2018). The fibril structure of collagen is achieved by covalent cross-linking, which depends on the hydroxylation state of telopeptide lysine residues (Yamauchi and Sricholpech, 2012). The fibrillar collagen has high mechanical resilience and plays a key role in providing mechanical support for connective tissues such as skin, tendons, and bones (Avila Rodriguez et al., 2018). It interacts with cells in connective tissues to regulate cell anchorage migration, proliferation, differentiation, and survival (Yang et al., 2004). As the major mechanical component in the extracellular matrix (ECM), its mechanical resilience structure gives collagen the ability to maintain the structural integrity of tissues and organs.

2.2 Biological characteristics of collagen

Collagen is considered a safe biomaterial due to its low immunogenicity. Despite concerns that it may induce an immune response as a material of animal origin, collagen is still considered a weak antigen (Furthmayr and Timpl, 1976). The presence of non-collagenous proteins (Delustro et al., 1986), cells and cell remnants (Esses and Halloran, 1983), and residues of cross-linking (Speer et al., 1980) all may be the cause of the

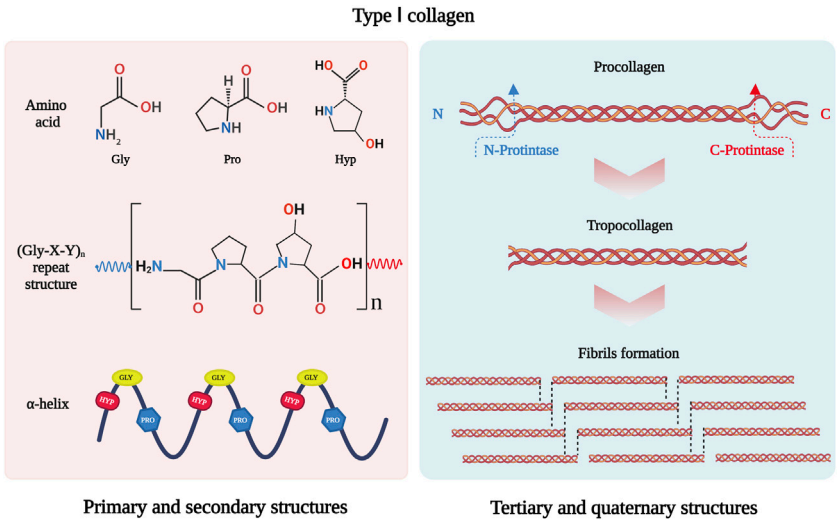

FIGURE 1
Schematic drawing of type I collagen structure. Gly-X-Y is the repeating peptide triplets. X and Y position is often occupied by proline and hydroxyproline. There α-chains are woven together to form procollagen with triple helix. Type I collagen is synthesized *in vivo* in the form of procollagen. The N- and C-terminal propeptides of procollagen are cleaved off by special enzymatic hydrolysis to form troprocollagen, and trigger spontaneous assembly to form fibrils. This figure was created with BioRender.com.

immune response. Studies have shown that the terminal non-helical regions might be the sites for inducing immune responses (Michaeli et al., 1969; Lynn et al., 2004). To reduce the immune response of collagen, the terminal non-helical regions could be removed by proteolytic enzyme treatment, known as atelocollagen (Vizarova et al., 1994). The immune response can also be avoided by selecting an appropriate source of collagen and the method of extracting collagen.

The excellent biodegradability and biocompatibility are also advantages of collagen as a biomaterial. Although collagen has a tight and firm triple helical structure that prevents hydrolysis by most proteases (Fields, 2013), the collagen degradation process can be achieved by cleaving the intact collagen fibers through special proteolytic hydrolysis (Jablonska-Trypuc et al., 2016). The members of the matrix metalloprotease (MMP) family (Amar et al., 2017) and cathepsin K (Drake et al., 2017) were two well-known mammalian interstitial collagenolytic enzymes, which could recognize and bind collagen fibrils, then cleave the individual strands of the triple helix after unwinding the collagen fibril (Aguda et al., 2014; Sprangers and Everts, 2019). The generated collagen fragments could be taken up by micropinocytosis or receptor-mediated endocytosis and subsequently degraded by lysosomal cysteine proteases (Sprangers and Everts, 2019). Furthermore, collagen is non-cytotoxic and biocompatible with various cells, supporting cell growth and cell differentiation *in vitro* (Zhang et al., 2021a; Hinman et al., 2021). Based on these biological characteristics, collagens have potential properties for tissue engineering applications.

2.3 Sources and extraction of collagen

Collagen is abundant in sources due to its widely existed in the dermis, tendons and bones of animals (Dong and Lv, 2016). It can be extracted from human tissues such as peripheral nerve tissue (Fujii et al., 1986) or placenta (Spira et al., 1994), as well as from traditional animal sources, generally rat, bovine, porcine, and sheep (Vidal et al., 2020). Among them, rat-tail tendon collagen has been widely used in early work due to its high purity and relatively simple extraction process (Gonzalez-Masis et al., 2020). Recently, marine animals are an emerging source of collagen extraction, which has the advantages of low cost, easy availability, and low risk of disease transfer (Liu et al., 2022b).

As an insoluble macromolecular structure *in vivo*, animal-derived collagen could be extracted by various methods, usually using chemical reagents to extract collagen, such as dilute acetic acid, neutral salt solution and alkali treatment (Matinong et al., 2022). Dilute acetic acid is an ideal collagen extraction reagent that results in higher extraction and retains the triple helix of collagen with non-helical regions. It is often combined with enzymatic hydrolysis to cleave the highly cross-linked bonds (Sorushanova et al., 2019). In addition, physical methods such as ultrasonic and microwave irradiation (MWI) could improve collagen extraction by accelerating chemical reactions (Jin et al., 2019; Petcharat et al., 2021).

Although natural collagen has a wide range of sources and an evolving extraction process, animal-derived material still carries the risks of inducing immune responses, batch-to-batch variability and disease transmission (Lee et al., 2021). To

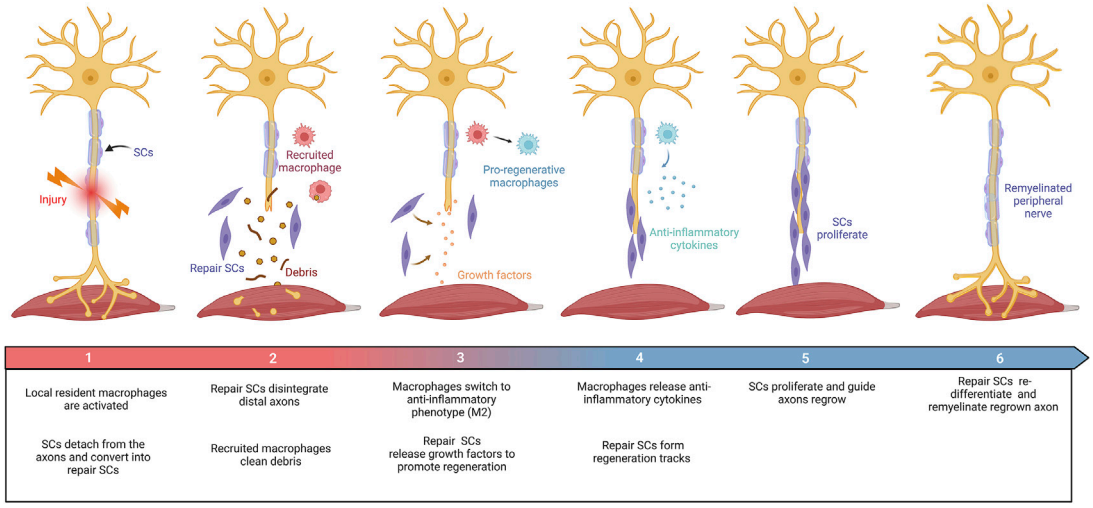

FIGURE 2
Schematic diagram summarizing the repair process in the PNI. Damage to peripheral nerves: (1) SCs were rapidly responded and converted into repair SCs. Local resident macrophages are activated. (2) Repair SCs disintegrate distal axons and recruit macrophages to clear debris. (3) Repair SCs release growth factors to promote axon regrowth. Macrophages switch to an anti-inflammatory phenotype (M2). (4) Repair SCs form regeneration tracks to guide axon regrowth. Macrophages secrete anti-inflammatory factors under the stimulation of the local injured microenvironment. (5) SCs proliferate and guide axon regeneration. (6) Finally, SCs transform into myelinating SCs and remyelinate the regenerated axon. This figure was created with BioRender.com.

avoid these concerns, a few safer methods have been proposed to synthesize collagen. Protein recombination is an emerging approach to the mass production of collagen. Various types of collagen could be produced in mammalian cells, insect cells, bacteria and yeast, transgenic animals, and transgenic plants (Dong and Lv, 2016; Avila Rodriguez et al., 2018). Advanced genetic engineering techniques facilitate efficient transgenic system for recombinant collagens co-expressed with both the alpha- and beta-subunits of a recombinant Prolyl 4-hydroxyprolin (P4H) to stabilize the triple-helix structure of collagen (Xu et al., 2011; Yu et al., 2014). In addition, collagen-like peptides can be achieved using synthetic strategies. This material resembles native collagen in its protein structure and folding (O'Leary et al., 2011; Kumar et al., 2014). Extensive sources of collagen and optimization of the extraction process ensure the great demand for collagen in tissue engineering.

3 The role of collagen in peripheral nerve regeneration

Axons in the peripheral nervous system can regenerate after damage. Peripheral nerve repair is a diverse and complex process (Figure 2). Schwann cell (SC) behaviors (such as migration, proliferation, differentiation, and myelination), recruitment and polarization of macrophages, and release of growth factors are critical for the regeneration of peripheral nerves after injury (Bassilios Habre et al., 2018). Growing evidence suggests that several members of the collagen played key roles in the peripheral nervous system, where they affected the behaviors of SCs and maintained the physiological function of peripheral nerves (Sund et al., 2001; Chernousov et al., 2006; Rasi et al., 2010; Chen et al., 2014). For instance, collagen α4 type V has promoted SC adhesion, spreading, and migration by binding its N-terminal domain to heparin, mediated by syndecan-3, induced actin cytoskeleton assembly, tyrosine phosphorylation, and activation of Erk1/Erk2 protein kinases of SCs (Chernousov et al., 2001; Erdman et al., 2002). The absence of collagen VI in mice resulted in the hypermyelination of the peripheral nervous system, induced the activation of myelin-related signaling pathways, such as P-FAK, P-AKT, P-ERK1, P-ERK2, and P-p38, and accompanied by inhibition including P-JNK and P-c-Jun (Chen et al., 2014). These results consistently imply that collagens have functions in peripheral nerve regeneration.

Indeed, collagen contributes to the regeneration of peripheral nerves regeneration (Figure 3). After nerve injury, the expression of various collagen types was upregulated in peripheral nerves, such as collagen VI and IV (Gantus et al., 2006; Chen et al., 2015; Isaacman-Beck et al., 2015). Collagen VI was identified as a novel regulator for peripheral nerve regeneration that promoted macrophage migration and polarization via AKT and PKA pathways (Chen et al., 2015). The sustained release of collagen enhanced macrophage recruitment and polarized macrophages toward the

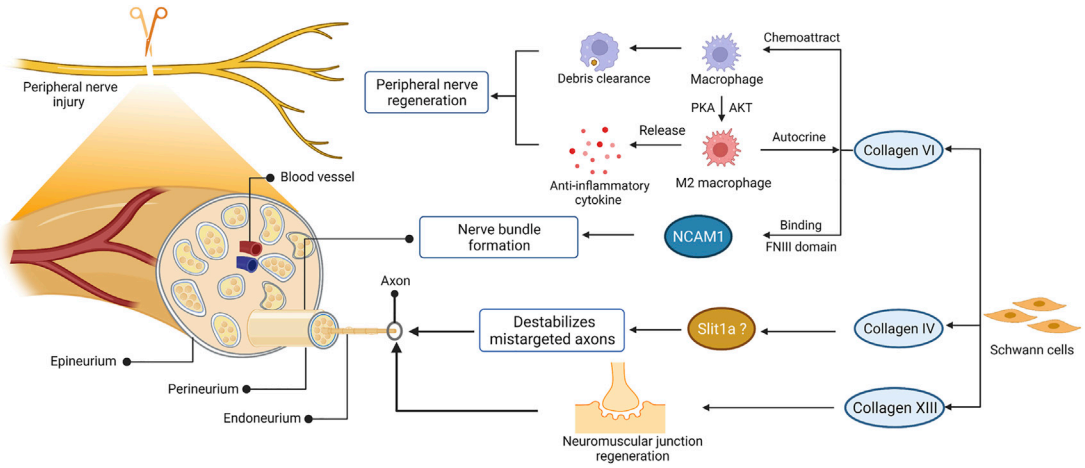

FIGURE 3
The role of collagen in peripheral nerve regeneration. The schematic representations of cross-sectional anatomy of the peripheral nerve and the role of collagen in peripheral nerve regeneration are shown on the left and right, respectively. This figure was created with BioRender.com.

M2 phenotype, thereby promoting nerve regeneration and functional recovery after sciatic nerve injury (Lv et al., 2017). Evidence has found that collagen VI also participated in regulating nerve bundle formation, mediated by direct binding to the FNIII domain of neural cell adhesion molecule 1 (NCAM1) in the extracellular space (Fang and Zou, 2021; Sun et al., 2022). As the substrate of lysyl hydroxylase 3, collagen4a5 destabilizes mistargeted axons to ensure target-selective regeneration *in vivo*, possibly via slit1a (Isaacman-Beck et al., 2015). Moreover, collagen XIII has been reported to affect synaptic integrity by binding the ColQ tail of acetylcholine esterase (Haronen et al., 2017). Further studies have confirmed its critical role in neuromuscular synapse regeneration and functional recovery after PNI (Zainul et al., 2018). Collectively, these observations suggest that collagen was required for the recruitment and polarization of macrophages, formation of nerve bundles, destabilization of mistargeted axons, and regeneration of neuromuscular synapses after PNI.

In particular, type I collagen is the most abundant and well-studied collagen among the various collagen types. It is the predominant type of collagen that exists in the peripheral nerve (Deal et al., 2012). After peripheral nerve injury, the endoneurial fibroblast is responsible for producing type I collagen (Siironen et al., 1992), which is thought to provide mechanical support for axonal growth and regeneration (Koopmans et al., 2009). In addition to the properties of natural polymers, such as excellent biocompatibility and degradability, type I collagen can be easily extracted from various animal sources and prepared into several physical forms according to special requirements. Thus, type I collagen is the most commonly used type of collagen in peripheral nerve reconstruction.

4 Design principles for advanced collagen-based nerve conduits

Based on the characteristics of collagen and its role in peripheral nerve development and regeneration, collagen is currently considered a suitable biomaterial for preparing nerve conduits to repair peripheral nerve injuries. However, their therapeutic effect is still not comparable to ANT. Thus, many attempts have been made to improve the physical properties, structure, and biological functions of collagen nerve conduits to mimic the *in vivo* microenvironment.

4.1 Improved physical properties

The physical properties of nerve conduits are known to strongly influence the regeneration process of peripheral nerves after transplantation (Salvatore et al., 2014). The nerve conduit must be able to provide mechanical support for the regenerated axon under pressure from surrounding tissues, and its degradation rate should also match the regeneration rate of the peripheral nerve (Harley et al., 2004). However, despite attracting great interest in nerve tissue engineering due to its excellent biological properties, natural collagen is limited by its poor mechanical strength and faster degradation rate *in vivo* (Itoh et al., 2002). Damage to assembly structure and natural cross-linking in the extraction process will lead to poorer mechanical properties and stability of extracted collagen than collagen in its natural state (Gu et al., 2019a). Therefore, cross-linked strategies were developed to improve the mechanical strength and stability of collagen (Bozkurt et al., 2009). Increased intermolecular cross-links between collagen molecules reduce the degrees of freedom

of its α-chains, thereby improving the thermal stability of collagen (Harrington and Von Hippel, 1961). Besides, the cleavage site of collagen can be masked by intermolecular cross-linking and enhance the ability of collagen to resist enzymatic degradation (Aldahlawi et al., 2016).

Based on the characteristics of various cross-linking methods, which can be defined into three classes: chemical, physical and enzymatic cross-linking. Chemical cross-linking is the most effective and widely used strategy due to its uniform and high degree of cross-linking. However, residues of chemical agents in collagen molecule, such as the cross-linking agent glutaraldehyde (GA), which was widely used in previous studies, might lead to cytotoxicity (Salvatore et al., 2014). The later proposed 1-ethyl-3-(3-dimethylaminopropyl) carbodiimide/N-hydroxysuccinimide (EDC/NHS) became the most widely used cross-linking method for collagen nerve conduits due to the removal of activated intermediates (Yao et al., 2010a; Yao et al., 2010b; Cao et al., 2013). Physical cross-linking is generally considered a simple and safe method, such as UV irradiation, MWI, and dehydro-thermal treatment (DHT) (Itoh et al., 2002; Ahmed et al., 2004; Haugh et al., 2009). It can avoid the introduction of exogenous toxic chemicals into tissues and cytotoxicity. Moreover, enzymatic cross-linking is promising as an effective method for collagen due to its precise kinetics of reaction and non-cytotoxic. Compared with chemical and physical cross-linking, enzymatic cross-linking is the most expensive strategy. In general, different cross-linking methods have different effects on the degree of cross-linking and safety performance (Itoh et al., 2002; Ahmed et al., 2005; Salvatore et al., 2014), and the time and temperature during the cross-linking process will also affect the physical properties of collagen (Harley et al., 2004). *In vivo* studies using nerve guides with varying degrees of cross-linking showed that the degree of cross-linking could significantly affect the ability of peripheral nerve regeneration (Bozkurt et al., 2012). Thus, for peripheral nerve injuries with varying degrees, mechanical properties and degradation rates need to be accurately controlled by cross-linking methods.

4.2 Various physical forms of collagen in nerve conduits

To optimize the structure of nerve conduits, collagen in various physical forms was used to prepare the walls or as an internal filler of nerve conduits for peripheral nerve repair, including hydrogels, filaments and fibers, films and membranes (Figure 4). Different physical forms of collagen have their advantages. To achieve better therapeutic effect, functional composite nerve conduits are often used in studies to combine the advantages of different physical forms of collagen.

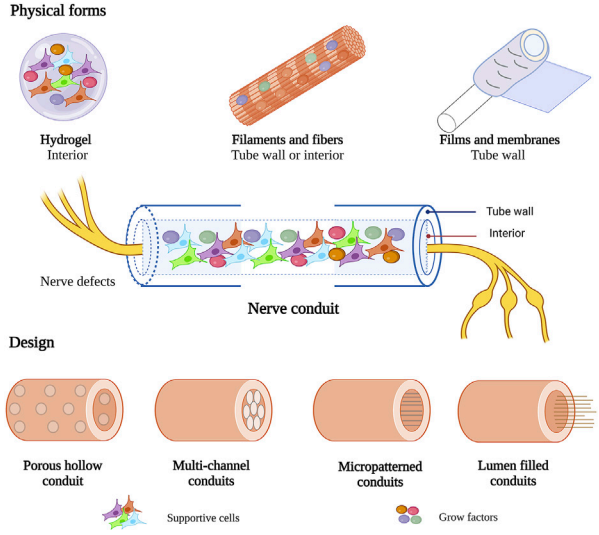

FIGURE 4
Various physical forms and design of collagen in nerve conduit. This figure was created with BioRender.com.

4.2.1 Hydrogels

Hydrogels are semi-solid structures containing networks formed by water-insoluble polymers, which serve as a three-dimensional (3D) substrate for nerve cell culture and have shown promise as scaffolds for nerve tissue engineering. As the ubiquitous structural component in the ECM, type I collagen can self-assemble into a fibrillar gel under physiological temperature and pH, providing cell adhesion, support, and structural networks (Drzewiecki et al., 2014). Its fibrillar structure and major role in ECM make collagen a suitable hydrogel material for mimicking the properties of neural tissue *in vivo*. Compared with conventional cultures, collagen hydrogels are more physiologically relevant to the structure and ECM *in vivo*, could provide adequate space for neural cell growth and migration, and ensure efficient cell-cell and cell-ECM communication (Antoine et al., 2014). The physical properties of collagen hydrogel, such as elasticity and mechanical strength, can also be tuned to match the particular physiological property of nerve cells or tissue (Mori et al., 2013; Antoine et al., 2014). Changes in the mechanical properties of collagen hydrogels significantly affected the morphological patterns, phenotypic progression and behaviors of nerve cells (East et al., 2009; Ribeiro et al., 2012; Balasubramanian et al., 2016). Therefore, these excellent biological and physiological properties of collagen hydrogels make them suitable as an inner filler for nerve conduits to provide a suitable growth environment for loaded cells. Stem cell-based therapy has received much attention in cell-transplantation therapy for PNI. The soft 3D-collagen hydrogel drove the conversion of mesenchymal stem cells (MSCs) into neuronal lineage by the activation of NOTCH

and PI3K-Akt signaling pathway (Zhang et al., 2021a; He et al., 2021), as well as contributed to the enhanced expression of neural phenotypes and release of neurotrophic factors in umbilical cord blood (UCB) cells and MSCs (Lee et al., 2014; Park et al., 2014). Further *in vivo* studies using collagen hydrogels loaded with human MSCs (Zhang et al., 2021a), SCs (Muangsanit et al., 2020), and bioactive molecules (Midha et al., 2003; Masand et al., 2012; Gonzalez-Perez et al., 2017; Samadian et al., 2019) significantly improved functional recovery and axonal regeneration. These results suggest that collagen hydrogel promoted the regeneration of peripheral nerves by providing support for the supportive cells and bioactive molecules within nerve conduits.

4.2.2 Filaments and fibers

Collagen fibers have often been used as nerve conduits' inner filler to load growth factors (Hayakawa et al., 2021). A previous study reported a new method for preparing linear-ordered collagen (LOC) fibers and considered it a good nerve guidance material (Lin et al., 2006). Compared to extracted collagen, collagen fibers prepared from aponeuroses could maintain the natural fiber structure and avoid the introduction of exogenous toxic compounds (Lin et al., 2006). Subsequent studies have achieved the combination of linear-ordered collagen scaffold (LOCS) and neurotrophins by fusing a collagen-binding domain (CBD) (Han et al., 2009) or laminin-binding domain (LBD) (Cao et al., 2011) in the N-terminal of neurotrophins. The sustained delivery of neurotrophins may provide a more favorable microenvironment for axon regeneration. These functional composite nerve conduits exhibited favorable mechanical properties and strongly promoted nerve regeneration and functional recovery in rodent and large animal models (Cao et al., 2013; Cui et al., 2014; Ma et al., 2014a; Yao et al., 2018). As well as an inner architecture for nerve guides, collagen fibers can be used to produce fibrous nerve conduits using many novel techniques. Single collagen fibers exhibited poor mechanical properties, while collagen microfibers fabricated by a microfluidic approach had excellent mechanical stability and thermal characteristics and showed excellent biocompatibility and growth-directing properties on the culture of neuronal NG108-15 cells, which indicates potential applications in peripheral nerve repair (Haynl et al., 2016). Moreover, collagen could be blended with synthetic polymers to improve mechanical properties and produce nanofibrous using electrospinning, 3D nanofibrous nerve conduits with highly longitudinal aligned nanofibers provided an optimal environment for axonal regeneration (Ouyang et al., 2013). Collagen fibers with additional topographical guidance further facilitated the neuronal response to injury and showed superior guidance for cell growth and neurite extension along the fibers (Hoffman-Kim et al., 2010).

4.2.3 Films and membranes

To avoid the destruction of the physical structure of natural collagen during the extraction process, several methods have been reported to prepare collagen membranes with oriented fibers structure from tendons (Dai et al., 2012; Alberti and Xu, 2013). The prepared collagen membranes could be wound around a tubular rod to form a nerve conduit, retaining the native triple-helix structure and strength of collagen fibers (Alberti et al., 2014). This collagen conduit supported directional nerve growth, resulting in a more mature SC phenotype, and may promote the formation of the correct connections in re-growing axons (Alberti et al., 2014). Collagen conduits prepared from flow-oriented collagen fibrils exhibited highly porous and mechanically robust properties. *In vivo* results confirmed the directing role of its micro-patterned structure in the adherence and proliferation of sprouting axons (Ahmed et al., 2004). Furthermore, a bilayer collagen membrane has been used to fabricate nerve conduits (Zhuang et al., 2016). This collagen membrane was composed of loosely arranged collagen fibers in the inner layer and dense tight fibers in the outer layer. Its unique structure could effectively prevent the growth of soft tissue into the conduits without affecting cell adhesion and the exchange of nutrients and metabolites, which is similar to the design of nerve conduits with gradient pores (Cerri et al., 2014). These collagen membranes with an oriented-fiber structure contributed to the directed growth of axon regeneration.

4.3 Design of collagen nerve conduits

Collagen nerve conduits have been used in nerve regeneration for over 40 years (Colin and Donoff, 1984). It has evolved from single conduits to functional composite nerve conduits. Several designs of collagen-based nerve conduits have been proposed to promote axon regeneration in PNI, including hollow conduits, multichannel conduits, micropatterned conduits, and lumen-filled conduits (Figure 4).

4.3.1 Hollow conduits

The hollow collagen conduit is the simplest design in the manufacturing process of nerve conduits. Its limitations include poor permeability of nutrient and growth factors and an inability to guide axonal growth (Yao et al., 2010b; Vijayavenkataraman, 2020). To optimize the structure of the hollow conduit, several modifications have been reported to make hollow collagen nerve conduits with porous properties, such as unidirectional freezing (Bozkurt et al., 2009), electrospinning (Ouyang et al., 2013), and freeze-drying (Lowe et al., 2016). The collagen scaffold with longitudinal guidance channels guided neurite outgrowth from adult DRG (Bozkurt et al., 2007) and facilitated the formation of "bands of Büngner" *in vitro* (Bozkurt et al., 2009). *In vivo* studies

using this collagen scaffold seeded with SC could effectively repair a 20-mm-long sciatic nerve gap in rats using an epineurial sheath tube (EST) technique (Bozkurt et al., 2011), with somatosensory and motor neurons extending their axons across the implant, similar to autografts (Bozkurt et al., 2012; Bozkurt et al., 2016). Moreover, 3D nanofibrous collagen nerve conduits formed by electrospinning not only have sufficient mechanical properties to support cell growth but also guide SC growth and axonal alignment during regeneration (Ouyang et al., 2013).

4.3.2 Multichannel conduits

Multichannel conduits with structural stability were designed to limit axonal dispersion and provide better guidance for nerve growth. A novel multistep process was reported to generate multichannel collagen conduits using cylindrical molds, followed by cross-linking with EDC and NHS (Yao et al., 2010a; Yao et al., 2010b). *In vitro* studies showed that 4- and 7-channel nerve conduits possessed favorable properties for nerve regeneration applications (Yao et al., 2010a). Further evaluation of nerve morphometry and the accuracy of regeneration in a 1-cm sciatic nerve gap indicated that 4-channel collagen conduits were considered the most suitable structure for peripheral nerve regeneration (Yao et al., 2010b). Furthermore, collagen conduits with a multichannel structure facilitated the loading of neurotrophic factors and supportive cells (Yao et al., 2013; Liu et al., 2021). The limitation of axonal dispersion on the multichannel structure combined with supportive cells or growth factors will be more beneficial to the regeneration of peripheral nerves.

4.3.3 Micropatterned conduits

Neurons could respond to topography in specific ways (Hoffman-Kim et al., 2010). Many studies have proved that porous scaffolds with micropatterns were important for arranging cells in predesigned locations and directing the regeneration of complex networks (Rieu et al., 2019; Yu et al., 2021; Zhang et al., 2022). Several novel approaches have been reported to prepare micropatterned collagen for PNI. A spinning technique could be used to produce highly porous tubular constructs. The micropatterned collagen scaffold (MPCS) has been reported to be prepared by a spinning technique (Harley et al., 2006), characterized by a radially oriented pore structure in the wall of the conduit. The special structure with a small outer and large inner pore ensured that cells could grow and migrate inside the conduits without infiltrating outside. *In vivo* studies using MPCS confirmed the enhanced nerve morphogenesis in a 10-mm sciatic nerve traumatic injury, and gene expression profiles revealed that known genes related to PNS regeneration were regulated with MPCS (Cerri et al., 2014). Furthermore, the gradient collagen micropatterns played different regulatory effects on SCs (Li et al., 2019), which indicate that micropatterns of collagen can be extended to different patterned structures to promote nerve regeneration.

4.3.4 Lumen-filled conduits

Collagen nerve conduits filled with fibers or hydrogel were more suitable for cell growth and incorporation of bioactive molecules (Li et al., 2018). LOC fibers were most widely filled in collagen nerve conduits, facilitating cell migration and guided nerve growth along the fibers. The collagen conduits filled with longitudinal collagen filaments successfully repaired a 30-mm sciatic nerve gap in dogs (Okamoto et al., 2010). The combination of this functional collagen-based nerve conduit with neurotrophin was further investigated (Cao et al., 2011; Shi et al., 2014): filled LOC fibers contributed to the sustained release of neurotrophin and strongly enhanced nerve regeneration and functional recovery (Cao et al., 2013; Ma et al., 2014a; Lu et al., 2015). Hydrogel was beneficial to the sustained release of neurotrophin. The axonal regeneration and functional recovery were similar to the autologous group using GelMA hydrogel-loaded glial cell-line derived neurotrophic factor (GDNF) (Zhuang et al., 2016). Hydrogels could also provide an excellent environment for the growth of supportive cells. Collagen conduits filled with fibrin-agarose hydrogels for loading adipose-derived mesenchymal stem cells (ADMSCs) resulted in enhanced functional recovery and nerve regeneration in the rat sciatic nerve gap (Carriel et al., 2013). The design of the inner filling of collagen nerve conduits provides a more permissive environment for cell growth and the binding of neurotrophic factors, thereby promoting axonal regeneration.

4.4 Collagen-based nerve conduits combined with bioactive components

4.4.1 Supportive cells

Collagen-based nerve conduit loaded with supportive cells is an effective way to promote nerve regeneration and functional recovery. Research mainly focuses on the beneficial effects of SCs and stem cells on PNI (Table 1).

4.4.1.1 Schwann cells

SCs are the principal glial cells that support neurons in the peripheral nervous system (PNS) and play a central role in peripheral nerve repair. After nerve transection, SCs from both proximal and distal nerve stumps dedifferentiated into repair SCs through the reprogramming process, followed by the release of neurotrophins (Madduri and Gander, 2010; Nocera and Jacob, 2020), proliferated and migrated into the nerve bridge, formed bands of Büngner to guide axon regeneration, and finally re-differentiated into myelinating SCs and remyelinated the regenerated axons (Jessen et al., 2015;

TABLE 1 Supportive cells fill in collagen material to repair PNI.

Cell type	Mechanism	Strategies	Outcomes	Nerve	Animal models
Schwan cells (SCs)	• Recruit macrophages (Zigmond and Echevarria 2019) • Secrete neurotrophic factors (Madduri and Gander, 2010)	• Collagen conduit with inner collagen skeleton (Keilhoff et al. 2003) • Collagen-based nerve guide with longitudinal guidance channels (Bozkurt et al. 2009, Bozkurt et al. 2012)	• Axon regeneration similar to autograft (Bozkurt et al. 2012, Burks et al. 2021) • Improved myelination (Berrocal et al. 2013, Burks et al. 2021)	• Sciatic nerve (Keilhoff et al. 2003, Bozkurt et al. 2012, Berrocal et al. 2013, Burks et al. 2021)	• Rat (Keilhoff et al. 2003, Bozkurt et al. 2012, Berrocal et al. 2013, Burks et al. 2021)
	• Form Büngner to guide the axonal regrowth (Nocera and Jacob, 2020) • Re-myelinate the regenerated axon (Nocera and Jacob, 2020)	• NeuraGen 3D collagen matrix conduits (Burks et al. 2021)	• Decreased muscle atrophy (Burks et al., 2021)		
Bone marrow-derived mesenchymal stem cells (BDMSCs)	• Differentiate into SC-like cells (Mimura et al. 2004, Cai et al. 2017) • Increase production of trophic factors (Novikova et al., 2011)	• Biodegradable collagen tube (Pereira Lopes et al. 2006) • Collagen conduits filled with differentiated mesenchymal stem cells (MSCs) (Ladak et al. 2011)	• Improved myelination and motor function recovery (Pereira Lopes et al. 2006) • Improved neurite outgrowth *in vitro* and motoneurons regeneration *in vivo* (Ladak et al. 2011)	• Sciatic nerve (Pereira Lopes et al. 2006, Ladak et al. 2011)	• Mice (Pereira Lopes et al. 2006) • Rat (Ladak et al. 2011)
Adipose-derived mesenchymal stem cells (ADMSCs)	• Differentiate into SC-like cells (Liu et al., 2022a) • Secrete neurotrophin (Lopatinaet al., 2011)	• Collagen nerve guide conduits containing a natural fibrin-agarose material (Carriel et al., 2013)	• Improved myelination and recovery of sensory and motor functions (Carriel et al., 2013)	• Sciatic nerve (Carriel et al., 2013)	• Rat (Carriel et al., 2013)
Human umbilical cord mesenchymal stem cells (hUC-MSCs)	• Differentiate into SC-like cells (Xiao and Wang, 2015) • Secrete various neurotrophic factors and deposit extracellular matrix proteins (Guo et al. 2015)	• Collagen conduit filled with longitudinally aligned collagenous fibers (Cui et al., 2018)	• Improved regeneration and functional recovery (Cui et al., 2018)	• Sciatic nerve (Cui et al., 2018)	• Dog (Cui et al., 2018)
Gingiva-derived mesenchymal stem cells (GMSCs)	• Differentiate into neural crest stem-like cells (NCSC) (Zhang et al. 2018), neural progenitor-Like Cells ((iNPCs) (Zhang et al. 2017) and Schwann cell precursor-like (SCP) cells (Zhang et al. 2021a) • Upregulation of NOTCH3 signaling pathway (Zhang et al. 2021a)	• 3D-collagen hydrogel (Zhang et al. 2021a)	• Improved functional recovery and axonal regeneration (Zhang et al. 2021a)	• Facial nerve (Zhang et al. 2021a)	• Rat (Zhang et al. 2021a)
Dental pulp stem cells (DPSCs)	• Differentiate into NCSC and SC-like cells (Al-Zer and Kalbouneh, 2015)	• Collagen conduits (Yamamoto et al. 2016)	• Improved myelination and revascularization (Yamamoto et al. 2016)	• Sciatic nerve (Yamamoto et al. 2016)	• Rat (Yamamoto et al. 2016)
Olfactory ensheathing cells (OECs)	• Remove degenerating axons via phagocytosis (Wewetzer et al. 2005, Bock et al. 2007)	• Collagen-chitosan conduits filled with a "PFTBA-OECs" enriched fibrin hydrogel (Zhu et al., 2014)	• Overcome the hypoxic status within nerve scaffolds (Zhu et al., 2014)	• Sciatic nerve (Zhu et al. 2014; Roche et al. 2017)	• Rat (Zhu et al. 2014, Roche et al. 2017, Gu et al. 2019b)
	• Secrete neurotrophic factors (Brouch et al., 2001)	• Biphasic collagen and laminin functionalized hyaluronic acid-based nerve guidance conduit (Roche et al., 2017) • Collagen sponge (Gu et al., 2019b)	• Improved axonal regeneration and functional recovery (Zhu et al., 2014, Gu et al., 2019b) • Improved clinical and electrophysiological outcomes (Roche et al., 2017)	• Facial nerve (Gu et al., 2019b)	
Neural stem cells (NSCs)	• Differentiate into cells of the neural lineage and SC-like cells (Tong et al., 2010)	• NT-3-supplemetned HA-Collagen composite conduit (Zhang et al., 2008)	• Re-innervations of damaged facial nerve (Zhang et al., 2008)	• Facial nerve (Zhang et al., 2008, Ma et al. 2017)	• Rabbit (Zhang et al., 2008)

(Continued on following page)

TABLE 1 (*Continued*) Supportive cells fill in collagen material to repair PNI.

Cell type	Mechanism	Strategies	Outcomes	Nerve	Animal models
	• Secrete various neurotrophic factors (Llado et al., 2004)	• Rat-tail collagen gel with the anchored bFGF (Ma et al., 2017)	• Functional recovery and nerve growth similar to autograft (Ma et al., 2017)		• Rat (Ma et al., 2017)

Nocera and Jacob, 2020). Thus, additional SC-seeding may provide a unique opportunity to promote axonal regeneration further.

The development of techniques for culturing SCs from adult rat and human materials make it possible to add SCs to neural grafts (Keilhoff et al., 1999; Keilhoff et al., 2000; Calderon-Martinez et al., 2002). Collagen nerve guide conduits containing SCs were used for a longer nerve gap. *In vivo* results showed that collagen nerve conduits supported SCs behaviors, such as adhered, survived, and proliferated on the inner surface, which suggests that collagen conduits seeded with SCs may be applied to repair extended nerve gaps (Keilhoff et al., 2003). In addition, the SCs' behaviors were regulated by the micropattern of collagen (Li et al., 2019). Collagen scaffolds with longitudinally oriented channels not only supported SC growth and migration but also guided SCs to align longitudinally along the channels, their framework highly supportive of peripheral nerve regeneration (Bozkurt et al., 2009; Bozkurt et al., 2012; Zhang et al., 2013). Further optimization of collagen nerve guide structure could provide a more suitable environment for SC growth and migration, thereby promoting axonal regeneration.

4.4.1.2 Stem cells

The limitations of *in vitro* culture of SCs led to the investigation of other cell types that may present similar SC phenotypes or provide neurotrophic support to promote axonal regeneration. Stem cells represent a class of cells capable of self-renewal, proliferation, and differentiation (Thomson et al., 1998). Previous studies have shown that stem cells promoted nerve regeneration through differentiating into specific cell types (Kingham et al., 2007; Arthur et al., 2008; Berrocal et al., 2013) and sustained releasing of neurotrophic factors (Sowa et al., 2012). These properties make stem cell-based therapies widely used in preclinical peripheral nerve repair. The roles of various types of stem cells in peripheral nerve regeneration have been investigated in collagen-based nerve conduits (Ladak et al., 2011; Sowa et al., 2012; Ma et al., 2017).

The most comprehensively studied stem cells in collagen nerve conduits are MSCs (Zhang et al., 2021b), which could differentiate into SC-like cells (Dezawa et al., 2001; Zhang et al., 2021a). MSCs exhibited an equivalent efficacy on neurite outgrowth and axon regeneration as SCs (Ladak et al., 2011). Various derived MSCs have been filled in collagen nerve conduits to investigate the efficacy in nerve regeneration, such as bone marrow-derived mesenchymal stem cells (BMSCs) (Pereira Lopes et al., 2006), ADMSCs (Carriel et al., 2013), human umbilical cord mesenchymal stem cells (hUC-MSCs) (Cui et al., 2018), and dental pulp stem cells (Yamamoto et al., 2016). Further *in vivo* studies using stem cells-loaded collagen conduits significantly improved the nerve regeneration and recovery of sensory and motor functions (Carriel et al., 2013), and the longitudinally aligned collagenous fibers loaded with hUC-MSCs resulted in greater myelin sheath formation and functional recovery (Cui et al., 2018).

Olfactory ensheathing cells (OECs) are specialized glial cells between SCs and astrocytes. The therapeutic efficacy of various collagen-based nerve conduits seeded with OEC for peripheral nerve injury has been investigated (Li et al., 2010; Guerout et al., 2011). Nerve regeneration and functional recovery were significantly improved using OEC therapy (Gu et al., 2019b). Increased nerve fibers, myelinated fibers, and myelin area were observed in the OEC group (Goulart et al., 2016). Increased oxygen levels within the nerve conduit contributed to the enhanced therapeutic effect of OECs on nerve regeneration (Zhu et al., 2014).

Furthermore, neural stem cells (NSCs) can differentiate into neurons and promote locomotor recovery in spinal cord-injured mice (Cummings et al., 2005). Various collagen scaffolds loaded with NSCs have shown remarkable therapeutic effects in spinal cord injury (Cummings et al., 2005; Jiang et al., 2020b). To improve the therapeutic effect after transplantation, basic fibroblast growth factor (bFGF) was anchored on heparinized collagen nerve conduits to promote neural stem/progenitor cell (NS/PC) proliferation. NS/PCs-bFGF conduits exhibited similar therapeutic effects to ANT in 8-mm rat facial nerve gaps (Ma et al., 2017). The internal environment of collagen nerve conduits suitable for stem cell growth needs to be further optimized.

4.4.2 Growth factors

Growth factors are involved in the regulation of various cellular processes. Combining collagen-based nerve conduits with growth factors could create a more appropriate microenvironment for nerve

TABLE 2 Growth factors fill in collagen material to repair PNI.

Growth factors	Mechanism	Strategies	Outcomes	Nerve	Animal models
Basic fibroblast growth factor (bFGF)	• Promotes neurite extension (Fujimoto et al., 1997) • Stimulates SCs proliferation (Wang et al., 2003)	• Linear ordered collagen scaffold (LOCS) filled with collagen binding bFGF (CBD-bFGF) (Ma et al. 2014a, Cui et al. 2014) • Oriented collagen tubes (Fujimaki et al., 2017) • Collagen conduits filled with CBD- bFGF (Wang et al., 2020) • Combine with CNTF (Cui et al., 2014)	• Sustained release (Ma et al. 2014a, Cui et al. 2014) • Guide axon growth, promote nerve regeneration and functional restoration (Ma et al. 2014a, Cui et al. 2014) • Improved nerve repair and recovery of motor function (Fujimaki et al., 2017) • Promote functional facial nerve recovery (Wang et al., 2020) • Synergistic effect (Cui et al., 2014)	• Sciatic nerve (Ma et al. 2014a, Fujimaki et al., 2017) • Facial nerve (Cui et al. 2014, Wang et al. 2020)	• Rat (Ma et al. 2014a, Fujimaki et al., 2017) • Minipigs (Cui et al. 2014) • Rabbit (Wang et al., 2020)
Ciliary neurotrophic factor (CNTF)	• Stimulate neurite outgrowth (Hartnick et al., 1996) • Increase the number of elongating axon tips (Sahenk et al., 1994) • Promote neurotransmitter synthesis (Cao et al., 2011)	• LOCS filled with laminin binding CNTF (LBD-CNTF) (Cao et al., 2011) • LOCS filled with CBD-CNTF (Cui et al. 2014; Lu et al., 2015) or LBD-CNTF (Cao et al., 2013) • Combine with bFGF (Cui et al. 2014), BDNF (Cao et al. 2013)	• Sustained release (Cao et al. 2011, Cao et al. 2013) • Guide axon growth, promote nerve regeneration and functional restoration (Cao et al., 2011) • Guide axon growth and improve nerve functional recovery (Cao et al., 2013) • Improved axon regeneration, SCs cell migration, remyelination and recovery rate (Lu et al., 2015) • Synergistic effect (Cao et al. 2013, Cui et al. 2014)	• Sciatic nerve (Cao et al., 2011) • Facial nerve (Cao et al. 2013, Cui et al. 2014, Lu et al. 2015)	• Rat (Cao et al. 2011, Cao et al. 2013) • Minipigs (Cui et al. 2014, Lu et al. 2015)
Brain-derived neurotrophic factor (BDNF)	• Promote neuronal growth and differentiation (Yang et al., 2015) • Neuronal survival (Hartnick et al., 1996) • Neuronal plasticity (Castren and Kojima, 2017)	• LOCS filled with CBD-BDNF or LBD-BDNF; Combine with CNTF (Cao et al., 2013)	• Sustained release (Cao et al., 2013) • Guided axon growth, promote functional restoration (Cao et al., 2013) • Synergistic effect (Cao et al., 2013)	• Facial nerve (Cao et al., 2013)	• Rat (Cao et al., 2013)
Glial cell line-derived neurotrophic factor (GDNF)	• Promote axonal elongation (Madduri et al., 2009) • Promote survival of both motor and sensory nerves (Ma et al., 2018)	• Collagen nerve conduits coated with layers of PLGA (Madduri et al., 2010b) • Bilayer collagen conduit filled with GDNF-loaded microspheres (Zhuang et al., 2016) • Immobilized on collagen nerve conduits by chemical conjugation (Ma et al., 2018) • Combine with NGF (Madduri et al., 2010b)	• Sustained release (Madduri et al. 2010b, Ma et al. 2018, Zhuang et al. 2016) • Improved axonal outgrowth and Schwann cell migration (Madduri et al., 2010b) • Axonal regeneration and functional recovery similar to autograft (Zhuang et al., 2016, Ma et al. 2018) • Synergistic effect (Madduri et al., 2010b)	• Sciatic nerve (Madduri et al., 2010b, Zhuang et al. 2016) • Facial nerve (Ma et al., 2018)	• Rat (Madduri et al. 2010b, Zhuang et al. 2016, Ma et al. 2018)
Nerve growth factor (NGF)	• Support neuron survival and direct neurite outgrowth (Kemp et al., 2011) • Induced extensive axonal branching (Madduri et al., 2009) • Regulate the receptivity of axons to myelination (Chan et al., 2004)	• Longitudinally oriented collagen conduit (Yao et al., 2018) • Combine with GDNF (Madduri et al., 2010b)	• Improved recovery of regenerated axons and muscle weight (Yao et al., 2018) • Synergistic effect (Madduri et al., 2010b)	• Sciatic nerve (Madduri et al. 2010b, Yao et al. 2018)	• Rat (Madduri et al., 2010b) • Dog (Yao et al., 2018)

(Continued on following page)

TABLE 2 (*Continued*) Growth factors fill in collagen material to repair PNI.

Growth factors	Mechanism	Strategies	Outcomes	Nerve	Animal models
Vascular Endothelial Growth Factor (VEGF)	• Vasculogenesis and angiogenesis (Lu et al., 2019) • Induced extensive neurite growth and branching (Guaiquil et al., 2014)	• Collagen tube filled with CBD-VEGF-immobilized collagen Fibers (Ma et al., 2014b)	• Sustained release (Ma et al., 2014b) • Guided axon growth, morphological and functional improvements similar to autograft (Ma et al., 2014b)	• Sciatic nerve (Ma et al., 2014b)	• Rat (Ma et al., 2014b)

regeneration. Recently, multiple concepts have focused on collagen as a nerve conduit with growth factors for nerve regeneration (Table 2). growth could be immobilized on collagen by chemical conjugation (Ma et al., 2018), heparin cross-linking (Ma et al., 2017; Zhang et al., 2021c), and fusion binding domain, such as the laminin-binding domain and collagen-binding domain (Cao et al., 2013). At present, the use of recombinant DNA technology to fuse a binding domain at the N/C-terminus of growth factors is a more popular method (Fujimaki et al., 2020).

4.4.2.1 Basic fibroblast growth factor

The bFGF is a member of the fibroblast growth factor family and is abundantly expressed in neural tissue. It played a crucial role in the mitogenesis and proliferation of SCs (Davis and Stroobant, 1990) and DRG neurons *in vitro* (Li et al., 2002) and stimulated persistent angiogenesis *in vivo* (Chu et al., 2011). Moreover, bFGF is involved in the early peripheral nerve regeneration by activating autophagy to accelerate myelin debris clearance (Li et al., 2020), and further *in vivo* study confirmed that the regulation of bFGF in autophagy was achieved by activating the PAK1 pathway in SCs (Hu et al., 2022). Therefore, it is considered as a growth factor that is beneficial for nerve regeneration. *In vivo* studies have confirmed the effect of collagen conduits combined with bFGF on axonal regeneration and functional recovery (Fujimaki et al., 2017). However, bFGF cannot play a long-term effect after transplantation due to its poor immobilization on collagen nerve conduits, so various strategies have been proposed to ensure its sustained release *in vivo*. Based on its high affinity for heparin (Sakiyama-Elbert and Hubbell, 2000; Yang et al., 2010), bFGF was immobilized on nerve conduits cross-linked with heparin, which facilitated the local sustained release of bFGF *in vivo* (Ma et al., 2017). A novel approach to improving the affinity of bFGF for collagen was also previously reported. The N-terminal of native bFGF was fused with a CBD, TKKTLRT, which could specifically bind to collagen (Li et al., 2011; Ma et al., 2014a). The sustained release of the bFGF further improved nerve regeneration *in vivo* (Cui et al., 2014; Wang et al., 2020).

4.4.2.2 Neurotrophins

Neurotrophins are a protein family associated with the survival of sensory and sympathetic neurons. They participate in regulating various aspects of neuronal development and function (Reichardt, 2006). Damage to peripheral nerves induces active cellular mechanisms that lead to the synthesis of neurotrophins in neurons and SCs to promote nerve regeneration (Richner et al., 2014). The two main receptors were tropomyosin receptor kinase (TrkA, Trk-B, and Trk-C) and P75NTR. Neurotrophins could activate the downstream targets of various signaling cascades by binding with their corresponding receptors to exert their multiple effects on neurorestoration. The signaling pathways involved in neurotrophins after nerve injury include PI3K/Akt, MAPK/ERK, JNK/c-Jun, and Rho A/ROCK (Li et al., 2020). Various neurotrophins were loaded on collagen scaffolds to investigate their promoting effects on peripheral nerve regeneration, such as brain-derived neurotrophic factor (BDNF) (Cao et al., 2013), ciliary neurotrophic factor (CNTF) (Cao et al., 2011; Lu et al., 2015), nerve growth factor (NGF) (Yao et al., 2018; Long et al., 2021), GDNF (Zhuang et al., 2016). To ensure the sustained release of neurotrophins *in vivo*, LBD (Cao et al., 2011), CBD (Cui et al., 2014), and chemical conjugation (Ma et al., 2018) were proposed for their immobilization on collagen. The combination of neurotrophins may have a synergistic effect on nerve regeneration. For instance, GDNF and NGF were functionally complementary in promoting axonal elongation and axonal branching (Madduri et al., 2009). Their combination exerted a synergistic effect on axonal growth (Madduri et al., 2010a; Madduri et al., 2010b). The combination of CNTF and BDNF within LOCS showed enhanced facial nerve regeneration and functional recovery (Cao et al., 2013). Thus, combining multiple neurotrophins and collagen nerve conduits may be a better treatment to repair PNI in the future.

5 Discussion

Nerve conduits prepared from several biomaterials offer a promising approach to promoting peripheral nerve regeneration, such as the natural polymers collagen, chitosan, and silk and the synthetic polymers poly-ε-caprolactone (PCL), poly-lactic-co-glycolic acid (PLGA), and poly-glycolic acid (PGA) (Pinho et al., 2016). Compared with synthetic biomaterials, natural polymeric proteins exhibit more excellent biocompatibility and biodegradability, and evoke a minimal inflammatory reaction after transplantation (Jiang et al., 2020a). Thus, natural polymers have attracted great attention in tissue engineering. The peripheral nerve is

surrounded by ECM *in vivo*, and its repair is a complicated process that requires cell-cell and cell-ECM interactions. Thus, simulating neural tissue in the natural microenvironment is an important factor in designing nerve conduits (Sarker et al., 2018). As the major component in the ECM of peripheral nerve, the fibrous structure of collagen can simulate native nerve tissue, creating a suitable microenvironment for nerve regeneration (Hosseinkhani et al., 2013). Compared with other natural polymers, collagen exhibited higher affinity for nerve cells (Cheng et al., 2003). Its semipermeable membrane structure allows the exchange of nutrients and metabolites while preventing the outward migration of cells within the conduits. In addition, collagen is the major component of FDA-approved artificial nerve conduits for the surgical reconstruction of the peripheral nerve due to its low antigenicity and immunogenicity (Kornfeld et al., 2019). Commercially available collagen nerve guides showed potential therapeutic effects for bridging larger nerve gaps (Bozkurt et al., 2017) and functional recovery in the clinic (Wangensteen and Kalliainen, 2010). Therefore, collagen is an extensively used natural polymer in preclinical *in vivo* studies, second only to chitosan (Gregory and Phillips, 2021). Collagen is considered a promising material for the preparation of nerve conduits as an alternative to autografts for PNI.

Over recent years, collagen nerve conduits have evolved from single hollow conduits to functional composite nerve conduits. Collagen nerve conduits loaded with bioactive components have shown improved biological performance due to mimicking biological processes following nerve injury *in vivo* (Carriel et al., 2013; Zhuang et al., 2016; Ma et al., 2017). However, some concerns remain to be considered. The emergence of stem cells overcame the poor proliferation and differentiation capacity of SCs, and collagen nerve conduits loaded with differentiated stem cells could induce more sciatic motoneurons regenerating axons *in vivo* (Ladak et al., 2011). However, nonscalable protocols control the transdifferentiation of stem cells. It is challenging to maintain the differentiated state of the stem cells *in vitro* under dynamic *in vivo* conditions (Uz et al., 2018). More efficient and scalable transdifferentiation procedures are required to precisely control the final fate of implanted stem cells loaded in collagen nerve conduits. In addition, although the sustained release of growth factors *in vivo* has been greatly improved by CBD, LBD, or chemical conjugation, more precise control methods still need to be investigated to control the release of growth factors in different stages of peripheral nerve repair. Furthermore, the combination of growth factors and supportive cells in collagen nerve conduits showed synergistic effects on PNI. For instance, anchored bFGF on collagen exhibited sustained mitogenic and anti-apoptotic effects on NS/PCs, the combination of bFGF and NS/PCs showed synergistic therapeutic effect in the restoration of facial nerve defects, similar to ANT (Ma et al., 2017). NGF is involved in stem cell growth. Incorporating HuMSCs and NGF further enhanced the repair effect of collagen scaffolds on recurrent laryngeal nerve injury (Pan et al., 2017). Thus, the combination of various bioactive components is a promising therapeutic strategy.

In conclusion, we summarize the characteristics of collagen as biomaterial and the roles of extensively studied collagen types in peripheral nerve regeneration. The optimization of collagen nerve conduits in terms of physical properties, structure and combination of bioactive components was further investigated. With the successive proposals of various therapeutic strategies, the therapeutic effects of collagen nerve conduit have been greatly improved, even similar to ANT (Ma et al., 2017; Burks et al., 2021; Long et al., 2021). However, it should be mentioned that the major clinical challenge is the repair of large nerve gaps. There are only a few studies on applying collagen nerve conduits in large animal models of PNI (Cui et al., 2014; Cui et al., 2018). Compared with rodent models, large animal models can be used to create longer gaps for preclinical evaluation, which is more closely applicable to the challenge of artificial nerve conduits in PNI. Therefore, the application of large animal models to evaluate the effects of functional collagen nerve conduits on peripheral nerve regeneration may accelerate the transition to the clinic in the future.

Author contributions

XL, XZ, MH, and DW wrote the manuscript. XL, XZ, MH, DW, ZJ, LS, YG, YJ, PL, YZ collected the references and prepared figures. All authors reviewed the manuscript.

Funding

This work was supported by the Jilin Health Commission Program under Grant 2020J05S, the Fundamental Research Funds for the Central Universities under Grant 2019JCKT-70, the Jilin Education Department Program under Grant JJKH20200950KJ, and the Jilin Scientific and Technological Development Program under Grant 20190103071JH, 202002006JC and 20210101010JC.

Conflict of interest

The authors declare that the research was conducted in the absence of any commercial or financial relationships that could be construed as a potential conflict of interest.

Publisher's note

References

Aguda, A. H., Panwar, P., Du, X., Nguyen, N. T., Brayer, G. D., and Bromme, D. (2014). Structural basis of collagen fiber degradation by cathepsin K. *Proc. Natl. Acad. Sci. U. S. A.* 111 (49), 17474–17479. doi:10.1073/pnas.1414126111

Ahmed, M. R., Venkateshwarlu, U., and Jayakumar, R. (2004). Multilayered peptide incorporated collagen tubules for peripheral nerve repair. *Biomaterials* 25 (13), 2585–2594. doi:10.1016/j.biomaterials.2003.09.075

Ahmed, M. R., Vairamuthu, S., Shafiuzama, M., Basha, S. H., and Jayakumar, R. (2005). Microwave irradiated collagen tubes as a better matrix for peripheral nerve regeneration. *Brain Res.* 1046 (1-2), 55–67. doi:10.1016/j.brainres.2005.03.022

Alberti, K. A., and Xu, Q. (2013). Slicing, stacking and rolling: fabrication of nanostructured collagen constructs from tendon sections. *Adv. Healthc. Mat.* 2 (6), 817–821. doi:10.1002/adhm.201200319

Alberti, K. A., Hopkins, A. M., Tang-Schomer, M. D., Kaplan, D. L., and Xu, Q. (2014). The behavior of neuronal cells on tendon-derived collagen sheets as potential substrates for nerve regeneration. *Biomaterials* 35 (11), 3551–3557. doi:10.1016/j.biomaterials.2013.12.082

Aldahlawi, N. H., Hayes, S., O'Brart, D. P. S., Akhbanbetova, A., Littlechild, S. L., and Meek, K. M. (2016). Enzymatic resistance of corneas cross-linked using riboflavin in conjunction with low energy, high energy, and pulsed UVA irradiation modes. *Invest. Ophthalmol. Vis. Sci.* 57 (4), 1547–1552. doi:10.1167/iovs.15-18769

Al-Zer, H., and Kalbouneh, H. (2015). Dental pulp stem cells-derived schwann cells for peripheral nerve injury regeneration. *Neural Regen. Res.* 10 (12), 1945–1946. doi:10.4103/1673-5374.172309

Amar, S., Smith, L., and Fields, G. B. (2017). Matrix metalloproteinase collagenolysis in health and disease. *Biochimica Biophysica Acta - Mol. Cell Res.* 1864, 1940–1951. doi:10.1016/j.bbamcr.2017.04.015

Antoine, E. E., Vlachos, P. P., and Rylander, M. N. (2014). Review of collagen I hydrogels for bioengineered tissue microenvironments: characterization of mechanics, structure, and transport. *Tissue Eng. Part B Rev.* 20 (6), 683–696. doi:10.1089/ten.teb.2014.0086

Arthur, A., Rychkov, G., Shi, S., Koblar, S. A., and Gronthos, S. (2008). Adult human dental pulp stem cells differentiate toward functionally active neurons under appropriate environmental cues. *Stem Cells* 26 (7), 1787–1795. doi:10.1634/stemcells.2007-0979

Avila Rodriguez, M. I., Rodriguez Barroso, L. G., and Sanchez, M. L. (2018). Collagen: A review on its sources and potential cosmetic applications. *J. Cosmet. Dermatol.* 17 (1), 20–26. doi:10.1111/jocd.12450

Balasubramanian, S., Packard, J. A., Leach, J. B., and Powell, E. M. (2016). Three-dimensional environment sustains morphological heterogeneity and promotes phenotypic progression during astrocyte development. *Tissue Eng. Part A* 22 (11-12), 885–898. doi:10.1089/ten.tea.2016.0103

Bassilios Habre, S., Bond, G., Jing, X. L., Kostopoulos, E., Wallace, R. D., and Konofaos, P. (2018). The surgical management of nerve gaps: Present and future. *Ann. Plast. Surg.* 80 (3), 252–261. doi:10.1097/sap.0000000000001252

Berrocal, Y. A., Almeida, V. W., Gupta, R., and Levi, A. D. (2013). Transplantation of Schwann cells in a collagen tube for the repair of large, segmental peripheral nerve defects in rats. *J. Neurosurg.* 119 (3), 720–732. doi:10.3171/2013.4.jns121189

Bock, P., Beineke, A., Techangamsuwan, S., Baumgartner, W., and Wewetzer, K. (2007). Differential expression of HNK-1 and p75(NTR) in adult canine Schwann cells and olfactory ensheathing cells *in situ* but not *in vitro*. *J. Comp. Neurol.* 505 (5), 572–585. doi:10.1002/cne.21519

Boni, R., Ali, A., Shavandi, A., and Clarkson, A. N. (2018). Current and novel polymeric biomaterials for neural tissue engineering. *J. Biomed. Sci.* 25 (1), 90. doi:10.1186/s12929-018-0491-8

Boruch, A. V., Conners, J. J., Pipitone, M., Deadwyler, G., Storer, P. D., Devries, G. H., et al. (2001). Neurotrophic and migratory properties of an olfactory ensheathing cell line. *Glia* 33 (3), 225–229. doi:10.1002/1098-1136(200103)33:3<225::aid-glia1021>3.0.co;2-y

Bozkurt, A., Brook, G. A., Moellers, S., Lassner, F., Sellhaus, B., Weis, J., et al. (2007). *In vitro* assessment of axonal growth using dorsal root ganglia explants in a novel three-dimensional collagen matrix. *Tissue Eng.* 13 (12), 2971–2979. doi:10.1089/ten.2007.0116

Bozkurt, A., Deumens, R., Beckmann, C., Olde Damink, L., Schugner, F., Heschel, I., et al. (2009). *In vitro* cell alignment obtained with a Schwann cell enriched microstructured nerve guide with longitudinal guidance channels. *Biomaterials* 30 (2), 169–179. doi:10.1016/j.biomaterials.2008.09.017

Bozkurt, A., Dunda, S. E., O'Dey Dm, D., Brook, G. A., Suschek, C. V., and Pallua, N. (2011). Epineurial sheath tube (EST) technique: an experimental peripheral nerve repair model. *Neurol. Res.* 33 (10), 1010–1015. doi:10.1179/1743132811y.0000000029

Bozkurt, A., Lassner, F., O'Dey, D., Deumens, R., Bocker, A., Schwendt, T., et al. (2012). The role of microstructured and interconnected pore channels in a collagen-based nerve guide on axonal regeneration in peripheral nerves. *Biomaterials* 33 (5), 1363–1375. doi:10.1016/j.biomaterials.2011.10.069

Bozkurt, A., Boecker, A., Tank, J., Altinova, H., Deumens, R., Dabhi, C., et al. (2016). Efficient bridging of 20 mm rat sciatic nerve lesions with a longitudinally micro-structured collagen scaffold. *Biomaterials* 75, 112–122. doi:10.1016/j.biomaterials.2015.10.009

Bozkurt, A., Claeys, K. G., Schrading, S., Rodler, J. V., Altinova, H., Schulz, J. B., et al. (2017). Clinical and biometrical 12-month follow-up in patients after reconstruction of the sural nerve biopsy defect by the collagen-based nerve guide Neuromaix. *Eur. J. Med. Res.* 22 (1), 34. doi:10.1186/s40001-017-0279-4

Burks, S. S., Diaz, A., Haggerty, A. E., Oliva, N. d. l., Midha, R., and Levi, A. D. (2021). Schwann cell delivery via a novel 3D collagen matrix conduit improves outcomes in critical length nerve gap repairs. *J. Neurosurg.*, 1–11. doi:10.3171/2020.8.JNS202349

Cai, S., Tsui, Y. P., Tam, K. W., Shea, G. K., Chang, R. S., Ao, Q., et al. (2017). Directed differentiation of human bone marrow stromal cells to fate-committed schwann cells. *Stem Cell Rep.* 9 (4), 1097–1108. doi:10.1016/j.stemcr.2017.08.004

Calderon-Martinez, D., Garavito, Z., Spinel, C., and Hurtado, H. (2002). Schwann cell-enriched cultures from adult human peripheral nerve: a technique combining short enzymatic dissociation and treatment with cytosine arabinoside (ara-C). *J. Neurosci. Methods* 114 (1), 1–8. doi:10.1016/s0165-0270(01)00493-9

Cao, J., Sun, C., Zhao, H., Xiao, Z., Chen, B., Gao, J., et al. (2011). The use of laminin modified linear ordered collagen scaffolds loaded with laminin-binding ciliary neurotrophic factor for sciatic nerve regeneration in rats. *Biomaterials* 32 (16), 3939–3948. doi:10.1016/j.biomaterials.2011.02.020

Cao, J., Xiao, Z., Jin, W., Chen, B., Meng, D., Ding, W., et al. (2013). Induction of rat facial nerve regeneration by functional collagen scaffolds. *Biomaterials* 34 (4), 1302–1310. doi:10.1016/j.biomaterials.2012.10.031

Carriel, V., Garrido-Gomez, J., Hernandez-Cortes, P., Garzon, I., Garcia-Garcia, S., Saez-Moreno, J. A., et al. (2013). Combination of fibrin-agarose hydrogels and adipose-derived mesenchymal stem cells for peripheral nerve regeneration. *J. Neural Eng.* 10 (2), 026022. doi:10.1088/1741-2560/10/2/026022

Castren, E., and Kojima, M. (2017). Brain-derived neurotrophic factor in mood disorders and antidepressant treatments. *Neurobiol. Dis.* 97, 119–126. doi:10.1016/j.nbd.2016.07.010

Cerri, F., Salvatore, L., Memon, D., Martinelli Boneschi, F., Madaghiele, M., Brambilla, P., et al. (2014). Peripheral nerve morphogenesis induced by scaffold micropatterning. *Biomaterials* 35 (13), 4035–4045. doi:10.1016/j.biomaterials.2014.01.069

Chan, J. R., Watkins, T. A., Cosgaya, J. M., Zhang, C., Chen, L., Reichardt, L. F., et al. (2004). NGF controls axonal receptivity to myelination by Schwann cells or oligodendrocytes. *Neuron* 43 (2), 183–191. doi:10.1016/j.neuron.2004.06.024

Chen, P., Cescon, M., Megighian, A., and Ronaldo, P. (2014). Collagen VI regulates peripheral nerve myelination and function. *FASEB J.* 28 (3), 1145–1156. doi:10.1096/fj.13-239533

Chen, P., Cescon, M., Zuccolotto, G., Nobbio, L., Colombelli, C., Filaferro, M., et al. (2015). Collagen VI regulates peripheral nerve regeneration by modulating macrophage recruitment and polarization. *Acta Neuropathol.* 129 (1), 97–113. doi:10.1007/s00401-014-1369-9

Cheng, M., Cao, W., Gao, Y., Gong, Y., Zhao, N., and Zhang, X. (2003). Studies on nerve cell affinity of biodegradable modified chitosan films. *J. Biomaterials Sci. Polym. Ed.* 14 (10), 1155–1167. doi:10.1163/156856203769231628

Chernousov, M. A., Stahl, R. C., and Carey, D. J. (2001). Schwann cell type V collagen inhibits axonal outgrowth and promotes Schwann cell migration via distinct adhesive activities of the collagen and noncollagen domains. *J. Neurosci.* 21 (16), 6125–6135. doi:10.1523/jneurosci.21-16-06125.2001

Chernousov, M. A., Rothblum, K., Stahl, R. C., Evans, A., Prentiss, L., and Carey, D. J. (2006). Glypican-1 and 4(V) collagen are required for schwann cell myelination. *J. Neurosci.* 26 (2), 508–517. doi:10.1523/jneurosci.2544-05.2006

Choi, J., Kim, J., Jang, J., Kim, H., and Choi, S. (2018). Decellularized sciatic nerve matrix as a biodegradable conduit for peripheral nerve regeneration. *Neural Regen. Res.* 13 (10), 1796–1803. doi:10.4103/1673-5374.237126

Chu, H., Gao, J., Chen, C. W., Huard, J., and Wang, Y. (2011). Injectable fibroblast growth factor-2 coacervate for persistent angiogenesis. *Proc. Natl. Acad. Sci. U. S. A.* 108 (33), 13444–13449. doi:10.1073/pnas.1110121108

Chung, L., Dinakarpandian, D., Yoshida, N., Lauer-Fields, J. L., Fields, G. B., Visse, R., et al. (2004). Collagenase unwinds triple-helical collagen prior to peptide bond hydrolysis. *EMBO J.* 23 (15), 3020–3030. doi:10.1038/sj.emboj.7600318

Colin, W., and Donoff, R. B. (1984). Nerve regeneration through collagen tubes. *J. Dent. Res.* 63 (7), 987–993. doi:10.1177/00220345840630071601

Cui, Y., Lu, C., Meng, D., Xiao, Z., Hou, X., Ding, W., et al. (2014). Collagen scaffolds modified with CNTF and bFGF promote facial nerve regeneration in minipigs. *Biomaterials* 35 (27), 7819–7827. doi:10.1016/j.biomaterials.2014.05.065

Cui, Y., Yao, Y., Zhao, Y., Xiao, Z., Cao, Z., Han, S., et al. (2018). Functional collagen conduits combined with human mesenchymal stem cells promote regeneration after sciatic nerve transection in dogs. *J. Tissue Eng. Regen. Med.* 12 (5), 1285–1296. doi:10.1002/term.2660

Cummings, B. J., Uchida, N., Tamaki, S. J., Salazar, D. L., Hooshmand, M., Summers, R., et al. (2005). Human neural stem cells differentiate and promote locomotor recovery in spinal cord-injured mice. *Proc. Natl. Acad. Sci. U. S. A.* 102 (39), 14069–14074. doi:10.1073/pnas.0507063102

Dai, X., Schalek, R., and Xu, Q. (2012). Staining and etching: a simple method to fabricate inorganic nanostructures from tissue slices. *Adv. Mat.* 24 (3), 370–374. doi:10.1002/adma.201103908

Davis, J. B., and Stroobant, P. (1990). Platelet-derived growth factors and fibroblast growth factors are mitogens for rat Schwann cells. *J. Cell Biol.* 110 (4), 1353–1360. doi:10.1083/jcb.110.4.1353

Deal, D. N., Griffin, J. W., and Hogan, M. V. (2012). Nerve conduits for nerve repair or reconstruction. *J. Am. Acad. Orthop. Surg.* 20 (2), 63–68. doi:10.5435/jaaos-20-02-063

Delustro, F., Condell, R. A., Nguyen, M. A., and McPherson, J. M. (1986). A comparative study of the biologic and immunologic response to medical devices derived from dermal collagen. *J. Biomed. Mat. Res.* 20 (1), 109–120. doi:10.1002/jbm.820200110

Dezawa, M., Takahashi, I., Esaki, M., Takano, M., and Sawada, H. (2001). Sciatic nerve regeneration in rats induced by transplantation of *in vitro* differentiated bone-marrow stromal cells. *Eur. J. Neurosci.* 14 (11), 1771–1776. doi:10.1046/j.0953-816x.2001.01814.x

Dong, C., and Lv, Y. (2016). Application of collagen scaffold in tissue engineering: Recent advances and new perspectives. *Polym. (Basel)* 8 (2), 42. doi:10.3390/polym8020042

Drake, M. T., Clarke, B. L., Oursler, M. J., and Khosla, S. (2017). Cathepsin K inhibitors for osteoporosis: Biology, potential clinical utility, and lessons learned. *Endocr. Rev.* 38 (4), 325–350. doi:10.1210/er.2015-1114

Drzewiecki, K. E., Parmar, A. S., Gaudet, I. D., Branch, J. R., Pike, D. H., Nanda, V., et al. (2014). Methacrylation induces rapid, temperature-dependent, reversible self-assembly of type-I collagen. *Langmuir* 30 (37), 11204–11211. doi:10.1021/la502418s

East, E., Golding, J. P., and Phillips, J. B. (2009). A versatile 3D culture model facilitates monitoring of astrocytes undergoing reactive gliosis. *J. Tissue Eng. Regen. Med.* 3 (8), 634–646. doi:10.1002/term.209

Erdman, R., Stahl, R. C., Rothblum, K., Chernousov, M. A., and Carey, D. J. (2002). Schwann cell adhesion to a novel heparan sulfate binding site in the N-terminal domain of alpha 4 type V collagen is mediated by syndecan-3. *J. Biol. Chem.* 277 (9), 7619–7625. doi:10.1074/jbc.m111311200

Esses, S. I., and Halloran, P. F. (1983). Donor marrow-derived cells as immunogens and targets for the immune response to bone and skin allografts. *Transplantation* 35 (2), 169–174. doi:10.1097/00007890-198302000-00012

Fang, Z., and Zou, J. L. (2021). Recombinant COL6 α2 as a self-organization factor that triggers orderly nerve regeneration without guidance cues. *Front. Cell. Neurosci.* 15, 816781. doi:10.3389/fncel.2021.816781

Faroni, A., Mobasseri, S. A., Kingham, P. J., and Reid, A. J. (2015). Peripheral nerve regeneration: experimental strategies and future perspectives. *Adv. Drug Deliv. Rev.* 82-83, 160–167. doi:10.1016/j.addr.2014.11.010

Fields, G. B. (2013). Interstitial collagen catabolism. *J. Biol. Chem.* 288 (13), 8785–8793. doi:10.1074/jbc.r113.451211

Fujii, K., Tsuji, M., and Murota, K. (1986). Isolation of peripheral nerve collagen. *Neurochem. Res.* 11 (10), 1439–1446. doi:10.1007/bf00966223

Fujimaki, H., Uchida, K., Inoue, G., Miyagi, M., Nemoto, N., Saku, T., et al. (2017). Oriented collagen tubes combined with basic fibroblast growth factor promote peripheral nerve regeneration in a 15 mm sciatic nerve defect rat model. *J. Biomed. Mat. Res. A* 105 (1), 8–14. doi:10.1002/jbm.a.35866

Fujimaki, H., Uchida, K., Inoue, G., Matsushita, O., Nemoto, N., Miyagi, M., et al. (2020). Polyglycolic acid-collagen tube combined with collagen-binding basic fibroblast growth factor accelerates gait recovery in a rat sciatic nerve critical-size defect model. *J. Biomed. Mat. Res.* 108 (2), 326–332. doi:10.1002/jbm.b.34391

Fujimoto, E., Mizoguchi, A., Hanada, K., Yajima, M., and Ide, C. (1997). Basic fibroblast growth factor promotes extension of regenerating axons of peripheral nerve. *in vivo* experiments using a Schwann cell basal lamina tube model. *J. Neurocytol.* 26 (8), 511–528. doi:10.1023/a:1015410023132

Furthmayr, H., and Timpl, R. (1976). Immunochemistry of collagens and procollagens. *Int. Rev. Connect. Tissue Res.* 7, 61–99. doi:10.1016/b978-0-12-363707-9.50008-3

Gantus, M. A., Nasciutti, L., Cruz, C., Persechini, P., and Martinez, A. (2006). Modulation of extracellular matrix components by metalloproteinases and their tissue inhibitors during degeneration and regeneration of rat sural nerve. *Brain Res.* 1122 (1), 36–46. doi:10.1016/j.brainres.2006.09.016

Gelse, K., Poschl, E., and Aigner, T. (2003). Collagens--structure, function, and biosynthesis. *Adv. Drug Deliv. Rev.* 55 (12), 1531–1546. doi:10.1016/j.addr.2003.08.002

Gonzalez-Masis, J., Cubero-Sesin, J. M., Guerrero, S., Gonzalez-Camacho, S., Corrales-Urena, Y. R., Redondo-Gomez, C., et al. (2020). Self-assembly study of type I collagen extracted from male Wistar Hannover rat tail tendons. *Biomater. Res.* 24 (1), 19. doi:10.1186/s40824-020-00197-0

Gonzalez-Perez, F., Cobianchi, S., Heimann, C., Phillips, J. B., Udina, E., and Navarro, X. (2017). Stabilization, rolling, and addition of other extracellular matrix proteins to collagen hydrogels improve regeneration in chitosan guides for long peripheral nerve gaps in rats. *Neurosurgery* 80 (3), 465–474. doi:10.1093/neuros/nyw068

Goulart, C. O., Angelo Durco, D. d. F. P., de Carvalho, L. A., Oliveira, J. T., Alves, L., Cavalcante, L. A., et al. (2016). Olfactory ensheathing glia cell therapy and tubular conduit enhance nerve regeneration after mouse sciatic nerve transection. *Brain Res.* 1650, 243–251. doi:10.1016/j.brainres.2016.09.021

Gregory, H., and Phillips, J. B. (2021). Materials for peripheral nerve repair constructs: Natural proteins or synthetic polymers? *Neurochem. Int.* 143, 104953. doi:10.1016/j.neuint.2020.104953

Grinsell, D., and Keating, C. P. (2014). Peripheral nerve reconstruction after injury: a review of clinical and experimental therapies. *Biomed. Res. Int.* 2014, 1–13. doi:10.1155/2014/698256

Gu, L., Shan, T., Ma, Y. x., Tay, F. R., and Niu, L. (2019a). Novel biomedical applications of cross-linked collagen. *Trends Biotechnol.* 37 (5), 464–491. doi:10.1016/j.tibtech.2018.10.007

Gu, J., Xu, H., Xu, Y. P., Liu, H. H., Lang, J. T., Chen, X. P., et al. (2019b). Olfactory ensheathing cells promote nerve regeneration and functional recovery after facial nerve defects. *Neural Regen. Res.* 14 (1), 124–131. doi:10.4103/1673-5374.243717

Guaiquil, V. H., Pan, Z., Karagianni, N., Fukuoka, S., Alegre, G., and Rosenblatt, M. I. (2014). VEGF-B selectively regenerates injured peripheral neurons and restores sensory and trophic functions. *Proc. Natl. Acad. Sci. U. S. A.* 111 (48), 17272–17277. doi:10.1073/pnas.1407227111

Guerout, N., Duclos, C., Drouot, L., Abramovici, O., Bon-Mardion, N., Lacoume, Y., et al. (2011). Transplantation of olfactory ensheathing cells promotes axonal regeneration and functional recovery of peripheral nerve lesion in rats. *Muscle Nerve* 43 (4), 543–551. doi:10.1002/mus.21907

Guo, Z. Y., Sun, X., Xu, X. L., Zhao, Q., Peng, J., and Wang, Y. (2015). Human umbilical cord mesenchymal stem cells promote peripheral nerve repair via paracrine mechanisms. *Neural Regen. Res.* 10 (4), 651–658. doi:10.4103/1673-5374.155442

Han, Q., Sun, W., Lin, H., Zhao, W., Gao, Y., Zhao, Y., et al. (2009). Linear ordered collagen scaffolds loaded with collagen-binding brain-derived neurotrophic factor improve the recovery of spinal cord injury in rats. *Tissue Eng. Part A* 15 (10), 2927–2935. doi:10.1089/ten.tea.2008.0506

Harley, B. A., Spilker, M., Wu, J., Asano, K., Hsu, H. P., Spector, M., et al. (2004). Optimal degradation rate for collagen chambers used for regeneration of peripheral nerves over long gaps. *Cells Tissues Organs* 176 (1-3), 153–165. doi:10.1159/000075035

Harley, B. A., Hastings, A., Yannas, I., and Sannino, A. (2006). Fabricating tubular scaffolds with a radial pore size gradient by a spinning technique. *Biomaterials* 27 (6), 866–874. doi:10.1016/j.biomaterials.2005.07.012

Haronen, H., Zainul, Z., Tu, H., Naumenko, N., Sormunen, R., Miinalainen, I., et al. (2017). Collagen XIII secures pre- and postsynaptic integrity of the

neuromuscular synapse. *Hum. Mol. Genet.* 26 (11), 2076–2090. doi:10.1093/hmg/ddx101

Harrington, W. F., and Von Hippel, P. H. (1961). The structure of collagen and gelatin. *Adv. Protein Chem.* 16, 1–138. doi:10.1016/s0065-3233(08)60028-5

Hartnick, C. J., Staecker, H., Malgrange, B., Lefebvre, P. P., Liu, W., Moonen, G., et al. (1996). Neurotrophic effects of BDNF and CNTF, alone and in combination, on postnatal day 5 rat acoustic ganglion neurons. *J. Neurobiol.* 30 (2), 246–254. doi:10.1002/(SICI)1097-4695(199606)30:2<246::AID-NEU6>3.0.CO;2-5

Haugh, M. G., Jaasma, M. J., and O'Brien, F. J. (2009). The effect of dehydrothermal treatment on the mechanical and structural properties of collagen-GAG scaffolds. *J. Biomed. Mat. Res. A* 89 (2), 363–369. doi:10.1002/jbm.a.31955

Hayakawa, N., Matsumine, H., Fujii, K., Osaki, H., Ueta, Y., Kamei, W., et al. (2021). Facial nerve regeneration with bioabsorbable collagen conduits filled with collagen filaments: An experimental study. *Regen. Ther.* 18, 302–308. doi:10.1016/j.reth.2021.08.006

Haynl, C., Hofmann, E., Pawar, K., Forster, S., and Scheibel, T. (2016). Microfluidics-produced collagen fibers show extraordinary mechanical properties. *Nano Lett.* 16 (9), 5917–5922. doi:10.1021/acs.nanolett.6b02828

He, J., Zhang, N., Zhu, Y., Jin, R., and Wu, F. (2021). MSC spheroids-loaded collagen hydrogels simultaneously promote neuronal differentiation and suppress inflammatory reaction through PI3K-Akt signaling pathway. *Biomaterials* 265, 120448. doi:10.1016/j.biomaterials.2020.120448

Hinman, S. S., Wang, Y., Kim, R., and Allbritton, N. L. (2021). *In vitro* generation of self-renewing human intestinal epithelia over planar and shaped collagen hydrogels. *Nat. Protoc.* 16 (1), 352–382. doi:10.1038/s41596-020-00419-8

Hoffman-Kim, D., Mitchel, J. A., and Bellamkonda, R. V. (2010). Topography, cell response, and nerve regeneration. *Annu. Rev. Biomed. Eng.* 12, 203–231. doi:10.1146/annurev-bioeng-070909-105351

Holmes, D. F., Lu, Y., Starborg, T., and Kadler, K. E. (2018). Collagen fibril assembly and function. *Curr. Top. Dev. Biol.* 130, 107–142. doi:10.1016/bs.ctdb.2018.02.004

Holmquist, B., Kanje, M., Kerns, J. M., and Danielsen, N. (1993). A mathematical model for regeneration rate and initial delay following surgical repair of peripheral nerves. *J. Neurosci. Methods* 48 (1-2), 27–33. doi:10.1016/s0165-0270(05)80004-4

Hosseinkhani, H., Hiraoka, Y., Li, C. H., Chen, Y. R., Yu, D. S., Hong, P. D., et al. (2013). Engineering three-dimensional collagen-IKVAV matrix to mimic neural microenvironment. *ACS Chem. Neurosci.* 4 (8), 1229–1235. doi:10.1021/cn400075h

Hu, B., Zhang, H., Xu, M., Li, L., Wu, M., Zhang, S., et al. (2022). Delivery of basic fibroblast growth factor through an *in situ* forming smart hydrogel activates autophagy in schwann cells and improves facial nerves generation via the PAK-1 signaling pathway. *Front. Pharmacol.* 13, 778680. doi:10.3389/fphar.2022.778680

Isaacman-Beck, J., Schneider, V., Franzini-Armstrong, C., and Granato, M. (2015). The lh3 glycosyltransferase directs target-selective peripheral nerve regeneration. *Neuron* 88 (4), 691–703. doi:10.1016/j.neuron.2015.10.004

Itoh, S., Takakuda, K., Kawabata, S., Aso, Y., Kasai, K., Itoh, H., et al. (2002). Evaluation of cross-linking procedures of collagen tubes used in peripheral nerve repair. *Biomaterials* 23 (23), 4475–4481. doi:10.1016/s0142-9612(02)00166-7

Jablonska-Trypuc, A., Matejczyk, M., and Rosochacki, S. (2016). Matrix metalloproteinases (MMPs), the main extracellular matrix (ECM) enzymes in collagen degradation, as a target for anticancer drugs. *J. Enzyme Inhib. Med. Chem.* 31, 177–183. doi:10.3109/14756366.2016.1161620

Jessen, K. R., Mirsky, R., and Lloyd, A. C. (2015). Schwann cells: Development and role in nerve repair. *Cold Spring Harb. Perspect. Biol.* 7 (7), a020487. doi:10.1101/cshperspect.a020487

Jiang, H., Qian, Y., Fan, C., and Ouyang, Y. (2020a). Polymeric guide conduits for peripheral nerve tissue engineering. *Front. Bioeng. Biotechnol.* 8, 582646. doi:10.3389/fbioe.2020.582646

Jiang, J. P., Liu, X. Y., Zhao, F., Zhu, X., Li, X. Y., Niu, X. G., et al. (2020b). Three-dimensional bioprinting collagen/silk fibroin scaffold combined with neural stem cells promotes nerve regeneration after spinal cord injury. *Neural Regen. Res.* 15 (5), 959–968. doi:10.4103/1673-5374.268974

Jin, H. X., Xu, H. P., Li, Y., Zhang, Q. W., and Xie, H. (2019). Preparation and evaluation of peptides with potential antioxidant activity by microwave assisted enzymatic hydrolysis of collagen from sea cucumber acaudina molpadioides obtained from zhejiang Province in China. *Mar. Drugs* 17 (3), 169. doi:10.3390/md17030169

Karsdal, M. A., Nielsen, S., Leeming, D., Langholm, L., Nielsen, M., Manon-Jensen, T., et al. (2017). The good and the bad collagens of fibrosis - their role in signaling and organ function. *Adv. Drug Deliv. Rev.* 121, 43–56. doi:10.1016/j.addr.2017.07.014

Keilhoff, G., Fansa, H., Schneider, W., and Wolf, G. (1999). *In vivo* predegeneration of peripheral nerves: an effective technique to obtain activated schwann cells for nerve conduits. *J. Neurosci. Methods* 89 (1), 17–24. doi:10.1016/s0165-0270(99)00034-5

Keilhoff, G., Fansa, H., Smalla, K. H., Schneider, W., and Wolf, G. (2000). Neuroma: a donor-age independent source of human schwann cells for tissue engineered nerve grafts. *Neuroreport* 11 (17), 3805–3809. doi:10.1097/00001756-200011270-00042

Keilhoff, G., Stang, F., Wolf, G., and Fansa, H. (2003). Bio-compatibility of type I/III collagen matrix for peripheral nerve reconstruction. *Biomaterials* 24 (16), 2779–2787. doi:10.1016/s0142-9612(03)00084-x

Kemp, S. W., Webb, A. A., Dhaliwal, S., Syed, S., Walsh, S. K., and Midha, R. (2011). Dose and duration of nerve growth factor (NGF) administration determine the extent of behavioral recovery following peripheral nerve injury in the rat. *Exp. Neurol.* 229 (2), 460–470. doi:10.1016/j.expneurol.2011.03.017

Kingham, P. J., Kalbermatten, D. F., Mahay, D., Armstrong, S. J., Wiberg, M., and Terenghi, G. (2007). Adipose-derived stem cells differentiate into a Schwann cell phenotype and promote neurite outgrowth *in vitro*. *Exp. Neurol.* 207 (2), 267–274. doi:10.1016/j.expneurol.2007.06.029

Koopmans, G., Hasse, B., and Sinis, N. (2009). Chapter 19: The role of collagen in peripheral nerve repair. *Int. Rev. Neurobiol.* 87, 363–379. doi:10.1016/S0074-7742(09)87019-0

Kornfeld, T., Vogt, P. M., and Radtke, C. (2019). Nerve grafting for peripheral nerve injuries with extended defect sizes. *Wien. Med. Wochenschr.* 169 (9-10), 240–251. doi:10.1007/s10354-018-0675-6

Kumar, V. A., Taylor, N. L., Jalan, A. A., Hwang, L. K., Wang, B. K., and Hartgerink, J. D. (2014). A nanostructured synthetic collagen mimic for hemostasis. *Biomacromolecules* 15 (4), 1484–1490. doi:10.1021/bm500091e

Ladak, A., Olson, J., Tredget, E., and Gordon, T. (2011). Differentiation of mesenchymal stem cells to support peripheral nerve regeneration in a rat model. *Exp. Neurol.* 228 (2), 242–252. doi:10.1016/j.expneurol.2011.01.013

Lee, J. H., Yang, S. H., Lee, E. J., and Kim, H. W. (2014). Carbon nanotube-collagen three-dimensional culture of mesenchymal stem cells promotes expression of neural phenotypes and secretion of neurotrophic factors. *Acta Biomater.* 10 (10), 4425–4436. doi:10.1016/j.actbio.2014.06.023

Lee, J. M., Suen, S. K. Q., Ng, W. L., Ma, W. C., and Yeong, W. Y. (2021). Bioprinting of collagen: Considerations, potentials, and applications. *Macromol. Biosci.* 21 (1), e2000280. doi:10.1002/mabi.202000280

Li, G. D., Wo, Y., Zhong, M. F., Zhang, F. X., Bao, L., Lu, Y. J., et al. (2002). Expression of fibroblast growth factors in rat dorsal root ganglion neurons and regulation after peripheral nerve injury. *Neuroreport* 13 (15), 1903–1907. doi:10.1097/00001756-200210280-00014

Li, B. C., Jiao, S. S., Xu, C., You, H., and Chen, J. M. (2010). PLGA conduit seeded with olfactory ensheathing cells for bridging sciatic nerve defect of rats. *J. Biomed. Mat. Res. A* 94 (3), 769–780. doi:10.1002/jbm.a.32727

Li, X., Sun, H., Lin, N., Hou, X., Wang, J., Zhou, B., et al. (2011). Regeneration of uterine horns in rats by collagen scaffolds loaded with collagen-binding human basic fibroblast growth factor. *Biomaterials* 32 (32), 8172–8181. doi:10.1016/j.biomaterials.2011.07.050

Li, R., Liu, Z., Pan, Y., Chen, L., Zhang, Z., and Lu, L. (2014). Peripheral nerve injuries treatment: a systematic review. *Cell biochem. Biophys.* 68 (3), 449–454. doi:10.1007/s12013-013-9742-1

Li, R., Li, Y., Wu, Y., Zhao, Y., Chen, H., Yuan, Y., et al. (2018). Heparin-poloxamer thermosensitive hydrogel loaded with bFGF and NGF enhances peripheral nerve regeneration in diabetic rats. *Biomaterials* 168, 24–37. doi:10.1016/j.biomaterials.2018.03.044

Li, G., Chen, S., Zeng, M., Kong, Y., Zhao, F., Zhang, L., et al. (2019). Hierarchically aligned gradient collagen micropatterns for rapidly screening Schwann cells behavior. *Colloids Surfaces B Biointerfaces* 176, 341–351. doi:10.1016/j.colsurfb.2019.01.019

Li, R., Li, D. h., Zhang, H. y., Wang, J., Li, X. k., and Xiao, J. (2020). Growth factors-based therapeutic strategies and their underlying signaling mechanisms for peripheral nerve regeneration. *Acta Pharmacol. Sin.* 41 (10), 1289–1300. doi:10.1038/s41401-019-0338-1

Lin, H., Chen, B., Wang, B., Zhao, Y., Sun, W., and Dai, J. (2006). Novel nerve guidance material prepared from bovine aponeurosis. *J. Biomed. Mat. Res. A* 79 (3), 591–598. doi:10.1002/jbm.a.30862

Liu, B., Kong, Y., Shi, W., Kuss, M., Liao, K., Hu, G., et al. (2022a). Exosomes derived from differentiated human ADMSC with the Schwann cell phenotype modulate peripheral nerve-related cellular functions. *Bioact. Mat.* 14, 61–75. doi:10.1016/j.bioactmat.2021.11.022

Liu, S., Xie, Y. Y., Wang, L. D., Tai, C. X., Chen, D., Mu, D., et al. (2021). A multichannel collagen scaffold loaded with neural stem cells for the repair of

spinal cord injury. *Neural Regen. Res.* 16 (11), 2284–2292. doi:10.4103/1673-5374.310698

Liu, S., Lau, C. S., Liang, K., Wen, F., and Teoh, S. H. (2022b). Marine collagen scaffolds in tissue engineering. *Curr. Opin. Biotechnol.* 74, 92–103. doi:10.1016/j.copbio.2021.10.011

Llado, J., Haenggeli, C., Maragakis, N. J., Snyder, E. Y., and Rothstein, J. D. (2004). Neural stem cells protect against glutamate-induced excitotoxicity and promote survival of injured motor neurons through the secretion of neurotrophic factors. *Mol. Cell. Neurosci.* 27 (3), 322–331. doi:10.1016/j.mcn.2004.07.010

Long, Q., Wu, B., Yang, Y., Wang, S., Shen, Y., Bao, Q., et al. (2021). Nerve guidance conduit promoted peripheral nerve regeneration in rats. *Artif. Organs* 45 (6), 616–624. doi:10.1111/aor.13881

Lopatina, T., Kalinina, N., Karagyaur, M., Stambolsky, D., Rubina, K., Revischin, A., et al. (2011). Adipose-derived stem cells stimulate regeneration of peripheral nerves: BDNF secreted by these cells promotes nerve healing and axon growth de novo. *PLoS One* 6 (3), e17899. doi:10.1371/journal.pone.0017899

Lowe, C. J., Reucroft, I. M., Grota, M. C., and Shreiber, D. I. (2016). Production of highly aligned collagen scaffolds by freeze-drying of self-assembled, fibrillar collagen gels. *ACS Biomater. Sci. Eng.* 2 (4), 643–651. doi:10.1021/acsbiomaterials.6b00036

Lu, C., Meng, D., Cao, J., Xiao, Z., Cui, Y., Fan, J., et al. (2015). Collagen scaffolds combined with collagen-binding ciliary neurotrophic factor facilitate facial nerve repair in mini-pigs. *J. Biomed. Mat. Res. A* 103 (5), 1669–1676. doi:10.1002/jbm.a.35305

Lu, J., Yan, X., Sun, X., Shen, X., Yin, H., Wang, C., et al. (2019). Synergistic effects of dual-presenting VEGF- and BDNF-mimetic peptide epitopes from self-assembling peptide hydrogels on peripheral nerve regeneration. *Nanoscale* 11 (42), 19943–19958. doi:10.1039/c9nr04521j

Lv, D., Zhou, L., Zheng, X., and Hu, Y. (2017). Sustained release of collagen VI potentiates sciatic nerve regeneration by modulating macrophage phenotype. *Eur. J. Neurosci.* 45 (10), 1258–1267. doi:10.1111/ejn.13558

Lynn, A. K., Yannas, I. V., and Bonfield, W. (2004). Antigenicity and immunogenicity of collagen. *J. Biomed. Mat. Res.* 71 (2), 343–354. doi:10.1002/jbm.b.30096

Ma, F., Xiao, Z., Chen, B., Hou, X., Dai, J., and Xu, R. (2014a). Linear ordered collagen scaffolds loaded with collagen-binding basic fibroblast growth factor facilitate recovery of sciatic nerve injury in rats. *Tissue Eng. Part A* 20 (7-8), 1253–1262. doi:10.1089/ten.tea.2013.0158

Ma, F., Xiao, Z., Meng, D., Hou, X., Zhu, J., Dai, J., et al. (2014b). Use of natural neural scaffolds consisting of engineered vascular endothelial growth factor immobilized on ordered collagen fibers filled in a collagen tube for peripheral nerve regeneration in rats. *Int. J. Mol. Sci.* 15 (10), 18593–18609. doi:10.3390/ijms151018593

Ma, F., Zhu, T., Xu, F., Wang, Z., Zheng, Y., Tang, Q., et al. (2017). Neural stem/progenitor cells on collagen with anchored basic fibroblast growth factor as potential natural nerve conduits for facial nerve regeneration. *Acta Biomater.* 50, 188–197. doi:10.1016/j.actbio.2016.11.064

Ma, F., Xu, F., Li, R., Zheng, Y., Wang, F., wei, N., et al. (2018). Sustained delivery of glial cell-derived neurotrophic factors in collagen conduits for facial nerve regeneration. *Acta Biomater.* 69, 146–155. doi:10.1016/j.actbio.2018.01.001

Madduri, S., and Gander, B. (2010). Schwann cell delivery of neurotrophic factors for peripheral nerve regeneration. *J. Peripher. Nerv. Syst.* 15 (2), 93–103. doi:10.1111/j.1529-8027.2010.00257.x

Madduri, S., Papaloizos, M., and Gander, B. (2009). Synergistic effect of GDNF and NGF on axonal branching and elongation *in vitro*. *Neurosci. Res.* 65 (1), 88–97. doi:10.1016/j.neures.2009.06.003

Madduri, S., Feldman, K., Tervoort, T., Papaloizos, M., and Gander, B. (2010a). Collagen nerve conduits releasing the neurotrophic factors GDNF and NGF. *J. Control. Release* 143 (2), 168–174. doi:10.1016/j.jconrel.2009.12.017

Madduri, S., di Summa, P., Papaloizos, M., Kalbermatten, D., and Gander, B. (2010b). Effect of controlled co-delivery of synergistic neurotrophic factors on early nerve regeneration in rats. *Biomaterials* 31 (32), 8402–8409. doi:10.1016/j.biomaterials.2010.07.052

Masand, S. N., Chen, J., Perron, I. J., Hammerling, B. C., Loers, G., Schachner, M., et al. (2012). The effect of glycomimetic functionalized collagen on peripheral nerve repair. *Biomaterials* 33 (33), 8353–8362. doi:10.1016/j.biomaterials.2012.08.018

Matinong, A. M. E., Chisti, Y., Pickering, K. L., and Haverkamp, R. G. (2022). Collagen extraction from animal skin. *Biol. (Basel)* 11 (6), 905. doi:10.3390/biology11060905

Michaeli, D., Martin, G. R., Kettman, J., Benjamini, E., Leung, D. Y. K., and Blatt, B. A. (1969). Localization of antigenic determinants in the polypeptide chains of collagen. *Science* 166 (3912), 1522–1524. doi:10.1126/science.166.3912.1522

Midha, R., Munro, C. A., Dalton, P. D., Tator, C. H., and Shoichet, M. S. (2003). Growth factor enhancement of peripheral nerve regeneration through a novel synthetic hydrogel tube. *J. Neurosurg.* 99 (3), 555–565. doi:10.3171/jns.2003.99.3.0555

Mimura, T., Dezawa, M., Kanno, H., Sawada, H., and Yamamoto, I. (2004). Peripheral nerve regeneration by transplantation of bone marrow stromal cell-derived Schwann cells in adult rats. *J. Neurosurg.* 101 (5), 806–812. doi:10.3171/jns.2004.101.5.0806

Mori, H., Takahashi, A., Horimoto, A., and Hara, M. (2013). Migration of glial cells differentiated from neurosphere-forming neural stem/progenitor cells depends on the stiffness of the chemically cross-linked collagen gel substrate. *Neurosci. Lett.* 555, 1–6. doi:10.1016/j.neulet.2013.09.012

Muangsanit, P., Day, A., Dimiou, S., Atac, A. F., Kayal, C., Park, H., et al. (2020). Rapidly formed stable and aligned dense collagen gels seeded with Schwann cells support peripheral nerve regeneration. *J. Neural Eng.* 17 (4), 046036. doi:10.1088/1741-2552/abaa9c

Nectow, A. R., Marra, K. G., and Kaplan, D. L. (2012). Biomaterials for the development of peripheral nerve guidance conduits. *Tissue Eng. Part B Rev.* 18 (1), 40–50. doi:10.1089/ten.teb.2011.0240

Noble, J., Munro, C. A., Prasad, V. S. S. V., and Midha, R. (1998). Analysis of upper and lower extremity peripheral nerve injuries in a population of patients with multiple injuries. *J. Trauma Inj. Infect. Crit. Care* 45 (1), 116–122. doi:10.1097/00005373-199807000-00025

Nocera, G., and Jacob, C. (2020). Mechanisms of Schwann cell plasticity involved in peripheral nerve repair after injury. *Cell. Mol. Life Sci.* 77 (20), 3977–3989. doi:10.1007/s00018-020-03516-9

Novikova, L. N., Brohlin, M., Kingham, P. J., Novikov, L. N., and Wiberg, M. (2011). Neuroprotective and growth-promoting effects of bone marrow stromal cells after cervical spinal cord injury in adult rats. *Cytotherapy* 13 (7), 873–887. doi:10.3109/14653249.2011.574116

Okamoto, H., Hata, K. I., Kagami, H., Okada, K., Ito, Y., Narita, Y., et al. (2010). Recovery process of sciatic nerve defect with novel bioabsorbable collagen tubes packed with collagen filaments in dogs. *J. Biomed. Mat. Res. A* 92 (3), 859–868. doi:10.1002/jbm.a.32421

O'Leary, L. E., Fallas, J. A., Bakota, E. L., Kang, M. K., and Hartgerink, J. D. (2011). Multi-hierarchical self-assembly of a collagen mimetic peptide from triple helix to nanofibre and hydrogel. *Nat. Chem.* 3 (10), 821–828. doi:10.1038/nchem.1123

Ouyang, Y., Huang, C., Zhu, Y., Fan, C., and Ke, Q. (2013). Fabrication of seamless electrospun collagen/PLGA conduits whose walls comprise highly longitudinal aligned nanofibers for nerve regeneration. *J. Biomed. Nanotechnol.* 9 (6), 931–943. doi:10.1166/jbn.2013.1605

Pan, Y., Jiao, G., Yang, J., Guo, R., Li, J., and Wang, C. (2017). Insights into the therapeutic potential of heparinized collagen scaffolds loading human umbilical cord mesenchymal stem cells and nerve growth factor for the repair of recurrent laryngeal nerve injury. *Tissue Eng. Regen. Med.* 14 (3), 317–326. doi:10.1007/s13770-017-0032-7

Park, J. W., Kang, Y. D., Kim, J. S., Lee, J. H., and Kim, H. W. (2014). 3D microenvironment of collagen hydrogel enhances the release of neurotrophic factors from human umbilical cord blood cells and stimulates the neurite outgrowth of human neural precursor cells. *Biochem. Biophys. Res. Commun.* 447 (3), 400–406. doi:10.1016/j.bbrc.2014.03.145

Pereira Lopes, F. R., Camargo de Moura Campos, L., Dias Correa, J., Balduino, A., Lora, S., Langone, F., et al. (2006). Bone marrow stromal cells and resorbable collagen guidance tubes enhance sciatic nerve regeneration in mice. *Exp. Neurol.* 198 (2), 457–468. doi:10.1016/j.expneurol.2005.12.019

Petcharat, T., Benjakul, S., Karnjanapratum, S., and Nalinanon, S. (2021). Ultrasound-assisted extraction of collagen from clown featherback (*Chitala ornata*) skin: Yield and molecular characteristics. *J. Sci. Food Agric.* 101 (2), 648–658. doi:10.1002/jsfa.10677

Pinho, A. C., Fonseca, A. C., Serra, A. C., Santos, J. D., and Coelho, J. F. J. (2016). Peripheral nerve regeneration: Current status and new strategies using polymeric materials. *Adv. Healthc. Mat.* 5 (21), 2732–2744. doi:10.1002/adhm.201600236

Rasi, K., Hurskainen, M., Kallio, M., Staven, S., Sormunen, R., Heape, A. M., et al. (2010). Lack of collagen XV impairs peripheral nerve maturation and, when combined with laminin-411 deficiency, leads to basement membrane abnormalities and sensorimotor dysfunction. *J. Neurosci.* 30 (43), 14490–14501. doi:10.1523/jneurosci.2644-10.2010

Reichardt, L. F. (2006). Neurotrophin-regulated signalling pathways. *Phil. Trans. R. Soc. B* 361 (1473), 1545–1564. doi:10.1098/rstb.2006.1894

Ribeiro, A., Vargo, S., Powell, E. M., and Leach, J. B. (2012). Substrate three-dimensionality induces elemental morphological transformation of sensory

neurons on a physiologic timescale. *Tissue Eng. Part A* 18 (1-2), 93–102. doi:10.1089/ten.tea.2011.0221

Ricard-Blum, S. (2011). The collagen family. *Cold Spring Harb. Perspect. Biol.* 3 (1), a004978. doi:10.1101/cshperspect.a004978

Richner, M., Ulrichsen, M., Elmegaard, S. L., Dieu, R., Pallesen, L. T., and Vaegter, C. B. (2014). Peripheral nerve injury modulates neurotrophin signaling in the peripheral and central nervous system. *Mol. Neurobiol.* 50 (3), 945–970. doi:10.1007/s12035-014-8706-9

Rieu, C., Parisi, C., Mosser, G., Haye, B., Coradin, T., Fernandes, F. M., et al. (2019). Topotactic fibrillogenesis of freeze-cast microridged collagen scaffolds for 3D cell culture. *ACS Appl. Mat. Interfaces* 11 (16), 14672–14683. doi:10.1021/acsami.9b03219

Roche, P., Alekseeva, T., Widaa, A., Ryan, A., Matsiko, A., Walsh, M., et al. (2017). Olfactory derived stem cells delivered in a biphasic conduit promote peripheral nerve repair in vivo. *Stem Cells Transl. Med.* 6 (10), 1894–1904. doi:10.1002/sctm.16-0420

Ruijs, A. C., Jaquet, J. B., Kalmijn, S., Giele, H., and Hovius, S. E. R. (2005). Median and ulnar nerve injuries: a meta-analysis of predictors of motor and sensory recovery after modern microsurgical nerve repair. *Plastic Reconstr. Surg.* 116 (2), 484–494. doi:10.1097/01.prs.0000172896.86594.07

Sahenk, Z., Seharaseyon, J., and Mendell, J. R. (1994). CNTF potentiates peripheral nerve regeneration. *Brain Res.* 655 (1-2), 246–250. doi:10.1016/0006-8993(94)91621-7

Sakiyama-Elbert, S. E., and Hubbell, J. A. (2000). Development of fibrin derivatives for controlled release of heparin-binding growth factors. *J. Control. Release* 65 (3), 389–402. doi:10.1016/s0168-3659(99)00221-7

Salvatore, L., Madaghiele, M., Parisi, C., Gatti, F., and Sannino, A. (2014). Cross-linking of micropatterned collagen-based nerve guides to modulate the expected half-life. *J. Biomed. Mat. Res. A* 102 (12), 4406–4414. doi:10.1002/jbm.a.35124

Samadian, H., Vaez, A., Ehterami, A., Salehi, M., Farzamfar, S., Sahrapeyma, H., et al. (2019). Sciatic nerve regeneration by using collagen type I hydrogel containing naringin. *J. Mat. Sci. Mat. Med.* 30 (9), 107. doi:10.1007/s10856-019-6309-8

Sarker, M. D., Naghieh, S., McInnes, A. D., Schreyer, D. J., and Chen, X. (2018). Regeneration of peripheral nerves by nerve guidance conduits: Influence of design, biopolymers, cells, growth factors, and physical stimuli. *Prog. Neurobiol.* 171, 125–150. doi:10.1016/j.pneurobio.2018.07.002

Shi, Q., Gao, W., Han, X., Zhu, X., Sun, J., Xie, F., et al. (2014). Collagen scaffolds modified with collagen-binding bFGF promotes the neural regeneration in a rat hemisected spinal cord injury model. *Sci. China Life Sci.* 57 (2), 232–240. doi:10.1007/s11427-014-4612-7

Siironen, J., SandbergM.Vuorinen, V., and RoyttaM. (1992). Expression of type I and III collagens and fibronectin after transection of rat sciatic nerve. Reinnervation compared with denervation. *Lab. Invest.* 67 (1), 80–87.

Sorushanova, A., Delgado, L. M., Wu, Z., Shologu, N., Kshirsagar, A., Raghunath, R., et al. (2019). The collagen suprafamily: From biosynthesis to advanced biomaterial development. *Adv. Mat.* 31 (1), e1801651. doi:10.1002/adma.201801651

Sowa, Y., Imura, T., Numajiri, T., Nishino, K., and Fushiki, S. (2012). Adipose-derived stem cells produce factors enhancing peripheral nerve regeneration: influence of age and anatomic site of origin. *Stem Cells Dev.* 21 (11), 1852–1862. doi:10.1089/scd.2011.0403

Speer, D. P., Chvapil, M., Eskelson, C. D., and Ulreich, J. (1980). Biological effects of residual glutaraldehyde in glutaraldehyde-tanned collagen biomaterials. *J. Biomed. Mat. Res.* 14 (6), 753–764. doi:10.1002/jbm.820140607

Spira, M., Liu, B., Xu, Z., Harrell, R., and Chahadeh, H. (1994). Human amnion collagen for soft tissue augmentation--biochemical characterizations and animal observations. *J. Biomed. Mat. Res.* 28 (1), 91–96. doi:10.1002/jbm.820280112

Sprangers, S., and Everts, V. (2019). Molecular pathways of cell-mediated degradation of fibrillar collagen. *Matrix Biol.* 75-76, 190–200. doi:10.1016/j.matbio.2017.11.008

Sullivan, R., Dailey, T., Duncan, K., Abel, N., and Borlongan, C. (2016). Peripheral nerve injury: Stem cell therapy and peripheral nerve transfer. *Int. J. Mol. Sci.* 17 (12), 2101. doi:10.3390/ijms17122101

Sun, J. H., Huang, M., Fang, Z., Li, T. X., Wu, T. T., Chen, Y., et al. (2022). Nerve bundle formation during the promotion of peripheral nerve regeneration: collagen VI-neural cell adhesion molecule 1 interaction. *Neural Regen. Res.* 17 (5), 1023–1033. doi:10.4103/1673-5374.324861

Sund, M., Vaisanen, T., Kaukinen, S., Ilves, M., Tu, H., Autio-Harmainen, H., et al. (2001). Distinct expression of type XIII collagen in neuronal structures and other tissues during mouse development. *Matrix Biol.* 20 (4), 215–231. doi:10.1016/s0945-053x(01)00134-2

Thomson, J. A., Itskovitz-Eldor, J., Shapiro, S. S., Waknitz, M. A., Swiergiel, J. J., Marshall, V. S., et al. (1998). Embryonic stem cell lines derived from human blastocysts. *Science* 282 (5391), 1145–1147. doi:10.1126/science.282.5391.1145

Tong, L., Ji, L., Wang, Z., Tong, X., Zhang, L., and Sun, X. (2010). Differentiation of neural stem cells into Schwann-like cells *in vitro*. *Biochem. Biophys. Res. Commun.* 401 (4), 592–597. doi:10.1016/j.bbrc.2010.09.107

Uz, M., Das, S. R., Ding, S., Sakaguchi, D. S., Claussen, J. C., and Mallapragada, S. K. (2018). Advances in controlling differentiation of adult stem cells for peripheral nerve regeneration. *Adv. Healthc. Mat.* 7 (14), e1701046. doi:10.1002/adhm.201701046

Vidal, A. R., Duarte, L. P., Schmidt, M. M., Cansian, R. L., Fernandes, I. A., de Oliveira Mello, R., et al. (2020). Extraction and characterization of collagen from sheep slaughter by-products. *Waste Manag.* 102, 838–846. doi:10.1016/j.wasman.2019.12.004

Vijayavenkataraman, S. (2020). Nerve guide conduits for peripheral nerve injury repair: A review on design, materials and fabrication methods. *Acta Biomater.* 106, 54–69. doi:10.1016/j.actbio.2020.02.003

Vizarova, K., Bakos, D., Rehakova, M., and Macho, V. (1994). Modification of layered atelocollagen by ultraviolet irradiation and chemical cross-linking: Structure stability and mechanical properties. *Biomaterials* 15 (13), 1082–1086. doi:10.1016/0142-9612(94)90094-9

Wang, S., Cai, Q., Hou, J., Bei, J., Zhang, T., Yang, J., et al. (2003). Acceleration effect of basic fibroblast growth factor on the regeneration of peripheral nerve through a 15-mm gap. *J. Biomed. Mat. Res.* 66 (3), 522–531. doi:10.1002/jbm.a.10008

Wang, P., Zhao, H., Yao, Y., Lu, C., Ma, J., Chen, R., et al. (2020). Repair of facial nerve crush injury in rabbits using collagen plus basic fibroblast growth factor. *J. Biomed. Mat. Res. A* 108 (6), 1329–1337. doi:10.1002/jbm.a.36905

Wangensteen, K. J., and Kalliainen, L. K. (2010). Collagen tube conduits in peripheral nerve repair: a retrospective analysis. *Hand (N Y)* 5 (3), 273–277. doi:10.1007/s11552-009-9245-0

Wewetzer, K., Kern, N., Ebel, C., Radtke, C., and Brandes, G. (2005). Phagocytosis of O4+ axonal fragments *in vitro* by p75- neonatal rat olfactory ensheathing cells. *Glia* 49 (4), 577–587. doi:10.1002/glia.20149

Xiao, Y. Z., and Wang, S. (2015). Differentiation of Schwannlike cells from human umbilical cord blood mesenchymal stem cells *in vitro*. *Mol. Med. Rep.* 11 (2), 1146–1152. doi:10.3892/mmr.2014.2840

Xu, X., Gan, Q., Clough, R. C., Pappu, K. M., Howard, J. A., Baez, J. A., et al. (2011). Hydroxylation of recombinant human collagen type I alpha 1 in transgenic maize co-expressed with a recombinant human prolyl 4-hydroxylase. *BMC Biotechnol.* 11, 69. doi:10.1186/1472-6750-11-69

Yamamoto, T., Osako, Y., Ito, M., Murakami, M., Hayashi, Y., Horibe, H., et al. (2016). Trophic effects of dental pulp stem cells on schwann cells in peripheral nerve regeneration. *Cell Transpl.* 25 (1), 183–193. doi:10.3727/096368915x688074

Yamauchi, M., and Sricholpech, M. (2012). Lysine post-translational modifications of collagen. *Essays Biochem.* 52, 113–133. doi:10.1042/bse0520113

Yang, C., Hillas, P. J., B??ez, J. A., Nokelainen, M., Balan, J., Tang, J., et al. (2004). The application of recombinant human collagen in tissue engineering. *BioDrugs* 18 (2), 103–119. doi:10.2165/00063030-200418020-00004

Yang, H. S., Bhang, S. H., Hwang, J. W., Kim, D. I., and Kim, B. S. (2010). Delivery of basic fibroblast growth factor using heparin-conjugated fibrin for therapeutic angiogenesis. *Tissue Eng. Part A* 16 (6), 2113–2119. doi:10.1089/ten.tea.2009.0673

Yang, J. W., Ru, J., Ma, W., Gao, Y., Liang, Z., Liu, J., et al. (2015). BDNF promotes the growth of human neurons through crosstalk with the Wnt/β-catenin signaling pathway via GSK-3β. *Neuropeptides* 54, 35–46. doi:10.1016/j.npep.2015.08.005

Yao, L., Billiar, K. L., Windebank, A. J., and Pandit, A. (2010a). Multichanneled collagen conduits for peripheral nerve regeneration: design, fabrication, and characterization. *Tissue Eng. Part C. Methods* 16 (6), 1585–1596. doi:10.1089/ten.tec.2010.0152

Yao, L., de Ruiter, G. C., Wang, H., Knight, A. M., Spinner, R. J., Yaszemski, M. J., et al. (2010b). Controlling dispersion of axonal regeneration using a multichannel collagen nerve conduit. *Biomaterials* 31 (22), 5789–5797. doi:10.1016/j.biomaterials.2010.03.081

Yao, L., Daly, W., Newland, B., Yao, S., Wang, W., Chen, B. K. K., et al. (2013). Improved axonal regeneration of transected spinal cord mediated by multichannel collagen conduits functionalized with neurotrophin-3 gene. *Gene Ther.* 20 (12), 1149–1157. doi:10.1038/gt.2013.42

Yao, Y., Cui, Y., Zhao, Y., Xiao, Z., Li, X., Han, S., et al. (2018). Efect of longitudinally oriented collagen conduit combined with nerve growth factor on nerve regeneration after dog sciatic nerve injury. *J. Biomed. Mat. Res.* 106 (6), 2131–2139. doi:10.1002/jbm.b.34020

Yu, Z., An, B., Ramshaw, J. A., and Brodsky, B. (2014). Bacterial collagen-like proteins that form triple-helical structures. *J. Struct. Biol. X.* 186 (3), 451–461. doi:10.1016/j.jsb.2014.01.003

Yu, X., Zhang, D., Liu, C., Liu, Z., Li, Y., Zhao, Q., et al. (2021). Micropatterned poly(D, L-lactide-Co-caprolactone) conduits with KHI-peptide and NGF promote peripheral nerve repair after severe traction injury. *Front. Bioeng. Biotechnol.* 9, 744230. doi:10.3389/fbioe.2021.744230

Zainul, Z., Heikkinen, A., Koivisto, H., Rautalahti, I., Kallio, M., Lin, S., et al. (2018). Collagen XIII is required for neuromuscular synapse regeneration and functional recovery after peripheral nerve injury. *J. Neurosci.* 38 (17), 4243–4258. doi:10.1523/jneurosci.3119-17.2018

Zhang, H., Wei, Y. T., Tsang, K. S., Sun, C. R., Li, J., Huang, H., et al. (2008). Implantation of neural stem cells embedded in hyaluronic acid and collagen composite conduit promotes regeneration in a rabbit facial nerve injury model. *J. Transl. Med.* 6, 67. doi:10.1186/1479-5876-6-67

Zhang, Y. G., Sheng, Q. S., Qi, F. Y., Hu, X. Y., Zhao, W., Wang, Y. Q., et al. (2013). Schwann cell-seeded scaffold with longitudinally oriented micro-channels for reconstruction of sciatic nerve in rats. *J. Mat. Sci. Mat. Med.* 24 (7), 1767–1780. doi:10.1007/s10856-013-4917-2

Zhang, Q., Nguyen, P. D., Shi, S., Burrell, J. C., Xu, Q., Cullen, K. D., et al. (2018). Neural crest stem-like cells non-genetically induced from human gingiva-derived mesenchymal stem cells promote facial nerve regeneration in rats. *Mol. Neurobiol.* 55 (8), 6965–6983. doi:10.1007/s12035-018-0913-3

Zhang, Q., Nguyen, P., Xu, Q., Park, W., Lee, S., Furuhashi, A., et al. (2017). Neural progenitor-like cells induced from human gingiva-derived mesenchymal stem cells regulate myelination of schwann cells in rat sciatic nerve regeneration. *Stem Cells Transl. Med.* 6 (2), 458–470. doi:10.5966/sctm.2016-0177

Zhang, X., Qu, W., Li, D., Shi, K., Li, R., Han, Y., et al. (2020). Functional polymer-based nerve guide conduits to promote peripheral nerve regeneration. *Adv. Mat. Interfaces* 7 (14), 2000225. doi:10.1002/admi.202000225

Zhang, Q., Nguyen, P., Burrell, J. C., Zeng, J., Shi, S., Shanti, R. M., et al. (2021a). Harnessing 3D collagen hydrogel-directed conversion of human GMSCs into SCP-like cells to generate functionalized nerve conduits. *npj Regen. Med.* 6 (1), 59. doi:10.1038/s41536-021-00170-y

Zhang, R. C., Du, W. Q., Zhang, J. Y., Yu, S. X., Lu, F. Z., Ding, H. M., et al. (2021b). Mesenchymal stem cell treatment for peripheral nerve injury: a narrative review. *Neural Regen. Res.* 16 (11), 2170–2176. doi:10.4103/1673-5374.310941

Zhang, J., Liu, X., Ma, K., Chen, M., Xu, H., Niu, X., et al. (2021c). Collagen/heparin scaffold combined with vascular endothelial growth factor promotes the repair of neurological function in rats with traumatic brain injury. *Biomater. Sci.* 9 (3), 745–764. doi:10.1039/c9bm01446b

Zhang, D., Li, Z., Shi, H., Yao, Y., Du, W., Lu, P., et al. (2022). Micropatterns and peptide gradient on the inner surface of a guidance conduit synergistically promotes nerve regeneration *in vivo*. *Bioact. Mat.* 9, 134–146. doi:10.1016/j.bioactmat.2021.07.010

Zhu, S., Ge, J., Wang, Y., Qi, F., Ma, T., Wang, M., et al. (2014). A synthetic oxygen carrier-olfactory ensheathing cell composition system for the promotion of sciatic nerve regeneration. *Biomaterials* 35 (5), 1450–1461. doi:10.1016/j.biomaterials.2013.10.071

Zhuang, H., Bu, S., Hua, L., Darabi, M. A., Cao, X., and Xing, M. (2016). Gelatin-methacrylamide gel loaded with microspheres to deliver GDNF in bilayer collagen conduit promoting sciatic nerve growth. *Int. J. Nanomedicine* 11, 1383–1394. doi:10.2147/ijn.s96324

Zigmond, R. E., and Echevarria, F. D. (2019). Macrophage biology in the peripheral nervous system after injury. *Prog. Neurobiol.* 173, 102–121. doi:10.1016/j.pneurobio.2018.12.001

Frontiers in
Bioengineering and Biotechnology

Accelerates the development of therapies, devices, and technologies to improve our lives

A multidisciplinary journal that accelerates the development of biological therapies, devices, processes and technologies to improve our lives by bridging the gap between discoveries and their application.

Discover the latest Research Topics

See more →

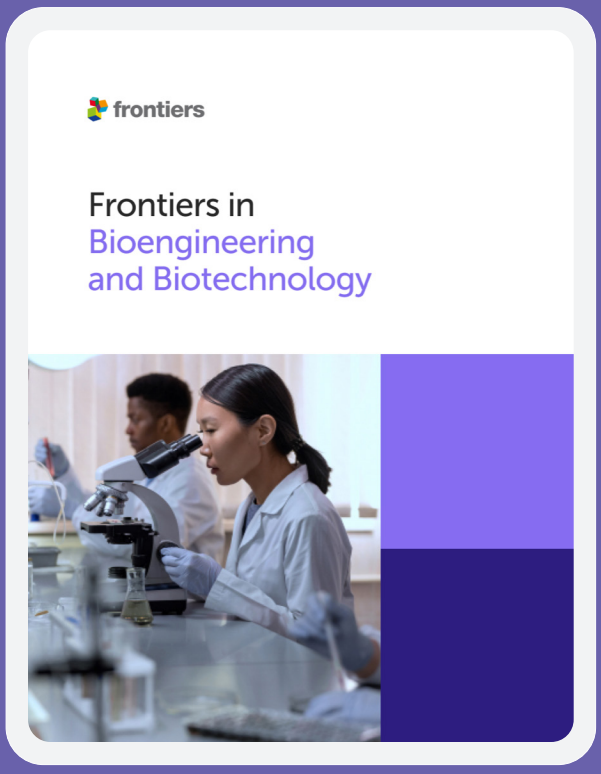

Frontiers

Avenue du Tribunal-Fédéral 34
1005 Lausanne, Switzerland
frontiersin.org

Contact us

+41 (0)21 510 17 00
frontiersin.org/about/contact